SHOUT
SHARE
IT

Volume 176 Number 2(S)

Marine Biological Laboratory
LIBRARY
MAY 15 1989
Woods Hole, Mass.

Ionic Currents in Development

An MBL Centennial Symposium Supplement to

THE BIOLOGICAL BULLETIN

Marine Biological Laboratory
LIBRARY
MAY 15 1989
Woods Hole, Mass.

Participants in Ionic Currents in Development Conference held at the Marine Biological Laboratory 3–6 September 1988: 1. Glen Winkel 2. Ben Peng 3. Julia Hush 4. Bob Wyman 5. Pamela Hayward 6. Yi-An Sun 7. Cynthia Troxell 8. Bill Lucas 9. Keerti Rathore 10. Nicolas Money 11. Jes Stollberg 12. Bill Parkinson 13. Yasunobo Okada 14. Arna Kerr 15. Richard Borgens 16. Pavel Kucera 17. Mary Jane Saunders 18. Laura MacGinitie 19. Joe Kunkel 20. Richard Nuccitelli 21. Richard Woodruff 22. Bill Diehl-Jones 23. Lionel Jaffe 24. Rachel Fink 25. Wiel Kuhtreiber 26. Barend Verachtert 27. Elizabeth Bowdan 28. Annelies Speksnijder 29. Danica Zivkovic 30. Shun-ichi Miyazaki 31. Robyn Overall 32. H. Hoch 33. Michele Miller Bever 34. Colin McCaig 35. Joe Vanable 36. Martin Steer 37. Hans Gruler 38. Shigetoshi Oiki 39. Darryl Kroph 40. Mark Eisenberg 41. Joachim Fisahn 42. Tim Ryan 43. Richard Staples 44. Rosemary White 45. Gene McGinnis 46. Hideaki Matsuoka 47. Steve Baumann 48. Ken Robinson 49. Wim Dictus 50. Mark Cooper 51. Rene Dohmen

Reference: *Biol. Bull.* **176(S)**: 3–4. (April, 1989, Suppl.)

Preface

Dear Reader:

The second conference on Ionic Currents in Development was held at the Marine Biological Laboratory here in Woods Hole on 3–6 September 1988; moreover, like the first one, it was (superbly!) organized by Richard Nuccitelli. Many of the speakers kindly agreed to furnish manuscripts covering their talks, and these are collected in this supplement to *The Biological Bulletin*. This introduction to it is intended to encourage you to read on; it is not a judicious precis.

In my mind, the highlight of this second conference on ionic currents was Woodruff's report that even a molecule as small as lucifer yellow can be electrophoresed across the bridge between *Drosophila* oocytes and their nurse cells. This finding considerably strengthens the idea that self-electrophoresis plays a significant role in establishing prepattern within eggs. It is true that Sun and Wyman failed to confirm the consistent pattern of extracellular currents previously reported around *Drosophila* follicles (Jaffe and Overall, 1985). However, Verachtert has recently confirmed direct microelectrode measurements of a standing voltage difference between the oocytes and nurse cells of *Drosophila* and (even more clearly) those of *Sarcophaga* (Verachtert, 1988). My own view is that the negative results of Sun and Wyman result from technical limitations. In this connection, two other conference participants told us of other recent findings that point toward transcytoplasmic self-electrophoresis (in *Xenopus* eggs; *cf.* Levine *et al.*, 1988), or at least indicate remarkably large steady transcytoplasmic voltage gradients (in illuminated internodal cells of *Chara*—Lucas and Fisahn, unpub.).

A related, interesting, and continuing issue is just how tight and how causal are the relationships between transcytoplasmic ion currents on the one hand and patterns of growth on the other. Gow presents evidence that patterns of electrical or net charge current through some fungal hyphae are only superficially related to their growth patterns; however, patterns of specific ion flow, as of hydrogen ions—or in other systems, calcium ions—may well be more tightly and indeed causally related to growth localization. For this reason, the paper (in progress) by Kühtreiber *et al.* on a calcium-specific vibrating probe may presage a considerable deepening of our understanding of developmental currents. This is particularly true because it should be only a short step from a calcium-specific vibrating probe to a proton-specific one and, indeed, to a whole line of ion-specific vibrating probes. Even without a vibrating proton probe, there is already evidence that proton currents are natural controls of growth in several plant systems. One thinks, for example, of Kropf's remarkable papers on fungal growth (*e.g.*, Kropf, 1986); moreover Miller's paper in this volume provides further evidence for the role of proton currents in normal root growth, Björkman's effectively uses a vibrating probe to further analyze graviperception in roots while Hush and Overall provide evidence for the role of proton (as well as calcium) currents in root wound healing.

Another fresh approach to elucidating the role of intracellular calcium gradients lies in the analysis of *long-term* responses to calcium buffer—particularly BAPTA-type buffer—injections. I have contributed an interim report on the "baptism" of fucoid eggs. This approach should help answer important questions raised by Kropf as well as by Brownlee about the exact role of calcium gradients within developing fucoid eggs. Three other very interesting systems where intracellular free calcium ion gradients may play a controlling role are growing pollen tubes, the synapse-forming muscle cell and the developing mollusc egg. Steer presents a very interesting review of calcium control of pollen growth; Peng and Zhu tell us more about postsynaptic differentiation while Zivkovic and Dohmen report their latest findings on currents—no

doubt including calcium currents—through developing snail eggs. Lest we focus too much on calcium and hydrogen ion currents, we should also consider the interesting report by Nawata *et al.* on the chloride-dominated currents through regenerating *Bryopsis* cells.

Finally, I should note several papers that further explore the effects of imposed, steady, electrical fields on cells: *e.g.,* that of Nuccitelli and Smart on neural crest migration, Stollberg and Fraser on the distribution of surface molecules in muscle cells, and that of Ryan *et al.* on such phenomena in tumor mast cells. Of course, such steady field effects may involve the indirect effects of induced intracellular calcium gradients as well as direct electrophoretic and electrosmotic effects. In particular the remarkable galvanotactic responses of neural crest cells to voltage drops as small as 0.4 mV per cell are likely to be mediated by local calcium ion influxes. Moreover, such cellular responses to small fields may well occur within whole organisms as well as *in vitro.* Chiang *et al.* present a very interesting approach to the possible role of skin wound fields in controlling wound healing.

—Lionel Jaffe

Literature Cited

Jaffe, L. F., and R. Overall. 1985. Patterns of ionic current through *Drosophila* follicles and eggs. *Dev. Biol.* **108:** 102–119.

Kropf, D. L. 1986. Electrophysiological properties of *Achlya* hypae. *J. Cell Biol.* **102:** 1209–1216.

Levine, E., R. Werner, and G. Dahl. 1988. Asymmetry of gap junction formation in *Xenopus* oocytes along the animal-vegetal axis. *Biophys. J.* **53:** 51a.

Nuccitelli, R. 1986. *Ionic Currents in Development.* Alan R. Liss, Inc., New York. 375 pp.

Verachtert, B. 1988. Electrical polarity in the ovarian follicles of *Sarcophaga bullata, Drosophila melanogaster* and *Locusta migratoria.* Ph.D. Thesis. Katholieke Universiteit Leuven.

Reference: *Biol. Bull.* **176(S):** 5–8. (April, 1989, Suppl.)

Calcium and Early Development in Fucoid Algae

DARRYL L. KROPF

Department of Biology, University of Utah, Salt Lake City, Utah 84112

Abstract. Understanding the mechanism by which a fertilized egg establishes an embryonic axis is of fundamental importance to the study of developmental biology. Much of what we have learned about axis formation in plants derives from investigations of fucoid algae. In this report I review the data concerning the role of Ca^{2+} in the early development of *Fucus* and *Pelvetia*. The evidence shows that Ca^{2+} plays an important role in germination and rhizoid growth, but its function in polarization remains uncertain.

Introduction

For over 100 years, brown algae of the order Fucales have served as model organisms for investigations of early development. The eggs of these algae are easily obtained, are relatively large (70–90 μm in diameter), and develop synchronously in culture. These features provide a unique opportunity to study the earliest events in plant zygotic embryogenesis. *Fucus* and *Pelvetia* are especially well suited for studies of the mechanism by which environmental gradients impose polarity on fertilized eggs. An egg, both before and soon after fertilization, bears no developmental axis. Approximately halfway through the first cell cycle the zygote acquires polarity and a number of external vectors, most notably unilateral light, can orient the polar axis. The newly formed axis determines the site at which the rhizoid will emerge from the cell body at germination. When zygotes are photopolarized with unilateral light, rhizoids form on the shaded hemisphere. The subsequent division is always perpendicular to the growth axis and delineates two cells of very different developmental fates. The rhizoid cell is the progenitor of the holdfast and the thallus cell gives rise to the fronds. The first cell cycle takes about one day to complete in *Fucus*.

Abbreviations: ASW, artificial seawater; EGTA, ethyleneglycol bis-(β-amino-ethyl ether) N,N,N^1,N^1-tetraacetic acid.

In 1923, E. J. Lund showed that imposed electric currents can orient the developmental axis and the position of rhizoid outgrowth in *Fucus* zygotes. More recent work by L. F. Jaffe and his colleagues R. Nuccitelli and K. R. Robinson has focused on an endogenous transcellular ionic current which is generated shortly after fertilization (for reviews see Jaffe, 1968; Jaffe *et al.*, 1975). These investigations and others suggested that the essence of polarization is the establishment of a transcellular Ca^{2+} current and a cytoplasmic Ca^{2+} gradient. However, we have recently obtained evidence which does not support this hypothesis. In this paper, I shall attempt to review briefly the literature and to discuss our present state of knowledge on the role of Ca^{2+} in fucoid embryogenesis.

Results and Discussion

Defining the stages of early development

Following fertilization of a fucoid egg it is useful to define carefully each stage of early development so that the role of Ca^{2+} in sequential events can be evaluated. For example, polarization is the process by which zygotes acquire a developmental axis. It can be further subdivided into two events, axis formation and axis fixation. Axis formation occurs from 5 to 9 h post-fertilization when *Fucus* zygotes are exposed to unilateral light (Kropf *et al.*, 1989). This initial polar axis is labile and can be reoriented by subsequent exposure to light vectors from different directions (Quatrano, 1973; Nuccitelli, 1978). Between 8 and 12 h, the axis becomes irreversibly fixed in space and can no longer be repositioned; this denotes axis fixation (Quatrano, 1973). Germination occurs between 13 and 17 h in *Fucus* and marks the initiation of tip growth. *Pelvetia* zygotes proceed through these developmental stages somewhat more rapidly and germinate between 9 and 12 h. It is important to note that germination is an expression of the developmental axis, but is not part of the polarization process. Polarization

and germination can be separated temporally using sucrose; zygotes form and fix an axis but cannot germinate in ASW containing 240 mg/ml sucrose (Quatrano, 1973).

Germination and rhizoid elongation

The rhizoid that emerges from the zygote at germination elongates by tip growth. Evidence indicates that calcium plays an important role in polarizing the extension of most tip-growing cells, and fucoid embryos are no exception. EGTA buffers that reduce the free Ca^{2+} concentration in ASW below 10^{-6} *M* completely block both germination and the elongation of preformed rhizoids, and Ca^{2+} channel blockers (La^{3+}, verapamil, and D600) do the same (Kropf and Quatrano, 1987). Measurements of localized fluxes demonstrate preferential uptake of $^{45}Ca^{2+}$ by rhizoids (Robinson and Jaffe, 1975), and, not surprisingly, Ca^{2+} also accumulates in the apex of emerging and elongating tips. This localization was initially determined by low-temperature autoradiography (Jaffe *et al.*, 1975; Gilkey and Jaffe, 1976). More recently, using Ca^{2+}-selective electrodes or quin-2 fluorescence, Brownlee and Wood (1986) found that the cytoplasmic Ca^{2+} concentration is nearly ten-fold greater in the apex than in the subapical cytoplasm. When visualized by CTC (chlorotetracycline) fluorescence, membrane-associated Ca^{2+} is also found to be localized at the germination site and in the apex of elongating tips (Kropf and Quatrano, 1987). Reductions in external Ca^{2+} that prevent tip elongation eliminate the apical CTC staining, suggesting that Ca^{2+} accumulation is required for sustained growth. Jaffe has recently shown that the internal Ca^{2+} gradient is also necessary for germination; BAPTA buffers inhibit the initiation of tip growth, presumably by collapsing the cytoplasmic Ca^{2+} gradient (pers. comm., Speksnijder *et al.*, 1989). Taken together, these data strongly support the tenant that localized Ca^{2+} transport and accumulation at the rhizoid site are essential for germination and tip elongation.

Polarization

Recent models postulate that formation of the embryonic axis is tantamount to the establishment of a cytoplasmic Ca^{2+} gradient (Quatrano *et al.*, 1979; Brawley and Robinson, 1985). It is thought that one of the earliest events is the redistribution of calcium channels such that they are concentrated at the future rhizoid site. This asymmetry establishes a Ca^{2+} current flowing into the presumptive rhizoid and out of the remaining zygote surface, which, in turn, gives rise to a cytoplasmic Ca^{2+} gradient oriented such that the more concentrated end resides at the future rhizoid site. Supportive and detractory evidence bearing on this hypothesis is analyzed below. Axis fixation is postulated to involve localized metabolic activation (Quatrano *et al.*, 1979; Brawley and Robinson, 1985) and/or the formation of transmembrane bridges (Kropf *et al.*, 1988). The involvement of Ca^{2+} in axis fixation has not been investigated extensively; what pertinent evidence there is is included in the following discussion.

Nuccitelli (1978) found that a transcellular ionic current begins to flow through the *Pelvetia* zygote during the period of axis formation (6 h post-fertilization) and that the site of inward current predicts the position of subsequent rhizoid outgrowth. Indirect evidence suggested that part of this inward current is carried by Ca^{2+}. The preferential uptake of Ca^{2+} into the presumptive rhizoid site during axis formation has been demonstrated directly. Robinson and Jaffe (1975) measured $^{45}Ca^{2+}$ fluxes in the two hemispheres of fertilized eggs and found preferential influx into the pre-rhizoid and preferential efflux from the pre-thallus. This asymmetry in Ca^{2+} fluxes is most intense 6 h post-fertilization, *i.e.*, at the time of axis formation, but remains throughout germination and rhizoid elongation (see above). These results provide a strong temporal correlation between calcium currents and axis formation, but do not address the issue of whether calcium is required for polarization.

One way to investigate calcium requirements is to remove calcium from the medium using EGTA buffers. We have recently taken this approach in *Fucus*. When cells were photopolarized in the presence of EGTA, well over 80% of the zygotes were able to form and to fix an axis in accordance with the light gradient even at extracellular Ca^{2+} concentrations calculated to be as low as 10^{-10} *M* (Kropf and Quatrano, 1987). Recall that tip growth and CTC fluorescence are inhibited below 10^{-6} *M* extracellular Ca^{2+}. Zygotes were also well polarized when exposed to EGTA for 2.5 h prior to photopolarization. In this case, 78% of zygotes treated with ASW containing 10^{-8} *M* free Ca^{2+}, and 83% of zygotes in ASW containing 10^{-10} *M* free Ca^{2+}, formed axes in accordance with the light vector and germinated on the shaded hemisphere. Eighty-four percent of untreated controls were polarized. Photopolarization in the presence of Ca^{2+}-channel blockers also does not prevent axis formation or fixation (Kropf and Quatrano, 1987). These results suggest that Ca^{2+} influx is not required for axis formation. If a cytoplasmic Ca^{2+} gradient is essential for axis formation, the zygotes must be capable of using internal stores (*e.g.*, mitochondria and endoplasmic reticulum) under conditions of Ca^{2+} deprivation.

We have also studied the distribution of membrane-associated calcium throughout early development in *Fucus* using CTC. During axis formation and fixation, membrane-associated Ca^{2+} is uniformly distributed about the cell cortex (Kropf and Quatrano, 1987); not

until germination does it accumulate at the rhizoid site. However, this may only indicate that CTC fluorescence does not reflect the pertinent Ca^{2+} pool within the cell, *i.e.*, the free, cytoplasmic Ca^{2+}. To date, other probes specific for cytoplasmic Ca^{2+} have not been used to investigate the Ca^{2+} distribution during axis formation in either *Fucus* or *Pelvetia*.

Externally imposed gradients have also been used to investigate the role of Ca^{2+} in early development. *Pelvetia* zygotes grown in the presence of a gradient of $CaCl_2$ or of the Ca^{2+}-ionophore A23187 form rhizoids toward the more concentrated end of the gradient (Robinson and Jaffe, 1976; Robinson and Cone, 1980). This suggests that an induced cytoplasmic Ca^{2+} gradient is sufficient to orient the axis. However, at least 15 other external gradients also polarize fucoid zygotes (Jaffe, 1968). In the context of ionic currents, I find it most intriguing that zygotes germinate on the high side of imposed pH and K^+ gradients (Jaffe, 1968), yet the role of these ions in polarization has not been fully investigated. Whether all the imposed gradients act via a common mechanism, and whether that mechanism involves Ca^{2+}, is unclear.

In my opinion, the results discussed above do not provide a clear picture of the role of calcium in polarization. A Ca^{2+} current begins to flow at the time of axis formation, but there is no direct evidence that an internal gradient is generated. If a cytoplasmic gradient is essential for axis formation, then zygotes must be able to establish it in the absence of Ca^{2+} influx, and presumably in the absence of a transcellular Ca^{2+} current. Although growth in external Ca^{2+} and A23187 gradients can be expected to generate cytoplasmic Ca^{2+} gradients, the significance of the polarization induced under these conditions is tempered by the observation that other ionic gradients are also effective in polarizing zygotes. Interpretation of the results is further complicated by the fact that much of the electrophysiological data comes from investigations of *Pelvetia*, while studies of calcium requirements have been done with *Fucus*.

Future research

I believe that three lines of investigation should be pursued to further our understanding of the role of Ca^{2+} in axis formation:

(1) Serious attempts must be made to measure the putative free, cytoplasmic Ca^{2+} gradient during axis formation. Different techniques, including Ca^{2+}-selective electrodes, aequorin, and fluorescent probes should be used so that the data can be compared and evaluated objectively. If a gradient is detected, attempts should be made to perturb it (perhaps using the BAPTA buffers Dr. Jaffe is currently investigating) in order to understand its relationship to axis formation. These experiments must be carefully designed to investigate axis formation as opposed to germination. It would also be informative to determine whether the gradient can be generated under conditions of Ca^{2+} deprivation.

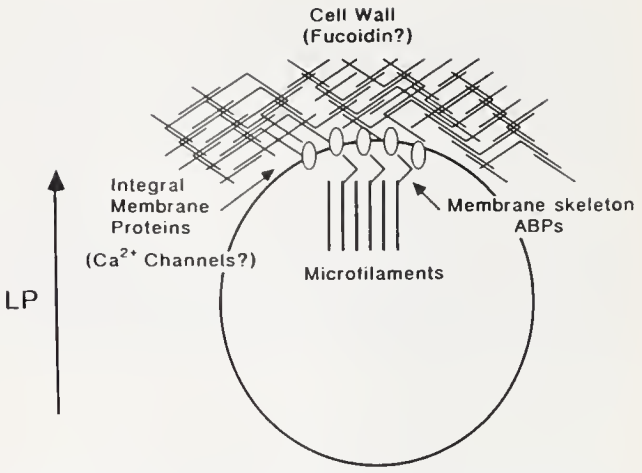

Figure 1. Model for axis fixation. A transmembrane bridge is localized at the presumptive rhizoid site on the shaded hemisphere in unilateral light. The direction of the light pulse is indicated by the arrow. Microfilaments are envisioned to be linked to integral membrane proteins via the membrane skeleton, which probably contains actin-binding proteins (ABPs). The integral membrane proteins associate with cell wall constituents. Much of the bridge may be composed of localized macromolecules. Microfilaments are localized in the rhizoid, as is the cell wall polysaccharide fucoidin F2. The membrane-spanning molecules may be Ca^{2+} channels, and these may also prove to be localized in the presumptive rhizoid. Drawing is not to scale.

(2) Much of the physiological information on early fucoid development has come from studies of *Fucus*. The transcellular current should be investigated during the early stages of *Fucus* development with the following questions in mind. Does the current flow during axis formation and does it precede and predict the site rhizoid emergence? How similar are the early currents in *Fucus* and *Pelvetia?* Does Ca^{2+} carry part of the early current? Manipulating the current by ion substitution and other procedures may provide important information that has not been forthcoming in studies of *Pelvetia*.

(3) Polarization of the embryonic axis certainly involves cytological and biochemical processes in addition to the transcellular current. These events need to be more fully investigated and the results integrated with the electrophysiological data. For example, axis fixation requires microfilaments (Quatrano, 1973) and cytological evidence shows that microfilaments localize to the presumptive rhizoid during fixation in both *Pelvetia* and *Fucus* (Brawley and Robinson, 1985; Kropf *et al.*, 1989). Experiments utilizing cytochalasins suggest that the localization of the filaments is necessary for axis fixation (Kropf *et al.*, 1989). Cell wall is also required for fixation, but not for formation, of the axis (Kropf *et al.*, 1988).

From these results we postulate that a localized transmembrane bridge from the microfilament cytoskeleton to the cell wall at the presumptive rhizoid may denote axis fixation (Fig. 1). Agents that perturb the organization of either the actin filament network or the cell wall would disrupt the bridge and block fixation, as observed. Microfilaments are envisioned to be linked indirectly to the plasma membrane via accessory proteins, such as actin-binding proteins. It is plausible that Ca^{2+} channels become localized in the plasma membrane at the rhizoid during axis formation (see above) and subsequently participate in the bridge by binding the accessory proteins.

Acknowledgments

I wish to thank Sonja Berge and Roswitha Hopkins who were involved in some of the research described. Most of all, I thank Dr. Ralph S. Quatrano in whose laboratory this research was conducted. His helpful advice and leadership were invaluable. This research was supported by an NSF Postdoctoral Fellowship in Plant Biology (No. DCB 8412389) to DLK, and NSF grant No. DCB 8511252 to RSQ.

Literature Cited

Brawley, S. H., and K. R. Robinson. 1985. Cytochalasin treatment disrupts the endogenous currents associated with cell polarization in fucoid zygotes: studies of the role of F-actin in embryogenesis. *J. Cell Biol.* **100:** 1173–1184.

Brownlee, C., and J. W. Wood. 1986. A gradient of cytoplasmic free calcium in growing rhizoid cells of *Fucus serratus*. *Nature* **320:** 624–626.

Gilkey, J. C., and L. F. Jaffe. 1976. Gradients of calcium ion concentration within *Pelvetia fastigiata* embryos. (Abstr.) *Biophys. J.* **16:** 110a.

Jaffe, L. F. 1968. Localization in the developing *Fucus* egg and the general role of localizing currents. *Adv. Morphog.* **7:** 295–328.

Jaffe, L. F., K. R. Robinson, and R. Nuccitelli. 1975. Calcium currents and gradients as a localizing mechanism. *ICN-UCLA Conference on Developmental Biology*, D. M. McMahon and C. F. Fox, eds. **2:** 135–147.

Kropf, D. L., S. K. Berge, and R. S. Quatrano. 1989. Actin localization during *Fucus* embryogenesis. *The Plant Cell* **1:** 191–200.

Kropf, D. L., B. Kloareg, and R. S. Quatrano. 1988. Cell wall is required for fixation of the embryonic axis in *Fucus* zygotes. *Science* **239:** 187–190.

Kropf, D. L., and R. S. Quatrano. 1987. Localization of membrane-associated calcium during development of fucoid algae using chlorotetracycline. *Planta* **171:** 158–170.

Lund, E. J. 1923. Electric control of organic polarity in the egg of *Fucus*. *Bot. Gaz.* **76:** 288–301.

Nuccitelli, R. 1978. Ooplasmic segregation and secretion in the *Pelvetia* egg is accompanied by membrane-generated electrical current. *Dev. Biol* **62:** 13–33.

Quatrano, R. S. 1973. Separation of processes associated with differentiation of two-celled *Fucus* embryos. *Dev. Biol.* **30:** 209–213.

Quatrano, R. S., S. H. Brawley, and W. E. Hogsett. 1979. The control of the polar deposition of a sulfated polysaccharide in *Fucus* zygotes. Pp. 77–96 in *Determinants of Spatial Organization*, S. Subtelny and I. R. Konigsberg, eds. Academic Press, New York.

Robinson, K. R., and R. Cone. 1980. Polarization of fucoid eggs by a calcium ionophore gradient. *Science* **207:** 77–78.

Robinson, K. R., and L. F. Jaffe. 1975. Polarizing fucoid eggs drive a calcium current through themselves. *Science* **187:** 70–72.

Robinson, K. R., and L. F. Jaffe. 1976. Calcium gradients and egg polarity. (Abstr.) *J. Cell Biol.* **70:** 37a.

Speksnijder, J. E., M. H. Weisenseel, T.-H. Chen, and L. F. Jaffe. 1989. Calcium buffer injections arrest fucoid egg development by suppressing calcium gradients. *Biol. Bull.* **176**(S): 9–13.

Reference: *Biol. Bull.* **176(S)**: 9–13. (April, 1989, Suppl.)

Calcium Buffer Injections Arrest Fucoid Egg Development by Suppressing Calcium Gradients

J. E. SPEKSNIJDER[1], M. H. WEISENSEEL[2], T.-H. CHEN[3], AND L. F. JAFFE[4]

Marine Biological Laboratory, Woods Hole, Massachusetts 02543

Abstract. The polarity of fucoid eggs is fixed when rhizoidal growth starts. A steady flow of calcium ions into the incipient tip is thought to establish a high calcium zone, which is needed for tip formation and outgrowth. To test this model, we injected six different BAPTA-type calcium buffers into *Pelvetia* eggs at about 3 to 7 h before outgrowth normally starts. Critical final cell concentration of each buffer proves to block outgrowth (as well as cell division) for up to two weeks.

The critical inhibitory concentration falls as the calcium dissociation constant, K_D, rises (and the buffers weaken) in the series of five buffers from 5,5′ dimethyl-bapta ($K_D = 0.4\ \mu M$) to 4,4′ difluoro-bapta ($K_D = 5\ \mu M$); then finally rises again with the weakest buffer tested, 5,5′ methylnitro-bapta ($K_D = 60\ \mu M$). Thus calcium buffers with a K_D of about $5\ \mu M$ prove most effective in blocking development. The effects of injecting a buffer do *not* depend upon the amount of coinjected calcium.

To analyze these results, we imagine that each buffer acts to facilitate free calcium diffusion and thus suppresses gradient formation. This model leads to an exact equation and prediction of the concentrations of various buffers needed to inhibit development. The data fit this equation rather well if it is assumed that the free calcium concentration in the incipient tip is normally kept at about $10\ \mu M$ and thus far above the general cytosolic level.

[1] Present address: Experimental Zoology Dept., Utrecht University, Padualaan 8, 3584 CH Utrecht, The Netherlands.

[2] Present address: Botanisches Institut der Universitat, Kaiserstrasse 2, Karlsruhe D-7500, Federal Republic of Germany.

[3] Present address: Botanical Institute, Academia Sinica, Nankang, Taipei, Taiwan, Republic of China.

[4] To whom all correspondence should be addressed.

Introduction

The localization of rhizoidal tip growth in the fucoid egg is a prototype of the localization problem in cellular development. The locus of tip growth can be determined by a variety of external stimuli. These varied stimuli are all thought to be amplified by the same positive feedback loop. This inner loop includes an influx of calcium ions into the nascent tip which, in turn, raises free calcium to a level far above the general cytosolic one. The evidence for this hypothesis is reviewed by Hepler and Wayne (1985).

Recently, Brownlee and Wood (1986) used calcium microelectrodes to measure a steady free calcium level of about $3\ \mu M$ within the growing tips of fucoid rhizoids—a level which is, indeed, far above the general cytosolic one. Nevertheless, there has been little evidence of either the existence or the need for a high calcium region in the nascent or incipient tip except for the observation that secretion (which is likely to be calcium-mediated) occurs there (Peng and Jaffe, 1976; Schroter, 1978). Because of this lack, the whole calcium hypothesis of tip localization has been seriously questioned by Kropf and Quatrano (1987).

Therefore, we reinvestigated the problem by injecting fucoid eggs at a stage well before tip localization with various calcium buffers. Our purpose was neither to change the free calcium level near the injection site nor to change the average free calcium level within the whole cytosol. Rather we aimed to inhibit the later development of calcium gradients and particularly the later formation of a high calcium region within the nascent tip. If such a high calcium region does indeed form and is needed, then appropriate buffer injections should block

tip formation. Here we report that microinjections of critical final cell concentrations of BAPTA-type buffers (Tsien, 1980) into *Pelvetia* eggs—particularly 1 to 2 m*M* dibromo BAPTA—permanently arrest development.

Materials and Methods

Ripe thalli of *Pelvetia fastigiata* were collected near Monterey, California. Gametes were obtained by exposing the thalli to a dark pulse after a light period of about 12–18 h (Jaffe, 1954). The BAPTA-type buffers were obtained from Molecular Probes.

At 5–9 h after fertilization, the eggs were injected via the quantitative, low pressure method of Hiramoto as described by Kiehart (1982). To minimize damage during pipette withdrawal, the eggs' turgor was reduced during injection by using seawater with 0.5 *M* mannitol added. Control eggs were injected with a background medium containing 550 m*M* mannitol, 200 m*M* KCl, and 5 m*M* HEPES, pH 7.0. Injections of up to about 15% of the egg volume did not disturb development and practically 100% of the injected controls developed as the uninjected ones. The buffer solutions contained 4 to 40 m*M* of BAPTA-type buffer and 0.1 mole of $CaCl_2$ per mole buffer except where counterindicated.

The final cytosolic concentrations of buffer were separately calculated for each injected egg taking the volume of injectate and egg into account and correcting for noncytosolic volume. The K_D's or dissociation constants of the BAPTA-type buffers were measured in 300 m*M* KCl solutions since this approximates the ionic strength of the cytosol. These values were taken from the unpublished data of R. Pethig, R. Payne, T.-H. Chen, E. Adler, and L. F. Jaffe.

Results

Qualitative observations

In control eggs cultured at 15°C, germination (*i.e.*, the initiation of rhizoidal tip growth) begins at about 12 h. In eggs injected with a critical final concentration of calcium buffer and cultured under the same conditions, germination is grossly delayed or permanently inhibited. Most of these arrested eggs remain dormant for one to two weeks. During this period they neither resume development nor die. In general, germination and division were tightly coupled: all of the eggs that germinated also divided; however, about 5 to 10% of those which failed to germinate nevertheless divided once.

Above the critical inhibitory concentration, eggs died within a day or two. Dead eggs were unmistakable on the basis of a combination of gross mottling, a change in color from olive green to brown, a gross layer of extracellular exudate, and the presence of numerous motile bacteria and protozoa attracted to the corpse.

Below the critical inhibitory buffer level, eggs developed normally. For example, in one experiment about half of the uninjected controls had begun apical differentiation by 11 days as marked by the formation of characteristic apical papillae; while one or two of four eggs injected to reach 1 to 2 m*M* BAPTA had likewise formed such papillae at this time.

Quantitative results

Figure 1 displays our main quantitative result. The mean inhibitory cytosolic buffer level *falls* steadily from 6.8 ± 1.9 m*M* to 1.2 ± 0.5 m*M* as the buffer's K_D rises from 0.40 μM (for 5,5′ dimethyl BAPTA) to 6.3 μM (for 4,4′ difluoro-BAPTA); then rises back up to 4.0 ± 0.3 μM for a buffer (5,5′ methylnitro BAPTA) with a K_D of 60 μM. These inhibitory concentrations are quite critical. Thus at day 2, half the eggs are dead at buffer concentrations only about 20 to 30% higher than the mean inhibitory ones.

Since the injections were done about 5 hours before germination normally begins and since inhibition usually lasts for at least a week it seems evident that the injected buffers do *not* work via their immediate effects on free calcium concentrations. If they did act in this way, their effects should depend upon the level of calcium in the injectate. So we checked this conclusion by injecting some eggs with media containing dibromo BAPTA without added calcium and some with media containing one mole of calcium per mole of the same buffer. We found no significant difference between the effects of injecting these two media and the main results of injecting this same buffer containing 0.1 mole of calcium per mole of buffer.

Analysis

We reason that a mobile calcium buffer acts by facilitating the diffusion of calcium away from a needed point of high calcium. The buffer does this by: (1) picking up free calcium at the high end of a steady gradient, (2) diffusing with its bound calcium to the low end where (3) the calcium is released, and (4) then diffusing back to the high end to pick up more calcium. This shuttle provides an alternate route for the diffusion of calcium down a gradient and thus effectively increases its diffusive mobility. Note that this cycle requires the buffer to be weak enough to release calcium at the low end of the gradient (step 3) as well as strong enough to pick it up at its high end (step 1). Therefore, a buffer is expected to be most effective when its K_D matches the (average) calcium level within the gradient. Injection of too strong a buffer with-

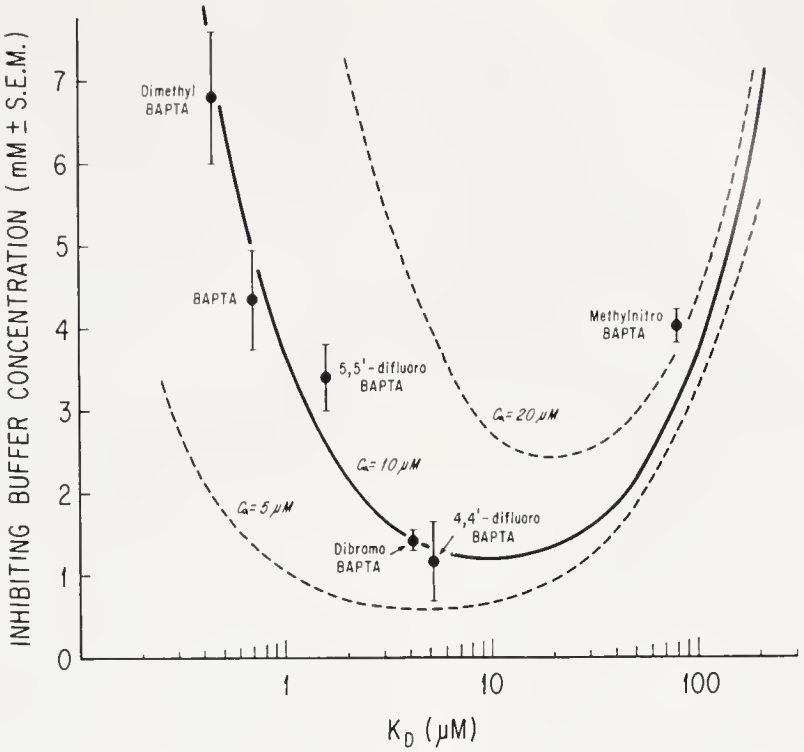

Figure 1. Critical inhibitory buffer concentration versus buffer dissociation constant, K_D. Each *data point* is an average of the final cytosolic buffer concentrations within all (*Pelvetia*) eggs that were still ungerminated on day 2, except for those injected with the apparently somewhat unstable 4,4'-difluoro BAPTA which were counted on day 1. The solid *line* is calculated from equation (1) with r = 1, C = 10 μM, $D_{Ca}/D_B = 17$; the dotted ones with C = 5 or 20 μM. From work in progress. Fuller results, including additional buffers, will be reported elsewhere.

out bound calcium will initially extract calcium from sources within and without the cell; but thereafter it will just sit, unable to release its bound calcium and will thus remain inert as yolk.

Because of their very high reaction rates (Quast *et al.*, 1984), we assume that a BAPTA-type buffer is everywhere in near local equilibrium with free Ca^{2+}. We may then ask how large the buffer-mediated or facilitated calcium flux, J_B, is between any two points as compared to the direct flux, J_{Ca}, of free Ca^{++}. Presumably the buffer will begin to effect the cell when these two fluxes become comparable.

A quantitative analysis of this model (to be presented elsewhere) yields the following equation:

$$B = rC \cdot (D_{Ca}/D_B) \cdot [(1 + F)^2/F] \qquad (1)$$

where:

B is the critical inhibitory buffer concentration;
r is J_B/J_{Ca} at this concentration;
C is the average concentration of free Ca^{++} in the region containing the gradient needed for development;
D_{Ca} and D_B are the cytosolic diffusion constants of *free* Ca^{++} and buffer, respectively; and
$F = K_D/C$ where K_D is the buffer's cytosolic dissociation constant.

In order to apply (1) to our data, we must assume that the fucoid egg is in a relatively steady state, *i.e.*, that the free Ca^{2+} in the cytosol turns over many times during the transitions considered. The following calculations indicate that this is a safe assumption: Figure 3 of Robinson and Jaffe (1975) indicates that the ungerminated *Pelvetia* egg turns over its calcium at about .054 picomoles/h. The total amount of free calcium in the cytosol may be reasonably estimated to be about 0.3 μM (Brownlee and Wood, 1986) times one third of the 400 pl egg volume or 1.2×10^{-4} picomoles. Dividing this by the turnover rate yields an estimated free calcium turnover time of only 8 s. The transitions involved in establishing a point of outgrowth seem to be the order of an hour and thus nearly a thousand times longer than this turnover time.

In order to apply (1), we must also estimate the ratio, D_{Ca}/D_B. D_B is reported to be 3.9×10^{-7} and 3.6×10^{-7}

cm^2/s for the BAPTA-type buffer, fura-2, within frog and barnacle muscle, respectively (Timmerman and Ashley, 1986; Baylor and Hollingworth, 1988). These values of D_B average 3.8×10^{-7} cm^2/s. D_{Ca} is reported to be 5.3×10^{-6} cm^2/s in *Myxicola* (worm) axoplasm and 7.5×10^{-6} cm^2/s in unsupported aqueous media of similar ionic strength (Donahue and Abercrombie, 1987; Harned and Owen, 1958). The former figure was obtained under conditions that clearly blocked active uptake but may not have fully blocked passive binding. It may therefore have somewhat underestimated the true value. However, the latter figure should overestimate it due to a lack of tortuosity. Hence we will use their average, 6.4×10^{-6} cm^2/s. Thus our best estimate of the ratio D_{Ca}/D_B to be put in (1) is $6.4 \times 10^{-6}/3.8 \times 10^{-7}$ or 17.

Finally, in Figure 1 we apply (1) to our data on the further assumption that germination is about half inhibited when the buffer-mediated and direct fluxes of Ca^{++} are equal, *i.e.*, when r = 1. One sees a rather good fit of (1) to the data if C, the (average) free Ca^{++} within the imagined gradient, is taken to be about 10 μM; but not if C is taken to be 5 or 20 μM.

Discussion

Tip growth

Figure 1 shows a rather good fit of the data to equation (1), which is obtained from our facilitated diffusion theory. We take this as strong evidence that the theory is essentially correct and that the nascent growth region both contains and needs free calcium of the order of 10 μM and thus far above the general cytosolic level.

This analysis then raises the question of just where the inferred high calcium zone is within ungerminated eggs. A number of considerations suggest that this high calcium zone lies just below the plasma membrane of the nascent tip. It is there that inflowing calcium first arrives. It is there that secretion as well as further influx must be controlled. It is there that (transient) high calcium occurs in active neurons (Gorman *et al.*, 1984; Simon and Llinas, 1985). And it is there that Kropf and Quatrano (1987) have seen strong chlorotetracycline fluorescence in just germinated *Pelvetia* eggs (see their Fig. 2a). Chlorotetracycline fluorescence is believed to indicate membrane-bound rather than free calcium; however, fluorescence from surface or near surface membranes may well reflect high calcium within the subsurface space.

Cell division

With few exceptions, *Pelvetia* eggs that failed to germinate likewise failed to divide; while those that did germinate divided normally. There is no reason to believe that the germination of fucoid eggs induces their division or visa versa. Normally, they germinate long before they divide; however, if germination is osmotically suppressed with high sugar concentrations, they will nevertheless undergo numerous divisions (Torrey and Galun, 1970). We would therefore infer that injected BAPTA-type buffers block cell division by blocking the formation of some comparable high calcium region which is quite separate from the one in either the nascent or active growth tip.

Cell death

Why do eggs that are overloaded with calcium buffer die in a day or two? We would imagine that the same reduction in subsurface calcium that blocks germination also speeds calcium influx. If this accelerated influx exceeds the egg's ability to pump calcium out, the cell will ultimately become overloaded with calcium and die of calcium poisoning. This hypothesis is quite consistent with what is known of calcium turnover in *Pelvetia* eggs. Thus it can be calculated from the data of Allen *et al.* (1972) that a *Pelvetia* egg contains a total of about 1.3 picomoles of intracellular calcium while we noted above that this egg turns over its calcium at about .054 picomoles/h. The ratio yields a turnover time of about one day. Moreover, acceleration of calcium influx by reduced subsurface calcium is a negative feedback mechanism that would seem to be essential for calcium control in almost any living cell and, in fact, is well known to exist in a wide variety of cells (Eckert and Chad, 1984).

Broader implications

Our results provide considerable confidence that injections of BAPTA-type buffers, together with equation (1), can effectively test for the actions of relatively steady free calcium gradients within cells. Much as cytochalasin immersal tests for the action of an actin cytoskeleton, so "baptism" may test for the actions of steady calcium gradients.

Most buffer injection studies have been effectively designed to immediately reset the calcium level (*e.g.*, see Gilkey, 1983). However, we would note one interesting exception which our facilitated diffusion theory may illuminate: Twigg *et al.* (1988) recently reported that injection of BAPTA into sea urchin eggs to reach "1.8 mM" blocks nuclear envelope breakdown in half of the injected eggs. Since this process would normally have occurred about 45 min after injection, a steady state analysis may well be applicable. These authors did not correct their 1.8 mM buffer figure for either noncytosolic volume or for inert impurities in the buffer. When this is done, one finally obtains a half inhibition value of about

4 mM BAPTA for nuclear envelope breakdown in sea urchin eggs. This figure is obviously within experimental error of the 4.4 ± 1.3 mM figure we find for the arrest of tip growth and cell division of BAPTA in fucoid eggs. We would therefore propose that the peak inner calcium level needed to support nuclear envelope breakdown in sea urchin eggs is likewise about 10 μM.

Acknowledgments

We thank Michael Kuhn of Molecular Probes for synthesizing 5,5′ methylnitro BAPTA. This work was supported by Grant No. HD18818 from the National Institutes of Health, Grant No. 88-37261-3984 from the United States Department of Agriculture as well as travel funds from the Academia Sinica for T.-H.C.

Literature Cited

Allen, R. D., L. Jacobsen, J. Joaquin, and L. F. Jaffe. 1972. Ionic concentrations in developing *Pelvetia* eggs. *Dev. Biol.* **27:** 538–545.

Baylor, S. M., and S. Hollingworth. 1988. Fura-2 calcium transients in frog skeletal muscle fibres. *J. Physiol.* **403:** 151–192.

Brownlee, C., and J. W. Wood. 1986. A gradient of cytoplasmic free calcium in growing rhizoid cells of *Fucus serratus*. *Nature* **320:** 624–626.

Donahue, B. S., and R. F. Abercrombie. 1987. Free diffusion coefficient of ionic calcium in cytoplasm. *Cell Calcium* **8:** 437–448.

Eckert, R., and J. E. Chad. 1984. Inactivation of Ca channels. *Prog. Biophys. Molec. Biol.* **44:** 215–267.

Gilkey, J. C. 1983. Roles of calcium and pH in activation of eggs of the medaka fish, *Oryzias latipes*. *J. Cell Biol.* **97:** 669–678.

Gorman, A. L. F., S. Levy, and D. Tillotson. 1984. Intracellular calcium measured with calcium-sensitive micro-electrodes and arsenazo III in voltage-clamped *Aplysia* neurones. *J. Physiol.* **353:** 127–142.

Harned, H. S., and B. B. Owen. 1958. *The Physical Chemistry of Electrolytic Solutions*. Reinhold, New York. 259 pp.

Hepler, P. K., and R. O. Wayne. 1985. Calcium and plant development. *Ann. Rev. Plant Physiol.* 36: 397–439.

Jaffe, L. F. 1954. Stimulation of the discharge of gametangia from a brown alga by a change from light to darkness. *Nature* **174:** 743.

Kiehart, D. P. 1982. Microinjection of echinoderm eggs. *Methods Cell Biol.* **25:** 13–31.

Kropf, D. L., and R. S. Quatrano. 1987. Localization of membrane-associated calcium during development of fucoid algae using chlorotetracycline. *Planta* **171:** 158–170.

Peng, H. B., and L. F. Jaffe. 1976. Cell wall formation in *Pelvetia* embryos; a freeze-fracture study. *Planta* **133:** 57–71.

Quast, U., A. M. Labhardt, and V. M. Doyle. 1984. Stopped-flow kinetics of the interaction of the fluorescent calcium indicator Quin 2 with calcium ions. *Biochem. Biophys. Res. Commun.* **123:** 604–611.

Robinson, K. R., and L. Jaffe. 1975. Polarizing fucoid eggs drive a calcium current through themselves. *Science* **187:** 70–72.

Schroter, K. 1978. Asymmetrical jelly secretion of zygotes of *Pelvetia* and *Fucus*. *Planta* **140:** 69–73.

Simon, S. M., and R. R. Llinas. 1985. Compartmentalization of the submembrane calcium activity during calcium influx and its significance in transmitter release. *Biophys. J.* **48:** 485–498.

Timmerman, M. P., and C. C. Ashley. 1986. Fura-2 diffusion and its use as an indicator of transient free calcium changes in single striated muscle cells. *FEBS Lett.* **209:** 1–8.

Torrey, J. G., and E. Galun. 1970. Apolar embryos of *Fucus* resulting from osmotic and chemical treatment. *Am. J. Bot.* **57:** 111–119.

Tsien, R. Y. 1980. New calcium indicators and buffers with high selectivity against magnesium and protons. *Biochemistry* **19:** 2396–2404.

Twigg, J., R. Patel, and M. Whitaker. 1988. Translational control of $InsP_3$-induced chromatin condensation during the early cell cycles of sea urchin embryos. *Nature* **332:** 366–369.

Reference: *Biol. Bull.* **176(S)**: 14–17. (April, 1989, Suppl.)

Visualizing Cytoplasmic Calcium in Polarizing Zygotes and Growing Rhizoids of *Fucus Serratus*

COLIN BROWNLEE

Marine Biological Association, The Laboratory, Citadel Hill, Plymouth, Devon PL1 2PB, U. K.

Abstract. Evidence for spatial variations in cytoplasmic free Ca^{2+} in tip-growing cells is briefly summarized. Methods are described for detecting such gradients using fura-2 with dual wavelength excitation fluorescence microscopy. Results so far indicate that gradients of Ca^{2+} are present in growing rhizoid cells but physiologically significant gradients have not yet been detected in the early stages of polarization.

Introduction

The *Fucus* zygote is an especially valuable organism for the study of the cellular events involved in the formation of a highly polarized structure from a non-polarized egg. The way in which factors such as light and external ionic gradients interact with the receptor mechanisms to dictate the axis of polarity and the direction of growth of the rhizoid cell are equally interesting. Based mainly on measurements of electrical current entry into cells using the vibrating probe, the role of an inwardly directed Ca^{2+} current leading to the establishment of a gradient of Ca^{2+} has been postulated (*e.g.*, Jaffe and Nuccitelli, 1977; Robinson and Cone 1980; Jaffe, 1986). The realization that free cytosolic Ca^{2+} is an important second messenger and regulator of cell functions has given new significance to this hypothesis.

Two distinct processes in the development of polarity in *Fucus* are beginning to emerge, namely the acquisition of a polar axis and the growth of the rhizoid cell associated with germination (see report by Kropf, this volume). The involvement of Ca^{2+} in germination and rhizoid growth is becoming clear. This process is calcium-dependent. Removing Ca^{2+} from the external medium or incubating zygotes in the presence of Ca^{2+} channel blockers inhibits rhizoid growth (Kropf and Quatrano, 1987). Indirect evidence for a gradient of free cytosolic Ca^{2+} in germinating zygotes has been provided by the use of ^{45}Ca autoradiography (Gilkey and Jaffe, 1976) and chlorotetracycline (Kropf and Quatrano, 1987). While these studies showed that total and membrane-bound Ca^{2+} were elevated in the growing rhizoid tip, it is difficult to assign a physiological function to such gradients. Using Ca^{2+}-selective electrodes, elevated levels of free Ca^{2+} were detected in the rhizoid tips of 2–3 day old *Fucus serratus* zygotes (Brownlee and Wood, 1986). The role of Ca^{2+} in the fixation of the polar axis of recently fertilized zygotes is less clear. Axis formation has been demonstrated in the absence of external Ca^{2+} and in the presence of Ca^{2+} channel blockers (Kropf and Quatrano, 1987). This may mean that the mechanism by which the Ca^{2+} channel gradient is established is Ca^{2+}-independent. This mechanism is likely to be membrane-associated since the actions of the variety of agents known to induce polarity (*e.g.*, light, external ionic and ionophore gradients) can only reasonably be explained in terms of their interaction with the cell membrane. The simplest mechanism involves the asymmetric insertion or activation of (Ca^{2+}?) channels at the site of future rhizoid outgrowth. It is important to know at what stage a cytosolic Ca^{2+} gradient can be detected and how this relates temporally to the fixation of the polar axis, *i.e.*, is a Ca^{2+} gradient the result of asymmetric channel activity or does it preceed it?

This report summarizes evidence for cytosolic Ca^{2+}

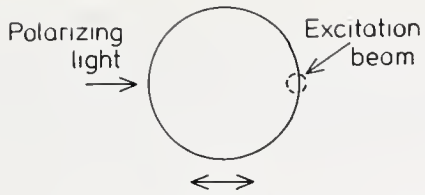

Figure 1. Schematic diagram of polarizing *Fucus* zygote showing method of excitation of fluorescently labelled cell.

gradients in polarized and polarizing zygotes using the fluorescent Ca^{2+} indicator fura-2. The spectral properties of fura-2 are such that the ratio of fluorescence following excitation with 350 (or 360) and 385 nm light is calcium-dependent. (Grynkievicz *et al.*, 1985; Tsien *et al.*, 1985; Cobbold and Rink, 1987).

Materials and Methods

Zygote growth and dye loading

Zygotes of *Fucus serratus* could not be loaded with fura-2 acetoxymethyl ester. Fura-2 free acid was injected iontophoretically via an intracellular electrode containing 1 m*M* fura-2 pentapotassium salt (Molecular Probes, Oregon) in distilled water (Brownlee and Pulsford, 1988). Tips of filamented microelectrodes were filled with fura-2 by briefly dipping the back end of the electrode in solution. A silver/silver chloride wire was inserted into the electrode. It was not necessary to backfill with electrolyte to achieve electrical contact. For injection of growing rhizoids, zygotes were germinated in filtered seawater on coverslips for two days in unilateral light. Microelectrodes were inserted from above by bending the electrode tips by 90°. Recently fertilized eggs and polarizing zygotes were held in 1% seawater agarose (ultra-low melting point, Sigma, U. K.) in unilateral light for varying periods prior to microinjection. Microinjection of polarizing zygotes was more difficult than growing rhizoids, apparently due to their lower turgor and thicker cell wall. Zygotes were held with a suction pipette during microinjection. Cells were observed during microinjection with a ×20 long working distance objective.

Fluorescence microscopy and image analysis

Fluorescence ratio images of growing rhizoids loaded with fura-2 and excited with 350 and 385 nm light were obtained as described in Brownlee and Pulsford (1988), using a Kontron (W. Germany) image analyzer. For detection of spatial variations in Ca^{2+} in recently fertilized polarizing zygotes, cells were observed with a modified M2 micromanipulation microscope (Microinstruments, U. K.), using a ×40 water immersion objective (Zeiss, W. Germany). Excitation was provided from a 150-watt xenon lamp source via a fluid light guide (Microinstruments, U. K.) into the fluorescence port of the microscope. Light (360 and 385 nm) was obtained with interference filters (Ealing Electrooptics, U. K.) held in a rotating disc in front of the light source. This was driven by a stepper motor controlled by a BBC microcomputer. Excitation light could be reduced to a 10-μm diameter spot using an iris diaphragm (Fig. 1). Emission at 510 nm was monitored with a photomultiplier tube (PM 9924B, EMI, U. K.).

Autofluorescence subtraction and 360/385 nm signal ratios were performed automatically by the microcomputer. Filters were alternated to give one ratio per second. By slowly moving the cell across the excitation beam, a profile of 360/385 nm ratio could be obtained. Alternatively, selected areas of the cell could be observed for varying times. Using this method of fluorescence measurement, Ca^{2+} data could be obtained with very low dye loading. This is desirable since fura-2 is known to chelate Ca^{2+} and high intracellular concentrations may dissipate any small gradients in the cell. Sufficient dye could be loaded into the cell after iontophoresing for only 30 s [*cf.* 3–5 min for imaging with an image-intensified TV camera (Brownlee and Pulsford, 1988)].

Results

Figure 2 shows a 350/385 nm ratio image of a fura-2-loaded rhizoid of *Fucus serratus*. Brighter areas represent higher Ca^{2+} levels. Ca^{2+} is elevated at the growing rhizoid tip. A full account of these experiments is given in Brownlee and Pulsford (1988). In summary, work with

Figure 2. 350/385 nm ratio image of a fura-2-loaded rhizoid cell. Bar = 10 μm.

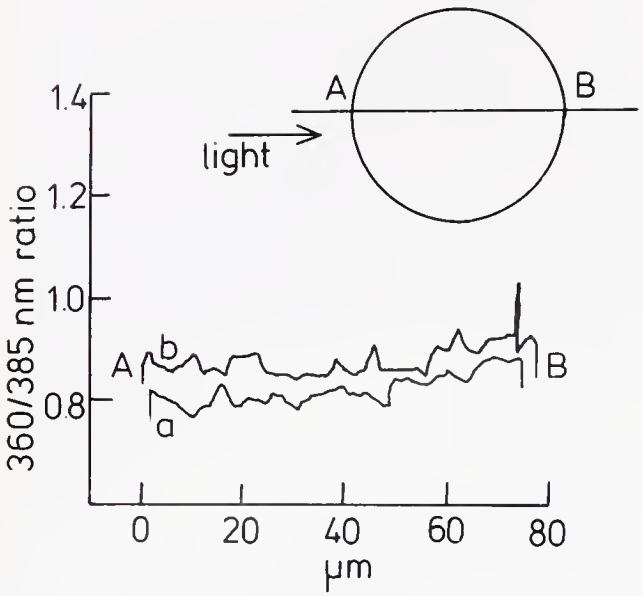

Figure 3. 350/385 nm ratio profiles across zygotes polarized for 5 h (a) or 7 h (b).

growing rhizoids has shown the following: (a) higher fura-2-visualized Ca^{2+} levels occur in about 50–60% of rhizoids so far studied. (b) Considerable variation in the pattern of Ca^{2+} distribution has been observed. (c) Verapamil reduced but did not abolish the magnitude of the gradient, though no effect could be observed with nifedipine. (d) Permeabilizing the cell by removing external Ca^{2+} via EGTA resulted in a loss of fura-2 from the cytoplasmic compartment, leaving a very low fluorescence in the (presumably) vacuolar compartment and perhaps allowing an assessment of the degree of dye sequestration by vesicles and vacuoles.

Figure 3 shows representative preliminary data for 360/385-nm ratio profiles taken across polarizing zygotes in unilateral light, 5 and 7 hours after fertilization as described in Materials and Methods. There is evidence from both profiles that Ca^{2+} is very slightly elevated at the shaded side of the zygote. However, the difference in terms of $[Ca^{2+}]$ concentration is very small. A provisional estimate based on *in vitro* calibration curves indicates that this difference is less than 100 n*M*.

Discussion

Work with Ca^{2+} electrodes and fluorescent indicators (Brownlee and Wood, 1986; Brownlee and Pulsford, 1987) suggests that the growing rhizoid cell of *Fucus serratus* has elevated levels of free cytoplasmic Ca^{2+} at the cell apex. There is also evidence from work using the fluorescent indicator quin-2 with pollen tubes that Ca^{2+} is elevated at the apex (Nobiling and Reiss, 1987). However, we have not observed any significant Ca^{2+} gradients in growing tomato root hairs (Clarkson *et al.*, 1988). This is perhaps not surprising since these cells show very vigorous cytoplasmic streaming which would tend to dissipate any Ca^{2+} gradient. The spatial resolution of our measuring system was not sufficient to detect any elevated Ca^{2+} in the apical one or two μm of the hair.

The very limited evidence so far available suggests that a physiologically significant gradient of cytoplasmic Ca^{2+} is not detectable up to 7 h after the onset of a polarizing stimulus, though slightly elevated levels are detectable at the shaded side of the zygote. It is possible that there is a highly localized region of elevated Ca^{2+} immediately adjacent to the membrane on the shaded side that is not resolved by our measuring system. Clearly, a very detailed time course needs to be carried out for up to 12 h after fertilization, when axis fixation is complete and germination begins. This needs to be coupled with information on the precise time of axis fixation (Kropf and Quatrano, 1987). More information is urgently needed on the changes in ultrastructure and membrane properties during axis fixation. Information gained from other methods of measuring cytoplasmic Ca^{2+} will be very valuable, particularly via the use of aequorin. Aequorin has the advantage that it does not partition into subcellular compartments. The fairly large and spherical nature of the *Fucus* zygote imposes limits on the degree of spatial resolution of fluorescence signals due to interference from surrounding regions. It is hoped that advances in confocal microscopy may in the future circumvent some of these problems.

While the data obtained so far are insufficient to allow us to make any firm conclusions, they are consistent with the hypothesis that polarization involves the incorporation of Ca^{2+} channels into the shaded side of the membrane (Kropf *et al.*, 1988) and that this is not dependent on the presence of a significant Ca^{2+} gradient. The slight differences in $[Ca^{2+}]$ observed here may reflect the gradual incorporation of such channels.

Acknowledgment

This work was supported by a grant-in-aid to the MBA from the Natural Environment Research Council.

Literature Cited

Brownlee, C., and A. L. Pulsford. 1988. Visualization of the cytoplasmic Ca^{2+} gradient in *Fucus serratus* rhizoids; correlation with cell ultrastructure and polarity. *J. Cell Sci.* **91**: 249–256.

Brownlee, C., and J. W. Wood. 1986. A gradient of cytoplasmic free

calcium in growing rhizoid cells of *Fucus serratus*. *Nature* **320:** 624–626.

Clarkson, D. T., C. Brownlee, and S. M. Ayling. 1988. Cytoplasmic calcium measurements in intact higher plant cells; results from fluorescence ratio imaging of fura-2. *J. Cell Sci.* **91:** 71–80.

Cobbold, P. H., and T. J. Rink. 1987. Fluorescence and bioluminescence measurements of cytoplasmic free calcium. *Biochem. J.* **248:** 313–328.

Gilkey, J. C., and L. F. Jaffe. 1976. Gradients of calcium ion concentration within *Pelvetia fastigiata* embryos. (Abstr.) *Biophys. J.* **16:** 110a.

Grynkiewicz, G., M. Poenie, and R. Y. Tsien. 1985. A new generation of calcium indicators with greatly improved fluorescence properties. *J. Biol. Chem.* **260:** 3440–3450.

Jaffe, L. F. 1986. Calcium and morphogenic fields. Pp. 271–288 in *Calcium and the Cell*, D. Evered and J. Whelan, eds. Wiley, Chichester.

Jaffe, L. F., and R. Nuccitelli. 1977. Electrical controls of development. *Annu. Rev. Biophys. Bioeng.* **6:** 445–476.

Kropf, D. L., B. Kloareg, and R. S. Quatrano. 1988. Cell wall is required for fixation of the embryonic axis in *Fucus* zygotes. *Science* **239:** 187–190.

Kropf, D. L., and R. S. Quatrano. 1987. Localization of membrane-associated calcium during development of fucoid algae using chlorotetracycline. *Planta* **171:** 158–170.

Nobiling, R., and H.-D. Reiss. 1987. Quantitative analysis of calcium gradients and activity in growing pollen tubes of *Lilium longiflorum*. *Protoplasma* **139:** 20–24.

Robinson, K. R., and R. Cone. 1980. Polarization of fucoid eggs by a calcium ionophore gradient. *Science* **207:** 77–78.

Tsien, R. Y., T. J. Rink, and M. Poenie. 1985. Measurements of cytosolic free calcium in individual small cells using fluorescence microscopy with dual excitation wavelengths. *Cell Calcium* **6:** 145–157.

Reference: *Biol. Bull.* **176(S)**: 18–20. (April, 1989, Suppl.)

Calcium Control of Pollen Tube Tip Growth

MARTIN W. STEER

Department of Botany, University College, Dublin, Ireland

Abstract. The role of calcium in pollen tube tip growth is reviewed. Calcium ions are essential for growth, but are inhibitory at high concentrations (above c. 10^{-2} *M*). Calcium intake is limited to the growing tip, and the inward flux of calcium appears to establish an ionic current within the surrounding medium. Cellular transport of calcium is reviewed against a background of the functional requirements for calcium ions. It is concluded that calcium-induced polarized tip growth depends on a dual control system: (1) intake through spatially localized calcium ion channels coupled with (2) cytoplasmic sequestration and transport from the tip region in organelles. This system maintains conditions appropriate for directed activity of the cytoskeleton and subsequent vesicle fusion at the growing tip.

Introduction

Pollen grains of many plant species germinate when placed in an artificial medium forming a pollen tube that extends by tip growth. Apart from non-permeant solutes (sucrose, polyethylene glycol, etc.), the medium need only contain the mineral ions of potassium, calcium, and borate with appropriate anions such as phosphate and nitrate or chlorine. The requirement for calcium is absolute, with growth only possible over a 1000-fold concentration range centered at about 5×10^{-4} *M* [Ca^{2+}] (Picton and Steer, 1983). Calcium enters at the tip of the tube, with other positive ions, mainly protons, leaving at the basal region (Weisenseel *et al.*, 1975).

Pollen tubes grown on such media exhibit an internal calcium gradient that ranges from high levels just behind the tip to low levels at the base, as measured by a variety of techniques. The gradients have been recorded as total (Reiss *et al.*, 1985), soluble cytoplasmic (Reiss and Nobiling, 1986), and membrane-associated calcium (Reiss and Herth, 1978). The Ca^{2+} gradients in all cases appear smooth, rather than stepped, with a sharp decline near the tip followed by a more gradual falling off towards the base.

Structurally, the tubes also exhibit a gradient of organelles, but this gradient is marked by sharply contrasted boundaries. A vesicle-rich zone at the tip is followed by a narrow band of mitochondria (Reiss and Herth, 1979). Behind this band the main part of the tube is occupied by streaming cytoplasm which is rich in the entire spectrum of organelles normally found in a plant cell.

The growth process ensures that new plasma membrane and carbohydrate wall components are added to the tip of the growing tube from secretory vesicles in a manner that results in the maintenance of tube diameter, apex shape, cell wall thickness, and direction of growth. This polarized growth process can be affected by a number of factors, that include interactions with calcium ions. Since disruption of the normal regulated supply of external calcium leads to immediate changes in the calcium gradients, it is not clear at which level calcium operates to control growth.

A sudden increase in the external calcium concentration to supraoptimal levels, or the addition of the calcium ionphore A23187 in the presence of optimal external calcium leads to the cessation of growth, but not wall deposition so that continued secretion builds a much thickened cell wall at the tip (Picton and Steer, 1983). Conversely, depriving the cells of calcium or application of the calcium-channel blocker nifedipine leads to a localized swelling at the tube tip (Reiss and Herth, 1985) with a thinning of the cell wall (Steer, in prep.).

Pollen tube growth depends on a forward growth process coupled with a restriction of lateral cell expansion so that a tube of more or less constant diameter is formed. The observed interactions between tip growth and various external conditions described above do not immediately lead to an understanding of the role of calcium in tip growth. This is because it is not possible to isolate the act of inflowing Ca^{2+} current through the membrane

from (1) the action of calcium on the immediate apical cytoplasmic environment and (2) from the cytoplasmic calcium transport system that establishes the observed internal gradient. All three factors (point of calcium entry, internal calcium gradient, local secretion of wall material) have been proposed, at one time or another, to be the decisive determinant of the polarized tip growth system (Sievers and Schnepf, 1981; Schnepf, 1986).

Calcium-Cell Wall Interaction

Calcium could control the tip extension process by stabilizing new cell wall components released from a localized part of the cell surface (Heslop-Harrison, 1987). Internal turgor pressure would cause expansion of the cell surface immediately beneath the newly secreted polymer (Sievers and Schnepf, 1981). Current information suggests that calcium binds with the cell wall components over a much lower range of calcium concentrations (10^{-6}–10^{-3} M) than that which affects tube growth rate (Baydoun and Brett, 1984). The reduction in growth rate with increasing external calcium ion concentration cannot then be ascribed to a wall-stiffening process preventing expansion. Further, the wall polymers released from secretory vesicles may already be saturated with calcium ions (Jaffe *et al.*, 1975; Heslop-Harrison *et al.*, 1985; Dorner *et al.*, 1987; Johnson, 1988).

Calcium-Vesicle Fusion Interaction

Calcium is required as one of the mediators of the process of vesicle fusion with the plasma membrane (Gomperts, 1987). The cytoplasmic calcium concentration appears to be regulated by the entry of external calcium ions through calcium channels in the plasma membrane (Reiss and Herth, 1985), although it is possible that existing calcium within the cell could facilitate the process of vesicle fusion. Polarized growth could then be achieved by restricting the calcium ion channels to a particular part of the cell surface. This part would then receive all the vesicles that would concentrate supply of new membrane and wall material at that point. Once established, such a polarity could be maintained by ensuring that the calcium channels had a relatively short functional lifetime and that vesicle membranes always contained new, active calcium channels. In this way membrane displaced laterally from the fusion area would not possess calcium channels, could not serve as fusion sites for vesicles, and thus would not expand the vesicle fusion site. Only the growth area itself would be capable of supporting new vesicle fusion events initiated by calcium arriving via the newly acquired calcium channels in its plasma membrane.

While this is an attractive idea it does not account for growth inhibition at high external calcium ion concentrations (Picton and Steer, 1983). This inhibition of elongation is not accompanied by a cessation of vesicle fusion. Indeed vesicles continue to fuse, at least for a few minutes, building up a thickened cell wall at the tip.

Calcium-Cytoskeleton Interaction

Studies on cytoplasmic cellular locomotion of animal and fungal cells from a range of multicellular and single-celled systems have demonstrated that the cytoskeleton is active in bringing about movement. This 'amoeboid movement' is strongly dependent on local calcium ion concentrations. The optimum calcium level allows a meshwork structure to actively move the whole cytoplasmic gel in relation to its substrate. Supra- and suboptimal concentrations can inhibit movement. The range of external calcium levels able to support growth in pollen tubes does not appear to be inconsistent with the range of external calcium concentrations affecting amoeboid movement. This process could therefore explain the interaction between external calcium and tube growth rate, but it cannot explain the growth polarity of the tube (Picton and Steer, 1982).

The local calcium ion concentration around the cytoskeleton is mediated by organelles that also transport the calcium in a basal direction. There are some indications that the mitochondrial zone may serve as a prime sink for the incoming calcium from the cell surface (Picton and Steer, 1985), though the endoplasmic reticulum has also been suggested to fill this role (Herth, pers. comm.). Excessive external calcium ion concentrations lead to large fluxes across the plasma membrane which could exceed the uptake capacity of these organelle systems, so that growth ceases (Picton and Steer, 1985). This constant intake and sequestering of calcium ions establishes a calcium ion gradient within the apical cytoplasm and on into the tube (Reiss *et al.*, 1985). It may also be responsible for the observed external calcium ion current (Weisenseel *et al.*, 1975).

Calcium Control of Pollen Tube Polarity and Tip Growth

The polarized growth of a pollen tube appears to result from a combination of calcium-dependent processes. The existence of positive feedback loops in the calcium-entry/vesicle-fusion system facilitates focusing of the growth processes to a single site on the cell surface. The incoming calcium at this site is effective in mobilizing the underlying cytoskeleton, promoting the forward growth process beneath the fusion site. The calcium-sequestering organelles establish a gradient of calcium ion concentration from the plasma membrane to the organelle membrane. This gradient is optimal for cytoskeleton activity, which moves the cell surface forward. The secre-

tory vesicles maintain the supply of new plasma membrane, new calcium ion channels, and new cell wall material to the expanding surface. The organelle system transports the calcium basally, probably by moving calcium-loaded organelles by cytoplasmic streaming, establishing a tip-to-base gradient. Mitochondrial activity in living pollen tubes is consistent with this role (Steer and Steer, 1989). The growth form is thus automatically tubular in the case of pollen tubes with a single area of membrane acting as a vesicle fusion site. Note that other forms could be generated by specifying more spatially distinct sites of calcium ion entry (Sievers and Schnepf, 1981; Schnepf, 1986).

The presence of a physical barrier to calcium ion access to the plasma membrane outer surface will assist the polarization process. Hence porate pollen grains can be regarded as more advanced, physiologically, than colpate pollen grains. The latter admit external calcium over a wide arc and permit the initial growth phase to occur as a bulge, rather than a tube. This early growth phase is exaggerated by the application of nifedipine, a calcium channel blocker, which forestalls the development of a preferred fusion site, and hence the formation of a normal tube (Reiss and Herth, 1985).

In summary, it is proposed that an ionic current of calcium ions enters at the pollen tube tip as a result of the localized positioning of calcium ion channels in the plasma membrane by secretory vesicle fusion at the tube apex. These processes create optimal conditions for growth mediated by the cytoskeleton at the calcium ion-entry site.

Literature Cited

Baydoun, E. A.-H., and C. T. Brett. 1984. The effect of pH on the binding of calcium to pea epicotyl walls and its implications for the control of cell extension. *J. Exp. Botany* **35:** 1820–1831.

Dormer, R. L., G. R. Brown, C. Doughney, and M. A. McPherson. 1987. Intracellular Ca^{2+} in pancreatic acinar cells: regulation and role in stimulation of enzyme secretion. *Biosci. Rep.* **7:** 333–344.

Gomperts, B. D. 1987. The dual effector system for exocytosis in mast cells: obligatory requirement for both Ca^{2+} and GTP. *Biosci. Rep.* **7:** 369–381.

Heslop-Harrison, J. S., J. Heslop-Harrison, Y. Heslop-Harrison, and B. J. Reger. 1985. The distribution of calcium in the grass pollen tube. *Proc. R. Soc. Lond B* **225:** 315–327.

Heslop-Harrison, J. 1987. Pollen germination and pollen tube growth. *Int. Rev. Cytol.* **107:** 1–78.

Jaffe, L. A., M. H. Weisenseel, and L. F. Jaffe. 1975. Calcium accumulations within the growing tips of pollen tubes. *J. Cell Biol.* **67:** 488–492.

Johnson, R. G. Jr. 1988. Accumulation of biological amines into chromaffin granules: a model for hormone and neurotransmitter transport. *Physiol. Rev.* **68:** 232–307.

Picton, J. M., and M. W. Steer. 1982. A model for the mechanism of tip extension in pollen tubes. *J. Theoret. Biol.* **98:** 15–20.

Picton, J. M., and M. W. Steer. 1983. Evidence for the role of Ca^{2+} ions in tip extension in pollen tubes. *Protoplasma* **115:** 11–17.

Picton, J. M., and M. W. Steer. 1985. The effects of ruthenium red, lanthanum, flourescein isothiocyanate and trifluoperazine on vesicle transport, vesicle fusion and tip extension in pollen tubes. *Planta* **163:** 20–26.

Reiss, H.-D., G. W. Grime, M. Q. Li, J. Takacs, and F. Watt. 1985. Distribution of elements in the lily pollen tip, determined with the Oxford scanning proton microprobe. *Protoplasma* **126:** 147–152.

Reiss, H.-D., and W. Herth. 1978. Visualisation of the Ca^{2+}-gradient in growing pollen tubes of *Lilium longiflorum* with chlorotetracycline fluorescence. *Protoplasma* **97:** 373–377.

Reiss, H.-D., and W. Herth. 1979. Calcium ionphore A23187 affects localised wall secretion in the tip region of pollen tubes of *Lilium longiflorum*. *Planta* **145:** 225–232.

Reiss, H.-D., and W. Herth. 1985. Nifedipine-sensitive calcium channels are involved in polar growth of lily pollen tubes. *J. Cell Sci.* **76:** 247–254.

Reiss, H.-D., and R. Nobiling. 1986. Quin-2 fluorescence in pollen tubes: distribution of free cytoplasmic calcium. *Protoplasma* **131:** 244–246.

Schnepf, E. 1986. Cellular polarity. *Ann. Rev. Plant Physiol.* **37:** 23–47.

Sievers, A., and E. Schnepf. 1981. Morphogenesis and polarity of tubular cells with tip growth. Pp. 265–299 in *Cytomorphogenesis in Plants* O. Kiermayer, ed. Springer-Verlag, Wein and New York.

Steer, M. W., and J. M. Steer. 1989. Pollen tube tip growth. *New Phytol.* (in press).

Weisenseel, M. H., R. Nuccitelli, and L. F. Jaffe. 1975. Large electrical currents traverse growing pollen tubes. *J. Cell Biol.* **66:** 556–567.

Reference: *Biol. Bull.* **176(S):** 21–24. (April, 1989, Suppl.)

Calcium Wave in Activating Hamster Eggs

SHUN-ICHI MIYAZAKI

Department of Physiology, Tokyo Women's Medical College, Kawada-cho, Shinjuku-ku, Tokyo, 162, Japan

Abstract. The activating hamster egg shows a series of periodic increases in intracellular free calcium concentration ($[Ca^{2+}]_i$) (Igusa and Miyazaki, 1986). The spatial distribution of the Ca^{2+} transients can be analyzed in single, aequorin-injected eggs by the photon-counting imaging method with a supersensitive TV camera system (Miyazaki *et al.*, 1986). A propagating increase in $[Ca^{2+}]_i$ is observed in the first response, starting from the sperm attachment site and spreading over the entire egg within 4–7 s. The Ca wave is repeated in the second and sometimes the third response, starting from the same focus, but spreading more rapidly (~2 s). In subsequent responses, $[Ca^{2+}]_i$ increases synchronously in the whole egg within 1 s.

A Ca^{2+} transient is induced in an all-or-none fashion by injection of either inositol 1,4,5-trisphosphate (IP_3) or Ca^{2+} ions into unfertilized eggs. The Ca^{2+} transient is due to release of Ca^{2+} from intracellular stores, and it is followed by a refractory period of 60–120 s. Injection of guanosine-5'-0-(3-thiotriphosphate) (GTPγS) causes a series of Ca^{2+} transients with a pattern similar to that upon insemination, but with remarkable attenuation of the $[Ca^{2+}]_i$ rise after 2–3 responses. Signal transduction involving activation of a GTP-binding protein and IP_3- and/or Ca^{2+}-induced Ca^{2+} release is considered to be responsible for the repeated Ca^{2+} transients.

Introduction

It is well known that a dramatic, transient increase in $[Ca^{2+}]_i$ occurs at the early stage of fertilization in various eggs. The biological significance of the Ca transient is to induce cortical granule exocytosis for polyspermy block and possibly to trigger other events at egg activation (Jaffe, 1985). In the sea urchin egg, the Ca^{2+} transient has been shown to be related to the increase in oxygen consumption and activation of NAD kinase (Epel, 1978). Gilkey *et al.* (1978) visualized the Ca transient in the medaka *Oryzias latipes* egg, using the Ca-dependent photoprotein, aequorin. They showed a Ca wave starting from the sperm attachment site and traveling across the egg cytoplasm. Recent development of the photon-counting imaging method enabled us to record photon-limited events and to analyze the distribution of Ca^{2+}-aequorin luminescence in single smaller eggs. As to the signal transduction of sperm-egg interaction causing the Ca^{2+} transient, recent studies of the sea urchin egg have shown the involvement of the activation of GTP-binding protein and polyphosphoinositide turnover (Turner *et al.*, 1986). Here, I shall describe repeated Ca^{2+} transients in the activating hamster egg and their spatial distribution in the egg cytoplasm. Then, I shall discuss the underlying mechanism in relation to the findings upon injection of IP_3, Ca^{2+}, and GTPγS.

Materials and Methods

Mature eggs obtained from superovulated female golden hamsters were freed from the zona pellucida by trypsin treatment. The diameter of the egg is about 72 μm. Eggs were injected with 20 pl of aequorin solution (9.6 mg/ml) and then inseminated by capacitated and acrosome-reacted sperm. Aequorin luminescence coming from the egg under the microscope was intensified by two-dimensionally arranged photon-counting tubes and visualized as light spots appearing momentarily on the TV screen (supersensitive TV camera system, Hamamatsu Photonics, C1966-20). The video-recorded raw image of the light spots was processed by the attached image processor using facilities such as continuous accumulation (accumulation of all light spots during a Ca^{2+} transient) or sequential accumulation (accumulation at every ⅛ to 1 s interval). The video-recorded, processed image was played back, and video frames were stopped one by one and then photographed at the desired moment (see Miyazaki *et al.*, 1986, for details).

In different experiments, IP_3 and guanine nucleotides were microinjected into unfertilized eggs by pressure or iontophoretically by current pulses, while Ca^{2+} transients were monitored by aequorin luminescence and/or by the hyperpolarizing response (HR) in membrane potential which is mediated by a Ca-activated K conductance (see Miyazaki, 1988, for details).

Results

Zona-free hamster eggs always become polyspermic, unless the number of applied sperm is specially limited. When the egg was inseminated by a single sperm that was applied near the egg through a glass capillary, the first Ca^{2+} transient occurred at about the time when flagellar motion of the sperm stopped, 10–30 s after the attachment to the egg surface. The increase in $[Ca^{2+}]_i$ began near the sperm attachment site and spread over the entire egg within 4–7 s (Miyazaki *et al.*, 1986). The calculated propagation velocity is 16–28 μm/s, if we assume that the Ca^{2+} wave travels along the egg surface. The velocity is more than 12 μm/s in the medaka fish (Gilkey *et al.*, 1978) or 8–10 μm/s in *Xenopus* (Busa and Nuccitelli, 1985). The $[Ca^{2+}]_i$ rise declined with almost even distribution and ceased in 12–17 s. The spreading $[Ca^{2+}]_i$ rise was repeated in the second and sometimes the third response, starting from the same focus, but spreading more rapidly (~2 s). In subsequent responses $[Ca^{2+}]_i$ increased synchronously in the whole egg within 1 s.

When additional sperm attached to the egg after the occurrence of the first response by the first sperm, the spread of $[Ca^{2+}]_i$ rise could take place from near the site of additional sperm attachment but only in the second or third response (Miyazaki *et al.*, 1986). The multiple foci for the initiation of $[Ca^{2+}]_i$ rise were not observed in responses following the third response, even when many sperm attached to an egg. Thus, it seems that the first 2–3 Ca^{2+} transients are triggered by the attached sperm, while subsequent ones are built up and repeated as the characteristics of inseminated eggs.

In the sea urchin egg, microinjection of IP_3 results in cortical granule exocytosis and fertilization membrane elevation (Whitaker and Irvine, 1984; Turner *et al.*, 1986). When IP_3 was injected into the unfertilized hamster egg under pressure, it induced a Ca^{2+} transient without measurable delay (Miyazaki, 1988). The $[Ca^{2+}]_i$ rise spread throughout the egg within 1 s. The Ca^{2+} transient was induced even in Ca-free medium, indicating that it is due to Ca^{2+} release from intracellular stores. The minimum effective concentration of IP_3 was 2 nM in the egg (assuming uniform distribution). When IP_3 was injected repeatedly with incremental current pulses, a Ca^{2+} release was induced in an all-or-none fashion (Miyazaki *et al.*, 1988). Once a Ca^{2+} release occurred, subsequent injection of IP_3 with the same current pulse failed to generate the next Ca^{2+} transient for 60–120 s: there is a transient refractory period. The critical injection current of IP_3 for induction of a Ca^{2+} release became higher during repeated injections.

In the hamster egg, a Ca^{2+} transient is reflected in the hyperpolarizing response (HR) in membrane potential, based on Ca-activated K channels (Miyazaki and Igusa, 1982). Injection of Ca^{2+} into the unfertilized hamster egg by current pulses induced a regenerative HR with an apparent threshold (Igusa and Miyazaki, 1983). This response was observed in Ca-free medium: the mechanism of Ca-induced Ca release appears to exist.

There are a number of reports that phosphodiesterase, which mediates the cleavage of phosphatidylinositol 4,5-bisphosphate (PIP_2) into IP_3 and diacylglycerol, is activated by ligand-receptor binding by way of a GTP-binding protein (G protein) (Stryer and Bourne, 1986). To activate a G protein, GTPγS, the hydrolysis-resistant analog of GTP, is usually used. Microinjection of GTPγS into the unfertilized hamster egg by pressure caused a Ca^{2+} transient with a delay of 160–200 s (Miyazaki, 1988). The minimum effective concentration was 12 μM in the egg. More than 50 μM GTPγS produced periodic Ca^{2+} transients with an initial delay of 25–40 s and intervals of 45–60 s. This pattern of repeated Ca^{2+} transients is similar to that induced by sperm. The difference is that the Ca^{2+} transients induced by GTPγS attenuated remarkably after the second or third response while the sperm-mediated Ca^{2+} transients do not. Analysis by aequorin luminescence revealed that the first 2–3 $[Ca^{2+}]_i$ rises upon injection of GTPγS covered the whole egg, but succeeding responses attenuated to a localized $[Ca^{2+}]_i$ rise. GTPγS could be injected repeatedly by current pulses, but additional injections of GTPγS by current pulses did not compensate the attenuated Ca^{2+} transients.

Preinjection of guanosine-5′-0-(2-thiodiphosphate) (GDPβS) inhibited the occurrence of both GTP-induced and sperm-mediated Ca^{2+} transients dose-dependently at similar concentration ranges. Therefore, it is very likely that the signal transduction of sperm-egg interaction causing repetitive Ca^{2+} transients involves a G protein-mediated process.

Discussion

The propagating Ca^{2+} wave in activating eggs was found to occur in a mammal. The first Ca^{2+} transient in activating hamster eggs is probably due to release of Ca^{2+} from intracellular stores, although it has not been confirmed because sperm-egg fusion does not occur in Ca-free medium. Intracellular Ca^{2+} release was induced in unfertilized hamster eggs by injection of either IP_3 or

Ca^{2+}. IP_3 is thought to be the initial inducer of Ca^{2+} release near the sperm attachment site. The propagating Ca^{2+} release could be successive local $[Ca^{2+}]_i$ rise based on Ca-induced Ca release. Swann and Whitaker (1986) proposed a recycling process in the sea urchin egg between Ca-stimulated production of IP_3 and IP_3-induced Ca release. The $[Ca^{2+}]_i$ rise in hamster eggs upon injection of IP_3 or Ca^{2+} spread so quickly over the whole egg that its propagation has not been clearly shown. More controlled injection is necessary.

The increase in $[Ca^{2+}]_i$ should induce cortical granule exocytosis. The material released from the cortical granules modifies the zona pellucida to become resistant for sperm penetration (Yanagimachi, 1977). This zona reaction seems to be the main mechanism for polyspermy block in the hamster egg. The electrical fast polyspermy block found in other species (Jaffe and Cross, 1986) seems to be unlikely, because sperm-egg fusion associated with the hyperpolarizing response could occur at any membrane potential between −160 and +50 mV (Miyazaki and Igusa, 1982).

The characteristic feature of the Ca^{2+} transient at fertilization of hamster eggs is the repeated Ca^{2+} wave in the second and sometimes the third response. The second and third responses are similar to the first one in the peak $[Ca^{2+}]_i$ (1–2 μM, measured with Ca-sensitive microelectrodes, Igusa and Miyazaki, 1986), as well as propagating increase of $[Ca^{2+}]_i$. To generate repeated Ca^{2+} transients, persistent production of IP_3 seems to be necessary: a single injection of IP_3 generated only one Ca^{2+} transient, even if the concentration was raised (Miyazaki, 1988). Injected IP_3 seems to be immediately turned over. Periodic Ca^{2+} transients were produced when IP_3 was applied continuously by leakage from an injection pipette with a blunt tip (Miyazaki *et al.*, 1988).

IP_3 is thought to be derived from polyphosphoinositide turnover. This process seems to be activated by a G protein, as also demonstrated in the sea urchin egg (Turner *et al.*, 1986). It remains to be elucidated how the G protein is activated by sperm-egg interaction. As to the supposed G protein, both pertussis toxin and cholera toxin neither stimulated nor inhibited the occurrence of both GTP-induced and sperm-mediated $[Ca^{2+}]_i$ rises (Miyazaki, 1988).

Activating hamster eggs show further Ca^{2+} transients following the third response at fairly constant intervals of 40–120 s. Even a single sperm is capable of producing these multiple Ca^{2+} transients, although the interval is a little longer than that in the case of multiple sperm (Miyazaki *et al.*, 1986). The series of Ca^{2+} transients was reduced in frequency and eventually stopped after perfusion of Ca-free medium (Igusa and Miyazaki, 1983). Correspondingly, injection of GTPγS did not produce the repetitive Ca^{2+} transients in Ca-free medium, except the first 1–2 responses (Miyazaki, 1988). Thus, the occurrence of repeated Ca^{2+} transients requires the presence of Ca^{2+} in the external medium. There is evidence that each Ca^{2+} transient is due to intracellular Ca^{2+} release and external Ca^{2+} is necessary to reload intracellular Ca^{2+} stores by Ca^{2+} influx (Igusa and Miyazaki, 1983). The refractory period of Ca^{2+} release revealed by injection of IP_3 or Ca^{2+} probably corresponds to the time required for reloading the Ca stores.

Our findings thus far indicate continuous Ca^{2+} influx across the plasma membrane in activating hamster eggs. There seems to be a G protein-mediated process for elevation of Ca^{2+} permeability in addition to the pathway for production of IP_3 and IP_3-induced Ca^{2+} release. The factor responsible for activating Ca channels may be the G protein itself, protein kinase C, or inositol 1,3,4,5-tetrakisphosphate (IP_4). Further study is necessary to identify the factor.

GTPγS should activate the G protein persistently because of its hydrolysis resistance. Correspondingly, injection of GDPβS interrupted the series of sperm-induced Ca^{2+} transients (Miyazaki, 1988). Therefore, the series of $[Ca^{2+}]_i$ rises upon fertilization requires persistent activation, not transient activation as a trigger, of the G protein-mediated process. Thus, it is likely that IP_3 is produced persistently and it induces Ca^{2+} release from reloaded stores. On the other hand, GTPγS-induced Ca^{2+} transients always attenuate to a localized $[Ca^{2+}]_i$ rise. Upon insemination, additional factor(s) may be involved in causing a synchronous Ca^{2+} release throughout the egg. Interestingly, the critical injection current of Ca^{2+} to induce Ca^{2+} release decreases tenfold after insemination (Igusa and Miyazaki, 1983): apparently, intracellular Ca^{2+} stores easily undergo Ca-induced Ca release.

Jaffe (1985) reviewed differences in the $[Ca^{2+}]_i$ rise at fertilization between deuterostome and protostome eggs. He proposed the generalization that in deuterostome eggs the $[Ca^{2+}]_i$ rise is due to propagating release of Ca^{2+} from intracellular stores whereas in protostome eggs it is due to continuous Ca^{2+} influx from external medium. In this respect, the hamster egg is interesting, because it includes both mechanisms, and furthermore, continuous Ca^{2+} influx appears to be linked to intracellular Ca^{2+} release in reloading the stores. It is likely that the continuous Ca^{2+} influx in protostome eggs is mediated by voltage-gated Ca channels, which are open during a sustained depolarization, and that the long-lasting increase in $[Ca^{2+}]_i$ is responsible for slow process of exocytosis (Jaffe, 1985). In the hamster egg, since the series of Ca^{2+} transients occurs irrespective of depolarization (Miyazaki and Igusa, 1982), other kinds of Ca channels may be activated by a G protein-mediated process. Exocytosis is also slow in hamster eggs, lasting for about 5–15 min

(Fukuda and Chang, 1978). The entire sperm, both head and tail, is incorporated into the egg cytoplasm by fusion of the sperm and egg membranes, taking a few hours. The prolonged $[Ca^{2+}]_i$ rise may be related to some activities of cytoskeletal systems.

The oscillatory or pulse-like repeated increase in $[Ca^{2+}]_i$ has been found in many different cell types and it is thought to be important for understanding of the relation between phosphoinositides and calcium signalling (Berridge *et al.*, 1988). The hamster egg is one of the good models for the study of the movement of Ca^{2+} ions in non-muscle cells.

Acknowledgments

The author is grateful to Dr. O. Shimomura, Marine Biological Laboratory, Woods Hole, for his generous gift of purified aequorin, and Drs. N. Hashimoto, Y. Yoshimoto, T. Kishimoto, and Y. Hiramoto for collaborating in the study of Ca^{2+} wave. He also thanks Drs. Y. Igusa and K. Swann for their collaboration in the iontophoretic injection of IP_3 and GTPγS.

Literature Cited

Berridge, M. J., P. H. Cobbold, and K. S. R. Cuthbertson. 1988. Spatial and temporal aspects of cell signalling. *Phil. Trans. R. Soc. Lond. B.* **320:** 325–343.

Busa, W. B., and R. Nuccitelli. 1985. An elevated free cytosolic Ca^{2+} wave follows fertilization in egg of the frog, *Xenopus laevis*. *J. Cell Biol.* **100:** 1325–1329.

Epel, D. 1978. Mechanism of activation of sperm and egg during fertilization of sea urchin gametes. *Curr. Top. Dev. Biol.* **12:** 185.

Fukuda, Y., and M. C. Chang. 1978. The time of cortical granule breakdown and sperm penetration in mouse and hamster eggs inseminated *in vitro*. *Biol. Reprod.* **19:** 261–266.

Gilkey, J. C., L. F. Jaffe, E. B. Ridgeway, and G. T. Reynolds. 1978. A free calcium wave traverses the activating egg of the medaka, *Oryzias latipes*. *J. Cell Biol.* **76:** 448–466.

Igusa, Y., and S. Miyazaki. 1983. Effects of altered extracellular and intracellular calcium concentration on hyperpolarizing responses of the hamster egg. *J. Physiol. (Lond.).* **340:** 611–632.

Igusa, Y., and S. Miyazaki. 1986. Periodic increase of cytoplasmic calcium in fertilized hamster eggs measured with calcium-sensitive electrodes. *J. Physiol. (Lond.).* **377:** 193–205.

Jaffe, L. F. 1985. The role of calcium explosions, waves and pulses in activating eggs. Pp. 127–165 in *Biology of Fertilization*, C. B. Metz and A. Monroy, eds. Academic Press, New York.

Jaffe, L. A., and N. L. Cross. 1986. Electrical regulation of sperm-egg fusion. *Annu. Rev. Physiol.* **48:** 191–200.

Miyazaki, S. 1988. Inositol 1,4,5-trisphosphate-induced calcium release and guanine nucleotide-binding protein-mediated periodic calcium rises in golden hamster eggs. *J. Cell Biol.* **106:** 345–354.

Miyazaki, S., N. Hashimoto, Y. Yoshimoto, T. Kishimoto, Y. Igusa, and Y. Hiramoto. 1986. Temporal and spatial dynamics of the periodic increase in intracellular free calcium at fertilization of golden hamster eggs. *Dev. Biol.* **118:** 259–267.

Miyazaki, S., and Y. Igusa. 1982. Ca-mediated activation of a K current at fertilization of golden hamster eggs. *Proc. Natl. Acad. Sci. USA* **79:** 931–935.

Miyazaki, S., Y. Igusa, and K. Swann. 1988. Involvement of GTP-binding protein in signal transduction of sperm-egg interaction at fertilization of hamster eggs. *J. Physiol. Soc. Jpn.* **50:** 390.

Stryer, L., and H. R. Bourne. 1986. G proteins: a family of signal transducers. *Annu. Rev. Cell Biol.* **2:** 391–419.

Swann, K., and M. Whitaker. 1986. The part played by inositol trisphosphate and calcium in propagation of the fertilization wave in sea urchin eggs. *J. Cell Biol.* **102:** 70–76.

Turner, P. R., L. A. Jaffe, and A. Fein. 1986. Regulation of cortical vesicle exocytosis in sea urchin egg by inositol 1,4,5-trisphosphate and GTP-binding protein. *J. Cell Biol.* **102:** 70–76.

Whitaker, M., and R. F. Irvine. 1984. Inositol 1,4,5-trisphosphate microinjection activates sea urchin eggs. *Nature.* **312:** 636–639.

Yanagimachi, R. 1977. Specificity of sperm-egg interaction. Pp. 255–295 in *Immunology of Gametes*, M. Edidin and M. H. Johnson, eds. Cambridge Univ. Press, Cambridge.

Reference: *Biol. Bull.* **176(S)**: 25–30. (April, 1989, Suppl.)

Measuring Cytoplasmic Calcium: A Review of Three Methods With Emphasis on the Practical Aspects of Their Use

R. J. CORK, A. F. STRAUTMAN, AND K. R. ROBINSON

Department of Biological Sciences, Purdue University, W. Lafayette, Indiana 47906

Abstract. We have used the three major techniques for measuring cytoplasmic calcium concentration to quantify calcium changes in a variety of cells during a number of developmental processes. In this paper, we describe our experiences with aequorin, calcium electrodes, and fluorescent calcium indicators. The *Xenopus* oocyte is used as the prime example throughout this discussion, as we have done all three types of measurements in oocytes.

Although each of these methods gives roughly the same value for the cytoplasmic calcium concentration in oocytes, each method has its own advantages and disadvantages when it comes to practical experiments. The particular problems with each of the methods are discussed in detail. We conclude that the choice of method depends on the type of information that is required. Calcium electrodes are probably the most precise method but are also the most technically difficult and only provide very localized measurements. Aequorin is quite suitable when an overall average of calcium levels in a cell is required but it is difficult to get good information on the spatial distribution of calcium. Fluorescent indicators are the most straightforward method to use and provide much information about the spatial distribution of calcium in cells as well as average levels in cell suspensions, however they are the most difficult to calibrate.

Introduction

When studying the consequences or regulation of steady ionic currents, the intracellular free calcium concentration ($[Ca^{2+}]_i$) is often an important cell parameter. Various methods exist for measuring $[Ca^{2+}]_i$, but all are technically demanding and each has its own advantages and disadvantages. The choice of a particular technique for measuring $[Ca^{2+}]_i$ in a specific cell depends on a number of factors. The ideal method should be non-invasive in that it should not change the very parameter it is trying to quantify. It should also have a lower detection limit of 10 n*M* or less with a desirable precision of at least ±10 n*M*. However, when considering a technique for a specific application, other factors such as the cell's size and shape, the complexity of the required equipment, cost in both time and money, and the ease of calibrating the measurements all become important.

There are few cell types that are suitable for all the different methods, so there have been few direct comparisons of them in the same cells (*e.g.*, Defeo and Morgan, 1986; David-Dufhilo *et al.*, 1988). We have employed three of the most widely used techniques—ion-specific electrodes, aequorin, and fluorescent indicators—to measure calcium levels in a variety of cell types including *Xenopus* oocytes and larval sea lamprey spinal cord axons. Full details of the results obtained with electrodes and aequorin in *Xenopus* oocytes have been published (Robinson, 1985; Cork *et al.*, 1987), and numerous research papers and reviews provide many theoretical and practical details of each of the techniques (*e.g.*, Blinks *et al.*, 1982). In this report, we shall discuss the relative merits of each of these techniques and, as all three methods have been employed in *Xenopus* oocytes, the discussion will concentrate on their use in oocytes; the results of the measurements will be presented as an example.

Materials and Methods

Cells

Oocytes were obtained from pieces of ovary surgically removed from mature *Xenopus laevis* females, anesthetized by hypothermia. Stage VI oocytes (≧1.2 mm diameter) were defolliculated manually with watchmaker's

forceps and stored in O-R2 solution (Wallace *et al.*, 1973). The composition of O-R2 is (in m*M*) NaCl 82.5, KCl 2.5, $CaCl_2$ 1.0, $MgCl_2$ 1.0, Na_2HPO_4, 1.0, HEPES 5.0, pH 7.6.

The entire brain and spinal cord of the larval sea lamprey, *Petromyzon marinus*, was removed and maintained in simple organ culture (Borgens *et al.*, 1980). The naturally flattened spinal cord is about 700 μm wide and 175 μm thick. The two Mauthner axons are 40 μm in diameter and were chosen for study because of their large size and their consistent location in the lateral margins of the spinal cord.

Ca^{2+}-sensitive microelectrodes

Ca^{2+}-sensitive microelectrodes were constructed using the methods described by Tsien and Rink (1981), with modifications by Busa and Nuccitelli (1985) and Robinson (1985). They were calibrated as described in Robinson (1985). The electrode tips were filled with a cocktail based on the neutral carrier ETH 1001 (Fluka Chemical Corporation, Hauppaunge, New York; Oehme *et al.*, 1976) and gelled with polyvinyl chloride. Micropipettes were pulled from 1.5 mm o.d. aluminosilicate glass, and the tips were broken to diameters of 1–2 μm. Micropipettes were then heated overnight at 225°C and silaned with trimethyl-(dimethyl-amino)-silane for 30 min at 225°C. More reliable electrodes were obtained by having a short column of ungelled sensor between the gelled sensor in the microelectrode tip and the pCa 6 solution in the rest of the microelectrode.

Microinjection

Defolliculated oocytes were transferred to Ca-free O-R2 for microinjection. Microinjection pipettes were pulled from 1.5-mm diameter capillaries with fibers (World Precision Instruments, New Haven, Connecticut), the tips were broken back to diameters of 6–12 μm, and the micropipettes were back filled with a few μl of either 1 mg/ml aequorin (from Dr. J. R. Blinks, Mayo Foundation, Rochester, Minnesota) in a buffer solution containing 150 m*M* KCl, 5 m*M* HEPES, 0.2 m*M* EGTA, pH 7.45, or 5 m*M* fura 2 (Molecular Probes, Eugene, Oregon) in a buffer containing 60 m*M* KCl, 6 m*M* NaCl, 3 m*M* $MgCl_2$, 5 m*M* HEPES, pH 7.4.

Oocytes were pressure-injected using a Picospritzer (General Valve, Fairfield, New Jersey) system. Typically, 2 or 3 pressure pulses of 20 lb/sq. in. for 200 ms were applied, each one injecting 2–6 nl. Injected volumes were calculated by measuring the diameter of solution droplets injected into paraffin oil before and after oocyte injection. After injection, oocytes were transferred back to O-R2 and left for 1–2 h to recover and to allow the indicator to diffuse throughout the cell.

In order to inject fura-2 into smaller cells, such as the lamprey axons, we developed an iontophoresis protocol. The tips of micropipettes (<1 μm tip diameter) are filled with a 24 m*M* solution of fura-2 free acid and the rest of the pipette is back-filled with 100 m*M* KCl. These microelectrodes are then used in a standard electrophysiological set-up (WPI 701 amplifier, Grass SD9 stimulator and Tektronix storage oscilloscope) and a Mauthner axon is impaled. If a membrane potential of −65 mV or more is observed, then fura-2 is iontophoresed into the axon by passing 5 nA square-wave pulses at 5 Hz for 7 min.

Experimental set-up for aequorin measurements

Single oocytes were mounted in a specially designed chamber which could be inserted into the end of the photomultiplier housing and held so that the cell was approximately 2 mm below the photocathode (Cork *et al.*, 1987). The photomultiplier tube, (Hamamatsu Corp. model R464S) was uncooled and operated at 775 volts. This tube was specially selected for low noise and under our experimental conditions had a dark count of 2–3 count s^{-1}. The rest of the light measuring equipment consisted of an amplifier/discriminator and a power supply/photometer (Pacific Precision Instruments, models AD126 and 126D, respectively). The analogue output of the photometer was recorded on a chart recorder.

Calibration of aequorin signals

The aequorin signals were calibrated according to Allen and Blinks (1978). At the end of an experimental run, the oocyte was lysed with 1% Triton X-100 and the total light emitted (L_{max}) was counted. The ratio of L to L_{max}, where L was the light signal recorded from the cell, was then used to convert the light counts to calcium concentrations using a calibration curve. The calibration curve was determined by measuring the light emitted from aequorin in a known calcium buffer (L) followed by the total light emitted when saturating calcium was added (L_{max}). The ionic composition of the calcium buffers used for the calibration was chosen to resemble the ionic composition of the oocyte cytoplasm, *i.e.*, 60 m*M* KCl, 6 m*M* NaCl, 1 m*M* $MgCl_2$, pH 7.4. For the L_{max} determination 60 m*M* $CaCl_2$ in 1% Triton X-100 was added.

Experimental set-up for fura 2 measurements

We have developed a microscope-based system for measuring fluorescence from single cells (Cork *et al.*, 1987). This system consists of a Leitz Diaphot microscope with a low noise photomultiplier tube (Hamamatsu R464S) connected through a photometer/photon counter (Pacific Precision Instruments, model 126D) to a chart recorder. The fluorescence excitation wavelength

can be selected by sliding a block containing the desired interference filter in front of the 100-W Hg-lamp. The wavelength of the measured fluorescence is determined by an interference filter mounted in the microscope. A pinhole in the projection lens at the image plane of the objective defines the area over which measurements are made; it also acts with an illumination iris in front of the excitation filters to restrict background fluorescence from above and below the focal plane (Koppel *et al.*, 1976).

For experiments on oocytes, we used a 505 nm interference filter with a 10 nm bandwidth to select the fura 2 fluorescence emission. The two excitation wavelengths were selected with a 352 nm (3 nm half bandwidth) filter and a 380 nm (10 nm half bandwidth) filter. The reduced bandwidth of the 352 nm filter was required to reduce contamination from the intense Hg-line at 365 nm, which decreased the sensitivity of the measurements to calcium changes. A 75 W xenon lamp, with a continuous rather than a line spectrum, was tried as an alternative solution to this problem; however, its output at 350 nm was much less than that obtained with the mercury lamp. To improve the 350 nm transmittance of the system, the thick glass condensing lens in front of the lamp was replaced with a fused silica lens (Oriel Corp.). The microscope objective used for a particular experiment is dependent on the geometry of the cell preparation, the required magnification, and the UV transmittance of the objective. For many applications, including the larval lamprey experiments, we found a 36× reflecting objective (Ealing Corporation, South Natick, Massachusetts) to be admirably suitable; we used a Leitz 50× Fluorezenz water immersion lens for the *Xenopus* oocyte experiments.

Calibration of the readings was done by determining values for the minimum (zero calcium) and maximum (saturating calcium) fluorescence ratio from calcium buffer solutions containing 2 μM fura-2. Ratios were converted to $[Ca^{2+}]_i$ values using the equation of Grynkiewicz *et al.* (1985);

$$[Ca^{2+}] = K_d \times \text{Scaling Factor} \times (R - R_{min})/(R_{max} - R) \quad (1)$$

Experiments were calibrated either just before or just after the series of experimental readings. Background fluorescence was determined from unloaded cells. Extraction of data from chart recordings, subtraction of background fluorescence, and calculation of ratios and calcium concentrations was performed with a microcomputer.

All experiments were done in a temperature controlled room at 20–22°C.

Table I

$[Ca^{2+}]_i$ values determined in Xenopus *oocytes using three different methods*

Method	$[Ca^{2+}]_i$ (nM)	S.D.	(n)	Reference
Ca-electrode	140	50	44	Robinson, 1985
aequorin	90	30	8	Cork *et al.*, 1987
fura-2 (wa)	110	50	10	This paper
fura-2 (wv)	160	55	8	This paper
fura-2 (al)	136	4	1	This paper

(wa) and (wv); measurements made from wild type (pigmented) oocytes, from the animal or vegetal hemispheres, respectively.

(al); measurements made from an albino oocyte. The value is the mean of the maximum $[Ca^{2+}]_i$ values determined at each of 3 locations (animal pole, vegetal pole, and equator).

Results and Discussion

The values determined for the calcium resting level in *Xenopus* oocytes with each of the three techniques are summarized in Table I. While the values determined with each of the three methods are not significantly different, when each of the values is judged on the basis of how long it took to get, how easy it was to determine, and how reliable it is expected to be, there are considerable differences between the three methods.

Electrodes

In principal, ion-selective electrodes are simple to construct and use. The currently available calcium resins, ETH 1001 and ETH 129 (Schefer *et al.*, 1986), have a lower detection limit of about 10 nM and possess sufficient selectivity to minimize interference from other cations, although there may be some generally unrecognized effects of cytoplasmic components such as organic anions (unpub. obs.). However, for intracellular experiments ion-selective microelectrodes have less than the quoted specifications and their use is restricted to those cells that are of suitable size and geometry to allow impalement. This is especially so in the case of calcium-selective microelectrodes, as it has generally proved extremely difficult to construct such microelectrodes with tip diameters less than 1 μm. In *Xenopus* oocytes, the very large size of the cells makes inserting electrodes relatively simple. The cells' size may even be somewhat of a disadvantage as ion-specific electrodes only detect the ionic activity in the immediate vicinity of the electrode tip. Therefore, in a cell the size of a *Xenopus* oocyte, where significant differences in calcium concentration may occur in different parts of the cell, the exact location of the electrode tip must be known. Impalement techniques are not yet that precise and, as far as oocytes are

concerned, it is almost impossible to position an electrode tip in the region less than 50 μm below the surface with any accuracy.

The major problems with the calcium microelectrodes were a lack of stability and shifting calibration after impalement and withdrawal. This makes their practical application time consuming and technically demanding. The success rate for completed experiments, where the electrodes had sufficient sensitivity and the calibration remained relatively stable throughout the experiment, was low (<10%).

One aspect of the microelectrodes construction that we are presently working on is improving the beveling technique to give better control over the size and shape of the electrode tip. The expectation is that this will allow us to make measurements in smaller cells with much improved reliability. Micropipettes must be beveled to achieve sufficiently sharp electrodes so as to avoid damage to the cells while retaining a large enough opening for good calcium response. We have developed a method that uses a turntable covered with an extremely fine abrasive film. The micropipette is mounted on a micromanipulator and an ultrasonic detector (designed and built by Dr. Eric Furgason, Electrical Engineering, Purdue University) is attached to the electrode. As the pipette is lowered onto the rotating turntable at an angle of ~45°, the ultrasonic detector picks up the ultrasonic (30 KHz) vibrations that are produced by the tip's contact with the abrasive and the operator hears an audio signal. This method allows extremely fine control of the degree of beveling and results in a very sharp, fine-tipped microelectrode with a nicely beveled point.

Aequorin

The use of aequorin to quantify the calcium levels in cells is, as with electrodes, limited by practical rather than theoretical considerations. Aequorin measurements are relatively insensitive to artifacts arising from changes in other ions and if care is taken in calibrating the measurements in appropriate media, the signals obtained from cells can be converted to calcium concentrations fairly simply. The chief difficulties with the use of aequorin to make calcium measurements arise from the practical limitations on detecting the low light levels emitted from [illegible]. The cells must be in a specially designed chamber with no stray light and they must be accessible to bathing media and the fairly sophisticated light [illegible] equipment. Methods involving imaging the [illegible] generally lose a large proportion of the signal [illegible], to obtain the best signal strength, and thus [illegible] the lower limit of $[Ca^{2+}]_i$ detectable, the ability to [illegible] the cells while measuring their calcium level [illegible] be sacrificed. This may create problems when it comes to interpreting the results because the light emitted by aequorin rises as the $[Ca^{2+}]_i$ to the power ~2.5 (Allen and Blinks, 1978). Light from any regions of higher $[Ca^{2+}]_i$ will therefore dominate the signal from the cell and the average value of $[Ca^{2+}]_i$ will be overestimated.

The use of aequorin has often been limited to observing transients in the calcium while the resting levels in cells have not been measured. Indeed, three of the previously published accounts of experiments using aequorin in *Xenopus* oocytes did not determine the resting levels (Belle *et al.*, 1977, Moreau *et al.*, 1980, Wasserman *et al.*, 1980). There are two major reasons why we were able to detect a resting level glow. First, we used albino oocytes that do not have the light absorbing pigment of the wild type and second, our chamber was specifically designed so that the cell was as close as possible to the photocathode and as much light as possible was reflected up into the photomultiplier.

Fluorescence measurements

The most recently developed methods for quantifying intracellular calcium are based on a family of fluorescent calcium probes introduced by Roger Tsien and co-workers (Tsien *et al.*, 1982, Grynkiewicz *et al.*, 1985). The principal indicator we have used is fura-2, although we have also used quin2 and indo-1. One of the main advantages of these dyes is their ability to be loaded into small cells without microinjection. Tsien (1981) proposed that these dyes could be best introduced into cells if they were esterified to acetoxymethyl groups that would be cleaved off by intracellular esterases leaving the parent compound trapped in the cytoplasm. While this method has worked well in many mammalian cell types, it has proved to be problematical in almost all plant cells (Cork, 1986; Bush and Jones, 1988) and some animal cells (Luckhoff, 1986). Even if the cells load, use of the AM esters may introduce artifacts into the measurements; the dye may compartmentalize within the cells (Malgaroli *et al.*, 1987) or incomplete hydrolysis may result in calcium-insensitive components (Scanlon *et al.*, 1987) that affect the calibration of signals. Consequently, wherever possible we have used both fura-2 and indo-1 in their free acid form and have microinjected them into cells. While there are some practical problems associated with loading cells, high background fluorescence from some cells, and the necessity to maximize the UV transmittance of the microscope, the principal problem with use of fura-2 and indo-1 is the calibration of the measurements in terms of absolute calcium concentrations.

Two questions need to be answered regarding calibration of fluorescence ratios. First, what values should be used for the constants in the calibrating equation (1), and

second, how appropriate are the values to intracellular measurements if they are determined from aqueous calcium standards? We routinely determine values for R_{min}, R_{max} and the scaling factor (S.F.) from aqueous calcium standards in a buffer chosen to resemble the intracellular ionic environment. We have used the value of 223 nM for the K_d (Grynkiewicz *et al.*, 1985), although this may not be the most appropriate value since it was determined for an ionic strength of 0.15 at pH 7.05 and 37°C, and our assumed intracellular milieu used for oocyte calcium standards is I = 0.1 at pH 7.6 and 22°C. We have yet to determine a better value but some of our preliminary data indicates that the K_d value should be lower and that the values for $[Ca^{2+}]_i$ may be lower than those shown in Table I, possibly 100 n*M* or less. At I = 0.114 M, pH 7.5, and 23°C, the fura-2/calcium dissociation constant was 104 n*M* (W. Busa, pers. comm.). Irrespective of what values are used in equation 1, the question remains whether the calibration values determined from aqueous calcium standards are appropriate to the intracellular indicator. It has been reported that either the fluorescence spectra or the calcium binding properties of fura-2 are sufficiently altered in an intracellular environment to make calibrations made in aqueous buffers inappropriate (Malgaroli *et al.*, 1987, David-Dufilho *et al.*, 1988). Whether this is due to some interaction with specific cytoplasmic components (Williams and Fay, 1986) or cell membranes, or is some general 'viscosity' effect (David-Dufilho *et al.*, 1988) is still not certain. However, what is apparent, is that the effect is variable. We have not observed any abnormally low levels of $[Ca^{2+}]_i$ in *Xenopus* oocytes, yet with bovine corneal cells or laval lamprey axons we have often seen apparent calcium levels below the minimum detection level for fura-2 determined from aqueous calcium standards (*i.e.*, the fluorescence ratio observed in the cells is close to, or below, the R_{min} value determined from standards). We have performed a direct comparison of the apparent calcium levels obtained with fura-2 and indo-1. The larval lamprey spinal cord has two Mauthner axons that run parallel along the lateral margins of the cord. We have filled one axon with fura-2 and the contralateral one with indo-1. The axons were filled with equal amounts of the dyes by iontophoresis, measurements were taken from both axons during the experiment, and both sets of data were calibrated with reference to the same calcium standards. The mean $[Ca^{2+}]_i$ resting level obtained with fura-2 was 24 n*M* while the axon filled with indo-1 had an apparent resting level of 416 n*M*. The very large difference between these two measurements gives us cause to believe that there are some dye-specific artifacts associated with making these measurements with fluorescent indicators. We believe that the levels obtained using fura-2 are too low while the apparent levels obtained using indo-1 seem too high. Further experiments to clarify these points are underway.

When using any of the fluorescent probes in *Xenopus* oocytes, one factor to be considered is the distribution of pigment (melanin) in the cells. The results shown in Table I are from wild-type oocytes in which we were specifically looking for a gradient in $[Ca^{2+}]_i$ between the animal and the vegetal hemispheres. Wild-type oocytes have a densely pigmented animal hemisphere and a vegetal hemisphere that has little or no pigmentation. The $[Ca^{2+}]_i$ in the animal hemisphere was apparently lower than that in the vegetal; however, signals from the animal hemisphere were greatly attenuated by the pigment layer and we considered the possibility that the pigment may have affected the measured calcium levels. Spectrophotometric measurements on melanin suspensions showed that the pigment's absorption at 350 nm was approximately 1.3× its absorption at 380 nm. Furthermore, tests using fura-2 in calcium standards with varying amounts of melanin showed that the melanin reduced the measured fluorescence ratio for a given calcium concentration. Besides a differential effect on the amount of exciting light at 350 nm and 380 nm and thus the emitted fluorescence at those excitation wavelengths, some of these tests also suggested that melanin may have some calcium binding properties that could lower the calcium concentration in the endoplasm of the animal hemisphere. These questions have not yet been resolved, but preliminary measurements have been made in albino oocytes that lack all the pigment. We find no difference in $[Ca^{2+}]_i$ between the two halves of the albino oocytes (Table I) but the use of albino oocytes presents other problems that make interpretation of these results difficult. First, it is not always possible to decide where the boundaries of the two hemispheres are in oocytes lacking the clear landmarks of pigment. Second, measurements taken by focusing the microscope above or below the cell's surface indicate there are differences in the apparent $[Ca^{2+}]_i$ at different levels in the oocytes. When observing a completely white opaque body through a microscope there are no landmarks on which to focus, so the location of the measurements in albino oocytes is uncertain.

In summary, probably the most accurate determinations of the resting $[Ca^{2+}]_i$ in *Xenopus* oocytes are those obtained using calcium-selective microelectrodes. However, they were the most technically demanding measurements to make, and microelectrodes are not very suitable for giving an overall picture of the calcium level in the cell. The measurements made using aequorin are probably the best for an average value from the whole cell although they do not give any information on any variations in $[Ca^{2+}]_i$ throughout the cell and they tend to emphasize regions of high calcium. For details on the

distribution of $[Ca^{2+}]_i$ in the cell, fluorescence measurements provide the most information although the absolute values obtained are probably the least reliable.

Literature Cited

Allen, D. G., and J. R. Blinks. 1978. Calcium transients in aequorin-injected frog cardiac muscle. *Nature* **273:** 509–513.

Bellé, R., R. Ozon, and J. Stinnakre. 1977. Free calcium in full grown *Xenopus laevis* oocyte following treatment with ionophore A23187 or progesterone. *Mol. Cell. Endocrinol.* **8:** 65–72.

Blinks, J. R., W. G. Weir, P. Hess, and F. G. Prendergast. 1982. Measurement of Ca^{2+} concentrations in living cells. *Prog. Biophys. Molec. Biol.* **40:** 1–114.

Borgens, R. B., L. F. Jaffe, and M. J. Cohen. 1980. Large and persistent electrical currents enter the transected lamprey spinal cord. *Proc. Natl. Acad. Sci. USA* **77:** 1209–1213.

Busa, W. B., and R. Nuccitelli. 1985. An elevated free cytosolic Ca^{2+} wave follows fertilization in eggs of the frog, *Xenopus laevis*. *J. Cell Biol.* **100:** 1325–1329.

Bush, D. S., and R. L. Jones. 1987. Measurements of cytoplasmic calcium in aleurone protoplasts using indo-1 and fura-2. *Cell Calcium* **8:** 455–472.

Cork, R. J. 1986. Problems with the application of quin-2-AM to measuring cytoplasmic free calcium in plant cells. *Plant Cell Environment* **9:** 157–161.

Cork, R. J., M. F. Cicirelli, and K. R. Robinson. 1987. A rise in cytosolic calcium is not necessary for maturation of *Xenopus laevis* oocytes. *Dev. Biol.* **121:** 41–47.

Cork, R. J., P. Reinach, J. Moses, and K. R. Robinson. 1987. Calcium does not act as a second messenger for adrenergic and cholinergic agonists in corneal epithelial cells. *Curr. Eye Res.* **6:** 1309–1317.

David-Dufilho, M., T. Montenay-Garestier, and M-A. Devynck. 1988. Fluorescence measurements of free Ca^{2+} concentration in human erythrocytes using the Ca^{2+}-indicator fura-2. *Cell Calcium* **9:** 167–179.

DeFeo, T. T., and K. G. Morgan. 1986. A comparison of two different indicators, quin2 and aequorin in isolated single cells and intact strips of ferret portal vein. *Pflugers Arch.* **406:** 427–429.

Grynkiewicz, G., M. Poenie, and R. Y. Tsien. 1985. A new generation of Ca^{2+} indicators with greatly improved fluorescence properties. *J. Biol. Chem.* **260:** 3440–3450.

Koppel, D. E., D. Axelrod, J. Schlessinger, E. L. Elson, and W. W. Webb. 1976. Dynamics of fluorescence marker concentration as a probe of mobility. *Biophys. J.* **16:** 1315–1329.

Luckhoff, A. 1986. Measuring cytosolic free calcium concentration in endothelial cells with indo-1: the pitfall of using the ratio of two fluorescence intensities recorded at different wavelengths. *Cell Calcium* **7:** 233–248.

Malgaroli, A., D. Milani, J. Meldolesi, and T. Pozzan. 1987. Fura-2 measurement of cytosolic free Ca^{2+} in monolayers and suspensions of various types of animal cells. *J. Cell Biol.* **105:** 2145–2155.

Moreau, M., J. P. Vilain, and P. Guerrier. 1980. Free calcium changes associated with hormone action in amphibian oocytes. *Dev. Biol.* **78:** 201–214.

Oehme, M., M. Kessler, and W. Simon. 1976. Neutral carrier Ca^{2+} microelectrode. *Chimia* **30:** 204–206.

Robinson, K. R. 1985. Maturation of *Xenopus* oocytes is not accompanied by electrode-detectable calcium changes. *Dev. Biol.* **109:** 504–508.

Scanlon, M., D. A. Williams, and F. S. Fay. 1987. A Ca^{2+}-insensitive form of fura-2 associated with polymorphonuclear leukocytes. *J. Biol. Chem.* **262:** 6308–6312.

Schefer, U., D. Amman, E. Pretsch, U. Oesch, and W. Simon. 1986. Neutral carrier based Ca^{2+}-selective electrode with detection limit in the subnanomolar range. *Anal. Chem.* **58:** 2282–2285.

Tsien, R. Y. 1981. A non-disruptive technique for loading calcium buffers and indicators into cells. *Nature* **290:** 527–528.

Tsien, R. Y., and T. J. Rink. 1981. Ca^{2+}-selective electrodes: a novel PVC-gelled neutral carrier mixture compared with other available sensors. *J. Neurosci. Methods* **4:** 73–86.

Tsien, R. Y., T. Pozzan, and T. J. Rink. 1982. Calcium homeostasis in intact lymphocytes: cytoplasmic free calcium monitored with a new intracellularly trapped fluorescent indicator. *J. Cell Biol.* **94:** 325–334.

Wallace, R. A., D. W. Jared, J. N. Dumont, and M. W. Sega. 1973. Protein incorporation by isolated amphibian oocytes. III. Optimum isolation conditions. *J. Exp. Zool.* **184:** 321–334.

Wasserman, W. J., L. H. Pinto, C. M. O'Connor, and L. D. Smith. 1980. Progesterone induces a rapid increase in $[Ca^{2+}]_i$ of *Xenopus laevis* oocytes. *Proc. Natl. Acad. Sci. USA* **77**(3): 1534–1536.

Williams, D. A., and F. S. Fay. 1986. Ca^{2+} and fura-2 in the nuclear environment of isolated smooth muscle cells. *J. Gen. Physiol.* **88:** 61a.

Reference: *Biol. Bull.* **176(S):** 31–35. (April, 1989, Suppl.)

Relationship Between Growth and the Electrical Current of Fungal Hyphae

NEIL A. R. GOW

Department of Genetics and Microbiology, Marischal College, University of Aberdeen, Aberdeen AB9 1AS, UK

Abstract. The hyphae of filamentous fungi exhibit a highly polarized mode of cell extension and all generate electrical currents around their hyphal tips. Of the 13 fungi that have been examined with the vibrating probe, 12 normally have positive electrical current entering the growing tip. However, the apical current is always outward in *Allomyces macrogynus*. In those organisms that have inward apical currents, outward currents are found occassionally and transiently in hyphae that extend at normal rates. There is no good correlation between either the extension rate or the length of the growing peripheral cell and the current density. These studies lead one to conclude that the relationship between the generation of an electrical current and the extension of a hypha is superficial and not essential. The association between the flow of protons, which carry most of the current in fungi, and cell extension may be tighter.

Comparison of the currents of three water molds *A. macrogynus, Blastocladiella emersonii* and *Achlya bisexualis* provides an insight to the probable role of the electrical current. *A. macrogynus* and *B. emersonii* both have rhizoids that may take up nutrients by proton-linked transport. The nutrients support growth of the sporangium and hypha, respectively, to which they are joined. In *A. bisexualis*, proton symport is responsible for nutrient transport into the hyphal tip. There seems to be an excellent correlation between the zones at which proton-coupled nutrient transport occurs and the regions where positive current enters these fungi. Therefore, the current may indicate local nutrient uptake rather than local cell growth.

Abbreviations: PGZ—peripheral growth zone.

Introduction

Investigations of ionic currents in fungi have centered on those found at the apices of hyphae and hyphal branches. The currents are normally steady, inward at the tip, and carried mainly by protons. Much effort has been devoted to the mechanism of generation of the current but here attention is turned to their biological significance. To date, three fungi have been examined in detail: *Achlya bisexualis*, a filamentous water mold (Kropf *et al.*, 1983, 1984; Gow *et al.*, 1984; Schreurs and Harold, 1988), *Neurospora crassa* (McGillivray and Gow, 1987; Takeuchi *et al.*, 1988), a mycelial ascomycete, and *Blastocladiella emersonii*, a chytidiomycetous fungus that forms branching rhizoids and a thallus-like sporangium (Stump *et al.*, 1980). Thirteen fungi have now been examined with the vibrating probe (Gow, 1987). Normally current enters the hyphal tips of the filamentous fungi or the rhizoids of *B. emersonii*, however transient outward currents have also been found at the growing tips of *A. bisexualis* (Kropf *et al.*, 1983) and *N. crassa* (McGillivray and Gow, 1987). Another water mold, *Allomyces macrogynus*, was recently investigated (Youatt *et al.*, 1988). This has hyphae like *A. bisexualis* and rhizoids like *B. emersonii*. Since these both have inward currents, we wondered whether *A. macrogynus* would follow the *Achlya* or the *Blastocladiella* pattern. A report of the findings follows.

Currents typically enter an apical zone of some hundreds of microns in length. The growing zone of a hypha in which cytoplasm provides the enzymes and new membrane for tip extension is a measurable parameter in mycelial fungi and has been called the "peripheral growth zone" (PGZ) (Trinci, 1971). This zone varies in length and volume according to the growth conditions but it

may be as small as the first 100 μm of the hypha or as much as a centimeter in length for some rapidly growing fungi. It is of interest to establish how the map of inward and outward current compares with the PGZ. Such a comparison is made here for three mycelial fungi. The pattern, shape, and magnitude of the transhyphal electrical current is discussed in relation to the polarity and kinetics of cell growth in fungi.

Materials and Methods

Organisms and culture conditions

A. bisexualis female strain T5, *N. crassa* strain RL21A, *Basidiobolus ranarum* (lab strain), and *A. macrogynus* strain 3.35 were all grown from agar blocks into liquid media as described previously (Gow, 1984; Youatt *et al.*, 1988). The medium for *B. ranarum* contained 20 g/l glucose and 5 g/l mycological peptone.

Measurements with the vibrating probe

A one-dimensional system using glass electrodes was used (Jaffe and Nuccitelli, 1974). Electrodes typically had a ball of between 15 and 25 μm diameter. Quadrature measurements were made at intervals or continuously. Signals were processed using a EG&G dual phase Princeton Applied Research 5208 lock-in amplifier. Current densities for all fungi were normally in the range of 0.1 to 1.0 $\mu A \cdot cm^{-2}$.

Determination of the peripheral growth zone

The PGZ was determined in three ways. (1) For *N. crassa* and *A. bisexualis*, the specific growth rate α of the organism was measured by determining the rate of increase in biomass in liquid culture. The PGZ is obtained from the following equation where Kr is the extension rate or radial growth rate of the hypha (Trinci, 1971).

$$PGZ = Kr/\alpha$$

(2) For *A. bisexualis* the PGZ was also determined by excising tips at increasingly distal locations and observing the effect on cell extension rate (Trinci, 1971). The minimum distance that the cut could be made from the tip without affecting the rate of hyphal extension was taken to be the PGZ. (3) For *B. ranarum*, the cytoplasm in the hypha migrates forward with extending tip leaving behind extensively vacuolated hypha to the rear (Robinow, 1963). The PGZ can be determined directly and is simply the observed length of the apical cytoplasmic compartment.

Results

Relationship between hyphal extension and electrical current

There is a very poor correlation between the extension rate of a hypha and the inward current density. Nongrowing hyphae with normal-sized currents have been reported in *N. crassa* and *Achlya ambisexualis* (McGillivray and Gow, 1987; Gow and Gooday, 1987). Takeuchi *et al.*, (1988) reported a correlation coefficient of only 0.36 between the rate of extension and the current density in this organism. In branching hyphae of *A. bisexualis*, transient outward currents have been reported at hyphae that maintained a normal extension rate (Kropf *et al.*, 1983). Recently Schreurs and Harold (1988) showed that *A. bisexualis* could be grown in media that supported normal growth but severely attenuated currents. Therefore quantitatively there is a poor correlation between current magnitude and the rate of hyphal extension. This does not support the view that the electrical current is a driving force for tip growth.

In Table I a qualitative study of the shape of the electrical current map is made by comparing the lengths of the zones of inward and outward current with the length of the actively growing portion of the hypha. This peripheral growth zone (PGZ) can be thought of as the equivalent of a "cell" for a filamentous fungus thus it is of interest to ascertain whether there is a relationship between the functional and electrically active growth zones.

In *N. crassa* and *A. bisexualis* the zone in which current entered the hypha was a small fraction of the PGZ. In *A. bisexualis* the complete map, comprising both inward and outward current, was approximately equal to the PGZ while in *B. ranarum* the zones of inward current and the PGZ were approximately the same (Table I). It was not possible to determine whether the whole current map coincided with the PGZ in *N. crassa* because currents could not be mapped well behind the tip where branching was profuse. There was also no indication that the length of the inward current zone was related to the extension rate. For example, with *N. crassa* the hyphae extended at twice the rate in malt extract medium than in Vogels minimal medium yet the zone of inward current was about the same. The error in making these measurements is large enough to prevent precise comparison but they do not suggest any firm relationship between the kinetic and electrical dynamics of cell growth.

Electrical currents in water molds

What is the biological significance of the vectorial flow of electrical current in fungi? The water molds include two major groups: the chytridiomycetes of which *B. em-*

Table I

Comparison of the growth of fungal hyphae and the associated endogenous electrical current

Organism	Medium	Current in (μm)	Current in + out (μm)	Extension rate (μm/h)	Peripheral growth zone (μm)	Method for PGZ*
N. crassa	MEM	240 ± 40	>1000	1250 ± 220	6900 ± 1100	1
N. crassa	VMM	290 ± 150	>1000	660 ± 120	6300 ± 1100	1
A. bisexualis	FYG	130 ± 110	800 ± 100	210 ± 120	920 ± 500	1
A. bisexualis	DMA	340 ± 70	880 ± 80	320 ± 20	600 ± 100	2
B. ranarum	MPG	350 ± 30	N.D.	210 ± 30	320 (max)	3

From: Gow, N. & MacCulloch, L.

MEM—Malt Extract Medium; VMM—Vogels Minimal Medium; PYG—peptone, yeast extract, glucose medium; DMA—Defined Medium Achlya; MPG—Malt extract, peptone, glucose medium.

* Methods 1, 2, and 3 are described in the Materials and Methods section. Values are means ± standard deviations. The temperature was 25 ± 1°C in each case.

ersonii and *A. macrogynus* are examples, and the oomycetes, which include *A. bisexualis*. Endogenous electrical currents have now been mapped with a vibrating probe in all three of these organisms and comparison of the current profiles provides a clue to significance of the electrical flux. Current flows into the rhizoids of *B. emersonii* (Stump *et al.*, 1980) and into the hyphal tip of *A. bisexualis* (Kropf *et al.*, 1983). *A. macrogynus* has both zhizoids and hyphae, so it was of interest to determine whether the flow of electrical current would be inward at the rhizoids or the hyphal tips or at both the rhizoids and the hyphae of this organism. Also, *A. macrogynus* is an intriguing model for cell polarity because in addition to the normal mode of tip extension the hyphae can also be made to grow with a reversed polarity (Cleary *et al.*, 1986).

The electrical current profiles around these three water molds is shown in Figure 1. Hyphae of *A. macrogynus*, whether extending or non-extending, had a steady outward current of around 0.1 $\mu A \cdot cm^{-2}$. Extension of these hyphae was slow (1–2 $\mu m \cdot min^{-1}$) but measurable. As with *B. emersonii*, positive current entered the rhizoids. This is the first example of a hypha with a constant outward current.

When hyphae were grown under conditions of partial oxygen starvation, the hyphae of *A. macrogynus* were narrow but extended at normal rates towards sites of higher oxygen tension (Fig. 2). Experimentally this was achieved by growing the organism on an agar surface that was covered with a glass coverslip. The hyphae grew up the oxygen gradient outwards towards the edge of the coverslip. Hyphae were allowed to grow into a well of liquid growth medium containing ascorbate to maintain a low oxygen tension, and the vibrating probe was placed in the well next to the hyphae. When the coverslip was removed and the medium was replaced with one without ascorbate, the oxygen gradient was abolished and the hyphae grew backwards by expanding the apex and then progressively more distal regions of the hypha (Fig. 2). This "reversed growth" involved active wall biosynthesis since it was completely inhibited by the specific chitin-synthase inhibitors polyoxin and nikkomycin. All this made no difference to the direction of current flow. The current was still outward even during reversed development. Again, there was no correlation between the electrical and growth polarities of this cell.

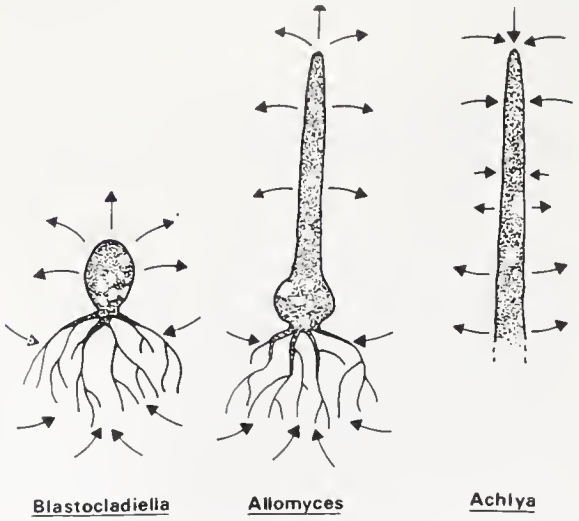

Figure 1. Pattern of flow of positive electrical current around three water molds measured with the vibrating probe. Inward currents enter the rhizoids of *Blastocladiella emersonii* (Stump *et al.*, 1980) and *Allomyces macrogynus* and the hyphal apex of *Achlya bisexualis*. It is suggested that these three sites are locations of ion-coupled nutrient transport. From Youatt *et al.* (1988) with permission.

Discussion

The direction and magnitude of current flow were not tightly correlated with the rate of cell extension or the length of the actively growing part of the hypha. With *A. macrogynus* the polarity of cell growth could effectively be reversed but this had no effect on the direction of the flow of the electrical current. These data indicate that electrical forces are not paramount in driving the expansion of the hyphal apex or maintaining cell polarity.

B. emersonii takes up nutrients preferentially in the rhizoids (Kropf and Harold, 1982) which are chemotropic towards them (Harold and Harold, 1980). The nutrients are used for growth of the rhizoids and for the sporangium. The rhizoids of *A. macrogynus* are also chemotropic towards amino acids (Youatt, Gow, and Gooday, unpubl.) and can also be presumed to be the principle site of nutrient adsorption (Fig. 3). In *A. bisexualis*, amino acid transport is localized at the hyphal tip (Gow *et al.*, 1984; Kropf *et al.*, 1984) (Fig. 3). Since nutrient transport in fungi is often linked to the influx of protons, one might expect to see inward currents at sites where nutrient transport is concentrated. An excellent correlation is demonstrated here between the sites of nutrient transport and the sites where inward currents are found in various water molds (see Figs. 1 and 3). These results imply that the inward electrical current relects local nutrient transport and not local cell growth.

In *A. bisexualis*, protons may continue to enter hyphal tips even when the electrical current turns from inward to outward (Gow *et al.*, 1984). It is possible that the outward currents at the apices of hyphae of *A. macrogynus* may be carried by an ion or ions other than protons. For example, it is conceivable that outward current at the hyphal tip may result from electrogenic potassium efflux, which masks continued proton influx at this site. This possibility is now under investigation. In this scheme of things it is the chemical component, not the electrical component, of circulating currents that may be significant in the control of cell polarity.

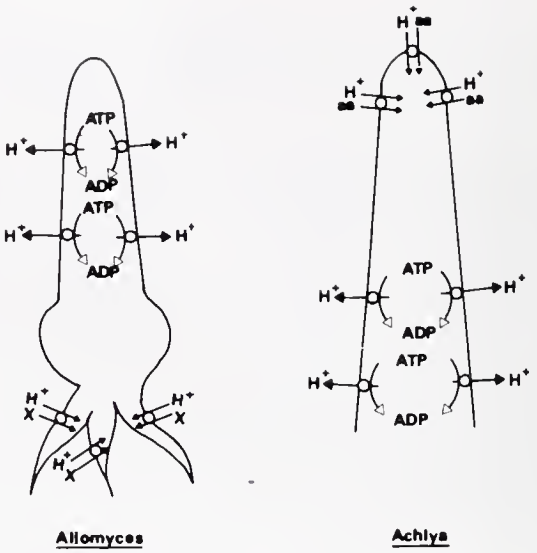

Figure 3. Suggested correlation between proton-coupled nutrient transport and the circulation of electrical current in *Allomyces macrogynus* and *Achlya bisexualis*. Symport of amino acids (aa) and other nutrients (X) is confined to the hyphal tip of *Achlya* and the rhizoids of *Allomyces*. The proton-pumping ATPases that drive the currents are probably excluded from these regions. Positive current enters sites of local nutrient transport, not local hyphal growth.

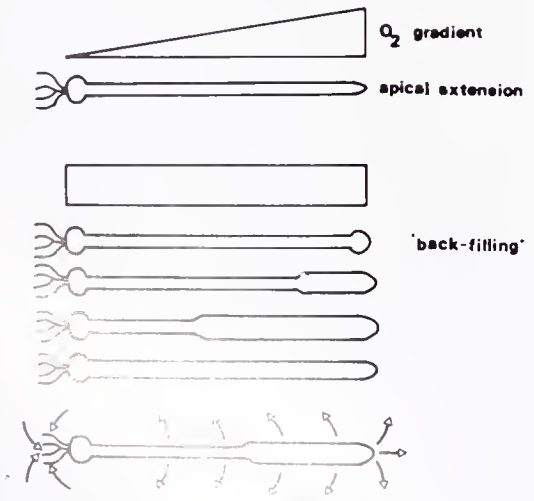

Figure 2. The electrical current associated with "reversed development" of *Allomyces macrogynus*. Hyphae were first grown in a gradient of limiting oxygen and were then allowed to undergo progressive hyphal widening from the tip to [illegible] oxygen-sufficient conditions.

Acknowledgments

This study was supported by grants from the SERC (GR/E 2943.4) and the University of Aberdeen Advisory Committee. I thank Jean Youatt, Graham Gooday, and Laura MacCulloch for their contributions to these studies.

Literature Cited

Cleary, A., J. Youatt, and T. P. O'Brien. 1986. Hyphal emergence and outgrowth of *Allomyces macrogynus* in aerated cultures. *Aust. J. Biol. Sci.* **46:** 241–254.

Gow, N. A. R. 1984. Transhyphal electrical currents in fungi. *J. Gen. Microbiol.* **130:** 3313–3318.

Gow, N. A. R. 1987. Polarity and branching in fungi induced by electrical fields. Pp. 25–41 in *Spatial Organisation in Eukaryotic Microbes*, R. K. Poole and A. P. J. Trinci, eds. IRL Press, Oxford.

Gow, N. A. R., and G. W. Gooday. 1987. Effects of antheridiol on growth, branching and electrical currents of hyphae of *Achlya ambisexualis*. *J. Gen. Microbiol.* **133:** 3531–3535.

Gow, N. A. R., D. L. Kroff, and F. M. Harold. 1984. Growing hyphae of *Achlya bisexualis* generate a longitudinal pH gradient in the surrounding medium. *J. Gen. Microbiol.* **130:** 2967–2974.

Harold, R. L., and F. M. Harold. 1980. Orientated growth of *Blastocladiella emersonii* in gradients of ionophores and inhibitors. *J. Bacteriol.* **144:** 1159–1167.

Jaffe, L. F., and R. Nuccitelli. 1974. An ultrasensitive vibrating probe for measuring steady extracellular currents. *J. Cell Biol.* **63:** 614–628.

Kropf, D. L., and F. M. Harold. 1982. Selective transport of nutrients via the rhizoids of the water mold *Blastocladiella emersonii*. *J. Bacteriol.* **151:** 429–437.

Kropf, D. L., M. D. A. Lupa, J. H. Caldwell, and F. M. Harold. 1983. Cell polarity: endogenous ion currents precede and predict branching in the water mold *Achlya*. *Science* **220:** 1385–1387.

Kropf, D. L., J. H. Caldwell, N. A. R. Gow, and F. M. Harold. 1984. Transcellular ion currents in the water mold *Achlya*. Amino acid proton symport as a mechanism of current entry. *J. Cell Biol.* **99:** 486–496.

McGillivray, A. M., and N. A. R. Gow. 1987. The transhyphal electrical current of *Neurospora crassa* is carried principally by protons. *J. Gen. Microbiol.* **133:** 2875–2881.

Robinow, C. F. 1963. Observations of cell growth, mitosis and division in the fungus *Basidiobolus ranarum*. *J. Cell Biol.* **17:** 123–152.

Schreurs, W. J. A., and F. M. Harold. 1988. Transcellular proton current in *Achlya bisexualis* hyphae: relationship to polarized growth. *Proc. Natl. Acad. Sci. USA* **85:** 1534–1538.

Stump, R. F., K. R. Robinson, R. L. Harold, and F. M. Harold. 1980. Endogenous electrical currents in the water mold *Blastocladiella emersonii* during growth and sporulation. *Proc. Natl. Acad. Sci. USA* **77:** 6673–6677.

Takeuchi, Y., J. Schmid, J. H. Caldwell, and F. M. Harold. 1988. Transcellular ion currents and extension of *Neurospora crassa* hyphae. *J. Membr. Biol.* **101:** 33–41.

Trinci, A. P. J. 1971. Influence of the width of the peripheral growth zone on the radial growth rate of fungal colonies on solid media. *J. Gen. Microbiol.* **67:** 325–344.

Youatt, J., N. A. R. Gow, and G. W. Gooday. 1988. Bioelectric and biosynthetic aspects of cell polarity in *Allomyces macrogynus*. *Protoplasma* **146:** 118–126.

Reference: *Biol. Bull.* **176(S)**: 36–40. (April, 1989, Suppl.)

Transcellular Ionic Currents During Primary Cell Wall Morphogenesis in *Micrasterias* and *Closterium*

CYNTHIA L. TROXELL

Division of Cellular and Molecular Biology, National Jewish Center for Immunology and Respiratory Medicine, 1400 Jackson Street, Denver, Colorado 80206

Abstract. The results of one- and two-dimensional vibrating probe studies of the desmids *Closterium* and *Micrasterias* have demonstrated that (i) transcellular ionic currents are detected only around cells that are undergoing primary cell wall morphogenesis, (ii) inward current is localized to regions of wall expansion, (iii) current densities maintain a steady level until growth slows with maturation of the primary cell wall pattern, and (iv) the currents are carried at least in part by Ca^{2+}, K^+, H^+, and Cl^- ions.

Introduction

The unicellular green algal desmids *Micrasterias* and *Closterium* are intriguing systems for the study of mechanisms controlling plant cell wall form (Tippit and Pickett-Heaps, 1974; Kallio and Lehtonen, 1981; Kiermayer, 1981; Staehelin and Giddings, 1982; Pickett-Heaps, 1983). A desmid cell has two symmetrical half cells joined at an isthmus. Each time a cell divides, it is bisected by a septum (cross wall) to produce asymmetric daughter cells. To regain interphase symmetry, each daughter must undergo a remarkable, patterned expansion of the cross wall. In *Closterium*, the septum expands [illegible] probably through tip growth, to regenerate the simple [illegible]rm of the mature cell. In *Micrasterias*, septum [illegible] accompanied by the appearance of clefts that [illegible] with a central polar lobe.

Although [illegible] controlling the pattern of primary expansion [illegible] derstood, localized wall expansion in gree[illegible] uated thus far is thought to be accompanied [illegible] ding localized influx of Ca^{2+} ions (reviewed [illegible] and Kircherer, 1981; Hepler and Wayne, [illegible] results of several studies (Brower and McIntos[illegible] Weisenseel, 1982; McNally *et al.*, 1983; Lehtonen, 1984) support the hypothesis that Ca^{2+} directs localized wall growth in *Micrasterias* and indicate that the desmids may be particularly favorable cells in which to investigate the electrical control of development. In this study, one- and two-dimensional vibrating probes (Jaffe and Nuccitelli, 1974; Scheffey, 1988) were used to map the ionic currents around *Micrasterias* and *Closterium* cells.

Materials and Methods

Algal cultures

Micrasterias and *Closterium* cells were cultured in a modified Waris medium (Waris, 1953) in which equimolar $CaCl_2$ was substituted for $CaSO_4$, as recommended by McNally *et al.* (1983) and to which 2.5 m*M* 2-(N-morpholino)ethanesulfonic acid (MES) and 50 ml/liter of soil water extract had been added. The pH of the medium was adjusted with KOH to 5.4 for *Micrasterias* cultures and to 6.0 for *Closterium* cultures. Cells were grown at 18°C on an 16-h light/8-h dark cycle, adjusted so that cell division and primary cell wall expansion occurred during the working day. Dividing cells selected for use in experiments were treated for 15 to 30 min with 1 Sigma unit of beta-glucuronidase (Sigma) reconstituted in Waris medium to remove the surface coat of mucilage, which can interfere with probe measurements. Dividing cells left in the beta-glucuronidase solution for longer periods completed wall expansion normally. During probe measurements, cells were maintained in modified Waris medium without soil extract. The specific resistivity of the medium was *ca.* 3.5×10^3 ohm·cm. The medium contained 1.0 m*M* KNO_3, 0.2 m*M* $MgSO_4$, 0.2 m*M* $(NH_4)_2HPO_4$, and 0.3 m*M* $CaCl_2$, and 2.5 m*M* MES.

The effects upon transcellular currents of media with altered ionic compositions or containing channel blockers or metabolic inhibitors were tested using a coupled syringe system. The system consisted of a 35-mm diameter Petri dish chamber to which inflow tube and outflow tubes were fitted. A sylastic insert in the dish reduced the volume of medium to be exchanged and more efficiently channeled the flow of medium from the input to the outflow tube. Two disposable 60-cc syringes served as reservoirs for media and were connected to the input tube by a three-way valve. The syringes could be quickly refilled or replaced as needed during experiments without disturbing the cell preparation. The exchanges were carried out by adjusting outflow and inflow rates so that the cells and probe in a preparation were always submerged. The system permitted the exchange of up to 0.5 cc of medium/s without disturbing the cells. Tests in which the dish was filled with a 1% neutral red solution showed that an exchange of 18 cc over a period of about 36 s was sufficient to exchange media. The probe was moved to a reference position during exchanges.

A "low-potassium" medium was made by replacing the KNO_3 in Waris medium with equimolar $Ca(NO_3)_2$. In a "low calcium" medium, $CaCl_2$ was replaced with equimolar $MgCl_2$. In some experiments, anthracine-9-carboxylic acid (Aldrich Chemical Co.), a Cl^- channel blocker (Palade and Barchi, 1977; Oberliethner *et al.*, 1983), was added to the medium at a final concentration of 100 μM. Gadolinium nitrate pentahydrate (Aldrich Chemical Co.) was added to the medium at a final concentration of 50 μM as a Ca^{2+} channel blocker (Bourne and Trifaro, 1982). These test media were of the appropriate pH (5.4 or 6.0) for the cell under investigation. Media of pH 5, 6, and 7 (buffered with MES) were used in substitution tests on *Closterium*. The resistivities of the test media were similar to the resistivity of regular Waris; however, measured current densities were corrected for slight differences in resistivity between normal and test media. *Closterium* cells were used for substitution experiments because these preparations were easier to work with.

Vibrating probe measurements

Ionic currents were measured using a vibrating probe (Jaffe and Nuccitelli, 1974; Scheffey *et al.*, 1983; Scheffey, 1986a, 1988). A one-dimensional probe was used for initial measurements of currents around *Micrasterias* and *Closterium* cells, for coarse and fine resolution mapping of trancellular current patterns and for ion substitution and drug studies. In addition, a two-dimensional probe (Scheffey, 1988) was used to map current patterns around *Closterium* cells. An excellent introduction to these techniques is available in Scheffey *et al.* (1983) and Scheffey (1986a, 1988). All experiments were conducted at the National Vibrating Probe Facility at the Marine Biological Laboratory, Woods Hole, Massachusetts.

Wire probe tips had diameters from 5 to 36 μm. The amplitude of probe vibration was set to the diameter of the probe tip in use, and the probes were vibrated perpendicular to the cell surface at frequencies in the range of 149 to 1842 Hz. Probe capacitance was checked frequently, and probes were replatinized or replaced when capacitance fell much below 1 nF in Waris medium or when noise levels became excessive. Lock-in quadrature response was monitored during experiments with the one-dimensional probe (Scheffey, 1986b) as an aid in detecting artifacts resulting from contact between the probe tip and mucilage secreted by the cells. Probe calibration was performed at the approximate depth in the preparation at which measurements were to be made.

Cell preparations were made as described previously (Troxell *et al.*, 1986). Transcellular current patterns during wall expansion were determined from one-dimensional probe measurements taken around 45 *Micrasterias* and 68 *Closterium* cells. In addition, 15 *Closterium* cells were mapped with a two-dimensional probe. One-dimensional probe measurements were recorded on chart records, and experiments were further documented with time-lapse video and/or 35 mm photographs. Two-dimensional probe data were stored on computer floppy disks and magnetic tape; data could be displayed as a printed log or as video images of cells upon which measured current vectors were plotted to the scale desired. Video displays of probe data were also recorded on Polaroid and 35-mm black and white and slide films.

Results

Correlation between currents and growth

Transcellular ionic currents were detected only in *Micrasterias* and *Closterium* cells undergoing primary cell wall expansion. Currents were observed to enter growing regions of the new semicell and to exit over the old semicell. Measurements of steady inward currents densities ranged from 0.7 to 5.4 $\mu A/cm^2$, and outward current densities ranged from 0.2 to 1.5 $\mu A/cm^2$ measured at 18 μm from the cell surface. Figure 1 shows typical one-dimensional probe measurements of the transcellular currents around a *Micrasterias* cell in the later stages of primary cell wall expansion. Currents measured in several *Micrasterias* cells from an early stage of wall expansion through completion of maturation of the primary wall pattern remained at a steady level and then decreased to background noise levels as wall expansion ceased with

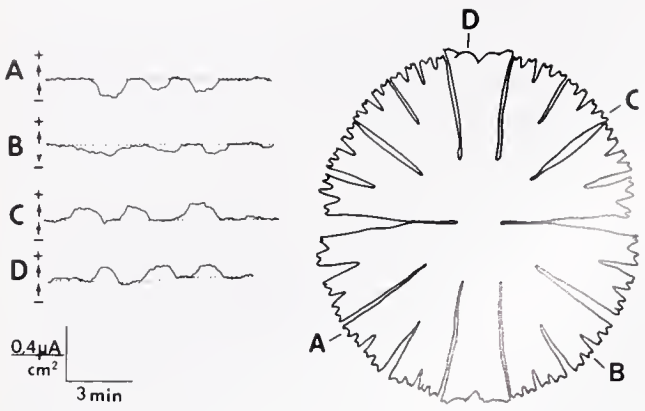

Figure 1. Ionic currents measured around a *Micrasterias thomasiana* cell with a one-dimensional vibrating probe. Outward current (−) is found over the old half cell (A, B), and inward current (+) is found over the nearly mature primary wall of the new half cell (C, D).

maturation of the primary wall pattern (data not shown). When the spatial resolution of the one-dimensional probe was maximized through the use of small probe tips (5–15 μm), more subtle details of the transcellular current patterns in biradiate and uniradiate *M. thomasiana* cells were observed. As the probe was moved from lobe to cleft to lobe over an expanding semicell, the corresponding current measurements showed inward current over the lobe tips, and slightly outward current over the intervening cleft. Because the lobe tips are about 5 μm across, which is near the limit of spatial resolution of the probe, it was not possible to determine whether changes in the current pattern at an expanding lobe tip precede the formation of a cleft as one would predict.

Primary cell wall expansion and semicell morphogenesis in the uniradiate variant of *M. thomasiana* differs from that of the normal biradiate cell in that lobes are formed only on one side of the expanding half cell; thus, the polar lobe of the resulting semicell thus has an exposed side. In uniradiate cells, current was observed to enter expanding lobe tips and exit over the parental semicell, as in biradiate forms; current was also found to leave over the lateral surface of the new polar lobe where a wing had not formed (data not shown).

The transcellular current pattern in growing *Closterium* cells is more graphically demonstrated in observations made on [illegible] cells with a two-dimensional vibrating probe; a typical current pattern is shown in Figure 2. Current appears to enter the tip region of the expanding primary cell wall and exit over the old semicell. No transcellular current was detected in observations of 5 interphase cells (data not shown).

Ionic dependence of the [illegible] currents

The results of ion substitution and channel blocker studies on *Closterium* cells summarized below, suggest that H^+, Cl^-, K^+, and Ca^{2+} ions may carry a portion of the current.

Treatment with anthracine-9-carboxylic acid. Both inward and outward currents decreased rapidly (20–64%) in cells treated with 100 μ*M* A-9-C, a chloride channel blocker. When the cells were returned to Waris medium, current decrease continued for a few minutes, and then currents recovered to their former levels.

The effects of low potassium medium. Both inward and outward currents decreased immediately (33–85%) in low potassium medium, but recovered rapidly when the cell was returned to Waris medium.

The effects of pH changes. Transcellular currents were dramatically affected by changing the pH of Waris me-

Figure 2. Current pattern around a *Closterium* cell undergoing primary wall expansion, mapped with a two-dimensional vibrating probe. Currents enter over the new half cell (N) and exit over the old half cell (O). The region where the old cell wall adjoins the new is marked by open arrowheads. Vectors indicate current density and directions; the vector base marks the probe position at the time of measurement. Vectors to the right of the cell are smaller because the cell-to-probe distance is proportionately larger. Scale vector (upper left) = 0.5 $\mu A/cm^{-2}$; scale bar = 60 μm.

dium plus or minus one pH unit. Both inward and outward currents decreased when the pH was raised from 6 to 7, and currents increased when the pH was lowered from 6 to 5; the effects of the pH changes were reversible.

The effects of low calcium medium. The effect upon currents measured around growing *Micrasterias* and *Closterium* cells of lowering the [Ca^{2+}] of Waris medium was distinctive. Upon exposure to the low-Ca^{2+} medium, inward currents showed a transient increase followed by a decrease over observation periods of about 5 min; outward currents were less effected, showing a slight decrease or even a slight increase. The effects of low calcium medium were reversible; upon return to normal Waris medium, current densities returned to normal levels. When cells were left in low calcium medium for longer period, the inward currents underwent more dramatic fluctuations, even reversing the direction of net ion flow; currents quickly stabilized to normal levels when the cells were returned to regular Waris medium.

The effect of gadolinium ions. The addition of 50 μM gadolinium nitrate to Waris medium as a calcium channel blocker resulted in current decreases of 50% or more of both inward and outward currents. The effects of gadolinium were somewhat reversible.

Discussion

Steady, transcellular ionic currents were found to enter the growing regions of semicells undergoing primary cell wall morphogenesis. They exited over non-growing regions of the old semicell or in regions of the new semicell, such as lobe clefts or the lateral side of the polar lobe, where wall-hardening prevents expansion. Currents maintained steady levels during wall expansion and decreased to background noise levels as primary wall morphogenesis reached completion.

The results of the ion substitution and channel blocker experiments on *Closterium* suggest that the transcellular current is carried in part by H^+, K^+, Cl^-, and Ca^{2+}, as has been found to be the case for a number of other plant cells (reviewed by Wiesenseel and Kircherer, 1982). An unexpected and intriguing result of the calcium ion substitution experiments with the desmids was the erratic fluctuation of the current at the growing tips when the cells were placed in a low calcium medium. The repeated reversal of the tip current from inward to outward in the low calcium medium suggests that extracellular calcium is required to maintain normal ion transport.

Of the ions that have been demonstrated to carry a portion of the current, calcium has the most probable significance for the localization of growth potential in expanding lobe tips. A localized intracellular increase in the concentration of calcium might facilitate secretion of vesicles containing wall materials by simple charge screening between the vesicle and plasma membranes, or might initiate and maintain a differentiation of an F-actin network in these cells. Such a network could direct secretory vesicles to the growing tips, as in the case of *Fucus* zygotes (Brawley and Robinson, 1985) or various fungal hyphae (reviewed by McKerracher and Heath, 1987).

Acknowledgements

This work was conducted at the National Vibrating Probe Facility at the Marine Biological Laboratory. Dr. Lionel Jaffe and Dr. Jeremy Pickett-Heaps provided valuable guidence, and Dr. Carl Scheffey, Mr. Alan Shipley, and Mr. Steve Dixon provided talented technical assistance.

Literature Cited

Bourne, G. W., and J. M. Trifaro. 1982. The gadolinium ion: a potent blocker of calcium channels and catecholamine release from cultured chromaffin cells. *Neuroscience* **7:** 1615–1622.

Brawley, S. H., and K. R. Robinson. 1985. Cytochalasin treatment disrupts the endogenous currents associated with cell polarization in fucoid zygotes: studies of the role of F-actin in embryogenesis. *J. Cell Biol.* **100:** 1173–1184.

Brower, D. L., and J. R. McIntosh. 1980. The effects of applied electric fields in *Micrasterias.* II. The distributions of cytoplasmic and plasma membrane components. *J. Cell Sci.* **42:** 279–290.

Giddings, T. H., and L. A. Staehelin. 1988. Spatial relationship between microtubules and plasma membrane rosettes during the deposition of primary wall microfibrils in *Closterium. Planta* **173:** 22–30.

Hepler, P. K., and R. O. Wayne. 1985. Calcium and plant development. *Annu. Rev. Plant Physiol.* **36:** 397–439.

Jaffe, L. F., and R. Nuccitelli. 1974. An ultrasensitive vibrating probe for measuring steady extracellular currents. *J. Cell Biol.* **63:** 614–628.

Kallio, P., and J. Lehtonen. 1981. Nuclear control of cytomorphogenesis in *Micrasterias.* Pp. 191–213 in *Cytomorphogenesis in Plants, Cell Biology Monographs 8,* O. Kiermayer, ed., Springer-Verlag, New York.

Kiermayer, O. 1981. Cytoplasmic basis of morphogenesis in *Micrasterias.* Pp. 147–189 In *Cytomorphogenesis in Plants, Cell Biol. Monographs 8,* O. Kiermayer, ed. Springer-Verlag, New York.

Lehtonen, J. 1984. The significance of Ca^{2+} in the morphogenesis of *Micrasterias* studied with EGTA, varapamil, $LaCl_3$ and calcium ionophore A23187. *Plant Sci. Lett.* **33:** 53–60.

McKerracher, L. J., and I. B. Heath. 1987. Cytoplasmic migration and intracellular organelle movements during tip growth of fungal hyphae. *Exp. Mycol.* **11:** 79–100.

McNally, J. G., J. D. Cowan, and H. Swift. 1983. The effects of the ionophore A23187 on pattern formation in the alga *Micrasterias. Dev. Biol.* **97:** 137–145.

Meindl, U. 1982. Local accumulation of membrane-associated calcium according to cell pattern formation in *Micrasterias denticulata,* visualized by chlorotetracycline fluorescence. *Protoplasma* **110:** 143–146.

Oberliethner, H., M. Ritter, F. Lang, and W. Guggins. 1983.

Anthracene-9-carboxylic acid inhibits renal chloride reabsorption. *Pflugers Arch.* **398:** 172–174.

Palade, P. T., and R. L. Barchi. 1977. On the inhibition of muscle membrane chloride conductance by aromatic carboxylic acids. *J. Gen. Physiol.* **69:** 879–896.

Pickett-Heaps, J. D. 1983. Morphogenesis in desmids: our present state of ignorance. *Mod. Cell Biol.* **2:** 241–258.

Scheffey, C. 1986a. Electric fields and the vibrating probe, for the u[illegible] initiated. Pp. xxv–xxxvii in *Ionic Currents in Development.* R. Nuccitelli, ed., Alan R. Liss, Inc. New York.

Scheffey, C. 1986b. Pitfalls of the vibrating probe technique, and what to do about them. Pp. 3–12 in *Ionic Currents in Development,* R. Nuccitelli, ed. Alan R. Liss, Inc. New York.

Scheffey, C. 1988. Two approaches to construction of vibrating probes for electrical current measurement in solution. *Rev. Sci. Instrum.* **59:** 787–792.

Scheffey, C., J. K. Foskett, and T. E. Machen. 1983. Localization of ionic pathways in the opercular membrane by extracellular recording with a vibrating probe. *J. Membr. Biol.* **75:** 193–205.

Staehelin, L. A., and T. H. Giddings. 1982. Membrane-mediated control of cell wall microfibrillar order. Pp. 133–147 in *Developmental Order: Its Origin and Regulation,* Alan R. Liss, Inc., New York.

Tippit, D. H., and J. D. Pickett-Heaps. 1974. Experimental investigations into morphogenesis in *Micrasterias. Protoplasma* **81:** 271–296.

Troxell, C. L., C. Scheffey, and J. D. Pickett-Heaps. 1986. Ionic currents during wall morphogenesis in *Micrasterias* and *Closterium.* Pp. 105–112 in *Ionic Currents in Development,* R. Nuccitelli, ed. A. R. Liss, Inc., New York.

Waris, H. 1953. The significance for algae of chelating substances in nutrient solutions. *Physiol. Plant.* **6:** 538–543.

Weisenseel, M. H., and R. M. Kircherer. 1982. Ionic currents as control mechanisms in cytomorphogenesis. Pp. 379–399 in *Cytomorphogenesis in Plants, Cell Biology Monographs 8,* O. Kiermayer, ed., Springer-Verlag, New York.

Reference: *Biol. Bull.* **176(S)**: 41–45. (April, 1989, Suppl.)

Ionic Currents During Regeneration of Thallus and Rhizoid From Cell Segments Isolated From the Marine Alga *Bryopsis*

TOMOKI NAWATA[1], TASUKU HISHINUMA[2], AND SHUNJI WADA

Biological Institute, Faculty of Science, Tohoku University, Sendai 980, Japan

Abstract. Cell segments isolated from the unicellular marine alga, *Bryopsis plumosa,* regenerated or protruded thallus (T) at one cut end and rhizoid (R) at the other cut end. Using a vibrating probe, we measured endogenous ionic currents associated with these events.

Prior to the protrusion of T and R, the currents changed in various ways. When the T and R protruded at the cut ends of the segments, we detected an inwardly directed current at the regions of T and R, and an outwardly directed current in other parts of the cell segment. Both currents were strongly affected by decreases in external concentrations of Cl^-, suggesting that a large part of the currents was carried by Cl^-. In addition, these currents decreased with a decrease in external concentrations of Mg^{2+}, and were also reversibly eliminated by two metabolic inhibitors. This evidence suggests that the Cl^--migration system involves an energy-dependent and Mg^{2+}-dependent process.

In parallel with the generation of these currents, turgor pressure reached a maximum prior to the protrusion of T and R. The relationship between the generation of the currents, the generation of the maximum turgor pressure, and the protrusion of T and R is discussed.

Introduction

Our knowledge of the relationship between endogenous (self-generated) ionic currents and growth and development in plants and animals has been increasing in recent years (*e.g.,* Nuccitelli, 1986), since Jaffe and Nuccitelli (1974) developed an ultrasensitive vibrating electrode.

The unicellular marine alga, *Bryopsis plumosa,* possesses not only a high capacity for the regeneration of whole plants from protoplasts (Tatewaki and Nagata, 1970) or from small pieces of algae (Nakazawa and Sasaki, 1982), but also possesses an apico-basal or thallus-rhizoid cellular polarity that is firmly established by microtubules (Mizukami and Wada, 1983).

So far, little is known about the bioelectro-ionic properties of algae (Munday, 1972). Our initial studies (Hishinuma, 1982), using a three-part chamber such as that used in studies of *Acetabularia* (Nova'k and Bentrup, 1972), suggested that regenerating or regenerated algae have a gradient of membrane potential along the T-R axis. This finding led us to investigate whether endogenous ionic currents are involved in the process of regeneration of T and R, as described below.

Materials and Methods

Alga and its culture

The marine alga *Bryopsis plumosa* was maintained in culture cups containing growth medium, which consisted of 250 ml natural seawater enriched with 2.5 ml of Provasoli's ES medium (McLachlan, 1973). The cups were placed under continuous illumination with 1200 lux from fluorescent tubes at 21–23°C. In the sea, the natural algae are pinnate in form. However, under our culture conditions the algae grew as cylindrical filaments, probably because the medium was never disturbed by shaking and the light intensity was insufficient. One end of the alga is called the rhizoid (R) and attaches to the bottom of the culture cup, and the other end is called the thallus (T) and grows up toward the surface of the growth medium.

[1] To whom all correspondence should be addressed. Present address: College of Medical Sciences, Tohoku University, Sendai 980, Japan.

[2] Present address: Department of Biology, Faculty of Science, Yamagata University, Yamagata 990, Japan.

Isolation of experimental materials

Filamentous algae (4–7 cm in length and 0.4–0.6 mm in diameter) were transferred to artificial seawater (ASW: 500 m*M* NaCl, 10 m*M* KCl, 10 m*M* $CaCl_2$, 20 m*M* $MgCl_2$, 30 m*M* $MgSO_4$, adjusted to pH 8.2 with 5 m*M* Tris-HCl), one of the tips of R was cut to release turgor pressure, and then both the whole of R and the tip of T were cut and removed with small scissors. The remainder of the filament was further cut into several segments of approximately 5 mm in length. The cut ends of each segment were closed by squashed cell walls, which were formed by cutting. The isolated segments were kept in ASW alone to minimize the multiplication of bacteria, which grew as contaminants during the electrical and pressure measurements. In this medium the segments regenerated T and R in the same way as those in the standard culture medium, and then grew normally, at least over two-week periods.

Measurement of endogenous currents

Our vibrating electrode system has been described in detail elsewhere (Nawata, 1984; Nawata and Sibaoka, 1987). The system is similar to that of Jaffe and Nuccitelli (1974), but the construction of the vibrating probe has been somewhat modified.

To examine the ion dependence of endogenous currents, we first prepared six modified ASWs, in which one ion at a time was excluded from ASW; in K^+-free ASW, KCl was replaced by NaCl; in Na^+-free ASW, NaCl was replaced by choline chloride; in Ca^{2+}-free ASW, $CaCl_2$ was replaced by $MgCl_2$; in Mg^{2+}-free ASW, both $MgCl_2$ and $MgSO_4$ were replaced by NaCl; in Cl^--free ASW, NaCl was replaced by CH_3CH_2COONa (sodium propionate) and other chlorides by the corresponding sulfates; and in SO_4^{2-}-free ASW, $MgSO_4$ was replaced by $MgCl_2$. By mixing any one of these media with ASW in different proportions, the concentration of a given specific ion could be varied. The pH of ASW, over the range from 6 to 9, was varied by addition of a small amounts of HCl or NaOH.

Specific resistivity of ASW and all of the experimental media was in the range of 24 to 38 Ω·cm. All experiments were conducted at 20–24°C and in white light (1125 lux) provided from the illumination apparatus of a light microscope.

Measurement of turgor pressure

Changes in turgor pressure of some segments were measured for five days after isolation, during the period of protrusion of T and R. A glass rod (ca. 20 μm in tip diameter) was glued to a movable arm of a high-sensitivity mechano-transducer (Transducer UL-2-240, Shinkoh Communication Industry Co., Ltd. Tokyo, Japan). The rod was gently rested against the surface of the segments immediately after they were isolated. Recovery of turgor pressure caused an increase in diameter of the segments, and as a result the rod was displaced upwards and the transducer generated the corresponding DC voltage. Use of different segments allowed the displacement to be calibrated against the absolute value of turgor pressure determined by the manometric method (Green and Stanton, 1967).

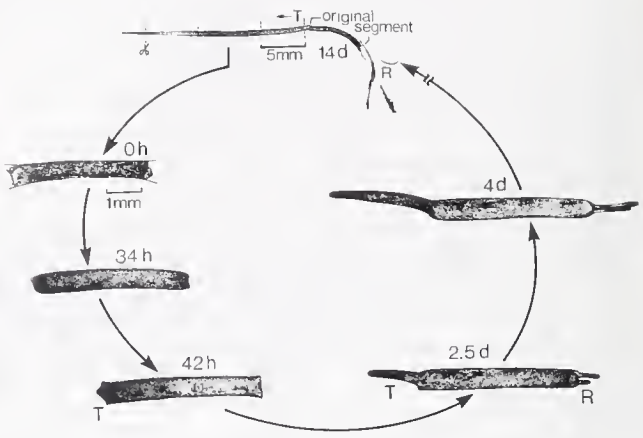

Figure 1. Regeneration cycle of a segment isolated from a *Bryopsis* cell. The filamentous alga cultured for 2 weeks (top) was cut into 3 segments. One of them was subsequently observed for 4 days; the photographs were taken at the times indicated. Protrusion of a new thallus (T) occurred 42 h after isolation, when there was still no sign of a rhizoid (R).

Results

Regeneration of T and R from isolated cell segments

A large part of the cellular volume of *Bryopsis* filaments is occupied by a central vacuole, so that a cytoplasmic layer is compressed against the cell wall. When the filament was cut into approximately 5-mm-long segments in ASW, the cytoplasmic layer retracted up to 3–4 mm along the cell wall (0 h in Fig. 1), and then the cytoplasm aggregated quickly to close the wound at both cut ends. This process resembled that of the wound healing observed in *Boodlea sp.* (La Claire II, 1982).

Membrane potential, which was recorded using a conventional glass microcapillary electrode, began to increase gradually until it reached approximately −40 mV (vacuolar side, negative) within 10 min of cutting of segments (unpub. data). This result suggests that new plasma and vacuolar membranes began to be formed on the surface of the aggregated cytoplasm. However, breakage and restoration of the new membranes occurred repeatedly at irregular intervals up to approximately 2 h after isolation.

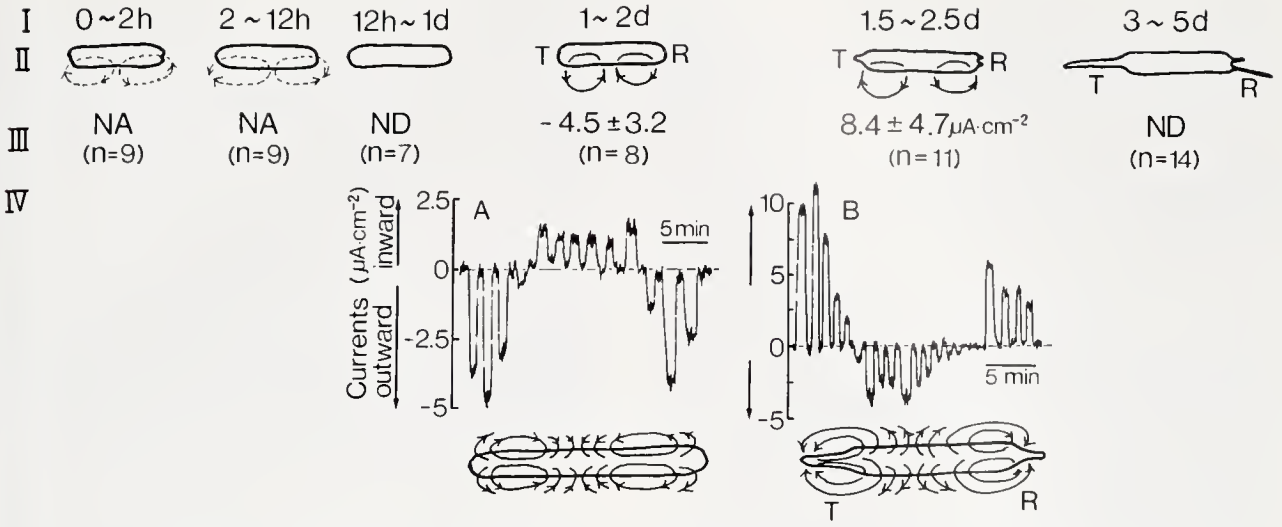

Figure 2. Schematic drawing of the pattern of ionic currents and representative measurements. Row I: time after isolation; II: pattern of currents detected; III: current density (mean ± standard deviation, n = number of experiments), all of which were measured at the thallus (T) end; NA, not applicable (see text); ND, not detectable. IV: Examples of current mappings made at 1–2 days (A) and 1.5–2.5 days (B) after isolation. The patterns detected currents are depicted on the outline of the cell segments. Arrows indicate the direction of currents.

Prior to the protrusion of T or R at either cut end, no significant morphological changes could be discerned (34 h in Fig. 1). However, observations using a fluorescent dye, Calcofluor White (a specific probe for β-linked glycosidic polymers) showed that the cytoplasmic surface of both cut ends could be stained positively 6–16 h after isolation, suggesting that a new cell wall was deposited during that time.

The time at which T and R protruded was in the range between 35 h (in the earliest case examined) to 60 h (in the latest case) after isolation. In the case shown in Figure 1, the protrusion of T became visible at 40 h, and that of R at 47 h. The new T-R polarity of the segment was consistent with that of the original filament. Subsequently, the tips of both T and R grew at a rate of approximately 0.5–1.0 mm per day, and the segments regained the form of cultured plants.

Generation of ionic currents and their orientation along the longitudinal axis

The ionic currents were mapped along the longitudinal axis of the segments; the probe was vibrated at a measuring position 50 μm away from the cell surface (at the center of vibration) and at a reference position 2 mm away from the cell surface. The results of 7–14 measurements at each cell stage are summarized in Figure 2, including examples of traces which were recorded before and after the protrusion of T and R.

During the first 1–2 h after isolation, inward currents which indicated an ionic flow from the outside toward the inside could sometimes be detected at both cut ends, but their peak values were rarely over 10 μA/cm^2. The currents appeared to be generated when the newly formed plasma and vacuolar membranes were suddenly broken.

During the next approximately 10 h, the currents that were measured at the cut ends of 24 segments decreased to less than 1.6 μA/cm^2, and their direction varied among segments. By the end of this period, these currents were reduced to the average noise level of our probe (about 0.4 μA/cm^2). One or two days after isolation, *i.e.*, approximately 0.5 days before the protrusion of either T or R, the currents flowed inwards over a large region of the segment and flowed outwards through both cut ends (1–2 days in Fig. 2).

At the time at which the protrusion of T and R was first discerned (1.5–2.5 days in Fig. 2), the direction of the currents was completely reversed, *i.e.*, the currents flowed inwards at the regions of T and R, while they flowed outwards in other regions of the original segments. These results were obtained from 10 segments out of a total 13 segments examined. The exact time at which the reversal of current occurred was not defined in the present study. The inward currents on the T side were somewhat stronger than those on the R side.

In the course of these measurements, we presumed that such currents continue to flow as long as the tip growth of T and R continues. However, when the T and

R grew to approximately 5 mm in length both the inward and outward currents were greatly reduced or had disappeared. The tip growth was subsequently maintained under conditions where no currents were detected.

Ion dependence of the inward currents detected at the region of new T

By varying the ionic composition of ASW, we examined the ion dependence of the currents that were detected during the protrusion of T and R (the period from 1.5–2.5 days in Fig. 2). The results for only the inward currents on the T side were described below, because the ion dependence of the other currents measured on the R side and in other regions of isolated segments gave almost identical results.

Exposure to K^+-, Na^+-, SO_4^{2-}-free ASW, or ASW at pH 6–9, had almost no effect on the magnitude of the currents for at least 60 min. When segments were exposed to Ca^{2+}-free ASW, twelve of the segments examined burst near the tips of the new T or R. Such segments rapidly lost all ionic currents. In the remaining 8 intact segments, the currents fell slowly by ~80% within 60 min. This result suggests that external Ca^{2+} is essential for maintaining the membrane structure, rather than for generation of the currents.

Changes in the concentration of Mg^{2+} ($[Mg^{2+}]$), over the range from 20 to 50 m*M*, did not have a major effect on the magnitude of the currents. However, when the $[Mg^{2+}]$ was decreased below 20 m*M* the currents decreased quickly and became almost zero within 5 min after the change. The currents were reversible, but not completely so.

Changes in the concentration of Cl^- ($[Cl^-]$), over the range from 10 to 570 m*M*, influenced the magnitude of the currents in two different ways. In 17 of the segments examined, the currents decreased toward zero with the decrease in $[Cl^-]$, and below 50 m*M* the currents became almost zero. In five other segments, the currents increased suddenly at a certain decreased $[Cl^-]$. Probably, such currents occurred as a result of leakage of the vacuolar sap, caused by imperceptible damage to membranes.

We also studied the effects of 1 m*M* 2,5-dinitrophenol (an inhibitor of respiration) and 30 μM 3-(3,4-dichlorophenyl)-1-methylurea (an inhibitor of photosystem II) dissolved in ASW on the currents. The currents were completely inhibited by each of these inhibitors within 3 min, and their removal from ASW allowed a gradual but complete recovery of the currents (30 min or more).

Recovery of turgor pressure

Changes in turgor pressure were monitored from the isolation of segments through the protrusion of T and R. A representative trace is shown in Figure 3. In this segment, turgor pressure began to increase approx. 0.8 days after isolation of the segment and reached a maximum value of 2.1 atmosphere at 2.3 days. At this point, the protrusion of T was observed for the first time. Soon after the T protruded, the protrusion of R occurred at the cut end opposite the T protrusion.

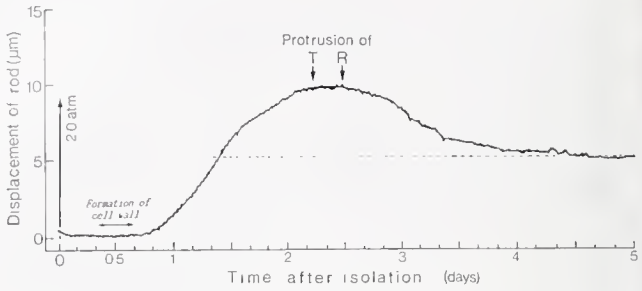

Figure 3. Time course of recovery of turgor pressure. The ordinate indicates the upward displacement of the glass rod and the calibrated turgor pressure. Protrusion of thallus occurred at the time indicated by T, and that of the rhizoid at the time indicated by R. Deposition of new cell wall on both cut ends seems to occur ~ 0.5 days after isolation.

After protrusion, both the T and R grew up to 0.1, 0.5, and 1.1 mm in length at 2.7, 4.0, and 4.7 days, respectively. The turgor pressure decreased gradually with the growth and fell to 1.6 atmosphere 5 days after isolation. This value of turgor pressure was maintained during subsequent growth (data not shown).

Discussion

The first visible sign that small segments isolated from *Bryopsis* filaments have begun to regenerate is a protrusion of T or R at either cut end of the segments (Fig. 1). However, the endogenous ionic currents could be clearly detected approximately 12 h before the visible morphological events occurred (1–2 days in Fig. 2). The spatial distribution of these currents changed totally by the time at which the T or R protruded. Thus, the relationship between these currents and the regeneration of T and R needs to be defined.

When either T or R could be discerned, ionic currents flowed inwards at both ends of the segment and flowed outwards at the central region of the segment (1.5–2.5 days in Fig. 2). Both the inward and outward currents continued to flow not only during the protrusion of T and R, but also during the initial growth of their tips. Therefore, it appears that the currents may play a role in the initial processes involved in the regeneration of T and R.

Changes in the external ionic composition showed that both the inward and outward currents were strongly affected by decreases in $[Cl^-]$, $[Mg^{2+}]$, or $[Ca^{2+}]$. In the

present study, the dependence on Ca^{2+} of these currents could not be clarified. Preliminary tracer experiments using radioactive Ca^{2+} indicate the accumulation of Ca^{2+} at the growing tips of T and R (unpub. data). It is possible that influx of Ca^{2+}, which might cause the accumulation of Ca^{2+}, was so small as to be undetectable as a Ca^{2+} current by our vibrating probe.

It is also unlikely that Mg^{2+} carried a major part of those currents, because Mg^{2+} generally possesses a low membrane permeability. Mg^{2+} may be required for activation of an energy-dependent ion transport system such as the Mg^{2+}-dependent proton pump in Chara (Shimmenn and Tazawa, 1977). If a similar Mg^{2+}-dependent ion transport system is present in *Bryopsis* segments, it is also possible to explain the fact that the two metabolic inhibitors examined rapidly eliminated the currents.

Therefore, we can hypothesize that a large part of the currents was carried by Cl^-. Furthermore, it is possible that Cl^- circulates through an inward-outward current pathway, because both the inward and outward currents responded to changes in $[Cl^-]$ in a similar way. The inward current may result from an efflux of Cl^- and the outward one from an influx of Cl^-. In the marine algae *Acetabularia* (Gradmann, 1970) and *Halycistis* (Graves and Gutknecht, 1977), Cl^- is taken up into the interior of cells by an active Cl^- pump. Thus, it seems likely that Cl^- was actively taken up into the segments of the marine algae *Bryopsis*. Consequently, Cl^- influx might be recorded as an outward current over the central region of the segments, while Cl^- efflux might be recorded as the inward current at the both cut ends, including the regions of T and R.

It has been shown that, in developing *Fucoid* eggs, an endogenous ionic current is partly carried by Ca^{2+} (Nuccitelli, 1978) and the current takes part in determination of the cell's polarity via a mechanism mediated by an intracellular distribution of microfilaments (Brawley and Robinson, 1985). The currents observed in Bryopsis segments, however, appeared to have no role in the determination of the cell's T-R polarity, because we could find no significant differences in magnitude and in ion dependence of the inward currents observed on the T side and the R side. Furthermore, the currents probably play no role in normal growth, because growth continued under conditions of no detectable currents (3–5 days in Fig. 2).

At the time at which the T and R protruded, the turgor pressure increased to approximately twice the value during subsequent normal growth of T and R (Fig. 3). It is noteworthy that the period of "increased" turgor pressure was compatible with the period when the currents continued to flow. The "increased" turgor pressure is probably caused by inflow of water coupled with some increases in the ionic concentration in the vacuole. We assume that Cl^- carried in by the outward current (Cl^- influx) participated in the increase in ionic concentration in the vacuole. In fact, the vacuolar concentration of Cl^- in the segments from which T and R protruded was approximately 60 m*M* higher than the external concentration of Cl^- (unpub. data). However, in the present study the process of accumulation of Cl^- could not be detected as an imbalance between the outward current (Cl^- influx) and the inward current (Cl^- efflux).

Literature Cited

Brawley, S. H., and K. R. Robinson. 1985. Cytochalasin treatment disrupts the endogenous currents associated with cell polarization in fucoid zygotes: studies of the role of F-actin in embryogenesis. *J. Cell Biol.* **100:** 1173–1184.

Gradmann, D. 1970. Einfluß von Licht, Temperature und Außenmedium auf das elektrische Verhalten von *Acetabularia crenulata*. *Planta* **93:** 323–353.

Graves, J. S., and J. Gutknecht. 1977. Chloride transport and the membrane potential in the marine alga, *Halicystis parvula*. *J. Memb. Biol.* **36:** 65–81.

Green, P. B., and F. W. Stanton. 1967. Turgor pressure: direct manometric measurement in single cells of *Nitella*. *Science* **155:** 1675–1676.

Hishinuma, T. 1982. Relationship between some electro-ionic properties and morphogenesis in *Bryopsis* cells (in Japanese). M.Sc. Thesis, Tohoku University.

Jaffe, L. F., and R. Nuccitelli. 1974. An ultrasensitive vibrating probe for measuring steady extracellular currents. *J. Cell Biol.* **63:** 614–628.

La Claire II, J. W. 1982. Cytomorphological aspects of wound healing in selected Siphonocladales (Chlorophyceae). *J. Phycol.* **18:** 379–384.

Munday, JR. J. C. 1972. Membrane potentials in *Bryopsis plumosa*. *Botanica Marina* **15:** 61–63.

McLachlan, J. 1973. Growth media—marine. Pp. 25–51 in *Handbook of Phycological Methods*, J. R. Stein, ed. Cambridge Univ. Press, Cambridge.

Mizukami, M., and S. Wada. 1983. Morphological anomalies induced by antimicrotubule agents in *Bryopsis plumosa*. *Protoplasma* **114:** 151–162.

Nakazawa, S., and R. Sasaki. 1982. Polarity disturbance in regeneration of *Bryopsis* by colchicine. *Bull. Yamagata Univ. Nat. Sci.* **10:** 313–317.

Nawata, T. 1984. A simple method for making a vibrating probe system. *Plant Cell Physiol.* **25:** 1089–1094.

Nawata, T., and T. Sibaoka. 1987. Local ionic currents controlling the localized cytoplasmic movement associated with feeding initiation of *Noctiluca*. *Protoplasma* **137:** 125–133.

Nova'k, B., and F. W. Bentrup. 1972. An electrophysiological study of regeneration in *Acetabularia mediterranea*. *Planta* **108:** 227–244.

Nuccitelli, R. 1978. Oöplasmic segregation and secretion in the *Pelvetia* egg is accompanied by a membrane-generated electrical current. *Dev. Biol.* **62:** 13–33.

Nuccitelli, R., ed. 1986. *Ionic Currents in Development. Progress in Clinical and Biological Research, Vol. 210.* Alan R. Liss, Inc., New York. (Proceedings of a Satellite Meeting of the Tenth International Congress of the International Society of Developmental Biologists).

Shimmenn T., and M. Tazawa. 1977. Control of membrane potential and excitability of *Chara* cells with ATP and Mg^{2+}. *J. Memb. Biol.* **37:** 167–192.

Tatewaki, M., and K. Nagata. 1970. Surviving protoplasts *in vitro* and their development in *Bryopsis*. *J. Phycol.* **6:** 401–403.

Reference: *Biol. Bull.* **176(S)**: 46–48. (April, 1989, Suppl.)

Ionic Currents Around Developing Embryos of Higher Plants in Culture

KEERTI S. RATHORE AND KENNETH R. ROBINSON

Department of Biological Sciences, Purdue University, West Lafayette, Indiana 47907

Plant cell and tissue cultures are being used extensively to study growth and early development of higher plants. This is because the egg cell of higher plants resides within the sporophyte and is difficult to isolate. Somatic embryogenesis offers an alternative that is being exploited by many investigators to produce large numbers of somatic embryos growing under controlled conditions. The development of somatic embryos in carrot tissue cultures was first demonstrated by Steward *et al.* (1958) and Reinert (1959). Asexual embryos develop from small embryogenic cell clusters (proembryos) that are growing in a medium containing the synthetic auxin 2,4-dichlorophenoxyacetic acid (2,4-D). Embryo development is initiated by removing very large cell clusters and single differentiated cells by filtration from a suspension culture and then transferring the small cell clusters at a low cell density to a medium lacking the 2,4-D. Embryos develop from these clusters and pass successively through globular, heart, and torpedo stages, which are similar to their zygotic counterparts (Fig. 1). This and another system, in which tobacco pollen have been induced to form haploid embryos, have now been used to investigate endogenous currents traversing developing higher plant embryos. The vibrating probe studies have allowed us to see the similarities between the embryos derived from the two systems and also made it possible to detect substantial physiological variability between the somatic embryos of the same species that are derived from different cultures.

Brawley *et al.* (1984) were the first to use the carrot somatic embryogenesis system to study the endogenous currents. They found that the current (flow of positive charge) enters the apical region and leaves the region near the presumptive radicle of the radially symmetric globular embryo. This electrical polarity precedes differentiation of vascular tissue and cotyledon development. The electrical polarity is maintained and strengthened during subsequent heart and torpedo stages. Current enters the cotyledons and it leaves the surface of the radicle. Similar electrical polarity was observed in globular and heart stage haploid embryos from tobacco pollen (Overall and Wernicke, 1986).

Recently, Gorst *et al.* (1987) showed that small cell clusters that were incubated in a medium containing 2,4-D possessed electrical polarity. The authors suggested that the electrical polarity was established in clusters undergoing apparently disorganized proliferation in the presence of 2,4-D, which is similar to that found in organized somatic embryos which form after removal of 2,4-D. On this basis, they concluded that the proliferating clusters are suppressed embryos and that their development into embryos represents progression rather than induction of embryogenesis. However, their results should be interpreted with some caution since the measurements were made on cell clusters after 8 days of culturing at a reduced density of 1000 clusters/ml. Borkird *et al.* (1986) showed that, in certain culture lines, limited embryonic development up to the globular stage was possible even in the presence of a low concentration of 2,4-D if the cell density was lowered. Probably a better way to test the interpretation of Gorst *et al.* (1987), which addresses a very important issue in our understanding of *in vitro* embryogenesis, would be to carry out current measurements with the proembryonic cell clusters immediately after isolating them from a suspension culture that is maintained at high cell density. The presence of electrical polarity at this stage would suggest an inherent mechanism that maintains polarity in the absence of any physical or chemical gradients in a suspension cultures.

We have confirmed and extended the findings of Brawley *et al.* (1984) with the heart and torpedo stage somatic embryos from culture lines of a cultivated vari-

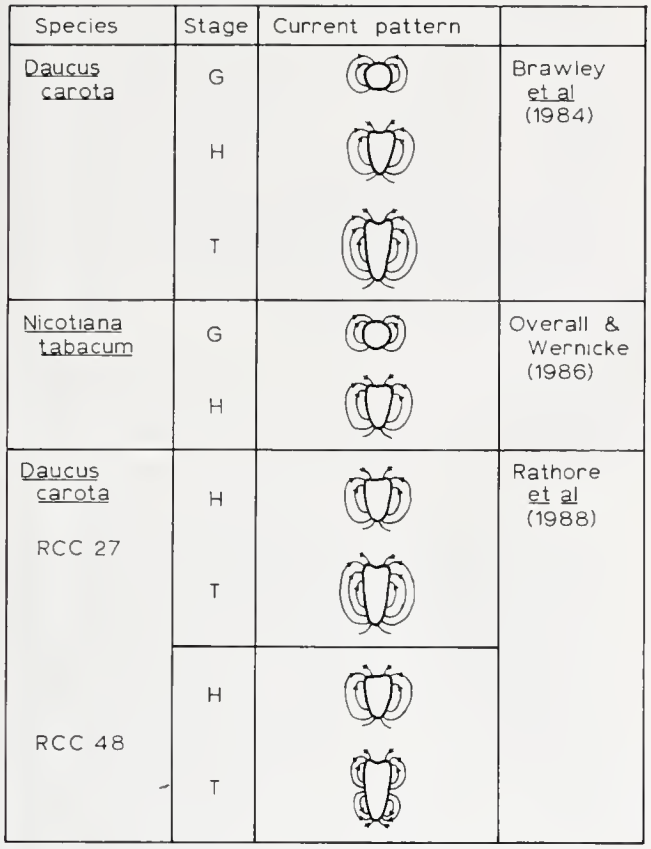

Figure 1. Patterns of electrical currents measured around developing embryos in culture at globular (G), heart (H), and torpedo (T) stages.

ety of *Daucus carota* (Rathore *et al.*, 1988). Two culture lines (RCC27 and RCC48) were used in our measurements. The heart stage embryos from both lines had inward current at the cotyledon and outward current at the radicle. Most torpedo stage embryos from RCC27 line also showed this current pattern. However, 5% of the embryos at the torpedo stage from this line had an additional inward current at the tip of the radicle. On the other hand, in all of the torpedo stage embryos from the faster developing RCC48 line that were tested, inward current was detected at the cotyledon as well as the tip of the radicle and outward current left from the middle region of the embryo. The development of inward current at the tip of the radicle is not surprising since, in the later stages of development, such as in a growing root of a seedling, current does enter the meristematic and cell elongation zone and leaves the region of maturing elongated cells (Weisenseel *et al.*, 1979; Miller *et al.*, 1986). It seems likely that somatic embryos from certain lines develop an inward current at the tip of the radicle at a rather early stage of their development. Somatic embryos, unlike zygotic embryos, frequently undergo precocious differentiation (Ammirato, 1987). It is possible that the differences in the current pattern reflect differences in the extent of differentiation in somatic embryos from the two culture lines. Our results also suggest that one should be careful in comparing the results of biochemical and molecular studies from various laboratories using different culture lines. Since only a small number of embryos are required, the use of vibrating probe also makes it possible to compare the development of zygotic embryos with that of somatic embryos.

Localized extracellular pH measurements around torpedo stage embryos from the RCC27 line showed that the regions adjacent to the cotyledon and radicle at the points of current entry and exit were 0.02 and 0.07 pH units more acidic than the bulk medium, respectively (Rathore *et al.*, 1988). This suggests that in addition to the electrical polarity, there is a pH gradient along the length of the embryo within the apoplast. Both could play a role in embryonic development. The electrical field set up across the embryo might result in polar transport of indole-3-acetic acid (IAA). Raven (1979) suggested that the longitudinal gradient of electrical potential difference (base positive to apex) in young shoots could maintain polar transport of IAA by causing asymmetric distribution of IAA^- uniporters to the basal side of the cell via lateral electrophoresis in the membrane (Jaffe, 1977; Poo and Robinson, 1977; Poo, 1981). He further suggested that, as a result of polar transport of IAA, the basal cells would be exposed to a higher IAA concentration and therefore have a more vigorous electrogenic H^+ extrusion than cells near the apex, resulting in a larger electrical potential difference across the plasmalemma of the basal than of the apical cells. Since the cells are connected to each other via plasmodesmata, there will be a flow of current from the apex to the base within the symplast. The return loop of this current would be in the apoplast which would set up an electrical potential difference as measured by electrodes in contact (via saline bridges) with the cell walls at the tip and base of a young shoot. A positive feedback mechanism of this kind may also exist in developing embryos. Schiavone (1988) recently provided indirect evidence for polar transport of IAA in somatic carrot embryos as early as heart stage. Schiavone and Cooke (1987) used inhibitors of polar transport of IAA to show that polar IAA transport was required for normal somatic embryo development. Polar transport of IAA has also been demonstrated in unripe zygotic embryos of *Phaseolus vulgaris* and *Acer pseudoplantanus* (Fry and Wangermann, 1976) and in hydrated, dormant embryo sections of *Pinus lambertiana* (Greenwood and Goldsmith, 1970). The studies discussed in this paper show quite clearly that electrical polarity is established at a very early stage of embryo development. The pH gradient observed along the embryonic

axis in the somatic embryos is also consistent with Raven's hypothesis. Thus, it is possible that the electrical polarity initiates and maintains polar transport in the developing embryos in a manner analogous to that proposed for shoots (Raven, 1979). The resultant IAA distribution, in interaction with other hormones, could affect embryonic development. In addition, the difference in extracellular pH could also affect cell growth via its influence on the cell wall (Rayle and Cleland, 1970). Finally, there may be a substantial difference in cytoplasmic pH between the radicle and cotyledon since the cells of the radicle appear to have a more active H^+-ATPase. As a result the cytoplasmic pH of radicle cells would be more alkaline than that of cotyledon cells. Many cellular functions are sensitive to pH, so this is another mechanism by which the currents might act to cause or amplify tissue polarity.

Literature Cited

Ammirato, P. V. 1987. Organizational events during somatic embryogenesis. Pp. 57–81 in *Plant Tissue and Cell Culture,* Green, C. E., Somers, D. A., Hackett, W. P., Biesboer, D. D., eds. Alan R. Liss, Inc., New York.

Borkird, C., J. H. Choi, and Z. R. Sung. 1986. Effect of 2,4-Dichlorophenoxyacetic acid on the expression of embryogenic program in carrot. *Plant Physiol.* **81:** 1143–1146.

Brawley, S. H., D. F. Wetherell, and K. R. Robinson. 1984. Electrical polarity in embryos of wild carrot precedes cotyledon differentiation. *Proc. Natl. Acad. Sci. USA* **81:** 6064–6067.

Fry, S. C., and E. Wangermann. 1976. Polar transport of auxin through embryos. *New Phytol.* **77:** 313–317.

Gorst, J., R. L. Overall, and W. Wernicke. 1987. Ionic currents traversing cell clusters from carrot suspension cultures reveal perpetuation of morphogenetic potential as distinct from induction of embryogenesis. *Cell Differ.* **21:** 101–109.

Greenwood, M. S., and M. H. M. Goldsmith. 1970. Polar transport and accumulation of indole-3-acetic acid during root regeneration by *Pinus lambertiana* embryos. *Planta* **95:** 297–313.

Jaffe, L. F. 1977. Electrophoresis along cell membranes. *Nature* **265:** 600–602.

Miller, A. L., J. A. Raven, J. I. Sprent, and M. H. Weisenseel. 1986. Endogenous ion currents traverse growing roots and root hairs of *Trifolium repens. Plant Cell Environment* **9:** 79–83.

Overall, R. L., and W. Wernicke. 1986. Steady ionic currents around haploid embryos formed from tabacco pollen in culture. Pp. 139–145 in *Ionic Currents in Development,* Nuccitelli, R., ed. Alan R. Liss, Inc., New York.

Poo, M-m. 1981. *In situ* electrophoresis of membrane components. *Ann. Rev. Biophys. Bioeng.* **10:** 245–276.

Poo, M-m., and K. R. Robinson. 1977. Electrophoresis of concanavalin A receptors along embryonic muscle cell membrane. *Nature* **265:** 602–605.

Rathore, K. S., T. K. Hodges, and K. R. Robinson. 1988. Ionic basis of currents in somatic embryos of *Daucus carota. Planta* **175:** 280–289.

Raven, J. A. 1979. The possible role of membrane electrophoresis in the polar transport of IAA and other solutes in plant tissues. *New Phytol.* **82:** 285–291.

Rayle, D. L., and R. Cleland. 1970. Enhancement of wall loosening and elongation by acid solutions. *Plant Physiol.* **46:** 250–253.

Reinert, J. 1959. Uber die Kontrolle der Morphogenes und die Induktion von Adventivembryonen an Gewebekulturen aus Karotten. *Planta* **53:** 318–333.

Schiavone, F. M. 1988. Microamputation of somatic embryos of the domestic carrot reveals apical control of axis elongation and root regeneration. *Development* **103:** 657–664.

Schiavone, F. M., and T. J. Cooke. 1987. Unusual patterns of somatic embryogenesis in the domesticated carrot: developmental effects of exogenous auxins and auxin transport inhibitors. *Cell Differ.* **21:** 53–62.

Steward, F. C., M. O. Mapes, and K. Mears. 1958. Growth and organized development of cultured cells. II. Organization in cultures grown from freely suspended cells. *Am. J. Bot.* **45:** 705–708.

Weisenseel, M. H., A. Dorn, and L. F. Jaffe. 1979. Natural H^+ currents traverse growing roots and root hairs of barley (*Hordeum vulgare* L.). *Plant Physiol.* **64:** 512–518.

Reference: *Biol. Bull.* **176(S)**: 49–55. (April, 1989, Suppl.)

The Use of Bioelectric Currents to Study Gravity Perception in Roots

THOMAS BJÖRKMAN

Department of Botany, KB-15, University of Washington, Seattle, Washington 98195

Abstract. Inhibitor-based studies of gravity perception in plants have yielded ambiguous results because gravitropism consists of many steps in series. Inhibiting any step eliminates gravicurvature; it cannot be shown whether gravity perception and transduction are affected by the inhibitory treatment. The use of the vibrating probe has allowed detection of a response that is measurable independent of stimulus transmission and growth, two post-transduction steps of gravitropism. This application of the vibrating probe requires particular attention to artifacts. Calmodulin action and auxin transport are both believed to be components of gravitropism and specific roles have been proposed for them in graviperception. The perception-dependent current measured with the vibrating probe is eliminated by inhibitors of calmodulin, but not by auxin inhibitors. Thus, the vibrating probe has made it possible to offer more direct evidence for a role of calmodulin in transduction, and to reject one for auxin transport in perception and transduction.

Introduction

Gravitropism is a complex process that occurs in heterogeneous tissues. Therefore it has been difficult to study the early events associated with gravity perception. Gravitropic curvature is a poor measure of perception because it can be inhibited or influenced by treatments that do not affect perception. Further, root curvature often has a time lag of approximately half an hour. Microscopic study of the perceiving cells is limited because no physiological response can be measured. This paper describes a method that detects a response to graviperception and transduction independently of the other steps in gravitropism.

Electrical changes around gravitropically responsive tissues have long been known (Schrank, 1945; Behrens *et al.*, 1982), although some have been artifacts or correlated with later steps in gravitropism (Woodcock and Wilkins, 1969). To develop these observations into a useful tool, a characteristic response associated with gravity perception had to be identified. A current specific to the perceiving region can be measured with a vibrating probe after gravistimulation. It has been described by Björkman and Leopold (1987a). This paper will further describe the technique and its validation.

The value of this technique of measuring graviperception is demonstrated in experiments testing proposed steps in perception. Numerous studies (reviewed by Roux and Serlin, 1987) based on measurements of curvature and calmodulin indicate that graviperception is not calmodulin dependent, but imply that transduction is altered through a calmodulin-dependent process from dia- to orthogravitropism. It has not been possible to test this hypothesis directly due to the problems outlined above. In this paper, this new electrical response is used to test the role of calmodulin in gravitropic transduction. Altered auxin transport is a likely component of root gravitropism (Jackson and Barlow, 1981). Evans *et al.* (1986) propose that the transport of auxin is altered in the graviperceptive cells. The technique described herein has also been applied to test this hypothesis (Björkman and Leopold, 1987b), and indicates that transduction is normal in the absence of auxin transport.

Materials and Methods

Plants

Three-day-old maize seedlings (*Zea mays* cv 'Merit'; Asgrow, Kalamazoo, Michigan) were used when the radicles were 25–35 mm long.

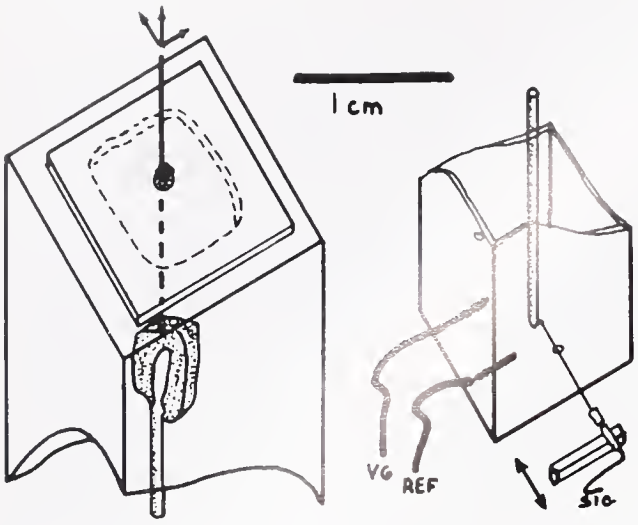

Figure 1. Detail of top and bottom of chamber showing how root tip was positioned and accessible to vibrating probe while preventing loss of solution when turned. Full description in Materials and Methods.

Vibrating probe

The chamber to hold the seedlings during the experiment had to meet several requirements: (1) the surface at the root tip had to be clear to allow precise microscopic observation of the root tip and the vibrating probe; (2) there had to be a means of positioning the seedling within the chamber during the experiment; (3) there had to be access for the vibrating probe and for a calibrating electrode; and (4) the chamber needed to be rotated 90° in either direction from the vertical without draining the solution from it.

The seedlings were held in a plexiglass chamber 10 × 10 mm at the base and 15 × 15 mm at the top; height 50 mm (Fig. 1). The upper surface had an opening large enough to insert the seedling; this opening was then covered with a lid using lanolin to make a strong and watertight seal. The lid had a 1-mm orifice through which a 24 gauge stainless steel cannula was passed and inserted into the endosperm of the seedling. The cannula needed to be small so that it displaced a minimum amount of solution when moved to position the root tip. The orifice was filled with lanolin to make a flexible and watertight seal. The external end of the cannula was attached to a micromanipulator, which allowed precise positioning of the seedling within the chamber.

Three mm from the bottom of the chamber, a 0.7-mm diameter hole was drilled in the side to allow access for the vibrating probe and the calibrating electrode. This configuration allowed measurement of the apical 3 mm of the root, the region examined in this study. The holes were large enough that a probe could successfully be passed through without touching the sides; probe vibration was axial. When the top of the chamber was sealed, solution would not drain out these holes, even when the chamber was turned on its side. While the seedling was being placed in the solution-filled chamber, these holes were covered with a small piece of Scotch tape (3M, St. Paul, Minnesota) which could easily be removed. There were two platinum black-coated platinum wires in the bottom of the chamber to serve as reference and virtual ground electrodes. The chamber and seedling manipulator were otherwise electrically isolated from the rest of the apparatus—any stray currents produced large artifacts.

The chamber and the vibrating probe were mounted on a rotatable plate (Newport Corp., Fountain Valley, California) so that the root tip was the center of rotation. On the plate were microtranslation stages (Newport) to allow positioning of the seedling and the probe in three dimensions. A stereomicroscope was fixed in front of the apparatus to observe the specimen at 50-fold magnification.

A suspending buffer was selected, which would allow normal root function while having a high resistivity to optimize the sensitivity of the vibrating probe. The medium contained 0.1 m*M* $CaCl_2$, 0.1 m*M* $MgCl_2$, 0.1 m*M* KCl, and 1 m*M* morpholinoethanesulfonic acid adjusted to pH 6 with KOH. The resistivity of this medium was 16 kOhm cm.

The electronics for the vibrating probe were built at the National Vibrating Probe Facility, Marine Biological Laboratory (Woods Hole, Massachusetts). The 25-μm probe tip was vibrated 25 μm in the axial direction. The signal from the probe was averaged with a time constant of 0.1 or 2 s. The signal was amplified so that a potential difference between the extremes of vibration of 1 μV produced a DC signal of 5 mV. Calibration of the probe was done at several distances 50 to 200 μm from the calibration electrode. Typically, a 1-mm deflection of the chart corresponded to 0.02 μA cm^{-2}, and the noise level was about 0.01 μA cm^{-2}. Measurements were made 100 μm from the root surface.

Results

Control for root surface artifacts

The surface of the maize root is covered with a mucopolysaccharide slime containing many charged carboxyl groups. The resulting surface charge could produce a response in the vibrating probe that is not due to ionic currents. Corn seedlings killed by incubating for 1 h in 8% gluteraldehyde produced no current, but approaches closer than 25 μm from the root cap caused typical sur-

face effects (Scheffey, 1986). Rotating the apparatus produced no signal.

Controls for physical artifacts

A current-generating, but gravity-insensitive control was needed to evaluate physical artifacts associated with turning the apparatus. These are important, both because of the high likelihood of generating false signals with the vibrating probe and because of the history of physical artifacts being identified as "the geoelectric effect" (Woodcock and Wilkins, 1969). Probable sources of artifacts were changes in the shape and position of the highly curved meniscus through which the probe shaft passed, and changes in the amplitude or direction of vibration with a change in position of the probe. These were in part avoided by periodically monitoring the out-of-phase signal. In addition, two controls were used: a platinum black-coated platinum wire of similar dimension and electrical activity as a root and a decapped (gravity-insensitive) root.

A 1-mm diameter platinum wire, insulated except for a 4-mm long section that was coated with platinum black, produced a predicable electric field when a current was passed through it to the virtual ground. With the vibrating probe positioned as for measurement on a root, the apparent current density remained constant before turning. On turning, the reference (zero current) value often shifted, occasionally taking up to one minute to stabilize at a new value. The calibration coefficient also changed on some runs. After one minute the readings were constant (Fig. 2). This artifact made recalibration at the end of the run essential and also rendered the measurements in the first minute after turning meaningless.

Maize root caps can be removed with minimal damage. Nevertheless, these roots generated inward currents at the tip of 2 to 10 μA cm^{-2}, compared to the usual 0 $\pm$ 1.5 μA cm^{-2}. This current continued for several hours. The large fields resulted in large differences in the apparent current with very small changes in probe position, thus artifacts of the expected size were not distinguishable from measurement error.

Response of roots

The radial current density measured 100 μm from the root surface was most inward at the tip and most outward 1000 to 1500 μm from the tip, approx. 3 μA cm^{-2} more outward than at the tip. This pattern was consistent, though the absolute values at the tip ranged from 1.5 inward to 1.5 μA cm^{-2} outward between roots.

The current associated with graviperception was a deviation from the initial pattern. At the tip of the cap (no graviperceptive cells) and in the elongating zone there was no deviation (Fig. 4a, b). Only adjacent to the columella was there an effect of gravistimulation (Fig. 4c). The response on the upper side was always distinct, beginning 3 to 4 minutes after gravistimulation, and rising to a new level 0.3 to 0.7 μA cm^{-2} more outward over 3 min. On the lower side, the response was highly variable from root to root, and therefore was not a useful diagnostic response for further experiments.

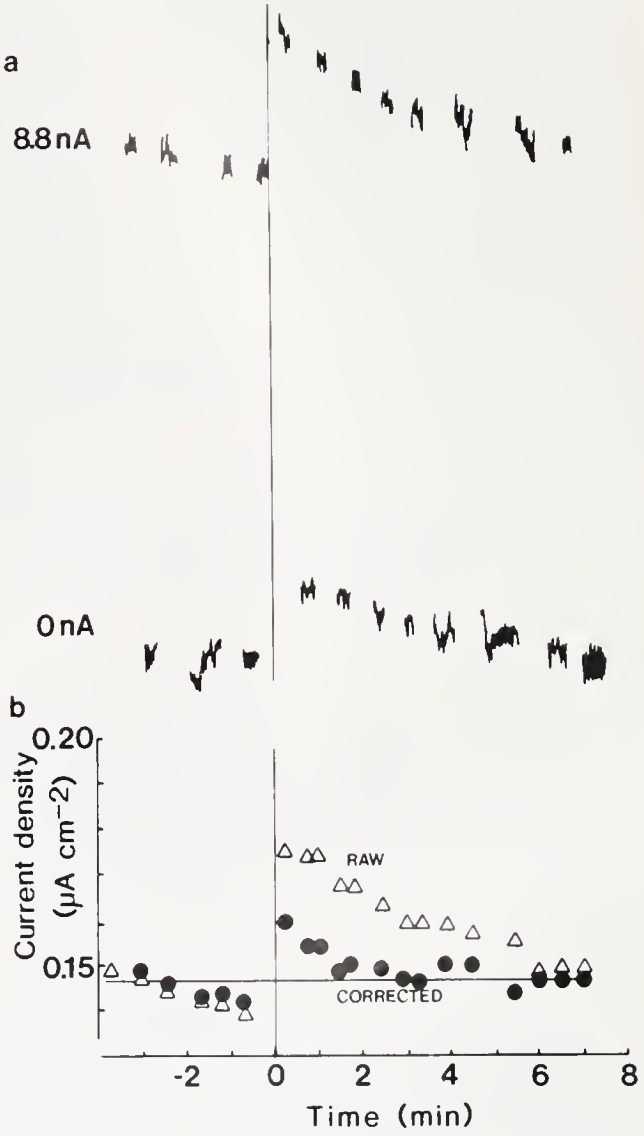

Figure 2. (a) Original trace of effect of turning apparatus while passing a constant current. (b) Measured current density assuming constant reference and calibration (△) or corrected for the shift in reference point and calibration coefficient (●). Horizontal line indicates actual current density. With correction, the artifact produced by turning is substantially eliminated after 1 min.

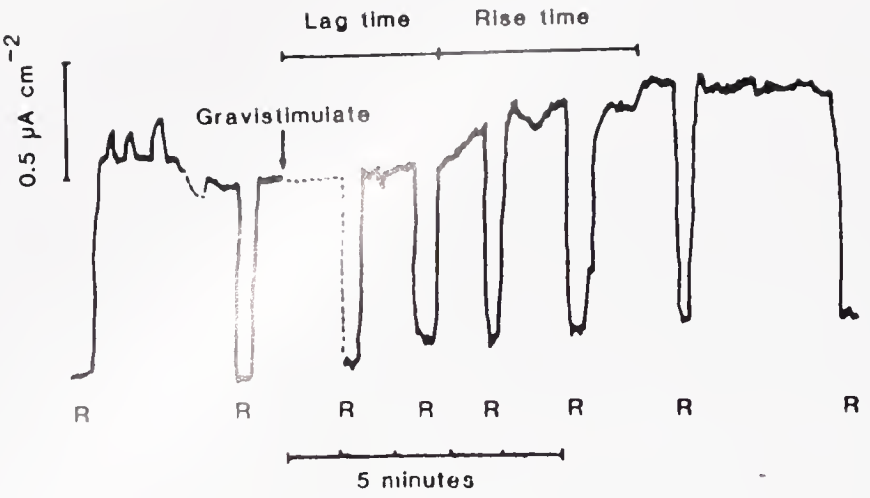

Figure 3. Original trace of current density at upper side of columella. R indicates when the probe was moved away from the root. This figure illustrates the characteristic current shift indicative of graviperception. Reproduced with permission from Björkman and Leopold (1987a).

Effect of inhibitors

Pretreatment of the roots for 10 min with calmodulin inhibitors calmidazolium (425 μM) and compound 48/80 (100 μg/ml), at doses that inhibit curvature but not growth or initial current distribution, completely eliminated the characteristic change in current (Fig. 5).

Pretreatment of the roots for 10 min with auxin transport inhibitors triiodobenzoic acid (10 μM) and naphthylphthalamic acid (NPA; 1 μM) likewise eliminated curvature but not growth. These treatments did not eliminate a change in current (Fig. 6). A statistical treatment presented in Björkman and Leopold (1987b) indicates that the responses after treatment with these inhibitors was the same as controls except that the response of the NPA-treated roots was delayed by about 3 min.

Discussion

In exploiting the "geoelectric effect" (Schrank, 1945) for the study of root graviperception, it must be estab-

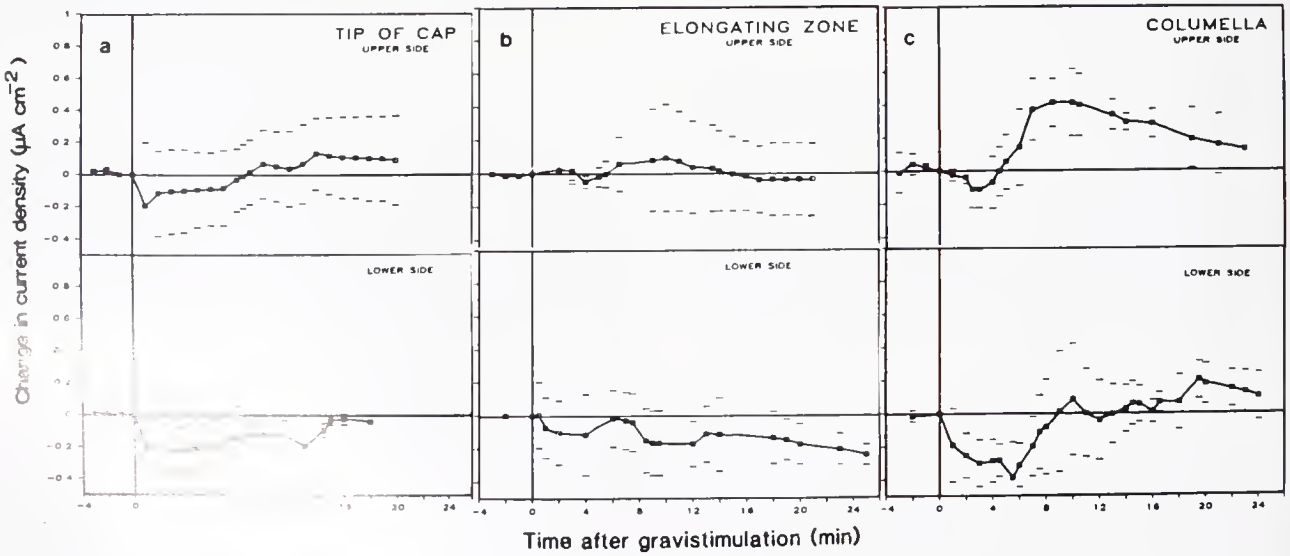

...urrent density after gravistimulation at different parts of the root. (a) Adjacent to ... of root cap. (b) Adjacent to elongating zone (1.5 mm from tip) which ultimately ... (c) Adjacent to graviperceptive columella. Bars indicate standard deviation. Positive current ... outward current. Redrawn with permission from Björkman and Leopold (1987a).

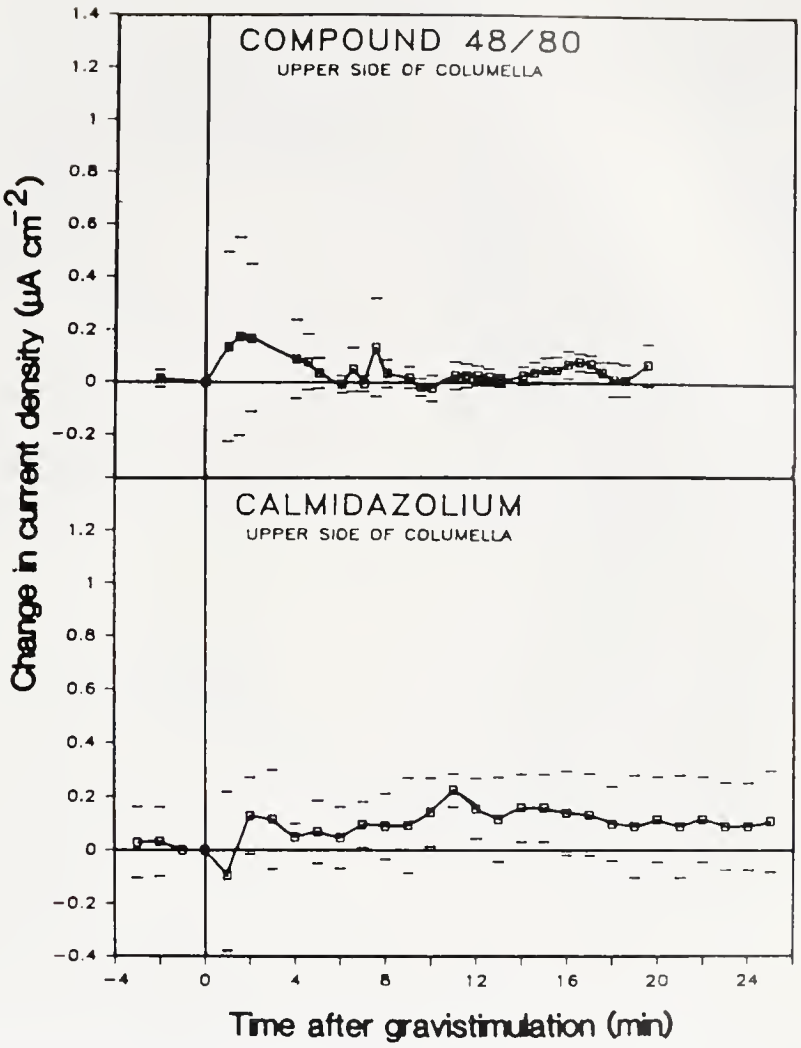

Figure 5. Effect of calmodulin inhibitors on current density. Bars indicate standard deviation. Positive current values indicate outward current. Redrawn with permission from Björkman and Leopold (1987b).

lished that the measured response is not a physical artifact (*e.g.*, Woodcock and Wilkins, 1969) nor a phenomenon associated with later stages of gravitropism as it is in shoots (Wilkins and Woodcock, 1965).

In conducting this experiment, two aspects of the apparatus are likely to introduce artifactual responses in the vibrating probe. First, the vibrating probe is passed through a small hole (radius 350 μm) having a meniscus of a corresponding radius of curvature. These conditions produce a static charge around the shank of the vibrating probe that can generate a signal in phase with the signal from the probe tip. Second, the apparatus is rotated 90°. Any change in alignment or vibration would change the signal.

Artifacts due to the meniscus were apparent only when the solution completely filled the orifice and the probe shank was near an edge of the orifice. When the meniscus was inside the chamber (*i.e.*, a small bubble) and the probed passed through the center of an air-filled orifice, no signal was registered. Turning the apparatus did cause both the zero-current output and the calibration coefficient to change. These stabilized within one minute after turning (Fig. 2) and then had to be remeasured. Therefore, these physical artifacts can be eliminated or corrected for.

To associate the response with perception, it must be appropriately correlated temporally and spatially. The response should occur roughly coincident with the presentation time (minimum stimulation to produce a response = 3 to 4 min in maize). Response caused by perception would take at least that long to occur. Likewise, responses appearing after the latent period (time for

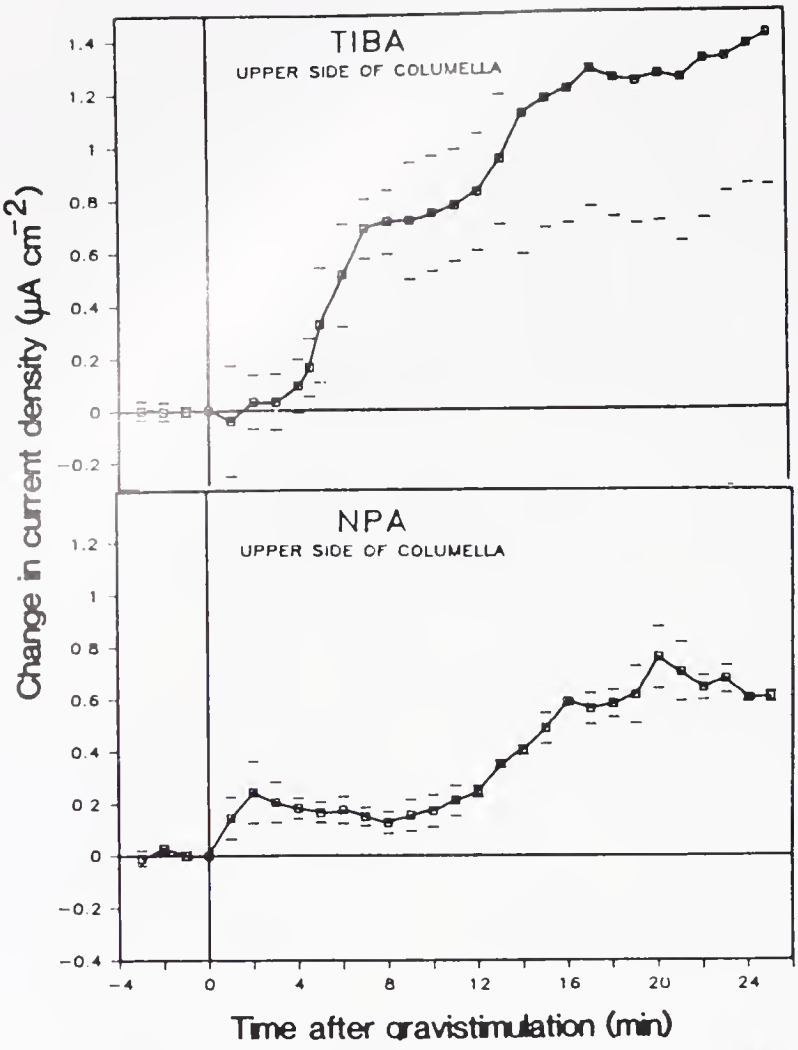

Figure 6. Effect of auxin-transport inhibitors on current density. Bars indicate standard deviation. Positive current values indicate outward current. Redrawn with permission from Björkman and Leopold (1987b).

differential growth to begin = 30 min in these roots) are probably associated with growth and cannot be attributed to perception with confidence. The response should also be associated with the tissue from which it originates. In the present experiment, an insensitive part of the root (top of cap) was used to measure non-specific changes, and the elongating zone for growth-related responses; the latter were responses adjacent to the graviperceptive columella. Thus there were nine combinations of time and position, only one of which fulfilled the criteria for a response associated with graviperception; only this combination produced a recognizable signal.

To be a useful diagnostic tool, the response must be consistent. On the upper side of the root cap, the current change was of a repeatable magnitude (0.5 μA cm^{-2} outward) with a repeatable rise time (3 min). On the lower side, the current did change, but not in a repeatable and recognizable manner. Therefore, only the current change on the upper side could be applied as a measure of graviperception. The response also occurs after artifacts due to turning have subsided. This technique will not work in tissues where the response is expected in under 1 min, *e.g., Lepidium* at 7 s (Behrens *et al.*, 1982) because the biological response would not be distinguished from artifacts of turning and because it would be difficult or impossible to realign the root with the probe and to get a stable reading before the biological response commenced.

This technique has been applied to test hypotheses about the physiology of graviperception which has not before been possible.

Acknowledgments

The author thanks L. F. Jaffe for valuable advice in designing the apparatus described herein and for providing the vibrating probe, and A. C. Leopold for advice and support. This work was funded by NASA (NSG-NAG-W3) and NIH (P41RR01395-SSS).

Literature Cited

Björkman, T., and A. C. Leopold. 1987a. An electric current associated with gravity sensing in maize roots. *Plant Physiol.* **84:** 841–846.

Björkman, T., and A. C. Leopold. 1987b. Effect of inhibitors of auxin transport and of calmodulin on a gravisensing-dependent current in maize roots. *Plant Physiol.* **84:** 847–850.

Behrens, H. M., M. H. Weisenseel, and A. Sievers. 1982. Rapid changes in the pattern of electric current around the root tip of *Lepidium sativum L. Plant Physiol.* **70:** 1079–1083.

Evans, M. L., K.-H. Hasenstein, and R. Moore. 1986. Gravity perception in plants. *Sci. Am.* **254**(12): 112–118.

Jackson, M. B., and P. W. Barlow. 1981. Root geotropism and the role of growth regulators from the cap: a re-examination. *Plant Cell Environ.* **4:** 107–123.

Roux, S. J., and B. S. Serlin. 1987. Cellular mechanisms controlling light-stimulated gravitropism: role of calcium. *CRC Crit. Rev. Plant Sci.* **5:** 205–236.

Scheffey, C. 1986. Pitfalls of the vibrating probe and what to do about them. Pp. 3–12 in *Ionic Currents in Development,* R. Nuccitelli, ed. Alan R. Liss, New York.

Schrank, A. R. 1945. Changes in the electrical polarity in the *Avena* coleoptile as an antecedent to hormone action in geotropic response. *Plant Physiol.* **20:** 133–136.

Wilkins, M. B., and A. E. R. Woodcock. 1965. Origin of the geoelectric effect in plants. *Nature* **208:** 990–992.

Woodcock, A. E. R., and M. B. Wilkins. 1969. The geoelectric effect in plant shoots. II. Sensitivity of concentration chain electrodes to reorientation. *J. Exp. Bot.* **20:** 687–697.

Reference: *Biol. Bull.* **176(S):** 56–64. (April, 1989, Suppl.)

Steady Ionic Currents Around Pea (*Pisum sativum* L.) Root Tips: the Effects of Tissue Wounding

JULIA M. HUSH AND ROBYN L. OVERALL

School of Biological Sciences, University of Sydney, N. S. W. 2006-Australia

Abstract. Using the vibrating probe, we measured the extracellular current pattern around 4-day-old pea (*Pisum sativum* L. var. Greenfeast) root tips. Currents of 1.0 μA cm^{-2} flow into the meristematic and elongating tip, and smaller currents (0.1 μA cm^{-2}) leave the mature zone basipetally behind this region. Wounding the root 3 mm from the root tip causes a very large (10 μA cm^{-2}) inward current at the wound site. This disrupts the normal extracellular current pattern around the root. This wound current is inhibitable, and we present evidence that H^+, and particularly Ca^{2+}, may be involved. The time course of these ionic current changes is described. We propose that this wound current plays a role in the establishment of a new polarity in the cortical cells adjacent to a wound in root tissue. Possible mechanisms are discussed.

Introduction

In higher plants, the development of a new axis of growth, such as in wound repair, characteristically involves periclinal divisions and a change in the orientation of cortical microtubules to perpendicular to the new axis of growth (review: Hardham, 1982). For example, in the *Datura* stem, the cortical microtubules and cellulose microfibrils in the cells adjacent to the wound undergo a 90° shift in their orientation (Flanders, 1985). Parenchyma cells adjacent to a wound in plant tissue commonly undergo reorganization of the protoplasm so that the predominant strands of cytoplasm and the plane of cell division become oriented parallel to the longitudinal axis of the plant organ. In effect then, the original direction of cellular polarity is shifted by 90° as a result of the wound stimulus. This phenomenon has been observed in large, vacuolated cells in the wounded tissues of various higher plant species (Sinnott and Bloch, 1940; Venverloo *et al.*, 1980, 1984; Flanders, 1985), as well as in parenchyma cells undergoing differentiation to form new vascular elements as a response to wounding of the stele (Sinnott and Bloch, 1945; Jacobs, 1970; Comer, 1978; Behnke and Schulz, 1980; Robbertse and McCully, 1979; Hardham and McCully, 1982a, b; Schultz, 1987).

It is not known what orchestrates these changes in cellular polarity adjacent to the wound. However, there is a strong body of evidence to suggest that steady ionic currents play a role in the establishment of polarities in a variety of systems (for review, see Nuccitelli, 1983). Indeed, ionic currents have been recently implicated in the process of wound healing and regeneration in higher plants (Gensler, 1979; Davies and Schuster, 1981; Chastain and Hanson, 1982; Davies, 1987; Miller *et al.*, 1988), and they are well established to initiate or control wound healing in amphibians (*e.g.*, Stump and Robinson, 1986).

This investigation aims to assess the role of steady ionic currents in the polarity shifts in higher plants that result from mechanically wounding tissue. Specifically, we establish the pattern of extracellular currents around growing root tips of *Pisum sativum* before and after mechanical wounding and attempt to identify the specific ions responsible for the wound current.

The significance of these findings is discussed in light of previous reports of ion current measurements around growing root tips (Weisenseel *et al.*, 1979; Björkman and Leopold, 1987a, b; Miller *et al.*, 1986, 1988), and also with respect to the changes in cell polarity, which are known to be induced by the wound incisions.

Materials and Methods

Plant material and root preparation

Pisum sativum L. var. Greenfeast (Yates and Co. Milperra, N. S. W., Australia) seeds were surface steril-

ized in 6% (W/V) NaClO for 5 min, rinsed four times in sterile dH_2O, and aseptically germinated in petri dishes containing 1% agar in ¼ strength modified Hoaglands solution (0.38 m*M* $MgSO_4 \cdot 7H_2O$; 0.34 m*M* $NaH_2PO_4 \cdot 2H_2O$; 0.7 m*M* $Ca(NO_3)_2 \cdot 4H_2O$; 1.00 m*M* KNO_3). Seeds were grown for 4 days at 20 ± 2°C in the dark.

Seedlings bearing roots 20–30 mm in length were placed into petri dishes (9 cm diameter). Care was taken not to disturb the orientation of the root so as to avoid gravitropic perturbations. A small perspex chamber (3 × 3 × 1 cm) was then positioned to enclose the root tip, which protruded into the center of the chamber via a hole slightly larger than the root, and sealed with white petroleum jelly, as in Figure 1a. Seedlings were then embedded in agar (1% in ¼ Hoaglands solution as above), which was poured into the dish at 35°C. Within 15 min, the agar had solidified and the perspex chamber was removed, leaving a small well around the root tip, in which the measuring medium (sterile ¼ Hoaglands solution) was placed (Fig. 1b). This preparation method ensured physical stability of the seedling throughout the measuring and wounding procedures. This physical stability was found to be crucial in order to obtain consistent current patterns. Seedlings were left in this position for 2 h before measurements were made. Submerging roots in the ¼ Hoaglands solution did not affect root growth rate when examined after 2, 24, and 48 hours ($P > 0.05$; 1-way analysis of variance). Prior to a measurement, the petri dish containing the horizontally oriented pea root was placed on a gliding stage of an inverted microscope (Nikon Diaphot) around which the vibrating probe was assembled. Roots were oriented horizontally during all experiments.

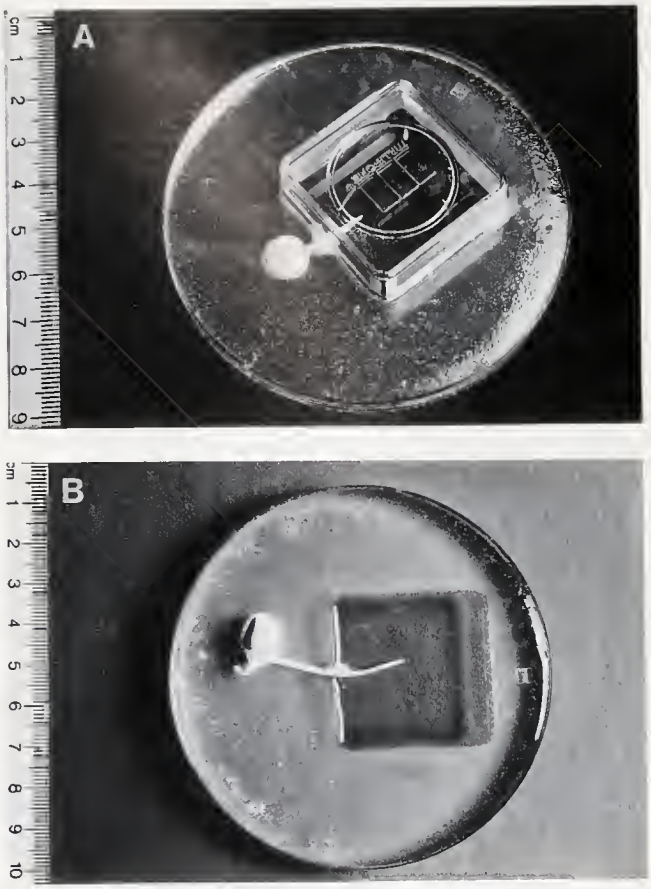

Figure 1. Preparation of pea roots for measurements with the vibrating probe. (A) The root tip is protected by a small perspex chamber as warm agar (1% in ¼ Hoaglands solution) is poured into the petri dish. (B) Once cooled, the agar supports and immobilizes the seedling and the chamber is removed, leaving an agar "well" into which bathing medium is poured.

Current measurements

Extracellular currents were measured with a standard one dimensional vibrating probe (Jaffe and Nuccitelli, 1974) using platinum wire probes with platinum black balls approximately 30 μm in diameter.

Current measurements were made by positioning the probe 50–100 μm from the root surface (Fig. 2) and then moving it back to a reference position approximately 8 mm away from the root. (Sometimes, the probe could not be brought as close as 50 μm due to cells sloughing from the root tip, in which case it was either positioned as close as possible, or else a measurement had to be missed.) This measuring procedure was repeated at 250 μm intervals around both sides of the root tip. All measurements were taken on the longitudinal median plane of the root.

Except for ion-substitution or channel-blocking experiments, measurements were made in ¼ Hoaglands solution, of approximately 28 Ωm resistivity. Replicate roots were measured in all experiments, and current densities at each root position calculated as means and standard errors (SEM) of these replicates. No current was detected around small wooden applicator sticks shaped to simulate a root tip, or small glass beads fixed to the bottom of the dish.

The pattern of steady ionic currents was mapped around the acropetal 4 mm of intact root tips and then again after wounding. The time course of the ionic current changes was followed, both around the whole root tip and specifically at the wound site itself, while roots were left in ¼ Hoaglands solution at 22°C. The sign convention refers to the movement of positive charge.

Wounding

Roots were wounded by cutting and removing a wedge of tissue 3 mm from the root tip, completely severing the stele. This procedure was done under a dissecting microscope while the root was set up in the petri dish in solu-

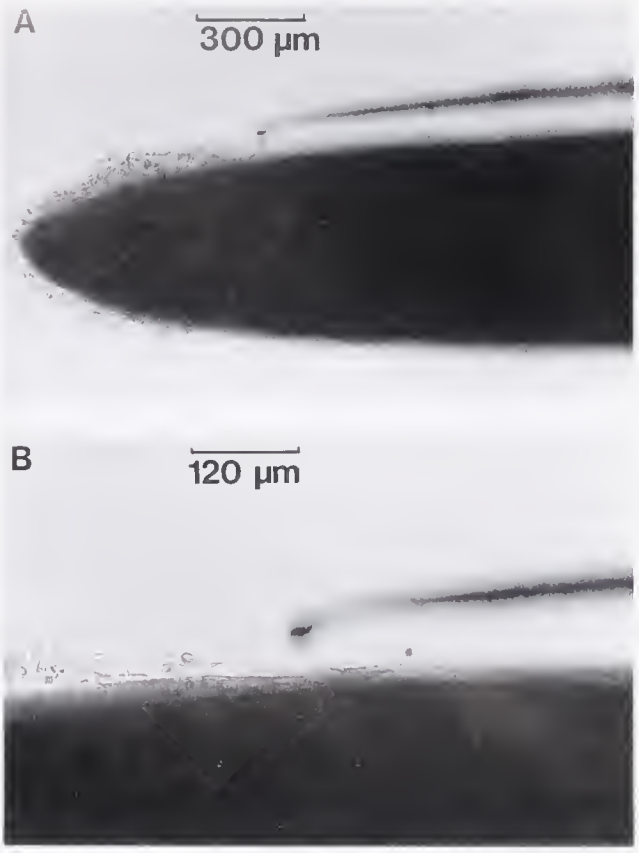

Figure 2. (A) The vibrating probe in position to measure current normal to the longitudinal axis of the pea root, as viewed from above. (B) Probe positioned at the root surface: higher magnification.

tion, and care was taken to avoid dislodging the root during the cutting process. Microscalpels were made for the wound incisions by placing a triangular-shaped piece of blade (cut from a single-edged razor blade) in a small slot cut at one end of a wooden applicator stick, and then applying a small drop of epoxy resin around the base of the blade to hold it in place. A fresh microscalpel was used for each wound and each blade was cleaned with alcohol before use.

Ion-substitution and channel-blocking experiments

The size of the wound current, about 5 min after wounding, was established in the control solution before flushing the 8-ml chamber with 20 ml of test solution. The current at the wound site was monitored in each test solution for about 5 min and then in the control solution again at the end of each trial.

Wherever possible, the control and test solution differed in the concentration of only one molecular species (Table I). The slightly altered resistivities of these media were taken into account when calculating current density values. The inorganic lanthanide ions La^{3+} and Gd^{3+}, and the organic species verapamil are known antagonists of calcium-mediated membrane function (dos Remedios, 1981). One hundred μM lanthanum was used on the basis of a report by Rincon and Hanson (1986), in which $LaCl_3$ strongly inhibited $^{45}Ca^{2+}$ influx in corn roots (K_m = 70 μM). Fifty μM gadolinium has been reported by Bourne and Trifaró (1982) to inhibit $^{45}Ca^{2+}$ uptake in chromaffin cells by 92% and Andrejauskas *et al.* (1985) found micromolar concentrations of verapamil to bind strongly to corn membranes. Lanthanum chloride was obtained from Sigma, gadolinium chloride from Pfaltz Bauer, Stamford, Connecticut, and verapamil was a gift from Knoll Pharmaceutical Co., Whippany, New Jersey.

Extracellular pH

Wounded roots were placed onto agar dishes containing the pH indicator bromocresol purple, which appears yellow at pH 5.2 and becomes purple at pH 6.8 (Edsall, 1969). 0.6% agar in ¼ Hoaglands solution was adjusted to pH 5.0 with HCl (10^{-1} M) and colored with 10 ml L^{-1} of bromocresol purple solution (7×10^{-4} M), resulting in a yellow/orange color (method modified from Weisenseel *et al.*, 1979). Dishes were placed on a fluorescent light box, and the color changes of the agar directly around the wound site were observed and recorded on color reversal (Fujichrome 100 ASA), and black and white negative (Kodak Panatomic-X 32 ASA) film.

Results

Ionic currents traversing the unwounded root

Three mm around the root tip a zone of large, inwardly directed current of about 1.0 $\mu A\ cm^{-2}$ exists, and is maximal 1.25–1.50 mm back from the root tip, in the elongation zone, where the current density reaches values as high as 1.7 $\mu A\ cm^{-2}$ (Fig. 3). Basipetal to this in the zone of differentiation, characterized by large, vacuolate cells which are no longer expanding, we measured smaller, outward currents on both sides of the root, and current density values were typically 0.1 $\mu A\ cm^{-2}$. The inward current seems to continue further along one side of the root than the other. This is an artifact due to the time taken to map currents growing around a rapidly growing root (the rate of root elongation in these conditions is approximately 15 mm per day).

On two occasions, roots displayed an anomalous current pattern for no apparent reason and these data were excluded from the statistical analyses.

Ionic currents after wounding

Immediately after wounding the root 3 mm back from the tip, a very large inward current with a peak of 14

Table I

Effects of ion-substitutions and ion-channel blockers on pea root wound currents

Trial	Alterations to ¼ Hoaglands: Test solution	Control solution	% of initial current[1]
$-Na^+$	$-NaH_2PO_4$ (34×10^{-5} *M*) $+KH_2PO_4$ (34×10^{-5} *M*)	+K Isethionate (34×10^{-5} *M*)	96 ± 2 (11)
$-K^+$	$-KNO_3$ (1×10^{-3} *M*) $+NaNO_3$ (1×10^{-3} *M*)	+Na Isethionate (1×10^{-3} *M*)	106 ± 2 (7)
$-Ca^{2+}$	+EGTA[2] (1×10^{-4} *M*)	nil	59 ± 12 (9)
$+Cl^-$	+KCl (3×10^{-4} *M*)	nil	107 ± 4 (15)
$+Gd^{3+}$	$+GdCl_3$ (5×10^{-5} *M*)	+KCl (3×10^{-5} *M*)	73 ± 3 (10)
$+La^{3+}$	$+LaCl_3$ (1×10^{-4} *M*)	+KCl (3×10^{-5} *M*)	50 ± 10 (11)
+verapamil	+verapamil (8×10^{-7} *M*) +verapamil (1×10^{-5} *M*)	nil nil	97 ± 5 (9) 92 ± 4 (11)
$-H^+$[3]	+HEPES[4] (5×10^{-3} *M*) pH 8.0	+MES[5] (5×10^{-3} *M*) pH 5.5	108 ± 5 (11)

[1] Mean percentages ± SEM (parentheses indicate number of cases studied). See Figure 6 for method of calculation.
[2] EGTA: glycoletherdiamine-N,N,N',N',-tetraacetic acid.
[3] pH of solutions was adjusted with 5 *M* KOH.
[4] HEPES: N-2-hydroxyethylpiperazine-N'-2-ethanesulfonic acid.
[5] MES: [2-(N-Morpholino)ethanesulfonic acid].

μA cm^{-2} was measured at the wound site (Fig. 4a). A consistent feature of this wound current is that the current density peak is not centered directly over the wound site, but slightly shifted acropetally by about 150 μm. Towards the basipetal end of the root, 500 μm from the wound center, the current changes direction and outward currents of the order of 1–2 μA cm^{-2} are found. By 1.5 h, this initial large inward current drops off, giving rise to outward currents of 1–2 μA cm^{-2}, and a shifted peak over the wound is still visible (Fig. 4b). Six h after wounding these secondary outward currents have diminished to 0.3 μA cm^{-2}, although the peak value is still markedly higher at 0.8 μA cm^{-2} (Fig. 4c). Also at this stage, inwardly directed currents of 0.6 μA cm^{-2} appear about 300 μm from the wound center, on the basipetal side of the wound. By 23 h (Fig. 4d), these inward cur-

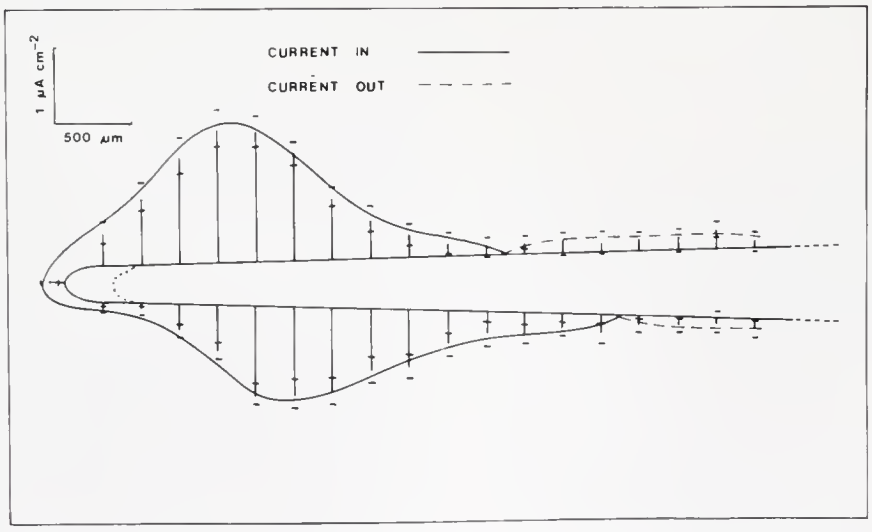

Figure 3. Current pattern traversing the 4-day-old pea root tip (diagrammatic representation of root as viewed from above the dish). Current density values are means (±SEM) from 13 roots measured.

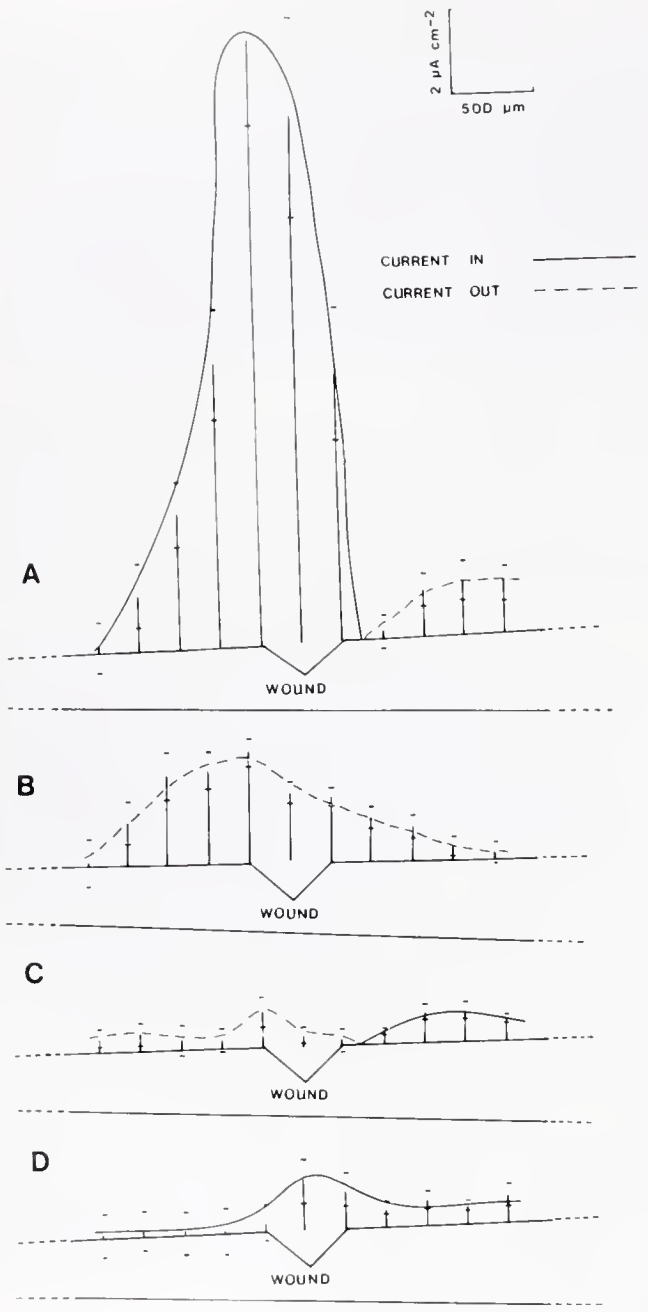

Figure 4. The effect of wounding the pea root 3 mm back from the tip: current patterns around the wound site (A) 2 min after wounding (mean ± SEM of 19 roots); (B) 1.5 h after wounding (mean ± SEM of 7 roots); (C) 6 h after wounding (mean ± SEM of 6 roots); (D) 23 h after wounding (mean ± SEM of 7 roots). Diagrammatic representation of the roots as viewed from above the dish.

rents are found exclusively around the wound area, a distinct peak of 1.2 μA cm⁻² still observable over the wound.

Five minutes after wounding, the root displays a distinct asymmetry in the pattern of transcellular ion currents (Fig. 5a). This persists at the wound site even after 1 h (Fig. 5b), although partial symmetry is restored around the rest of the root tip by this time.

Ionic composition of the wound current

Table I shows that there is no apparent effect on the wound current, of altering the levels of Na^+, K^+, Cl^-, or H^+ in the bathing medium. A very slight wound current enhancement appears to result from reducing external K^+ or H^+ levels, or increasing Cl^- concentration. However, lowering external Ca^{2+} (via 10^{-4} *M* EGTA) dramatically reduced the current (by about 40%) as did reasonable concentrations of two Ca^{2+} ion analogues and channel blockers: 100 μ*M* La^{3+} cut the current by 50% (Fig. 6) and 50 μ*M* Gd^{3+} by about 30%. These results strongly suggest that a Ca^{2+} current or Ca^{2+}-controlled current may be involved in the wound response. The effects of verapamil, a different type of calcium channel antagonist, were slight; it is possible that only concentrations higher than the micromolar range employed here, would be effective.

Extracellular pH

Wounded roots placed on agar plates containing bromocresol purple caused a strong pH shift in the agar directly around the wound, as indicated by the appearance of a strong purple band in the agar within a few minutes, which is focussed at the wound site (Fig. 7a). By 20 min the alkaline region is more diffuse (Fig. 7b), and after 45–60 min there is virtually no trace of the band at all. These results suggest that wounding causes an H^+ influx (or OH^- efflux) specifically into the wounded region of the root. The exact timing of this reaction in the medium was recorded accurately on color reversal film, which is not reproduced here. This result appears to conflict with the previous finding that an increase of 2.5 pH units in the bathing medium does not reduce the extracellular ionic current over the wound (Table I), as would be expected if an influx of H^+ ions resulted from wounding. This is discussed below.

Discussion

We have established that steady ionic currents traverse growing *Pisum sativum* roots: current densities of about 1 μA cm^{-2} flow into the zone of cellular elongation behind the root cap, while basipetally behind this, smaller currents (0.1 μA cm^{-2}) flow out of the more mature region. This agrees with previous reports of extracellular currents around horizontally growing roots of barley (Weisenseel *et al.*, 1979), *Trifolium* and *Nicotiana* (Miller *et al.*, 1986, 1988), and there is only slight variation in current magnitude and distribution between these pat-

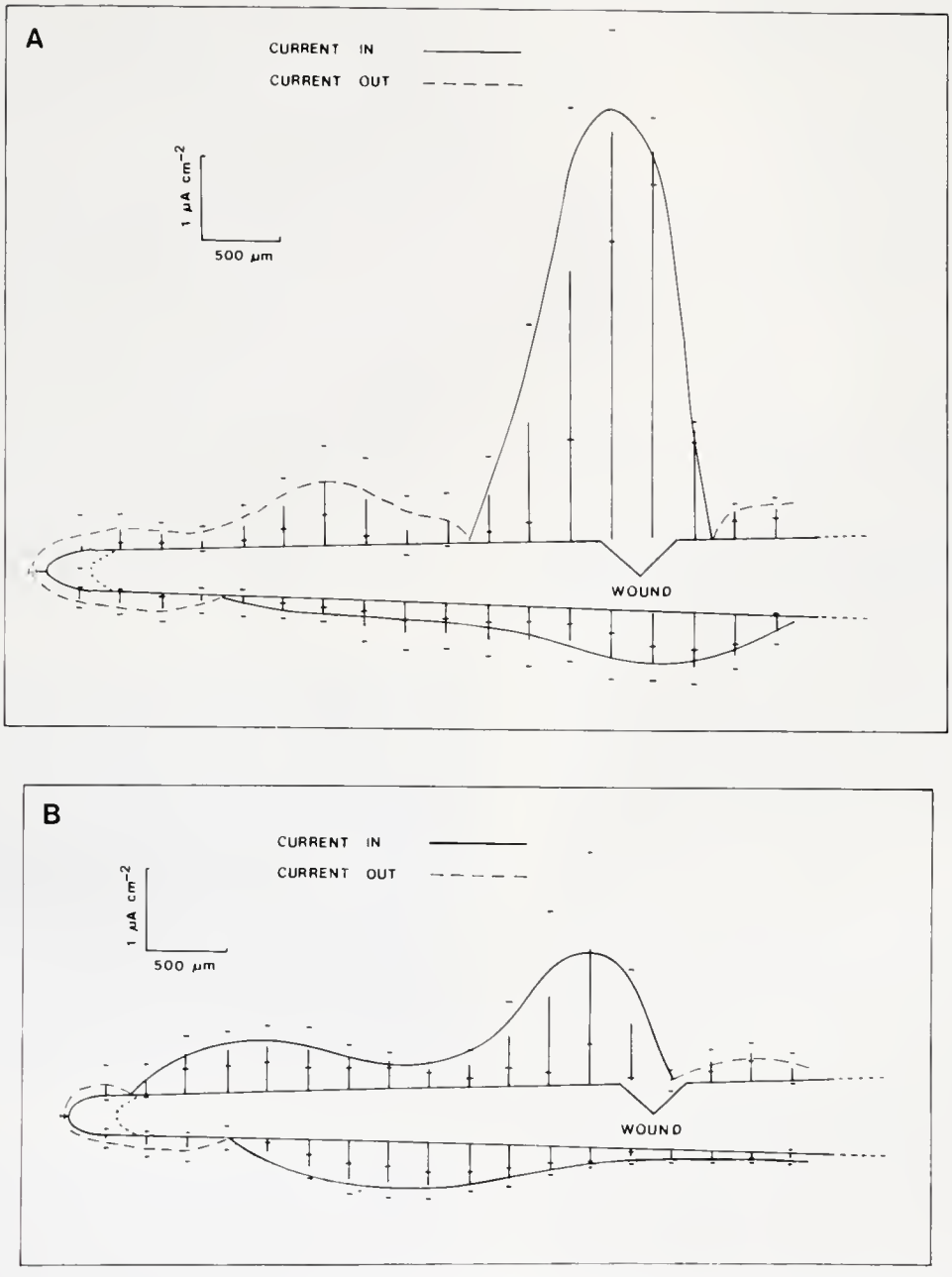

Figure 5. The effect of wounding the pea root 3 mm back from the tip: current patterns traversing the whole root tip (A) 5–10 min after wounding (mean ± SEM of 4 roots); (B) 1 h after wounding (mean ± SEM of 4 roots). Diagrammatic representation of the roots as viewed from above the dish.

terns. These findings are also similar to those in a series of pioneering studies of surface potentials in onion roots by Lund (1947) and in bean roots by Scott (1967) with respect to the size of surface current densities and their correlation with the different physiological zones of the root.

The large positive current in the order of 10 μA cm^{-2} that enters a newly wounded region in pea roots is of a similar magnitude to the wound current described for *Nicotiana* (Miller *et al.*, 1988). The fact that this current is inhibitable dismisses any argument that the increased current density at the wound site is an artifact caused by exudate from the severed vascular tissue.

The wound current displayed by newly injured pea roots appears to involve a Ca^{2+} influx since the reduction of external Ca^{2+} and the addition of La^{3+} and Gd^{3+} result in a significant decrease of the wound current. This agrees with data for corn roots in which injuries such as

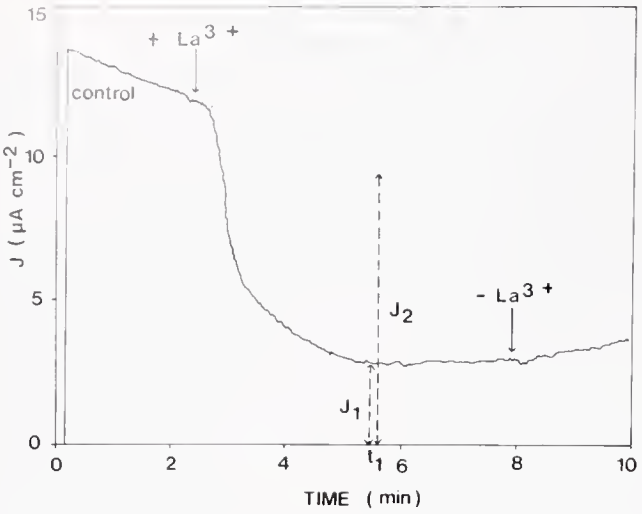

Figure 6. Representative record of wound current inhibition by the calcium ion channel blocker lanthanum (10^{-4} *M*); note the steady decline in the control wound current established in Figure 4. Calculation of ion substitution and channel blocking effects:

J_1 = steady value of the wound current due to change in concentration of molecular species x.

t_1 = time at which J_1 is reached.

J_2 = theoretical value of undisturbed wound current at time t_1 (determined by extrapolation from control current).

$(J_1/J_2) \times 100$ = % of initial current.

cutting, chilling, or rubbing increase $^{45}Ca^{2+}$ influx (Zocchi and Hanson, 1982; Rincon and Hanson, 1986). The fact that verapamil had only a slight effect may be because this organic blocker does not strongly inhibit Ca^{2+} channel activity in root plasma membranes: Rincon and Hanson (1986) also found micromolar concentrations of verapamil to poorly inhibit $^{45}Ca^{2+}$ fluxes into injured corn root cells, and Hagiwara and Byerly (1983) have reported that although verapamil and D-600 are effective in blocking the Ca^{2+} current of vertebrate heart and smooth muscle, they are much less effective against the Ca^{2+} channels of other membranes, which are sensitive to the inorganic lanthanide blockers. However, the precise nature of Ca^{2+} involvement in the wound current is not easily determined: the lanthanide inhibition does suggest that an influx of the Ca^{2+} ion occurs, but the possibility that Ca^{2+} controls other ion fluxes in this situation, cannot be ruled out.

Our experiments using the pH indicator dye bromocresol purple, although not quantitative, provide good evidence for an H^+ influx following wounding in pea roots, and this same result has been reported for wounded corn roots (Chastain and Hanson, 1982), using the same method. In apparent contradiction to this was the result from our experiments to test the effect of raising external pH on the wound current. It is probable that the high buffering of the solutions was unnecessary and masked any reduction in H^+ influx incurred by the bathing medium pH change. Some earlier studies concerned more with the effects of excision on ion transport in root segments demonstrated a decrease in the electrogenic H^+ efflux, which was reported to reverse to an H^+ influx following more effective injury stimuli (Gronewald and Hanson, 1980; Chastain and Hanson, 1982). These ionic fluxes would probably depolarize the membrane potential of the cells near the wound. Indeed, cells near a freshly cut surface in barley roots depolarize by 90 millivolts (Mertz and Higinbotham, 1976). Cutting roots into segments caused a reduction in K^+ influx in barley (Glass, 1978) and corn (Gronewald and Hanson, 1980; Chastain and Hanson, 1982). Our data, which suggests that there is a minimal involvement of K^+ in the wound current, is consistent with these findings.

The small outward currents that appear over the wound site from about 2 to 6 h after wounding are inter-

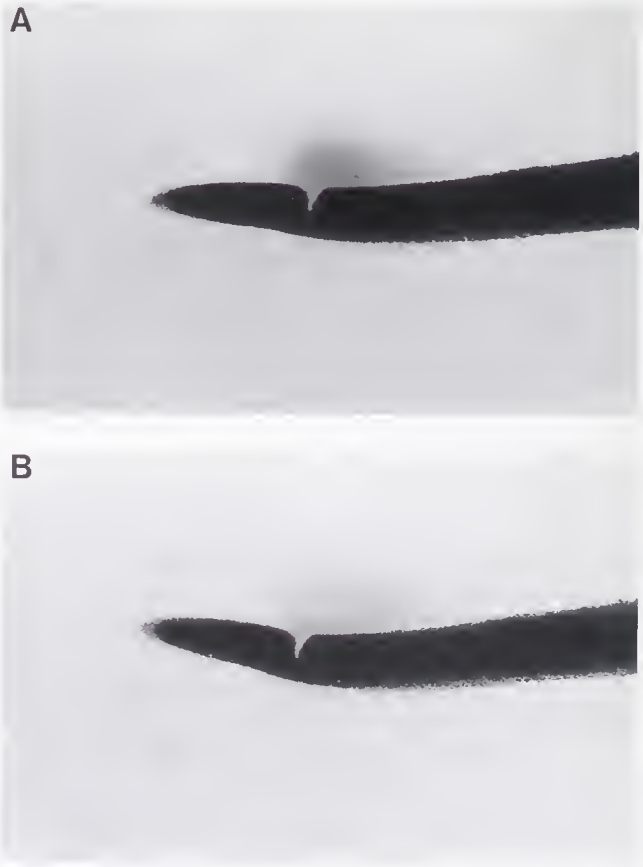

Figure 7. Effects of wounding the pea root tip on extracellular pH. The root is viewed from above a fluorescent light table so as to observe the color changes of the bromocresol purple indicator (70 m*M* in 0.6% agar + ¼ Hoaglands solution). The dark band of agar surrounding the wound indicates a rise in extracellular pH; (A) 5 min after wounding; (B) 20 min after wounding.

esting: although other electrogenic events are almost certainly involved, it is possible that this phase represents a Ca^{2+} efflux, since the elevation of free Ca^{2+} in the cytosol will stimulate Ca^{2+}-ATPase pumping (Marmé, 1983), until the free Ca^{2+} in the cytosol is restored to control levels.

We suggest that the drastic changes in current pattern that occur upon wounding may orchestrate the change in polarity in the cells near the wound.

In wounded pea roots specifically, division of the cortical cells occurs in a plane roughly parallel to the axis of the future strands of vascular tissue (*i.e.*, the longitudinal axis), and small bands of microtubules (thought to be equivalent to the pre-prophase band) are found at sites corresponding to the future planes of the periclinal divisions (Hardham and McCully, 1982a). We are presently investigating the timing involved with this development of a new cortical cell polarity, using immunocytochemical staining techniques to examine the shifts in orientation of interphase microtubule arrays.

The current may affect the cells directly, by changing local intracellular ion concentrations, which in turn modulate various enzymes and cytoskeletal elements. Specifically, if cytosolic calcium levels are increased by a Ca^{2+} influx as a result of wounding, then an intracellular Ca^{2+} gradient may serve to determine the new polar axis, possibly via effects on the cortical microtubules, the polymerization of which is known to be sensitive to Ca^{2+} levels (Weisenberg, 1972). There is convincing evidence that intracellular Ca^{2+} gradients resulting from Ca^{2+} currents play a causal role in polar axis establishment in the tip-growing plant cells of *Pelvetia* eggs (Robinson and Cone, 1980) and germinating *Lilium* pollen grains (Reiss *et al.*, 1985). Experiments to artificially induce polarity changes in unwounded root tissue, or inhibit polarity changes by artificially blocking the Ca^{2+} currents, are planned. Alternatively, the effect of these currents may be an indirect one: the distribution of ionic current in the unwounded root may generate an extracellular voltage potential in the longitudinal direction of the root, which is the direction of cell elongation and division in this tissue; wounding may stimulate a shift in the direction of this voltage gradient by 90°, to the transverse direction, via the large inward current into the wounded side of the root. This shift may act as an electrical signal, which individual cells perceive and correspondingly alter their direction of cellular orientation and of division. We are at present investigating the effect of wounding on both transverse and longitudinal extracellular root potentials.

Acknowledgments

This work was supported by an ARGS grant to R. L. Overall. J. M. Hush gratefully acknowledges the support from the Linnean Society of New South Wales, of a Joyce Vickery Research Grant, and a Linnean Macleay Fellowship.

Literature Cited

Andrejauskas, E., R. Hertel, and D. Marmé. 1985. Specific binding of the calcium antagonist [^{3}H] verapamil to membrane fractions from plants. *J. Biol. Chem.* **260:** 5411–5414.

Behnke, H.-D., and A. Schulz. 1980. Fine structure, pattern of division and course of wound phloem in *Coleus blumei*. *Planta* **150:** 357–365.

Björkman, T., and A. C. Leopold. 1987a. An electric current associated with gravity sensing in maize roots. *Plant Physiol.* **84:** 841–846.

Björkman, T., and A. C. Leopold. 1987b. Effect of inhibitors of auxin transport and of calmodulin on a gravisensing-dependent current in maize roots. *Plant Physiol.* **84:** 847–850.

Bourne, G. W., and J. M. Trifaró. 1982. The gadolinium ion: a potent blocker of calcium channels and catecholamine release from cultured chromaffin cells. *Neuroscience* **7:** 1615–1622.

Chastain, C. J., and J. B. Hanson. 1982. Control of proton efflux from corn root tissue by an injury-sensing mechanism. *Plant Sci. Lett.* **24:** 97–104.

Comer, A. E. 1978. Pattern of cell division and wound vessel member differentiation in *Coleus* pith explants. *Plant Physiol.* **62:** 354–359.

Davies, E. 1987. Action potentials as multifunctional signals in plants: a unifying hypothesis to explain apparently disparate wound responses. *Plant Cell Environment* **10:** 623–631.

Davies, E., and A. Schuster. 1981. Intercellular communication in plants: evidence for a rapidly generated, bidirectionally transmitted wound signal. *Proc. Natl. Acad. Sci. USA* **78:** 2422–2426.

dos Remedios, C. G. 1981. Lanthanide ion probes of calcium-binding sites on cellular membranes. *Cell Calcium* **2:** 29–51.

Edsall, J. T. 1969. In *CO_2: Chemical, Biochemical and Physiological Aspects*, R. E. Forster, ed. NASA, Washington DC.

Flanders, D. J. 1985. Cell response to tissue wounding in stems of *Datura stramonium* L. Ph.D. Thesis, Australian National University, A. C. T. Australia.

Gensler, W. 1979. Electrochemical healing similarities between animals and plants. *Biophys. J.* **27:** 461–466.

Glass, A. D. M. 1978. Influence of excision and aging upon K^+ influx into barley roots. *Plant Physiol.* **61:** 481–483.

Gronewald, J. W., and J. B. Hanson. 1980. Sensitivity of the proton and ion transport mechanisms of corn roots to injury. *Plant Sci. Lett.* **18:** 143–150.

Hagiwara, S., and L. Byerly. 1983. The calcium channel. *Trends Neurosci.* **6:** 189–193.

Hardham, A. R. 1982. Regulation of polarity in tissues and organs. Pp. 377–403 in *The Cytoskeleton in Plant Growth and Development*, C. Lloyd, ed. Academic Press, NY.

Hardham, A. R., and M. E. McCully. 1982a. Reprogramming of cells following wounding in pea (*Pisum sativum* L.) roots. I. Cell division and differentiation of new vascular elements. *Protoplasma* **112:** 143–151.

Hardham, A. R., and M. E. McCully. 1982b. Reprogramming of cells following wounding in pea (*Pisum sativum* L.) roots. II. The effects of caffeine and colchicine on the development of new vascular elements. *Protoplasma* **112:** 152–166.

Jacobs, W. P. 1970. Regeneration and differentiation of sieve tube elements. *Int. Rev. Cytol.* **28:** 239–273.

Jaffe, L. F., and R. Nuccitelli. 1974. An ultrasensitive vibrating probe for measuring steady extracellular currents. *J. Cell Biol.* **63:** 614–625.

Lund, E. J. 1947. *Bioelectric Fields and Growth.* University of Texas Press, Austin. Pp. 1–391.

Marmé, D. 1983. Calcium transport and functions. In *Encyclopedia of Plant Physiology,* Lauchli, A. and R. L. Bieleski, eds. Vol. 15: 599–625. Springer-Verlag, Berlin.

Mertz, S. M. Jr., and N. Higinbotham. 1976. Transmembrane electropotential in barley roots as related to cell type, cell location, and cutting and aging effects. *Plant Physiol.* **57:** 123–128.

Miller, A. L., J. A. Raven, J. I. Sprent, and M. H. Weisenseel. 1986. Endogenous ion currents traverse growing roots and root hairs of *Trifolium repens. Plant Cell Environment* **70:** 1079–1083.

Miller, A. L., E. Shand, and N. A. R. Gow. 1988. Ion currents associated with root tips, emerging laterals and induced wound sites in *Nicotiana tabacum:* spatial relationship proposed between resulting electric fields and phytophthoran zoospore infection. *Plant Cell Environment* **11:** 21–25.

Nuccitelli, R. 1983. Transcellular ion currents: signals and effectors of cell polarity. *Mod. Cell Biol.* **2:** 451–481.

Reiss, H.-D., W. Herth, and R. Nobiling. 1985. Development of membrane—and calcium—gradients during pollen germination in *Lilium longiflorum. Planta* **163:** 84–90.

Rincon, M., and J. B. Hanson. 1986. Controls on calcium ion fluxes in injured or shocked corn root cells: importance of proton pumping and cell membrane potential. *Physiol. Plant.* **67:** 576–583.

Robbertse, P. J., and M. E. McCully. 1979. Regeneration of vascular tissue in wounded pea roots. *Planta* **145:** 167–173.

Robinson, K. R., and R. Cone. 1980. Polarization of fucoid eggs by a calcium ionophone gradient. *Science* **207:** 77–78.

Schulz, A. 1987. Sieve-element differentiation and fluorosceine translocation in wound-phloem of pea roots after complete severence of the stele. *Planta* **170:** 289–299.

Scott, B. I. H. 1967. Electric fields in plants. *Annu. Rev. Plant Physiol.* **18:** 409–418.

Sinnott, E. W., and R. Bloch. 1940. Cytoplasmic behaviour during division of vacuolate plant cells. *Proc. Natl. Acad. Sci.* **26:** 223–227.

Sinnott, E. W., and R. Bloch. 1945. The cytoplasmic basis of intercellular patterns in vascular differentiation. *Am. J. Bot.* **32:** 151–156.

Stump, R. F., and K. R. Robinson. 1986. Ionic current in *Xenopus* embryos during neuralation and wound healing. Pp. 223–230 in *Ionic Currents in Development.* R. Nuccitelli, ed. Alan R. Liss Inc., NY.

Venverloo, C. J., L. Goosen-de Roo, P. C. van Spronsen, and K. R. Libbenga. 1984. Cell division in *Nautilocalyx* explants. III. Effects of 2,6-dichloro-benzonitrile on phragmasome, band of microtubules and cytokinesis. *J. Plant Physiol.* **116:** 225–234.

Venverloo, C. J., P. H. Hovenkamp, A. J. Weeda, and K. R. Libbenga. 1980. Cell division in *Nautilocalyx* explants. I. Phragmasome, preprophase band and plane of division. *Z. Pflanzenphysiol.* **100:** 161–174.

Weisenberg, R. C. 1972. Microtubule formation *in vitro* in solutions containing low calcium concentrations. *Science* **177:** 1104–1105.

Weisenseel, M. H., A. Dorn, and L. F. Jaffe. 1979. Natural H^+ currents traverse growing roots and root hairs of barley (*Hordeum vulgare* L.). *Plant Physiol.* **64:** 512–518.

Zocchi, G., and J. B. Hanson. 1982. Calcium influx into corn root cells as a result of cold shock. *Plant Physiol.* **70:** 318–319.

Reference: *Biol. Bull.* **176(S)**: 65–70. (April, 1989, Suppl.)

Ion Currents and Growth Regulators in Plant Root Development

ANDREW L. MILLER

National Vibrating Probe Facility, Marine Biological Laboratory, Woods Hole, Massachusetts 02543

Abstract. Factors that promote (low pH and fusicoccin) or reduce (high pH and IAA) the elongation rate of intact primary roots of *Zea mays* cv. Golden Bantam increased or decreased, respectively, the density of positive current flowing into the meristematic and elongating tissues of the developing root apex. Mature non-growing root regions generated the outward limb of the current loop. Ion-substitution and pH-profile experiments suggested that the bulk of the ion current was carried by H^+. Calcium ions did not carry a significant portion of the current, but calcium appeared to regulate the proton circulation since the current density was larger in calcium-depleted media. Increased root elongation at low pH was associated with increased current density and a basipetally extended zone of inward current. Conversely, decreased elongation at high pH was associated with a reduced current density and a more restricted zone of inward current. The fungal toxin fusicoccin increased the current density of the inward limb of the ion current and increased root extension. Concentrations of IAA that reduced growth also reduced the density of the inward current and shortened the inward current zone. The effects of both fusicoccin and IAA were dependent on the pH of the bathing medium.

Introduction

The electrical activities of plant roots are the subject of a considerable literature spanning more than 200 years (see bibliography by Rosene, 1947). The possible role of bioelectric fields as an integrating force in plant development was suggested by Schrank (1945), who proposed that root-generated potential differences might effect the distribution of growth regulators. Considerable effort has been invested in elucidating aspects of the chemical control of root growth mediated by growth regulators. Part of this research has resulted in the "acid growth hypothesis of auxin action" (Cleland, 1980). According to this hypothesis, IAA initiates cell enlargement by causing cells to excrete hydrogen ions. The consequent acidification of the cell wall is proposed to result in the loosening of the wall matrix to an extent which allows turgor-driven cell expansion. However, there have been several reports showing that intact roots generate areas of high pH around their growing tips (Weisenseel, Dorn and Jaffe, 1979; O'Neil and Scott, 1983). Initially, the fungal toxin fusicoccin (FC) was thought to provide a key to understanding the mechanism of auxin action since it appeared to mimic some of the effects of IAA (Marre, 1985). However, evidence now suggests that different mechanisms may be responsible for the similar reactions observed when auxin or FC are applied exogenously to tissues (Kutschera and Schopfer, 1985).

The present study exploited the non-invasive nature, high resolving power, and spatial resolution of a vibrating probe to investigate the magnitude, direction, and ionic composition of the electrical current generated by the primary root tips of intact *Zea* seedlings. The effects of changes in external pH and exogenously applied FC and IAA on this current are also determined. The interrelationships between endogenous current, external pH, growth regulatory substances, and root development are discussed.

Materials and Methods

Roots of *Zea mays* cv. Golden Bantam were examined with a vibrating probe when immersed in experimental media based on APW (Artificial Pond Water: 1.0 mol m^{-3} NaCl, 0.1 mol m^{-3} KCl, and 0.1 mol m^{-3} $CaCl_2$). Solutions used during ion-substitution experiments were isosmotic; K^+ and Ca^{2+} were replaced with Na^+, Na^+ with K^+, and Cl^- with SO_4^{2-}. EGTA at 1.0 mol m^{-3} was added to the Ca^{2+}-free medium to reduce further the ex-

traceliular calcium concentration. Media pH's were adjusted to 3.0, 5.0, 6.0, 6.5, or 7.0 using 0.1 mol m^{-3} HCl or NaOH (KOH in the case of the Na^{2+}-free medium, and H_2SO_4 for the Cl^--free medium). The media used in the IAA experiments were similar to those described above but for the addition of 10^{-4} *M* IAA (Sigma Chemical Co.). At this concentration, IAA inhibits primary root growth in *Zea* and causes an increase in the pH of the bathing medium (Evans *et al.*, 1980). Fusicoccin (Sigma Chemical Co.) was added to the various APW-based media at 10^{-6} *M* final concentration. This concentration promotes root elongation of *Zea* (Pilet, 1976). All media were air-saturated and equilibrated at 20°C prior to experimentation.

Caryopsis of *Zea* were sown in seed trays between double layers of paper tissues soaked in APW. These were kept in darkness at 18–20°C for four days. Seedlings that had developed similar root lengths were selected and placed in 1 liter pots containing aerated APW for 24 hours prior to experimentation.

Intact seedlings were used exclusively during experimentation, and mounted according to Miller *et al.* (1988). The magnitudes and patterns of the ion currents generated by growing roots of *Zea* were measured with a vibrating probe as described by Miller *et al.* (1988). Roots were either scanned at 250-μm intervals from the root tip back some 4–5 mm to mature root regions (Figs. 1, 3, 5), at similar intervals across the zone where current changes from inward to outward (Fig. 2) or, again at similar intervals, across a 2-mm region representing the peak of the inward current zone (Figs. 4, 6).

To identify which ion(s) were carrying the external limb of the ion current, two approaches were adopted. First, the component ions of APW were selectively removed from the bathing medium. This was achieved by mapping the current with a root bathed in one medium, then flushing a new medium minus a particular ion through the measuring chamber and rapidly re-mapping the current profile. The media used in these substitutions experiments were described earlier. The second approach was to map the current pattern and density in media of different pH's (3, 5, 6, & 7). The time-scale of both the ion-substitution and pH-profile were minimized as much as possible to avoid the longer term effects of changes in the ionic environment or in the external pH on endogenous current generation. Root extension rate measurements were made on an inverted microscope with a micrometer eye-piece.

Results

Pattern of ion-current generation

Three zones could be distinguished with respect to the direction of current flow relative to the surface of the root

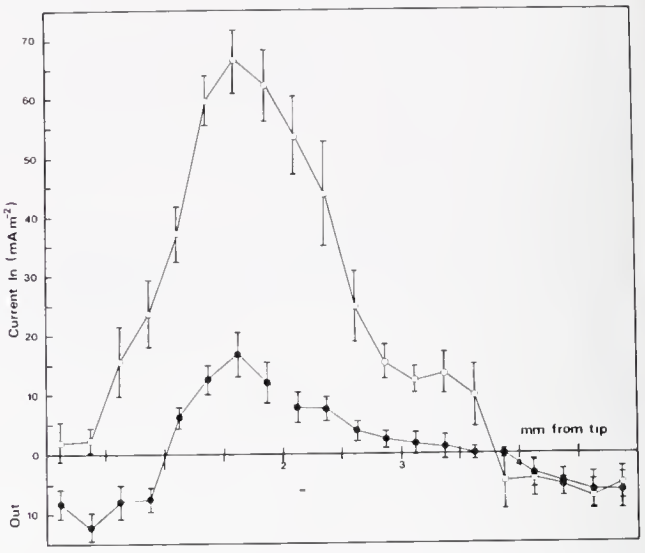

Figure 1. Pattern and density of ion current traversing 6-day-old *Zea* roots growing horizontally in APW at pH 6.0 (●). Stimulation of inward current resulting from replacement of APW with APW + 10^{-6} *M* FC (○) at pH 6.0. Averages from 6 experiments ±SEM.

(Fig. 1). (i) A zone of outward current associated with the root cap. (ii) A zone of strong inward current beginning with the meristematic tissue and peaking approximately at the region of maximum cell elongation. (iii) A second major region of outward current that was associated with the region of the root where cells were elongating much less vigorously and entering into a post-elongating phase. This indicates the beginning of mature root tissue. Where "outward current" is subsequently mentioned in the text it refers specifically to that associated with the mature cells of the root and not the root cap.

Ion-substitution experiments

The elimination of Na^+, K^+, and Cl^- from the measuring medium had little effect on the inward current, reducing mean peak inward current densities (MPICD) by 7%, 17%, and 15%, respectively (Fig. 2). On the other hand, the removal of Ca^{2+} resulted in a small increase in the MPICD in the order of some 15%. The current cross-over point, where inward current switches to outward current, was maintained (except after K^+-substitution) at approximately to same distance from the root apex (2.75–3.25 mm). These results suggest that these inorganic ions carry little of the inward current associated with the developing primary root tip of *Zea*. From this one can infer that the electrical current may be due mainly to a circulating flux of protons.

Relationship between current density, pH and root growth

To support the suggestion that protons were carrying most of the inward current, the magnitude and pattern

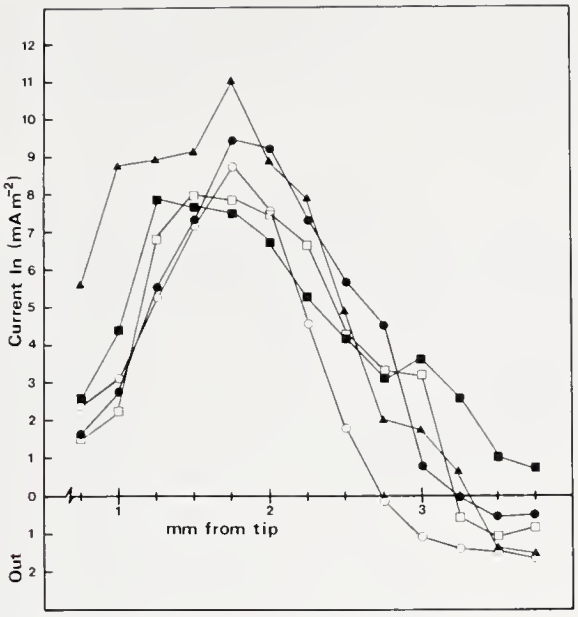

Figure 2. Ion substitution experiment on *Zea* in APW. Six-day-old seedlings were used with the media adjusted to pH 6.0. The effect on the current density and pattern of removing Na^+ (○), K^+ (■), Cl^- (□), and Ca^{2+} (▲) compared to an APW control (●) is shown. Each point represents the mean value from three separate ion-substitution experiments.

of the circulating current was monitored rapidly while the extracellular pH was adjusted between 3.0 and 7.0 (Fig. 3). Increasing the external pH resulted in an immediate reduction of the current density and a decrease in the elongation rate of the root (Table I). Roots exposed to more acidic pH's generated larger current densities and extended faster. These observations supported the proposal that protons carried the major component of the inward current and indicated a correlation between growth rate, pH, and current density. There also appeared to be a basipetal extension of the zone of inward current as the external pH fell and an acropetal compression of it as the pH increased.

Effects of fusicoccin on the root-generated ion current and root growth

The effect of 10^{-6} *M* fusicoccin on the ion current is illustrated in Figure 1. At pH 6.0, fusicoccin induced an approximate 3-fold increase in the inward limb of the current with little or no apparent stimulation of the outward limb over the length of root examined. Fusicoccin treatment also reversed the small outward current associated with the root cap. The current cross-over point was unaltered following fusicoccin treatment. The current profiles displayed in Figure 4 illustrates the relationship between fusicoccin, pH, and current density. At pH 7.0,

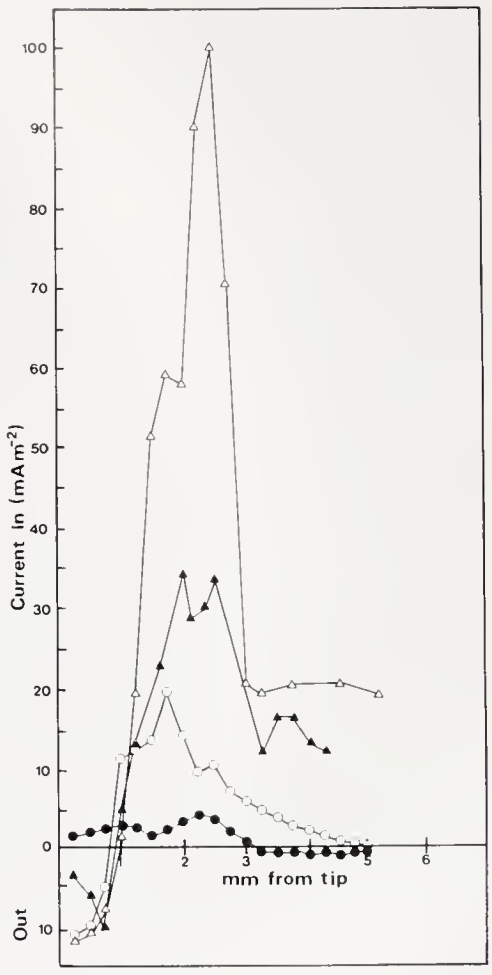

Figure 3. The relationship between the pH of the APW bathing medium and the pattern and density of current traversing a 6-day-old *Zea* root is illustrated. Media at pH 3.0 (△), 5.0 (▲), 6.0 (○), and 7.0 (●) were flushed through the measuring chamber.

fusicoccin induces an approximated 8-fold increase in current density, at pH 6.0, a 3-fold increase, and at pH 5.0 an approximate doubling. Fusicoccin stimulated the growth of intact *Zea* roots to varying degrees, being most

Table I

Elongation rates of primary root tips of Zea

	Growth Rate (μm min^{-2} ± SEM)		
pH	APW	APW + 10^{-4} *M* IAA	APW + 10^{-6} *M* FC
3.0	26.67 ± 3.45	26.72 ± 3.64	31.30 ± 4.24
5.0	16.69 ± 3.38	7.35 ± 2.27	16.59 ± 0.57
6.0	8.06 ± 0.38	2.53 ± 0.56	17.82 ± 1.64
6.5	7.81 ± 2.89	1.44 ± 0.43	11.01 ± 0.27
7.0	6.91 ± 0.57	0.90 ± 0.45	7.15 ± 0.20

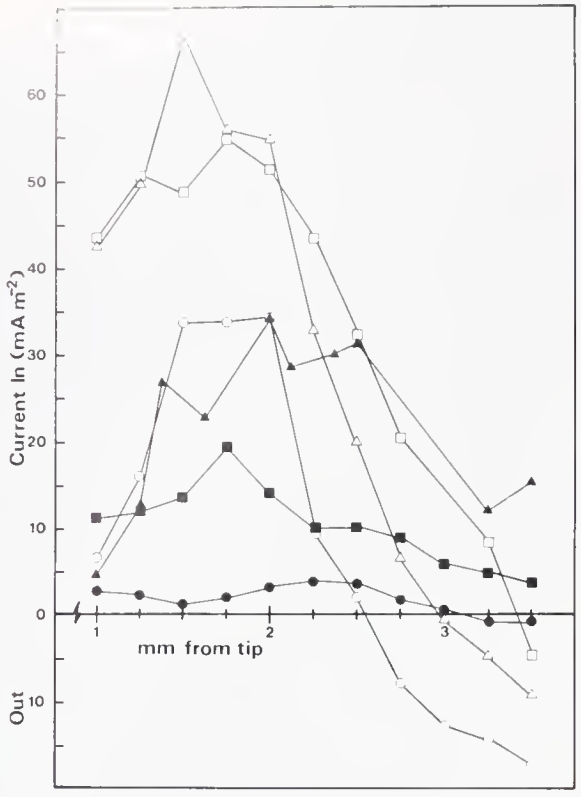

Figure 4. The enhanced root-generated current induced by 10^{-6} *M* FC at pH 5.0 (△), 6.0 (□), and 7.0 (○) are compared with their respective APW controls (▲), (■) and (●). Six-day-old seedlings were utilized.

effective at pH 6.0, where it induced more that a doubling of the elongation rate. At the upper (pH 7.0) and lower (pH 3.0) limits of the pH range, the promotive effects of fusicoccin on growth were not so apparent in comparison with controls (Table 1). It was clear that the absence of K^+ had little effect on the enhanced inward current density over the length of the root examined (Fig. 5).

Effects of IAA on the root-generated ion current and root growth

It was clear that the exogenous presence of 10^{-6} *M* IAA at pH 5.0, and 7.0 reduced the density of the inward current. IAA also induced a shift towards the root apex in the cross-over point (*i.e.*, acropetally compressed the inward current). The effects of IAA were again influenced by the pH of the experimental media. With the exception of growth rates measured at pH 3.0, the growth of *Zea* roots was inhibited by the presence of IAA. This inhibition appeared to be pH-dependent, with greater inhibition at high pH. As shown previously (Miller, 1988), the reduction in growth rate resulting from the pH of the bathing medium (in the absence of IAA) was also associated with a reduction in inward current density and an acropetal compression of the region of the root associated with inward current.

Discussion

The ion current pattern detected in the medium surrounding primary root tips of *Zea* indicated clearly that positive current flowed into those parts of the root that were responsible for division, differentiation, and growth: the meristematic and elongating tissues. Mature root regions were responsible for generating the bulk of the outward current. These results are consistent with previous investigations of root growth made with vibrating electrodes (Weisenseel *et al.*, 1979; Behrens *et al.*, 1982; Miller *et al.*, 1986, 1988; Miller and Gow, 1989). The suggestion that H^+ ions may be a major component carrying the endogenous current supports earlier reports where protons have been identified as the major current-carrying ion in both freshwater and terrestrial plants (Weisenseel *et al.*, 1979; Brawley *et al.*, 1984; Dorn and Weisenseel, 1984). This apparent influx of H^+ ions into the apex of intact *Zea* roots would appear to be at odds with the acid growth hypothesis. However, there is evidence that *Zea* root-tip segments acidify their bathing medium and respond to low pH (Edwards and Scott, 1974). It was recently reported that H^+ ions flow into the apex of intact *Zea* roots as far back as 3 mm from the tip (Bjorkman and Leopold, 1987). This region of current influx can be considered to be well within the elongation zone of *Zea* (Pilet and Senn, 1980). The proposition that roots generate a region of high pH around their growing tips is not new (Weisenseel *et al.*, 1979), and such alkaline environments correspond to the region of maximum

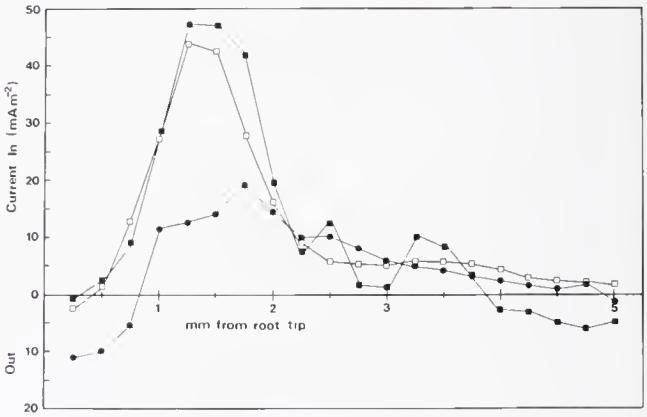

Figure 5. The effect of removing K^+ on FC-stimulated inward current. Current was mapped around 6-day-old *Zea* roots in the following sequence: APW control (●), APW + 10^{-6} M FC (■) followed by APW − K^+ + 10^{-6} *M* FC (□).

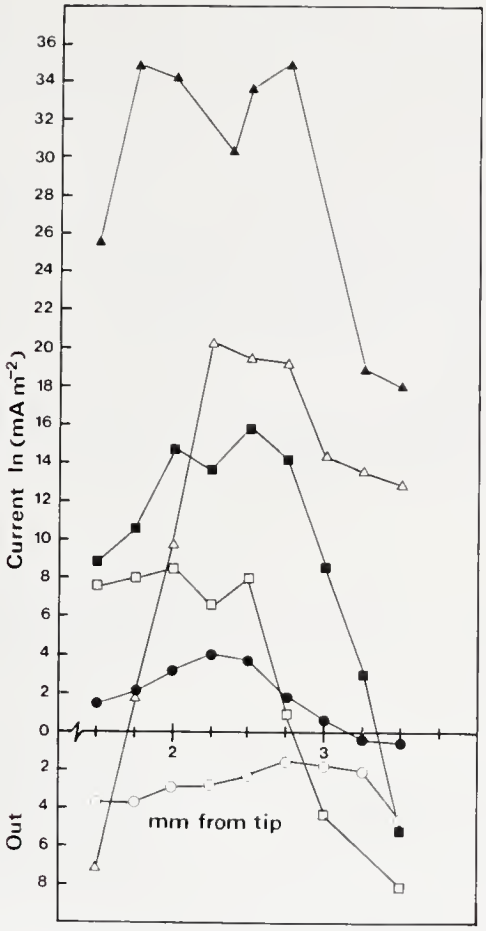

Figure 6. Effect of exogenously applied 10^{-4} *M* IAA on the current pattern generated by 6 day old *Zea* roots. The effects of IAA at pH 5.0 (△), 6.5 (□), and 7.0 (○) are compared with their respective APW controls: (▲), (■), and (●).

cell elongation (O'Neil and Scott, 1983). It is significant that in all cases where an alkalinization of the growing tip environment has been reported, intact plants were used as experimental material. In some experiments, activation of growth in root segments by low pH and low pH-inducing factors (*i.e.*, IAA and fusicoccin) may have resulted from accelerated recovery from excision or abrasion injury (Hanson and Trewavas, 1982).

It is difficult to reconcile the proposition that fusicoccin enhances just a proton influx with more than a decade of work suggesting it stimulates energy-linked net H^+ efflux (Marre, 1985). Although we detected no fusicoccin-induced stimulation of the outward current in the apical 5 mm of roots (Fig. 5), this represents only a small portion of the total root surface area of a 6-day-old seedling. Therefore, our data may represent only one limb of an enhanced ion circulation stimulated by fusicoccin. Some concern has been expressed about the validity of comparing results obtained from exposing fusicoccin to excised tissues, to those derived (as in this case) from intact tissues (Gronewald, Cheeseman and Hanson, 1979). In addition, little consideration has been given to the effect of fusicoccin on tissues of different developmental states. Where this has been taken into account, it would appear that the capacity of root tissues to acidify their bathing medium in the presence of fusicoccin increases with the age and the differentiation of the root (Gabella and Pilet, 1979). The integration of the effects of fusicoccin on intact roots into a spatially separated yet balanced flux may explain the observed lack of cytostolic pH perturbation experienced in the presence of fusicoccin (Roberts *et al.*, 1981). The stimulated inward current in the presence of fusicoccin was clearly not due to increased K^+ uptake (Marre, 1985), as removal of K^+ ions from the measuring medium had no significant effect on the enhanced inward current density.

The presence of exogenous IAA caused a reduction in the inward current density at all pH's examined. The effectiveness of IAA in reducing inward current density falls with decreasing pH. IAA also caused an acropetal shift of the point where inward switches to outward current, thereby reducing the volume of tissue traversed by an inward current.

In general, factors that promoted (low pH and fusicoccin) or reduced (high pH and IAA) the elongation of intact primary roots of *Zea*, increased or decreased respectively the density of current flowing into meristematic and elongating tissues. The effective stimulation of elongation by fusicoccin did not show any linear pattern as pH is reduced from pH 7.0 to 3.0. However, the effect of fusicoccin on inward current density did show a trend across this pH range; the amount of fusicoccin-induced current enhancement fell as pH was reduced. Therefore, there appears to be a complex relationship between applied fusicoccin, pH, and root metabolism (including growth).

There also appears to be a complex relationship between external pH, pCa, applied IAA, and root elongation (Hasenstein and Evans, 1986). The uptake of IAA (and therefore its cytosolic concentration) may be pH-dependent (Martin and Pilet, 1987). In addition, what effect exogenous IAA has on intact roots may depend both on the concentration of IAA and on the initial elongation of the root. Pilet and Saugy (1987) have reported that slow growing roots were all inhibited by exogenous IAA (at any concentration), whereas the elongation of fast growing roots may even have been promoted by IAA at low concentrations. These observations are reflected in the IAA related data presented in Table I. At pH 7.0, when the roots were growing slowly, the effect of 10^{-4} *M* IAA was to reduce the elongation rate of the root by some 90%. However, at pH 3.0, IAA had a negligible effect on elongation. It is not clear whether this is due to the initial

elongation rate of the root as influenced by the pH of the bathing medium, the effect of pH on the uptake kinetics of IAA, or a combination of both.

It is suggested that the root-generated ionic current associated with the primary root tips of *Zea* is due primarily to the circulation of protons, with Ca^{2+} ions perhaps playing a regulatory role. The extension rate of the root generally correlated with the density of current entering actively dividing and elongating cells. Factors that promoted (low pH and fusicoccin) or restricted (high pH or IAA) root growth, enhanced or reduced the root generated current, respectively.

Literature Cited

Behrens, H. M., M. H. Weisenseel, and A. Seivers. 1982. Rapid changes in the pattern of electrical current around the root tip of *Lepidium sativum* L. following gravistimulation. *Plant Physiol.* **70:** 1079–1083.

Bjorkman, T., and A. C. Leopold. 1987. An electrical current associated with gravity sensing in maize roots. *Plant Physiol.* **84:** 841–846.

Brawley, S. H., D. F. Wetherell, and K. R. Robinson. 1984. Electrical polarity in embryos of wild carrot proceeds cotyledon differentiation. *Proc. Natl. Acad. Sci. USA* **81:** 6064–6067.

Cleland, R. E. 1980. Auxin and H^+-excretion: the state of our knowledge. Pp. 71–78 in *Plant Growth Substances,* F. Skoog, ed. Springer, Berlin, Heidelberg, New York.

Dorn, A., and M. H. Weisenseel. 1984. Growth and current pattern around internodal cells of *Nitella flexilis* L. *J. Exp. Bot.* **35:** 373–383.

Edwards, K. L., and T. S. Scott. 1974. Rapid growth response of corn root segments: effect of pH on elongation. *Planta* **119:** 27–37.

Evans, M. L., T. J. Mulkey, and M. J. Vesper. 1980. Auxin action on proton influx in corn roots and its correlation with growth. *Planta* **148:** 510–512(s).

Gabella, M., and P-E. Pilet. 1979. Effects of fusicoccin on the maize root elongation and on the pH of the medium. *Z. Pflanzen.* **93:** 23–30.

Gronewald, J. W., J. M. Cheeseman, and J. B. Hanson. 1979. Comparison of the responses of corn tissues to fusicoccin and washing. *Plant Physiol.* **63:** 255–259.

Hanson, J. B., and A. Trewavas. 1982. Regulation of plant cell growth: the changing perspective. *New Phytol.* **90:** 1–18.

Hasenstein, K-H., and M. L. Evans. 1986. Calcium dependence of rapid auxin action in maize roots. *Plant Physiol.* **81:** 439–443.

Kutschera, U., and P. Schopfer. 1985. Evidence against the acid growth theory of auxin action. *Planta* **163:** 494–499.

Marre, E. 1985. Fusicoccin- and hormone-induced changes of H^+ extrusion: physiological implications. Pp. 439–460 in *Frontiers of Membrane Research in Agriculture,* J. B. St. John, E. Berlin, and P. C. Jackson, eds. Rowman and Allanheld, Totowa.

Martin, H. V., and P-E. Pilet. 1987. Effect of pH on IAA uptake by maize root segments. *Plant Physiol.* **83:** 262–264.

Miller, A. L., J. A. Raven, J. I. Sprent, and M. H. Weisenseel. 1986. Endogenous ion currents traverse growing roots and root hairs of *Trifolium repens. Plant Cell Environ.* **9:** 79–83.

Miller, A. L., E. Shand, and N. A. R. Gow. 1988. Ion currents associated with root tips, emerging laterals and induced wound sites in *Nicotiana tabacum:* spatial relationship proposed between resulting electrical fields and phytophthoran zoospore infection. *Plant Cell Environ.* **11:** 21–25.

Miller, A. L., and N. A. R. Gow. 1989. Correlation between profile of ion-current circulation and root development. *Physiol. Plant.* **75:** 102–108.

O'Neil, R. A., and T. K. Scott. 1983. Proton flux and elongation in the primary roots of barley (*Hordeum vulgare*). *Plant Physiol.* **73:** 199–201.

Pilet, P-E. 1976. Fusicoccin and auxin effects on root growth. *Plant Sci. Lett.* **7:** 81–84.

Pilet, P-E., and M. Saugy. 1987. Effect on root growth of endogenous and applied IAA and ABA. *Plant Physiol.* **83:** 33–38.

Pilet, P-E., and A. Senn. 1980. Root growth gradients: a critical analysis. *Z. Pflanzen.* **99:** 121–130.

Roberts, J. K. M., P. M. Ray, N. Wade-Jardetzky, and O. Jardetzky. 1981. Extent of intracellular pH changes during H^+ extrusion by maize root-tip cells. *Planta* **152:** 74–78.

Rosene, H. F. 1947. A bibliography of continuous bioelectric currents and bioelectric fields in animals and plants. Pp. 301–391 in *Bioelectric Fields and Growth,* E. J. Lund, ed. University of Texas Press, Austin.

Shrank, A. R. 1945. Changes in electrical polarity in the *Avena* coleoptile as an antecedent to hormone action in geotropic response. *Plant Physiol.* **20:** 133–136.

Weisenseel, M. H., A. Dorn, and L. F. Jaffe. 1979. Natural H^+ currents traverse growing roots and root hairs of barley (*Hordeum vulgare* L.). *Plant Physiol.* **64:** 512–518.

Reference: *Biol. Bull.* **176(S):** 71–78. (April, 1989, Suppl.)

Charge-Dependent Molecular Movement Through Intercellular Bridges in *Drosophila* Follicles

RICHARD I. WOODRUFF

Department of Biology, West Chester University, West Chester, Pennsylvania 19383

Abstract. The steady-state membrane potentials of the nurse cells of *Drosophila melanogaster* incubated in a Ringer's solution containing 2.5 m*M* K^+ averaged 5.2 mV more negative than those of oocytes to which they were attached by intercellular bridges (n = 159; $P < 0.001$, paired t-test). In sodium azide, the resting potentials of the two cells diminished from a range of −50 to −70 mV to an average of −10 mV, and the trans-bridge difference disappeared. Therefore, the trans-bridge difference is dependent upon metabolic energy. Lucifer yellow CH, when microinjected into either nurse cells or oocytes, became distributed in less than 30 min in a manner to be expected for a negatively charged fluorochrome in an electrically polarized system. Polarity was even more striking in this study than reported earlier for *Drosophila* follicles incubated in a higher K^+ medium (Woodruff *et al.*, 1988).

Introduction

In living cells, electrical currents can influence the distribution of charged molecules. This concept, so elegantly proposed by Jaffe (1969) as a consequence of the electrical currents he had shown to flow through the developing *Fucus* egg, has been most graphically demonstrated in the ovarian complexes of insects. There it has been visualized through the use of a number of fluorescein-conjugated or rhodamine-conjugated proteins (Woodruff and Telfer, 1973; 1980; Woodruff and Anderson, 1984; Woodruff *et al.*, 1988).

Charge-dependent movement has been shown in the polytrophic follicles of *Hyalophora* to manifest itself across the nurse cell-oocyte intercellular bridges (Woodruff and Telfer, 1973, 1980) and in the telotrophic ovaries of *Oncopeltus faciatus* (Woodruff and Anderson, 1984), *Dysdercus intermedius* (Munz and Dittmann, 1987), and *Rhodnius prolixus* (Telfer *et al.*, 1981) within the syncitial tropharium (particularly between the core and peripheral nurse cells). In each of these insects, the charge-dependent movement is accompanied by electrical gradients that correlate with the direction in which a charged molecule's movement is enhanced.

The polytrophic follicles of *Drosophila* are morphologically and functionally similar to those of *Hyalophora*, with nurse cells providing large amounts of RNA, while the oocyte accumulates yolk from the blood by endocytosis. While extrafollicular currents around the follicles had been recorded (Bohrmann *et al.*, 1984; 1986a; Jaffe and Overall, 1985), when Bohrmann *et al.* (1986b) and Sun and Wyman (1987) measured the membrane potentials and Bohrmann and Gutzeit (1987) studied the influence of charge on the distribution of microinjected fluorescent probes, they were unable to confirm the results seen in *Hyalophora*. However, Woodruff *et al.* (1988), using the same incubation medium as Bohrmann *et al.*, recently reported an average −2.5 mV potential difference between nurse cells and the individual oocyte to which each was attached. They also found that microinjected positively charged fluorescent protein detectably crossed the oocyte-nurse cell bridges only from the oocyte to the trophic cells, while its methylcarboxylated, negatively charged form migrated detectably only in the opposite direction.

In this paper I show: that when the measurements are made in Sun and Wyman's medium the potential difference between oocytes and their attached nurse cells is even greater than previously reported by Woodruff *et al.*; that most of the resting potential of both oocytes and nurse cells is Azide-sensitive and thus dependent on metabolic energy; that the influence or charge on molecular distribution is also energy dependent; and that Lucifer yellow CH, which can more easily be injected into cells than fluorescent proteins, can be used to study this charge-dependent movement.

Materials and Methods

Animals

Drosophila melanogaster (Oregon red) individuals were raised on standard *Drosophila* medium. Flies were removed from the culture each day. The following day, all newly emerged flies were transfered to a new culture tube, to be used on the third day after emergence. Chilled, unetherized females were decapitated and immersed in dissecting/incubation medium for removal of ovaries. The ovaries were transfered by pipette to a dish containing medium with collagenase (see below), where they were incubated at room temperature for a brief period of about five minutes (Sun and Wyman, 1987). This enzyme digestion softens the basement membrane (also called "tunica propria," King, 1970) and allows much easier penetration with microelectrodes. After separation, follicles were transfered by a transfer pipette consisting of heat-pulled polyethelene tubing (Intermedic) attached to a 10-μl Hamilton syringe, to an open-top chamber for electrophysiology, or to a Kiehart chamber (Kiehart, 1981) for microinjection. The "open" side of a Kiehart chamber was sealed with vegetable oil to prevent evaporation. If iontophoretic injection is planned, the Ag-AgCl ground wire must be inserted before the oil seal is made. Inserting the ground through the oil coats and insulates the wire.

Solutions

The dissection/incubation solution was that used by Sun and Wyman (1987) and consisted of (m*M*): sodium glutamate, 50; $MgCl_2$, 15; $CaSO_4$, 5; KCl, 2.5; glucose, 10; Hepes, 5; fructose, 10; sucrose to adjust medium to 300 mOsmols. For enzyme digestion, 1 mg/ml of collagenase (Sigma) was added to this medium. Lucifer yellow, a gift from Walter Stewart, or purchased from Sigma, was used as a 1% solution in distilled water. Both sources were satisfactory.

Electrophysiology

Three molar KCl capillary glass electrodes with tip resistances of 25–35 Mohms were attached to World Precision Instruments (WPI) 750 dual microprobe electrode holders and preamplifiers. The output from each WPI preamplifier was attached to a Tektronix 5103 storage oscilloscope, and also to a Hewlett-Packard 3476B digital multimeter, which allowed a digital readout to 0.1 mV of potential values. Impalement of cells was accomplished by bringing the electrodes into contact with the appropriate cells and then "ringing" each electrode by a momentary increase in capacitance compensation. With oocyte measurements in particular, care was taken to insure that penetration was into the intended cell and not into the epithelium. This was confirmed visually and also electrically by the effect on the other impaling electrode of a 1 nA current pulse.

Microinjections

While previous microinjections (Bohrmann and Gutzeit, 1987; Woodruff *et al.*, 1988) had been accomplished by pressure, the Lucifer yellow used in the present study could be iontophoresed into the cells. Although this study employed a custom-built constant current source, Lucifer yellow can be injected using a nine volt radio battery as the power source. Following insertion of the dye electrode into the target cell, sufficient current was used to cause the cell to become, at the end of a 2-min injection, easily seen on the video monitor while using fluorescence optics.

Microscopy/video

Electrophysiology was performed on an Olympus CK2 inverted microscope modified for transmitted oblique illumination. Two stage-mounted Narishige model MO-501 Emerson-type micromanipulators carried the electrode holders. For microinjection, a Olympus IMT (1) inverted microscope with epi-illumination for fluorescence was used. This microscope also was fitted for transmitted oblique illumination. Trans-oblique and/or fluorescent images were captured with a Dage-MTI 65 Newvicon video camera employing autogain and autoblack level, and recorded on a JVC BR-9000U ½ inch VHS time-lapse video recorder. No special video enhancement equipment was used. One of the Narishige micromanipulators described above was employed.

Estimation of relative Lucifer yellow concentrations

The length through the tissue of both the exciting and emitted light rays, as well as the opacity of the tissue, affect the strength of the fluorescent signal. These variables make attempts to determine the concentration of a single fluorochrome rather imprecise. Estimates of the relative concentration of Lucifer yellow between injected nurse cells or oocytes and their bridged partners were made in the following manner. Lucifer yellow was diluted until the strength of its fluorescent emission from a 0.8 mm I.D. capillary tube matched that seen in the injected cells. Identical tubes were filled with two-fold, four-fold, and eight-fold dilutions of this solution. Each dilution tube was placed next to the original on the stage of the fluorescence microscope, and the original together with each tube in turn was photographed from the video monitor with the same conditions of brightness, contrast, exposure, and development used to photograph cells. Photomicrographs of cell fluorescence were then

compared to these standards to give an estimate of the Lucifer yellow concentration in the bridged cell relative to that of the injected cell.

Results

Determination of electrode reliability

A special concern with dual-electrode microelectrophysiology is whether the electrodes have equal gain. To insure maximum confidence that the equipment yielded valid readings, the following strategies were employed. (1) At the start of each day, electrodes were balanced and both were used to impale a single oocyte or nurse cell to insure that both gave equal readings. This test was repeated several times a day. (2) Throughout this study, readings were accepted only if neither electrode showed more than 1 mV drift when electrodes were removed from the cells being measured. (3) In several cases, (>30%) both electrodes were withdrawn and checked to confirm 1 mV or less drift, minor re-zeroing was performed if necessary and the electrodes were reinserted to confirm the original reading. If lower values were found, only these values were used in compiling the data. However, values recorded were always simultaneously paired readings of the oocyte and attached nurse cell. (4) A more rigorous test was conducted on ten follicles selected at random (one each day on ten separate days). After balancing, electrodes were first brought into contact with the oocyte, then a nurse cell. Penetration was accomplished by ringing each electrode, oocyte first, then nurse cell. After the potentials and the intercellular differences were recorded, the electrodes were withdrawn and checked for drift (Fig. 1). They were then reinserted as above, but in the opposite order to check the possibility that the order of impalement influenced the cell potentials and hence the intercellular difference. Electrodes were withdrawn into the medium and reinserted in the original order, and withdrawn yet again. Finally the two electrodes were inserted into the oocyte to determine that they continued to give the same readings when in a common cytoplasm. Eight of the ten follicle readings subjected to this procedure passed all criteria. One of the ten failed when, prior to final simultaneous insertion into the oocyte, the nurse cell electrode developed a 4-mV drift. Another failed when, on third impalement, the oocyte had depolarized and was 8-mV less negative than during the previous two impalements.

The electrical gradient between oocytes and nurse cells

Since each nurse cell is attached to a particular oocyte, it is the difference between these two cells that is of paramount importance. It is particularly important to recognize this if the cell resting potentials vary considerably,

Figure 1. Polaroid screen-camera photograph of the oscilloscope screen during measurement of the steady-state potentials of an oocyte (−70 mV), and one of its attached nurse cells (−75 mV). At the start of the recording both electrodes were balanced. At "a" one electrode was brought into contact with the oocyte the positive deflection shown was often observed and is believed to be an artifact caused by stretching of the membrane across the tip of the electrode. At "b" the other electrode is placed in contact with the nurse cell. At "c" and "d" the oocyte and nurse cell electrodes respectively were "rung" by an increase in capacitance compensation and entered their cells. At "e" the oscilloscope channel recording the nurse cell was inverted to identify the nurse cell trace. The oocyte electrode ("f") and the nurse cell electrode ("g") were withdrawn, their return to zero confirming that neither had undergone drift during the measurement.

as they do in insect follicles. As in the earlier study by Woodruff *et al.* (1988), my study employed the paired t-test for compairing nurse cell and oocyte potentials. For 159 paired measurements from 81 different stage 10 follicles there was an average oocyte to nurse cell potential difference of -5.2 ± 5.1 mV, $P = <0.001$. The large standard deviation is primarily the result of several measurements in which the difference was as much as −21 mV. In 10 of the 159 measurements the oocyte was more electronegative than the attached nurse cell; in 12 measurements the oocyte and attached nurse cell had equal potentials. For the remaining 127, an electrical gradient of −1 to −21 mV, nurse cell negative, was revealed (Fig. 1). In this medium, the average oocyte potential was -60.6 ± 10.8 mV, while the average for the nurse cells was -65.8 ± 10.2 mV (Table I). The follicles were sensitive to changes in aK^+_0 of the medium (data not shown), but with a slope of less than 58 mV/decade change in concentration, indicating the presence of at least one other permeant ion.

Ten follicles were entered without the aid of collagenase digestion. These follicles displayed the same steady-state potentials as did those which had been subjected to enzyme digestion. Nor did addition of collagenase to the incubation medium appear to effect any change in the steady-state potentials of a follicle being measured at the time. However, untreated follicles were vastly harder to

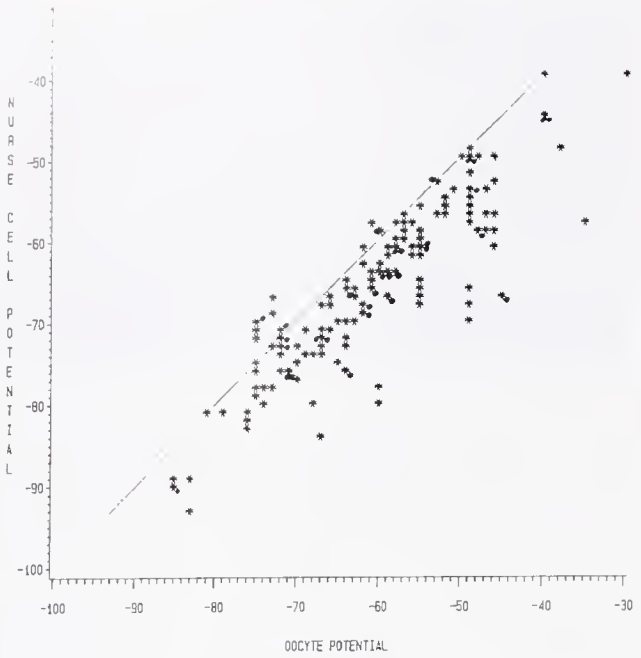

Figure 2. Nurse cell potential plotted against oocyte potential for 159 paired measurements. Satellite dots affixed to the * indicate additional pairs with the same values. The line has been drawn through the equipotential values, points below the line show nurse cell negative to oocyte.

enter without causing damage. Enzyme-treated follicles routinely had input resistances in excess of 1 Mohm, while those entered without prior enzyme digestion had resistances estimated to be on the order of 200–500 Kohms.

Stage 8–9 follicles were less intensely studied, but for 66 cases the mean difference was −5.5 ± 5.7 mV and $P = <0.001$, with an average oocyte potential of −60.7 ± 12.2 mV and an average nurse cell potential of −66.3 ± 10.3 mV. They also had input resistances of over 1 Mohm.

Energy dependence of the resting potential

Sodium azide can be used to suppress cytoplasmic ATP levels (Lowman, 1965a). A 10-m*M* concentration, the same concentration used to affect electrogenic pumps in *Neurospora* (Slayman, 1965b), has been used to reveal that about [illegible] membrane potential in *Hyalophora* is dependent upon metabolic energy (Stynan *et al.*, 1988). To determine the trans-bridge potential and a portion of the steady-state potentials of oocytes and nurse cells in *Drosophila* dependent upon metabolic energy, follicles were [illegible] medium containing 10 m*M* azide. Within [illegible] contact with azide, the potentials had decreased [illegible] the average potential for 15 azide-treated oocytes was −10.6 ± 2.6 mV and for 35 nurse cells it was −9.8 ± 2.9 mV. There was no significant difference when the measurements were analyzed by paired t-test. It would appear that 83% or more of the steady-state potential and all of the trans-bridge potential relies upon metabolic energy.

Iontophoresis of Lucifer yellow

Lucifer yellow microinjected into a nurse cell was detectable within 5 min in the oocyte (Figs. 3a–b, 4a–c, 5). In fact, the influence of the nurse cell-oocyte bridge gradient is so effective on this very mobile, negatively charged molecule that over a period of 30 minutes it appeared more concentrated in the oocyte than in the injected nurse cell (Figs. 4, 5). In the video record, no further noticeable change showed after 20 min, indicating that the distribution had either reached or was quite close to the final equilibrium concentrations. Comparison with relative concentration standards explained above indicated that the equilibrium concentration in the oocyte was greater than that in the nurse cell, but that the difference was less than two-fold. Similar results were seen in 25 follicles. When the fluorochrome was injected into an oocyte, it appeared to remain there, as can be seen in Figure 3c–d and Figure 4d–f. Oocyte injections were made in 25 different follicles. In none of these follicles was the dye detectable in the nurse cells at the level of sensitivity employed.

Injection of the dye into cells incubating in medium containing 10 m*M* azide revealed the energy-dependence of the bridge polarity (Fig. 6). Within 4 min the dye could be seen in the lowest tier of nurse cells. The dye was visible in the second tier at 16 min and often began to show in all but the most anterior nurse cells.

Table I

Oocyte to nurse cell potential differences and steady-state potential for stage 10 follicles (in mV)

n = 159
% Nurse cell negative to oocyte = 79.9
% Nurse cell positive to oocyte = 6.3
% Nurse cell and oocyte equally electronegative = 7.5
Average nurse cell to oocyte potential difference = −5.157 ± 5.06
$P = <0.001$ (paired t-test)

	oocyte	nurse cell
Minimum mV	−30*	−40*
Maximum mV	−85‡	−93**
Mean	−60.6	−65.7
Std dev	±10.8	±10.2

* Same follicle.
‡ Nurse cell was −90.
** Oocyte was −83.

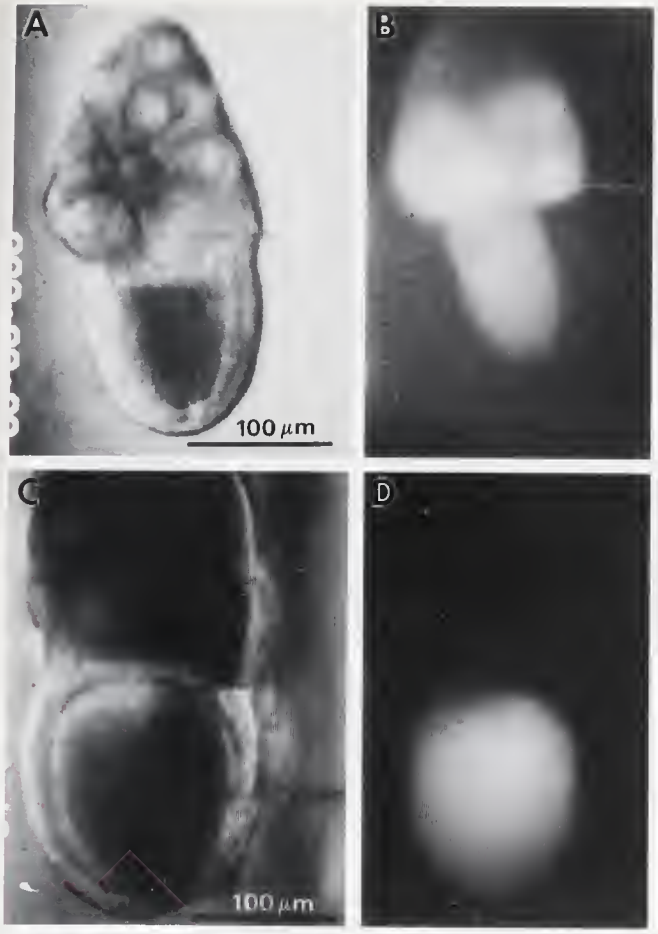

Figure 3. Photographs from the video screen of trans-oblique illumination and Fluorescence images recorded with a newvicon camera showing Lucifer yellow injected *Drosophila* follicles. The injection needle can be seen impaling a nurse cell in A. B is the fluorescence image taken 15 min after the injection. Note the lack of detectable dye-coupling. In C the injection was into an oocyte. D is the fluorescence image recorded 20 min later.

This experiment was repeated 10 times with the same results in each case.

An additional observation emerging from these experiments was the undetectability of dye-coupling between the oocyte and the follicle epithelial cells (Figs. 2–6). This facilitated the interpretation of dye movement through the intercellular bridges because it ruled out the possibility of an indirect route of migration between oocyte and nurse cells via the epithelium.

Discussion

The results confirm a charge-dependent polarizing effect operating within the nurse cell-oocyte intercellular bridges. This effect, previously shown to modulate the movement of positive or negative microinjected proteins (Woodruff *et al.*, 1988), also influences the distribution of Lucifer yellow CH, a small, highly mobile, negatively charged molecule soluble in the aqueous phase of the cytosol (Stewart, 1978). Dye injected into the oocyte does not cross the intercellular bridges into nurse cells in detectable amounts, but when injected into nurse cells it not only detectably crosses into the oocyte, but actually becomes more concentrated there. Furthermore, the results confirm, in a very different incubation medium, the electrical gradient described for *Drosophila* by Woodruff *et al.* (1988) and suggested to be responsible for enforcing this polarity.

An important observation made during this study concerned the level of dye detection. When dye injection into an oocyte had made the cell clearly fluorescent on the video screen, viewing through the oculars revealed a low level of fluorescence that was above autofluorescence in some nurse cells. This low level remained undetectable with the video system. Because the newvicon camera is not as sensitive as the dark-adapted eye, less dye needed to be injected into a cell when it was observed through the oculars. And at this reduced dye level no nurse cell fluorescence was observed. Presumably, with a SIT camera, one would again be able to detect some dye in nurse cells, until the level of injection was further reduced to match the increased sensitivity of the detection equipment. Such observations underscore the fact that the polarized nature of the nurse cell-oocyte bridges does not completely preclude the movement of charged molecules, but rather affects the equilibrium concentration of such molecules on either side of the bridge (Jaffe, 1977; Telfer *et al.*, 1981).

The effectiveness of the ability of the electrical gradient to influence concentrations is strikingly illustrated in Figure 5, showing the movement of Lucifer yellow from an injected nurse cell. The dye not only moves detectably into the oocyte, but eventually becomes more concentrated there. The observation is made possible by an apparent absence of adsorption to cytoplasmic structures, which is a chronic problem with the fluorescent protein probes that we have used to demonstrate polarity. While Lucifer yellow will eventually bind to cytoplasmic structures, it remains free in the aqueous phase of the cytosol for at least 30 min (deLaat *et al.*, 1980).

Concerning the relative concentrations of fluorochrome among cells of the follicle: when a nurse cell was microinjected with Lucifer yellow, the fluorochrome entered the oocyte and eventually caused brighter fluorescence there than in the injected cell. Comparison with the standards described in Materials and Methods suggested the eventual equilibrium concentrations were reached when the apparent concentration in the oocyte was more than 1:1 but less than two-fold greater than that in the injected nurse cell. Lucifer yellow CH is a dili-

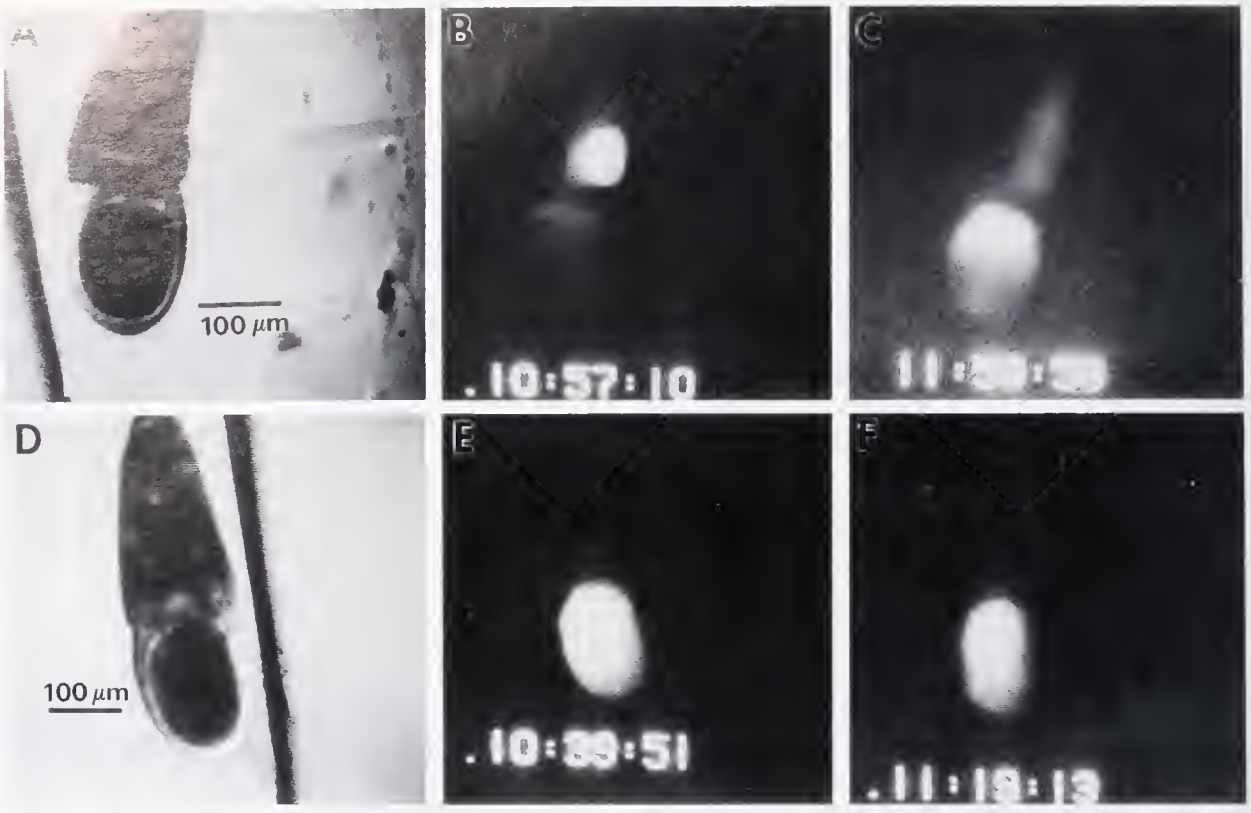

Figure 4. Photographs taken from the video screen. A, B, and C show an injection of Lucifer yellow into a nurse cell, followed by a 1-h incubation. The negative fluorochrome migrates via the intercellular bridge into the oocyte, becoming more concentrated there. The uneven appearance of the oocyte fluorescence in C is an artifact of the recording. D, E, and F show that, when injected into an oocyte and incubated, in this case for 48 min, no detectable levels of dye are seen in the nurse cell.

thium salt (Stewart, 1978) and thus in solution would have two negative charges. From the Nernst equation we would expect for a molecule with a $^{-2}$ charge that: Voltage = $29\text{mV} \cdot \log [C_1/C_2]$. Thus a potential difference of 5-mV should bring about a 1.5-fold difference in the equilibrium concentrations, while an 8-mV potential difference would bring about a two-fold difference in the equilibrium concentrations. Given the unknown variables such as the opacity of the different cells, the estimated [illegible] than two-fold difference seems to fit the expected [illegible]es. That no further change was observed after 20 min [illegible]rgument against bulk flow of materials from nurse [illegible] oocyte being a major factor in the distribution [illegible]rome.

In 1 h, oocyte-[illegible]cles had not yet reached equilibrium con[illegible]xpected for the average measured 5-mV pote[illegible]ence. Presumably this was due to the electr[illegible]focused at the oocyte-nurse cell bridges, op[illegible]position to the diffusion gradient, and thus [illegible] establishment of the equilibrium concentra[illegible] they were not yet achieved during the tim[illegible]ervation. That ATP suppression by treatment with azide allowed a detectable spread of the fluorochrome from oocyte to nurse cells confirms that the observed asymmetry of equilibrium concentrations is dependent on metabolic energy.

Varying values have appeared in the literature concerning the magnitude of the steady-state potentials in *Drosophila* oocytes. Bohrmann *et al.* (1986) reported that oocytes incubated in Robb's medium (aK_0 40 m*M*) had a potential of −21 mV, and Woodruff *et al.* (1988) reported a −23.9 mV average for oocytes incubated in that same medium. In a medium with lower (8.6 m*M*) aK_0, O'Donnell (1988) reported a steady-state potential for *Drosophila* of −40 mV, while in a similar medium Miyazaki and Hagawara (1976) reported an average potential of −65 mV for unfertilized eggs. Sun and Wyman (1987) reported development of the medium used in the present study, and found an average potential for 27 stage-10 oocytes of −85.2 mV. The −60 mV average for the 81 stage-10 oocytes in the present study is below the average value found by Sun and Wyman, although some values as high as −85 mV were encountered.

The saline solutions employed in these studies span

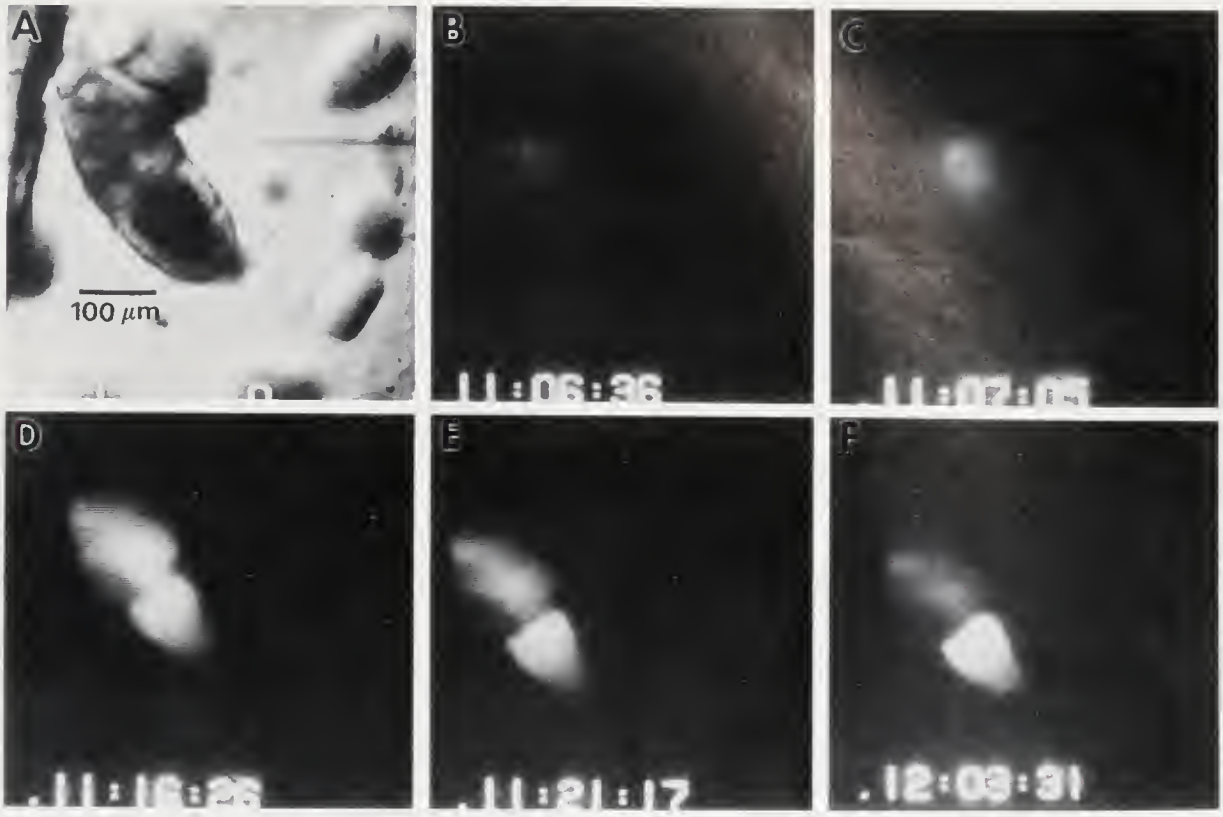

Figure 5. Excerpts from the video time-lapse record showing the migration of the negatively charged fluorochrome Lucifer yellow from an injected nurse cell into the oocyte. During this nearly 1-h incubation, the concentration of dye becomes greatest in the oocyte. Difference in path length causes fluorescence to appear brighter at the anterior end than at the narrow posterior end.

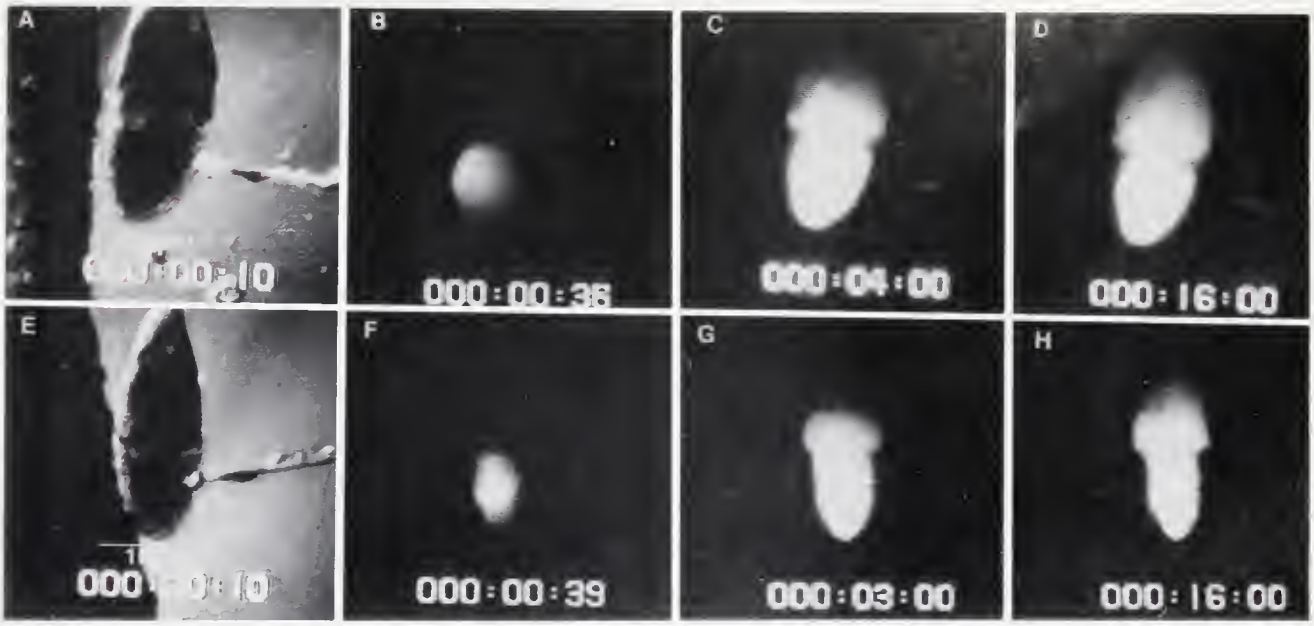

Figure 6. Excerpts from the video time-lapse records of two follicles injected into their oocytes with Lucifer yellow and incubated in the presence of Na-azide. Deprived of normal levels of ATP the follicles are unable to confine the negative dye to the oocyte.

the 25 m*M* aK_0 measured in *Drosophila* blood by Van Der Meer and Jaffe (1983), a potassium level that would presumably yield membrane potentials most similar to those *in vivo*. In both 40-m*M* and 2.5-m*M* aK_0, an average nurse cell negative electrical gradient occurs. However, its magnitude varies with the magnitude of the cell steady-state potentials. Thus in saline in which the average steady-state potential was −24 mV, the average trans-bridge voltage difference was −2.3 mV, while in saline in which the steady-state potentials were over twice as large the trans-bridge potential difference had also doubled. The effects of incubation in azide also has shown that the steady-state potentials, the nurse cell-oocyte electrical gradients, and the distribution of charged molecules between oocyte and attached nurse cells is dependent upon metabolic energy.

Intriguing for the future will be the use of various *Drosophila* mutants to explore the physiological effects of the electrical difference between oocytes and nurse cells, a direction dependent upon identification of a mutant in which the gradient fails to occur. Also, the apparent lack of dye-coupling suggests that it will be informative to investigate the nature of follicle epithelial cell-oocyte interaction.

Acknowledgments

This research was supported by grants from NSF (DB-18617) and West Chester University (RAPC 9014).

Literature Cited

Bohrmann, J., U. R. Heinrich, A. Dorn, K. Sander, and H. O. Gutzeit. 1984. Electrical phenomonena and their possible significance in vitellogenic follicles of *Drosophila melanogaster*. *J. Embryol. Exp. Morph.* **8**(suppl): 151.

Bohrmann, J., A. Dorn, K. Sander, and H. O. Gutzeit. 1986a. The extra-cellular electrical current and its variability in vitellogenic *Drosophila* follicles. *J. Cell Sci.* **81**: 189–206.

Bohrmann, J., and H. O. Gutzeit. 1987. Evidence against electrophoresis as the principal mode of protein transport in vitellogenic follicles of *Drosophila*. *Development* **101**: 279–288.

Bohrmann, J., E. Huebner, K. Sander, and H. O. Gutzeit. 1986b. Intercellular electrical potential measurements in *Drosophila* follicles. *J. Cell Sci.* **81**: 207–221.

Jaffe, L. F. 1969. On the centripetal course of development, the *Fucus* egg, and self-electrophoresis. *Dev. Biol.* suppl. **3**(A. Land, ed.): 83–111.

Jaffe, L. F. 1977. Electrophoresis along cell membranes. *Nature* **265**: 600–602.

Jaffe, L. F., and R. Overall. 1985. Patterns of ionic current through *Drosophila* follicles and eggs. *Dev. Biol.* **108**: 102–119.

Kiehart, D. P. 1981. Microinjections of *Echinoderm* eggs. Apparatus and procedure. Pp. 13–31 in *Methods and Perspectives in Cell Biology. The Cytoskeleton*, L. Wilson, ed. Vol. 25 part B, *Biological Systems and Functional Methods*. Academic Press, Orlando, FL.

King, R. C. 1970. *Ovarian Development in* Drosophila malanogaster. Academic Press, Inc., New York.

de Laat, S. S., L. G. J. Tertoolen, A. W. C. Dorrensteijn, and J. A. M. van den Biggelaar 1980. Intercellular communication patterns are involved in cell determination in early molluscan development. *Nature* **287**: 546–548.

Miyazaki, S-I., and S. Hagiwara. 1976. Electrical properties of the *Drosophila* egg membrane. *Dev. Biol.* **53**: 91–100.

Munz, A., and F. Dittmann. 1987. Voltage gradient and microtubules both involved in intracellular protein and mitochondria transport in the telotrophic ovarioles of *Dysdercus intermedius*. *Roux's Arch. Dev. Biol.* **196**: 391–396.

O'Donnell, M. J. 1988. Potassium channel blockers unmask electrical excitability of insect follicles. *J. Exp. Zool.* **245**: 137–143.

Slayman, C. L. 1965a. Electrical properties of *Neurospora crassa*. Effects of external cations on the intracellular potential. *J. Gen. Physiol.* **49**: 69–92.

Slayman, C. L. 1965b. Electrical properties of *Neurospora crassa*. Respiration and the intracellular potential. *J. Gen. Physiol.* **69**: 93–116.

Stewart, W. W. 1978. Functional connections between cells as revealed by dye-coupling with a highly fluorescent napthalimide tracer. *Cell* **14**: 741–759.

Stynan, D., R. I. Woodruff, and W. H. Telfer. 1988. The effects of ionophores on vitellogenin uptake in *Hyalophora* oocytes. *Arch. Insect Biochem. Physiol.* **8**: 261–276.

Sun, Y. A., and R. J. Wyman. 1987. Lack of an oocyte to nurse cell voltage difference in *Drosophila*. *Neuroscience* **13**(2): 1139.

Telfer, W. H., R. I. Woodruff, and E. Huebner. 1981. Electrical polarity and cellular differentiation in meroistic ovaries. *Am. Zool.* **21**: 675–686.

Van Der Meer, J. M., and L. F. Jaffe. 1983. Elemental composition of the perivitelline fluid in early *Drosophila* embryos. *Dev. Biol.* **95**: 249–252.

Woodruff, R. I. 1979. Electrotonic junctions in *Cecropia* moth ovaries. *Dev. Biol.* **69**: 281–295.

Woodruff, R. I., and K. L. Anderson. 1984. Nutritive cord connection and dye-coupling of the follicular epithelium of the growing oocytes in the telotrophic ovarioles in *Oncopeltus fasciatus*., the milkweed bug. *Roux's. Arch. Dev. Biol.* **193**: 158–163.

Woodruff, R. I., J. H. Kulp, and E. D. LaGaccia. 1988. Electrically mediated protein movement in *Drosophila* follicles. *Roux's Arch. Dev. Biol.* **197**: 231–238.

Woodruff, R. I., and W. H. Telfer. 1973. Polarized intercellular bridges in ovarian follicles of the *Cecropia* moth. *J. Cell Biol.* **58**: 172–188.

Woodruff, R. I., and W. H. Telfer. 1980. Electrophoresis of proteins in intercellular bridges. *Nature* **286**(No. 5768): 84–86.

Reference: *Biol. Bull.* **176(S):** 79–85. (April, 1989, Suppl.)

The *Drosophila* Egg Chamber: External Ionic Currents and the Hypothesis of Electrophoretic Transport

YI-AN SUN AND ROBERT J. WYMAN

Department of Biology, Yale University, New Haven, Connecticut 06511

Abstract. In insect egg chambers the nurse cells produce cytoplasm which is transported into the oocyte. It has been proposed that the transport is driven by an electrophoretic current resulting from a voltage gradient produced by the egg chamber. There are contradictory reports concerning the existence of significant voltage gradients. Any internal current must have a return pathway. An extracellular current surrounding the egg chamber that is in the *opposite* direction to that required for the return of an electrophoretic current has been reported, but other authors have not found such a consistent current.

We used the vibrating probe to measure the extracellular currents surrounding 50 egg chambers during the stage of maximum transport. Our set of measurements was predominantly characterized by small and variable currents. Most of the measurements were on the order of 1 microampere/cm^2, and no particular pattern of current flow was consistently evident. Although it was possible to pick out some egg chambers that appeared to show patterns of current flow, approximately equal numbers of egg chambers showed patterns of opposite types, and most showed no pattern at all. Our data do not support the presence of a consistent pattern of ionic current.

Introduction

The *Drosophila* egg chamber contains a syncytium of 15 nurse cells and 1 oocyte. These cells are enclosed in an epithelial layer of follicle cells. The nurse cells produce cytoplasm which is transported by an unknown mechanism into the oocyte. It has been proposed that the cytoplasmic proteins are driven from the nurse cells into the oocyte by an electrophoretic current (Woodruff *et al.*, 1988). A voltage gradient produced by the egg chamber is hypothesized to drive the electrophoretic current from nurse cells to oocyte within the egg chamber. Such a voltage gradient has been reported for *Hyalophora cecropia* (a moth) (Woodruff and Telfer, 1973, 1974, 1980), for the blow-fly *Sarcophaga* (Verachtert and De Loof, 1989), and for *Drosophila* (Woodruff *et al.*, 1988). On the other hand, no significant potential difference was found in *Drosophila* by Bohrmann *et al.* (1986b).

Any current from nurse cell to oocyte must be part of a loop completed by a return pathway. Jaffe and Woodruff (1979), in *cecropia,* and Overall and Jaffe (1985) in *Drosophila* reported an extracellular current surrounding the egg chamber which is in the *opposite* direction to that required for the return of an electrophoretic current. As a possible way of preserving the electrophoretic hypothesis, Overall and Jaffe (1985) proposed that there may be an intense, but totally internal, current loop that returns both the electrophoretic current and the external current. Verachtert and De Loof (1989) proposed a different internal current loop model. Two attempts have been made to peel away the follicular epithelium and measure this hypothesized internal current. In these peeled preparations, contradictory results were obtained. Woodruff *et al.* (1986), in *cecropia,* found an outward current and Bohrmann *et al.* (1986a), in *Drosophila,* found an inward current. Both measurements were made with the probe positioned over the nurse cells. Bohrmann *et al.* (1986a) also repeated the external vibrating probe measurements, they found the currents to be smaller than previously reported and very variable. They concluded that "the possibility that external currents may also play a role in developmental processes during oogenesis [was] . . . less attractive."

Because of the great interest in the electrophoretic theory and in *Drosophila* developmental biology in general, we tried to resolve this conflict over the presence or absence of consistent external currents by also carrying out vibrating probe measurements. Since maximum nurse

Figure 1. Stage-10 egg chamber with typically sized currents. Image of the probe, while it is vibrating, is seen at the upper right. At the beginning of the measurements on each egg chamber, reference measurements were taken at the probe position shown; any currents recorded at this position were considered as electronic biases and subtracted from all following measurements. For measurements around the egg chamber, the length and direction of the arrow represent the magnitude and direction of current signal. Arrowheads are plotted even if current vector is too small to be seen. At the end of measurements on each egg chamber, reference measurements were again taken at various points far from the egg chamber; these measurements give an idea of the magnitude of the electronic drift of the probe during the course of measurements. The small arrow to the lower left of the egg chamber is such a reference measurement. Some egg chambers at younger stages can be seen trailing off to the lower right. The scale bar (upper left) represents 3 $\mu A/cm^2$ for the current vectors and represents 80 microns for the size of the egg chamber.

cell-to-oocyte transport is occurring during egg chamber developmental stage 10 (King, 1970), we focussed our measurements on this stage. Overall and Jaffe (1985) reported on 12 stage-10 egg chambers. These showed maximal inward currents, ranging from 3 to 62 $\mu A/cm^2$ at various places in the anterior hemisphere of the egg chamber. Bohrmann *et al.* (1986a) studied 84 stage-10 egg chambers. They found currents "normally in the range of only 0.1–5 $\mu A/cm^2$" and maximally 10–20 $\mu A/cm^2$.

Materials and Methods

The Canton-S strain of *Drosophila melanogaster* (wild type) were used. They were reared in vials partly filled with a gelatinous mass consisting of 82% water, 9% molasses, 7% cornmeal, 1% yeast, and 0.65% agar cooked at 95°C for 20 min (Doane, 1967). On alternate days of a weekly cycle, the fungicides Tegasept M or propionic acid (0.5%) were added. Just before use extra yeast was added on top of the medium. Adult flies were transferred to fresh vials daily. Eggs collected in these vials were allowed to incubate at room temperature until emergence of the adults. Newly emerged females were transferred to new vials and used as a source of egg chambers on the second or third day.

Females were lightly anesthetized with ether, and restrained with microstaples in a Sylgard dish. Saline (see below) was added and the abdomens opened. The ovaries were dissected out and transferred to a new dish. The ovarioles were teased apart and oocytes isolated. Care was taken to never touch the egg chambers with any dissecting tool. The egg chambers adhered to glass cover slips that had either been coated with polylysine or simply cleaned with ethanol. To position the egg chambers flat on the surface, a stage 14 oocyte would be held by its "ears" (= the dorsal, or chorionic, appendages) and the body of the oocyte used to gently tap down the experimental egg chamber.

Experiments were done predominantly in Robb's medium (Robb, 1969) since this was used by Overall and Jaffe (1985) and by Bohrmann *et al.* (1986) or in a medium developed by us (see below). Our medium was optimized for egg chamber development from stage 9 or 10 to stage 14. In our medium about 50% of egg chambers develop from stage 10 to 14. A lesser percentage, about 20%, develop from stage 9. Failing to find large currents in these media, we also tried Robb's saline (Robb, 1969), then a medium suggested by L. Jaffe, and a saline optimized by us for electrophysiology. Our first batch of Robb's medium (a gift from W. H. Petri, Boston College) had been kept frozen for some time. Since large currents were not found in this medium, L. Jaffe suggested to us that it may have deteriorated. Accordingly, we prepared and used a new batch of Robb's medium. Significant differences in the results were not noted with any of the media.

Composition of the media (Sun and Wyman medium)

NaOH: 45 m*M*; KOH 14 m*M*; $CaCl_2$: 8 m*M*; $MgCl_2$: 13 m*M*; $MgSO_4$: 2 m*M*; NaH_2PO_4: 0.25 m*M*; $NaHCO_3$: 1 m*M*; HEPES Acid: 10 m*M*; glutamic acid: 45 m*M*; glucose: 20 m*M*; fructose: 10 m*M*; sucrose: 20 m*M*; phenol red: 2 mg; yeastolate: 2 g (Difco Labs, Detroit, Michigan); Lactalbumin hydrolysate 2 g (Gibco Labs, Grand Island, New York). Add distilled water to make up to 750 ml. Add this to 250 ml of Medium M199 (w/o $NaHCO_3$) (Sigma Tisue Culture Reagents M5017) to make one liter. For culture take 90 ml of above and add 10 ml of fetal bovine serum. Protein from serum was found to rapidly coat vibrating probe and make it inoperable. During experiments replace serum with 10 ml of 2 m*M* sucrose solution. In both cases adjust pH to 7.1 with NaOH or HCl. *Sun and Wyman saline:* NaCl: 58.5 m*M*;

Table I

Signals recorded with vibrating probe around stage-10 egg chambers

Current density—component normal to surface—$\mu A/cm^2$													
Oocyte half						Nurse cell half							
Inward vectors		Outward vectors		All vectors		Inward vectors		Outward vectors		All vectors		Pattern	
n	Mean ± S.E.	n	Mean ± S.E.	n	Mean ± S.E.	n	Mean ± S.E.	n	Mean ± S.E.	n	Mean ± S.E.	elements?	Fig #
3	0.21 ± .06	6	0.56 ± 0.11	9	+0.37 ± 0.13	6	1.38 ± 0.78	3	0.32 ± 0.12	9	−0.82 ± 0.58	None	5B
0		5	1.44 ± 0.15	5	+1.44 ± 0.15	3	1.63 ± 0.16	0		3	−1.63 ± 0.16	Reverse	6A
0		6	1.46 ± 0.60	7	+1.46 ± 0.60	5	1.13 ± 0.34	3	1.02 ± 0.73	8	−0.32 ± 0.50	Reverse	6D
3	0.59 ± 0.27	1	1.08	5	−0.14 ± 0.36	5	2.02 ± 0.29	1	0.41	6	−1.61 ± 0.47	None	
3	0.77 ± 0.25	1	0.27	4	+0.64 ± 0.22	7	0.97 ± 0.14	1	0.27	8	−0.88 ± 0.15	Reverse	6B
5	0.54 ± 0.14	2	1.12 ± 0.04	7	−0.07 ± 0.03	4	0.58 ± 0.18	0		4	−0.58 ± 0.18	None	
6	0.50 ± 0.13	5	1.02 ± 0.21	11	+0.19 ± 0.26	4	0.61 ± 0.12	0		4	−0.61 ± 0.12	None	
5	1.11 ± 0.34	3	0.63 ± 0.36	8	−0.46 ± 0.47	8	3.82 ± 1.02	1	2.73	9	−3.09 ± 1.15	None	
5	0.92 ± 0.20	2	2.38 ± 0.20	7	+0.02 ± 0.63	9	0.78 ± 0.18	0		9	−0.78 ± 0.18	None	
5	0.89 ± 0.33	3	0.72 ± 0.33	8	−0.29 ± 0.37	8	3.88 ± 1.09	1	1.90	9	−3.66 ± 0.99	None	
5	1.01 ± 0.35	4	0.61 ± 0.26	9	−0.29 ± 0.36	0		6	0.76 ± 0.24	6	+0.76 ± 0.22	Return	7D
5	5.48 ± 1.54	8	1.38 ± 0.37	13	−1.32 ± 1.17	5	0.48 ± 0.23	1	0.54	6	−0.32 ± 0.26	None	
2	0.40 ± 0.14	6	0.40 ± 0.13	8	+0.20 ± 0.16	4	0.67 ± 0.13	4	0.24 ± 0.04	8	−0.21 ± 0.18	Reverse	6C
3	0.23 ± 0.04	3	1.24 ± 0.19	6	+0.51 ± 0.34	12	0.87 ± 0.15	0		12	−0.87 ± 0.15	None	
3	1.54 ± 0.60	4	0.56 ± 0.09	7	−0.34 ± 0.48	2	1.63 ± 0.82	5	0.90 ± 0.20	7	+0.18 ± 0.52	None	
7	0.82 ± 0.20	0		7	−0.82 ± 0.20	2	0.23 ± 0.04	6	0.75 ± 0.28	8	+0.52 ± 0.26	Return	7B
5	3.26 ± 0.46	3	0.76 ± 0.15	8	−1.71 ± 0.79	0		8	2.59 ± 0.45	8	+2.59 ± 0.45	Return	7A
6	5.61 ± 1.06	2	3.64 ± 0.92	8	−3.28 ± 1.71	0		12	2.08 ± 0.19	12	+2.08 ± 0.19	Return	
3	0.40 ± 0.11	4	1.29 ± 0.52	7	+0.64 ± 0.46	0		5	1.22 ± 0.27	5	+1.22 ± 0.27	None	
7	0.64 ± 0.14	3	0.39 ± 0.17	10	−0.33 ± 0.19	7	0.77 ± 0.15	0		7	−0.77 ± 0.15	None	5A
9	0.73 ± 0.18	0		9	−0.73 ± 0.18	5	1.28 ± 0.24	8	0.74 ± 0.11	14	+0.01 ± 0.29	Return	7C
3	0.59 ± 0.05	7	1.17 ± 0.30	11	+0.81 ± 0.26	0		10	1.26 ± 0.12	10	+1.26 ± 0.12	None	5C
6	0.43 ± 0.05	2	0.20 ± 0.06	9	−0.17 ± 0.12	1	0.27	10	0.46 ± 0.07	12	+0.41 ± 0.07	Return	
7	3.68 ± 0.91	0		7	−3.68 ± 0.91	3	0.67 ± 0.62	3	1.13 ± 0.12	6	+0.90 ± 0.30	Return	3
4	0.61 ± 0.20	2	0.30 ± 0.03	6	−0.31 ± 0.22	3	0.48 ± 0.04	3	0.22 ± 0.08	6	+0.12 ± 0.15	None	1
0		9	0.76 ± 0.07	9	+0.76 ± 0.07	8	0.74 ± 0.13	0		8	−0.74 ± 0.13	Reverse	2
1	0.27	6	0.64 ± 0.08	7	+0.51 ± 0.15	12	0.61 ± 0.06	0		12	−0.61 ± 0.06	Reverse	
5	2.18 ± 0.49	0		5	−2.18 ± 0.49	1	0.81	4	1.98 ± 0.45	5	+1.42 ± 0.65	Return	
5	1.80 ± 0.40	0		5	+1.80 ± 0.40	0		4	1.92 ± 0.55	4	+1.92 ± 0.55	None	
3	0.42 ± 0.06	8	0.37 ± 0.04	12	+0.15 ± 0.11	4	0.41 ± 0.09	5	0.44 ± 0.13	10	+0.06 ± 0.16	None	5D
3	0.21 ± 0.03	5	0.90 ± 0.14	9	+0.43 ± 0.20	5	0.83 ± 0.19	2	0.41 ± 0.05	9	−0.37 ± 0.21	Reverse	
11	0.61 ± 0.13	2	0.37 ± 0.19	14	−0.43 ± 0.14	4	0.66 ± 0.09	14	0.59 ± 0.12	9	−0.09 ± 0.28	None	
5	1.92 ± 0.78	6	0.90 ± 0.28	11	−0.38 ± 0.57	3	1.30 ± 0.63	4	0.75 ± 0.21	7	−0.13 ± 0.45	None	
5	0.20 ± 0.03	5	0.23 ± 0.05	10	+0.02 ± 0.08	0		9	0.57 ± 0.06	9	+0.57 ± 0.06	None	

In the two "All Vectors" columns + indicates an outward average while − indicates an inward average.

KCl: 2.7 m*M;* $CaCl_2$: 5 m*M;* $MgCl_2$: 17 m*M;* pH: 7.1. *As suggested by L. Jaffe:* NaCl: 100 m*M;* KCl: 25 m*M;* $CaCl_2$: 10 m*M;* $MgCl_2$: 15 m*M;* pH: 7.1.

Measurements were performed at the National Vibrating probe facility at the Marine Biological Laboratory in Woods Hole (Dr. Lionel Jaffe, director). We used both of the two dimensional vibrating probes at the facility. The computerized apparatus produces a picture of the oocyte with the current vectors superimposed. It also prints out a list of the position of the probe at the time of measurement, the X and Y components of the current vector, and the total length and angle of the resultant current vector.

Results

We took vibrating probe measurements from 50 stage-10 egg chambers. Each egg chamber generated a different pattern of measurements; there is no "typical" pattern to present. However, there was a typical magnitude of the currents. The measurements made around an egg chamber that had typically *sized* current vectors is shown in Figure 1. The arrows represent the magnitude and direction of the currents at different points. The currents in this preparation were all less than 1.14 microamperes/cm^2 and no particular pattern of current flow is evident. In 34 of our cases (Table I), measurements and photographs were taken in the same horizontal plane as shown

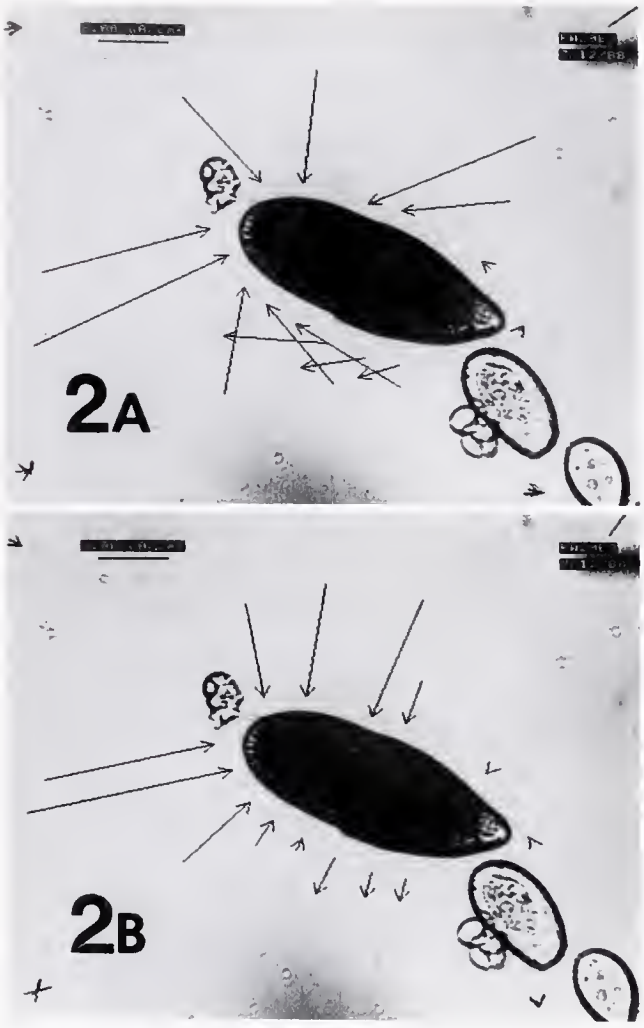

Figure 2. Stage-10 egg chamber showing our best example of a current pattern that could be responsible for returning an intrafollicular transport current. Scale bars: 3 μA/cm^2; 80 microns. (A) Vectors, as originally obtained, showing two dimensions of current flow. (B) Normalized vectors showing only current component perpendicular to egg chamber surface.

in Figure 1; measurements taken with the eggs oriented vertically showed similarly sized currents and no particular pattern (further examples are shown in Figs. 5A–D). Table I presents data on the current vectors around the anterior and around the posterior hemispheres (see below). Most of the measurements were on the order of 1 microampere/cm^2. This magnitude is at or below the limit of reproducibility of the measurements. No consistent direction of current flow appeared in our set of measurements. By simply averaging all the vectors over each half of the egg chamber we found that 10 egg chambers had mean inward currents over the oocyte half and mean outward currents over the nurse cell half. Eleven egg chambers had average currents in the reverse direction.

The vectors in Figure 1 are the resultant vectors derived from a probe vibrating in two dimensions. Previous reports have used measurements from a one dimensional probe; in these reports only the component of current normal to the egg chamber surface was measured. Of course, having both dimensions of data provides a better basis for evaluating the presence or absence of a pattern. However, to compare our data with those previously reported, it was possible for the cases shown in Table I, to resolve our vectors into normal (perpendicular to the egg chamber surface) and parallel components. Figures 2 and 3 show the vectors before and after the normalization procedure.

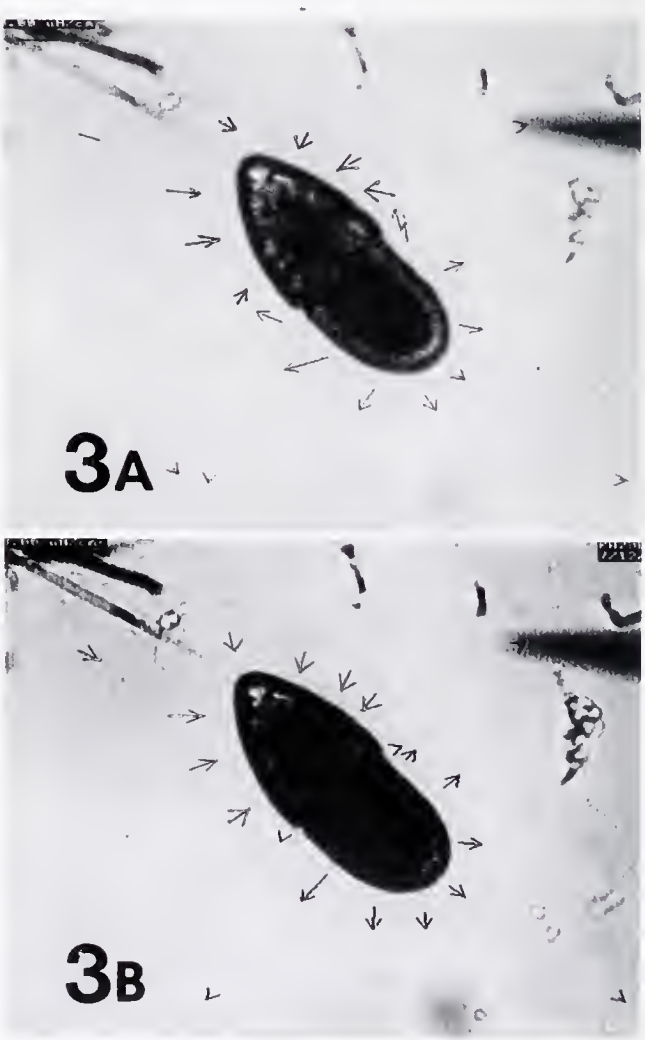

Figure 3. Stage-10 egg chamber showing our best example of a current pattern that is the reverse of that shown in Figure 2. These currents are similar in pattern, but smaller in size than those shown in Figure 4 of Overall and Jaffe (1985). Scale bars: 3 μA/cm^2; 80 microns. (A) Vectors, as originally obtained, showing two dimensions of current flow. (B) Normalized vectors showing only current component perpendicular to egg chamber surface.

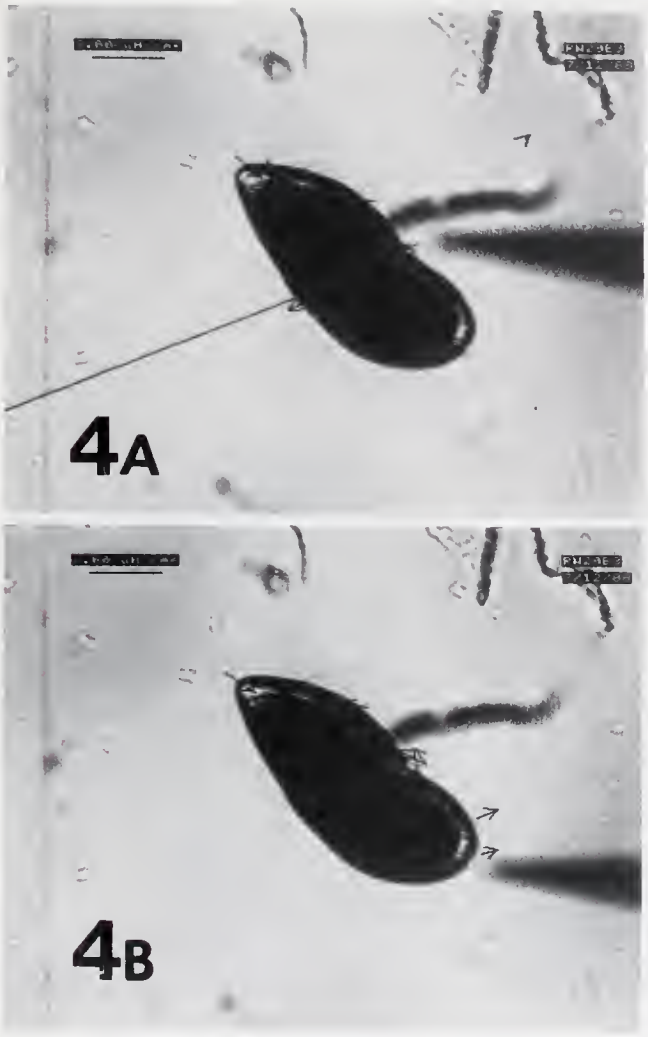

Figure 4. Stage-10 egg chamber with currents induced by contact with the vibrating probe. The photographs were taken while the probe was vibrating. The size of the probe tip and the magnitude of its vibration can be compared with the size of the egg chamber. Scale bars: 3 $\mu A/cm^2$; 80 microns. (A) The probe made contact at the upper right equator of the egg chamber and induced a large (117 $\mu A/cm^2$) inward injury current. The base of the current vector runs through the egg chamber and is not visible. It extends out of the field of view to the lower left. (B) Twenty-three minutes later, several measurements were again taken at the wound site. They are now less than 1.0 $\mu A/cm^2$.

To prepare Table I, vectors over the oocyte half and the nurse cell half were considered separately. All current vectors were first normalized. In most cases each half had both inward and outward vectors. Table I presents the mean and standard error of the normal component for vectors whose normal component was outward and for those whose normal component was inward; the mean and standard error for all vectors (including those which were parallel to the egg surface and therefore had a zero normal component) are also presented.

Even though our set of measurements was predominantly characterized by small and variable currents, it was possible to pick out some egg chambers that appear to show patterns of current flow. Although all the currents were of small size, the current flow around some egg chambers appeared to be predominantly inward near the oocyte pole and predominantly outward over the nurse cell pole. This pattern (called "return") would be what is required for extra-follicular return of an electrophoretic current. Other egg chambers (called "reverse") appeared to be surrounded by oppositely directed currents; these are similar to the nurse cell inward patterns found by Overall and Jaffe (1985). Our "best" examples of these two categories are shown in Figures 2 and 3 (further examples are shown in Figs. 6A–D, 7A–D). The maximum normal current vector in a "return" type pattern (oocyte inward) was 9.1 microamperes/cm^2. The maximum normal current vector found in a "reverse" type pattern (nurse cell inward) was 4.1 microamperes/cm^2 compared to 62 microamperes/cm^2 in the best case pattern of the same type from Overall and Jaffe (1985). If measurements from egg chambers with even smaller current vectors or less clear patterns than those shown in Figures 2 and 3 were to be assigned to either category, it might be possible to say that an additional seven egg chambers have some elements of the "return" type pattern and an additional six have some elements of the "reverse" type pattern. To infer that a pattern actually exists for this many cases, one would have to accept as patterned the currents around egg chambers where the average vector was only 0.29 microamperes/cm^2 ("return" type patterns) or 0.21 microamperes/cm^2 ("reverse" type patterns). The change in our reference vectors (control measurements taken far from the egg chamber) from beginning to end of a set of measurements was often larger than these magnitudes, so assignment of pattern at this level is clearly marginal. Yet a third pattern that occurred sometimes showed the largest vectors to be outwardly directed from the equator of the egg chamber (the oocyte—nurse cell boundary). Measurements from the majority of egg chambers could not be assigned to any category.

The possibility that some of the measurements were due to injury currents must always be considered. To generate a controlled and localized injury, we used the vibrating probe itself. Since the dimension of the probe tip is about 10–15 micrometers and its vibration amplitude is approximately the same, it can be used to distend the membrane by those dimensions. We moved the probe toward the surface of the oocyte until it barely touched. The injury currents produced in this way (Fig. 4A) were an order of magnitude larger (117 microamperes/cm^2) than anything else we measured. However, in our medium, with high calcium and magnesium, the injury current declined and was below 1 microampere/cm^2 within 30 min (Fig. 4B). Healing may be less rapid in

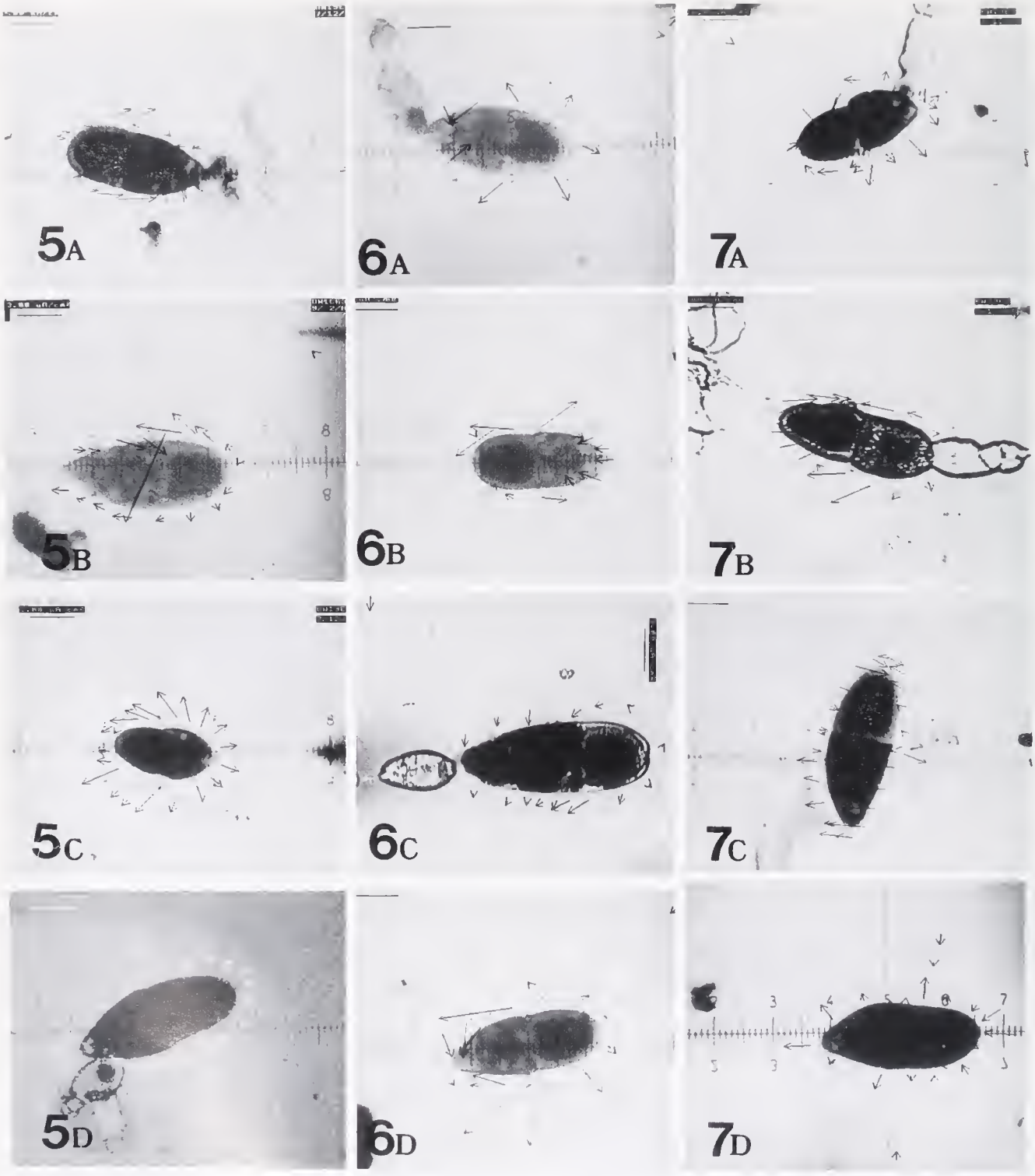

Figures 5, 6, and 7. These figures show a variety of egg chambers and the currents measured around them. Vectors have not been normalized. Column 6 shows egg chambers with some aspects of the "reverse" pattern while column 7 shows egg chambers with some aspects of the "return" pattern. Column 5 shows egg chambers that could not be assigned to either column 6 or 7. Although the egg chambers of column 6 and 7 are labelled "reverse" or "return" in Table I, and are typical of those so labelled, we do not mean to imply that a clear pattern exists. For instance the limits of assignment are clearly stretched for 6B, which shows current inward to the nurse cells, but does not show outward current from the oocyte, and for 7C, which shows current inward at the oocyte, but not outward from the nurse cells. Scale bars: 3 $\mu A/cm^2$ except for 5D which is 2 $\mu A/cm^2$ and 7D which is 10 $\mu A/cm^2$.

Robb's medium and saline, which is very low in divalent cations. This type of injury can thus be recognized by its extreme magnitude, very focal localization, and time course of healing. We do not know how to recognize injury currents that may be due to more diffuse injuries or those caused by distensions smaller than 15 micrometers.

Discussion

Our data do not show the presence of a consistent pattern of ionic current surrounding the stage-10 *Drosophila* egg chamber. Our results are concordant in magnitude with those found by Bohrmann *et al.* (1986), but we were unable to find the larger currents reported by Overall and Jaffe (1985). We found small size and great variability in the signals; we could not find a consistent current pattern arising out of the unpatterned background. There are a variety of differences in the procedures used by the three different groups. These include strain of flies, feeding regimen, anaesthetic used, dissection procedure, and vibrating probe used. We conclude that the variables involved in this phenomenon are not yet well enough understood to establish the conditions in which the different magnitudes and patterns of current flow found by different researchers can be obtained.

Acknowledgments

We are especially grateful to the director of the National Vibrating Probe Facility, Dr. Lionel Jaffe, to the managing director, Mr. Alan Shipley, and to staff member Mr. Eric Karplus. Without their efficient, competent, and friendly help this research could not have been completed.

Literature Cited

Bohrmann, J., A. Dorn, K. Sander, and H. Gutzeit. 1986a. The extracellular electrical current pattern and its variability in vitellogenic *Drosophila* follicles. *J. Cell Sci.* **81:** 189–206.

Bohrmann, J., E. Huebner, K. Sander, and H. Gutzeit. 1986b. Intracellular electrical potential measurements in *Drosophila* follicles. *J. Cell Sci.* **81:** 207–221.

Doane, W. W. 1967. *Drosophila.* Pp. 219–244 in *Methods in Developmental Biology,* F. Wilt and N. Wessels, eds. Crowell, New York.

Jaffe, L. F., and R. I. Woodruff. 1979. Large electrical currents traverse developing *Cecropia* follicles. *Proc. Natl. Acad. Sci. USA* **76:** 1328–1332.

King, R. C. 1970. *Ovarian Development in* Drosophila melanogaster. Academic Press, New York. 227 pp.

Overall, R., and L. F. Jaffe. 1985. Patterns of ionic current through *Drosophila* follicles and eggs. *Dev. Biol.* **108:** 102–119.

Robb, J. A. 1969. Maintenance of imaginal wing disks of *Drosophila melanogaster* in chemically defined media. *J. Cell Biol.* **41:** 876–885.

Verachtert, Barend, and Arnold De Loof. 1989. Intra- and extracellular electric fields of vitellogenic polytrophic insect follicles. *Biol. Bull.* **176**(S): 000–000.

Woodruff, R. I., and W. H. Telfer. 1973. Polarized intercellular bridges in ovarian follicles of the cecropia moth. *J. Cell Biol.* **58:** 172–188.

Woodruff, R. I., and W. H. Telfer. 1974. Electrical properties of ovarian cells linked by intercellular bridges. *Ann. N. Y. Acad. Sci.* **238:** 408–419.

Woodruff, R. I., and W. H. Telfer. 1980. Electrophoresis of proteins in intercellular bridges. *Nature* **286:** 84–86.

Woodruff, R. I., E. Huebner, and W. H. Telfer. 1986. Ion currents in *Hyalophora* ovaries: the role of the epithelium and the intercellular spaces of the trophic cap. *Dev. Biol.* **117:** 405–416.

Woodruff, R. I., J. H. Kulp, and E. D. LaGaccia. 1988. Electrically mediated protein movement in *Drosophila* follicles. *Roux's Arch. Dev. Biol.* **197:** 231–238.

Reference: *Biol. Bull.* **176(S):** 86–90. (April, 1989, Suppl.)

Pattern and Composition of Ionic Currents Around Ovarioles of the Hemipteran, *Rhodnius prolixus* (Stahl)

W. DIEHL-JONES AND E. HUEBNER

Department of Zoology, University of Manitoba, Winnipeg, Manitoba Canada R3T 2N2

Abstract. Two-dimensional vibrating probe analysis of extracellular currents around *Rhodnius prolixus* ovarioles correlated with an earlier one-dimensional analysis but revealed asymmetrical circumferential current patterns and large tangential currents. Na^+, K^+, and Ca^{+2} have been tentatively identified as the major ions involved in these currents, with Na^+ being the major ion involved in current efflux.

Introduction

A variety of insect ovarioles have been shown to possess ionic currents with the pattern of current flow generally correlated with developmental events (Jaffe and Woodruff, 1979; Overall and Jaffe, 1985; Huebner and Sigurdson, 1986; Kunkel, 1986; Verachtert and De Loof, 1986). Several possible roles have been attributed to extracellular ion currents, among them intracellular transport, regulation of vitellogenesis and chorionation, and establishment of pattern formation (Jaffe, 1981; Gutzeit, 1986). A thorough understanding of the current patterns and pathways in these tissues is necessary before direct links between ion currents and developmental events can be established. In addition, the question arises as to whether voltage and/or ion gradients are causative factors influencing development, or whether they are merely epiphenomena of other morphogenetic processes (Harold, 1986). Consequently, it is also necessary to characterize the current-carrying ions and the manner in which they cross the cell membrane.

Huebner and Sigurdson (1986) previously used the one-dimensional vibrating probe to map at least two current circuits in intact ovarioles of the hemipteran insect *Rhodnius prolixus*. We now present preliminary data from an ongoing two-dimensional (2-D) vibrating probe analysis of extracellular currents around *Rhodnius* ovarioles, and initial findings on the ionic composition of these currents.

Materials and Methods

Ovarioles of adult *Rhodnius prolixus* were dissected in a modified *Rhodnius* Ringers (O'Donnell, 1985) and desheathed immediately prior to each experiment. This saline was chosen over that initially used by Huebner and Sigurdson (1986) because the new saline sustained contractions and extracellular currents over a longer period than the previous Ringers (unpub. results) and with the elimination of $NaHCO_3$ the vibrating probe electrode tip stayed cleaner in the new Ringers. Ovarioles were placed in a plexiglass flow-through recording chamber based partly on a design by Elizabeth Bowden and Alan Shipley. It consisted of a lower specimen chamber and an upper fluid reservoir; medium could be exchanged either by means of a peristaltic pump or through a push-pull syringe system. Platinum-blacked reference and ground electrodes were incorporated into the chamber, and temperature could be monitored with a small thermistor (YSI). The recording chamber attached to a plexiglass gliding stage on an inverted phase contrast microscope (Zeiss IM35). The microscope and probe manipulator assembly rested on a vibration-free table (Micro-G).

Two-dimensional vibrating probe measurements were made with equipment purchased from the Vibrating Probe Company (Davis, California); this consisted of a low noise differential FET preamplifier (gain = 10) connected to a two phase lock-in amplifier (Model NR-2000). Lock-in outputs were digitized with a Labmaster A-D converter (Tekmar Co., Solon, Ohio), and were analyzed by an IBM PCXT computer. Video images were recorded with an AG-6050 Panasonic time lapse recorder. In-phase and quadrature outputs were monitored on a dual channel oscilloscope (Telequipment). A glass current-injecting microelectrode linked to a WPI iontophoresis module were used for probe calibration.

The 2-D current pattern around ovarioles at different

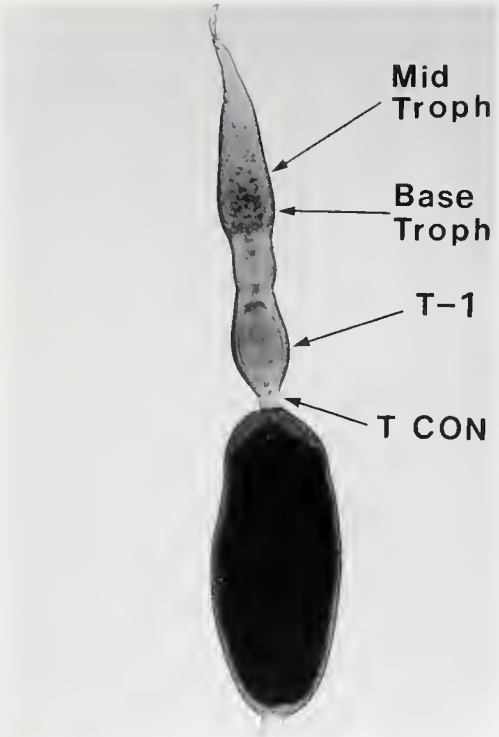

Figure 1. Recording positions used for ion substitution and inhibitor experiments. T CON = T-connective; T-1 = T-1 or penultimate follicle; Base Troph = base of tropharium; Mid Troph = middle of tropharium (micrograph from Telfer *et al.*, 1981).

stages of development was mapped along the length of each ovariole and at 4 circumferential positions. This was accomplished by attaching a suction pipette to the pedicel at the base of the terminal follicle (nearest the oviduct) and by placing a glass weight on the terminal filament. After recording along one side of an ovariole, it was rotated 90° on the longitudinal axis and measurements repeated along the length. As a reference point each ovariole was oriented according to the position of the trophic cord in the penultimate or T-1 oocyte. Approximately 5 ml of fresh Ringers was perfused through the recording chamber each time an ovariole was rotated.

For the ion substitution and inhibitor experiments, ovarioles in late vitellogenesis (T-follicle length = 1000–1500 μm) were affixed to glass slides coated with high molecular weight poly-L lysine (Sigma). Recordings were made at four locations along the ovariole: the T-connective (T CON), which usually displayed strong outward currents; the middle of the penultimate (T-1) follicle, which usually exhibited influxes at this stage; the basal portion of the tropharium (Base Troph); and the middle of the tropharium (Mid Troph) (Fig. 1). Both of the latter positions usually exhibited current influxes.

Initial current measurements were made in control Ringers, after which 10 ml, or roughly three times the volume of the recording chamber, of experimental medium was exchanged over a 2-min interval with a push-pull syringe system. Recordings were then repeated at 10-min intervals over 30 min. Following this, experimental media were replaced with control Ringers and the measurements repeated. Composition of the experimental media is listed in Table I. A one-way analysis of variance was used to determine if current magnitudes were significantly different from controls ($P > 0.05$).

Results

2-D current patterns

Due to limited space, this report will only present selected aspects of the current pattern around ovarioles in early, middle, and late stages of vitellogenesis. In general, results obtained in the present study with the 2-D vibrating probe correspond well with that obtained in an earlier study (Huebner and Sigurdson, 1986). However, an examination of currents around the circumference of each ovariole revealed radial asymmetries in current pattern and strong longitudinal components of current vectors which had been previously undetected. A typical early vitellogenic ovariole (T-follicle length = 400–500 μm) exhibited a stronger current efflux over the area opposite to the trophic cord than over other sides at the same position (Fig. 2A–D). In the same ovariole, current entered the region around the T-1 or penultimate follicle over the area closest to the trophic cord while current influx was apparent on the other three quadrants. In a typical mid-vitellogenic ovariole (T-follicle length = 800–900 μm), current efflux at the T-connective and influx over the tropharium showed marked increases from that observed in earlier stages (Fig. 3A–D). Inward currents were observed in the lower third of the tropharium over the area next to the T-connective. In addition,

Table I

Composition of experimental media (concentrations in mmol l^{-1})

	Control	Na^+-free	K^+-free	Mg^{+2}-free	Ca^{+2}-free
NaCl	129	—	129	129	129
KCl	8.6	8.6	—	8.6	8.8
$MgCl_2$	8.5	8.5	8.5	—	8.5
$CaCl_2$	2	2	2	2	—
Glucose	34	34	34	34	34
BIS-TRIS	15	15	15	15	15
Choline Cl	—	129	129	—	—
$MnCl_2$	—	—	—	8.5	—
$BaCl_2$	—	—	—	—	2

Saline containing cobalt (10 mmol l^{-1}) was made by direct addition to control. pH was adjusted to 6.8 by addition of 1 *N* HCl.

* Bis (2-hydroxyethyl)imino tris (hydroxymethyl) methane. Salines were made equi-osmotic by addition of glucose.

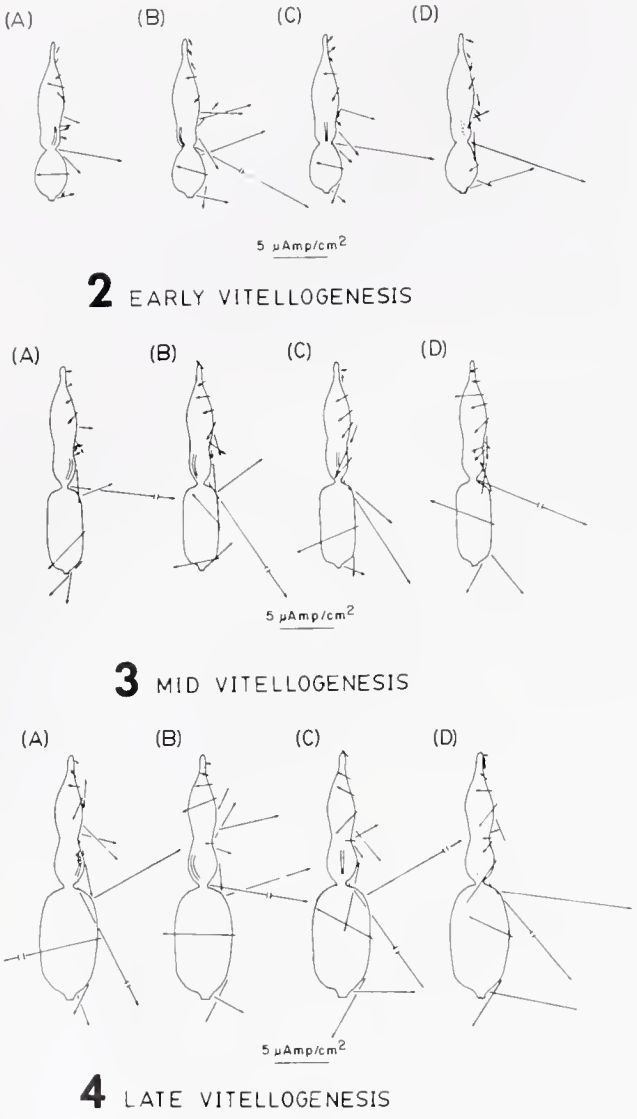

Figure 2. Extracellular current pattern around an early vitellogenic ovariole. (a) = side next to trophic cord; (b) = side opposite to trophic cord; (c) = side 90° clockwise from the trophic cord; (d) = side 90° counterclockwise from the trophic cord. Direction and length of the arrows indicate the direction and magnitude of current density.

Figure 3. Extracellular current pattern around a mid vitellogenic ovariole. Position information in Figure 2.

Figure 4. Extracellular current pattern around a late vitellogenic ovariole. Position information in Figure 2.

entry currents in the prefollicular regions 90° to the right and left of the trophic cord were stronger than have been hitherto reported, and had large longitudinal components.

Around a typical late vitellogenic ovariole (T-follicle length = 1000–1500 μm), current influx over the tropharium increased markedly, and larger (5–8 μA/cm²) currents than have been previously reported were observed over the T-1 follicle; these currents had large tangential components (Fig. 4A–D).

Ion substitutions

Replacement of Na^+ with choline, an impermeant cation, resulted in significant decreases in current efflux at the T-connective and no significant changes in current influx (Fig. 5). Furthermore, current influxes at the T-connective were observed in three of the six ovarioles. Gross signs of tissue swelling were observed in all ovarioles by 10 min post-exposure. By 40 min post-exposure, or 10 min after being returned to control saline, the T-connective current returned to normal values while current influxes at the other three recording positions were slightly, but not significantly, elevated. By contrast, replacement of K^+ with choline had no significant effect on current magnitude (results unpub.). The addition of Co^{+2}, a Ca^{+2} channel blocker, resulted in a significant decrease in current efflux at the T-connective, but did not significantly alter current influx (Fig. 5). Replacement of Ca^{+2} with Ba^{+2}, however, yielded a significant increase of current influx over the tropharium, but did not significantly alter current efflux at the T-connective. Replacement of Mg^{+2} with Mn^{+2} did not result in any significant differences in current density (unpub. results).

Ion inhibitors

Exposure to ethacrynic acid, an inhibitor of Na^+ transport not dependent on K^+ (Gee, 1976), caused a significant decrease in both current influx and efflux, the change being most noticeable at the T-connective (Fig. 5). Ouabain, a Na^+/K^+ ATPase inhibitor (Kline *et al.*, 1983), did not cause significant changes in current efflux, but resulted in a dramatic increase in current influx over the tropharium by 20 min post-exposure; this effect was reversed by 60 min post-exposure, or by 30 min recovery in control Ringers (Fig. 5). Current efflux in ovarioles exposed to TEA, which blocks voltage-dependent and some Ca^{+2}-dependent K^+ channels (O'Donnell, 1986), showed a marked decrease, and did not fully recover after perfusion of control Ringers. Current influx over the tropharium was slightly but not significantly elevated after perfusion of control Ringers. Ovarioles exposed to 4-aminopyridine, a K^+ channel blocker (O'Donnell, 1986), showed a significant decrease in current density at the T-connective only by 30 min post-exposure; an increase in current efflux at the base of the tropharium was significant only at 50 min. Exposure of ovarioles to furosemide, which inhibits Cl^- transport (Komukai *et al.*, 1985), resulted in a significant increase in current influx by 20 and 30 min post-recovery in control Ringers (Fig. 5).

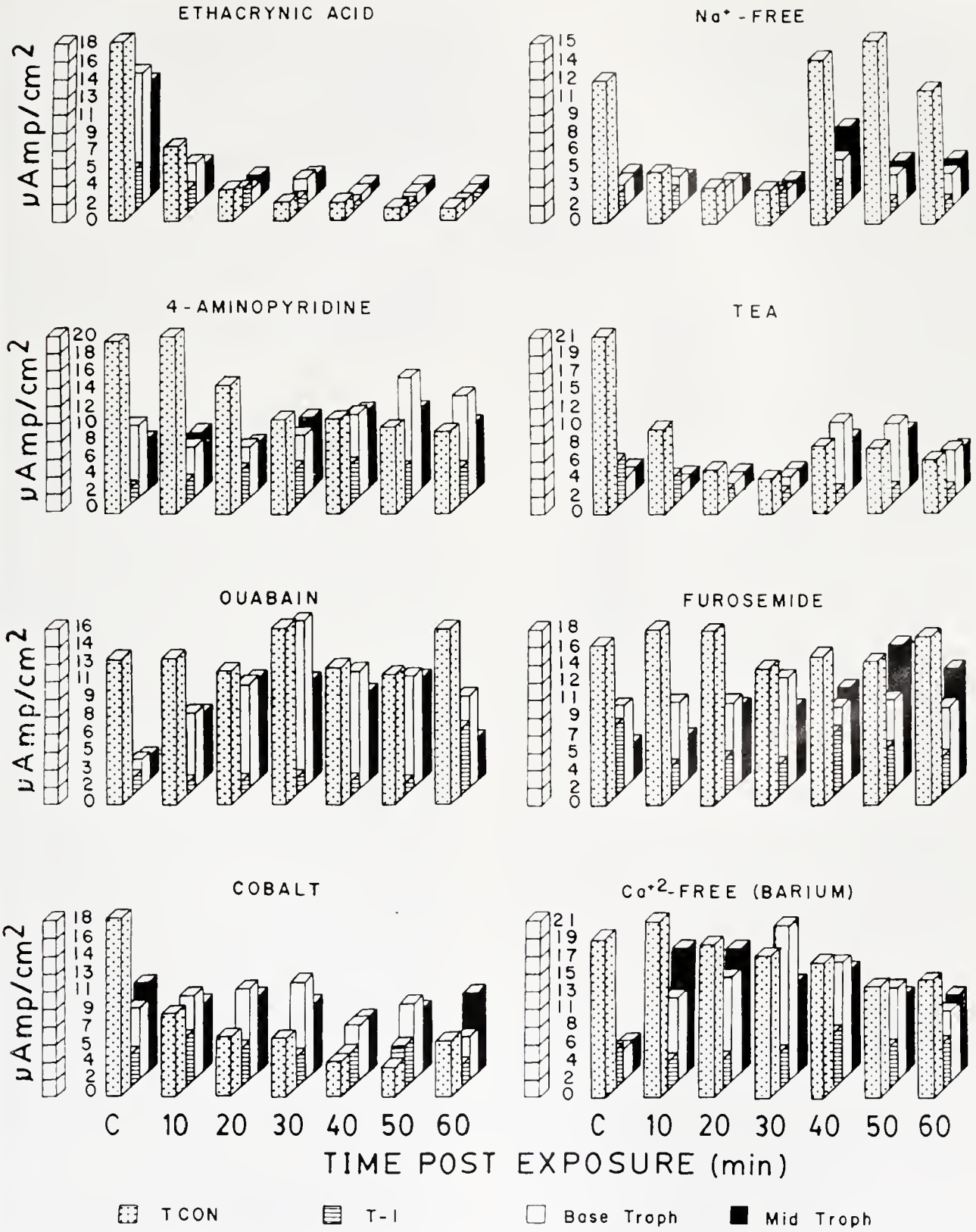

Figure 5. Effect of ion substitutions and inhibitors on extracellular currents at the T-connective (T-con), T-1 follicle (T-1), basal portion of the tropharium (Base Troph) and middle of the tropharium (Mid Troph). Five replicates per experiment. C = control medium. At times 10, 20, and 30 post exposure ovarioles were in experimental media, after which the medium was replaced with control medium.

Discussion

Preliminary data from our 2-D vibrating probe analysis of *Rhodnius* ovarioles compared well with previous data, although the current pathways now appear to be more complex than previously shown. Novel findings emerging from our present study include the apparent radial asymmetry in current direction and magnitude, and the large tangential inward currents at the T-1 follicle which were hitherto undetected by the 1-D vibrating probe. It is tempting to speculate on a link between current asymmetry and the trophic cord; this would have implications in the electrophoretic migration of charged molecules which has been demonstrated in *Rhodnius* and Cecropia ovarioles (Telfer *et al.*, 1981); however, further experimentation is clearly necessary before a definitive link is possible. The discovery of the large tangential component of some influx currents over the T-1 follicle and also over the tropharium may be of importance in completely delineating the current pathways in *Rhodnius* ovarioles.

At least three ionic species are involved in the extracellular currents around *Rhodnius* ovarioles: Na^+, K^+, and Ca^{+2}. From evidence obtained thus far, it is likely that Na^+ leaves the T-connective via an active transport mechanism not dependent on K^+. The situation for Ca^{+2} and K^+ has not yet been resolved. A passive entry of Ca^{+2} is suggested by the increase in inward current over the tropharium in Ca^{+2}-free Ringers containing Ba^{+2}. Barium has a hydrated radius similar to that of Ca^{+2}, and is well known to substitute for Ca^{+2} in action potentials (Reuter, 1973). L-type Ca^{+2} channels have an even higher permeability for Ba^{+2} ions (Bean, 1985). A passive Ca^{+2} influx is somewhat inconsistent with the finding that Co^{+2} decreased exit currents at the T-connective while not affecting entry currents at the tropharium. However, O'Donnell (1985) has shown the presence of inward-rectifying Ca^{+2} channels in *Rhodnius* ovarioles. Finally, the possibility also exists that Ca^{+2} may gate still other channels (Peterson *et al.*, 1986).

It is likely that K^+ is also one of the current-carrying ions in the outward flux at the T-connective; both voltage- and Ca^{+2}-gated channels may be involved, since 4-aminopyridine caused a decrease in outward current at the T-connective, but significantly less than that caused by TEA. Ouabain did not reduce current density at the T-connective but increased current efflux over the tropharium suggesting that neither K^+ nor Na^+ currents are dependent on Na^+/K^+-ATPase, but that the inward current over the tropharium is regulated by an equilibrium maintained by this ubiquitous pump.

Fluctuations in current density over the tropharium after exchange of experimental medium for *Rhodnius* Ringers suggest that the inward current may passively follow changes in permeability of other ions and may be responsive to changes in the Goldman equilibrium. Further experiments (including the use of other inhibitors and ion substitutes) are presently underway to refine our understanding of the nature of ion currents around *Rhodnius* ovarioles. Once these have been fully defined, and the origin of ionic currents determined, it will be possible to establish more adequately the link between ion currents and developmental events such as intracellular transport, vitellogenesis, etc.

Acknowledgments

The authors thank Al Shipley and Guy Desrocher for helpful technical advice and Alex Szalai for assistance with data analysis. This research was supported by an NSERC operating grant to EH.

Literature Cited

Bean, B. P. 1985. Two kinds of calcium channels in canine atrial cells. Differences in kinetics, selectivity, and pharmacology. *J. Gen. Physiol.* **86:** 1–30.

Gee, J. D. 1976. Fluid secretion by the Malpighian tubules of the Tsetse fly *Glossina morsitans:* the effects of ouabain, ethacrynic acid and amiloride. *J. Exp. Biol.* **65:** 323–332.

Gutzeit, H. O. 1986. Transport of molecules and organelles in meroistic ovarioles of insects. *Differentiation* **31:** 155–165.

Harold, F. M. 1986. Transcellular ion currents in tip-growing organisms: where are they taking us? Pp. 359–366 in *Ionic Currents in Development,* R. Nuccitelli, ed. Alan R. Liss, Inc., New York.

Huebner, E., and W. Sigurdson. 1986. Extracellular currents during insect oogenesis: special emphasis on telotrophic ovarioles. Pp. 155–163 in *Ionic Currents in Development,* R. Nuccitelli, ed. Alan R. Liss, Inc., New York.

Jaffe, L. F. 1981. The role of ionic currents in establishing developmental pattern. *Phil. Trans. R. Soc. Lond. B* **295:** 553–566.

Jaffe, L. F., and R. I. Woodruff. 1979. Large electrical currents traverse developing Cecropia follicles. *Proc. Natl. Acad. Sci. USA* **76:** 1328–1332.

Kline, D., K. R. Robinson, and R. Nuccitelli. 1983. Ion currents and membrane domains in the cleaving *Xenopus* egg. *J. Cell Biol.* **97:** 1753–1761.

Komukai, M., A. Fujiwara, Y. Fujino, and I. Yosumasu. 1985. The effects of several ion channel blockers and calmodulin antagonists on fertilization-induced acid release and $^{45}Ca^{2+}$ uptake in sea urchin eggs. *Exp. Cell Res.* **159:** 463–472.

Kunkel, J. G. 1986. Dorsoventral currents are associated with vitellogenesis in cockroach ovarioles. Pp. 165–172 in *Ionic Currents in Development,* R. Nuccitelli, ed. Alan R. Liss, Inc., New York.

O'Donnell, M. J. 1985. Calcium action potentials in the developing oocytes of an insect, *Rhodnius prolixus. J. Exp. Biol.* **119:** 287–300.

Overall, R., and L. F. Jaffe. 1985. Patterns of ionic current through *Drosophila* follicles and eggs. *Dev. Biol.* **108:** 102–119.

Peterson, O. H., I. Findlay, K. Suzuki, and M. J. Dunne. 1986. Messenger-mediated control of potassium channels in secretory cells. *J. Exp. Biol.* **124:** 33–52.

Reuter, H. 1973. Divalent cations as charge carriers in excitable membranes. *Prog. Biophys. Molec. Biol.* **26:** 1–43.

Telfer, W. H., R. I. Woodruff, and E. Huebner. 1981. Electrical polarity and cellular differentiation in meroistic ovaries. *Am. Zool.* **21:** 675–686.

Verachtert, B. and A. DeLoof. 1986. Electrical fields around the polytrophic ovarian follicles of *Sarcophaga bullata* and the panoistic follicles of *Locusta migratoria.* Pp. 173–179 in *Ionic Currents in Development,* R. Nuccitelli, ed. Alan R. Liss, Inc., New York.

Reference: *Biol. Bull.* **176(S):** 91–95. (April, 1989, Suppl.)

Intra- and Extracellular Electrical Fields of Vitellogenic Polytrophic Insect Follicles

BAREND VERACHTERT AND ARNOLD DE LOOF

Zoological Institute, Naamsestraat 59, 3000 Leuven, Belgium

Abstract. Dye-coupling of lucifer yellow between follicle cells and germ cells of the vitellogenic polytrophic follicles of *Sarcophaga bullata, Drosophila melanogaster,* and *Manduca sexta* does not always occur. The electrical field around the follicles of *Sarcophaga bullata* can be modified by altering the ionic composition of the Ringer solution. We propose general model that suggests possible pathways for both intracellular and extracellular current loops.

Introduction

The germ cells of vitellogenic polytrophic insect follicles form a syncytium of one oocyte and a number of nurse cells (typically 7 or 15). Despite the fact that these form a cluster of genetically identical sibling cells, the developing follicle can be characterized as a highly polarized differentiating system.

The polyploidy of the nuclei of the nurse cells can be up to 1024C in *Sarcophaga bullata* (Cardoen *et al.*, 1986) and 30,000C in *Hyalophora cecropia* (Berry, 1982). The value for the germinal vesicle of *Sarcophaga bullata* is 4C. The nuclei of the nurse cells synthesize most of the RNA of the follicle; this RNA is transported unidirectionally towards the oocyte. The follicle cells in the epithelium that surrounds the follicle have a 4C to 16C polyploidy. Sequestration of the vitellogenins from the haemolymph takes place in the oocyte only. The follicle cells are the site of the intraovarian synthesis of the vitellogenins in *Drosophila* (Brennan *et al.*, 1982) and *Sarcophaga* (Huybrechts *et al.*, 1983; Geysen *et al.*, 1987). The differential migration and differentiation of the follicle cells is another asymmetrical aspect of the architecture of the follicle. During the nurse cell collapse, the nurse cells inject their cytoplasmic contents into the oocyte.

The electrical polarity of the system has been described already in a number of species such as *Hyalophora cecropia* (Woodruff and Telfer, 1973; Jaffe and Woodruff, 1979), *Drosophila melanogaster* (Overall and Jaffe, 1985; Bohrmann *et al.*, 1986a, b; Sun and Wymann, 1987; Woodruff *et al.*, 1988) and *Sarcophaga bullata* (Verachtert and De Loof, 1986, 1988).

In this report, we describe an absence of dyecoupling of lucifer yellow between follicle cells and the underlying oocyte of follicles of *Manduca sexta, Drosophila melanogaster,* and *Sarcophaga bullata.* By altering the composition of Ringer solution, the electrical field around all vitellogenic stages of *Sarcophaga* follicles can be modified. We also present a model that suggests possible pathways for both the intra- and the extracellular current loops.

Materials and Methods

Individual follicles were carefully dissected from the ovaries of *Drosophila melanogaster* and *Sarcophaga bullata.* The follicles of *Manduca sexta* were left in their ovarioles with the ovariole sheath removed. The experiments were carried out in the appropriate Ringer solutions at room temperature.

Drosophila melanogaster

Robb's medium (Robb, 1969).

Sarcophaga bullata

S-Ringer: NaCl 121.5 m*M*, KCl 10 m*M*, NaH_2PO_4 1 m*M*, $NaHCO_3$ 10 m*M*, $MgCl_2$ 0.7 m*M*, $CaCl_2$ 2.2 m*M*. The solutions were aerated with 95% O_2/5% CO_2 pH 6.8. In the experimental Ringer solution (E-Ringer) the K^+- and Cl^--concentration were varied according to the Donnan equilibrium so that their produce remained constant: $[K^+][Cl^-] = 1373$ mM^2 (see also Boyle and

Conway, 1941). NaCl 21.9 m*M*, NaH_2PO_4 1 m*M* $NaHCO_3$ 10 m*M*, $MgCl_2$ 0.12 m*M*, $CaCl_2$ 0.37 m*M*, $CaSO_4$ 8.3 m*M*, $MgSO_4$ 0.83 m*M*, Na_2SO_4 3.3 m*M* K_2SO_4 30 m*M*, sucrose 127 m*M*; 95% O_2/5% CO_2; pH 6.8.

Manduca sexta

KCl 40 m*M*, $MgCl_2$ 15 m*M*, $CaCl_2$ 5 m*M* and Tris-succinate 110 m*M*, pH 6.2.

Pressure injection

We used an Eppendorf SL42 Microinjector System to inject lucifer yellow (3% in aqua destillata). The injection pipette was mounted on a hydraulic micromanipulator (Narishige MO-108). Volumes of 10–30 pl were injected into either the oocyte or the nurse cells of follicles of *Sarcophaga bullata*.

The injected follicles were examined by epiillumination fluorescence on a Nikon diaphot-TMD inverted microscope with the appropriate filter cassette.

Vibrating probe

The extracellular electrical field was measured using a one dimensional vibrating probe (Jaffe and Nuccitelli, 1974) with parylene coated metal electrodes. Some experiments were performed with a two-dimensional vibrating probe set up at Woods Hole.

The measurements were performed in a small dish filled with Ringer solution (1 ml). The Ringer solutions were exchanged with syringes while the follicles remained at the same place. After exchange, the probe was allowed to equilibrate for at least 20 min.

Results and Discussion

Dye injection

When lucifer yellow was pressure injected in either the oocyte or the nurse cell compartment of a follicle of *Sarcophaga bullata*, the dye quickly spread throughout the whole follicle in less than 15 min. Sometimes, a few nurse cells were excluded from being stained. Similar observations have been made on *Drosophila melanogaster* and *Manduca sexta* vitellogenic follicles (Fig. 1.).

The spread of lucifer yellow from one germ cell (oocyte or nurse cells) to another occurred via the intercellular bridges or ring channels between the cells. These ring channels form large cytoplasmic connections and present no barrier to the diffusion of lucifer yellow.

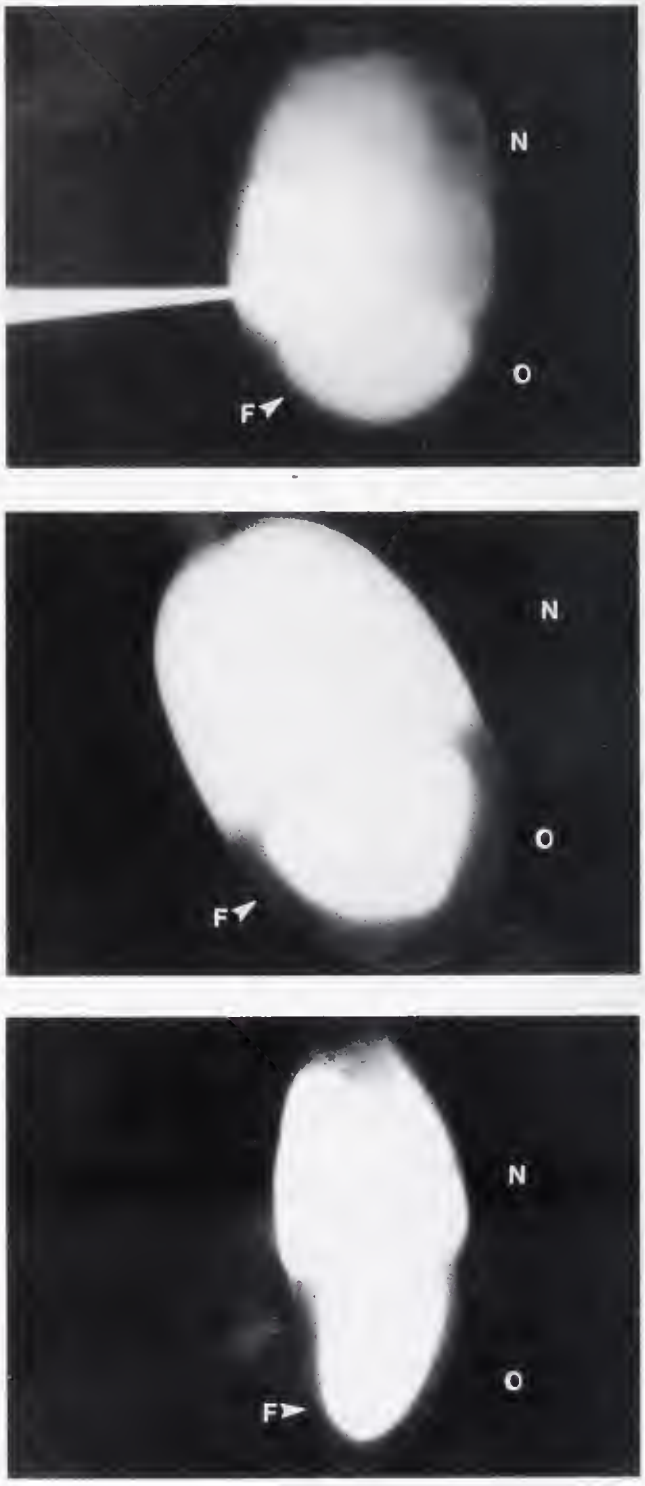

Figure 1. Injection of lucifer yellow into (top) a nurse cell of an early vitellogenic 4A follicle of *Sarcophaga bullata*, (middle) the oocyte of a vitellogenic follicle of *Manduca sexta*, and (bottom) a nurse cell of a vitellogenic 10B follicle of *Drosophila melanogaster*. In each case, the oocyte (O) is at the bottom of the photograph; the nurse cell compartment is at the upper side. The follicle cells (F) around the oocyte do not stain with lucifer yellow.

In *Manduca* and *Drosophila*, dyecoupling of lucifer yellow between follicle cells and the underlying germ cells did not occur. In *Sarcophaga*, dyecoupling was usually observed in 4A follicles and sometimes in 4B and 4C follicles.

These observations confirm partially those of Woodruff (1979) who found that fluorescein, injected in either the oocyte or the nurse cells of *Hyalophora cecropia* follicles, spread to the surrounding follicle cell layer. Dyecoupling of rhodamine between the oocyte and the columnar epithelial follicle cells of *Drosophila melanogaster* was mentioned by Bohrmann and Gutzeit (1987).

In the telotrophic ovariole of the milkweed bug, *Oncopeltus fasciatus*, dyecoupling (lucifer yellow) of epithelial cells to the oocyte begins coincidentally with cord severance and the onset of vitellogenesis (Woodruff and Anderson, 1984).

The question about the generality of the dye-coupling phenomenon between the epithelial follicle cell layer and the maturing oocyte in a follicle remains unanswered.

Nevertheless, we would like to suggest that the lack of dye-coupling in some test systems shows that the epithelial layer and the underlying oocyte can form independent electrical compartments.

Modification of the extracellular electrical field

Only quantitative changes. The electrical field was first measured in S-Ringer. The current densities of the electrical field, after perfusion with E-Ringer (with reduced Cl^- and increased K^+), decreased from 83% to 0% measured at the same locations in S-Ringer. After E-Ringer was exchanged for S-Ringer again, the measured current densities were comparable to those of the original field and sometimes even slightly higher (4A: 10 out of 18 experiments; 4B: 8 of out 15 experiments; 4C: 6 out of 21 experiments).

Quantitative and qualitative changes. In a number of experiments (4A: 8 out of 18; 4B: 6 out of 15; 4C: 14 out of 21), the current densities in E-Ringer not only declined but also reversed direction over a part or the whole of the field. The current was now entering the oocyte surface and leaving the nurse cell compartment. After E-Ringer was exchanged for S-Ringer again, the original situation was re-established.

Some follicles only displayed a partially reversed field. Analysis of the data of the 4C follicles suggests that the concave (future dorsal) side of the follicle reverses its field followed by the convex (future ventral) side. Subsequently, the reversal goes from the middle part of the follicle towards both poles. It seems that the reversal of the electrical field goes through a gradual succession of different stages. It is unclear why several follicles only undergo a partial reversal.

In a few experiments (4B: 1 out of 14; 4C: 1 out of 21), the field strength was increased in E-Ringer while the polarity remained unchanged.

A model for the electrical current patterns of polytrophic insect follicles

The model takes into account two premises: (1) The experimental data on the electrophysiology of different test systems (*Hyalophora cecropia, Drosophila melanogaster* and *Sarcophaga bullata*) reflect similar underlying basic mechanisms. (2) In the model there may be two electrically independent systems: the epithelial follicle cell layer around a vitellogenic follicle and the centrally located oocyte and nurse cell syncytium. The model suggests a possible pathway for the currents through and around the follicle and is illustrated in Figure 2a.

The model divides the total current flux into two main current loops. The first loop is generated by the follicular epithelium over the trophic cap. The current is pumped through this epithelium towards the subepithelial space where it joins the current leaving the nurse cells. From there it is deviated to the subepithelial space over the oocyte. Then, part of the current leaks out of the epithelium and the loop is closed around the outside of the follicle. The second current loop is generated by the membranes of oocyte and nurse cells, either by a separation in activity of ion pumps or ion channels or both. The current leaks out or is pumped out of the nurse cells and follows the same pathway in the subepithelial space as the current of the first loop. When it arrives at the oocyte surface, part of it leaks into or is pumped into the oocyte and the current loop is closed through the cytoplasmic bridge.

The extracellular field around the follicle has the same main features in all the different species and is not largely modified during progressive vitellogenesis (Jaffe and Woodruff, 1979; Overall and Jaffe, 1985; Verachtert and De Loof, 1986; Bohrmann *et al.*, 1986a). Moreover, the sense of the extracellular field opposes the intracellular potential gradient. The measurements of the extracellular field around individual follicles of each species show a high variability. These observations make it hard to understand how the intracellular potential gradient can be the direct consequence of the extracellular field (or vice versa).

Jaffe and Woodruff (1979) proposed a model of the steady current pattern through a *Hyalophora cecropia* follicle. Overall and Jaffe (1985) suggested a similar model for *Drosophila melanogaster*. The battery of the observed currents is proposed to be an ion pump lying within the nurse cell face of the furrow membrane. With the data of Woodruff and Telfer (1973) and Jaffe and Woodruff (1979), it can be calculated that the ion pumps

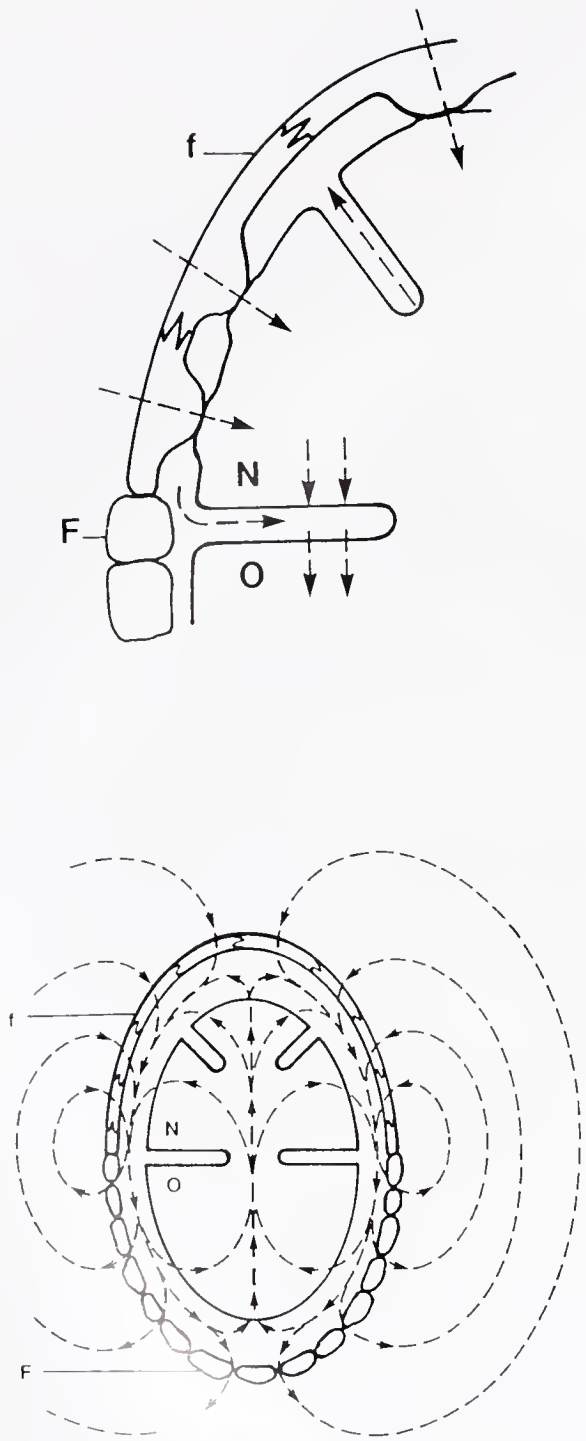

Figure 2. Model for the ionic current patterns of a vitellogenic polytrophic insect follicle. Bottom: [illegible] current loops; top: additional currents allowed for by the model. O: oocyte, N: nurse cells, F: cylindrical follicle cells, f: squamous follicle cells. The follicle cells are represented, separated from the oocyte and the nurse cells, for clarity.

would have to generate an average membrane current in the furrow of the order of magnitude of 100 $\mu A/cm^2$ to 1 mA/cm^2 to retain the bridge current. This is a high value for the activity of ion pumps. If the model of Jaffe and Woodruff (1979) were to apply to other polytrophic follicles from other species, a potential gradient between oocyte and nurse cells should necessarily occur in all species and stages. One would also expect to find a concomitant variability for the measurements of the membrane potential as for the measurements of the extracellular electrical field. Since this is not the case, the model of Jaffe and Woodruff (1979) does not completely explain all the data observed.

The extrafollicular field originates on the surface of the follicle. Therefore, the follicle cells must have a modulating, if not generating, contribution to this field. Woodruff *et al.* (1986) measured the extracellular currents of vitellogenic follicles of *Hyalophora cecropia* with patches of the epithelium overlying the trophic cap removed. Under these conditions, the current over the trophic cap is reversed: it is now directed outward. From microinjection experiments of lucifer yellow in the subepithelial spaces, the same authors conclude that the follicular epithelium over the trophic cap presents a barrier to ion movement.

Another line of evidence that should be taken into account are the dye-coupling experiments. Woodruff (1979) has shown fluorescein and electrical coupling between oocytes in adjacent follicles of *Hyalophora cecropia*. Bohrmann and Gutzeit (1987) found rhodamine coupling between follicle cells and the oocyte of *Drosophila melanogaster*. Our results on follicles of three different species show that dyecoupling between the follicle cells and the germ cells does not always occur. The generation of the extracellular field can be explained, however, even in the presence of open gap junctions, which make an electrical junction between the different cell types.

Woodruff *et al.* (1986) suggested a model where the extracellular currents around the nurse cell cap flow directly through the epithelial layer into the nurse cells. They have also suggested that a return current would flow through the intercellular spaces surrounding the nurse cells to an as yet undefined target in the vitellogenic end of the follicle.

In our model, we can allow for a direct current between follicle cell layer and nurse cells. A current through the intercellular spaces surrounding the nurse cells also seems to be possible, but is of the opposite sign as proposed by Woodruff *et al.* (1986). Finally, the model of Jaffe and Woodruff (1979) can be fitted into our model (Figure 2b).

Both current loops can be regulated independently and do not influence each other in a direct way.

Literature Cited

Berry, S. J. 1982. Maternal direction of oogenesis and early embryogenesis in insects. *Annu. Rev. Entomol.* **27:** 205–227.

Bohrmann, J., and H. Gutzeit. 1987. Evidence against electrophoresis as the principal mode of protein transport in vitellogenic ovarian follicles of *Drosophila*. *Development* **101:** 279–288.

Bohrmann, J., A. Dorn, K. Sander, and H. Gutzeit. 1986a. The extracellular current pattern and its variability in vitellogenic *Drosophila* follicles. *J. Cell Sci.* **81:** 189–206.

Bohrmann, J., E. Huebner, K. Sander, and H. Gutzeit. 1986b. Intracellular electrical potential measurements in *Drosophila* follicles. *J. Cell Sci.* **81:** 207–221.

Boyle, P. J., and E. J. Conway. 1941. Potassium accumulation in muscle and associated changes. *J. Physiol.* **100:** 1–63.

Brennan, M. D., A. J. Weiner, T. J. Gorasky, and A. P. Mahowald. 1982. The follicle cells are the major site of vitellogenin synthesis in *Drosophila melanogaster*. *Dev. Biol.* **89:** 225–236.

Cardoen, J., L. Schoofs, D. Broekaert, H. Van Mellaert, B. Verachtert, and A. De Loof. 1986. Polyploidization and localization of poly(A)$^+$ RNA in the different cell types of the vitellogenic meroistic ovary of the fleshfly, *Sarcophaga bullata*. *Histochemistry* **85:** 305–312.

Geysen, J., J. Cardoen, and A. De Loof. 1987. Distribution of yolk polypeptides in the follicle cells during the differentiation of the follicular epithelium in *Sarcophaga bullata* egg follicles. *Development* **101:** 33–43.

Huybrechts, R., J. Cardoen, and A. De Loof. 1983. "In vitro" secretion of yolk polypeptides by the fat body and ovaries of *Sarcophaga bullata* (Diptera, Calliphoridae). *Ann. Soc. R. Zool. Belg.* **T113**(Suppl. 1): 309–317.

Jaffe, L. F., and R. Nuccitelli. 1974. An ultrasensitive vibrating probe for measuring steady extracellular currents. *J. Cell Biol.* **63:** 614–628.

Jaffe, L. F., and R. I. Woodruff. 1979. Large electrical currents traverse developing Cecropia follicles. *PNAS* **76:** 1328–1332.

Overall, R., and L. F. Jaffe. 1985. Patterns of ionic current through *Drosophila* follicles and eggs. *Dev. Biol.* **108:** 102–119.

Robb, J. A. 1969. Maintenance of imaginal wing discs of *Drosophila melanogaster* in chemically defined media. *J. Cell Biol.* **41:** 876–885.

Sun, Y. A., and R. J. Wyman. 1987. Lack of an oocyte to nurse cell voltage difference in *Drosophila*. *Neuroscience* **13:** 1139.

Verachtert, B., and A. De Loof. 1986. Electrical fields around the polytrophic ovarian follicles of *Sarcophaga bullata* and the panoistic follicles of *Locusta migratoria*. Pp. 173–179 in *Ionic Currents in Development*. Alan R. Liss, Inc., New York.

Verachtert, B., M. Amelinckx, and A. De Loof. 1988. Potassium and chloride dependence of the membrane potential of vitellogenic follicles of *Sarcophaga bullata* (Diptera). *J. Insect Physiol.* (in press).

Woodruff, R. I. 1979. Electrotonic junctions in Cecropia moth ovaries. *Dev. Biol.* **69:** 281–295.

Woodruff, R. I., and K. L. Anderson. 1984. Nutritive cord connection and dye coupling of the follicular epithelium to the growing oocytes in the telotrophic ovarioles on *Oncopeltus fasciatus*, the milkweed bug. *Roux's Arch. Dev. Biol.* **193:** 158–163.

Woodruff, R. I., E. Huebner, and W. H. Telfer. 1986. Ion currents in *Hyalophora* ovaries: the role of the epithelium and the intercellular spaces of the trophic cap. *Dev. Biol.* **117:** 405–416.

Woodruff, R. I., and W. H. Telfer. 1973. Polarized intercellular bridges in ovarian follicles of the Cecropia moth. *J. Cell Biol.* **58:** 172–188.

Woodruff, R. I., J. H. Kulp, and E. D. LaGaccia. 1988. Electrically mediated protein movement in *Drosophila* follicles. *Roux's Arch. Dev. Biol.* **197:** 231–238.

Reference: *Biol. Bull.* **176(S):** 96–102. (April, 1989, Suppl.)

Modeling Currents About Vitellogenic Oocytes of the Cockroach, *Blattella germanica*

J. G. KUNKEL AND E. BOWDAN

Zoology Department, University of Massachusetts, Amherst, Massachusetts 01003

Abstract. An insect oocyte with a disc-shaped sink of current on its ventral surface during a vitellogenic phase of development is used to demonstrate modeling of expected currents arising from a mathematically defined source. A simple model with an analytical solution for the expected currents is compared to a more complex model in which expectations are computed by mathematical integration. The currents about two oocytes of different pattern type are interpreted in light of the two models.

Introduction

Ionic currents surrounding an insect oocyte may have a role in the physiology and development of the future embryo (Jaffe, 1986). The vibrating probe makes it possible to describe such currents in terms of their spatial pattern and intensity. During vitellogenesis the cockroach oocyte, a simple panoistic insect oocyte, has a sink of inward current at its ventral surface and a complimentary exit of current more broadly from the dorsal surface (*cf.*, Kunkel, 1986; Kunkel *et al.*, 1986). However, because the probe is non-invasive and is vibrating, current is measured at positions remote from the actual cell membrane. Typically the probe vibrates one probe diameter, making it in fact impossible to approach a source closer than 25 μ with the center of vibration of a 25-μ probe. Thus, a display of fields of current vectors measured at any distance from the oocyte gives an incomplete characterization of even this relatively simple pattern with respect to the cell surface. This is because current measurements made at discrete positions remote from the cell surface are weighted integrations of current from all membrane sources, with local sources more heavily weighted for two reasons: first, as indicated by equation (1) the contribution of current from each point on the cell falls off with the square of its distance from the measuring point and second, only the components in the directions of the probe's two vibration axes are measured.

It is crucial to understand the relationship between measured current patterns in the medium and current sources flowing through a membrane. With such an understanding, rapid and repeated sampling of current fields about cells would then lead to knowledge about the patterned ionic flux through the membrane and hence through the cell.

So far the mathematics of patterns of currents has only been applied by a few investigators in the field, and only in simple cases (Jaffe *et al.*, 1974; Betz and Caldwell, 1984). Freeman and *et al.* (1985) examined a more complex model. We introduce here an attempt to establish an approach with a slightly more complex system that changes over time. We expect this will lead to the sequential building of mathematical models, which will allow us to describe the current properties of any membrane system examined by means of the non-invasive vibrating probe technique.

Making sense of these fields of currents requires practice with simple models of hypothesized phenomena. Often, examining physical and mathematical models of the patterns and strengths of currents about well-defined, three-dimensional objects allows more insights than can be achieved by examining non-ideal natural examples. However, the models will only provide insight when they accurately describe and predict natural phenomena.

If current, i, emanates from a single point source, as is the case for one standard calibration procedure, then the radial current density 'I' is inversely proportional to the square of the radial distance 'k' from the source:

$$I = i/(4 \cdot pi \cdot k^2) \qquad (1)$$

In an isotropic medium then, potential drops perceived by the probe can be automatically interpreted as

current densities at the probe's position. This simple model does not estimate current density at the 'point' source, much less from multiple point or irregularly shaped sources. However this formula (1) can be used in conjunction with a model or knowledge of current patterns passing through a particular source, to integrate, on a point-by-point basis, what the current density measurable at some external point should be. For the orifice of a glass electrode used to inject a known current the inverse calculation of the source current density is simple, dividing the total current on the sphere of radius 'k' by the area of the orifice. Integration formulae have been developed predicting local currents remote from simple non-point sources (Freeman *et al.*, 1985; Purcell, 1985). The inverse operation of predicting what the source is like based on remote measurements is the crux of biological use of the vibrating probe. We examine two models of disc sources of current and apply these models to interpreting the disc-shaped sinks of current we hypothesize to be on the ventral surface of cockroach oocytes.

Materials and Methods

Measurements of current density around, and at different distances from, oocytes were made using the 2-D vibrating probe at the National Vibrating Probe Facility, Woods Hole. The medium used was a simplified version of Landureau's tissue culture medium and contains 4 m*M* $CaCl_2$; 14 m*M* KCl; 5 m*M* $MgSO_4$; 145 m*M* NaCl; 11 m*M* H_3PO_3, to buffer the medium at pH 6.8; 110 m*M* sucrose, to give an osmolarity of 390 mOsm; 12.5 mg/100 ml penicillin; 0.5 mg/100 ml streptomycin. Individual ovarioles of the German cockroach, *Blattella germanica,* were dissected, in this medium, from first parturition females which had access to food for 2–5 days. [Growth of oocytes is initiated by feeding the females at 30°C, the temperature for the maximum growth rate of this species. Newly metamorphosed females, which have been fed for 4 days, for example, have oocytes approximately ⅔ of the way through the vitellogenic phase, measuring 1.2–1.3 mm, and will be ovulated in 2 days (Kunkel, 1973)]. A single ovariole was dissected from an ovary and was then carefully positioned in an 8-ml plastic petri dish filled with medium. A layer of mineral oil over the medium's surface prevented evaporative convection of the medium. A heating coil and thermal probe in the oil layer maintained the preparation at 30°C. Oocytes prepared in this manner have exhibited stable currents for up to 10 h.

An XYZ coordinate system describes location. The X dimension is parallel to the length of the oocyte. Positive x-values are anterior, negative are posterior relative to the adult and the future embryo. The Y dimension defines the dorsal ventral axis of the future embryo, ventral values being positive and dorsal negative. The X-Y plane with z = 0 is defined as the mid-sagittal plane through the oocyte. The Z dimension is lateral.

Two oocytes provided the data used in this study (Fig. 1). Although similar in size this time represents a transition in the current pattern which is correlated with oocyte growth. One (oocyte #1, 1.1 mm) was probed repeatedly close along the ventral mid-sagittal surface. Current densities from the other (oocyte #2, 1.2 mm) were first measured also close along the ventral mid-sagittal surface. Subsequent measurements were then made at various distances away from the surface, in the mid-sagittal plane. Additional measurements were made close to the oocyte to check that the currents remained stable. The data collected consisted of the x, y, and (z = 0) position of the probe, and the resolved x- and y-currents, I_x and I_y. From I_x and I_y the mid-sagittal total current, I_t, and the angle of the resultant current vector in the X-Y plane were calculated; these are plotted in Figure 1. This 'total current' cannot include an I_z component since the probe does not vibrate in that direction. Thus the I_t vector for the 2-D vibrating probe describes only two of the three dimensions of measurable current at a point in space remote from a three-dimensional source. However, I_x and I_y do benefit from point sources located in the Z direction (Fig. 3.)

Data from the PDP 11/23 system at the NVPF was captured on an MS/DOS computer configured as a terminal of the PDP 11/23 and stored on floppy disc. Further data analysis was made with a 80286 computer fitted with a 80287 math coprocessor using both commercial and custom designed software. MathCad was useful for numerical integrations of equations using circular coordinates. Custom software included a vector and cell outline plotting program and a contour fitting program written in Turbo Pascal.

Results

The first model that was examined is described by the equation:

$$I_y = 2\ \text{pi}\ I_r(1 - [k/\text{sqrt}(k^2 + a^2)]) \qquad (2)$$

which predicts the current, I_y, measured remote from a disc shaped source of radius 'a', current density 'I_r' at radial distance 'r' on the disc surface, at a distance 'k' along the Y-axis normal to the center of the disc at (x, y, z) = (0, 0, 0) (Purcell, 1985). Along this axis both I_x and I_z are zero. Thus, the true total current is equivalent to both I_t and I_y. It should be noted that in this model, and also in model II, that I_r is a constant for $r < a$; but this could change in future models in which a non-uniform disc is considered. Relative to the central axis, the disc source is radially symmetric and thus the integral equations are

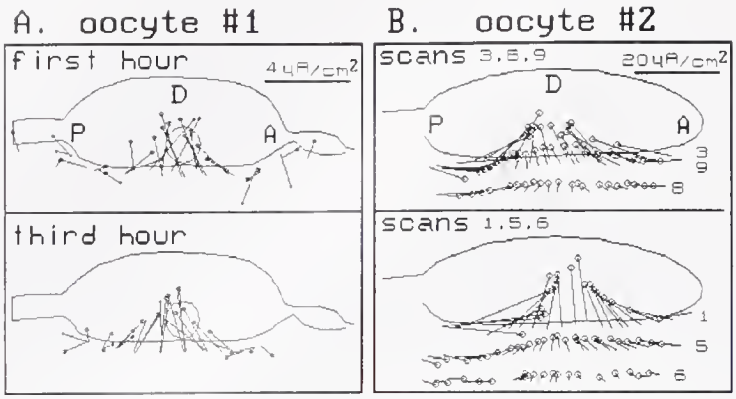

Figure 1. Outlines of two oocytes with local total current density vectors measured with a 2-dimensional vibrating probe. A circle marks the head of each vector. The base of each vector indicates the point of measurement. The length and direction of the displayed vector are computed as the sum of the x- and y-current vectors. A scale bar in the upper right corner for each oocyte indicates the vector callibration. (A) Oocyte #1 (1.1 mm)—repeated scans close to the mid sagittal ventral surface. (B) Oocyte #2 (1.2 mm)—measurements made at various distances away from the mid sagittal ventral oocyte surface. N. B. The current vectors of these oocytes are an order of magnitude smaller than those of Kunkel (1986). The discrepancy is due to an error in a computer program being developed at the earlier time. This error has since been corrected.

simple and can be solved analytically. Equation (2) is that analytic solution (Purcell, 1985).

In applying model I to experimental situations the distance, k, from the surface and the current I_y at position (x, y, z) = (0, k, 0) are measurable. The radius and density of the current source on the surface are estimated by fitting the 'a' and 'I_r' parameters of equation (2) to observed (k, I_y) data. The greatest current density, I_y, emanating from oocyte #2 was measured in the central region. Total current densities at positions above the surface measured from this region were fitted to equation (2) and the radius of the disc source was calculated to be 125 μ and current density on the disc to be 3 $\mu A/cm^2$. The data fit well to the theoretical curve (Fig. 2) with the exception of those values measured during the first and last (9th) scans. Fit of scans 1 and 9 are substantially improved if a linear time-dependent decay rate (1/3 per h) is added to the equation. Measurement ended after scan 9 because it became obvious that the currents had begun to deteriorate at that time. Deterioration is evident from the positions of these data with respect to the theoretical curve, scan 1 data lie above the curve, scan 9 lie below. Model I cannot be fit to oocyte #1 data since scans were not done at varying distances from the source.

Subsequently, model II, a more flexible and complex extension of model I, was examined. This first step in increasing complexity is described by equations (3) and (4), which are based on Figure 3. They describe the normal, I_y, and tangential, I_x, currents measured along the X-axis at a distance y above a model disc of uniform current density. With x = 0, model II is identical to model I; but when x is not equal to zero, the equations to be integrated are not rotationally symmetric, have no analytic solution, and thus must be integrated mathematically. Equations (3) and (4) allow the estimation of I_y and I_x at any point off the central axis by means of point-by-point mathematical integration of the current coming from all points (x, 0, z) on a source surface measured at the point (x, y, z) (Fig. 3). In practice, since the model disc's source is symmetric about (x, y, z) = (0, 0, 0), computations were simplified by making computations only for external points in the X-Y plane in what would correspond to the mid-sagittal plane of an oocyte, z = 0. Theoretical isopotential lines generated by these equations are shown in Figures 4 and 5. These figures demonstrate very clearly that I_x has maxima and minima corresponding to the edges of the disc source. Figure 5A especially shows that these peaks can be diagnostic of the size of this disc. In addition, the model of total current, $I_t = I_x + I_y$, predicts a plateau for large diameter discs probed close to the surface (Fig. 5B). In this case close would correspond to a distance that is a small fraction of the probed disc diameter, 2 units for a radius 10 disc.

Model II expectations were applied to the observed data from oocytes 1 and 2 (Fig. 6). The data from oocyte #1 are shown in Figure 6A. The plot of tangential current, I_x, shows clear maxima and minima indicating, if model II is accurate, that the source of inward current has a diameter of about 500 μ. This value correlates well with the size implications of Figure 1. However, for this oocyte, minimum I_x is not symmetric with maximum I_x, as an ideal disc would exhibit. This suggests that the effective source (that is, either its shape or the distribution of pumps or channels) is not a perfect disc nor mir-

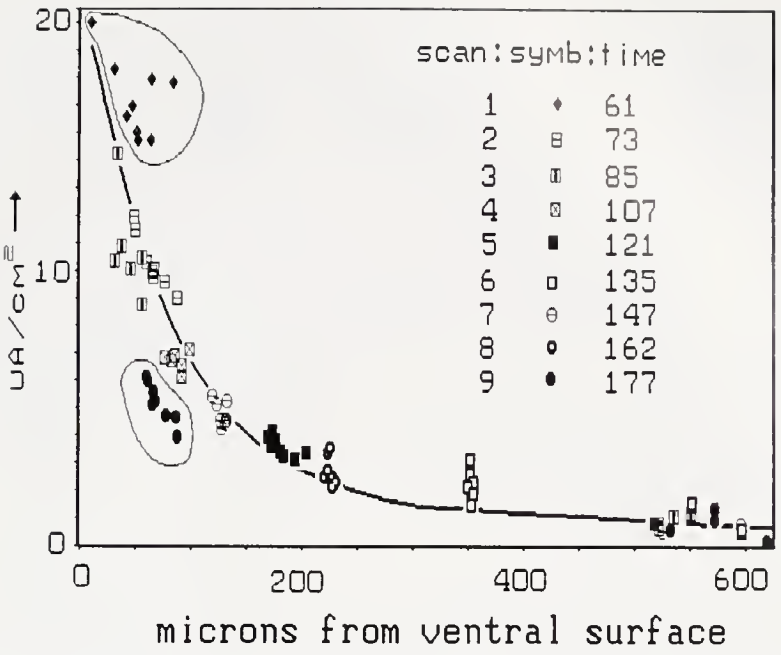

Figure 2. Theoretical current density generated by equation (2) (see text), using a disc source radius 125 μ and a source current density of 3 $\mu A/cm^2$, is plotted as a solid line. The observed data of oocyte #2 are superimposed. Each scan is plotted using a distinct symbol and the start time of the scan is tabulated in minutes from disection time. The outlined measurements above and below the curve are those of scans #1 and #9 respectively (see text).

ror symmetric along the X-axis. This is supported by the plot of I_y, the normal current, which shows a displaced maximum. The relatively sharp peak of I_y also suggests that the maximum inward current is highly focused in this oocyte. No plateau of the total current, I_t, is perceived, additional support for the suggestion that the disc is non-uniform. The size of the disc is large enough such that probing at the typical distance from the ovariole surface, 35 μ, at the disc center should result in a measured current density in the medium about 5–6 times the membrane level current density. This would suggest that the true current density at the disc center of oocyte 1 is closer to 0.5–1 $\mu A/cm^2$ and closer to 3 $\mu A/cm^2$ for oocyte 2.

Plots of scan 1 data from the second oocyte (Fig. 6B) suggest a differently shaped source. The plots of I_x have no sharply defined maxima and minima, which suggests that there is inward current across the major part of the ventral surface (*i.e.*, 900–1000 μ) and it is not focused. This is in contradiction to the prediction of model I (which suggested a source 250 μ in diameter) but correlates more reasonably with what is intuitively observed in Figure 1. Again, minimum I_x is not quite symmetric with the maximum I_x. The plot of I_y has a broad plateau, which again indicates that the center of inward current is not focused. Plots of I_t for this oocyte are flat, indicative of a broad and relatively uniform unfocused current source. In comparing oocyte 1 and 2, the membrane level current grew from 1 to 3 $\mu A/cm^2$ and the area of the inward current increased by a factor of 2–3. The trend suggested by these two exemplars was observed overall in a substantially larger sample of oocytes, which will be reported elsewhere in a developmental context.

Discussion

Adequate interpretations of non-invasive physical measurements about cells depend upon appropriate models of the sources. Model I, equation (2), describes the decay of current along the normal axis, perpendicular to the center of a disc source and yields an estimate of the radius and the current density of the disc. It is sensitive enough to indicate deterioration of the source, but it has some restrictive limitations. The first is that measurements must be made along an axis normal to the cell surface, a position and direction that may be difficult to know under experimental conditions or that may shift with time or with changing conditions. We know that the borders of the disc (current reversal from inward to outward) shifts somewhat from scan to scan; but we do not yet know whether this, for example, corresponds to shifts in the center of the disc or to local changes in the disc border. The second limit of model I is that only the average radius of a source can be sensed so that asym-

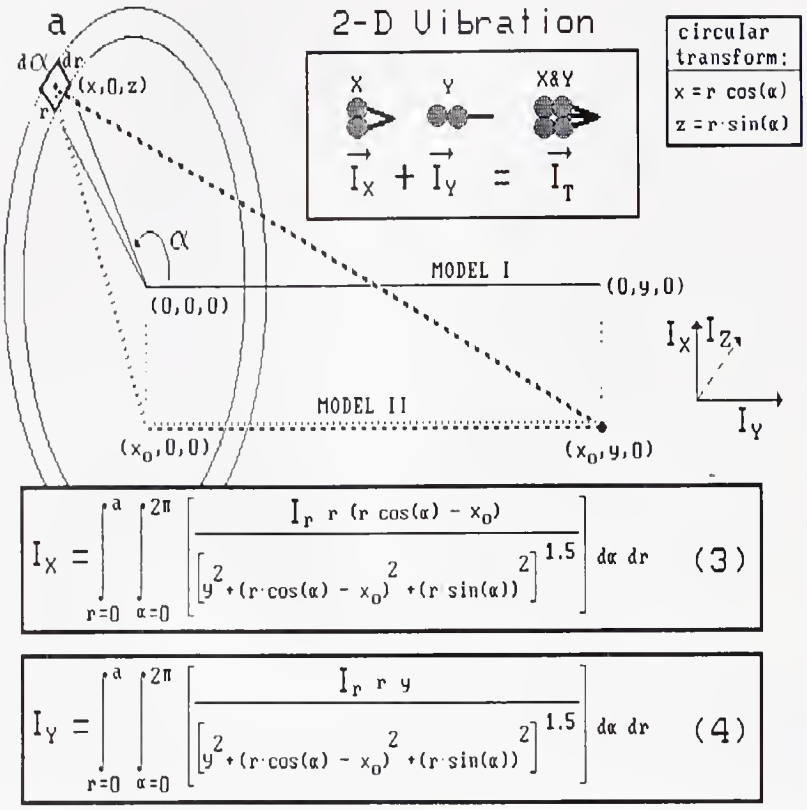

Figure 3. Physical model for equations (3) and (4). These indicate the 3-D disc source located on the ventral surface of a hypothetical oocyte measured by the probe in 2 dimensions: X, Y, Z—the three dimensions of space. A disc source of current is located in the X-Z plane on the ventral oocyte surface with its center at (x, y, z) = (0, 0, 0). X is parallel to the length of the oocyte on which the disc is located. Y is normal to the disc at its center. The X and Z axes are tangential to the disc surface. The vibrating probe vibrates in two dimensions, X and Y only. The X coordinate at the point of measurement is designated x_0. A dashed line outlines a right triangle in 3-space whose legs are y in the Y-dimension, $(r\cdot\cos(\alpha) - x_0)$ in the X-dimension and $(r\cdot\sin(\alpha))$ in the Z-dimension.

α = angle, in radians, used to transform the XZ coordinates (x, 0, z) into circular coordinates (α, r).

a = radius of the disc, in arbitrary units.

r = the radius at a particular point on the source.

I_r = 1 μA/(area unit)^2 for r < a, the current density through the disk at a particular radius, r.

metries such as those suggested by departures from the more complex model II cannot be demonstrated. Equation (2) is limited to relatively small discs on a cell surface because distortions of a disc, due to, for example, cell curvature, will lead to substantial departures of the predicted curve from ideal behavior. Since the theoretical curve (2) has only two parameters dictating its form, it is difficult to ascribe departures in the shape of the curve to a particular departure of a disc from its ideal form.

Equations (3) and (4) describing model II are more robust in their ability to detect a divergence of observed data from ideal predictions and are, in general, more informative. The equation of the tangential current I_x (3) indicates the limits of the source independently and so can detect an asymmetric source. For small disc sources the equation for current normal to the disc surface, I_y (4), provides a means of calculating the membrane-level current. Point-by-point integral equations can model irregularly shaped sources limited only by the ingenuity of the defining equations for the surface of integration and the current density function, $I_r = I(x, 0, z) = 1\ \mu A/cm^2$ for r < a in this case. Such an ability to model currents is necessary to relate patterns of remotely measured currents to the distributions and densities of functioning ion channels and pumps. Application of model II to the data collected from the two oocytes indicates that the sink of

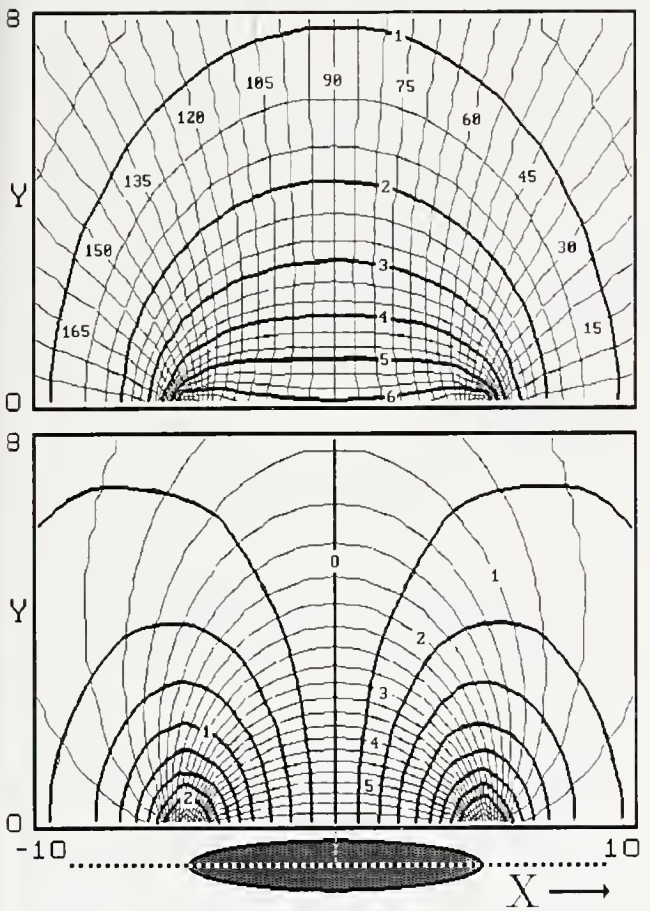

Figure 4. Predicted currents, generated from equations (3) and (4): current density at source held at 1 μA/unit^2 on a disc of radius 5 units. (Bottom Panel) Isopotential contours for tangential, (I_x, thick contours) and normal, (I_y, thin contours) current densities. Below the contour plot is a representation of the disc source; a dotted line through the disc represents the location of the scan. (Top Panel) Isopotential contours for total current density (It, thick contours) and contours of equal angles (thin contours) subtended by the vectors.

inward current from the smaller oocyte is smaller and more tightly focused than that from the larger oocyte. This may be simply interoocyte variability or it may be a developmental change. Clearly, however, model II can quantitate the difference.

Thus, model II provides substantially more information than model I and allows for relatively easy extension to more complex models. However, it too has its limitations. Like the first model, it may overestimate current density at the disc surface by as much as 2·pi. This is because measurements made include substantial lateral contributions especially when the disc radius is large, even if the measurements are made as close to the surface of the disc as possible (1 probe diameter). This corruption of local measurements by lateral components argues for routine measurement of the decay of current away from the surface to increase the ability to use modeling to predict the shape of the current source. A greater density of measurements at closer intervals along the surface can achieve similar ends. Sparse data are difficult to model with high resolution. In particular, geometric conditions increasing the number of measurements of either I_y or I_x may be preferable. As in model I, model II equations (3) and (4) assume a flat disc source while the oocyte surface is, of course, curved. Thus, we need to develop models that take more advanced geometry into account. This is not a difficult problem when mathematical integration is used as we did for model II. In spite of these limitations, model II is able to improve our interpretation of the observed currents about oocytes #1 and #2. It further provides an approach by which subtle changes of current pattern measured during develop-

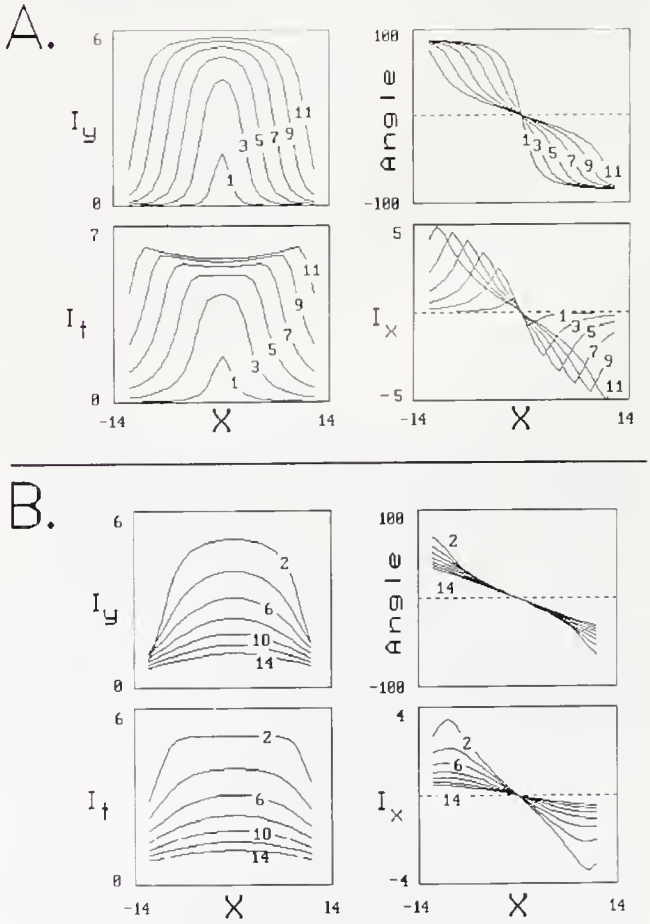

Figure 5. Calculated current densities: current density at source = 1 μA/unit^2; measured along the X axis: (A) I_x, I_y, I_t and the angles of the vectors from discs of radius 1–11 arbitrary units; at 1 distance unit above the disc source. (B) I_x, I_y, I_t and angles from a disc, radius 10 units; predicted for 1 to 14 Y distance units above the disc source.

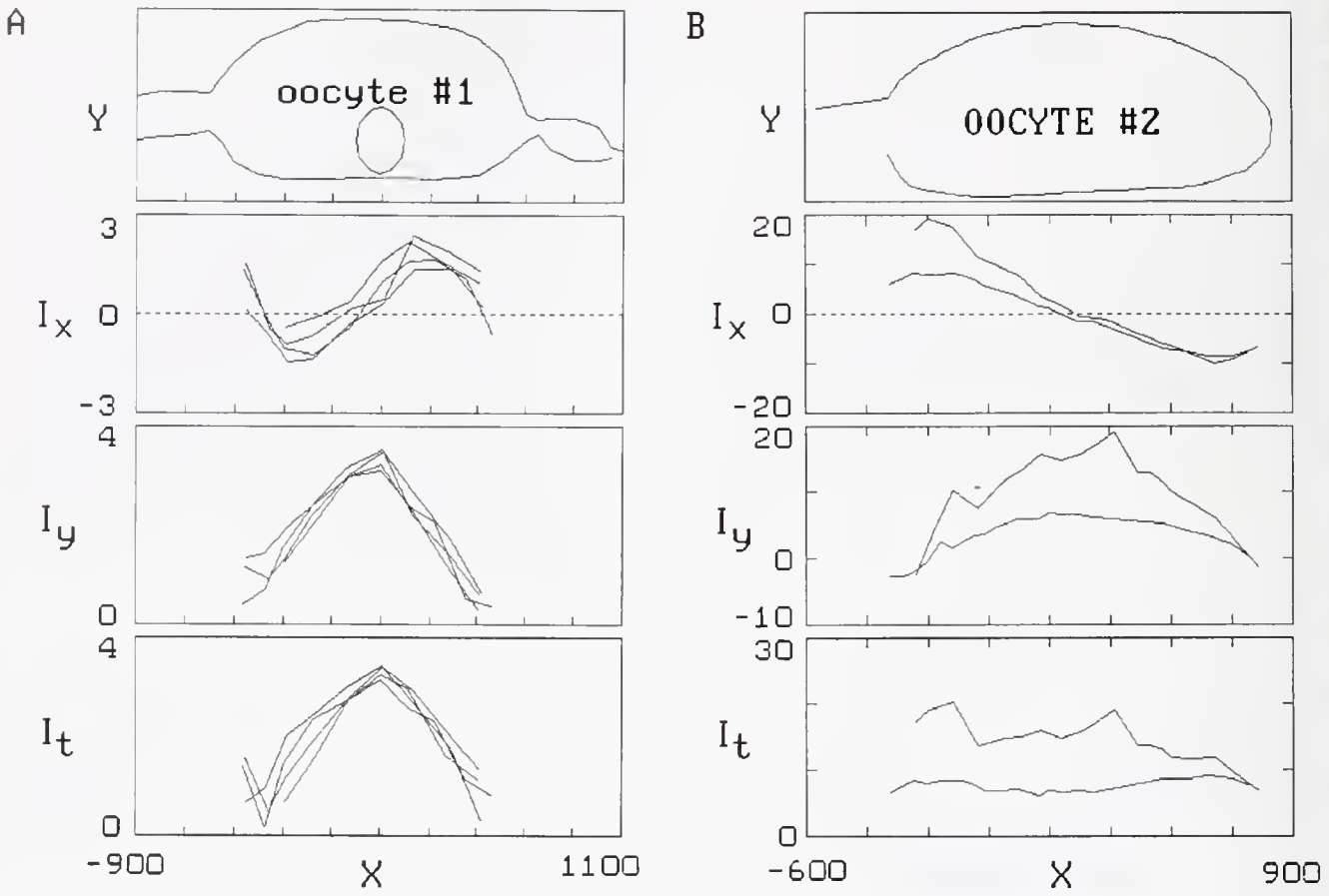

Figure 6. Observed data interpreted according to the model of I_x, I_y and I_t plotted under oocyte outlines for (A) Oocyte #1; (B) Oocyte #2

ment or caused by experimental manipulations may be interpreted with greater insight. Thus, a better understanding of the physiology of the oocyte should be possible.

Acknowledgments

We are grateful to Dr. L. Jaffe and the staff of the NVPF, especially A. Shipley and S. Dixon. This work was supported in part by NSF grant #DCB-851781

Literature Cited

Betz, W. J., and J. H. Caldwell. 1984. Mapping electrical currents around skeletal muscle with a vibrating probe. *J. Gen. Physiol.* **83:** 143–156.

Freeman, J. A., P. B. Manis, G. J. Snipes, B. N. Mayes, P. C. Samson, J. P. Wikswo, and D. B. Freeman. 1985. Steady growth cone currents revealed by a novel circularly vibrating probe. *J. Neurosci. Res.* **13:** 257–283.

Jaffe, L. F. 1985. Extracellular current measurements with a vibrating probe. *TINS-December 1985* **8:** 517–521.

Jaffe, L. F. 1986. Ventral activation process in insect oocytes. *Nature* **321:** 386.

Jaffe, L. F., K. Robinson, and B. F. Picologlou. 1974. A uniform current model of the endogenous current in an egg. *J. Theor. Biol.* **45:** 593–595.

Kunkel, J. G. 1973. Gonadotrophic effect of juvenile hormone in *Blattella germanica:* a rapid, simple quantitative bioassay. *J. Insect Physiol.* **19:** 1285–1297.

Kunkel, J. G. 1986. Dorsoventral currents are associated with vitellogenesis in cockroach ovarioles. Pp. 165–172 in *Ion Currents in Development,* R. Nucitelli, ed. Alan R. Liss, NY.

Kunkel, J. G., R. Koenig, H. Kindle, and B. Lanzrein. 1986. Ion Flux during vitellogenesis and patterning of insect oocytes. *Adv. Invert. Reprod* **4:** 101–108.

Purcell, E. M. 1985. Electricity and Magnetism. *Berkeley Physics Course,* Vol. 2, 2nd edition. 484 pp. McGraw-Hill, NY.

Reference: *Biol. Bull.* **176(S)**: 103–109. (April, 1989, Suppl.)

Ionic Currents in *Lymnaea stagnalis* Eggs During Maturation Divisions and First Mitotic Cell Cycle

D. ZIVKOVIC AND M. R. DOHMEN

Department of Experimental Zoology, University of Utrecht, Padualaan 8, 3584CH Utrecht, The Netherlands

Abstract. The eggs of the mollusc *Lymnaea stagnalis* generate weak extracellular ionic currents, which have been mapped from oviposition through first cleavage. Throughout this period the current is inward in the animal hemisphere, with highest density at the animal pole, and outward in the vegetal hemisphere, with highest density at the vegetal pole. Peak current densities are measured at the time of first and second polar body formation. During anaphase and telophase of the first mitotic cell cycle, the outward current at the vegetal pole reaches its minimum density and its direction is reversed in most eggs, whereas the inward current at the animal pole gradually increases. This coincides with the segregation of the so-called animal pole plasm to the animal pole (Raven, 1970).

The organic calcium channel blockers diltiazem and D600 cause abnormal maturation division(s) and/or first cleavage. At the same time they reduce and eventually abolish the associated ionic currents. These results suggest the existence of a cell-cycle correlated, calcium-dependent component of ionic currents in *Lymnaea* eggs.

Introduction

In eggs of most organisms, polar axes such as animal-vegetal, anterior-posterior, and dorsal-ventral are established during oogenesis, maturation, or shortly after fertilization (Davidson, 1986; Gerhart *et al.*, 1983). The mechanisms responsible for the induction and maintenance of the polar organization are still largely unknown.

In many molluscan eggs, including *Lymnaea stagnalis*, the apico-basal polarity of the oocyte in the ovary corresponds to the animal-vegetal axis of the mature egg, which in turn corresponds to the anterior-posterior axis of the developing embryo (van den Biggelaar, 1983; Raven, 1967). Thus, it is conceivable that the animal-vegetal polarity originates from the asymmetric intercellular contacts between the oocyte and the surrounding ovary cells, by a process of imprinting stable structural features into the plasma membrane and/or the cortex of the oocyte. Such stable features occur in eggs of several species. In molluscs, the most extensively studied species in this respect, *Nassarius reticulatus*, shows a polar distribution of intramembrane particles and polar differences in the mobility of membrane lipids (Speksnijder *et al.*, 1985a, b). Similarly, the distribution of ion channels and pumps may also be non-homogeneous in the plasma membrane of egg cells (Nuccitelli, 1983). As a result, asymmetric extracellular electric fields could be generated that might contribute to the establishment or maintenance of polar phenomena in eggs (Jaffe, 1982).

We have studied the ionic currents occurring in the egg of *Lymnaea stagnalis* during maturation and the first mitotic cell cycle. In view of the probable involvement of intracellular calcium ion gradients and the associated electric fields in axis establishment as described for *Fucus* eggs (Jaffe, 1986; Robinson and Jaffe, 1975) and because of postulated importance of intra- and extracellular calcium in the meiotic and mitotic cell cycles, we have investigated the role that calcium ions might play in these currents. For this purpose we used the organic calcium channel blockers diltiazem and D600.

Materials and Methods

Lymnaea stagnalis is a freshwater hermaphrodite pulmonate snail. The eggs are fertilized internally. Spontaneously laid eggs were decapsulated in filtered copper-free tap water (CFTW), which normally contains about 0.7 m*M* calcium. After a few rinses the eggs were transferred to plastic Petri dishes (Costar, Cambridge, Massachusetts) containing the desired measuring medium. The

eggs adhere spontaneously to the bottom of the dish, so they should be oriented in the desired position before they touch the bottom of the dish. Once attached the eggs can no longer be manipulated without plasma membrane damage and cytolysis.

Measuring media

Eggs were measured in filtered CFTW supplemented with 2 m*M* $CaCl_2$, pH 8.2–8.4, and specific resistivity of about 1200 Ω/cm. Another medium used was copper-free tapwater containing 2 m*M* $CaCl_2$ buffered with 3–5 m*M* HEPES(Na) of pH ranging from 7.0 to 8.5 adjusted with 0.1 *N* HCl or 1 *N* NaOH as required. In both media, eggs developed normally until gastrulation although the cell cycles were extended with approximately 10% as compared with control eggs in their capsules. The HEPES-buffered medium was used when studying the effect of pH on ionic currents and in studies using drugs that cause a pH shift in non-buffered conditions.

To determine whether extracellular calcium is needed for the generation of ionic currents in *Lymnaea*, eggs were treated with organic calcium-channel inhibitors; D600 (methoxy-verapamil hydrochloride) (Sigma, St. Louis, Missouri) at 0.1 m*M* or diltiazem-hydrochloride (Sigma) at 2 m*M*. Both substances are readily soluble in copper-free tapwater containing 2 m*M* $CaCl_2$. Treatments were initiated by perfusion of the media through the measuring chamber containing the eggs in copper-free tapwater with or without 2 m*M* $CaCl_2$ added. Perfusion with D600 was carried out 20 min before first polar body formation in the controls, and perfusion with diltiazem at the onset of first polar body formation. Applied in these concentrations, and at these particular times, both drugs had a maximal inhibitory effect on polar body formation and the associated peak current.

All measurements were made at 25°C, and fresh medium was perfused through the measuring chamber at regular intervals during the experiments. Data from different measurements at corresponding cell cycle times expressed in percentages were pooled and averaged. The phases of the cell cycle were determined from the data reported by van den Biggelaar (1971).

The second meiotic cycle was defined as the period between the anaphase of the first maturation division (P1 in the figures) and the anaphase of the second maturation division (P2 in the figures). The first mitotic division cycle was defined as the interval between the anaphase of the second maturation division (P2) and the onset of the first cleavage (K1). We could not define the first maturation cycle as part of it takes place in the gonads of the snail; therefore the cell cycle time was expressed in minutes instead of percentage (Fig. 2A).

Measurement of extracellular currents

The extracellular vibrating probe (Jaffe and Nuccitelli, 1974) was used to measure electrical currents around eggs of *Lymnaea*. In our set up, the one-dimensional vibrating probe system constructed for use of glass probes (The Vibrating Probe Co., Davis, California) was modified for use of parylene insulated metal probes. The additional equipment was purchased from Applied Electronics (Falmouth, Massachusetts). Measurements were made with probes that had platinum black balls with a diameter of 15–20 μm, which corresponds to about 10% of the egg diameter. The probes were vibrated with amplitudes of 15–30 μm.

Current densities for all measurements are indicated as detected at the actual measuring position with the center of vibration approximately 40 μm away from the egg surface. Minor deviations in the distance of the probe to the egg surface were due to the continuously changing geometry of cleaving eggs. No corrections were made for these deviations. Currents were mapped around the whole egg with emphasis on the animal and vegetal pole. The minimum recording time at one measuring site was 0.5 min with a lock-in amplifier time constant of 3 s. Between two measurements the probe was moved to a reference position typically 200 μm away from the egg surface. Current direction as indicated in the figures refers to the flow of positive charge. In the figures representing single measurements at the animal (A) and the vegetal (V) pole, the designations for current as upward and downward mean that the downward deflection from the reference line when the probe is above the animal pole indicates inward current, while the downward deflection indicates outward current when the probe is positioned under the vegetal pole.

Preparation of whole mounts

Eggs were fixed in Zenker, stained with gallocyanin/chromalum, and embedded in Canada balsam as described for *Nassarius reticulatus* by Speksnijder *et al.* (1985a).

Results

We have mapped steady electrical currents around *Lymnaea* eggs through both maturation divisions and the first mitotic cell cycle. During this entire period the currents show a polar pattern, being inward in the animal hemisphere and outward at the vegetal pole. The outward current has its highest density (200–600 nA/cm^2) at the vegetal pole, and the inward current is concentrated at the animal pole, where it ranges from 200 to 600 nA/cm^2 and occasionally attains even 1 μA/cm^2 (Fig. 3A). The egg surface laterally from the vegetal pole

shows an outward current of about 50 nA/cm^2. Laterally from the animal pole, including the equator area, inward current of about 50 nA/cm^2 is measured.

In certain areas of the egg surface we have detected current density approaching the technical detection limit of the measuring system, which is about 20–40 nA/cm^2 in our media. Such currents were considered to be zero and could not be included in calculations for inward/outward current balancing. It was therefore not possible to satisfy limits for inward/outward current compensation as discussed for *Drosophila* follicles and eggs by Overall and Jaffe (1985).

Maturation divisions

The earliest possible measurements were made at about 40 min before the extrusion of the first polar body, when the meiotic spindle still resides in the center of the zygote (Fig. 1A). At this time we measured an outward current at the vegetal pole ranging from 100–200 nA/cm^2 and no current at the animal pole. An inward current at the animal pole was first detectable at metaphase, when the meiotic aster becomes anchored in the cortex of the animal pole, which is at about 20 min before the extrusion of the first polar body (Figs. 1B, 2A).

Maximum current density at both animal and vegetal pole was concurrent with telophase, when the nascent polar body was bulging out maximally (Fig. 1D; T in Fig. 2B; V2 and A2 in Fig. 3A), and usually occurred slightly earlier at the animal pole than at the vegetal pole (T in Fig. 2B).

Before the extrusion of the first polar body was completed (Fig. 1E), the current density decreased to about 100 nA/cm^2 and remained at this level until the formation of the second polar body (T in Fig. 2C).

Figure 2B shows the average current density profile during the second maturation division. The current pattern at about the time of second polar body formation (Figs. 2C, 3B) is comparable to that measured at the time of first polar body formation (Figs. 2B, 3A). During telophase of the second meiotic division (T in Fig. 2C), the vegetal outward current was generally somewhat weaker, and the animal inward current somewhat stronger than at the time of the first meiotic telophase (T in Fig. 2B).

First mitotic division

The mean current density profile is given in Figure 2C. At the beginning of the G2 phase, there is a slight increase in average inward current at the animal pole to about 250 nA/cm^2. During the last 20% of the cell cycle, corresponding to anaphase and telophase, the current at the vegetal pole is reversed from outward to inward in most eggs.

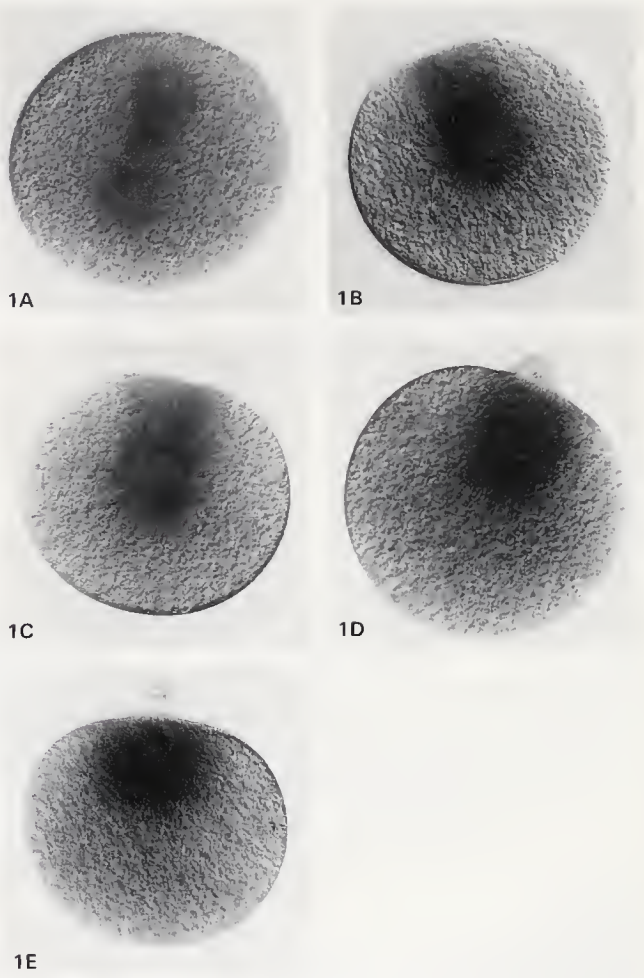

Figure 1A–E. Nomarski micrographs of gallocyanin/chromalum stained whole mounts of eggs in prometaphase (A), metaphase (B), anaphase (C), telophase (D) and during the extrusion of the first polar body (E). The eggs were fixed at 9, 39, 49, 59, and 60 min after oviposition for A, B, C, D, and E, respectively. The timing concerns development of decapsulated eggs in CFTW + 2 m*M* $CaCl_2$.

Treatment with calcium channel blockers

Diltiazem. In eggs incubated from about anaphase of the first meiotic cycle in copper-free tapwater containing 2 m*M* $CaCl_2$ and 2 m*M* diltiazem, the extrusion of the first polar body was generally complete and at the time of second polar body formation there was a bulging out of cytoplasm resembling the second polar body. However, this plasm was immediately resorbed and the second polar body never formed. When $CaCl_2$ was not added to CFTW, first polar body was not completely extruded and was subsequently resorbed. A representative measurement of such a treatment is shown in Figure 4A. The current density decreased abruptly from 250 to 50 nA/cm^2 within 10% of the cell cycle after perfusion with diltiazem, and within 25% of the cell cycle it reached zero

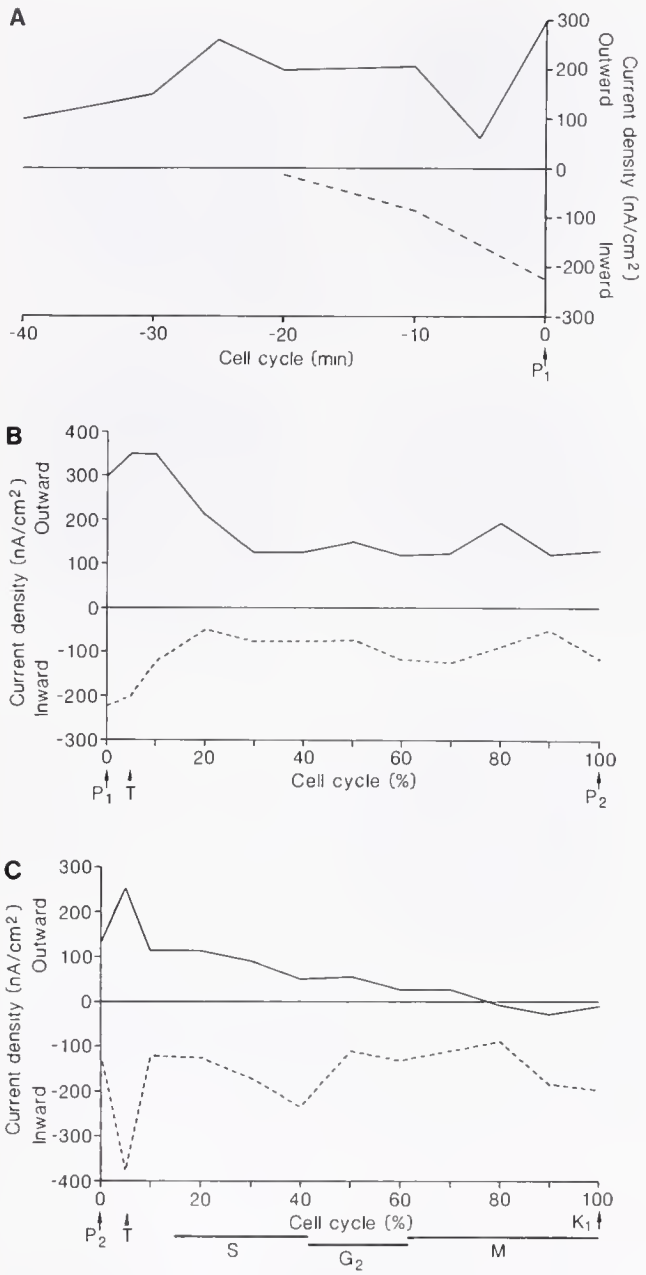

Figure 2A–C. Mean ionic current densities at the animal (– – –) and the vegetal (——) pole of *Lymnaea* eggs based on measurements made in copper-free tapwater (CFTW) supplemented with 2 m*M* $CaCl_2$. Mean current density during: (A) About 40 minutes preceeding the anaphase of the first meiosis (P1), 10 measurements. Current at the animal pole becomes first measurable at about 20 min prior to anaphase of the first meiosis (P1), and remains inward during the entire period. (B) The second meiotic cell cycle, from anaphase of the first (P1) until anaphase of the second (P2) meiosis, 15 measurements. (C) The first mitotic cell cycle, from anaphase (P2) of the second meiosis until the onset of the first cleavage (K1), 11 measurements. Maximum current densities occur during telophase (T) of the meiotic divisions. Current at the vegetal pole is outward to zero until anaphase/telophase of the first cleavage cycle (M), when it reverses to inward in most eggs. Note that the cell cycle time is expressed in percentage in Figure 2B and 2C, and in min in Figure 2A.

level. This current peak was much shorter, the decrease in current more abrupt, and the minimum current density lower than in an egg in the medium without diltiazem (Fig. 3A). Perfusion with CFTW containing 5 m*M* $CaCl_2$ after the decrease in current was not able to restore the current or to rescue polar body formation or cleavage.

When eggs were incubated continously in CFTW containing from 0.1 to 1.0 mM diltiazem, concentration dependent effects were as follows from about 40 min before the first polar body formation in the controls. No effect on polar body formation and the associated currents was found with 0.1 and 0.2 m*M* diltiazem. In 0.3 and 0.35 m*M* diltiazem, first and second polar body formation was attempted synchronously with the control eggs in CFTW. However, both polar bodies were resorbed after incomplete cytokinesis. The current pattern in 0.3 m*M* diltiazem was normal and fell to zero only after resorption of the second polar body, and in 0.35 m*M* no current was detectable from about 10 min after the onset of incubation. Therefore, it seems that at the concentration of 0.35 m*M* diltiazem there is an uncoupling of an (incomplete) meiotic telophase from the concurrent ionic currents that exist in the media without the inhibitor. At the higher concentrations of diltiazem there was an attempted first polar body formation followed by resorption. The second polar body never formed and the current at the vegetal pole was reversed. At the concentrations of 0.3, 0.35, and 0.5 m*M* diltiazem, the eggs lysed within 2.5 h after the onset of incubation. Finally, in 1 m*M* diltiazem polar bodies did not form, the current at the vegetal pole was reversed and the eggs lysed within 1 h (data not shown).

D600. Incubation of eggs with D600, another organic calcium channel blocker, in concentrations higher than 0.5 m*M* caused cytolysis within an hour of treatment. Incubation in 0.1 m*M* D600 in CFTW containing 2 m*M* $CaCl_2$ before the extrusion of the second polar body resulted in current abolishment and abortive first cleavage. When incubation was initiated about 20 min before first polar body formation in the controls, the first and second polar bodies were formed at the same time as in the controls. However, the first mitotic cell cycle was extended for about 30% and resulted in partial cleavage and subsequent cytolysis.

The ionic current pattern as shown for an individual egg in Figure 4B was comparable to that in normal media (Fig. 3A) However, the current density was reduced, with peak densities of less then 200 nA/cm^2 at telophase of the first (V2 in Fig. 4B) and second meiotic cycle (data not shown). The density in the remainder of the cell cycle did not exceed 100 nA/cm^2. At 40% of the mitotic cycle, equivalent to 150 min after the onset of incubation, the vegetal current decreased to zero, while currents lower

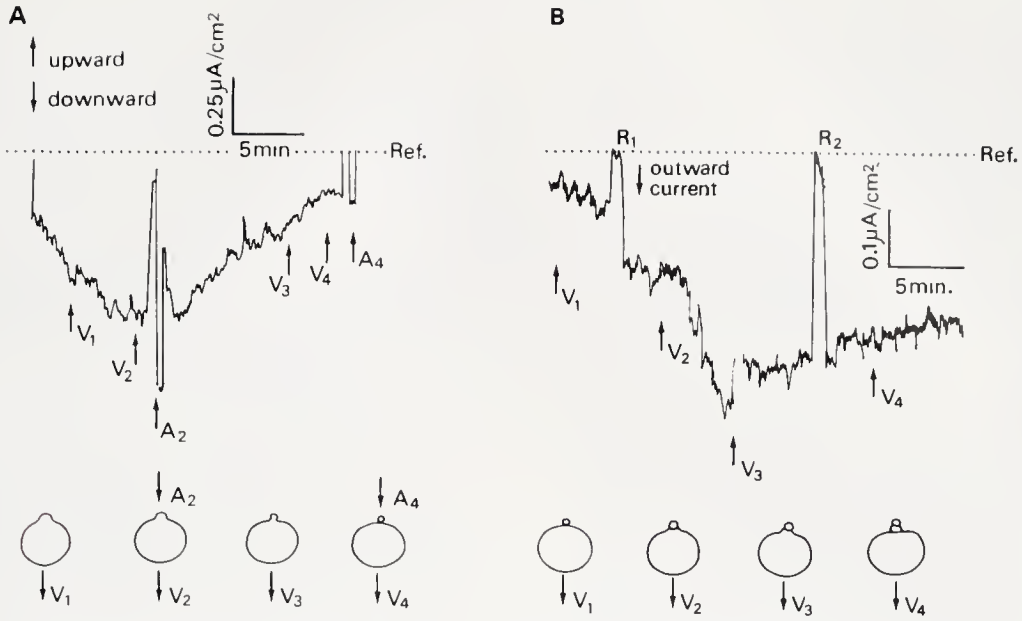

Figure 3A–B. Current density profiles at the vegetal (V) and at the animal (A) pole of individual *Lymnaea* eggs measured in CFTW + 2 m*M* $CaCl_2$. (A) Anaphase (V1) through telophase (V2 an V3) to complete extrusion of first polar body (V4). (B) Current trace is shown of another egg from metaphase (V1) through anaphase (V2) and telophase (V3) to complete extrusion (V4) of second polar body.

The dotted line connects the reference measurements and is not the actual measurement of the reference level. In Figure 3B, the probe was moved to a reference position R1, typically 200 μm away, about 8 min before the maximal current density at V3 was measured and again to R2 about 6 minutes thereafter. Note that the current is outward (downward) at the vegetal pole (V), and inward (downward) at the animal pole (A), with highest densities at telophase.

than 50 nA/cm^2 were measured at the animal pole (data not shown).

Discussion

We have measured current densities ranging in individual eggs from 200 to 600 nA/cm^2 at both poles of the *Lymnaea* egg. These currents are rather weak as compared with other known developmental currents (Nuccitelli, 1986) and often approach the detection limit of the technique. However, the results clearly show an animal-vegetal difference in current pattern and density. In addition, current pattern and density vary during the cell cycle.

It has been shown, using techniques other than the vibrating probe, that cell cycle-dependent changes in membrane ion permeabilities occur (Boonstra *et al.*, 1982; Rodeau and Vilain, 1987). Changes in intracellular ion concentrations have been reported particularly for protons (Busa and Nuccitelli, 1984) and for calcium ions (Poenie *et al.*, 1985). In view of these intracellular ionic changes it would not be surprising if the cell cycle were to be associated with extracellular ionic currents.

Experiments with D600 and diltiazem indicate the importance of extracellular calcium for the process of maturation and cleavage. When standard micromolar concentrations of the inhibitors are used (Lee and Tsien, 1983) disturbances of cell division occur late with respect to the onset of the treatment, although the associated currents are rapidly reduced (Fig. 4B). This could mean that only partial inhibition of calcium channels is achieved, maybe due to competition with calcium ions in the medium, as reported for mouse oocytes (Yoshida, 1986). It is also possible that intracellular calcium temporarily compensates for the lack of calcium influx. It is known that *Lymnaea* eggs pretreated for half an hour with 0.05–0.1 *M* $CaCl_2$ and then transferred into distilled water may show a normal cleavage pattern and thus it was speculated that *Lymnaea* eggs can accumulate calcium (Raven and Mighorst, 1946).

Preliminary results with TMB-8, an antagonist of intracellular calcium release, suggest that there is indeed a correlation between intracellular free calcium and external ionic currents. However, preliminary results of substitution experiments in which calcium was replaced by equimolar magnesium in a defined artificial medium show that the peak currents associated with the meiotic divisions still occur. However, these currents are somewhat weaker (200 nA/cm^2 at the maximum), and the

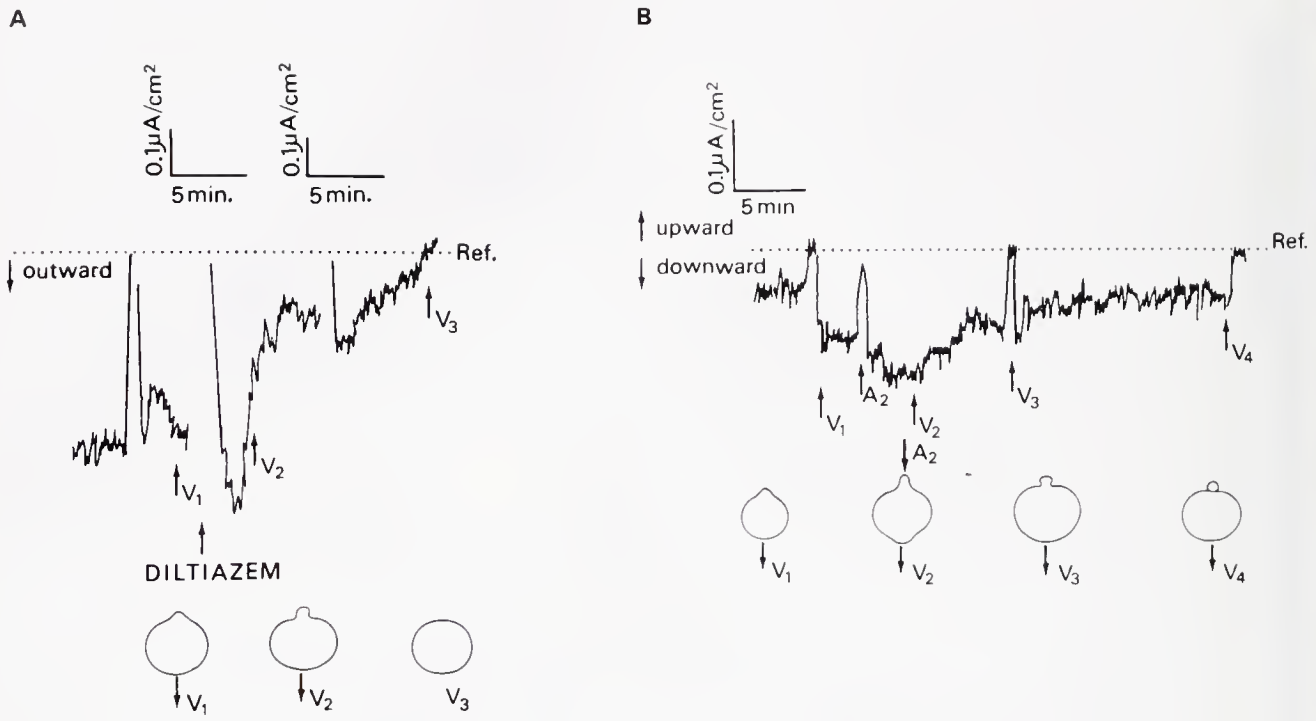

Figure 4A–B. (A) Current density profile at the vegetal pole (V) of a *Lymnaea* egg perfused with 2 m*M* diltiazem in CFTW at early telophase (V1) of the first meiotic division. The current decreased within 10% of the cell cycle (V2) and disappeared within 25% of the cell cycle (V3). Note that after perfusion with diltiazem the current density scale changed due to the lower resistivity of this medium. (B) The current density profile at the animal (A) and vegetal (V) pole of an egg incubated in 0.1 m*M* D600 in CFTW + 2 m*M* $CaCl_2$. Incubation was initiated 20 min prior to first meiotic anaphase in the controls. A maximum density of about 170 nA/cm² was measured at telophase (V2) of the first meiotic cell cycle. However, this maximum density was reduced if compared to the controls in medium without D600. Note that the current is outward (downward) at the vegetal pole (V), and inward (downward) at the animal pole (A).

peak is not associated with maximum bulging out of the polar bodies as in the controls, but occurs a few minutes later. This suggests that other ions than calcium are also components of the ionic current.

We do not know if the currents described here are causally related to the animal-vegetal polarity of the egg. However, some interesting correlations between polar events in the egg and current pattern have emerged from this study. First, the absence of current at the animal pole before first polar body formation (Fig. 2A) coincides with a stage during which animal/vegetal polarity is not yet firmly established, as shown in another mollusc, *Limax* (Guerrier, 1968). Second, the onset of the inward current at the animal pole just before first polar body formation (Fig. 2A) coincides with the anchoring of the meiotic aster at the animal pole. This might be the trigger for the increase of ion fluxes there. Third, there is a significant temporal coincidence between the segregation of the so-called animal pole plasm at about one hour after second polar body formation (Raven, 1970) on the one side, and a minimal outward current at the vegetal pole associated with a gradual increase in inward current at the animal pole (Fig. 2C) on the other. Finally, inward current is always measured preceeding and concurrent with the formation of the contractile ring during polar body formation and at first cleavage. These inward currents might bring about a local increase in free calcium for the formation of the contractile ring.

Acknowledgments

We thank Prof. Dr. N. H. Verdonk and Prof. Dr. J. A. M. van den Biggelaar for helpful suggestions concerning this manuscript. The Department of Image-Processing and Design is thanked for its photographic services. The Doctor Catharine van Tussenbroek Foundation is thanked for subsidizing D.Z.'s travel to the Ionic Currents in Development Conference.

Literature Cited

Biggelaar, J. A. M. van den. 1983. Origin of spatial organization. Pp. 179–213 in *The Mollusca, Vol. 3, Development,* N. H. Verdonk,

J. A. M. van den Biggelaar, and A. S. Tompa, eds. Academic Press, New York.

Biggelaar, J. A. M., van den. 1971. Timing of the phases of the cell cycle with tritiated thymidine and feulgen cytophotometry during the period of synchronous divisions in *Lymnaea*. *J. Embryol. Exp. Morph.* **26:** 351–366.

Boonstra, J., C. L. Mummery, J. J. E. van Zoelen, P. T. van der Saag and S. W. de Laat. 1982. Monovalent cation transport during the cell cycle. *Anticancer Res.* **2:** 265–274.

Busa, W. B., and R. Nuccitelli. 1984. Metabolic regulation via intracellular pH. *Am. J. Physiol.* **246:** R409–R438.

Davidson, E. H. 1986. *Gene Activity in Early Development,* 3rd Ed. Academic Press, New York.

Gerhart, J., S. Black, R. Gimlich, and S. Scharf. 1983. Control of polarity in the amphibian egg. Pp. 261–286 in *Time, Space and Pattern in Embryonic Development,* W. R. Jeffery and R. A. Raff, eds. Liss, New York.

Guerrier, P. 1968. Origine et stabilité de la polarité animale-vegetative chez quelques Spiralia. *Ann. Embryol. Morphogen.* **1:** 119–139.

Jaffe, L. F. 1982. Developmental currents, voltages, and gradients. Pp. 183–215 in *Developmental Order: Its Origin and Regulation,* S. S. Subtelny and P. B. Green, eds. Alan R. Liss, New York.

Jaffe, L. F. 1986. Calcium and morphogenetic fields. Pp. 271–281 in *Calcium and the Cell,* D. Evered and J. Whelan, eds. Wiley and Sons, Chichester, UK.

Jaffe, L. F., and R. Nuccitelli. 1974. An ultrasensitive vibrating probe for measuring steady extracellular currents. *J. Cell. Biol.* **63:** 614–628.

Lee, K. S., and Tsien, R. W. 1983. Mechanisms of calcium channel blockade by verapamil, D600, diltiazem and nitrendipine in single dialysed heart cells. *Nature* **302:** 790–794.

Nuccitelli, R. 1983. Transcellular ion currents: signals and effectors of cell polarity. Pp. 451–481 in *Modern Cell Biology, Vol. 2.* Alan R. Liss, New York.

Nuccitelli, R. 1986. Ionic currents in development. *Progress in Clinical and Biological Research, Vol. 210.* Alan R. Liss, New York.

Overall, R., and L. F. Jaffe. 1985. Patterns of ionic current through *Drosophila* follicles and eggs. *Dev. Biol.* **108:** 102–119.

Poenie, M., J. Alderton, R. Y. Tsien, and R. A. Steinhardt. 1985. Changes of free calcium levels with stages of the cell division cycle. *Nature* **315:** 147–149.

Raven, C. P. 1967. The distribution of special cytoplasmic differentiations of the egg during early cleavage in *Lymnaea stagnalis*. *Dev. Biol.* **16:** 407–437.

Raven, C. P., and J. C. A. Mighorst. 1946. *Proc. Koninkl. Ned. Akad. Wetenschap.,* **49:** 1003–1010.

Raven, C. P. 1970. The cortical and subcortical cytoplasm of the *Limnaea* egg. *Int. Rev. Cytol.* **28:** 1–43.

Robinson, K. R., and L. F. Jaffe. 1975. Polarizing fucoid eggs drive a calcium current through themselves. *Science* **187:** 70–72.

Rodeau, J. L., and J. P. Vilain. 1987. Changes in membrane potential, membrane resistance, and intracellular H^+, K^+, Na^+ and Cl^- activities during the progesteron-induced maturation of urodele Amphibian oocytes. *Dev. Biol.* **120:** 481–493.

Speksnijder, J. E., M. M. Mulder, M. R. Dohmen, W. J. Hage, and J. G. Bluemink. 1985a. Animal-vegetal polarity in the plasma membrane of a molluscan egg: a quantitative freeze-fracture study. *Dev. Biol.* **108:** 38–48.

Speksnijder, J. E., M. R. Dohmen, L. G. J. Tertoolen, and S. W. de Laat. 1985b. Regional differences in the lateral mobility of plasma membrane lipids in a molluscan embryo. *Dev. Biol.* **110:** 207–216.

Yoshida, S. 1986. Effects of the calcium channel blocker diltiazem on the excitability of mouse oocytes. *Gamete Res.* **13:** 309–316.

Reference: *Biol. Bull.* **176(S)**: 110–117. (April, 1989, Suppl.)

Large Ionic Currents Leave the Primitive Streak of the 7.5-Day Mouse Embryo

GLEN K. WINKEL AND RICHARD NUCCITELLI

Department of Zoology, University of California, Davis, California 95616

Abstract. During mouse gastrulation, underlying mesoderm cells contribute to the future embryonic endoderm, though the mechanism of this morphogenetic process is not well understood. We have utilized the two-dimensional vibrating probe to investigate the relationship between transembryonic ionic currents and the underlying cellular morphogenetic rearrangements. We were able to detect strong outward currents along the midline of the embryo, with inward currents completing the current loop via the extraembryonic endoderm. The average maximum current density for 21 embryos was 21.2 $\mu A/cm^2$ situated over the developing foregut region. This outward current sometimes reached magnitudes of 60 $\mu A/cm^2$ and could be detected superior to Reichardt's membrane when it was left intact during the dissection. The outward current gradually decreased as the probe was moved posterior to the foregut and turned inward just beyond the hindgut and rostral to the foregut over the extraembryonic endoderm. These currents were stable over several hours and were temperature-sensitive, gradually decreasing as the temperature was lowered. Neither amiloride nor ouabain blocked or decreased these currents, though the lack of an effect may have been due to restricted access of these drugs to internal epithelia. The outward current was dramatically increased if an artificial leak was created. This suggests that the observed currents are due to a passive leak of ions through leaky junctions along the midline. Such leaky junctions would be expected to occur at regions in which extensive cellular rearrangements were occurring due to breakage and reformation of cellular junctions as would occur during gastrulation in this region.

Introduction

The process of gastrulation in the mouse embryo is poorly understood. Previous experiments have demonstrated that the embryonic ectoderm of the mouse embryo retains the capacity of forming endodermal derivatives if transferred to ectopic sites (Skreb *et al.*, 1976). Evidence from chimeric embryos derived from blastocyst injection experiments also suggest a similar conclusion (Gardner and Rossant, 1979). Likewise, there is little evidence that the visceral embryonic endoderm contributes to the fetal endoderm (Gardner, 1982; Hogan and Tilly, 1981; Diwan and Stevens, 1976). Therefore, it is generally believed that the endoderm is derived from the underlying mesoderm or primitive streak. This event is believed to occur in a manner similar to chick embryo gastrulation in which the mesoderm cells laterally displace the hypoblast cells and subsequently form the embryonic endoderm (Rosenquist, 1972). However, this morphogenetic movement has never been directly observed in the mouse embryo. Nakatsuji and Snow (1986) used Normarski DIC optics to observe directly mesoderm cells in the 7-day mouse embryo. They reported that mesoderm cells migrate away from the primitive streak, however they did not examine the movement of mesoderm cells into the endoderm layer.

Recently, experiments using horseradish peroxidase as a lineage tracer have indicated that the embryonic endoderm has a dual origin, being derived both from the visceral embryonic endoderm as well as the underlying mesoderm (Lawson *et al.*, 1986; Lawson and Pedersen, 1987). These lineage experiments also demonstrate that significant morphogenetic rearrangements occur during gastrulation in the mouse embryo. Such tissue rearrangements suggest that cellular junctions must be broken and re-established within the overlying epithelium. This would result in a leaky epithelium through which various ions could escape causing detectable transembryonic ionic currents. Such ionic currents have already been detected leaving the primitive streak of the chick embryo

(Jaffe and Stern, 1979). Therefore we should be able to identify those regions where gastrulation is occurring by locating regions of current leakage. In this paper we describe experiments in which we used the 2-dimensional vibrating probe to detect and localize the ionic current pattern of the 7.5-day postimplanation mouse embryo.

Materials and Methods

Recovery of embryos

Three CD-1 (Charles River) females were placed with one male CD-1 mouse and were checked daily for evidence of pregnancy by the presence of a vaginal semen plug (Day of plug equal to day 0.5). Plugged female mice were then transferred to separate cages and late on the afternoon of day 7.5 were killed by cervical dislocation. Uterine tubes with decidual swellings were removed, the individual swellings were cut apart with dissecting scissors and the decidua were dissected out from the uterine tubes. The embryonic egg cylinders were carefully removed from the decidua with fine tweezers (with Reichardt's membrane intact) and placed in Dulbecco's phosphate-buffered saline. Using a pair of extra fine forceps, Reichardt's membrane was carefully dissected away. Any embryos damaged during dissection were discarded. Well developed 7.5-day embryos were transferred to 35 mm petri dishes containing 2.5 ml of Dulbecco's modified Eagle medium (DMEM, Gibco, 430-1600) supplemented with 30% fetal bovine serum (FBS, Sigma). These were placed within a 100 mm petri dish with 1 ml of distilled water in the dish and incubated for 2 h at 37°C with 5% CO_2 (v/v).

Two-dimensional vibrating probe

The two-dimensional vibrating probe was used with a 20 μm platinum tip vibrated in a 20 μm circle by two piezoelectric reeds mounted at right angles (Nuccitelli, 1986). The signal from the vibrating electrode was connected to a low noise differential FET preamplifier with a gain of 100. The output of the preamp was connected to a two-phase lock-in amplifier that detects both in-phase and quadrature components of the signal (Model NR-2000, Vibrating Probe Co.). An A-D converter (Labmaster TM40 PGH, Scientific Solutions) digitizes the signal, which is analysed by an IBM PC-XT computer. The computer calculates the average current vector and displays a graphic vector in real time over the video image of the embryo being studied (Nuccitelli, 1986). The vector angles and magnitude were stored on a hard disk while the video images with computer graphics were stored on video tape for further analysis.

The magnitude of the vector normal to the surface plane of the embryo was calculated as follows: the relative angle of the surface was measured from the screen image of the embryo by drawing a line tangent to the surface at the probe measuring point. The angle of this line was subtracted from the calculated vector angle and the magnitude was recalculated. These vectors represent the outward and inward currents normal to the surface for the purpose of comparison of currents from different embryos and making comparative graphs.

The vibrating electrode was calibrated by measuring the current pattern around a microelectrode through which 2–5 nA of current was injected. A single embryo was placed in the probe chamber with 1 ml DMEM with 25 m*M* HEPES and 33% fetal bovine serum (FBS) heated to 37°C with an air curtain incubator mounted beneath the stage. The chamber temperature was measured with a temperature probe held adjacent to the embryo with a micromanipulator. The surface of the chamber was covered with 1 ml paraffin oil (Thomas scientific) to prevent evaporation and the vibrating probe was lowered into the chamber. A fire-polished holding pipette attached to a Narashige micromanipulator was used to orient and fix the embryo in the preferred orientation using mild suction.

For microelectrode recording and penetrations, a second Narashige micromanipulator was placed opposite the holding pipet. A 10 MΩ pipet was filled with 3 *M* KCl and positioned adjacent to the vibrating probe. The ionic current pattern was recorded prior to penetration, during impalement, and after the microelectrode was withdrawn, to determine whether an artifically created leak in the embryo would lead to an increase in the observed ionic current.

Scanning electron microscopy

7.5-day embryos were washed in Dulbecco's phosphate-buffered saline and then immersed in a solution of 3% glutaraldehyde in 0.1 *M* Na Cacodylate for 6 h. After fixation, specimens were rinsed in cacodylate buffer twice and post-fixed in 2% osmium tetraoxide in 0.1 *M* Na cacodylate for 2 h at room temperature. Dehydration was performed through graded alcohols ending in two changes of absolute anhydrous ethanol. Critical point drying was accomplished in a Bomar model APC-900/Ex critical point dryer with Matheson bone-dry CO_2. Embryos were mounted on studs with silver paste and gold coated in a Technics Hummer sputter coater V until a 150–200 Angstrom coating was achieved. Scanning electron microscopy was performed in a Cambridge Stereoscan-150 microscope at 20 kV with a 100 μm aperture.

Figure 1. Light micrograph of representative late 7.5-day mouse embryos. Upper right embryo in optical para-saggital section shows several features of the mouse embryo. The foregut (fg) is still developing while the hindgut (hg) is just beginning to invaginate. The archenteron (ar) is just anterior to the swelling anterior to the hindgut. Several somites (so) are visible along the midline. The outline of the amnion (am) is barely visible. Lower left embryo shows a frontal optical section of the foregut. Neural folds (nf) are the most visible feature. Head folds (hf) can be seen through the yolksac endoderm. The arrow denotes the anterior border of the foregut from which the heart will eventually develop. Bar = 0.1 mm.

Results

The three-dimensional nature of the mouse embryo made its orientation a crucial factor for obtaining reproducible current patterns. Therefore only embryos that could be correctly positioned were used for recording purposes. We further insured that the midline of the embryo was positioned properly using the head fold structures to optically orient the embryo in a para-saggital position (Fig. 1). Several embryonic structures were also used to determine the recording points of the probe. We used seven routine recording positions (Fig. 2). Beginning at the ectoplacental cone, we studied three extraembryonic positions, with the third position nearest the amnionic junction denoting the extraembryonic-to-embryonic transition. Then, continuing from the foregut, we recorded adjacent to four embryonic positions: the foregut, two midgut locations, and the hindgut. The current pattern measured around a representative embryo (Fig. 2a) shows that the maximal outward current is over the foregut. We recorded outward current densities at the foregut that sometimes exceeded 60 $\mu A/cm^2$ (S.E.M.), although the average of outward currents from 21 embryos was 20.2 ± 0.4 $\mu A/cm^2$ (Fig. 3). Both anterior and posterior to the foregut region the current density gradually decreased. At the anterior extraembryonic junction the current often abruptly reversed becoming inward. Posteriorly, toward the hindgut, the current also decreased and sometimes changed to an inward current. However, the recordings in this region proved to be more variable, and we were often unable to record from this region based upon the orientation of the probe relative to the embryo. When the embryo was reoriented and rescanned with the probe, the region of inward-to-outward current shift was variable, although the current usually turned inward just past the hindgut and towards the ectoplacental cone region the current was always strongly inward. The maximal inward current was always closest to the ectoplacental cone region (4.8 $\mu A/cm^2$). However, there were a few cases of outward current (2/21) in this region. Since the current was predominately inward if the ectoplacental cone was left intact and always strongly outward if removed, it is possible that this outward current may have been due to leakage from a tear in the extraembryonic endoderm during the dissection.

When the embryo was repositioned and rotated in the frontal plane, we recorded outward current that was largest over the midline and declined gradually within 50 μm to either side (Fig. 2b). This suggests a transembryonic current pattern leaving the embryonic region of the embryo, strongest along the midline, and returning via the extraembryonic yolk sac endoderm.

We performed several experiments to determine the nature of these ionic currents. Holding the chamber temperature constant, we recorded the current over the foregut. Under constant-temperature conditions, the magnitude of the current leaving the foregut was stable over a two-hour observation period. In another experiment, the air curtain incubator was turned off while the outward current was measured. During this 21-min period, the chamber temperature dropped from 36.5 to 29°C. Meanwhile, the maximal outward current decreased from 13.0 $\pm$ 0.4 $\mu A/cm^2$ to 3.6 $\pm$ 0.1 $\mu A/cm^2$. This demonstrates that the maintenance of the outward current requires a stable physiological temperature.

The observation that the outward currents diminished with a decrease in temperature, suggested the involvement of active transport, possibly the Na^+/K^+-ATPase. Therefore we investigated whether ouabain, a specific

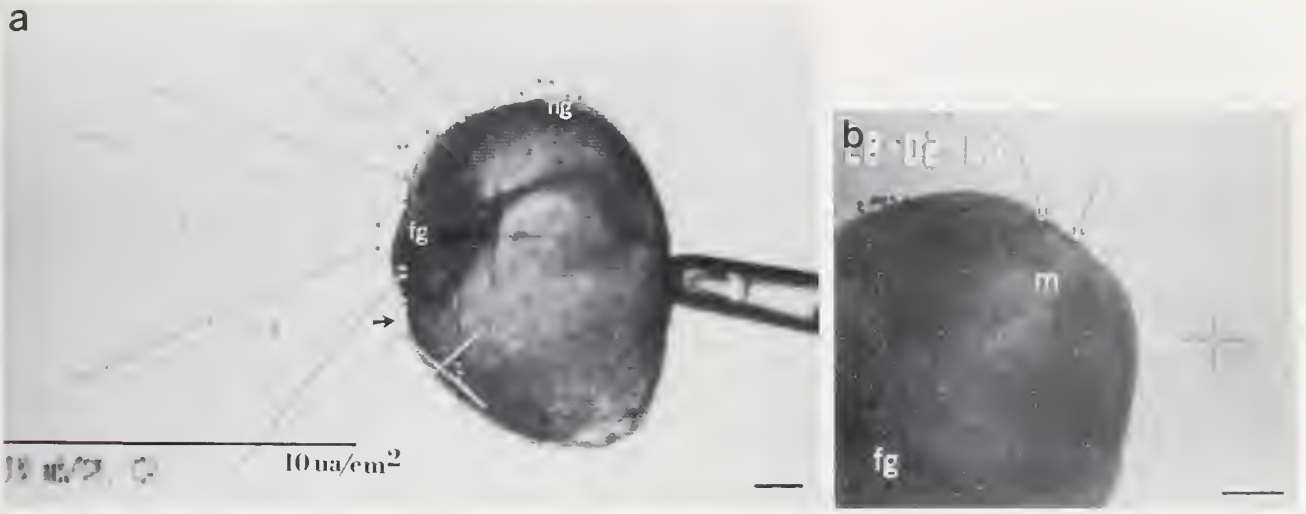

Figure 2. (a) Parasaggital view of 7.5-day embryo in the recording chamber with the computer vectors superimposed over the video image. The mouse embryo is held from the right with a fire-polished holding micropipet. The IBM-XT computer displays the current vector at each position. The magnitude of the current is represented by the length of the vector, while the direction of the vector shows the current direction. Note that maximum outward current is detected over the developing foregut (fg). As the probe is moved both anterior and posterior to the foregut the outward current decreases. Anterior to the foregut, an arrow marks the juncture between the embryonic and extraembryonic region. At this juncture note how the outward current abruptly reverses direction and the current vectors now point inward. Posterior to the hindgut (hg) note how the current vectors gradually begin to turn inward, representing an inward ionic current. Bar = 0.1 mm. (b) Three current vectors recorded from a 7.5-day embryo in frontal orientation. The foregut is in the foreground, while the hindgut is hidden. The current vectors indicate that the maximal current is outward along the midline, and falls off sharply as the probe is moved laterally towards the yolk sac (ys). Bar = 0.1 mm.

ATPase inhibitor (Borland and Tasca, 1974), would interfere with the current pattern. In our initial experiments, we added 100 μM ouabain to the media, after we had done a control recording of the current pattern. However, we observed no change in the current pattern even after a few hours of exposure to ouabain. Similarly, culture of embryos in 100 μM ouabain had no developmental effect on the embryos. We also attempted to use amiloride to block Na^+ channels and the Na^+/H^+ transporter (Simchowitz and Cragoe, 1986). After an 18-min stable recording period with the probe, 0.1 ml of 500 μM amiloride was added to the recording chamber to give a final concentration of 50 μM. The outward current was then monitored for a further 30-min interval. We observed no changes in the current relative to the reference current. However, these results are not conclusive as neither of these inhibitors may have reached the internal membranes where the Na^+ channels and the Na^+/K^+ ATPase reside.

The large magnitude of these ionic currents suggested that they might play some role during development, possibly by affecting migration of certain embryonic cells during gastrulation. As the mouse embryo *in situ* is completely surrounded by the parietal yolk sac (Reichardt's membrane) and the decidua, our *in vitro* conditions may not have been indicative of the normal current pattern. Both this membrane and the decidua could further restrict these currents forcing them along the plane of the embryo surface, rather than away from the surface as our current measurements indicated. Therefore, in a few embryos, we left Reichardt's membrane intact during the dissection to see how the current pattern would be affected. In two embryos, we recorded the current with Reichardt's membrane intact. In both embryos, the current pattern was similar to those without the membrane. Inward current was recorded over the extraembryonic endoderm, while outward current was detected emanating from the midline of the embryonic portion. The maximum outward current at the foregut was 3.8 ± 0.7 $\mu A/cm^2$, while the maximum inward current was -6.3 ± 0.8 $\mu A/cm^2$. For another embryo, the maximum inward and outward current was 5.3 ± 0.4 $\mu A/cm^2$ and -13.4 ± 0.8 $\mu A/cm^2$, respectively. Thus, in both these cases, the outward current pattern appeared to be reduced over the embryonic portion, while the extraembryonic inward current was less affected.

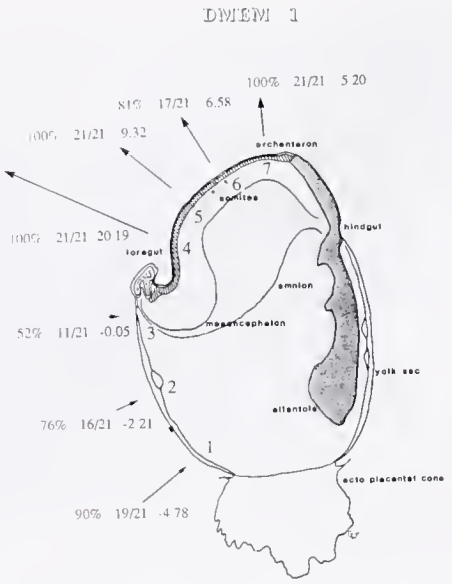

Figure 3. Diagramatic display of results from studies of 21 postimplantation mouse embryos. The numbers (1–7) along the inner margin of the embryo represent the probe recording positions. At each position the length of the arrow represents the average current vector ($\mu A/cm^2$) of all of the embryos. The numbers beneath each vector show the number and percent of embryos exhibiting current with this polarity. In a few embryos the detected current polarity was opposite to the average orientation. Note that at the embryonic/extraembryonic junction the inward current was more variable and likewise the average inward/outward magnitude was reduced. The point of maximum outward current was observed to be over the developing foregut, while the maximal inward current was over the extraembryonic yolk sac nearest the ectoplacental cone.

To further characterize the nature of these currents, we tested whether an artificially created leak, such as in puncture of the embryonic epithelium by a micropipet, would result in an outward current greater than that observed with an intact epithelium. This is indeed the case and in an embryo exhibiting a typical outward foregut current of 11.5 $\mu A/cm^2$, we recorded currents of 41.8, 11.5, and 15.5 $\mu A/cm^2$ at 2, 4, and 6 min after puncture with a micropipet. The larger value recorded initially supports the interpretation that the outward current is a passive leakage current. After a short interval of time this current stabilized to a value similar to that before injury, suggesting that the leak was repaired after a few minutes. This observation supports the hypothesis that outward current at the primitive streak is a passive leak due to the reduced junctional resistance along the embryonic midline (Jaffe and Stern, 1979).

The above experiments suggested that we might be detecting ionic currents caused by ions leaking from the amnionic cavity at junctional regions of low resistance. It is possible that these regions of low resistance may correspond to the site of gastrulation or other cellular rearrangements. Therefore, we utilized scanning electron microscopy to examine the cell morphology overlying the embryonic midline to detect areas of cellular rearrangement or other obvious discontinuities in the epithelium. The endoderm overlying the embryonic portion of the embryo was typically flattened and squamous with small micro plicae (Fig. 4a, b). There were no obvious cellular discontinuities along the midline of the embryo from foregut to hindgut, except in the region of the archenteron (Fig. 4c). This particular region was not associated with any significant changes in the current pattern. In fact it is unusual that such a major morphological discontinuity had no effect on the observed current pattern. This result suggests that morphological alterations at the gross level are not easily correlated with the observed ionic current pattern.

Discussion

Gastrulation in the mouse embryo involves the rearrangement of cells along the midline of the embryonic region of the embryo. At various regions along the midline, the underlying mesoderm is closely associated with the overlying endoderm (Poelman, 1981; Tam and Meier, 1982). We have shown that the current along the midline is predominantly outward, suggesting a leakage of ions through areas of reduced junctional resistance possibly due to cellular remodeling. Over the foregut of the embryo we detected the largest outward currents suggesting that either the cellular junctions were more leaky in this region or that the underlying driving force was greater. Evidence from the chick embryo showed that the epiblast or ectoderm of the chick embryo was the source of the current as it contained the Na^+/K^+ ATPase responsible for the generation of the ionic gradients (Stern, 1982; Stern and MacKenzie, 1983). In the mouse embryo, there is a greater mass of ectoderm (neural ectoderm) underlying the foregut region due to the formation of the developing brain (Jacobson and Tam, 1982). The enhanced ion flux generated by this expanse of neural ectoderm could be the basis of the larger outward current over the foregut. McCaig and Robinson (1982) showed that transepidermal currents began at neurulation in the frog. Thus the neural ectoderm could be the source of the currents that would increase as neurulation begins. This idea is supported by the observation that in younger mouse embryos, in which the head fold (neural ectoderm) was not fully developed, the outward current over the foregut region was reduced. An alternative explanation is that the fairly massive cell death occurring in the midline (Poelmann, 1981) could provide a region of low resistance resulting in a localized increase in current density.

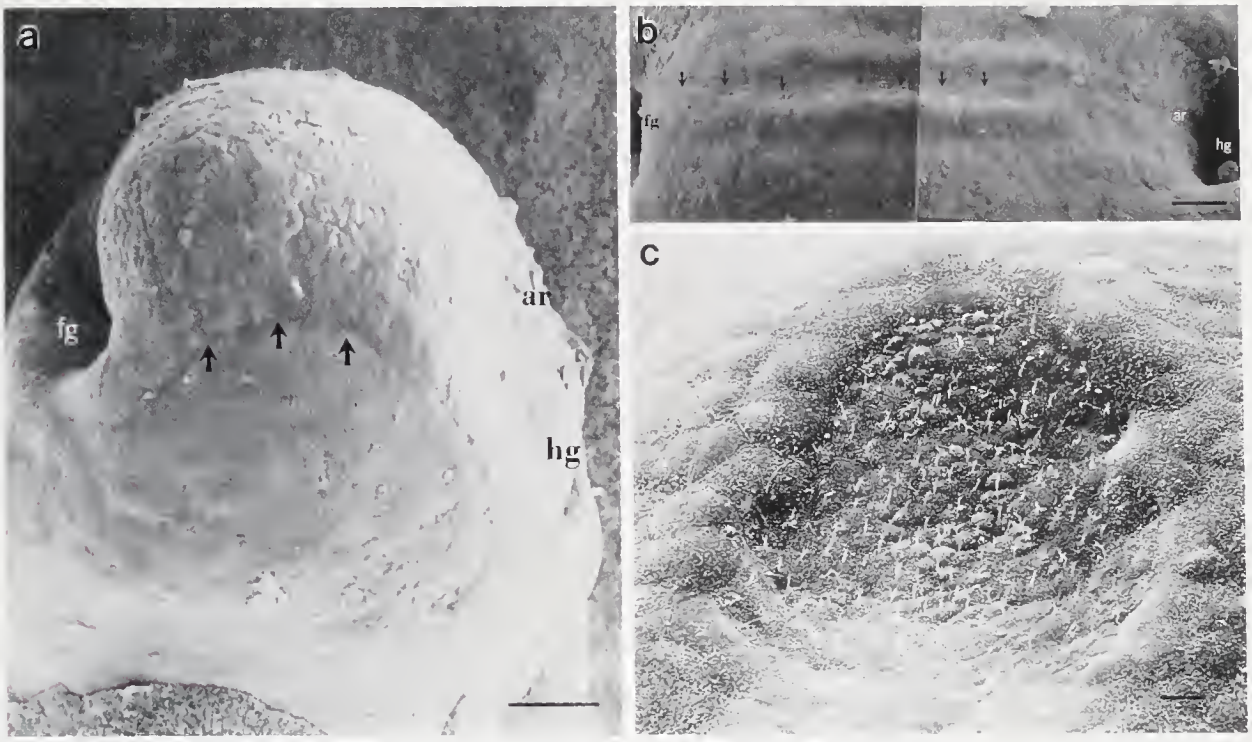

Figure 4. Scanning electron micrograph of overlying endoderm of a typical 7.5-day embryo. (a) View of whole embryo for orientation. The foregut (fg) is to the left and the hindgut (hg) is to the right. The embryonic endoderm spans the whole embryo from foregut to hindgut with the only epithelial discontinuity over the archenteron. Bar = 0.1 mm. (b) A frontal view of the region between the foregut and hindgut show that the endoderm is continuous. In particular, the cells overlying the foregut are not morphologically different from the endoderm cells over the midline. However, at the archenteron there is a break in the endoderm and different cells appear to be protruding. Bar = 50 μm. (c) Magnified view of the archenteron region. Note that the underlying cells are morphologically quite different from the endoderm cells. They are smaller and have a single cilium protruding from the cell. In cross-section (not shown) these cells are columnar compared to the squamous endoderm cells (see Poelman, 1981). Bar = 10 μm.

The inward current pattern also showed variations in magnitude. The extraembryonic currents in general were smaller than the embryonic currents. However, the extraembryonic endoderm, through which the outward current completes the current loop (Fig. 5), has a greater surface area than the embryonic region. Therefore, one would expect to see currents larger in magnitude emanating from the embryo, with smaller currents returning via the extraembryonic endoderm. The inward current was always maximal nearest to the ectoplacental cone region. This observation reinforces the proposition that the extraembryonic endoderm is a pumping epithelium. In cross section the extraembryonic endoderm is increasingly more columnar toward the ectoplacental cone (Snell and Stevens, 1966; Snow, 1976) and the number and density of microvilli are also higher in that region (Tamarin and Boyde, 1976; Tam and Meier, 1982). Therefore, as the extraembryonic endoderm develops into a more effective pumping epithelium, one might expect that the inward currents generated would also increase.

In our experiments we were unable to determine the source of these currents, however since a decrease in temperature also reduced the current, it is likely that some of the currents are generated by an active transport mechanism. The fact that a break in the epithelium caused a dramatic increase in the outward current suggests a passive leakage of ions out of the embryonic region, which implies that the ionic pumps may be situated in the extraembryonic endoderm. Eventually we plan to localize the Na^+/K^+-ATPase with [^{3}H] ouabain, as did Stern and MacKenzie (1983) who found that the ATPase was situated on the basal surfaces of the embryonic epiblast. Additionally, they found that the Na^+/K^+-ATPase was also located apically at the primitive streak, suggesting an active pumping of ions outward from the streak (Stern and MacKenzie, 1983). Although none of the inhibitor drugs we applied had any effect on these currents,

Figure 5. Composite diagram of the ionic current pattern in the 7.5-day mouse embryo. The current is outward along the embryonic midline, while the maximal outward current is primarily over the foregut. This transembryonic current will then complete the current loop returning as inward current via the extraembryonic endoderm.

they may not have had access to internal epithelia. Therefore in future experiments we plan to inject ATPase inhibitors and channel-blocking drugs into the amniotic cavity to bypass this limitation. Furthermore, we would like to determine which ionic species are responsible for the majority of the ionic current. Thus we are conducting ionic substitution experiments to establish the ionic character of these currents (Winkel and Nuccitelli, 1987).

The morphology of the endoderm overlying the primitive streak and anterior to the head process had little relationship to the detected current pattern. In scanning electron micrographs, the cells in the midline appear continuous from the foregut, where the outward current is greatest, to the archenteron where the outward current is reduced. Despite the fact that there is a hiatus in the endoderm at the archenteron, as the cells of the head process emerge (Poelman, 1981; Tam and Meier, 1982), the outward currents are not affected by this morphological discontinuity. Therefore, changes in morphology overlying the embryonic regions of the mouse embryo are apparently unrelated to the ionic and junctional changes occurring within the epithelium.

The ionic current pattern demonstrated here may be indicative of a morphogenetic event, such as gastrulation in the mouse embryo, and may even be influencing morphogenetic cellular rearrangements as gastrulation proceeds. The currents we detected are strong ionic currents. Currents on the order of 20 to 40 $\mu A/cm^2$ recorded 20 μM from the cell surface translate into higher currents at the cell surface of the epithelium. Currents of this magnitude could generate significant electric fields along cells in the primitive steak region that could guide cell movement. Studies in the chick have shown that fields as low as 10 mV/mm can direct migration of cells towards the cathode (Erickson and Nuccitelli, 1984). Similarly, the mesoderm cells in the mouse embryo may be responsive to the electric fields generated by ionic currents along the midline. In the chick embryo, the current leaves the primitive streak with chick mesoderm cells traveling against the current. However, in the mouse embryo, the mesoderm cells would be migrating in the same direction as the current. The possibility that mouse mesoderm cells are responsive to electric fields *in vivo* remains to be demonstrated.

Acknowledgments

The authors thank Jerry Morgan for technical assistance with the scanning electron microscope. This work was supported in part by NIH grant 22594 to R.N.; G.W. was supported by NIH reproductive biology training grant #HD 07131.

Literature Cited

Borland, R. M., and R. J. Tasca. 1974. Activation of a Na^+-dependant amino acid transport system in preimplantation mouse embryos. *Dev Biol.* **36:** 169–183.

Diwan, S. B., and L. C. Stevens. 1976. Development of teratomas from the ectoderm of mouse egg cylinders. *J. Natl. Cancer Inst.* **57:** 937–942.

Erickson, C. A., and R. Nuccitelli. 1984. Embryonic fibroblast motility and orientation can be influenced by physiological electric fields. *J. Cell Biol.* **98:** 296–307.

Gardner, R. L. 1982. Investigation of cell lineage and differentiation in the extraembryonic endoderm of the mouse embryo. *J. Embryol. Exp. Morph.* **68:** 175–198.

Gardner, R. L., and J. Rossant. 1979. Investigation of the fate of 4.5 day post-coitum mouse inner cell mass cells by blastocyst injection. *J. Embryol. Exp. Morph.* **52:** 141–152.

Hogan, B. L. M., and R. Tilly. 1981. Cell interactions and endoderm differentiation in cultured mouse embryos. *J. Embryol. Exp. Morph.* **62:** 379–394.

Jacobson, A. G., and P. P. L. Tam. 1982. Cephalic neurulation in the mouse embryo analyzed by SEM and morphometry. *Anat. Rec.* **203:** 375–396.

Jaffe, L. F., and C. D. Stern. 1979. Strong electrical currents leave the primitive streak of chick embryos. *Science* **206:** 569–571.

Lawson, K. A., J. J. Meneses, and R. A. Pedersen. 1986. Cell fate and cell lineage in the endoderm of the presomite mouse embryo, studied with an intracellular tracer. *Dev. Biol.* **115:** 325–339.

Lawson, K. A., and R. A. Pedersen. 1987. Cell fate, morphogenetic movement and population kinetics of embryonic endoderm at the time of germ layer formation in the mouse. *Development* **101:** 627–652.

McCaig, C. D., and K. R. Robinson. 1982. The ontogeny of the tran-

epidermal potential difference in frog embryos. *Dev. Biol.* **90:** 335–339.

Nakatsuji, N., and M. H. L. Snow. 1986. Cinemicrographic study of the cell movement in the primitive-streak-stage mouse embryo. *J. Embryol. Exp. Morph.* **96:** 99–109.

Nuccitelli, R. 1986. A two-dimensional vibrating probe with a computerized graphics display. Pp. 13–20 in *Ionic Currents in Development,* A. R. Liss, Inc., New York.

Poelman, R. E. 1981. The head process and the formation of the definitive endoderm in the mesoderm. *Anat. Embryol.* **162:** 41–49.

Rosenquist, G. C. 1972. Endoderm movements in the chick embryo between the early short streak and head process stage. *J. Exp. Zool.* **180:** 95–104.

Simchowitx, L., and E. J. Cragoe, Jr. 1986. Inhibition of chemotactic factor-activated Na^+/H^+ exchange in human neutrophils by analogues of amiloride: structure-activity relationships in the amiloride series. *Molec. Pharmacol.* **30:** 112–120.

Skreb, N., A. Svajger, and B. Levak-Svajger. 1968. Developmental potentialities of the germ layers in mammals Pp. 27–39 in *Embryogenesis in Mammals* (Ciba Foundation Symph. 40), Elsevier, Amsterdam.

Snell, G. D., and L. C. Stevens. 1966. Early embryology. Pp. 205–245 in *Biology of the Laboratory Mouse,* E. L. Green, ed. Dover Pub. Inc., New York.

Snow, M. H. L. 1976. Embryo growth during the immediate postimplantation period. Pp. 53–66 in *Embryogenesis in Mammals* (Ciba Foundation Symph. 40), Elsevier, Amsterdam.

Stern, C. D., and D. O. MacKenzie, 1983. Sodium transport and the control of epiblast polarity in the early chick embryo. *J. Embryol. Exp. Morph.* **77:** 73–98.

Tam, P. P. L., and S. Meier. 1982. The establishment of a somitomeric pattern in the mesoderm of the gastrulating mouse embryo. *Am. J. Anat.* **164:** 209–225.

Tamarin, A., and A. Boyde. 1976. Three-dimensional anatomy of the 8-day mouse conceptus: a study by scanning electron microscopy. *J. Embryol. Exp. Morph.* **36:** 575–596.

Winkel, G. K., and R. Nuccitelli, 1987. Strong ionic currents leave the midline of the 7.5-day postimplantation mouse embryo. *J. Cell Biol.* **105:** 256a.

Reference: *Biol. Bull.* **176(S):** 118–122. (April, 1989, Suppl.)

Extracellular Electrical Currents in the Chick Blastoderm

PAVEL KUČERA AND YVES DE RIBAUPIERRE

Institute of Physiology, Medical Faculty of the University of Lausanne, CH-1005 Lausanne, Switzerland

Abstract. Extracellular electrical currents were recorded using a computer-controlled scanning vibrating electrode from gastrulating chick blastoderms cultured *in vitro*. On the ventral surface, currents of 10–20 $\mu A/cm^2$ diverged from the area opaca and turned around the margin of blastoderm across the vitelline membrane. Weaker currents (1–10 $\mu A/cm^2$) converged to the anterolateral area pellucida and penetrated it in the ventrodorsal direction. On the dorsal surface, currents returned to the area opaca from the margin and from the center of area pellucida. During development, the pattern of currents remained similar on the dorsal surface while the leaky area on the ventral surface progressively extended to all the periphery of area pellucida. The intensity of currents in the blastoderm oscillated with a period of 5 to 6 min. This spatio-temporal organization of extracellular currents is compared to physiological activities of embryonic cells in different regions of the blastoderm.

Introduction

The chick blastoderm is a discoidal structure formed by the ecto-, meso-, and endodermal cell layers. The embryonic cells show a remarkable functional differentiation in energy metabolism (Raddatz and Kučera, 1983, 1988; Kučera *et al.*, 1984), mechanical behavior (Kučera and Burnand, 1987a) and formation of extracellular matrix (Monnet-Tschudi *et al.*, 1985). This differentiation, observed already during the first day of incubation, is related to the position of cells within the blastoderm and may depend on relatively simple intercellular communications such as diffusion of metabolites and ions (Kučera and Monnet-Tschudi, 1987). Experiments using the vibrating probe (Jaffe and Stern, 1979) and radioisotopes (Stern and MacKenzie, 1983) have suggested the existence in the embryo of organized electrical currents probably linked to sodium flux across the epiblast.

Recently, by using the voltage-clamp technique, we showed that both areas of the blastoderm—the extraembryonal area opaca and the embryonal area pellucida—actively transport sodium but differ in their electrophysiological properties. The former area generates stronger and regularly oscillating short-circuit current. The latter area is more leaky and generates weaker and rather stable current (Kučera and Katz, 1988).

In this paper, the extracellular distribution of these currents is studied in the whole chick blastoderm using a technique of vibrating electrode (Jaffe and Nucitelli, 1974).

Materials and Methods

Blastoderms at stages 4 to 8 of Hamburger and Hamilton, obtained from eggs preincubated for 18 to 24 hours, were excised with the vitelline membrane, cleaned from the adhering yolk, and mounted in incubation chambers casted from silicone. The vitelline membrane was stretched over a ring protruding from the bottom of the chamber and fixed by a steel ring. The space under and over the preparation was filled with a Tyrode solution of the same composition. Blastoderms were mounted mostly in the inverted position, *i.e.*, with the ventral side up. In those mounted in the upright position, the vitelline membrane was left either intact or circularly opened to expose the ectoderm of the embryo. The chamber was inserted in a thermostabilized support and maintained at 36.5°C. This culture, allowing a normal development for at least three additional days, has been extensively used and described in detail (Kučera and Burnand, 1987b).

The thermostabilized preparation was fixed on a motorized table controlled by a microcomputer (Fig. 1, left). Before each record, a preliminary step-to-step scan was

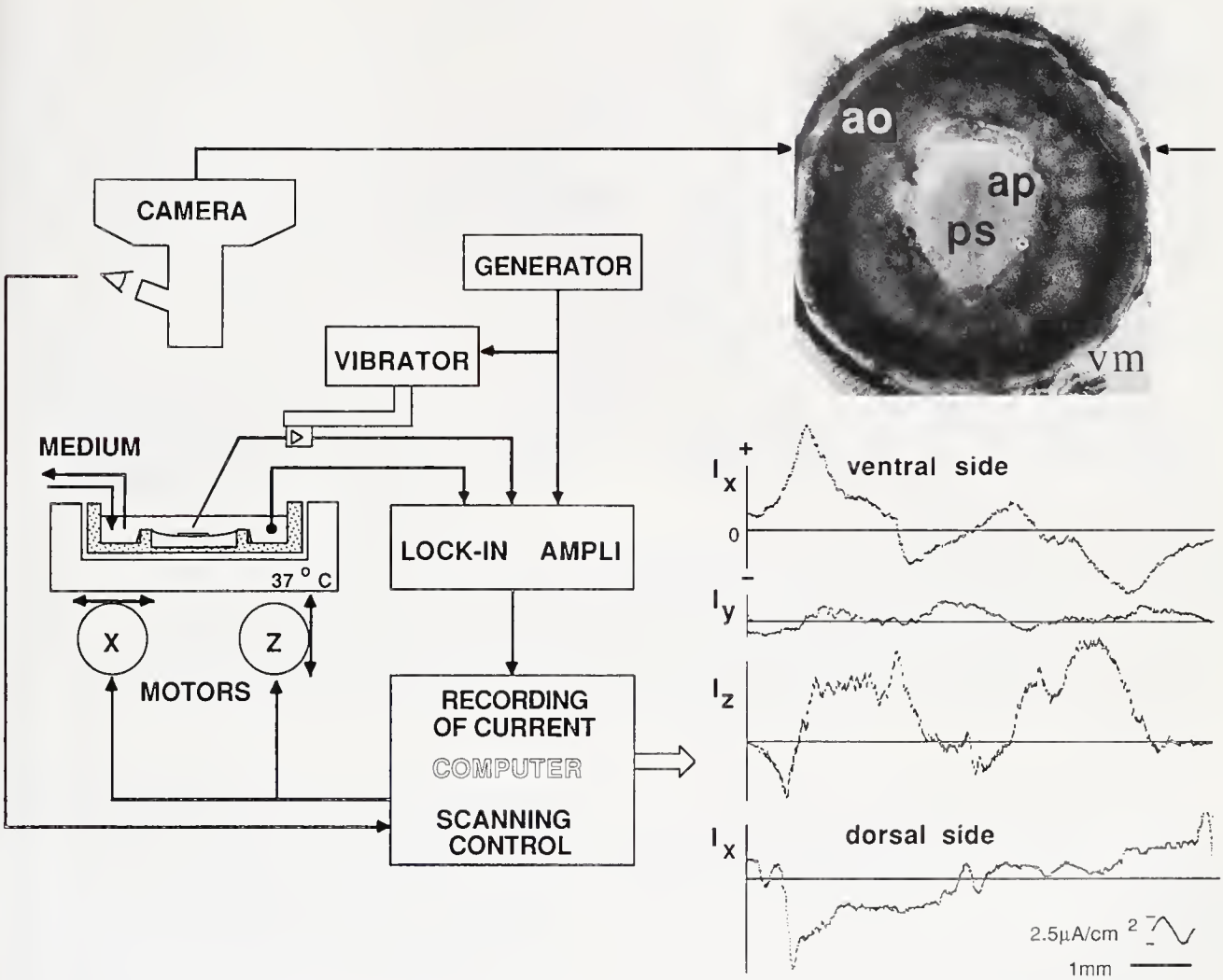

Figure 1. Scanning of extracellular currents in the blastoderm. Left: the experimental set up. The blastoderm attached to vitelline membrane is spread over the ring at the bottom of the chamber (stippled). The electrode (bent needle) vibrates in parallel or vertically to the plane of the preparation. Right top: photograph of the blastoderm of stage 4 of Hamburger and Hamilton. Right bottom: currents recorded using vibrations parallel (Ix), transversal (Iy), and vertical (Iz) to the direction of scanning. These profiles correspond to the level indicated on the photograph by the two arrows.

done to adjust and memorize a constant distance (mostly 125 μm) from the preparation to the electrode tip. A profile interpolated from these measurements was used to control the height of the table during the scan done at 6 mm/min. Visual control and photographs of the preparation were done using a binocular microscope.

The electrode was made of a bent tungsten wire insulated with glass and the tip (about 5 μm) was plated with gold. The electrode was inserted into a miniature amplifier fixed on the oscillating arm of an ECG scriptor. The frequency of driving oscillation (around 180 Hz) was adjusted to produce a stable resonance of the vibrating electrode and the amplitude of vibration was held at 250 μm. The potential difference between the extreme positions of the electrode tip was detected by using a lock-in amplifier with a time-constant of 0.1 s. The calibrations were done in the Tyrode solution between two square parallel electrodes generating a sinusoidal current of 2.5 μA/cm^2.

Each scan was done twice with the vibration parallel and, after 90° rotation of the probe, transversal to the direction of scanning. The corresponding currents were labelled Ix and Iy. The vectorial sum of these two components, parallel to the preparation was superimposed on the image of preparation (Fig. 2).

A frequency of about 200 Hz elicited at the tip of the bent needle a circular oscillation in the plane perpendicular to the preparation. In some cases, this mode was used and the detection phase adjusted to measure the vertical current (Iz).

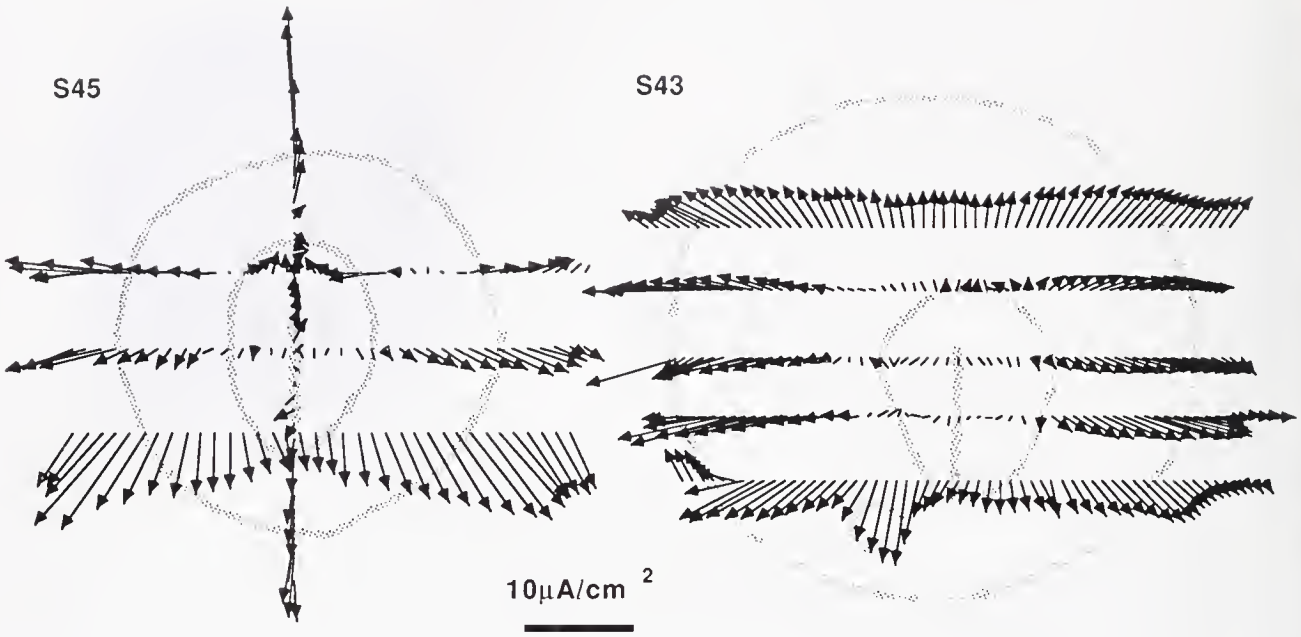

Figure 2. Maps of the extracellular currents parallel to the ventral surface of the blastoderm. Divergent pattern of strong currents in the area opaca contrasts with weak currents in the area pellucida. In the S45, at the intersection of vertical and superior scans, the currents converge into the proamniotic region. In the S43, strong currents flow towards a hole made in the posterior area opaca.

Results

Twenty-two embryos were considered: 17 mounted in the inverted position, 5 in the upright position.

Spatial pattern in the stage 4

The blastoderm of the stage 4 (Fig. 1, upper right) consists of the central area pellucida in which the primitive streak indicates the axis of the embryo and of the peripheral area opaca (loaded with yolk), the marginal cell of which attaches to the vitelline membrane. Examples of currents recorded from the ventral side of the blastoderm and from left to right are shown in Figure 1 (lower right).

The currents were already detectable outside of the blastoderm, at about 1 mm from the margin. Here, the Ix and Iz, positive and negative, respectively, indicate that the current flowed from the area opaca and traversed the vitelline membrane in ventrodorsal direction. The Ix were always maximal near the margin and then attenuated towards the area pellucida. The Iz was now positive, indicating that the current was emerging from the area opaca in the dorsoventral direction. In the area pellucida, the negative Ix and nul or slightly negative Iz indicate that the current converged towards the axis of the blastoderm and might eventually cross it in a ventrodorsal direction. The currents were bilaterally symmetrical.

The profiles recorded from the dorsal surface of the stage 4 show currents flowing towards the area opaca from the outside of blastoderm and from the center of area pellucida (Fig. 1, lower right).

The maps of vectors resulting from the addition of ventral Ix and Iy components are illustrated in Figure 2. They show that the blastoderm behaves mostly as a source of divergent currents with the exception of the anterior horseshoe-shaped part of the area pellucida (future proamnios) which seems to drain currents from the adjacent regions.

Temporal aspects

In embryos of different stages of development, the dorsal pattern of currents remained similar to that described above, *i.e.*, large centripetal and minor centrifugal currents flowing towards the area opaca. In contrast, the ventral pattern in the center of blastoderm was rapidly changing. Namely, the regions where the current penetrated ventrodorsally through the tissue became larger and better delimited as shown in Figure 3 (left). In one very young stage 4, the current actually converged upon the area pellucida (upper profile) but at the stage of fully developed primitive streak, it spread out from it (middle profile) and was in part directed towards the proamniotic region. From the stage 5, progressively all the peripheral area pellucida drained the current (lower profile).

Within a given embryo, the current spontaneously

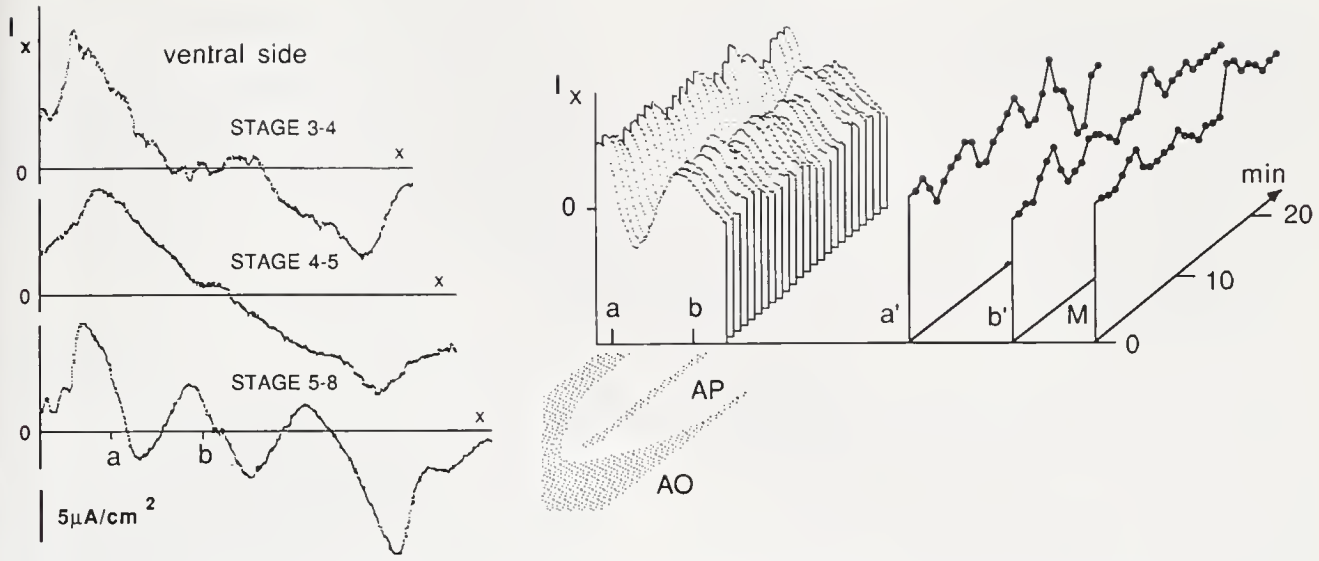

Figure 3. Temporal evolution of the ventral currents. Left: profiles recorded at the mid-level of primitive streak in successive stages of development (interval of 6 h). The area pellucida changes from a current sink to a current source, while two sinks appear laterally. The left one is located in between the a and b. Right: profiles recorded at 54-s intervals over the region a-b, covering the boundary between the area opaca and area pellucida (see the stippled scheme). The currents recorded at the points a and b and plotted with respect to time (a', b') reveal 4.5 oscillations in 24 min. This periodicity is suggested even in the fluctuations of the mean value (M) of all the points of the scan.

fluctuated on the scale of minutes. Rather regular variations, with a period of about 5 to 6 min, were observed over the internal part of area opaca (Fig. 3, right). This phenomenon was less expressed in the area pellucida. Nevertheless, all points of the scans, even if averaged, indicated the same periodicity.

All currents in the blastoderm were abolished after 45 min in the presence of 10^{-4} mol/l ouabain (not shown).

Discussion

The current profiles show that the entire extraembryonal area opaca is traversed dorsoventrally by electrical currents, which leave its ventral side and return to its dorsal side mainly around the margin of blastoderm and to a smaller extent also through the area pellucida. Jaffe and Stern (1979) made local recordings from the dorsal face of area pellucida at stages 3–4 and found mostly centrifugal currents up to 20 μA/cm^2. Our values are slightly lower but in excellent agreement with the data from voltage-clamp experiments showing that the area opaca is rather tight (400–1000 Ω cm^2 and generates relatively high transembryonic sodium current and potential (16–22 μA/cm^2, about 8 mV, respectively) while the area pellucida is rather leaky (200–400 Ω cm^2) and generates lower transembryonic current and potential (about 8 μA/cm^2 and 2mV, respectively) (Kučera and Katz, 1988). Under our conditions, similar to the situation in ovo, the cells are actually stretched by the tension actively generated in the blastoderm (Kučera and Burnand, 1987). The stretching decreases not only the amount of transporting sites per unit area of the embryo but also the paracellular resistance (unpub. results) and hence the current density.

Jaffe and Stern (1979) found that the primitive streak allows for ventrodorsal currents. This finding is confirmed by the scans from the dorsal, but not from the ventral, side of blastoderm. In fact, the streak behaves ventrally as a current source. Furthermore, the leaks in the lateral parts of the area pellucida do not seem to be present dorsally. At present, we have no knowledge about the currents within the embryonic cavity and think that the currents generated by the both areas are short-circuited through the endoderm and ectoderm of the area pellucida.

Thus the ring-shaped area opaca generates two families of current loops arranged in a toroidal manner. The loops in the external torus diverge ventrally towards the periphery, cross the edge of blastoderm, and converge upon the dorsal side of area opaca. These currents are strong and radially symmetrical. The loops forming the internal torus converge ventrally and anteriorly, cross the anterolateral limits of area pellucida, pass through the embryonal cavity, emerge from the ectoderm in a fountain-like manner, and close on the dorsal surface of

area opaca. These currents are weak and bilaterally symmetrical. The two systems of loops, especially the external one, can show oscillations with a period very comparable to that measured in short-circuited conditions, *i.e.*, about 5 min (Kučera and Katz, 1988).

Could there be any physiological correlates to such a spatio-temporal organization of currents in the blastoderm?

Studies done in the area opaca (Monnet-Tschudi *et al.*, 1985; Kučera and Burnand, 1987; Kučera and Monnet-Tschudi, 1988; Monnet-Tschudi and Kučera, 1988) have shown that (1) in the internal zone, the ectodermal cells are stretched, show organized myosin filaments, and form a dense punctated pattern of extracellular fibronectin (this zone is traversed by dorsoventral currents which very likely correspond to active sodium transport); (2) in the external zone, the ectodermal cells are permanently contracted, do not show organized myosin but their extracellular matrix is arranged radially sometimes in very long filaments in which the fibronectin staining decreases towards the periphery (in this zone, the currents flow radially and in parallel to the blastoderm); and (3) at the margin of blastoderm, the ectodermal edge cells attach to the vitelline membrane and migrate upon it, show no organized myosin and fenestrated basement membrane (this zone is traversed by ventrodorsal currents).

Studies done in the area pellucida (Kučera and de Ribaupierre 1982; Kučera and Burnand, 1987a) have shown that (1) tissue viscosity (possibly reflecting the state of cytoskeletal elements) oscillates with a period of about 5 min; (2) migration of mesodermal cells leaving the primitive streak is saccadic with a period of about 5 min; and (3) repetitive local field stimulations (anode ventrally) leads to contractions and ectopic accumulation of cells in the mesodermal layer.

Thus, indeed, to each pattern of cell behavior might be correlated a particular pattern of extracellular currents and the embryonal cells do react in response to experimentally induced electrical currents. However interesting these observations may be, the possible role of such currents as mediators of epigenetic information in the morphogenesis remains still to be experimentally demonstrated.

Acknowledgments

We thank Miss E. Cano for the explantations and technical help, Mr. Ch. Haeberli for the conception of the data acquisition system, and Mr. M. Jade for the construction of the scanning table. This work was supported by the grant 3.418-0.86 from the Swiss National Science Foundation.

Literature Cited

Jaffe, L. F., and R. Nuccitelli. 1974. An ultrasensitive vibrating probe for measuring steady extracellular currents. *J. Cell. Biol.* **63:** 614–628.

Jaffe, L. F., and C. D. Stern. 1979. Strong electrical currents leave the primitive streak of chick embryos. *Science* **206:** 569–571.

Kučera, P., and Y. de Ribaupierre. 1982. In situ recording of mechanical behaviour of cells in the chick embryo. Pp. 433–444 in *Progress in Clinical and Biological Research, Vol. 85B: Embryonic Development,* M. M. Burger and R. Weber, eds. A. R. Liss, New York.

Kučera, P., E. Raddatz, and A. Baroffio. 1984. Oxygen and glucose uptakes in the early chick embryo. Pp. 299–309 in *Respiration and Metabolism of Embryonic Vertebrates,* R. S. Seymour, ed. Dr W. Junk Publ., Dordrecht/Boston/London.

Kučera, P., and M-B. Burnand. 1987a. Mechanical tension and movement in the chick blastoderm as studied by real time image analysis. *J. Exp. Zool.* Suppl. **1:** 329–339.

Kučera, P., and M-B. Burnand. 1987b. Routine teratogenicity test that uses chick embryos in vitro. *Teratogen. Carcinogen. Mutagen.* **7:** 427–447.

Kučera, P., and F. Monnet-Tschudi. 1987. Early functional differentiation in the chick embryonic disc: interaction between mechanical activity and extracellular matrix. *J. Cell Sci.* Suppl. **8:** 415–431.

Kučera, P., and U. Katz. 1988. Sodium current clock in the early chick embryo. *Experientia* **44** (Suppl. 20th Annual meeting of USGEB):A34.

Monnet-Tschudi, F., M.-B. Burnand, P. Favrod, M. Capt, C. Verdan, and P. Kucera. 1985. Fibronectin in the area opaca of the young chick embryo. *Cell Tissue Res.* **241:** 85–92.

Monnet-Tschudi, F., and P. Kučera. 1988. Myosin, Tubulin and laminin immuno-reactivity in the growing area opaca of the chick embryo. *Anat. Embryol.* **79:** 157–164.

Raddatz, E., and P. Kučera. 1983. Mapping of the oxygen consumption in the gastrulating chick embryo. *Respiration Physiol.* **51:** 153–166.

Raddatz, E., and P. Kučera. 1988. CO_2 production of the chick embryo during the first day of post-laying development. *Respiration Physiol.* **71:** 133–145.

Stern, C. D., and D. O. MacKenzie. 1983. Sodium transport and the control of epiblast polarity in the early chick embryo. *J. Embryol. Exp. Morphol.* **77:** 73–98.

Reference: *Biol. Bull.* **176(S):** 123–125. (April, 1989, Suppl.)

Electric Currents Associated With Directed Migration of Fibroblasts

SHIGETOSHI OIKI, TAKAKO OHNO-SHOSAKU[1], AND YASUNOBU OKADA[2]

Department of Physiology, Kyoto University Faculty of Medicine, Kyoto 606, Japan

Abstract. Cultured mouse fibroblasts (L cells) respond to a complement subcomponent, Clq, with hyperpolarizations and exhibit chemotaxis toward this ligand. Using a vibrating probe extracellular recording technique, we have studied whether extracellular electric currents are associated with directed migration or chemotaxis of the fibroblasts. The fibroblasts under directed migration were obtained in wounded monolayer cultures. Extracellular electric currents were too small to be detected around these migrating cells by means of a vibrating platinum black electrode (about 30 μm in diameter). To converge the current around migrating cells to a narrow space, a disk-like coverslip (with a central hole of 1 mm in diameter) was laid over wounded cultures. Thus, sizable electric currents (0.1–2.4 $\mu A/cm^2$) could be recorded at an aperture opening of the coverslip on wounded cultures in a weakly conductive medium. The currents always flowed to the leading front of the migrating cells. No current was detected on non-migrating fibroblasts. A chemoattractant (Clq) added in front of migrating cells induced biphasic changes in the electric current.

Introduction

Fibroblasts migrate into a wound and play a central role in the healing process (Ross, 1968). Recently we (Oiki and Okada, 1988) showed that cultured mouse fibroblasts (L cells) respond with chemotaxis and hyperpolarizations to a subcomponent of the complement Cl component, Clq, which is accumulated in areas of inflammation (Appel *et al.*, 1978). There is a possibility that extracellular electric fields are associated with polarized fibroblasts, which are exhibiting electrical membrane responses, under chemotactic migration to a wound. The purpose of this paper is to detect electric fields around fibroblastic L cells migrating to a wound by the vibrating probe technique (Jaffe and Nuccitelli, 1974) and to examine effects of Clq on the extracellular electric current.

A preliminary account of some of these results has been given in abstract form (Oiki *et al.*, 1985a).

Materials and Methods

Mouse fibroblastic L cells were cultured in Fischer medium (Nissui Co.) supplemented with 10% bovine serum. Studies with vibrating probes were made using the monolayer cells cultured for 5 to 7 days in 3.5-cm plastic petri dishes (Falcon). A wound model was obtained by scraping away the central or circumferential part of the confluent cell sheet (see Fig. 3). After 3- to 5 h-culture, fibroblasts under directed migration were found at the periphery of the wound. After replacing a culture medium with a control or a low-conductivity saline of about 2 ml, extracellular electric fields were measured with a vibrating electrode (Vibrating Probe Co., Davis, California), according to Jaffe and Nuccitelli (1974). Vibrating electrodes with a spherical platinum black (about 30 μm in diameter) were made as described by Nawata (1984). The probe was vibrated in a horizontal plane at about 150 Hz between two extracellular points about 30 μm apart at 25°C. The output voltage from a lock-in amplifier was recorded on a chart recorder through a prefilter with a time constant of 1 s. To detect electric fields derived from migrating fibroblasts, the probe was placed around the cells (especially at the leading front end) or at the edge of the aperture opening of a disk-like coverslip laid over the monolayer cells (see Results). The control saline contained (in mM) 137.5 NaCl, 4.2 KCl, 0.5 $MgCl_2$, 0.9 $CaCl_2$, 10 HEPES-NaOH (pH 7.3), and 10 mannitol (resistivity 56 Ω-cm). The low-conductivity sa-

[1] Present address: Department of Physiology, Osaka Medical College, Takatsuki City, Osaka 569, Japan.

[2] Author to whom reprint request should be addressed.

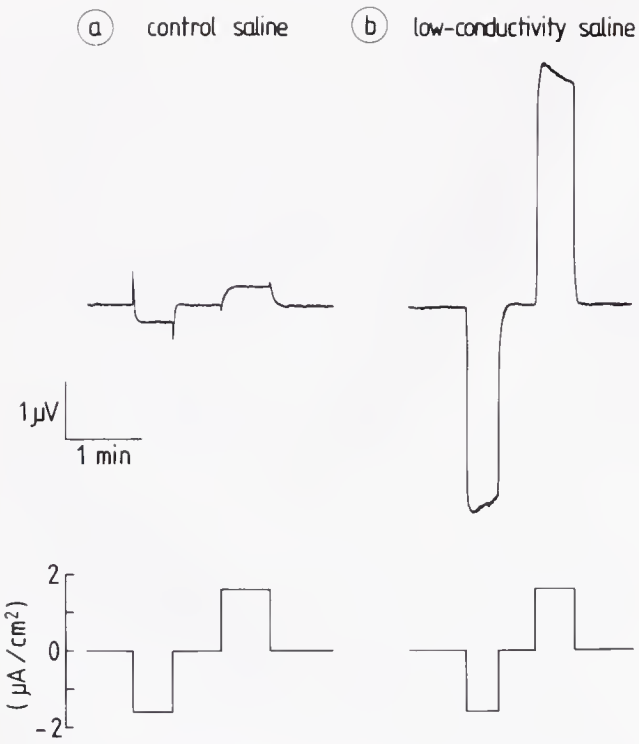

Figure 1. Responses of the vibrating probe to the known current density (±1.6 μA/cm^2) in the control (a) and the low-conductivity salines (b).

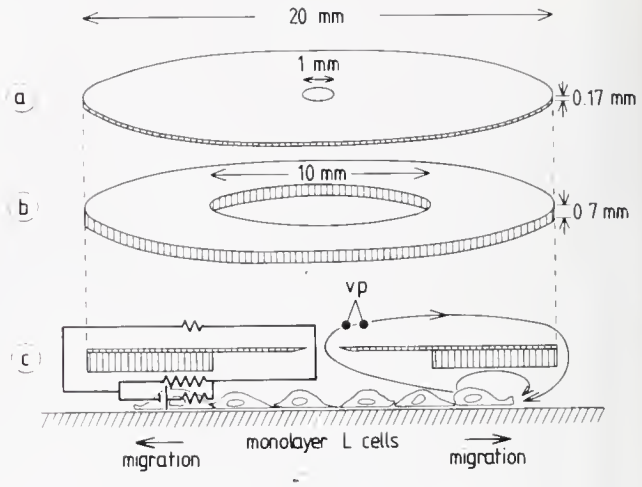

Figure 2. Schematic drawing of an apparatus to converge the current around migrating cells to a narrow space. The device (c) consists of a disk-like coverslip (a) with a central hole (the upper edge of which should be sharp to eliminate a "barrier artifact") and a plastic disk spacer (b). Both disks were glued with each other with epoxyresin. The spacer was directly laid over monolayer cells around the circular wound edge without crashing them. The extracellular currents around cells migrating into the wound (centrifugally, in this scheme) can be converged to the aperture opening of a coverslip, because the resistance via a space between the migrating cells at the wound edge and the disk-like plastic spacer must be very high, as illustrated in c. The current thus converged was measured by a vibrating probe (*vp*) at the edge of the aperture. A "barrier artifact" was never observed, when the probe was horizontally vibrated above a horizontal plane at the coverslip in the vicinity of the aperture opening.

line (resistivity 0.7 kΩ-cm) was obtained by replacing NaCl in the control saline with 270 m*M* mannitol. The calibration of the output of the vibrating system was made by applying known current densities in both salines in each experiment (Fig. 1). Freshly isolated human Clq (Oiki and Okada, 1988) was administered to the cells at the final dose of 100 μg/ml.

Results

Wounding a monolayer resulted in cell migration only at the periphery of the wound within 3–5 h. At the leading front end of migrating L cells, the ruffling structure (lamellipodia), which is a locomotion organ of fibroblasts (Abercrombie *et al.*, 1970), was always observed. Around these migrating fibroblasts (even at the leading front end), vibrating probes failed to detect extracellular currents in a control or a low-conductivity saline. In an attempt to converge the scanty current, if present, to a narrow space, a disk-like device with a central hole (1 mm in diameter) was directly laid over monolayer cells migrating from the circular wound edge (Fig. 2). This device consists of a disk-like coverslip glued on a plastic disk spacer. At the edge of the aperture opening of a coverslip, currents in the range of 0.08 to 3 μA/cm^2 (mean ± S.E.: 0.64 ± 0.24 μA/cm^2, n = 11) were consistently recorded on wounded cultures in a weakly conductive saline (Fig. 3). On the uninjured confluent cultures, currents were never recorded even using such a current-converging device. Immediately after wounding, the current could not be detected on the cells that had not yet exhibited migrating morphology. When the central area of monolayers

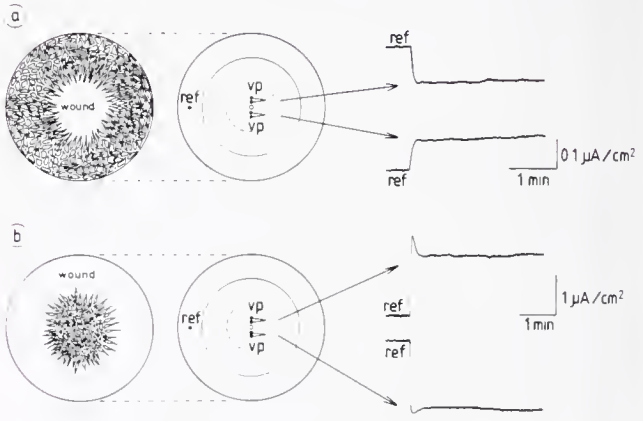

Figure 3. Representative recordings of extracellular currents flowing to a leading front end of the migrating L cells in the wounded monolayers. Significant currents were detected when the vibrating probe was translocated from the vicinity of a reference electrode (at *ref*) to the edge of the aperture opening (at *vp*).

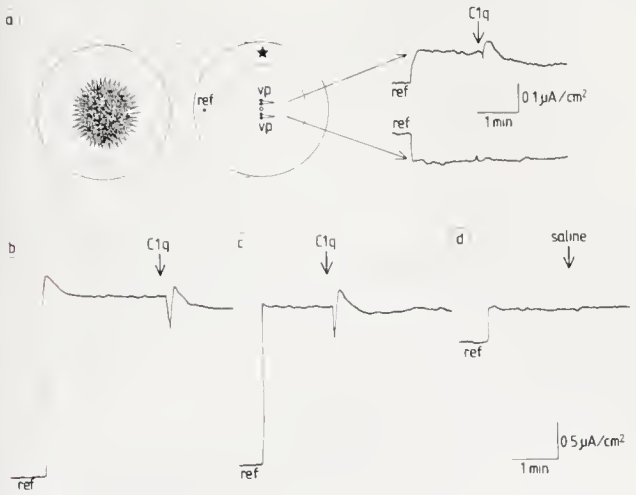

Figure 4. Clq-induced changes in the extracellular fields derived from L cells migrating into the wound (a–c). Addition of the saline (the Clq solvent) alone induced no response (d). Clq (100 μg/ml) or the solvent saline was added at the front of centrifugally migrating L cells (at *asterisk*) at the time indicated by arrows. *vp* and *ref* are the same as those in Figures 2 and 3. Note that the extracellular current flowing to the leading front end of migrating fibroblasts increased (the peak amplitude of 0.05–0.23 $\mu A/cm^2$) for about 20 s after the brief decrease upon the Clq application.

was wounded and thus the cells were found to centripetally migrate, the aperture opening above the wound area was always the sink for current (Fig. 3a). In contrast, the opening above the intact part of monolayers was the source, when the circumferential area was scraped away and the cells were found to move centrifugally (Fig. 3b, Fig. 4a).

When a complement subcomponent Clq, which is a chemoattractant for L cells and evokes hyperpolarizing responses in the cells (Oiki and Okada, 1988), was administered in front (but not at the rear: Fig. 4a, bottom trace) of the migrating L cells, biphasic changes in the profile of extracellular fields were observed in all three experiments (Fig. 4). In the saline without cells or on the unwounded monolayer culture, the Clq responses were not observed.

Discussion

The present data obtained with vibrating probes clearly indicate that extracellular electric currents are endogenously associated with fibroblasts migrating into a wound and that the sink for current was concentrated at the leading front end of L cells in motion. Similarly, steady inward currents were observed at the tips of growth cones in retinal ganglion cells (Freeman *et al.*, 1985). Steady currents were also observed around moving amoebas (Nuccitelli *et al.*, 1977), though the direction was opposite to those around migrating fibroblasts. It is also noteworthy that embryonic quail fibroblasts respond to exogenous electric currents by migrating towards the cathodal end of the field (Erickson and Nuccitelli, 1984).

A chemotactic factor for fibroblasts, Clq, induced biphasic changes in the electric fields. This ligand induces hyperpolarizing responses due to transient increases in the Ca^{2+}-activated K^+ conductance in L cells (Oiki *et al.*, 1985b; Oiki and Okada, 1988). Since deprivation of extracellular Ca^{2+} or application of a Ca^{2+} channel blocker, nifedipine, inhibited these hyperpolarizing responses, Ca^{2+} influxes are likely involved in the chemoattractant-induced hyperpolarizing responses (Oiki *et al.*, 1985b; Oiki and Okada, 1988). Therefore, there is a possibility that activation of currents through Ca^{2+} channels and/or Ca^{2+}-activated K^+ channels is responsible for the Clq-induced changes in the extracellular electric current around migrating fibroblasts. More evidence is needed to identify the ion channel species responsible for the electric field associated with fibroblast migration and chemotaxis.

Literature Cited

Abercrombie, M., J. E. M. Heaysman, and S. M. Pegrum. 1970. The locomotion of fibroblasts in culture. II. Ruffling. *Exp. Cell Res.* **60:** 437–444.

Appel, G., F. Silva, C. Pirani, J. Meltzer, and D. Estes. 1978. Renal involvement in systemic lupus erythematosus: a study of 56 patients emphasizing histologic classification. *Medicine* **57:** 371–410.

Erickson, C. A., and R. Nuccitelli. 1984. Embryonic fibroblast motility and orientation can be influenced by physiological electric fields. *J. Cell. Biol.* **98:** 296–307.

Freeman, J. A., P. B. Manis, G. L. Snipes, B. N. Mayes, P. C. Samson, J. P. Wikswo, and D. B. Freeman. 1985. Steady growth cone currents revealed by a novel circularly vibrating probe: a possible mechanism underlying neurite growth. *J. Neurosci. Res.* **13:** 257–283.

Jaffe, L. F., and R. Nuccitelli. 1974. An ultrasensitive vibrating probe for measuring steady extracellular currents. *J. Cell Biol.* **63:** 614–628.

Nawata, T. 1984. A simple method for making a vibrating probe system. *Plant Cell Physiol.* **25:** 1089–1094.

Nuccitelli, R., M.-M. Poo, and L. F. Jaffe. 1977. Relations between ameboid movement and membrane-controlled electrical currents. *J. Gen. Physiol.* **69:** 743–763.

Oiki, S., and Y. Okada. 1988. Clq induces chamotaxis and K^+ conductance activation coupled to increased cytosolic Ca^{2+} in mouse fibroblasts. *J. Immunol.* **141:** 3177–3185.

Oiki, S., T. Ohno-Shosaku, and Y. Okada. 1985a. Measurements of extracellular electric currents around migrating fibroblasts by means of a vibrating probe. *Cell Struct. Funct.* **10:** 516.

Oiki, S., S. Ueda, and Y. Okada. 1985b. Increases in cytosolic free Ca^{2+} induced by ATP, complement and β-lipoprotein in mouse L fibroblasts. *Biochem. Biophys. Res. Commun.* **132:** 290–298.

Ross, R. 1968. The fibroblast and wound repair. *Biol. Rev. Camb. Philos. Soc.* **43:** 51–96.

Reference: *Biol. Bull.* **176(S)**: 126–129. (April, 1989, Suppl.)

Ionic Control of Postsynaptic Differentiation in Muscle

H. BENJAMIN PENG AND DING-LIANG ZHU*

Laboratories for Cell Biology, Department of Cell Biology and Anatomy, University of North Carolina, Chapel Hill, North Carolina 27599

Abstract. The formation of acetylcholine receptor (AChR) clusters in cultured *Xenopus* muscle cells can be effected by polycation-coated latex beads. In a manner resembling innervation, the beads induce AChR clustering discretely at the bead-muscle contacts. In this study, we examined the role of intracellular Ca^{2+} and pH on the development of this postsynaptic-type specialization. A transient increase in intracellular Ca^{2+} was immediately elicited when the muscle cell was stimulated by the beads. This Ca^{2+} transient is a necessary condition for the activation of the clustering process. In addition, the polycations on the beads caused a cytoplasmic alkalinization which also appeared to be necessary for the AChR clustering to take place. These studies indicate that the signaling of postsynaptic differentiation at the neuromuscular junction may be mediated by an ionic mechanism.

Introduction

Synapses are the fundamental building blocks of the neuronal machine. The neuromuscular junction (NMJ) of vertebrate skeletal muscle is the best example of chemical synapse. Its presynaptic element is made up of a nerve terminal specialized in the exocytosis of acetylcholine. The postsynaptic element on muscle is composed of membrane plaques containing acetylcholine receptors (AChRs) at a high density and a highly specialized extracellular matrix which anchors proteins, such as cholinesterase, essential for synaptic transmission. The exact registration of the pre- and postsynaptic elements at the neuromuscular junction ensures the speed and fidelity of information transfer.

During development, processes of motoneurons grow toward muscle cells to establish the NMJ. *In vitro*, a number of stimuli can mimic the yet unidentified endogenous signal in inducing postsynaptic differentiation. These include chemical stimuli, such as conditioned media and extracts from neuronal tissues, and physical stimuli, such as constant electric field and positively charged beads (Peng, 1987; Bloch and Pumplin, 1988). Among them, the positively charged beads represent the only stimulus that can effect a local development of the synaptic apparatus in the same manner as innervation. When applied to cultured muscle cells, these beads induce the formation of AChR clusters and the accumulation of acetylcholinesterase at the bead-muscle contacts (Peng *et al.*, 1981; Peng and Cheng, 1982; Peng *et al.*, 1988). When applied to neuronal cultures, they induce the formation of presynaptic-type specializations along the bead-neurite contacts (Peng *et al.*, 1987). Thus, it is of great interest to understand the nature of the signal for synaptic differentiation conveyed by the beads to the targets. In this communication we describe our work on understanding the signal for postsynaptic development.

Materials and Methods

Cell culture and the induction of AChR clustering by beads

Myotomal muscle cells were isolated from *Xenopus laevis* embryos according to published methods (Peng and Nakajima, 1978). They were cultured on coverglass in Steinberg's medium supplemented with 10% L-15 (Leibovitz) medium and 1% fetal bovine serum at room temperature. To induce the formation of AChR clusters, 1–10 μm polystyrene latex beads coated with polyornithine or polylysine were added to the culture (Peng and Cheng, 1982). Following an incubation period ranging from 1 to 48 h, the culture was labeled with tetramethylrhodamine-conjugated α-bungarotoxin (R-BTX), fixed

* Present address: Department of Pharmacology, INSERM U.7, 161 Rue de Sevres, 75015 Paris, France.

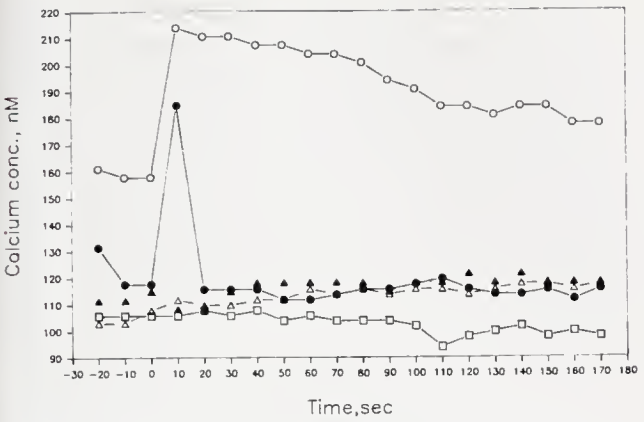

Figure 1. Changes in intracellular Ca^{2+} when muscle cells were treated with latex beads. The beads were added at time 0. After the establishment of the bead-muscle contact, the measurements were carried out at 10-s intervals for a duration of 3 min. Open and solid circles: cells treated with polyornithine-coated beads; open triangles: cell treated with uncoated beads; squares: cell treated with polyornithine-coated beads in Ca^{2+}-free medium; solid triangles: cell treated with polyornithine-coated beads in medium containing 50 μM verapamil.

with 95% ethanol at −20°C, and mounted on a slide. AChR clusters were examined by fluorescence microscopy and their relationship to the beads were assessed by phase contrast. The efficacy of the beads in inducing the formation of clusters was quantified by scoring the percentage of bead-muscle contacts that were positive in R-BTX fluorescence.

Measurement of intracellular calcium

Ratio imaging of fura-2-loaded cells was used to measure intracellular Ca^{2+}. This method and its application to *Xenopus* muscle cultures have been described (Tsien *et al.*, 1985; Zhu and Peng, 1988). Briefly, the culture was loaded with fura-2 AM (10 μM) for 30 min in the dark and then washed. Fluorescence images of the cells, which were excited at 340 and 380 nm and detected at >520 nm, were digitally recorded with a light-sensitive video camera interfaced with an image processing system. After background subtraction and noise reduction through thresholding, the ratio of 340 and 380 nm images was calculated for each pixel. From the ratio image, the mean gray level of the cell was calculated. It was calibrated with respect to Ca^{2+} concentration according to the method of Grynkiewicz *et al.* (1985).

Measurement of intracellular pH

Ratio imaging of carboxyfluorescein (BCECF)-loaded cells was used to measure the intracellular pH (Paradiso *et al.*, 1987). The cells were loaded with the ester form of the dye. Fluorescence images at excitation wavelengths of 440 and 490 nm were obtained and their ratio was calculated according to the method outlined above. From the ratio image, the mean gray scale of the cell was calculated. This gray scale was calibrated by equilibrating the intracellular pH with extracellular pH standards after treating the culture with 10 μM nigericin and 150 mM KCl (Chaillet and Boron, 1985).

Results

Increase in intracellular calcium accompanying the onset of AChR clustering

We showed previously that deprivation of extracellular Ca^{2+}, either by Ca^{2+}-free medium or by Ca^{2+} antagonists, including divalent cations such as cobalt, nickel, and manganese and organic compounds such as verapamil and D-600, suppresses the bead-induced clustering of AChRs (Peng, 1984). This suggests that an influx of Ca^{2+} is a necessary condition for AChR clustering. Recently, we examined the change in intracellular Ca^{2+} when the muscle cells were stimulated by polycation-coated beads (Zhu and Peng, 1988). As shown in Figure 1, an increase in intracellular Ca^{2+} was seen immediately after the bead-muscle contact. This increase, ranging from 5–57% of the resting level, occurs throughout the cytoplasm. It returns to the resting level with a time course of about 3 min. Removal of extracellular Ca^{2+} or addition of Ca^{2+} antagonist verapamil abolished this increase. Uncoated beads, which do not induce AChR clustering, also failed to cause this Ca^{2+} transient (Fig. 1).

Relationship of intracellular pH and AChR clustering

Recently we found that the bead-induced AChR clustering is sensitive to extracellular Na^+ concentration. When it was raised to 100 mM from our normal medium concentration of 60 mM, the cluster formation was sup-

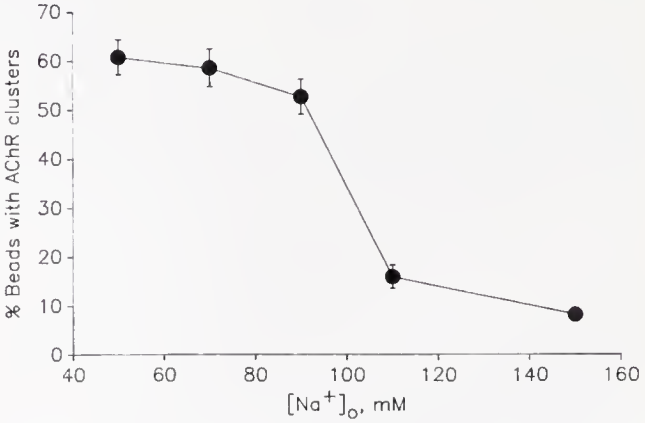

Figure 2. Effect of extracellular Na^+ on the formation of AChR clusters induced by polyornithine-coated beads.

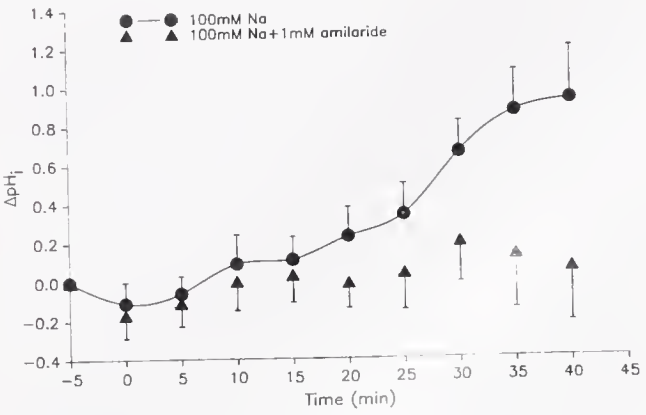

Figure 3. Changes of intracellular pH as a function of extracellular Na^+ concentration.

pressed (Fig. 2). Raising the extracellular tonicity of the normal Na^+ medium by sucrose to the same level of the high Na^+ medium did not suppress AChR clustering. Thus, this effect could not be attributed to an increase in osmotic pressure. This suppression due to high Na^+ could be reversed by 1 m*M* amiloride, which inhibits the Na^+-H^+ exchange in the plasma membrane (Aronson, 1985). Furthermore, application of 10–20 m*M* NH_4Cl, a weak base which causes rapid elevation of cytoplasmic pH, suppressed the bead-induced formation of AChR clusters. These results suggest that the intracellular pH may be involved in the regulation of bead-induced cluster formation. This was tested by intracellular pH measurements. When the extracellular Na^{2+} was elevated from 60 m*M* to 100 m*M*, there was a cytoplasmic alkalinization of 0.9 pH units over a 45 min period; this could be suppressed by 1 m*M* amiloride (Fig. 3). Bath application of polycations, such as polylysine or polyornithine, also effected a large alkalinization of the cytoplasm (Fig. 4).

Discussion

These studies show that an increase in intracellular Ca^{2+} is a necessary condition for the induction of AChR clustering induced by polycation-coated beads. Deprivation of extracellular Ca^{2+} also inhibits the formation of AChR clusters induced by nerve (Henderson *et al.*, 1984), by molecules extracted from the basement membrane of nicotinic synapses (Wallace, 1988), or by constant electric field (Stollberg and Fraser, 1988). Thus, all these stimuli may cause an opening of the Ca^{2+} channels in the plasma membrane. The calcium influx resulting from this action may trigger the process of AChR clustering. Our previous studies have also shown that calmodulin may mediate the bead-induced process in *Xenopus* muscle cells (Peng, 1984). Recent evidence shows that the basement extract-induced AChR clustering in chick myotubes may be mediated by protein kinase C (Wallace, 1988). Thus, a protein kinase system may be one of the targets of this Ca^{2+} signal.

Although we do not yet know the molecular mechanism of postsynaptic activation, it is conceivable that the highly positively charged surface of the beads may cause a local perturbation of the electric field across the lipid bilayer and thus affect voltage-dependent ion channels. Recent works show that the amino acid sequence of voltage-dependent sodium, calcium, and potassium channels all contain the "S4" domain, which is highly enriched in positively charged amino acid residues: every third amino acid in this domain is an arginine or a lysine residue (Catterall, 1986). One theory postulates that this domain of the channel is transmembrane and serves as the voltage sensor responsible for channel gating (Catterall, 1986). We postulate that, in addition to voltage, it may also be sensitive to perturbation by the positively charged surface of the beads. The high efficacy of the polycation-coated beads in activating the postsynaptic development suggests that molecules with such attributes may be involved in postsynaptic induction *in vivo*.

In addition to Ca^{2+}, our studies show that an increase in cytoplasmic pH is also a necessary step in the activation of AChR clustering induced by polycation-coated beads. Global cytoplasmic alkalinization prior to bead application, either by an increase in Na^+ influx or by weak bases, overwhelms the local stimulatory effect of the beads and results in refractoriness of AChR clustering. In contrast to the Ca^{2+} transient, the increase in pH takes much longer to develop and is long lasting. Thus, it may not be involved in the triggering of the postsynaptic development. Alkalinization of the cytoplasm also accompanies the fertilization of animal eggs (Johnson and Epel, 1981; Webb and Nuccitelli, 1981) and the activa-

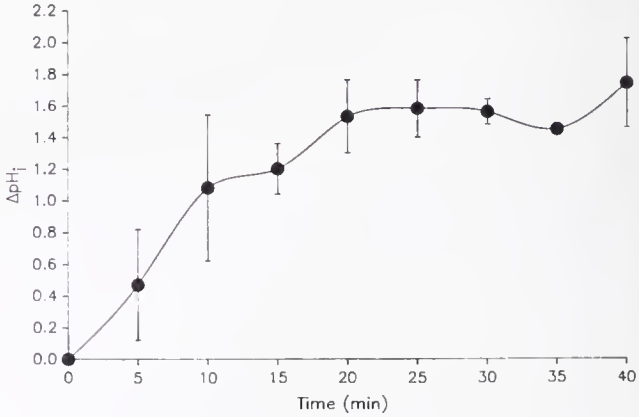

Figure 4. Effect of polyornithine on intracellular pH. 12 μg/ml polyornithine was added to the bath at time 0 and the intracellular pH was monitored at 5 min intervals.

tion of fibroblasts by growth factors (Moolenaar *et al.*, 1983). Such cytoplasmic alkalinization may lead to an increase in protein or DNA synthesis and a reorganization of the cytoskeleton (Busa, 1986).

Although we have not detected a local change in either Ca^{2+} or pH at sites of bead-muscle contacts, the fact that AChR clustering occurs discretely at these sites suggests the existence of a local signaling process. Local ion fluxes elicited by the bead or by the nerve can conceivably activate second messenger systems which not only can lead to postsynaptic development at the site of stimulation but also can influence a global change throughout the muscle cell to effect a series of innervation-related changes, such as elimination of extrasynaptic AChR clusters (Moody-Corbett and Cohen, 1982; Kuromi and Kidokoro, 1984; Peng, 1986) and myofibril differentiation (Kidokoro and Saito, 1988).

Acknowledgments

This investigation was supported by NIH grant NS23583 and the Muscular Dystrophy Association.

Literature Cited

Aronson, P. S. 1985. Kinetic properties of the plasma membrane Na^+-H^+ exchanger. *Ann. Rev. Physiol.* **47:** 545–560.

Bloch, R. J., and D. W. Pumplin. 1988. Molecular events in synaptogenesis: nerve-muscle adhesion and postsynaptic differentiation. *Am. J. Physiol.* **254:** C345–C364.

Busa, W. B. 1986. Mechanisms and consequence of pH-mediated cell regulation. *Ann. Rev. Physiol.* **48:** 389–402.

Catterall, W. A. 1986. Voltage-dependent gating of sodium channels: correlating structure and function. *TINS* **9:** 7–10.

Chaillet, J. R., and W. F. Boron. 1985. Intracellular calibration of a pH-sensitive dye in isolated perfused salamander proximal tubules. *J. Gen. Physiol.* **86:** 765–794.

Grynkiewicz, G., M. Poenie, and R. Y. Tsien. 1985. A new generation of Ca^{2+} indicators with greatly improved fluorescence properties. *J. Biol. Chem.* **260:** 3440–3450.

Henderson, L. P., M. A. Smith, and N. C. Spitzer. 1984. The absence of calcium blocks impulse-evoked release of acetylcholine but not de novo formation of functional neuromuscular synaptic contacts in culture. *J. Neurosci.* **4:** 3140–3150.

Johnson, C. H., and D. Epel. 1981. Intracellular pH of sea urchin eggs measured by the dimethyloxazolidinedione (DMO) method. *J. Cell Biol.* **89:** 284–291.

Kidokoro, Y., and M. Saito. 1988. Early cross-striation formation in twitching *Xenopus* myocytes in culture. *Proc. Natl. Acad. Sci. USA* **85:** 1978–1982.

Kuromi, H., and Y. Kidokoro. 1984. Nerve disperses preexisting acetylcholine receptor clusters prior to induction of receptor accumulation in *Xenopus* muscle cultures. *Dev. Biol.* **103:** 53–61.

Moody-Corbett, F., and M. W. Cohen. 1982. Influence of nerve on the formation and survival of acetylcholine receptor and cholinesterase patches on embryonic *Xenopus* muscle cells in culture. *J. Neurosci.* **2:** 633–646.

Moolenaar, W. H., R. Y. Tsien, P. T. Van Der Saag, and S. W. De Laat. 1983. Na^+/H^+ exchange and cytoplasmic pH in the action of growth factors in human fibroblasts. *Nature* **304:** 645–648.

Paradiso, A. M., R. Y. Tsien, and T. E. Machen. 1987. Digital image processing of intracellular pH in gastric oxyntic and chief cells. *Nature* **325:** 447–450.

Peng, H. B. 1984. Participation of calcium and calmodulin in the formation of acetylcholine receptor clusters. *J. Cell Biol.* **98:** 550–557.

Peng, H. B. 1986. Elimination of preexistent acetylcholine receptor clusters induced by the formation of new clusters in the absence of nerve. *J. Neurosci.* **6:** 581–589.

Peng, H. B. 1987. Development of the neuromuscular junction in tissue culture. *CRC Critical Rev. Anat. Sci.* **1:** 91–131.

Peng, H. B., and P.-C. Cheng. 1982. Formation of postsynaptic specializations induced by latex beads in cultured muscle cells. *J. Neurosci.* **2:** 1760–1774.

Peng, H. B., P.-C. Cheng, and P. W. Luther. 1981. Formation of ACh receptor clusters induced by positively charged latex beads. *Nature* **292:** 831–834.

Peng, H. B., K.-X. Gao, M.-Z. Xie, and D.-Y. Zhao. 1988. Development of acetylcholinesterase induced by basic polypeptide-coated latex beads in cultured *Xenopus* muscle cells. *Dev. Biol.* **127:** 452–455.

Peng, H. B., D. R. Markey, W. L. Muhlach, and E. D. Pollack. 1987. Development of presynaptic specializations induced by basic polypeptide-coated latex beads in spinal cord cultures. *Synapse* **1:** 10–19.

Peng, H. B., and Y. Nakajima. 1978. Membrane particle aggregates in innervated and noninnervated cultures of *Xenopus* embryonic muscle cells. *Proc. Natl. Acad. Sci. USA* **75:** 500–504.

Stollberg, J., and S. E. Fraser. 1988. Acetylcholine receptors and concanavalin A-binding sites on cultured *Xenopus* muscle cells: electrophoresis, diffusion, and aggregation. *J. Cell Biol.* **106:** 1723–1734.

Tsien, R. Y., T. J. Rink, and M. Poenie. 1985. Measurement of cytosolic free Ca^{2+} in individual small cells using fluorescence microscopy with dual excitation wavelengths. *Cell Calcium* **6:** 145–157.

Wallace, B. G. 1988. Regulation of agrin-induced acetylcholine receptor aggregation by Ca^{++} and phorbol ester. *J. Cell Biol.* **107:** 267–278.

Webb, D. J., and R. Nuccitelli. 1981. Direct measurement of intracellular pH changes in *Xenopus* eggs at fertilization and cleavage. *J. Cell Biol.* **91:** 562–567.

Zhu, D.-L., and H. B. Peng. 1988. Increase in intracellular calcium induced by the polycation-coated latex bead, a stimulus that causes postsynaptic-type differentiation in cultured *Xenopus* muscle cells. *Dev. Biol.* **126:** 63–70.

Reference: *Biol. Bull.* **176(S):** 130–135. (April, 1989, Suppl.)

Extracellular Calcium Levels Strongly Influence Neural Crest Cell Galvanotaxis

RICHARD NUCCITELLI AND TANYA SMART

Zoology Department, University of California, Davis, California 95616

Abstract. We have been studying the response of neural crest cells from 56-h-old quail embryos to small, imposed d.c. electrical fields. These cells exhibit directed translocation or galvanotaxis towards the negative pole of fields as low as 7 mV/mm. With an average cell length of 60 μm, these cells respond to fields as low as 0.4 mV along their length. A significant change in the average cosine of the cellular translocation distribution can be detected as early as 7 min after field application for all field strengths greater than 10 mV/mm. Extracellular Ca^{2+} is not required for the motility of these cells as long as extracellular Mg^{2+} is increased to 10 m*M*. However, the galvanotaxis response does appear to require Ca^{2+} influx since it is completely blocked by the addition of either 10 m*M* Mg^{2+} or 100 μM Gd^{3+}. Moreover, the galvanotaxis response is partially reversed by the complete removal of extracellular Ca^{2+}.

Introduction

The directed translocation of cells by an electrical field has been termed "galvanotaxis." During the past six years there has been a surge of activity in this area of research because embryonic neural crest cells from avians and amphibians (Nuccitelli and Erickson, 1983; Stump and Robinson, 1983; Cooper and Keller, 1984), fibroblasts from aves and mammals (Erickson and Nuccitelli, 1984, 1986; Yang *et al.*, 1984), and epithelial cells from amphibians and fish (Luther *et al.*, 1983; Cooper and Schliwa 1985, 1986a, b) all exhibited this behavior. All of these cells respond to rather small, physiological d.c. electric fields by exhibiting enhanced migratory activity toward the negative pole of the electric field. Two other responses are perpendicular alignment and elongation, but both of these generally require higher field strengths of at least 150 and 400 mV/mm, respectively. It is interesting that the perpendicular alignment response has been found in all cell types investigated, even when the directed migration is absent. It appears to be due to the selected retraction of lamellipodia facing the positive pole and begins within a few minutes of field application (Erickson and Nuccitelli, 1984).

In the present study we concentrated on the translocation response of neural crest cells from the quail embryo and found their response to be more consistent than that of somitic fibroblasts from the same embryo (Gruler and Nuccitelli, 1986). We determined that the galvanotactic response can be completely suppressed by Ca^{2+} channel blockers and is reversed in the absence of extracellular Ca^{2+}.

Materials and Methods

Eggs from a colony of Japanese quail (*Coturnix coturnix japonica*) were incubated in a humidified incubator at 37°C for 56 h. Procedures for dissecting and culturing neural tubes were similar to those described previously (Loring *et al.*, 1981). Briefly, embryos were removed from the eggs, rinsed in Locke's saline solution, and transferred to dishes containing 2% agar in Locke's saline. A portion of the posterior embryonic trunk consisting of the most posterior 10–12 somites was dissected out using sharpened tungsten needles. These trunk segments were rinsed in Hank's balanced salt solution (HBSS, Gibco) buffered with 10 m*M* N-2-hydroxyethylpiperazine-N'-2-ethanesulfonic acid (Hepes, Gibco) (pH 7.3). The HBSS was removed and 2 ml warm (37°C) pancreatin (Gibco) was added. Tubes were gently agitated with a pipet to loosen tissue adhesions. As soon as the somites began to separate from the neural tubes, the tissue was transferred to fresh HBSS. This process routinely occurred in less than two minutes. The somites, surface ectoderm, notochord, and adjacent mesenchyme were dissected from the tubes with sharpened tungsten needles.

Two to four neural tubes free of adherent tissue were placed on a 25 × 6 mm sterile glass coverslip in a 35 mm plastic petri dish containing approximately 1.5 ml of culture medium (see below) and incubated at 37°C in a humidified atmosphere of 10% CO_2 in air for 16 or 18 hours. During this time, the neural crest cells emigrated from the neural tube onto the coverslips to form outgrowths. Neural tubes were removed from the coverslips just prior to experimentation, leaving isolated outgrowths.

Culture media

Modified F12 (Gibco) was supplemented with 10% by volume of fetal calf serum (FCS:Gibco), 3.5% of 14-day chick embryo extract (50% in HBSS), 1 ml of penicillin-streptomycin (Gibco: 5000 IU penicillin, 5 mg streptomycin sulfate/ml), 1 ml of 200 m*M* L-glutamine (Gibco; rehydrated with sterile glass distilled water). The volume of the last two ingredients specified is for a 100-ml aliquot of modified F12.

When the cells were placed in the chambers, the culture medium was replaced with F12, to which had been added only 1% penicillin-streptomycin, and 10 m*M* Hepes buffer to minimize the possible effects of serum protein gradients generated by electrophoresis.

Galvanotactic chambers

Chambers employed for imposing an electric field were identical to those described previously (Erickson and Nuccitelli, 1984, fig. 1). The average height of chambers varied between 120–150 μm. Chambers were sealed with tape and silicone high vacuum grease. Experimental medium was added initially to only one well of the chamber. Fluid was added to the remaining well only after flow into that well had occurred indicating a clear path for fluid flow over the cells. The voltage across each chamber was measured at 30-min intervals by inserting Ag-AgCl electrodes into the wells on either end, and the current passing over the cells was monitored continuously with an ammeter. Ten-cm-long agar bridges separated the electrodes supplying the current from the wells of the chamber.

Filming procedure

Cells were observed with phase contrast optics on an inverted microscope at 250× and their movements were recorded using a video camera and time-lapse recorder. Fields of cells to be studied were chosen from those regions in which the cells were well dispersed to reduce the influence of contact inhibition. Cells that were clustered in each field were not used for subsequent analysis. Experiments were usually conducted for two hours in the electric field. Total cell displacement was measured from the position each cell was in at the beginning of the observation period to its location at the end of two hours. A digitizing pad (Houston Instruments) and an IBM PC XT were used to analyze the cell displacement using plastic transparencies onto which the beginning and end points of the cell displacements were copied from the video screen. To quantitate the directionality of the average cellular translocation, the angle that each cell moved with respect to the imposed electric field direction was used. Specifically, the cosine of this angle would be equal to one if the cell moved right along the field toward the negative pole, zero if the cell moved perpendicular to the field direction, and minus one if the cell moved directly toward the positive pole of the field. By taking the average of all the cosines, one can quantitate the average directionality of movement. If as many cells moved toward the positive pole as toward the negative pole, the average cosine would be zero. This average was calculated for each distribution from the equation, $\Sigma_i \cos \theta_i/N$, where θ is the angle between the field axis and the cellular translocation direction and N is the total number of cells. Discrepancies in the average cosine determined from the time course analysis when compared to the 120-minute analysis are a result of some cells entering or leaving the field during the experiment. To eliminate these cells from the total time analysis would have caused a bias against the most responsive cells, so the final point of observation was taken as the point where they left the screen. In the time course analysis, once a cell had left the video screen it could no longer be included in the average cosine.

Results

Embryonic neural crest cells from two-day-old quail embryos are extremely sensitive to imposed d.c. electric fields. These cells migrate towards the negative pole of such a field (Fig. 1) and non-random migration can be detected for fields as low as 5 to 7 mV/mm. Since the average length of these cells is 60 ± 20 μm (SD, n = 60), they are responding to fields as low as 0.4 mV along the length of the cell or 0.2 mV across the membranes facing either pole of the field.

The time course of this response was studied by analyzing the time-lapse video tapes of the cellular response at various intervals after field application. A significant change in the average cosine of the cellular distribution could be detected as early as 7 min after field application for fields greater than 10 mV/mm (Fig. 2). Field strengths of 7 and 10 mV/mm required 60 and 30 min, respectively, to generate a significant asymmetry in the translocation response. Thus, the cellular response is quite rapid and exhibits a very steep dependence on field strength

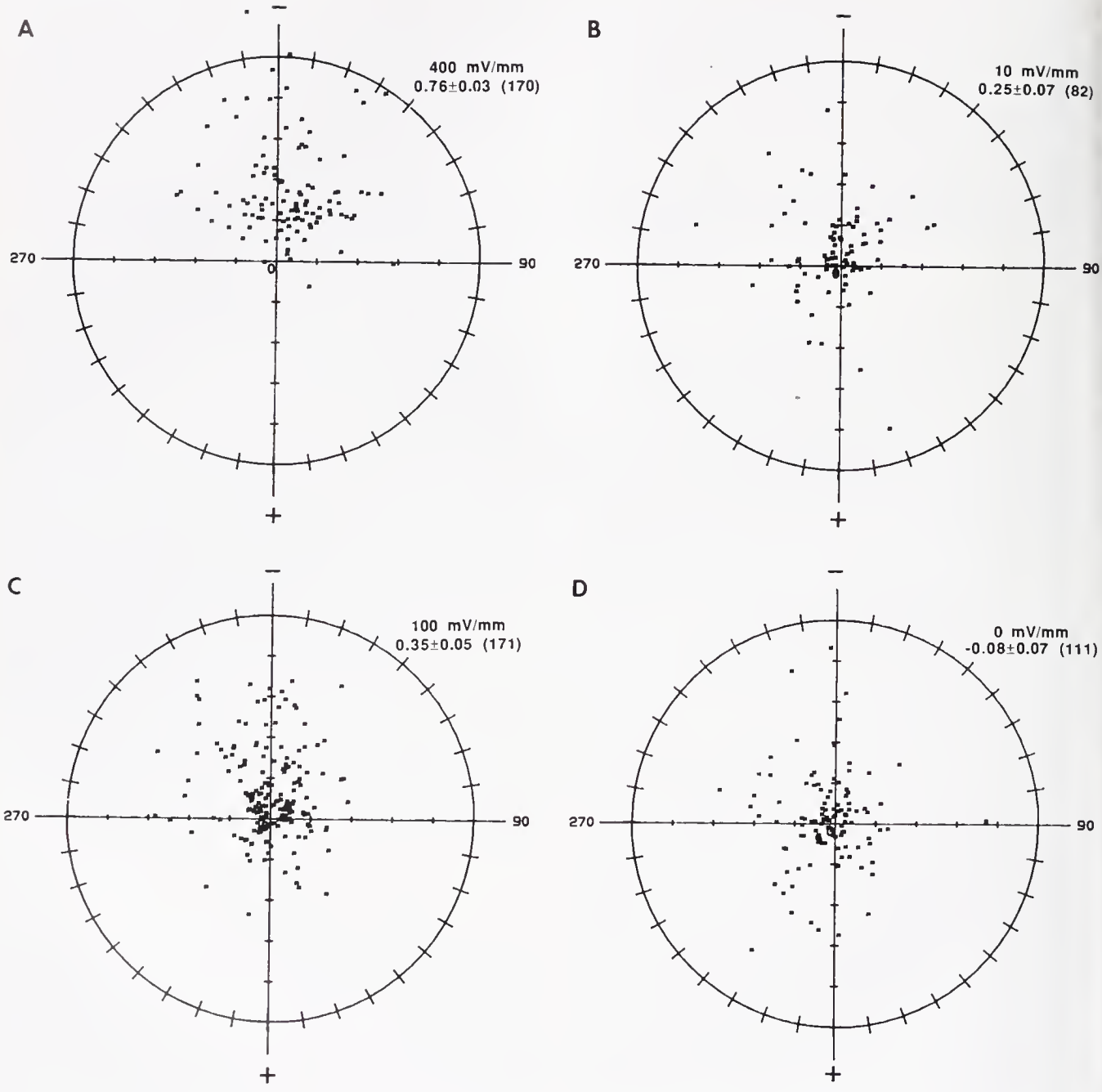

Figure 1. The translocation response of 56-h-old neural crest cells during a 2-h period in the indicated electric field strength. After tracing from a video screen the position of each cell before and after 2 hours in the field, the initial point was placed at the origin and the final location plotted as a single point on the circular graph. The radius of each circle represents 1 mm of translocation distance and the average cell length is 60 μm. The applied field strength, average cosine of the distribution plus or minus the standard error of the mean, and the number of cells plotted are indicated to the upper right of each distribution. A. 400 mV/mm. B. 10 mV/mm. C. 100 mV/mm. D. 0 mV/mm.

with the shoulder of the response between 10 and 50 mV/mm.

It has been reported that fish epidermal cells depend on Ca^{2+} influx to generate polarity of movement during galvanotaxis (Cooper and Schliwa, 1986b). Our investigations indicate that the same is true for avian neural crest cells. One cannot simply place these cells in a solution of F12 medium in which all of the Ca^{2+} has been

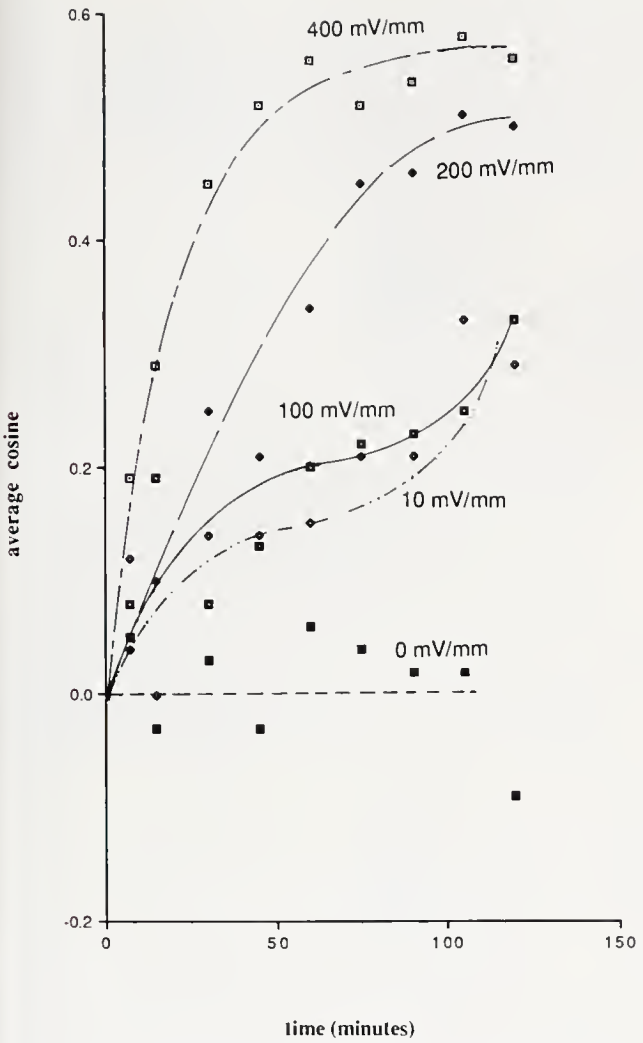

Figure 2. The time course of the galvanotactic response. The average cosine of the translocation distribution was measured at various times after field application for the four field strengths indicated. The rate of approach to the final average cosine is much steeper at the higher field strengths than at the lower ones.

removed by the addition of the Ca^{2+} chelator, EGTA, because the cells promptly round up and stop moving. However, this is not due to the absolute requirement of Ca^{2+} for cell motility because the addition of Mg^{2+} (increasing from 0.6 to 10 m*M*) prevents the rounding up in the absence of Ca^{2+} and the cells move quite well. Therefore, we studied the galvanotaxis response under these conditions. When the Mg^{2+} is raised to 10 m*M* without changing the external Ca^{2+} level, the galvanotaxis response is no longer observed and the degree of translocation is reduced (Fig. 3B). This blockage of the galvanotaxis response by Mg^{2+} was a surprise because Mg^{2+} is not a very efficient Ca^{2+} channel blocker. However, at these high levels where its concentration is 30-fold higher than that of Ca^{2+}, it might be blocking calcium's access to channels. In support of this interpretation, an identical result was obtained when only 100 μM of the much more specific Ca^{2+} channel blocker, Gd^{3+}, was added (Fig. 3C). Again the galvanotaxis response is blocked and the net translocation of most cells is reduced compared to controls.

The response to the removal of external Ca^{2+} in the high Mg^{2+} medium (Fig. 3D) is perhaps the most surprising result. Under these conditions, most cells move in the reverse direction toward the positive pole of the applied field. This reversal of direction of migration is reminiscent of the observation by Cooper and Schliwa (1986b) who found a reversed response when extracellular Co^{2+} was used to block Ca^{2+} and the Ca^{2+} ionophore, A23187, was added.

Discussion

Embryonic quail neural crest cells appear to be an ideal cell type for the study of galvanotaxis. These cells are exquisitely sensitive to d.c. electric fields, responding to fields as small as 0.4 mV per cell length. This response is found in all cell cultures without the variability in response found with quail somitic fibroblasts (Gruler and Nuccitelli, 1986). This observed sensitivity to such low field strengths suggests that these cells may use information from endogenous electric fields within the embryo as one of the guiding factors in their migration. These cells normally migrate towards the negative pole of the imposed field. Here we report a Ca^{2+}-dependence for this directed migration.

External calcium is not required for neural crest cell motility

A requirement for extracellular Ca^{2+} for the movement of fibroblasts and epithelial cells has been documented (Gail *et al.*, 1973; Moore and Pastan, 1979; Strohmeier and Berieter-Hahn, 1984; Mittal and Bereiter-Hahn, 1985). The addition of up to 3 m*M* external Mg^{2+} was not found to substitute for calcium in the maintenance of motility in the three types of mammalian fibroblasts or in chick embryo fibroblasts used in those studies. However, we find that the addition of 10 m*M* external Mg^{2+} to our neural crest cells allows them to translocate quite normally in Ca^{2+}-free medium. This is very useful because it allows us to more thoroughly study the role of Ca^{2+} in the galvanotaxis response.

Calcium dependence of galvanotaxis

The mechanism of neural crest galvanotaxis appears to be quite sensitive to Ca^{2+} movements across the plasma membrane. Thus, if the external $[Ca^{2+}]$ is left unmodified, and other ions that are known to compete with

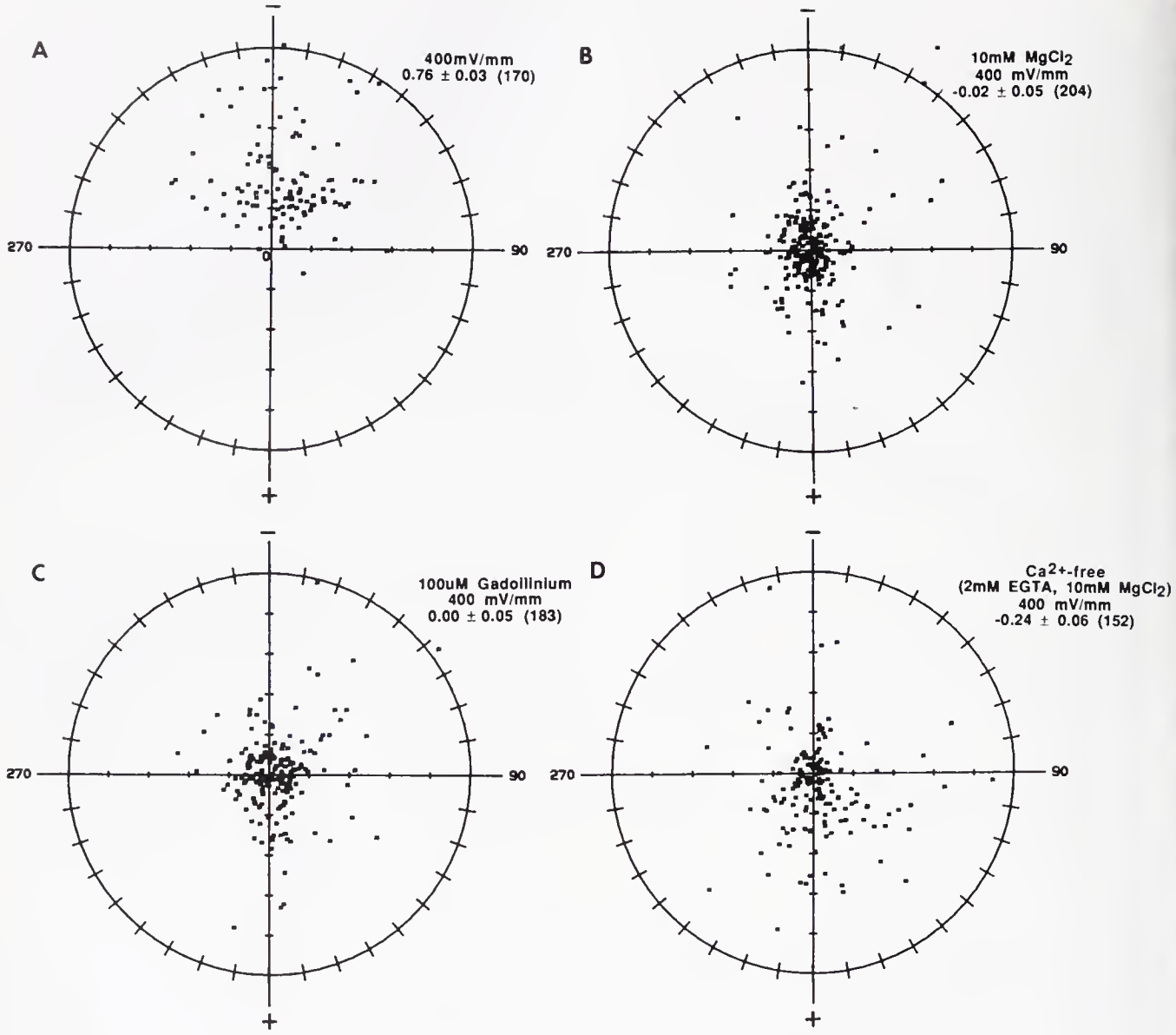

Figure 3. The translocation response of 2-day-old neural crest cells during a 2-h period in an imposed d.c. field of 400 mV/mm. The scale marks on the axes represent 200 μm and the average cell length is 60 μm. A. Control in normal F12 medium. B. F12 was supplemented with 10 mM Mg^{2+} in normal Ca^{2+}. C. F12 was supplemented with 100 μM gadolinium. Gadolinium is a potent Ca^{2+} channel blocker. D. F12 was supplemented with 10 mM Mg^{2+} and extracellular free Ca^{2+} was removed (3 mM EGTA added).

Ca^{2+} for entry or to block its entry are added, the directed translocation can be completely blocked while the average cell motility is only partially reduced. Interestingly, the complete removal of Ca^{2+} from the external medium does not simply block galvanotaxis, but reverses the direction of translocation toward the positive pole. Since this response clearly cannot involve Ca^{2+} influx, it suggests that other factors must be involved. What factors would be influenced by removing external Ca^{2+}? In most cells with large surface-to-volume ratios, removing external Ca^{2+} rapidly reduces intracellular Ca^{2+}. Indeed, we have preliminary results using the fluorescent probe, fura-2, that this is the case in neural crest cells as well. Thus, the response mechanism might be sensitive to intracellular Ca^{2+} levels. One hypothesis is that gradients in the concentration of intracellular Ca^{2+} are involved in the signal transduction process. Perhaps the electric field somehow increases the permeability of the plasma membrane to Ca^{2+} at the cathode-facing side of the cell, increasing the $[Ca^{2+}]$ below the membrane in that region

and biasing cell movement in that direction. When the cell finds itself in Ca^{2+}-free medium, the same permeability gradient would allow Ca^{2+} to leak out of the cell more rapidly at the cathode-facing side of the cell and this would lead to a *reversed* intracellular concentration gradient of Ca^{2+}. This could lead to the observed reversal in the galvanotaxis response under these conditions.

Literature Cited

Cooper, M. S., and R. E. Keller. 1984. Perpendicular orientation and directional migration of amphibian neural crest cells in DC electrical fields. *Proc. Natl. Acad. Sci. USA* **81:** 160–164.

Cooper, M. S., and M. Schliwa. 1985. Electrical and ionic controls of tissue cell locomotion in direct current electric fields. *J. Neurosci. Res.* **13:** 223–244.

Cooper, M. S., and M. Schliwa. 1986a. Motility of cultured fish epidermal cells in the presence and absence of direct current electric fields. *J. Cell Biol.* **102:** 1384–1399.

Cooper, M. S., and M. Schliwa. 1986b. Transmembrane Ca^{2+} fluxes in the forward and reversed galvanotaxis of fish epidermal cells. *Prog. Clin. Biol. Res.* **210:** 311–318.

Erickson, C. A., and R. Nuccitelli. 1984. Embryonic fibroblast motility and orientation can be influenced by physiological electric fields. *J. Cell Biol.* **98:** 296–307.

Erickson, C. A., and R. Nuccitelli. 1986. Role of electric fields in fibroblast motility. Pp. 303–310 in *Progress in Clinical and Biological Research,* Vol. 210, R. Nuccitelli, ed. Alan R. Liss, Inc. New York.

Gail, M. H., Ch. W. Boone, and C. S. Thompson. 1973. A calcium requirement for fibroblast motility and proliferation. *Exp. Cell Res.* **79:** 386–390.

Gruler, H., and R. Nuccitelli. 1986. New insights into galvanotaxis and other directed cell movements: an analysis of the translocation distribution function. *Prog. Clin. Biol. Res.* **210:** 337–347.

Loring, J., B. Glimelius, C. Erickson, and J. A. Weston. 1981. Analysis of developmentally homogeneous neural cell populations *in vitro*. *Dev. Biol.* **82:** 86–94.

Luther, P. W., H. B. Peng, and J. J.-C. Lin. 1983. Changes in cell shape and actin distribution induced by constant electric fields. *Nature* **303:** 61–64.

Mittal, A. K., and J. Bereiter-Hahn. 1985. Ionic control of locomotion and shape of epithelial cells: I. Role of calcium influx. *Cell Motility* **5:** 123–136.

Moore, L., and I. Pastan. 1979. Calcium requirement for movement of cultured cells. *J. Cell. Physiol.* **101:** 101–108.

Nuccitelli, R., and C. A. Erickson. 1983. Embryonic cell motility can be guided by physiological electric fields. *Exp. Cell Res.* **147:** 195–201.

Strohmeier, R., and J. Bereiter-Hahn. 1984. Control of cell shape and locomotion by external calcium. *Exp. Cell Res.* **154:** 412–420.

Stump, R. F. and K. R. Robinson. 1983. *Xenopus* neural crest cell migration in an applied electrical field. *J. Cell Biol.* **97:** 1226–1233.

Yang, W.-P., E. K. Onuma, and S.-W. Hui. 1984. Response of C3H/10T1/2 fibroblasts to an external steady electric field stimulation. *Exp. Cell Res.* **155:** 92–104.

Reference: *Biol. Bull.* **176(S)**: 136–139. (April, 1989, Suppl.)

On the Mechanism of Nerve Galvanotropism

COLIN D. McCAIG

Department of Physiology, Marischal College, University of Aberdeen, Aberdeen AB9 1AS, Scotland

Abstract. The mechanism whereby nerves turn towards the cathode in a small applied electric field has been investigated. The distribution of filopodia on the growth cone is suggestive of a pivotal role in orientation. However, nerves denuded of all filopodia by treatment with cytochalasin D continued to grow and to turn towards the cathode. Nerves treated with neuraminidase showed robust galvanotropic responses, which may call into question the role of cell surface receptor redistribution in orientation. The calcium channel blocker cobalt inhibited orientation, while simultaneous treatment of nerves with cobalt and the calcium ionophore A23187 resulted in nerves turning towards the anode; a reversal of galvanotropism. Localized entry of calcium, predominantly on one side of the growth cone, may underlie galvanotropism.

Introduction

It is well established that developing and regenerating nerves show remarkable orientation responses to a small applied electric field (McCaig, 1988). However, the underlying mechanisms remain unclear. Two observations are pertinent. First, more filopodia are found on the cathodal-facing side of growth cones, a response which precedes and predicts turning behavior (McCaig, 1986). By determining the distribution of tension at the growth cone, filopodia generally are regarded as essential sensors and transducers of anisotropic environmental conditions. Second, pretreatment of *Xenopus* neurites with concanavalin A (con A) blocks subsequent galvanotropism (Patel and Poo, 1982). In addition there is growing interest in calcium's role in determining growth cone motility and nerve orientation (Cohan *et al.*, 1987). Recent experiments provide new insight into the mechanisms controlling the turning behavior of nerves developing in an applied electric field.

Materials and Methods

Cultures of dissociated neural tubes from Stage 20 *Xenopus laevis* were prepared as described previously (Hinkle *et al.*, 1981; McCaig, 1987). Neurones were seeded into chambers of defined geometry, preconstructed on the base of plastic tissue culture dishes. Neurones began to extend processes within about 4 h. In general, aspects of control growth were assessed before the normal culture medium was replaced with one containing a test solution. At this stage the electric field was applied and repeated photographs taken of pre-selected cells in the continuous presence of drug plus electric field. Nerves selected for study initially projected at angles $< 30°$ to the "perpendicular" (*i.e.* perpendicular to the long axis of the chamber and hence the vector of the applied field). This allowed maximum scope for orientation in the field. The culture chambers were connected to the constant power supply by long agar-salt bridges, thus isolating the cells from potential electrode products. The applied field strength was measured directly with a voltmeter.

The angles of growth of neurites were measured from prints magnified 400×. A line was projected through the center of the growth cone to meet a line drawn perpendicular to the lines of force of the electric field. Neurites projecting perpendicular to the field had a value of 0°, those projecting directly towards anode or cathode, ±90° respectively. When nerves showed a sustained deviation of growth of $> \pm 10°$ this was taken as an orientation response. Neurite length was the distance between the phase bright soma and the center of the phase dark growth cone. It did not include the length of filopodia. The distribution of filopodia was counted on each print viewed under a dissecting microscope. This was done only on neurites that projected roughly perpendicularly (±30°) as the field was applied and were therefore most likely to undergo orientation.

Table I

The effects of various treatments on the rates of growth (μm/h), orientation response and distribution of filopodia on nerves exposed to a small electric field (70–110 mV/mm)

Treatment	Rate of growth (μm/h)			Orientation			Filopodial distribution		
	Control	Experimental	[n]	Turn to cathode (left)	Turn to anode (right)	No response	To cathode (left)	To anode (right)	[n]
E alone	26 ± 2	25 ± 2	[85]	75%	5%	20%	4.9 ± 0.4*	2.5 ± 0.2	[16]
E + Cyto D	24 ± 4	3 ± 2	[54]	62%	2%	36%	Not present		
E + Con A	23 ± 3	10 ± 2	[18]	6%	6%	88%	Not assessed		
E + Co^{++}	21 ± 3	7 ± 1	[29]	21%	0%	79%	9.3 ± 0.6*	5.6 ± 0.4	[19]
E + A23187	35 ± 9	3 ± 6	[12]	92%	0%	8%	3.2 ± 0.4	3.0 ± 0.9	[8]
E + CO^{++}] + A23187]	22 ± 4	7 ± 2	[21]	5%	62%	33%	3.5 ± 0.3*	2.4 ± 0.2	[35]
							* $P < 0.001$		
Control	30 ± 3	24 ± 4	[70]	22%	20%	58%	1.9 ± 0.1	2.1 ± 0.1	[35]

Each individual nerve was selected from a particular culture and photographed repeatedly over time (see Methods). The number analysed (n) therefore does not represent the number of nerves per culture dish, but a random selection of nerves taken from many culture dishes.

Drug concentrations used were cytochalasin D 0.1–0.25 μg/ml; con A 80 μg/ml; neuraminidase 1 and 10 μg/ml; Co 5 m*M*/l; A23187 10 or 15 μ*M*/l.

Results

Filopodia are not necessary for galvanotropism.

Most neurites exposed to cytochalasin D (CD, 0.05 – 0.25 μg/ml) rapidly lost all of their filopodia and advanced much more slowly. Nevertheless, continued growth did occur, and in cells exposed to an applied electric field (100 mV/mm), two thirds of neurites turned towards the cathode (Table I; Fig. 1). Thus, contrary to expectation, neurites were capable of galvanotropic responses in the absence of growth cone filopodia.

A role for the cell surface in galvanotropism?

In confirmation of Patel and Poo (1982), pretreatment of neurones with con A inhibited orientation to an applied electric field. Nerve growth slowed down but showed no deviation in direction of growth throughout 16 h of exposure to the field (Table I).

In an applied electric field, con A receptors rapidly redistribute within the plane of the membrane to accumulate on the cathodal-facing side of neurones and myoblasts (Poo and Robinson, 1977; Patel and Poo, 1982). This redistribution is inhibited by con A pretreatment and has led to the suggestion that redistribution of IMPS may be a prerequisite for nerve galvanotropism (Patel and Poo, 1982). Pretreatment of *Xenopus* myoblasts with neuraminidase, which reduces surface negativity, causes fluorescently labelled con A to redistribute to the anodal-facing membrane (McLaughlin and Poo, 1981). If this also happened in the neuronal membrane, then pretreatment of nerves with neuraminidase might be expected to reverse the direction of galvanotropism, if indeed redistribution of IMPS in some way controls orientation.

Nerves were allowed to grow out then exposed to neuraminidase (1–10 μg/ml) for 0.5–1 h before switching on the electric field. Both the field and neuraminidase were

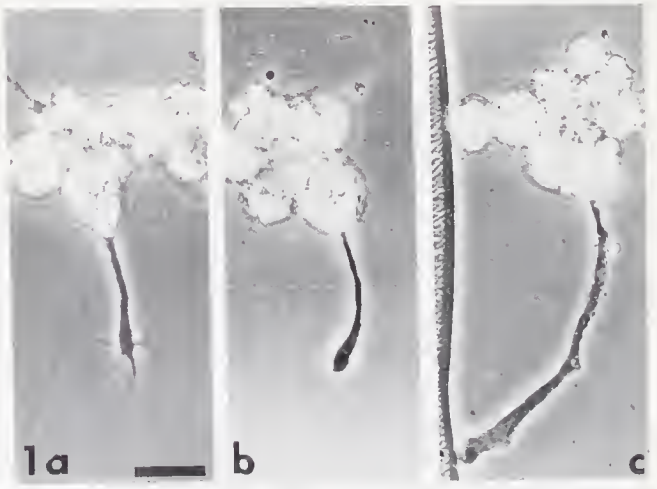

Figure 1. (a) Control nerve 35 min before exposure to CD and electric field. Scale bar = 25 μm. (b) Same nerve 7 min after simultaneous and continuous exposure to CD (0.15 μg/ml) and 110 mV/mm. All filopodia have collapsed and the nerve is beginning to orient towards the cathode at left. (c) Same nerve after 13 h continuous exposure to 0.15 μg/ml CD and 110 mV/mm. The nerve still lacks filopodia and has oriented slowly towards the cathode (left). Culture dishes were scored to assist relocation of cells. A score is seen at left and may have impeded further growth.

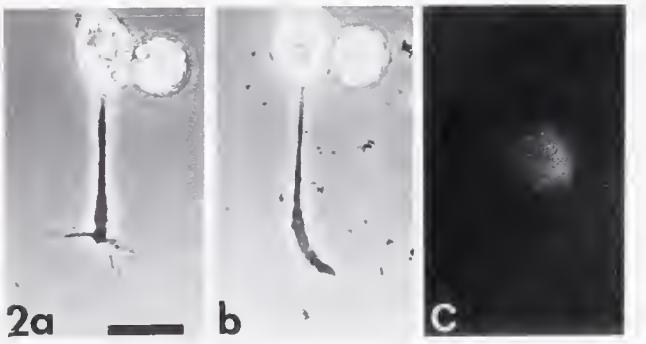

Figure 2. (a) Control nerve. Scale bar = 25 μm. (b) Same nerve after 84 min exposure to Co^{++} (5 m*M*), A23187 (10 μM) and 110 mV/mm. Nerve has oriented towards the anode at right. (c) Fluorescence micrograph of neuronal cell body after 1 h exposure to Co^{++} (5 m*M*), A23187 (15 μM), and 100 mV/mm and fixed in culture medium + 4% formaldehyde. Under UV excitation A23187 is fluorescent and is localized predominantly on the anodal-facing side of cells (right). Cells fixed but not exposed to A23187 showed no autofluorescence.

present throughout the ensuing 16 h. Interestingly, the rate of nerve growth almost doubled during the first 2 h in the field, and 88% of nerves turned towards the cathode (35/40; Table 1). Therefore, procedures that may reverse the field-induced asymmetry of the con A receptors did not influence galvanotropism.

A role for Ca^{++} in galvanotropism?

Elongating neurites were exposed to the calcium channel blocker Co^{++} (5 m*M*) and simultaneously to an applied electric field. Co^{++} significantly slowed nerve advance, although slow rates of growth were maintained over a 12-h period. Around 80% of processes showed no orientation to the electric field (23/29).

An intriguing method for reversing the galvanotaxis of fish keratocytes similarly points to a role for calcium (Cooper and Schliwa, 1986) and has been applied to *Xenopus* neurites. Orientation was inhibited in the presence of Co^{++}. The calcium ionophore A23187 did not affect orientation; 11/12 nerves turned towards the cathode. When these procedures were combined (*i.e.*, 5 m*M* Co^{++} plus 15 μM A23187 plus 100 mV/mm), 62% of nerves showed reversed galvanotropism and turned towards the anode (13/21). Examination of neuronal somata under UV excitation revealed that fluorescence from the ionophore was predominant in the anodal-facing half of cells (Fig. 2; Table I).

Discussion

Nerves orient to a variety of environmental cues, largely by unknown mechanisms. Both a gradient of nerve growth factor and a small applied electric field induce filopodial asymmetry which precedes and predicts orientation (Gundersen and Barrett, 1980; McCaig, 1986). It has been assumed that contractile events within filopodia bias the net vector of tension exerted at the growth cone and in this way influence turning. However, pharmacological treatment of nerves with CD removes filopodia, and yet blunt-ended neurites continue to orient towards the cathode. Clearly, filopodia must be permissive and not instructive. This conclusion is borne out by the observations that filopodia were predominant cathodally on Co^{++}-treated growth cones that did not orient, were distributed symmetrically on cells that oriented towards the cathode (A23187), and were present predominantly on the cathodal side of growth cones that oriented towards the anode (Table I).

If filopodia are not essential to galvanotropism, what of other mechanisms? Since the observation that con A pretreatment blocks both redistribution of IMPS and nerve orientation, it has been assumed that the distribution of cell surface receptors in some way regulates orientation. This may not be true. Neuraminidase treatment might be expected to cause con A receptors to accumulate on the anodal side of the growth cone, given its effect on myoblasts (McLaughlin and Poo, 1981). If this occurred, it certainly did not prevent nerves from showing the normal cathodal galvanotropic response. In a parallel study, we have been examining the distribution of organelles within myoblasts exposed to similar electric fields (McCaig and Dover, 1988). We have found that it is by no means only the cell surface constituents that translocate. Mitochondria, microfilaments, ribosomes, and yolk granules all assume asymmetric distributions in cells exposed to electric fields. An ultrastructural study of nerves in an applied electric field is underway and may elucidate further the control mechanisms in orientation.

Calcium is known to control aspects of growth cone motility (Cohan *et al.*, 1987), and localized currents carried by calcium have been recorded from the filopodia of advancing retinal neurites (Freeman *et al.*, 1985). The present results show that calcium entry through voltage-sensitive channels may be involved in turning behavior, since neurites continued to grow slowly in the presence of Co^{++}, but did not orient. This is in apparent contradiction to previous work showing galvanotropism occurring in calcium-free media (Robinson and Muncy, 1986). Further support for Ca^{++} involvement in orientation comes from experiments in which reversed galvanotropism was induced by a procedure likely to increase Ca^{++} entry anodally. Co^{++}-blocked neurites treated with A23187, which may accumulate on the anodal sides of cells, turned towards the anode.

There are two ways by which cells exposed to electric fields could use external calcium asymmetrically to produce the normal response of cathodal orientation. The first involves translocation of calcium channels predomi-

nantly to the cathodal side of the neurite, although a question about the role of the cell surface has been raised. The second could involve local depolarization and an increase in calcium channel conductance predominantly on the cathodal side. There is no direct evidence for either proposal.

In conclusion, nerve galvanotropism does not require filopodia, may not require redistribution of IMPS, and may depend on an asymmetric entry of calcium at the growing tip.

Acknowledgments

I am grateful for the support of the MRC, Action Research for the Crippled Child, and the International Spinal Research Trust.

Literature Cited

Cohan, C. S., J. A. Connor, and S. B. Kater. 1987. Electrically and chemically mediated increases in intracellular calcium in neuronal growth cones. *J. Neurosci.* **7:** 3588–3599.

Cooper, M. S., and M. Schliwa. 1986. Transmembrane calcium fluxes in the forward and reversed galvanotaxis of fish epidermal cells. Pp. 311–318 in *Ionic Currents in Development,* R. Nuccitelli, ed. A. R. Liss, NY.

Freeman, J. A., P. B. Manis, G. J. Snipes, B. N. Mayes, P. C. Samson, J. P. Wikswo Jr., and D. B. Freeman. 1985. Steady growth cone currents revealed by a novel circularly vibrating probe: a possible mechanism underlying neurite growth. *J. Neurosci. Res.* **13:** 257–283.

Gundersen, R. W., and J. N. Barrett. 1980. Characterization of the turning response of dorsal root neurites towards nerve growth factor. *J. Cell Biol.* **87:** 546–554.

Hinkle, L., C. D. McCaig, and K. R. Robinson. 1981. The direction of growth of differentiating neurones and myoblasts from frog embryos in an applied electric field. *J. Physiol.* **314:** 121–135.

McCaig, C. D. 1986. Dynamic aspects of amphibian neurite growth and the effects of an applied electric field. *J. Physiol.* **375:** 55–69.

McCaig, C. D. 1987. Spinal neurite reabsorption and regrowth *in vitro* depend on the polarity of an applied electric field. *Development* **100:** 31–41.

McCaig, C. D. 1988. Nerve guidance: a role for bioelectric fields? *Prog. Neurobiol.* **30:** 449–468.

McCaig, C. D., and P. J. Dover. 1988. On the mechanism of myoblast orientation in an applied electric field. *Biol. Bull.* **176:** 000–000.

McLaughlin, S., and M-m. Poo. 1981. The role of electro-osmosis in the electric-field-induced movement of charged macromolecules on the surfaces of cells. *Biophys. J.* **34:** 85–93.

Patel, N. B., and M-m. Poo. 1982. Orientation of neurite growth by extracellular electric fields. *J. Neurosci.* **2:** 483–496.

Poo, M-m., and K. R. Robinson. 1977. Electrophoresis of concanavalin A receptors in the embryonic muscle cell membrane. *Nature* **265:** 602–605.

Robinson, K. R., and L. Muncy. 1986. Neurite growth and responses to electric fields in calcium-free media. Pp. 279–284 in *Ionic Currents in Development,* R. Nuccitelli, ed. A. R. Liss, NY.

Reference: *Biol. Bull.* **176(S)**: 140–144. (April, 1989, Suppl.)

On the Mechanism of Oriented Myoblast Differentiation in an Applied Electric Field

COLIN D. McCAIG AND PHILIPPA J. DOVER

Department of Physiology, Marischal College, University of Aberdeen, Aberdeen AB9 1AS, Scotland

Abstract. We are investigating the mechanism of perpendicular differentiation of myoblasts in an applied electric field. Electric fields have latent effects in this regard. Perpendicular alignment can occur at least an hour after the field has been switched off. Polarization of the axis of development was a Ca^{++}-dependent process, being blocked by Co^{++} and mimicked by a unilateral source of the calcium channel agonist Bay K8644. Surprisingly, several types of organelles became distributed asymmetrically within the cytoplasm of oriented and orienting cells. Whether these asymmetries underpin orientation, together with the explanation for organelle asymmetry, are unclear.

Introduction

The myoblasts that form the somites of *Xenopus laevis* elongate from spherical cells into cigar-shaped, bipolar cells both *in vivo* and *in vitro*. *In vivo*, elongation occurs in the presence of skin and probably neural tube-driven currents; somitic myoblasts develop perpendicular to the resulting endogenous electric fields (Robinson and Stump, 1984). In culture, *Xenopus* myoblasts also elongate perpendicular to a small applied electric field (Hinkle *et al.*, 1981). The mechanism is unknown. Since this original observation, a variety of cell types has been shown to assume perpendicular orientation in an applied field. In many cases these cells then showed migratory galvanotactic behavior (Erickson and Nuccitelli, 1984; Stump and Robinson, 1983; Cooper and Schliwa, 1986). By contrast, it is only the forming axis of elongation that is influenced in *Xenopus* myoblasts; once elongation has occurred, cells remain with a fixed position and orientation. One proposed explanation for the perpendicular alignment of epithelial cells suggests that cells assume this orientation to minimize membrane potential perturbations that occur across the anodal and cathodal facing membranes (hyperpolarization and depolarization respectively, Cooper and Keller, 1984).

We report results that make this an unlikely explanation for myoblast orientation. We also show that the intracellular distribution of organelles in field-exposed myoblasts is asymmetric. Both perpendicular orientation and organelle asymmetry may be calcium-dependent phenomena. We suspect that an asymmetric distribution of organelles in some way underlies perpendicular orientation.

Materials and Methods

The somites of stage 19/20 *Xenopus* were dissected out and disaggregated in divalent ion-free media. Dissociated myoblasts were dispersed into preconstructed chambers formed by gluing strips of cover glass onto the base of a plastic tissue culture dish, as described previously (Hinkle *et al.*, 1981). Once a roof of cover glass was applied, chambers measured 60 × 10 × 0.5 mm. Cells were grown in a standard culture medium prepared with 20% Liebowitz L15 medium (Hinkle *et al.*, 1981). Electric fields were applied using 15-cm long Agar-salt bridges. In all experiments myoblasts orientation was assessed relative to the long axis of the chambers and hence to the lines of electrical force. Cells were measured as either forming an angle > or <45° to the horizontal (long axis). An index of orientation was calculated by dividing the difference between these values by their sum. If all cells were perpendicular to the field this ratio would be one. If as many cells were perpendicular as were parallel, the ratio would be zero. Orientation ratios of 0.2–0.25 (or higher) are usually derived from data that give clear statistical differences if paired *t*-tests are applied to the raw data. Values of this sort are taken to represent significant levels of orientation.

Rhodamine phalloidin was used as a fluoresent stain

Table I

Degree of orientation of myoblasts elongating during various treatments

Treatment	Time (h)	Number	Number of myoblasts oriented >45° (1)	Number of myoblasts oriented <45° (2)	(1) − (2) / (1) + (2)
Control	5	8	14 ± 3	13 ± 3	0.04
Control	18	8	52 ± 8	54 ± 10	0.02
E Alone	5	4	57 ± 14	22 ± 6	0.44
E 6 min	5	10	20 ± 3	9 ± 2	0.38
CD + E 4 h(Off/W.O.)	18	7	242 ± 20	132 ± 15	0.27
Co^{++} + E	5	10	85 ± 19	78 ± 17	0.04
Agar + Bay K8644 (2.8×10^{-5} M)	18	13	46 ± 9	25 ± 4	0.30

E = the applied electric field; in all cases this was 100–130 mV/mm. The time given represents the number of hours of culture before assessing cell orientation. The numbers of culture dishes assessed is shown also.

E 6 min represents experiments in which myoblasts were exposed to the applied field for only the first 5–10 min (mean 6 min) after the roof had been affixed to the chambers. The first cells began to elongate about an hour later (*i.e.*, well after the field had been switched off) and orientation was assessed after 5 hours in culture.

for F-actin (Molecular Probes Inc.). Cells were fixed and stained simultaneously by replacing normal culture medium with one containing 3.7% formaldehyde, 5 units/ml rhodamine phalloidin, and 50 μg/ml palmitoyl for 20 min at 4°C. Chambers were washed through with culture medium and this replaced with a phosphate buffered saline/glycerol mixture in a 1:1 ratio. Rhodamine 123, a fluorescent stain specific for mitochondria (Johnson *et al.*, 1980), was used at 10 μg/ml in culture medium. Staining was for 30 min, followed by two brief washes in culture medium.

In a few experiments the effects of a unilateral source of chemical impregnating a block of agar (1.3%) was tested on myoblasts elongating within a mm of the source (see McCaig, 1986, for detailed method). Briefly, liquid agar containing the dissolved test substance was plated out into one half of the culture chamber and allowed to set. Dissociated myoblasts were plated into the liquid culture medium within a mm of the agar front and the chamber lid applied. Over the next 1–12 hours, myoblasts elongated in the presence of a gradient of substance diffusing out of the agar block, as demonstrated previously using India ink.

Results

The cellular influence of an applied electric field can be "remembered"

The idea that cells minimize the dimension presented to the field to minimize membrane potential perturbations across oppositely facing membranes was tested for myoblasts in two ways. Both involved field application before elongation had occurred, but no field as elongation/orientation was taking place.

The effects of a brief period of exposure to an electric field. In control and experimental cultures, the first myoblasts elongated within about 50 min–1 h of plating out into the chambers. A brief exposure to an electric field during this time, that is before any elongation had occurred, nevertheless was effective in orienting cell differentiation (Table I, Fig. 1a). Table I shows the combined results from 10 culture chambers that were exposed to the electric field for only the first 6 min after the chamber

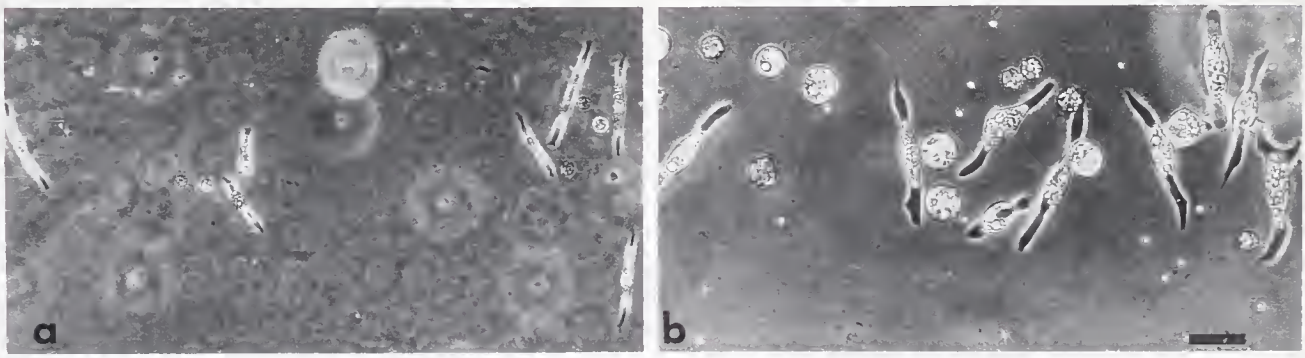

Figure 1. (a) Spherical myoblasts exposed to 100 mV/mm for their first 10 min in culture begin to elongate about 1 h later. Most orient perpendicular to the previously applied electric field; cathode at left. (b) Myoblasts exposed to 1 μg/ml cytochalasin D and 120 mV/mm for 4 h fail to elongate. If CD is washed out and the electric field is switched off (at 4 h) simultaneously, cells begin to elongate about an hour later. Cells assessed 19 h after plating have oriented perpendicular to the applied electric field; cathode at left. Scale bar = 100 μm in a, 50 μm in b.

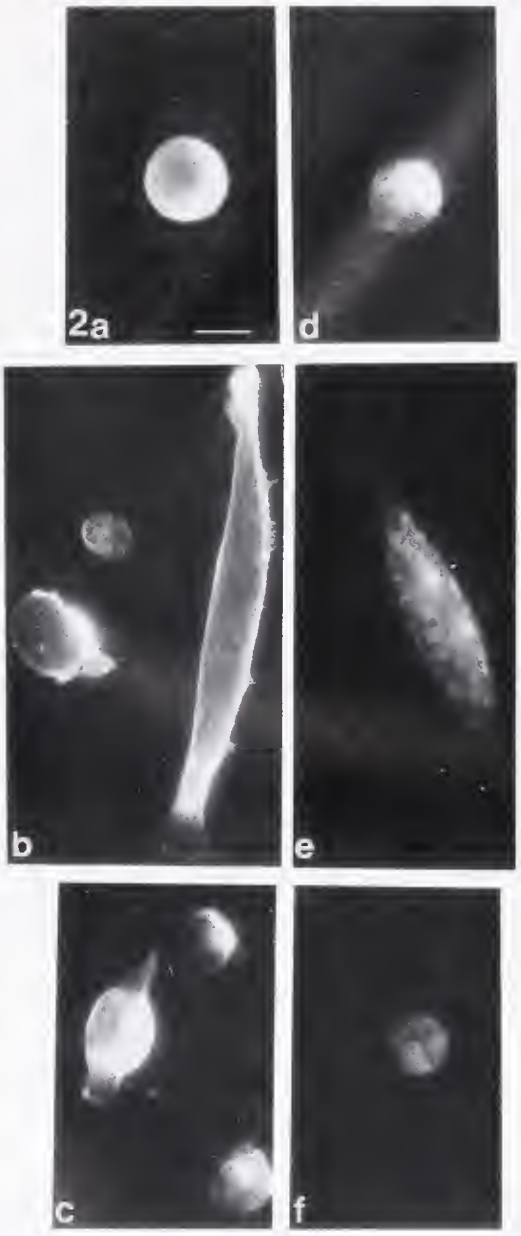

Figure 2. (a–c) Rhodamine phalloidin labelling of F-actin. (a) Spherical myoball after 6 h at 105 mV/mm. (b) Perpendicularly oriented myoblast after 4.5 h at 150 mV/mm. (c) Elongating myoblast after 30 min at 200 mV/mm. In all cases, F-actin labelling is predominant on the anodal-facing side of cells (right). (d–f) Rhodamine 123 labelling of live cells to locate mitochondria. (d) Spherical myoball after 5 h at 110 mV/mm. (e) Perpendicularly oriented myoblast after 5 h at 110 mV/mm. (f) Spherical myoball after 50 min at 200 mV/mm. In all cases, fluorescence associated with mitochondria is predominant on the anodal-facing side of cells. Scale bar = 25 μm throughout.

roof had been applied. This shows that myoblast orientation could occur in cultures that had only been exposed to an electric field for 5–10 min, fully 1 h before most cells had begun to elongate.

The effects of exposure to an electric field during periods of suppressed elongation. Microfilament disruption with cytochalasin D (CD) had variable effects on cell orientation in an electric field. At 0.1–0.2 μg/ml perpendicular orientation was unaffected; at 0.5 μg/ml it was inhibited, although interestingly elongation still occurred. One μg/ml completely suppressed all elongation with cells remaining spherical for at least 24 h.

Cells were exposed simultaneously to 1 μg/ml CD, to prevent elongation and to an applied electric field ($\sim$100 mV/mm) for 4 h. The field was switched off and CD washed out and replaced by normal culture medium. The first cells began to elongate about an hour later and more did so over the ensuing 24 h or so. Such cultures showed considerable degrees of orientation, not disimilar to the value found in an electric field alone (Table 1, Fig. 1a).

Perpendicular alignment is a calcium-dependent phenomenon and may involve asymmetric distribution of intracellular organelles

When developing myoblasts were exposed to an electric field in the presence of 5 m*M* cobalt chloride, no orientation occurred; roughly equal numbers of cells elongated perpendicular and parallel to the field (Table I, Fig. 1c). Cells were stained with fluorochromes to determine the distribution of microfilaments and mitochondria. Rhodamine phalloidin specifically stains for F-actin. This was distributed symmetrically in control cells but was present predominantly on the anodal side of cells exposed to an applied electric field for 18 h, 5 h, or even 1 h (Fig. 2a, b, c). Similarly Rhodamine 123, which is a specific probe for mitochondria, revealed anodal accumulations of mitochondria after a 1 h exposure to an electric field (Fig. 2d, e, f). Preliminary electron microscopy has extended these observations to relative accumulations of ribosomes beneath the anodal-facing cell membrane (not shown). The field-induced anodal accumulation of F-actin microfilaments was inhibited in cultures exposed to cobalt (Fig. 3a); these cultures showed no orientation. Therefore, both field-induced orientation and organelle asymmetry may depend on asymmetric calcium entry, predominantly on the depolarized cathodal-facing side of myoblasts.

We have tested this hypothesis by exposing differentiating myoblasts to a unilateral source of the calcium channel agonist Bay K8644 (Bayer). With this present at a concentration of 2.8×10^{-5} *M* in a 1.3% agar slab, myoblasts developed predominantly perpendicular to the lines of diffusion of Bay K8644 from the agar (Table I, Fig. 3b). In addition, preliminary electron microscopy revealed that microfilaments and mitochondria were also distributed asymmetrically in these cells. After 18 h,

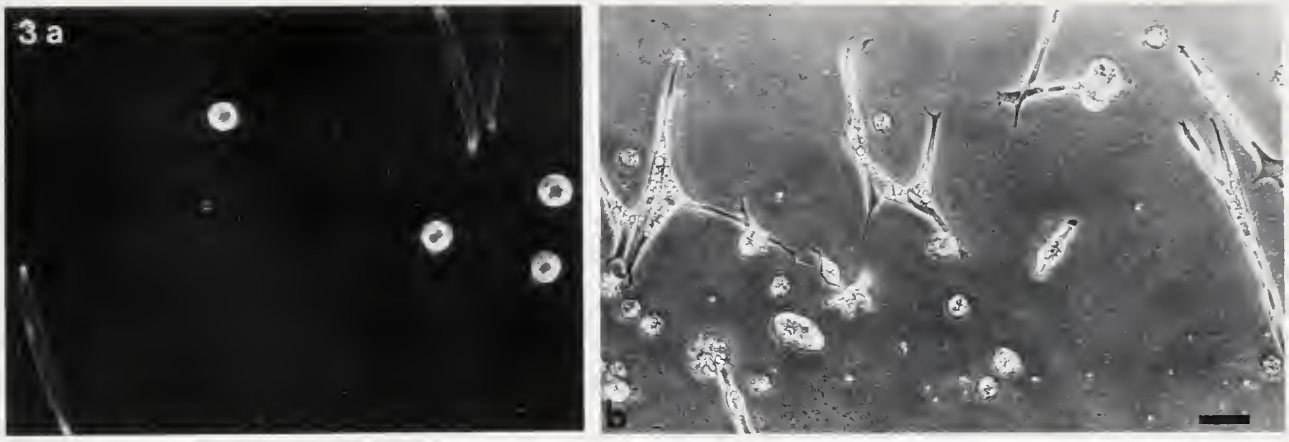

Figure 3. (a) Rhodamine phalloidin staining of myoblasts after 5 h at 100 mV/mm + 5 m*M*/l Co^{++}. F-actin staining appears uniform. (b) Myoblasts exposed to a unilateral agar source of the calcium channel agonist Bayer K8644 (2.8×10^{-5} *M*/l; at left) elongate perpendicular to the lines of diffusion from the agar slab. Scale bar = 50 μm.

accumulations of both were present on the side of cells furthest away from the agar source of Ca^{++} channel agonist.

Discussion

Several cell types assume a perpendicular orientation in an applied electric field (Robinson, 1985, for review). A unifying mechanistic proposal suggests that cells behave in this way to limit the membrane potential perturbations experienced at anodal and cathodal-facing membranes (Cooper and Keller, 1984). Such behavior is conceivable for cells that alter an already differentiated shape in response to field application. However, it cannot explain the directed differentiation of *Xenopus* myoblasts. These cells oriented perpendicularly when no electric field was present, provided they had been exposed previously to an applied field.

In general there are three ways in which an electric field may influence cell functioning. By altering the membrane potential, various voltage-sensitive ion conductances may be altered. For instance, cathodal-facing membranes will be depolarized and this may increase calcium entry on that side while reducing calcium conductance on the hyperpolarized, anodal side of the cell. External voltage drops can redistribute membrane proteins involved in transmembrane ion conductance resulting again in internal ionic asymmetries. The third possibility is that a small proportion of the external voltage drop (10^{-5}–10^{-3} depending on membrane resistance) exists as a potential drop within the cell. For applied field strengths in the physiological range, this value would usually only be of the order of microvolts and would not be expected to cause redistribution of charged cellular components (see Jaffe, 1969, 1979, for discussion of exceptional circumstances). We report that organelle redistribution does occur.

We have shown that galvanic orientation in myoblasts is a calcium-dependent process. Calcium may enter these differentiating cells predominantly on the cathodal side, either because of voltage sensitive conductance changes, or a cathodal accumulation of calcium channels, or both. This could create an intracellular gradient of calcium that asymmetrically activated selected cell functions. In support of this view, we have demonstrated that other experimental situations designed to unilaterally raise intracellular calcium also caused perpendicular alignment.

In addition, we have evidence that several intracellular components redistribute, both in the presence of a small electric field and when asymmetric calcium entry may be imposed on elongating myoblasts (Bay K8644 experiments). Although this work is preliminary, mitochondria, actin microfilaments, and ribosomes all appeared concentrated on the side of cells opposite the expected sites of increased calcium entry. That is, opposite the cathodal-facing membrane and further away from the agar source of calcium agonist. There is good experimental evidence for the translocation of charged integral membrane components (IMPS) in applied electric fields (Poo, 1981). Similar movements of charged intracellular components have been thought likely only between specialized cells, *e.g.*, insect ovarian follicles (Woodruff and Telfer, 1980). Unless the surface movements of IMPS are causal in the cellular redistributions of organelles, these results are difficult to explain as the effects of transcytoplasmic Donnan-type potentials. Such potentials could arise following asymmetric influx of ions, immobi-

lization of these as an intracellular gradient (*e.g.*, Ca^{++}) while mobile counter ions established a substantial potential drop (Jaffe, 1969, 1979; Jaffe *et al.*, 1974). This analysis predicts that sites of Ca^{++} leak into cells will be electropositive with the opposite sites of lower Ca^{++} concentration, electronegative. We appear to have accumulations of some negatively charged organelles on the "wrong" side of the cell to be explained by intracellular Donnan potentials. Therefore, we expect a complex interplay between the applied electric field and intracellular organelle transport processes. Whatever the mechanism, this work draws attention to field-induced organelle asymmetries in cells where the calculated cytoplasmic voltage drop would not be expected to produce these effects. Finally, both the proposed asymmetric entry of Ca^{++} and the establishment of a transcytoplasmic voltage drop should be measurable.

Acknowledgments

We thank the Medical Research Council, Action Research for the Crippled Child, and the International Spinal Research Trust for financial support.

Literature Cited

Cooper, M. S., and R. E. Keller. 1984. Perpendicular orientation and directional migration of amphibian neural crest cells in dc electrical fields. *Proc. Natl. Acad. Sci. USA* **81:** 160–164.

Cooper, M. S., and M. Schliwa. 1986. Motility of cultured fish epidermal cells in the presence and absence of direct current electric fields. *J. Cell. Biol.* **102:** 1384–1399.

Erickson, C. E., and R. Nuccitelli. 1984. Embryonic fibroblast motility and orientation can be influenced by physiological electric fields. *J. Cell Biol.* **98:** 296–307.

Hinkle, L., C. D. McCaig, and K. R. Robinson. 1981. The direction of growth of differentiating neurones and myoblasts from frog embryos in an applied electric field. *J. Physiol.* **314:** 121–135.

Jaffe, L. F. 1969. On the centripetal course of development, the *Fucus* egg and self-electrophoresis. *Dev. Biol. Suppl.* **3:** 83–111.

Jaffe, L. F. 1979. Control of development by ionic currents. In *Membrane Transduction Mechanisms,* R. A. Cone and J. E. Dowling, eds. Raven Press, NY.

Jaffe, L. F., K. R. Robinson, and R. Nuccitelli. 1974. Local cation entry and self-electrophoresis as an intracellular localization mechanism. *Ann. N.Y. Acad. Sci.* **238:** 372–389.

Johnson, L. V., M. L. Walsh, and L. B. Chen. 1980. Localization of mitochondria in living cells with rhodamine 123. *Proc. Natl. Acad. Sci. USA* **77:** 990–994.

McCaig, C. D. 1986. Myoblasts and notochord influence the orientation of somitic myoblasts from *Xenopus laevis*. *J. Embryol. Exp. Morphol.* **93:** 121–131.

Poo, M-m. 1981. *In Situ* electrophoresis of membrane components. *Ann. Rev. Biophys. Bioeng.* **10:** 245–276.

Robinson, K. R. 1985. The responses of cells to electrical fields: a review. *J. Cell. Biol.* **101:** 2023–2027.

Robinson, K. R., and R. F. Stump. 1984. Self-generated electrical currents through *Xenopus* neurulae. *J. Physiol.* **352:** 339–352.

Stump, R. F., and K. R. Robinson. 1983. *Xenopus* neural crest cell migration in an applied electric field. *J. Cell Biol.* **97:** 1226–1233.

Woodruff, R. I., and W. H. Telfer. 1980. Electrophoresis of proteins in intercellular bridges. *Nature* **286:** 84–86.

Reference: *Biol. Bull.* **176(S)**: 145–149. (April, 1989, Suppl.)

Elongation of Initially Non-Polar Protoplasts is Oriented by Electric Fields

ROSEMARY G. WHITE AND ROBYN L. OVERALL

School of Biological Sciences, University of Sydney, N.S.W. 2006, Australia

Abstract. When regenerating *Mougeotia* protoplasts, suspended in agar, are cultured for 20–24 h in a 7 mV/cell D.C. field, their growth axes tend to parallel the field. This may indicate either rotation of the regenerates by the field or polarization of the protoplasts and hence polarization of their microtubules which lie perpendicular to the growth axis and regulate elongation.

Introduction

The cylindrical shape of many plant cells is established by the helical or transverse orientation of cellulose microfibrils in the cell wall. The relatively inelastic microfibrils are laid down approximately perpendicular to the axis of cell expansion. This specific orientation of the microfibrils is thought to be controlled, in turn, by the regular helical or transverse orientation of microtubules in the peripheral cytoplasm adjacent to the plasma membrane (for review see Heath and Seagull, 1982). Thus the growth axis of the cell, and hence the tissue composed of these cells, is established by the constraints of the microtubule and microfibril arrangement in component cells. We know nothing of the mechanism that initiates the development of this growth axis.

The spherical protoplasts of the green alga *Mougeotia* are an ideal system in which to study this process because they readily deposit a new cell wall and revert to their original cylindrical cell shape (Marchant and Fowke, 1977; Marchant and Hines, 1979). In addition, the reorganization of the microtubules during the establishment of the axis, and the accompanying cellulose deposition, have been characterized (Galway and Hardham, 1986), as summarized in Fig. 1.

The orientation of the developing axes in naturally occurring spherical plant cells, such as the *Fucus* egg or *Lilium* pollen, can be manipulated by the application of external electric fields (Jaffe and Nuccitelli, 1977). In this study, we ask if the orientation of the axis of a typical vegetative cylindrical plant cell, namely that of *Mougeotia*, can also be affected by the application of an external field. In other studies in our laboratory, it has been shown that light and gravity have no effect on the orientation of the developing axis in protoplasts of *Mougeotia* (Hyde, 1987).

Materials and Methods

Plant material

Mougeotia sp. filaments, originally collected from the Botanic Gardens, Canberra, were obtained from M. E. Galway, A.N.U., Canberra. Filaments were cultured in a soil-water medium using either a soil substrate (Pringsheim, 1946) or a substrate of 1% agar in soil-water extract. The latter method reduced contamination of cultured protoplasts. Soil-water extract was obtained by autoclaving garden soil (with no added fertilizer, herbicides or pesticides) in distilled water (1:3 soil:water) for 20 min. A pinch of $CaCO_3$ was added to every 500 g of soil.

Protoplast preparation

Consistent protoplast yields have been obtained by modifying a purification routine of Galway and Hardham (1986). Briefly, *Mougeotia* filaments were collected on a gauze filter and rinsed with sterile water. Cell walls were digested in the dark using 2% cellulase (Onozuka), 1% driselase (Yakult), and 0.4% macerase (Calbiochem) in 400 m*M* sorbitol, 10 m*M* $CaCl_2$, 3 m*M* $MgSO_4$, 25 m*M* MES/TRIS buffer (pH 5.6) containing 0.5% bovine serum albumin (Sigma) for 2.5 to 3 h on a rotary shaker at 60 rpm. Dextran (mw 17,200; Sigma) was then added to a final concentration of 3%, the solution was centrifuged at $100 \times g$ for 10 min and floating protoplasts were removed. A solution of 1% Dextran in 1/8 protoplast maintenance medium (1/8 PMM: 350 m*M* sorbitol, 1.25 m*M* $CaCl_2$, 0.5 m*M* $MgSO_4$, 10 m*M* MES/TRIS pH 6.1)

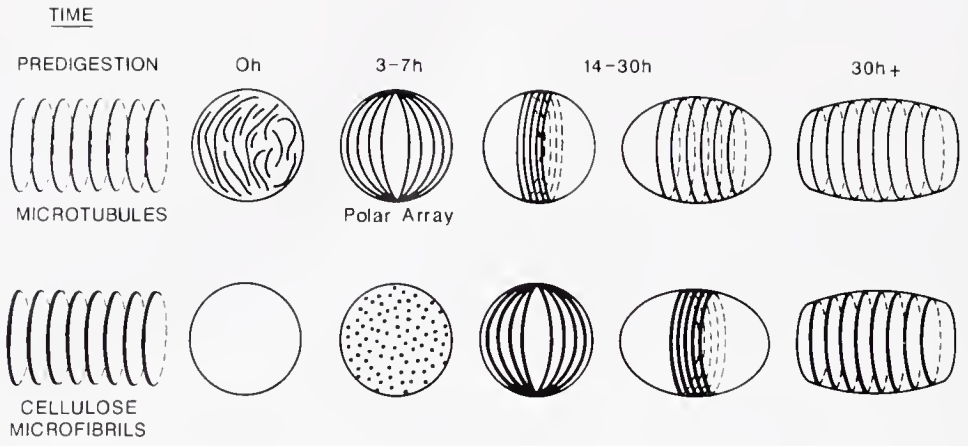

Figure 1. Organization of microtubules and cell wall microfibrils in protoplasts of the green alga *Mougeotia* at intervals after protoplast isolation. (Adapted from Galway and Hardham, 1986).

or 1/4 PMM (350 m*M* sorbitol, 2.5 m*M* $CaCl_2$, 1 m*M* $MgSO_4$, 15 m*M* MES/TRIS pH 6.1) was layered onto the protoplast suspension, then 1/8 PMM or 1/4 PMM layered on top. Protoplasts were centrifuged for 10 min at 100 × *g* and those at the interface between the top and second layer were removed and rinsed 3 times with 1/8 or 1/4 PMM. To the final suspension was added 1.5% sea plaque agarose (FMC Corp., Rockland, Maine) in 1/8 or 1/4 PMM, to a final concentration of 0.75% agarose. The protoplasts in PMM-agarose were cultured in field chambers 0.05 cm deep × 0.7 cm wide × 4 cm long.

Application of electric fields

Fields were applied via Ag/AgCl salt bridges connected via agar (1% Bacto-Agar) tubes (47 cm long; bore 0.45 or

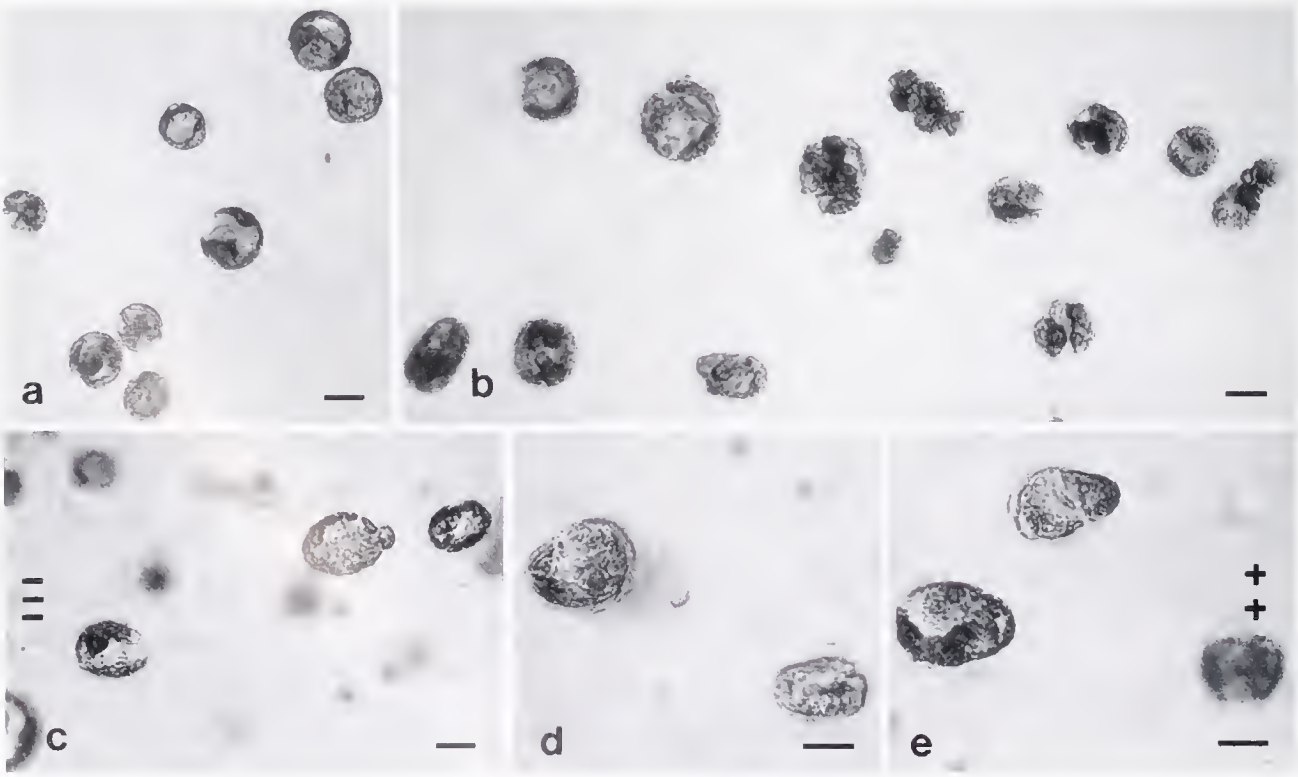

Figure 2. Immediately after isolation, *Mougeotia* protoplasts are spherical (a). After 20 h, untreated protoplasts showed random orientation of elongation (b); elongation was parallel to an applied field of 2 V cm^{-1} (c, d, e). −, location of cathode; +, location of anode. Bar = 20 μm.

Table I

Analysis of the effect of steady electric fields on growth axis orientation of regenerating Mougeotia *protoplasts*

Treatment	No. protoplasts (no. experiments)	Rayleigh's R value	Critical R value
Fields (2 V cm^{-1})	661 (6)	232.1	44.5
Fields (0.3 V cm^{-1})	354 (3)	19.7	32.6
Controls	397 (10)	25.6	37.4

If the calculated R is less than the critical $R_{0\,05,n}$ then it can be said that there are no significant angular trends at $P = 0.05$, where n = no. protoplasts (see Ch. 2 in Zar, 1974).

0.6 cm) as described by Erickson and Nuccitelli (1984). Resistivity of media was 1800 (1/8 PMM) or 1000 (1/4 PMM) ohm cm. Field strength was measured immediately and monitored throughout the experiments. Chambers were left at 20°C in a light intensity (42 μ Einstein $m^{-2} \cdot s^{-1}$) at which normal elongation of protoplasts occurred. After 16 to 20 h, the chambers were removed from the fields and the axis of elongation of the protoplasts was recorded using a Bioquant Hipad digitizing tablet (R & M Biometrics, Nashville, Tennessee) linked to a Bioquant II software package on an Apple IIE microcomputer.

Microtubule immunofluorence

Many attempts to stain microtubules in protoplasts that were either embedded in agarose or attached with 0.1 mg ml^{-1} poly-L-lysine (Sigma) to one side of the field chambers were unsuccessful. Finally, protoplasts were grown in chambers as described above, except that agarose was omitted from the growth medium, *i.e.*, the protoplasts were suspended in 1/8 PMM during the experiment. After field treatment, protoplasts were stained for microtubules as described by Galway and Hardham (1986).

Results

Protoplast elongation in electric fields

Protoplasts elongated parallel to the direction of an applied electric field with a field strength of 2 V cm^{-1} (Fig. 2). There was an extremely significant trend in the distribution of angles of elongation in the field treated protoplasts (Rayleigh's R test, $P = 0.001$) but not in the controls which were not subjected to fields (Rayleigh's R test, $P = 0.05$; Table I). With a field strength of 0.3 V cm^{-1}, angles of elongation were not significantly different from controls (Rayleigh's R test, $P = 0.05$).

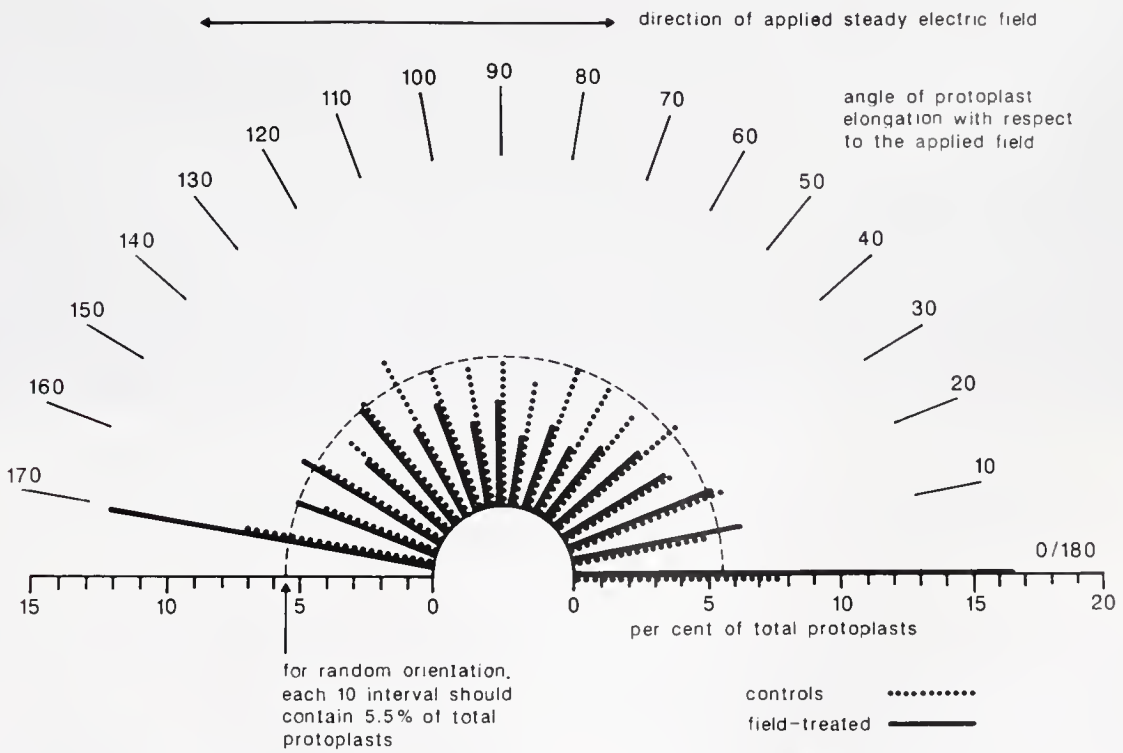

Figure 3. Frequency histogram of growth axis orientation of regenerating *Mougeotia* protoplasts. The percentage of protoplasts in a 10° window centered at 10° intervals is plotted.

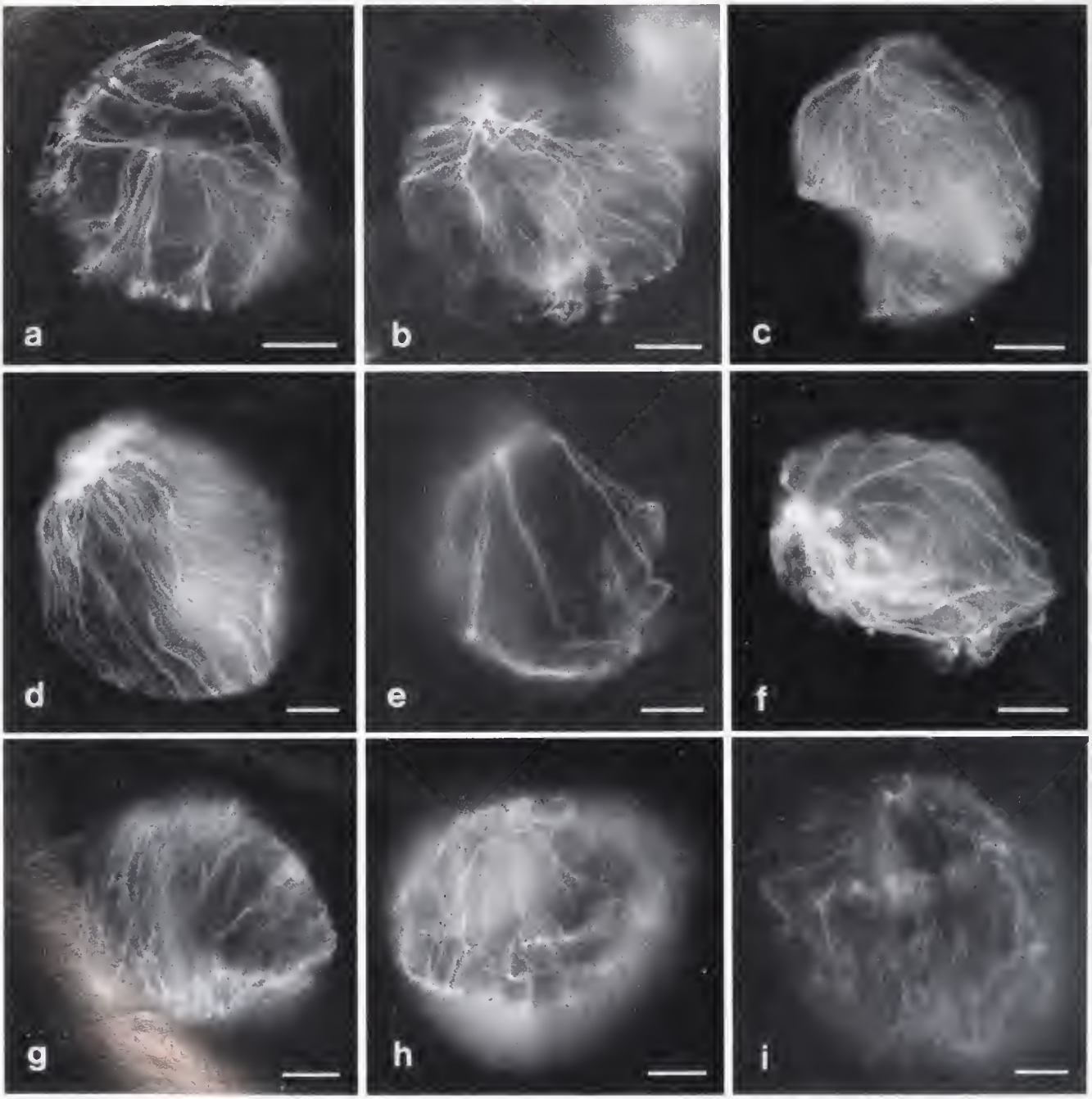

Figure 4. Microtubule immunofluorescence of *Mougeotia* protoplasts. Microtubules are arranged randomly 30 min after isolation in untreated protoplasts (a). Microtubule foci appeared by 3 h in both controls (b) and field treated protoplasts (c, f). By 18 h, almost all protoplasts showed two distinct foci in controls (d) and in fields (e, i). The microtubules appeared to be aggregated in fewer strands in field-treated protoplasts. By 20–24 h in controls (g), and 17–20 h in fields (h), some protoplasts had begun to elongate (compare Fig. 1). Bar = 10 μm.

The frequency histogram of angular orientations in 2 V cm^{-1} field strength is presented in Figure 3. Protoplasts were not randomly oriented after field treatment and there was a small, but not significant tendency for control protoplasts to be aligned parallel to the edges of the chamber.

Development of microtubule arrays in protoplasts grown in applied fields

Preliminary experiments showed that development of the polar array of microtubules was similar in untreated protoplasts and in protoplasts grown in applied electric

fields (2 V cm^{-1}; Fig. 4). However, subsequent development of the meridian band of microtubules, and establishment of the transverse array typical of cells in intact *Mougeotia* filaments, appeared to be accelerated by field treatments.

Discussion

The exact threshold field strength that affects the orientation of the elongation axis in *Mougeotia* protoplasts has not been determined, but it lies between 1 and 7 mV per cell. This is within the range of field strengths that affect the development of an axis in other plant cells (Jaffe and Nuccitelli, 1977).

The elongation of *Mougeotia* protoplasts is controlled by the orientation of the cellulose microfibrils and ultimately by the orientation of the microtubular arrays. Elongation is perpendicular to the band of aggregated microtubules. For the elongation to be parallel to the field, the two foci (poles) of the initial polar array must be formed at positions of equal potential within the field. If poles were formed so that the axis connecting them were parallel to the field, elongation perpendicular to the aggregated meridian microtubules could never be parallel to the field, as all meridians pass through the poles of the array. For elongation parallel to the field, the aggregated meridian microtubules must also be placed at positions of equal potential within the field.

Unfortunately, attempts to verify these inferences about the orientation of microtubular arrays in applied electric fields by immunofluorescent labeling of the cytoskeleton of *Mougeotia* protoplasts, while maintaining them in a fixed position, have been unsuccessful. Nevertheless, we have shown that all the usual microtubular arrays do at least form in the field treated protoplasts.

The fact that the development of the axis in this vegetative plant cell can be manipulated by electric fields opens the possibility that endogenous ionic currents play a role in the establishment and maintenance of this axis. We plan to investigate the pattern of extracellular currents around regenerating protoplasts and filaments of *Mougeotia*. Indeed, steady ionic currents and the voltages they generate may be the polarizing influence which brings about the parallel alignment of cortical microtubules perpendicular to the long axis of many plant cells.

Acknowledgments

We thank Leila Blackman for technical assistance. Supported by grants from the Australian Research Council and the University of Sydney.

Literature Cited

Erickson, C. A., and R. Nuccitelli. 1984. Embryonic fibroblast motility and orientation can be influenced by physiological electric fields. *J. Cell Biol.* **98:** 296–307.

Galway, M. E., and A. R. Hardham. 1986. Microtubule reorganization, cell wall synthesis and establishment of the axis of elongation in regenerating protoplasts of the alga *Mougeotia*. *Protoplasma* **135:** 130–145.

Heath, I. B., and R. W. Seagull. 1982. Orientated cellulose fibrils and the cytoskeleton: A critical comparison of models. Pp. 163–184 in *The Cytoskeleton in Plant Growth and Development*, C. W. Lloyd, ed. Academic Press, New York.

Hyde, G. J. 1987. Spatial organisation and orientation in *Mougeotia* protoplasts. Hons. Thesis, University of Sydney.

Jaffe, L. R., and R. Nuccitelli. 1977. Electrical controls of development. *Annu. Rev. Biophys. Bioeng.* **6:** 445–476.

Marchant, H. J., and L. C. Fowke. 1977. Preparation, culture and regeneration of protoplasts from filamentous green algae. *Can. J. Bot.* **55:** 3080–3086.

Marchant, H. J., and E. R. Hines. 1979. The role of microtubules and cell wall deposition in elongation of regenerating protoplasts of *Mougeotia*. *Planta* **146:** 41–48.

Pringsheim, E. G. 1946. The biphasic or soil-water culture method for growing algae and flagellata. *J. Ecol.* **33:** 193–204.

Zar, J. H. 1974. *Biostatistical Analysis.* Prentice-Hall, New Jersey.

Reference: *Biol. Bull.* **176(S):** 150–156. (April, 1989, Suppl.)

Electrophoresis of Cytoplasmic Molecules Through Gap Junctions by Externally Applied Electric Fields

MARK S. COOPER[1], JOHN P. MILLER[2], AND SCOTT E. FRASER[3]

[1]*Howard Hughes Medical Institute, Yale University School of Medicine, Section of Molecular Neurobiology, New Haven, Connecticut 06510,* [2]*Department of Zoology, University of California, Berkeley, California 94720,* [3]*Department of Physiology and Biophysics, University of California, Irvine, California 92717*

Abstract. External electric fields are efficiently conducted into the cytoplasmic interior of extended chains of cells that are electrotonically coupled by gap junctions. For chains of cells or tissues that are much longer than their electrical length constant, the cytoplasmic electric field within the center of the ensemble is identical in magnitude to the externally applied field. Over a period of time, this internal electric field should cause a intercellular redistribution of charged molecules that are permeant to gap junctions, within the coupled tissue. This prediction was confirmed experimentally by observing the directed migration of 6-carboxyfluorescein (negatively charged) within the electrotonically coupled lateral giant neurons of a crayfish nerve cord under the influence of externally applied DC electric fields. To determine whether such redistributions could occur in developing epithelial tissues, hydra were exposed to DC electric fields, after charged fluorescent dyes had been loaded into their ectoderm. In this electrotonically coupled tissue, the fluorescent dyes also underwent an electrophoretic redistribution in response to externally applied fields. To facilitate the future use of electric fields as an experimental means to redistribute intracellular constituents in developing tissues, mathematical relationships are presented that predict the time course and steady-state concentration profiles of molecules undergoing intercellular electrophoresis.

Introduction

The mechanisms by which endogenous and applied electric fields affect the physiology and pattern formation of developing organisms are strongly determined by how electric field lines are spatially partitioned within cells and tissues. This partitioning of electric field lines is, in general, dictated by the specific core conductor and cable properties of the cellular ensemble in question. In this paper, we examine how externally applied electric fields can influence the movement and concentration profiles of charged intracellular molecules within the coupled cytoplasms of tissue cells connected by gap junctions. We show experimentally that externally applied electric fields can be used as experimental tools to control the transjunctional fluxes of charged molecules across open gap junctions. The ability to control intercellular diffusion by externally applied fields potentially offers a new means of determining whether the transfer of signal molecules across gap junctions is involved in the pattern formation of developing tissues.

Briefly, we discuss the following issues in this paper:

(1) The conduction of electrical current through cell membranes into the cytoplasmic interior of an electrotonically coupled tissue.

(2) The cytoplasmic electric field profile, which arises from the passage of current through the cytoplasm and gap junctions of the coupled tissue.

(3) Recent experimental observations of a directed electrophoretic movement of charged cytoplasmic molecules through gap junctions within tissues exposed to an externally applied electric field.

(4) Theoretical analysis of the steady-state molecular concentration asymmetries which should develop in tissues resulting from long-term intercellular electrophoresis under the influence of external electric fields.

(5) An experimental method to distinguish between developmental biological effects originating from (a) the electrophoretic segregation of molecules within cells or

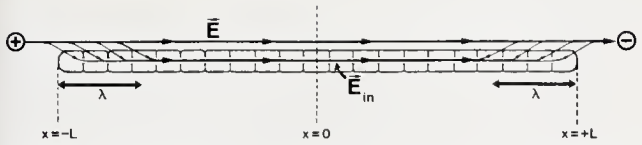

Figure 1. Conduction of external electric fields into the cytoplasmic interior of cells coupled by gap junctions. A chain of tissue cells (length 2L with electrical length constant λ), coupled electrotonically with gap junctions, will react as a long leaky cable to an externally applied electric field E. Current that is conducted through cell membranes will flow between cells via their gap junctions. The flow of electrical current within the ensemble is associated with a cytoplasmic electric field E_{in} which will exert an electrophoretic force on charged intracellular molecules.

cell membranes, and (b) the perturbation of the membrane potential induced by the electric field, and subsequent active membrane responses to this perturbation.

Cytoplasmic electric fields and intercellular electrophoresis

The electrical behavior of single cells, as well as chains of cells coupled by gap junctions, is well modelled by a finite length (2L), leaky cable. When such a cable is placed in an externally applied electric field, current from the external medium is conducted through cell membranes into the interior of a cellular ensemble. The resulting internal electric field depends strongly on the electrical space constant, λ, and is given by the following expression (Cooper, 1984):

$$E_{in} = E[1 - \cosh(x/\lambda)/\cosh(L/\lambda)]. \quad (1)$$

In the center of cellular ensembles that are much longer than their electrical length constant (λ), the internal electric field (E_{in}) is identical in magnitude to that of the externally applied field (E). If the resistance of junctional membranes within cellular ensembles is significantly larger than the electrical resistance of bulk cytoplasm, the cytoplasmic potential drop is no longer a continuous function as expressed in Equation 1. Instead, as the resistance of the junction membrane increases, the electrical potential drop within the cytoplasm becomes progressively localized to the gap junctions (Brink and Barr, 1977; Plonsey and Barr, 1986). Whether the cytoplasmic electric field is uniformly distributed within the cytoplasm, or becomes concentrated at junctional cell membranes, an electrophoretic force acts on intracellular molecules which tends to drive intracellular charged molecules toward one end of the cable.

Materials and Methods

We used the electrotonically coupled lateral giant neurons of the crayfish abdominal nerve cord as an experi-

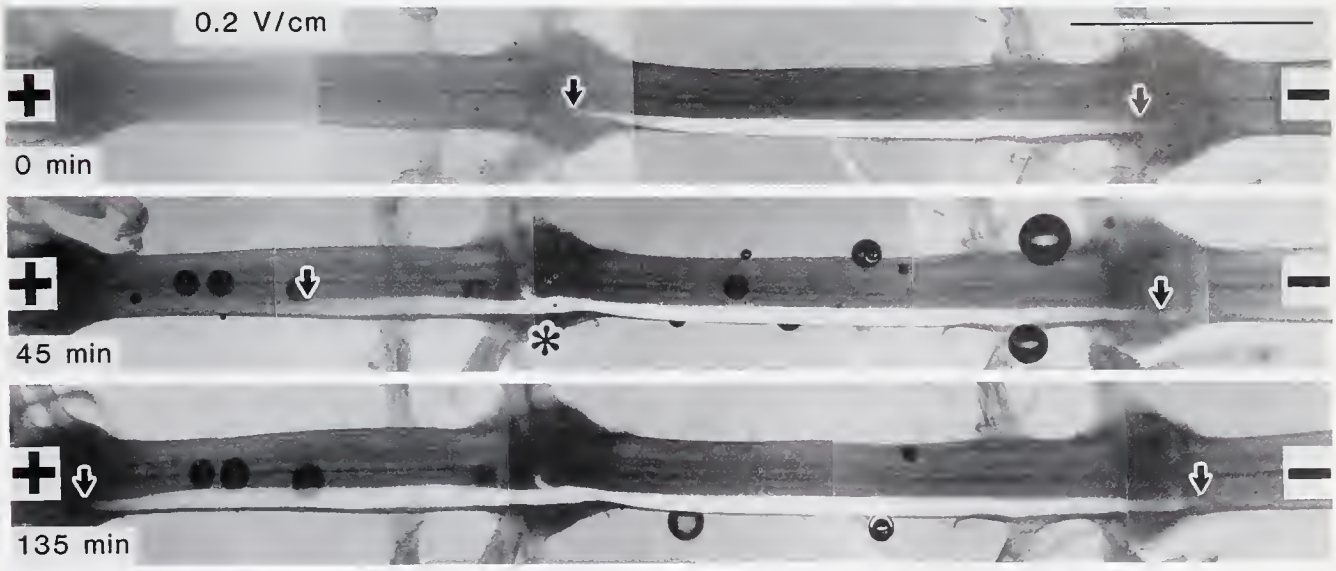

Figure 2. Intercellular electrophoresis of charged molecules through gap junctions. 0 min. 6-carboxyfluorescein has been injected (15 min prior to photo) into a lateral giant neuron. The microelectrode has been pulled just outside of the cell to mark the center of the dye fill. An extracellular electric field of 200 mV/cm is subsequently applied. At 45 and 135 min after field application, the center of the dye has been displaced toward the anode. The position of the gap junction that connects the lateral giant neurons of adjacent nerve cord segments is marked by an asterisk. Scale bar = 2 mm. A similar movement of the dye center toward the positive electrode was seen consistently in fields of 200 mV/cm, at a rate of $v = 0.8 \pm 0.3$ mm/h ($n = 4$). This directed movement was distinct ($P < 0.005$, two-tailed t-test) from control experiments where no movement of the dye center was observed; $v = 0.1 \pm 0.2$ mm/h ($n = 3$).

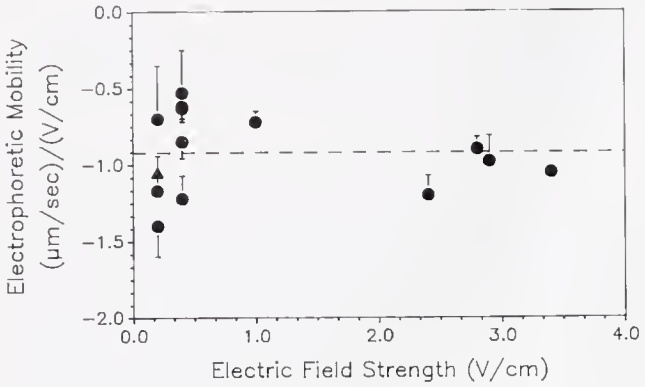

Figure 3. Intercellular electrophoretic mobility of 6-carboxyfluorescein. The observed electrophoretic mobility of 6-carboxyfluorescein is plotted as a function of applied electric field strength. All values represent mobility measurements based on movements within the central four segments of the nerve cord. In a given experiment, the center of the dye fill, defined as the midpoint between the two edges of the region visibly containing dye, moved linearly with time. The velocity of the dye's movement (mean displacement in time) divided by the applied electric field strength yields the dye's electrophoretic mobility, m. Standard deviation bars are associated with each mean mobility (2–9 observations/experiment), except for one experiment (triangle) where only a single timepoint was recorded. At 3.4 V/cm, the standard deviation bar was too small to be portrayed with the mean (-1.05 ± 0.03 μm/s per V/cm; 5 observations). The mean mobility for all experiments performed (dashed line) was $m = -0.92 \pm 0.27$ μm/s per V/cm ($n = 14$ experiments; representing a total of 65 individual observations of dye movement). By convention, a negative mobility refers to electrophoretic migration towards the positive electrode (Poo, 1981). Through linear regression analysis, the electrophoretic mobility was found to be independent ($P < 0.025$, t-test) of electric field strength. This is consistent with a linear electrophoretic field interaction.

mental system to test for intercellular electrophoresis. On each side of the nerve cord, six lateral giant neurons are linked end to end by non-rectifying gap junctions, making a cable approximately 3 cm long, with an electrical length constant of $\lambda = 2.6$ mm. Watanabe and Grundfest (1961) have measured the total axoplasmic resistance of crayfish lateral giant neurons to be approximately 500 kΩ, and the resistance of their junctional membranes to be 300 kΩ. In the presence of a longitudinal current within the coupled chain of neurons, the elevated resistance of the junctional membranes will result in some localization of the cytoplasmic voltage drop to the junctional regions (see Brink and Barr, 1977; Plonsey and Barr, 1986); however, the internal electric field profile within the chain of lateral giants, exposed to a uniform external electric field, is well approximated by the theoretical profile predicted by Equation 1.

Abdominal nerve cords of the crayfish *Procambarus clarkii* were isolated by standard methods (Furshpan and Potter, 1959) and pinned into a Sylgard coated chamber ($0.4 \times 0.5 \times 0.7$ cm). A chilled (4°C) Crayfish Ringers (m*M* composition: NaCl 207, KCl 5, $MgCl_2$ 3, $CaCl_2$ 14, HEPES 2, pH 7.4) was perfused through the chamber at a rate of 3–4 ml/min. Several segments of the nerve cord were then desheathed. Individual lateral giant axons were impaled with a micropipet containing a 3% solution of 6-carboxyfluorescein, and were injected with the dye using pressure and/or iontophoresis.

Uniform DC electric fields of 0.2–3.4 V/cm were applied parallel to the axis of the nerve cords using 20-cm agar-saline bridges coupled to the ends of the Sylgard coated chamber. To further isolate the experimental preparation from electrolysis products, each bridge was in turn coupled to a 200-ml beaker filled with Ringers buffered with 50 m*M* HEPES, a second 20-cm agar-saline bridge, and a second beaker containing 50 m*M* HEPES-buffered Ringers, and a 4 cm^2 Ag/AgCl plate electrode.

The position of the injected dye was recorded using a motorized epifluorescence microscope (Jacobs and Mil-

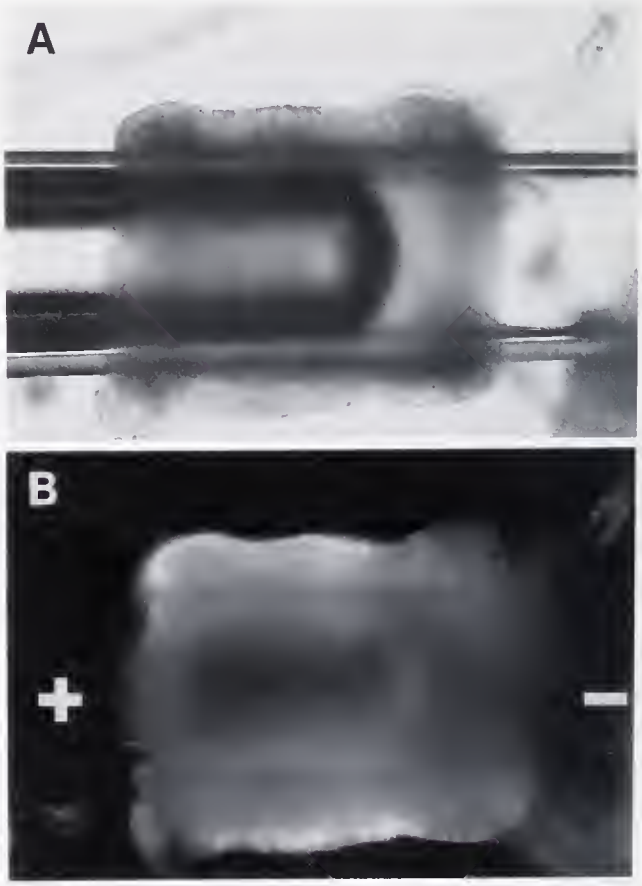

Figure 4. Electrophoretic redistribution of a charged fluorescent dye within the coupled ectoderm of hydra. Negatively charged calcein was loaded into hydra ectodermal cells using an electroporator, and the hydra was strung onto a glass fiber. (A) Phase image of the hydra on the glass fiber. (B) distribution of the calcein dye after exposure to a 1 V/cm electric field for 20 min. The negatively charged calcein is asymmetrically distributed toward the positive electrode or anode.

Table I

Electric field induced redistribution of calcein in hydra

Electric field strength (V/cm)	Asymmetric	Marginal	Symmetrical
0.0	0	0	12
1.0@	7	3	6
1.0*	3	3	3
1.0#	4	2	4
Total	14	8	13

Hydra were classed as asymmetric if they showed a decisive gradient in the distribution of calcein when compared with the initial distribution of calcein (@) or the distribution of either tetramethylrhodamine cadaverine (*) or rhodamine dextran (#). Those that were in any way questionable were classed as marginal. All observations were made after the hydra were placed in the experimental chamber and exposed to an electric field of 1.0 V/cm or 0.0 V/cm for 20 min.

ler, 1985). To quantify the movements of the injected dye under the influence of applied fields, position measurements were made of the center of the dye fill, defined as the midpoint between the anode- and cathode-facing edges of the visible dye bolus. We judged this to be the most accurate means of determining dye movement from our photographic data, because it is largely unaffected by the fluorescent dye slowly leaking from the cells, or by bleaching of the dye under repeated epifluorescence illumination.

A similar chamber was used to observe intercellular electrophoresis in the coupled ectoderm of hydra. Dyes were loaded into the cells of individual *Hydra attenuata* by electroporation. Hydra were placed in a cuvette containing 200 μl of hydra medium (1 m*M* $CaCl_2$, 1 m*M* $NaHCO_3$, 10 μ*M* EDTA), 2.5 m*M* calcein (negatively charged) and either 2.5 m*M* tetramethylrhodamine cadaverine (5(and 6)-((n-(aminopental)amino)carbonyl)tetramethylrhodamine) (positively charged) or 0.5 m*M* rhodamine dextran (positively charged, but too large to pass through junctional membranes). All fluorescent dyes were obtained from Molecular Probes (Eugene, Oregon). Two platinum wire electrodes (1 mm diameter, spaced 1 cm apart) were lowered into the cuvette solution and used to apply an electric discharge from a Promega X-Cell 450 Electroporation Unit (1 s train of pulses from a 300 mfd capacitor bank charged to 100 volts). The hydra were then removed from the cuvette, washed three times with hydra medium, and allowed to recover for 20 min in the dark. To orient hydra in an applied electric field, several organisms were strung longitudinally onto a glass filament that had been fire-polished to a blunt point using a microforge. The glass filament holding the hydra was secured in the electric field chamber using small pieces of dental wax. Current was applied to the chamber containing hydra medium via agar-saline bridges made with hydra medium buffered with 50 m*M* HEPES, pH 7. The distribution of the dyes within the hydra ectoderm was determined using an epifluorescence microscope. Because of the sensitivity of the cells to phototoxic byproducts from the bleaching of the fluorescence dyes, illumination of the hydra was kept to a minimum. Images of the cytoplasmic dye distributions were recorded using either a low-light level video camera (SIT) or 35 mm film.

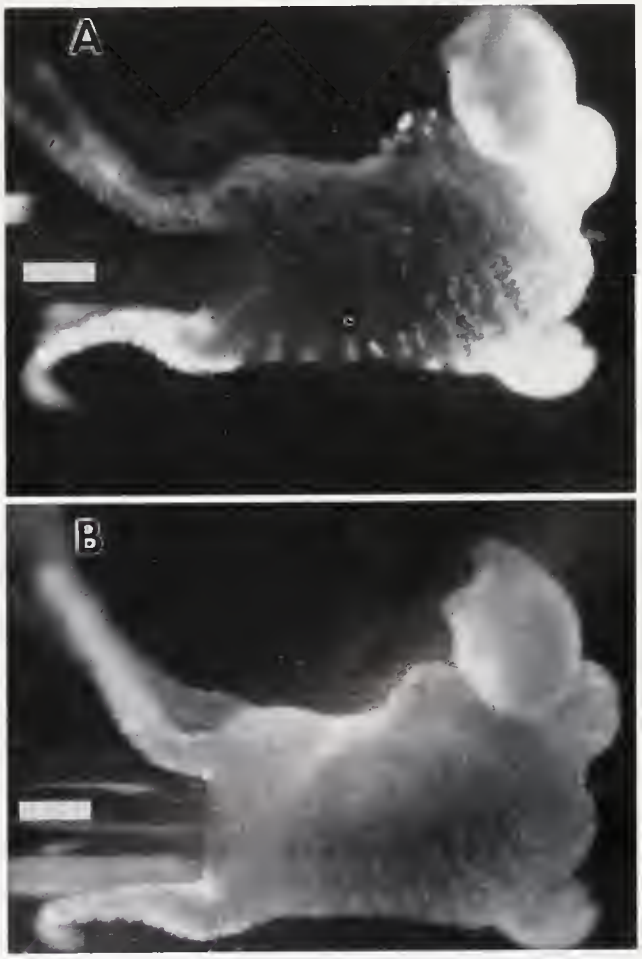

Figure 5. Electrophoretic redistribution of oppositely charged fluorescent dyes in hydra. Negatively charged calcein and positively charged tetramethylrhodamine cadaverine were loaded into hydra ectodermal cells using an electroporator. The hydra was strung onto a glass fiber and was placed in a 1 V/cm electric field for 20 min. (A) Calcein redistributed toward the positive electrode, producing a visible asymmetry between the head and the base of the body column. (B) Tetramethylrhodamine cadaverine shows a small asymmetry within the body column, with slightly more dye accumulating near the cathode (−electrode). In visualizing the concentration asymmetries, the tentacles and hydroid bud (near the base) should be viewed as separate compartments from the hydra body, since they are not aligned in the electric field, can move independently of the body column, and may not be well coupled to the body ectoderm in terms of molecular diffusion.

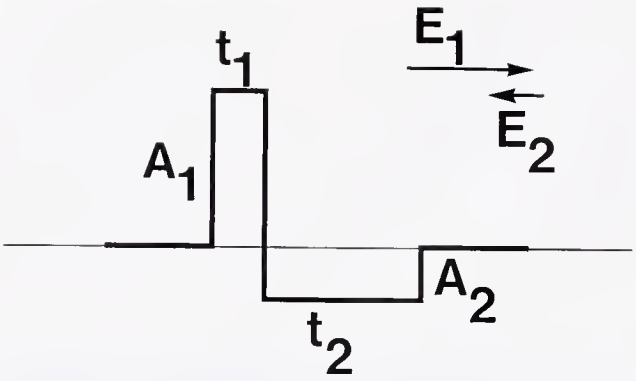

Figure 6. Waveform for distinguishing non-linear from linear processes. An asymmetric alternating electric waveform applied to tissues serves as a method to excite non-linear or threshold processes, such as action potentials, predominantly on one side of the tissue. The first phase of the waveform provides a supranormal stimulus that induces larger membrane potential perturbations than the second phase of the waveform. However, the entire waveform produces no net polarization for processes that are linear in electric field strength, such as electrophoresis. Linear effects are cancelled because the amplitude and duration of the two phases of the stimulus are designed such that the time-averaged amplitude of the applied electric field is zero, *i.e.*, $A_1/A_2 = t_2/t_1$.

Results and Discussion

Figure 2 illustrates the movement of injected 6-carboxyfluorescein within the electrotonically coupled lateral giant neurons of a crayfish nerve cord exposed to an externally applied DC electric field of 200 mV/cm. Under the influence of the electric field, the dye steadily migrated from the cell in which it was injected, through a gap junction (within the ganglion), and into the cytoplasm of the lateral giant neuron of the adjacent nerve cord segment. During a given experiment, this directed migration of dye toward the anode occurred at a constant rate which was directly proportional to the applied electric field strength. In experiments using electric fields ≥ 1 V/cm, the dye bolus was observed to pass through several segments of the nerve cord, with no obvious retardation of dye movement at the gap junctions which couple adjacent lateral giant neurons (Cooper *et al.*, 1989). In the absence of an applied electric field, an injected dye bolus slowly spreads out symmetrically by diffusion from the injection site (Fig. 2 at 0 min., before field). By normalizing the velocity of dye movement to the strength of the applied electric field, an electrophoretic mobility for 6-carboxyfluorescein within the cytoplasm of the crayfish lateral giant neurons can be determined. Figure 3 illustrates that the electrophoretic mobility for 6-carboxyfluorescein is constant, -0.92 ± 0.27 μm/s per V/cm ($n = 14$), over a nearly 20-fold range of field strengths (0.2–3.4 V/cm).

When placed in an electric field of 1 V/cm, a directed redistribution of charged dye molecules was also observed to occur within the electrotonically coupled cells of the hydra ectoderm. The negatively charged and highly mobile dye, calcein, was observed, in many cases, to redistribute towards the anode within 20 min of exposure to the electric field (Fig. 4; Table I). To determine if the final distribution of the calcein resulted from a field-induced redistribution, it was compared to the distribution in the same animals of a positive dye, tetrameylrhodamine cadaverine, or a junction impermeable dye, rhodamine dextran. These two dyes displayed either no significant asymmetry (rhodamine dextran) or a slight asymmetry towards the cathode (tetramethylrhodamine cadaverine) (Fig. 5). This suggests that the non-uniform distribution of calcein is not the product of non-uniform loading of the dyes or field-induced leakage of the dyes from the cells. Furthermore, hydra, which were briefly observed with the epifluorescence microscope before the application of the electric field, showed no major or systematic non-uniformities in the loading of the calcein (Table I).

Detailed analysis of the rates of redistribution of the calcein and determination of its steady-state profile in hydra, was hampered by the gradual sequestration of dye into cellular vacuoles, which occupy up to 90% of the cell volume (Fraser *et al.*, 1987). From examination of the hydra that failed to demonstrate calcein redistribution, it appears likely that sequestration of the dye into vacuoles was responsible. In addition, it should be noted that the intercellular mobilities of the dyes are difficult to compare on the basis of charge since the effective dye mobility is influenced by both the sequestration of the dye and its binding to intracellular constituents. Despite these limitations for quantitative analyses, the clear asymmetry of the calcein distribution observed in some of the hydra following exposure to an electric field suggests that small, charged intracellular molecules can be redistributed within a developing tissue by externally applied electric fields.

The exposure to the electric field appears to be non-deleterious. In response to the initial application of the external electric field, the hydra contracted their body columns; however, within minutes the animals relaxed their body columns and began waving their tentacles. Even after continued exposure to the electric field for several hours, the animals remained active, suggesting a lack of adverse effects of the electric field on the organism's physiology.

Steady-state molecular profiles

As charged molecules are driven to one end of a cellular ensemble, such as is illustrated in Figure 1, the electrophoretic flux of molecules induced by the electric field will eventually become counterbalanced by back-diffu-

sion. In steady-state, this is represented by the one-dimensional electrodiffusion equation:

$$mCE_{in} = D(dC/dx) \quad (2)$$

where C, m, and D are the concentration, intercellular electrophoretic mobility, and intercellular diffusion coefficient of the charged cytoplasmic molecule, respectively. m and D are lumped variables that refer to the averaged movement of molecules as they pass through a chain of coupled cytoplasms and gap junctions. Integrating equation 2 (Dwight, 1961; integrals 82.1 and 677.101), using equation 1 for the cytoplasmic electric field, one obtains the steady-state concentration profile of the charged cytoplasmic molecules:

$$C(x) = \alpha \exp\{(mE/D)[x - \lambda \sinh(x/\lambda)/\cosh(L/\lambda)]\} \quad (3)$$

where m is the intercellular electrophoretic mobility of the charged cytoplasmic molecule and α is a normalization constant requiring that the total number of molecules within the cytoplasm is conserved during exposure to the field (Cooper *et al.*, 1989).

A steady-state concentration asymmetry index can be defined as the ratio of the concentration of molecules at opposite ends of the tissue:

$$A = C(+L)/C(-L) = \exp\{(2mE/D)[L - \lambda \tanh(L/\lambda)]\} \quad (4)$$

Upon rearrangement, a useful expression is obtained that predicts the electric field necessary to create a given steady-state concentration asymmetry between the two ends of the tissue:

$$E = (D/2m) \ln A/[L - \lambda \tanh(L/\lambda)] \quad (5)$$

The approximate time τ necessary to establish this steady-state profile is the time it takes the average internal electric field within the cable to move a molecule from one end of the cable to the other (Cooper *et al.*, 1989):

$$\tau = (2L/m)\Big/\left[(1/2L)\int_{-L}^{+L} E_{in}dx\right] = 2L^2/\{mE[L - \lambda \tanh(L/\lambda)]\}. \quad (6)$$

For the case in which the cellular ensemble is much longer than the electrical length constant (*i.e.*, $L \gg \lambda$), equation 4 can be approximated by:

$$A = \exp(2mEL/D) \quad (7)$$

or

$$A = \exp(mV/D) \quad (8)$$

where $V = 2LE$ is the total voltage drop across the length of the tissue. The concentration asymmetry is essentially a Boltzmann distribution, and of the same mathematical form as equations derived separately by Jaffe (1977) and Poo (1981) for the steady-state distribution of charged molecules within cell membranes arising from surface electrophoresis. For an electrotonically coupled tissue, one would expect larger concentration asymmetries to arise from intercellular electrophoresis across the length of the tissue than from surface electrophoresis of charged molecules within individual cell membranes. This is due to the fact that small (<1500 MW) cytoplasmic molecules are free to move through gap junctions the entire length of the tissue, whereas the electrophoresis of surface molecules is confined to the dimensions of a single cell. In other words, 2L in equation 7 is much larger for intercellular electrophoresis through an ensemble of cells than the distance 2L for surface electrophoresis. However, the smaller diffusion coefficient of molecules within the cell membrane ($D \cong 10^{-9}$ cm^2/s) will tend to accentuate the concentration asymmetries on the cell surface as opposed to the concentration asymmetries of the more mobile cytoplasmic molecules ($D \cong 10^{-5}$–10^{-6} cm^2/s) within the tissue cytoplasm. For a given electric field, the magnitudes of the concentration asymmetries, either on the cell surface or in the cytoplasm, depend on the factor (2Lm/D) for the specific molecular environment.

Distinguishing mechanisms of electric field interaction

Besides polarizing cells and tissues by redistributing charged mobile molecules on the cell surface or within cell cytoplasm, externally applied electric fields also produce shifts in transmembrane potential which can evoke active membrane responses from both excitable and non-excitable cells. For the one-dimensional chain of cells illustrated in Figure 1, these membrane potentials shifts can be approximated by (Brink and Barr, 1977; Cooper, 1984; Chan and Nicholson, 1986):

$$V(x) = -E\lambda \sinh(x/\lambda)/\cosh(L/\lambda). \quad (9)$$

These membrane potential perturbations alter the driving forces for transmembrane ion fluxes and may induce voltage-gated ion channels to alter their conductance. Thus, an applied electric field could influence the pattern formation or morphogenesis of a tissue by directly acting on its electrophysiology.

Since an electric field can simultaneously affect transmembrane ion fluxes, the topography of cell membranes, and the distribution of cytoplasmic molecules within electrotonically coupled tissues, it is important to develop experimental methods of distinguishing which electric field interaction(s) is dominant in producing a specific biological response to an electrical stimulus. To first order, electrophoretic effects should be directly pro-

portional to the applied electric field strength. Although shifts in membrane potentials are also linear in the applied electric field strength (see Equation 9), the acute physiological responses resulting from membrane potential perturbations frequently stem from non-linear and/or threshold processes, such as the modification of ionic conductances or the initiation of action potentials. For linear processes, symmetrical alternating field waveforms (sinusoidal or square-wave), should not initate polarizing effects on cellular physiology, since the time average of the effects are zero (*e.g.*, no net electrophoresis). Such alternating waveforms have been previously used as diagnostic tools to distinguish biological responses originating from membrane potential perturbations, as opposed to effects stemming from the electrophoresis of membrane components (Jaffe and Nuccitelli, 1977). However, in certain instances, a symmetric alternating waveform might not serve as a decisive test to reveal effects originating from active membrane responses to the membrane potential perturbations generated by a DC electric field.

The use of an asymmetric alternating waveform, such as is illustrated in Figure 6, offers a possible means to determine whether a biological response to an applied field is due to a linear or non-linear mechanism. Similar to the symmetric waveform, the asymmetric alternating waveform will produce no net reaction for a linearly responding system (*e.g.*, no net electrophoresis). However, the first phase of the waveform (t_1) produces a supranormal stimulus (*i.e.*, exceeding the mean absolute amplitude) when compared to the second phase of the waveform (t_2). Thus, for any non-linear process, such as the firing of an action potential, one end of the tissue will be predominantly stimulated. Therefore, a waveform of the type shown in Figure 6 should be a useful assay for determining whether a non-linear or a non-linear transduction mechanism is involved in generating a specific biological response to a DC electric field. Linear processes, such as an electrophoretic mechanism, would yield no response to the asymmetric waveform because they require the time-averaged electric field be non-zero to produce a net polarization of molecular distributions.

In conclusion, the ability to redistribute charged cytoplasmic molecules through open gap junctions with externally applied electric fields provides a new method of controlling the fluxes and intercellular profiles of putative morphogens within developing tissues over prolonged periods of time. Within the context of appropriate control experiments, it may be feasible to use the unique, long-range polarizing actions of electric fields to selectively analyze the roles that gap junctions and intercellular diffusion play in pattern formation and morphogenesis.

Acknowledgments

We thank H. Bode and C. Teragawa (U. C. Irvine) for their kind gifts of hydra. This work was supported by a NASA Postdoctoral Research Associate Award NAGW-70 to M.C., NSF Grant BNS 85-19416 to J.M., and NSF Grant DCB 85-10891 to S.F.

Literature Cited

Brink, P., and L. Barr. 1977. The resistance of the septum of the median giant axon of the earthworm. *J. Gen. Physiol.* **69:** 517–536.

Chan, C. Y., and C. Nicholson. 1986. Modulation by applied electric fields of Purkinje and stellate cell activity in the isolated turtle cerebellum. *J. Physiol. (Lond.)* **371:** 89–114.

Cooper, M. S. 1984. Gap junctions increase the sensitivity of tissue cells to exogenous electric fields. *J. Theor. Biol.* **111:** 123–130.

Cooper, M. S., J. P. Miller, and S. E. Fraser. 1989. Electrophoretic repatterning of charged cytoplasmic molecules within tissues coupled by gap junctions by externally applied electric fields. *Dev. Biol.* **132:** 179–188.

Dwight, H. B. 1961. *Tables of Integrals and Other Mathematical Data.* MacMillan Publishing Company, Inc., New York.

Fraser, S. E., C. R. Green, H. R. Bode, and N. B. Giula. 1987. Selective disruption of gap junctional communication interferes with a patterning process in *Hydra. Science* **237:** 47–55.

Furshpan, E. J., and D. D. Potter. 1959. Transmission at the giant motor synapses of crayfish. *J. Physiol. (Lond.)* **145:** 289–325.

Jacobs, G. A., and J. P. Miller. 1985. Functional properties of individual neuronal branches isolated *in situ* by laser photoinactivation. *Science* **228:** 344–346.

Jaffe, L. F. 1977. Electrophoresis along cell membranes. *Nature (Lond.)* **265:** 600–602.

Jaffe, L. F., and R. Nuccitelli. 1977. Electrical controls of development. *Ann. Rev. Biophys. Bioeng.* **6:** 445–476.

Plonsey, R., and R. C. Barr. 1986. Inclusion of junctional elements in a linear cardiac model through secondary sources: application to defibrillation. *Med. Biol. Eng. Comp.* **24:** 137–144.

Poo, M-m. 1981. In situ electrophoresis of membrane components. *Ann. Rev. Biophys. Bioeng.* **10:** 245–276.

Watanabe, A., and H. Grundfest. 1961. Impulse propagation at the septal and commisural junctions of crayfish lateral giant neurons. *J. Gen. Physiol.* **45:** 267–308.

Reference: *Biol. Bull.* **176(S)**: 157–163. (April, 1989, Suppl.)

Electric Field-Induced Redistribution of ACh Receptors on Cultured Muscle Cells: Electromigration, Diffusion, and Aggregation

JES STOLLBERG AND SCOTT E. FRASER

Department of Physiology and Biophysics, College of Medicine, University of California, Irvine, California 92717

Abstract. *Xenopus* myoball cultures were used to examine the lateral migration and clustering of acetylcholine receptors in response to electric fields. In contrast to concanavalin A binding sites, which behave in a manner explained by electromigration and diffusion, acetylcholine receptors form stabile aggregates at the cathode-facing cell pole. Interestingly, receptor aggregation continues there after termination of the field. This post-field receptor aggregation is consistent with the action of a specific diffusion-trap mechanism mediated by adhesion or cohesion events on the cell surface.

The simplest hypothesis for the triggering of receptor aggregation is that receptors are accumulated in response to the electric field and, once past a threshold density, autoaggregation is initiated. This model was tested by examining field-induced distributions of receptors following enzymatic treatment to reverse the electromigration of receptors. After neuraminidase treatment, and exposure to electric fields, receptor distributions were consistent with reversed electromigration (towards the anodal cell pole) but continued to show receptor aggregation at the cathodal cell pole. We conclude that the diffusion-trapping of acetylcholine receptors requires the participation of non-receptor molecules. In addition to providing a useful experimental tool in these studies, electric fields may play a role in receptor clustering at the neuromuscular junction.

Introduction

The accumulation of specific molecules at forming synapses is an important problem in developmental neurobiology. Only specific types of nerve terminals can induce this localization, suggesting that the mechanisms involved may play a role in the developmental specificity of neuronal connections. The induction of acetylcholine receptor (AChR) clusters at the developing neuromuscular junction is a well-studied example of such localization. Prior to innervation, AChRs and other components are distributed diffusely; clustering begins shortly after neuronal contact both *in vivo* (Blackshaw and Warner, 1976; Creazzo and Sohal, 1983) and *in vitro* (Frank and Fischbach, 1979; Kidokoro *et al.*, 1980; Role *et al.*, 1987). Lateral migration of diffusely distributed receptors makes a significant contribution to receptor clustering (Anderson and Cohen, 1977; Frank and Fischbach, 1979; Kuromi and Kidokoro, 1984; Ziskind-Conhaim *et al.*, 1984; Role *et al.*, 1985; Stollberg and Fraser, 1988).

The use of electric fields to perturb the distribution of membrane molecules on a cell surface permits biophysical studies of the lateral migration and aggregation properties governing these molecules (Jaffe, 1977; Poo and Robinson, 1977; Poo *et al.*, 1978). This approach permits a controlled experimental manipulation which is non-invasive, and which triggers receptor clustering independently of added factors or cell contacts. In particular, myoball (spherical muscle cell) cultures have been used to advantage in testing theoretical predictions concerning electromigration, diffusion, and aggregation of concanavalin A (con A) binding sites and AChRs (Orida and Poo, 1978, 1980, 1981; Poo *et al.*, 1979; McLaughlin and Poo, 1981; Stollberg and Fraser, 1988).

We report here the use of digitally analyzed videomi-

Abbreviations α-Bgt, alpha-Bungarotoxin; AChR, acetylcholine receptor; con A, concanavalin A; FLR-con A fluorescein labeled concanavalin A; TMR-α-Bgt, tetra-methyl-rhodamine labeled alpha-Bungarotoxin.

croscopy to extend the accuracy and resolution of data describing the distribution of AChRs after exposure to electric fields. The use of these techniques permits rigorous comparison to theoretical predictions based on electromigration and diffusion. Experiments presented here document and dissect the mechanisms underlying an intriguing finding—AChRs, accumulated at the cathode-facing cell pole in an electric field, continue to aggregate there after termination of the field.

Materials and Methods

Reagents, culture system

Reagents and culture preparation were as described previously (Stollberg and Fraser, 1988). In brief, myotomal cells were dissected from stage 18–20 *Xenopus laevis* embryos (Nieuwkoop and Faber, 1962) in collagenase/Steinberg's solution, dissociated in Ca^{++}/Mg^{++}-free Steinberg's solution, and maintained on sterile coverslips in drops of culture medium for 1 day at 24°C.

Experimental manipulations

Neuraminidase incubations were carried out in 50 μl of Steinberg's solution, pH 6.6. In the event of subsequent trypsin digestion, the neuraminidase solution was removed and replaced with 50 μl of 0.1% trypsin in Steinberg's solution, pH 7.8. Following pre-field treatments (where indicated), the cultures were returned to culture medium and assembled into chambers with internal dimensions of $6 \times 1 \times 0.02$ cm. Following the electric fields, cultures were given the indicated post-field periods, chilled, and labeled with 300 nM tetra-methyl-rhodamine labeled alpha-Bungarotoxin (TMR-α-Bgt), 25 μg/ml fluorescein labeled con A (FLR-con A) in culture medium. The cultures were then rinsed with 1 ml of culture medium, and kept on ice until video images were acquired.

Data analysis

Data analysis techniques were as previously described (Stollberg and Fraser, 1988). In brief, fluorescent images were viewed through a Zeiss Universal microscope, gathered by a SIT video camera (RCA [Lancaster, Pennsylvania] model No. TC1030), and stored on video cassettes (Sony U-matic video cassette recorder [Tokyo, Japan] models VO-5600 and VO-5800). Videotape images were digitized using a Digisector DS-88 board from Microworks (Del Mar, California) modified to permit decreased contrast settings. The position of a cell within the digital image was identified by cursor positioning at the top, bottom, left, and right of the video image of the cell. Digital images were corrected on a pixel-by-pixel basis for spatial aberrations in the illumination, optics, and video tube. Pixels corresponding to the annulus of a given cell image were identified, along with their angular position (θ) with respect to the electric field (see Fig. 1). This information was used to estimate the binding site density as a function of θ, expressed as a percentage of the average receptor density on the cell surface. The extent of redistribution under different conditions was compared using an Asymmetry index (Orida and Poo, 1978; Poo *et al.*, 1979), defined as

$$A = (C_{180} - C_0)/(C_{180} + C_0).$$

The asymmetry index was calculated using intensities at the 1st and 16th sectors as approximations to C_0 and C_{180}, respectively (see Fig. 1).

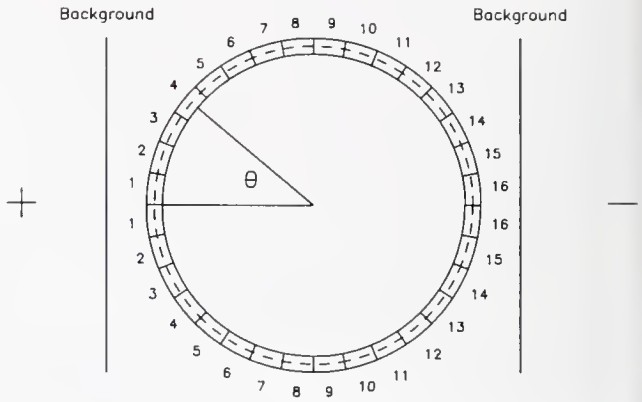

Figure 1. Scale diagram of the image analysis scheme. The dashed-line circle indicates the boundary of the cell image. The solid circles represent the tolerance (±5% of the radius) within which pixels must lie to be accepted. For each pixel within this tolerance, the angle with respect to the anode (θ) is found and the corrected intensity (less background) is sorted into one of 16 sectors representing θ.

Theoretical considerations

The electrophoretic force acting on a cell-surface molecule depends on the molecule's net extracellular charge. Electric fields will also induce an electro-osmotic flow toward the cathodal cell pole due to the negative charge on the cell surface; the magnitude of this effect depends on the net surface charge (the zeta potential; see McLaughlin and Poo, 1981). Thus, the tendency of a given molecule to move in response to electric fields can be altered by treating the cell surface with agents such as neuraminidase, which remove negatively charged sialic acid residues. We will use the term "electromigration" to refer to the net response of molecules to the forces of electrophoresis and electro-osmosis.

Under "ideal" conditions (spherical, non-conducting cells; no interaction between sites), the distribution of cell-surface sites at steady-state in an electric field is a balance between the actions of electromigration and

diffusion (Jaffe, 1977; Poo *et al.*, 1979; McLaughlin and Poo, 1981). The density of sites as a function of θ (C_θ) is

$$C_\theta = f_m \cdot \alpha \cdot \exp(-\beta \cdot \cos\theta) + (1 - f_m) \cdot C_i, \text{ where}$$

$$\alpha = \beta \cdot C_i / \sinh(\beta), \quad \beta = 1.5 \cdot E \cdot r \cdot m/D,$$

r is the cell radius, C_i the initial molecular concentration, E the field strength, f_m the fraction of mobile sites, m the electromigration mobility constant, and D the diffusion constant (Stollberg and Fraser, 1988). The two parameters m/D and f_m were allowed to vary in fitting this model to data (all other parameters being measured quantities).

Results

Methodological considerations

As shown previously, the video-microscopic assay is linear over a substantial range of ligand concentrations, and after the pixel-by-pixel correction scheme (see Materials and Methods), the assay is independent of pixel position within the image (Stollberg and Fraser, 1988). The same study also indicated that the binding of fluorescent ligands is independent of binding-site density over the range of densities encountered in these experiments. Analysis of experiments was performed only when the data were within the linear range of the assay.

Concanavalin A binding sites

FLR-con A labeled sites were seen to migrate towards the cathode-facing pole of cells in electric fields. The time-course of asymmetry development in the electric field is well fit by an exponential with $\tau \approx 12$ min (Stollberg and Fraser, 1988), and is close to maximal after 40 min. The steady-state distributions of FLR-con A binding sites following fields of 0, 1, 2, and 4 V/cm for 40 min are shown in Figure 2. The solid lines represent the least-squares fit of the theoretical model (see Materials and Methods) to the four experimental conditions. The figure illustrates a good agreement between data and the theory over this range of field strengths (Fig. 2, legend).

After termination of a field of 4 V/cm, the asymmetry of con A binding site distributions was seen to decay exponentially to approximately 0 (*i.e.*, to a nearly uniform distribution). The rate of this asymmetry decay was used to estimate the diffusion constant of the average site, and gave a value of $D \approx 2.3 \times 10^{-9}$ cm^2/s, in good agreement with the approximation of D obtained from the rate of asymmetry development in a field (Stollberg and Fraser, 1988). Thus, in terms of asymmetry development and decay, and the distribution of sites in the steady-state, con A binding sites behave "ideally" (as predicted by the theoretical model) in fields ranging from 0 to 4 V/cm. However at higher field strengths, con A binding sites showed less asymmetry in the steady-state than would be

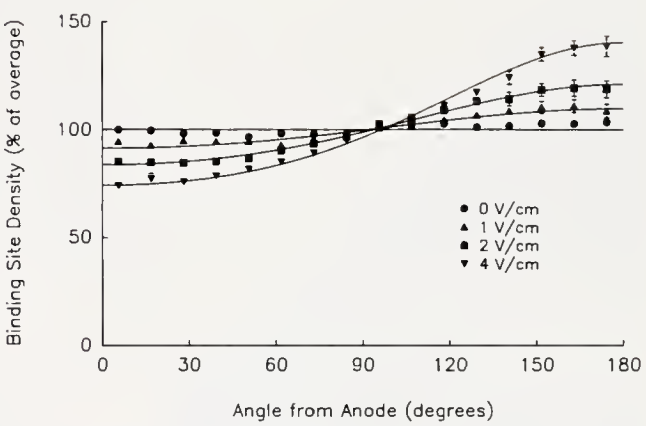

Figure 2. Steady-state distributions of con A binding sites after electric fields of 0–4 V/cm. Cultures were subjected to the indicated electric fields for 40 min and analyzed for the distribution of con A binding sites as described. Data represent means ± standard errors for 3–6 experiments, each consisting of 7–14 scanned cells. Curves, the least-squares fit of the predicted distribution (see Materials and Methods) to the combined data from 1, 2, and 4 V/cm. m/D = 64 ± 8 V^{-1} and f_m = 0.48 ± .05; $\chi_{(45)}^2 = 67$.

predicted by the model on the basis of the data from 0 to 4 V/cm, and also failed to return completely to a uniform distribution after termination of the field (Stollberg and Fraser, 1988).

Acetylcholine receptors—native conditions

AChR distributions were found to deviate significantly from ideal behavior in response to all electric field paradigms. An example of such a distribution is shown in Figure 3; it is not well fit by the model under discussion (Fig. 3, legend). Furthermore, the minimum receptor density under these conditions occurs not at the anode-facing cell pole, as would be expected if ideal behavior dominated the distribution, but at about 115 degrees (Fig. 3, arrow). These non-ideal behaviors suggest that some other phenomenon (besides electromigration and diffusion) contributes to the observed receptor distribution.

To further analyze receptor behavior, distributions were monitored following application of electric fields and a post-field relaxation period. Unlike con A binding sites, which return to a uniform distribution after termination of the field, the receptors continue to aggregate at the cathode-facing cell pole (Stollberg and Fraser, 1988). In the same study it was shown that receptor aggregation is due to lateral migration of receptors, is insensitive to disruption of cytoskeletal elements, and is sensitive to trypsin digestion. Thus, the data are consistent with a diffusion-trap mechanism of receptor aggregation (Edwards and Frisch, 1976) mediated by adhesion or cohesion events on the extracellular surface. In principle the

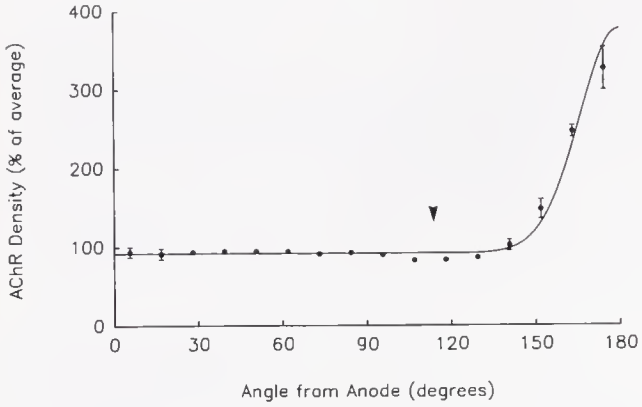

Figure 3. Distribution of AChRs after exposure to an electric field. Cultures were exposed to a field strength of 8 V/cm for 80 min, then labeled with TMR-α-Bgt and analyzed as described. Curve, the least-squares fit of the model distribution to this data; in obtaining even this poor fit m/D and f_m are forced to implausibly large and small values, respectively. m/D = 831 ± 83 V^{-1}, f_m = 0.084 ± .002, $\chi_{(13)}^2$ = 170. Arrow, approximate location of minimum receptor density.

triggering of the diffusion trap could be due to (i) field-induced concentration of receptors, (ii) field-induced concentration of some other molecules, or (iii) voltage-sensitive mechanisms (see Discussion).

Acetylcholine receptors—enzymatic modification

To test the relationship between electromigrational concentration of receptors and post-field aggregation (hypothesis i above), cells were exposed to neuraminidase treatments reported to reverse the electromigration of AChRs (Orida and Poo, 1978). The result from such experiments is shown in Figure 4, and shows a strikingly bimodal distribution. The inset frequency histogram of minimum density location shows that this is not due to the averaging of two cell populations, but rather is a feature common to individual cells. The accumulation of receptors at both cell poles under these conditions is a novel finding, presumably missed in earlier experiments in which the asymmetry index was used to characterize the resulting distribution (Orida and Poo, 1978; McLaughlin and Poo, 1981).

The bimodality of the AChR distribution implies two opposed tendencies, and the shape suggests a combination of ideal electromigration and receptor aggregation. An estimate of the contribution made by electromigration is shown by the dashed curve of Figure 4. By subtracting this distribution from that of the data, we arrive at an estimate of the contribution made by aggregation (Fig. 4, dotted curve). The curve is qualitatively similar to the receptor distribution (dominated by aggregation) shown in Figure 3, strengthening the view that the distribution of Figure 4 represents a combination of ideal electromigration (towards the anodal cell pole) and diffusion-trapping of receptors (at the cathodal pole).

To further test this hypothesis, the distribution of receptors on neuraminidase-treated cells was monitored following a post-field relaxation period. In accord with the above interpretation, receptor densities were seen to *in*crease at the cathode-facing pole and *de*crease at the anode-facing pole during the post-field relaxation period (Stollberg and Fraser, submitted). The density decrease at the anodal pole clearly indicates that elevated AChR density is insufficient to induce receptor aggregation.

Previous studies indicated that the receptor aggregation seen as a consequence of exposure to electric fields can be blocked by treatment of the cultures with trypsin (Stollberg and Fraser, 1988). Together with the above analysis, this suggests that pretreatment with neuraminidase *and* trypsin should result in an ideal distribution with a maximum at the anodal pole. Quantitative results from several such experiments are shown in Figure 5. The distribution is reasonably well described by the theoretical model (Figure 5, legend), indicating that the AChRs have indeed been converted to ideally behaving sites via the trypsin treatment.

If receptors behave ideally after treatment with neuraminidase and trypsin, the distributions should decay

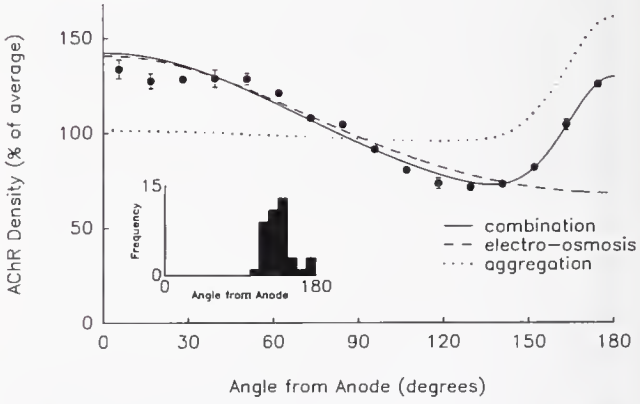

Figure 4. Distribution of AChRs following neuraminidase treatment, and exposure to an electric field. Cells were treated with 0.2 U/ml neuraminidase for 40 min and subjected to a field of 8 V/cm for 80 min. The distribution is bimodal, indicating receptor accumulation at both anode- and cathode-facing poles. Data are from 4 experiments, each consisting of 9–11 scanned cells. Inset, frequency histogram showing the positions of minimal receptor density among the cells. The majority of the cells are seen to have minima located in the 120–150 degree region. Solid curve, theoretical fit for the sum of two ideally behaving populations: 1st population, m/D = 632 ± 54 V^{-1}, f_m = 0.027 ± .002; 2nd population, m/D = −21 ± 1 V^{-1}, f_m fixed at 0.97 (else the algorithm forced the value over 1.0); $\chi_{(12)}^2$ = 64. Dashed curve, theoretical result fit by eye to left-half of the data, yielding m/D = −19 V^{-1} (f_m = 0.8, from data of Fig. 5). Dotted curve, estimated distribution of receptors resulting from aggregation alone—this curve is the difference between the solid and dashed curves.

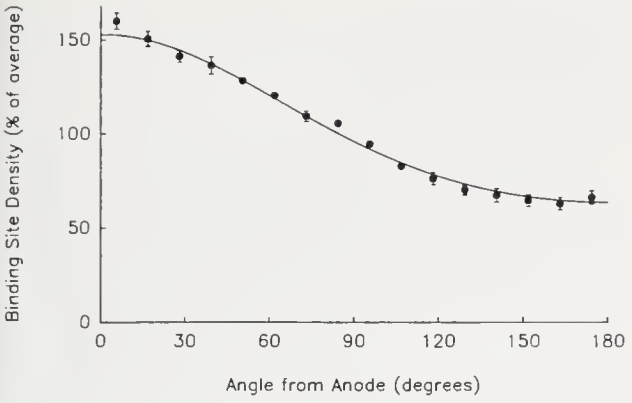

Figure 5. Steady-state distribution of AChRs following treatment with neuraminidase and trypsin. Cells were incubated with 0.2 U/ml neuraminidase for 40 min, 0.1% trypsin for 20 min, and then exposed to a field of 8 V/cm for 40 min. Curve, theoretical fit to ideal electro-osmotic distribution. $m/D = -28 \pm 1\ V^{-1}$, $f_m = 0.8$, $\chi_{(15)}^2 = 27$. Data are from 4 experiments, each consisting of 7–12 analyzed cells.

back to uniformity after termination of the electric field. Furthermore, the development of asymmetry with time in the field, and the decay of asymmetry following field termination, should show exponential kinetics giving independent estimates of the receptor diffusion constant. Quantitative estimates of the development and decay of receptor asymmetries have been made, and give good agreement on a receptor diffusion constant of $\approx 1.2 \times 10^{-9}$ cm^2/s (Stollberg and Fraser, in prep.). The agreement between these two estimates is reassuring, and is consistent with the characterization of AChR behavior as ideal following treatment with neuraminidase and trypsin.

Discussion

Redistribution of FLR-concanavalin A binding sites

The steady-state model describing the distribution of ideal (non-interacting) sites describes the experimental distribution of con A binding sites quite well over a four-fold range of field strengths (Fig. 2). It should be emphasized that the same values for the two free parameters (m/D, f_m) were used to generate the four curves in Figure 2, providing a rigorous test of the model. The behavior of con A binding sites at or below 4 V/cm appears ideal both in terms of these steady-state distributions, and by the relaxation to near-symmetry following field termination. Thus, the assumptions of the theoretical model (spherical, non-conducting cells; non-interacting sites) appear to apply in this range of field strengths.

The asymmetry seen at 8 V/cm is larger than that at 4 V/cm, but less than expected based on the theoretical model and the data from fields of 0–4 V/cm (Stollberg and Fraser, 1988). A similar attenuation of the expected asymmetry at higher field strengths has been reported for IgE and con A binding sites on rat basophilic leukemia cells (Ryan *et al.*, 1988). Further experiments will be necessary to illucidate the biophysics behind the non-ideal behavior of these sites at higher field strengths (see Stollberg and Fraser, 1988). Of greater relevance to the behavior of AChRs (see below) is the observation that con A binding sites behave ideally over a considerable range of field strengths.

Redistribution of acetylcholine receptors

In contrast to con A binding sites, AChRs were found to behave non-ideally in response to electric fields. The distribution of receptors immediately after exposure to electric fields is poorly fit by theoretical predictions based on ideal behavior, and even this poor fit requires implausibly large and small values for m/D and f_m, respectively (Fig. 3). Additionally, the minimum receptor density is adjacent to the region of receptor accumulation (Fig. 3, arrow), whereas an electromigration model predicts that this should occur at the anodal pole. The location of this minimum suggests the operation of a diffusion-trap mechanism, in which the trapping of AChRs at the cathode-facing pole leads to depletion in neighboring regions via diffusion-mediated migration. This interpretation is consistent with the observations that field-induced receptor aggregation (1) continues after termination of the field, (2) is due to lateral migration of receptors, and (3) is not affected by drugs disrupting the cytoskeleton (Stollberg and Fraser, 1988). We should note that elevated receptor densities might represent the action of a single trap, or of many traps too small for individual resolution.

Previous experiments have shown that trypsin blocks field-induced receptor asymmetries, and disperses receptor aggregates initiated by electric fields (Orida and Poo, 1980, 1981). Accordingly, experiments were undertaken to analyze the effects of trypsin on the post-field accumulation of receptors. Trypsin digestion throughout the experiment, as a pre-treatment, or at the start of the post-field period was shown to block post-field aggregation of receptors (Stollberg and Fraser, 1988). The likely mechanism for this effect is a disruption of adhesion or cohesion events stabilizing receptor clusters, and is consistent with a diffusion-trap mechanism of aggregation.

The simplest model accounting for the above observations is that the electromigration of AChRs toward the cathodal pole triggers the aggregation event there. This hypothesis holds that, above some threshold density, receptor-receptor interactions are sufficient to induce aggregation. The proposition is quite attractive with respect to its simplicity and generality (Poo, 1981; for theoretical development see Gershon, 1978). There are only two other ways in which receptor clustering might be trig-

gered in this system. First, the electromigration of some other molecules might be responsible for receptor aggregation. Second, a voltage-sensitive mechanism might be involved; at 8 V/cm a spherical cell of radius 20 μm will experience a 16 mV depolarization at the cathode-facing pole.

The data depicted in Figure 4 represent the receptor distributions of cells treated with neuraminidase, subjected to fields, and analyzed with no post-field relaxation period. The resulting bimodal distribution of receptors is a property of most individual cells, rather than a population phenomenon (Fig. 4, inset; see also Results). The direction of electromigration has been reversed (by neuraminidase treatment) and is now toward the anodal pole, while the diffusion-trapping of receptors proceeds at the cathodal pole as before. This interpretation is supported by the dissection of the experimental distribution into two distributions, one of which behaves ideally, while the other is characteristic of receptor aggregation (Figure 4, dashed and dotted curves). As additional support for this view, it was found that receptor density increases at the cathodal pole, but decreases at the anodal pole following field termination (Stollberg and Fraser, in prep.).

If neuraminidase treatment results in the opposition of electromigration and aggregation, cells incubated with neuraminidase (to reverse electromigration) and trypsin (to block aggregation) should show ideal, but reversed receptor distributions. Figure 5 depicts the results from such experiments under near steady-state conditions. The distribution is consistent with ideal electromigration. Furthermore, the asymmetric distributions obtained under these conditions decay back to uniformity after termination of the electric field, in accordance with the prediction of the theoretical model (Stollberg and Fraser, in prep.). Together these observations support the interpretation that electromigration has been reversed, while diffusion-trapping of receptors has been eliminated. The conversion of AChRs to ideally behaving sites permits measurement of the receptor diffusion constant by the rates of approach to, and decay from, the steady-state receptor distribution. The results from such experiments provide an estimated diffusion constant of about 1.2×10^{-9} cm^2/s (Stollberg and Fraser, in prep.). This value is easily large enough to account for the receptor aggregation seen in *Xenopus* myoball cultures (Stollberg and Fraser, 1988), and is similar to that found for AChRs on cultured *Xenopus* muscle cells (2.6×10^{-9} cm^2/s; Poo, 1982), and for extrajunctional AChRs in *Xenopus* tadpole muscle ($1.5–4 \times 10^{-9}$ cm^2/s; Young and Poo, 1983), as measured by recovery of ACh sensitivity. However, our estimate is considerably larger than the AChR diffusion constant from *Xenopus* muscle cultures (2.5×10^{-10} cm^2/s; Kuromi *et al.*, 1985) and cultured rat myotubes (5×10^{-11} cm^2/s; Axelrod *et al.*, 1976) as determined by photobleaching recovery methods.

The triggering of AChR aggregation

The simple hypothesis that receptor aggregation is triggered via an increase in the concentration of receptors is excluded by the results discussed above. Although a significant receptor accumulation takes place at the anode-facing pole in neuraminidase-treated cultures (Fig. 4), the receptor concentration decreases in this region after termination of the field (Stollberg and Fraser, in prep.). Thus, elevated receptor density is not sufficient to induce aggregation. Furthermore, receptor aggregation proceeds at the cathode-facing pole despite the lowering of receptor density there due to electromigration (Stollberg and Fraser, in prep.). Thus, the local accumulation of AChRs is neither sufficient nor necessary as a trigger for subsequent receptor aggregation.

There are only two remaining mechanisms of receptor aggregation that are consistent with the findings presented here. First, the aggregation may be triggered by the electromigrational accumulation of some other molecules (or by a distinct subpopulation of AChRs). This possibility is not ruled out by the results from the neuraminidase experiments (Fig. 4); one need only postulate that the relevant molecules carry charges such that their electromigration remains toward the cathodal pole under these conditions. A second class of mechanism for the triggering of receptor aggregation depends on the depolarization of the cathodal pole membrane associated with the application of electric fields (approx. 16 mV at 8 V/cm). Under such a model, the adhesion or cohesion events responsible for receptor aggregation could be controlled by voltage-sensitive channels. Experiments based on the different predictions of these two remaining hypotheses are currently underway. The experimental system is ideally suited to further examination of the mechanisms of receptor aggregation by virtue of the simplicity and rapid response of the aneural *Xenopus* myoball system, and the quantitative nature of the analysis.

Relevance of electric fields to receptor clustering in vivo

The usefulness of the model system described here does not depend on the assumption that electric fields are involved in the *in vivo* clustering of receptors. However, it is likely that such fields do occur *in vivo* (Fraser and Poo, 1982). In brief, acetylcholine is released from nerve terminals soon after contact with the muscle (Kidokoro *et al.*, 1980; Xie and Poo, 1986), *i.e.*, before and during the clustering of receptors. From the point of view of the neighboring cell surface, the extracellular region exposed to acetylcholine will be at a negative potential, as the activated receptors increase the local conductance

to the cell interior. Thus, the orientation of the electric field is appropriate to induce a receptor trap in the region of acetylcholine binding. An attractive feature of such a model is the positive feedback inherent in such a process—local excitation causes receptor aggregation, which causes greater local excitation, and so on.

Despite the appealing simplicity of such a mechanism, several important questions remained to be addressed about the response of AChRs to externally applied fields before the proposed *in vivo* mechanism can be tested. Most critical is the interaction between the strength, duration, and duty cycle of fields in determining the threshold for the induction of receptor clustering. Pulsed field protocols have been used to dissect the behavior of con A binding sites under these conditions (Lin-Liu *et al.*, 1984); these kinds of experiments need to be undertaken with respect to the initiation of receptor diffusion-traps. It should also be noted that, whereas in the case of externally applied electric fields the intracellular field is essentially zero, this will not be true in the case of endogenously generated fields. Accordingly, the contribution made by the internal fields to electromigration of other molecules (possibly) involved in receptor-trapping may have to be taken into account. The model system described here should prove invaluable both for dissection of the biophysics of receptor aggregation, and investigation of the possible role of electric fields in receptor clustering at the developing neuromuscular junction.

Literature Cited

Anderson, M. J., and M. W. Cohen. 1977. Nerve-induced and spontaneous redistribution of acetylcholine receptors on cultured muscle cells. *J. Physiol. Lond.* **268:** 757–773.

Axelrod, D., P. Ravdin, D. E. Koppel, J. Schlessinger, W. W. Webb, E. L. Elson, and T. R. Podleski. 1976. Lateral motion of fluorescently labeled acetylcholine receptors in membranes of developing muscle fibers. *Proc. Natl. Acad. Sci. USA* **73:** 4594–4598.

Blackshaw, S., and A. Warner. 1976. Onset of acetylcholine sensitivity and endplate activity in developing myotome muscles of *Xenopus*. *Nature* **262:** 217–218.

Creazzo, T. L., and G. S. Sohal. 1983. Neural control of embryonic acetylcholine receptor and skeletal muscle. *Cell Tissue Res.* **228:** 1–12.

Edwards, C., and H. L. Frisch. 1976. A model for the localization of acetylcholine receptors at the muscle endplate. *J. Neurobiol.* **7:** 377–381.

Frank, E., and G. D. Fischbach. 1979. Early events in neuromuscular junction formation *in vitro*. Induction of acetylcholine receptor clusters in the postsynaptic membrane and morphology of newly formed nerve-muscle synapses. *J. Cell Biol.* **83:** 143–58.

Fraser, S. E., and M-m. Poo. 1982. Development, maintenance, and modulation of patterned membrane topography: models based on the acetylcholine receptor. *Curr. Top. Dev. Biol.* **17:** 77–100.

Gershon, N. D. 1978. Model for capping of membrane receptors based on boundary surface effects. *Proc. Natl. Acad. Sci. USA* **75:** 1357–1360.

Jaffe, L. F. 1977. Electrophoresis along cell membranes. *Nature* **265:** 600–602.

Kidokoro, Y., M. J. Anderson, and R. Gruener. 1980. Changes in synaptic potential properties during acetylcholine receptor accumulation and neuronspecific interactions in *Xenopus* nerve-muscle cultures. *Dev. Biol.* **78:** 464–483.

Kuromi, H., and Y. Kidokoro. 1984. Nerve disperses preexisting acetylcholine receptor clusters prior to induction of receptor accumulation in *Xenopus* muscle cultures. *Dev. Biol.* **103:** 53–61.

Lin-Liu, S., W. R. Adey, and M-m. Poo. 1984. Migration of cell surface concanavalin A receptors in pulsed electric fields. *Biophys. J.* **45:** 1211–1218.

McLaughlin, S., and M-m. Poo. 1981. The role of electro-osmosis in the electric-field-induced movement of charged macromolecules on the surfaces of cells. *Biophys. J.* **34:** 85–93.

Nieuwkoop, P. D., and J. Faber. 1962. *Normal Table of* Xenopus laevis. North Holland Publishing Co., Amsterdam.

Orida N., and M-m. Poo. 1978. Electrophoretic movement and localization of acetylcholine receptors in the embryonic muscle cell membrane. *Nature* **275:** 31–35.

Orida, N., and M-m. Poo. 1980. On the developmental regulation of acetylcholine receptor mobility in the *Xenopus* embryonic muscle membrane. *Exp. Cell Res.* **130:** 281–290.

Orida, N., and M-m. Poo. 1981. Maintenance and dissolution of acetylcholine receptor clusters in the embryonic muscle cell membrane. *Dev. Brn. Res.* **1:** 293–298.

Poo, M-m., and K. R. Robinson. 1977. Electrophoresis of concanavalin A receptors along embryonic muscle cell membrane. *Nature* **265:** 602–605.

Poo, M-m., W-j. H. Poo, and J. W. Lam. 1978. Lateral electrophoresis and diffusion of concanavalin A receptors in the membrane of embryonic muscle cell. *J. Cell. Biol.* **76:** 483–501.

Poo, M-m., J. W. Lam, N. Orida, and A. W. Chao. 1979. Electrophoresis and diffusion in the plane of the cell membrane. *Biophys. J.* **26:** 1–22.

Poo, M-m. 1981. *In situ* electrophoresis of membrane components. *Ann. Rev. Biophys. Bioeng.* **10:** 245–276.

Poo, M-m. 1982. Rapid lateral diffusion of functional ACh receptors in embryonic muscle cell membrane. *Nature* **295:** 332–334.

Role, L. W., V. R. Matossian, R. J. O'Brien, and G. D. Fischbach. 1985. On the mechanism of acetylcholine receptor accumulation at newly formed synapses on chick myotubes. *J. Neurosci.* **5:** 2197–2204.

Role, L. W., D. Roufa, and G. D. Fischbach. 1987. The distribution of acetylcholine receptor clusters and sites of transmitter release along chick ciliary ganglion neurite-myotube contacts in culture. *J. Cell Biol.* **104:** 371–379.

Ryan, T. A., J. Myers, D. Holowka, B. Baird, and W. W. Webb. 1988. Molecular crowding on the cell surface. *Science* **239:** 61–64.

Stollberg, J. and S. E. Fraser. 1988. Acetylcholine receptors and concanavalin A-binding sites on cultured *Xenopus* muscle cells: Electrophoresis, diffusion, and aggregation. *J. Cell Biol.* **107:** 1397–1408.

Xie, Z-p., and M-m. Poo. 1986. Initial events in the formation of neuromuscular synapse: rapid induction of acetylcholine release from embryonic neuron. *Proc. Natl. Acad. Sci. USA* **83:** 7069–7073.

Young, S. H., and M-m. Poo. 1983. Rapid lateral diffusion of extrajunctional acetylcholine receptors in the developing muscle membrane of *Xenopus* tadpole. *J. Neurosci.* **3:** 225–231.

Ziskind-Conhaim, L., I. Geffen, and Z. W. Hall. 1984. Redistribution of acetylcholine receptors on developing rat myotubes. *J. Neurosci.* **4:** 2346–2349.

Reference: *Biol. Bull.* **176(S):** 164–169. (April, 1989, Suppl.)

Molecular Interactions on the Cell Surface Revealed by Electrophoresis

TIMOTHY RYAN, JEFFREY MYERS*, AND WATT W. WEBB**

*Department of Physics, *Chemistry, and **Applied and Engineering Physics, Cornell University, Ithaca, New York 14853*

Introduction

The intriguing finding of Jaffe and Stern and others (Jaffe and Stern, 1979) that strong ionic currents can be detected in the vicinity of developing embryos and the observation that the migratory and/or growth patterns of cells separated from explanted embryonic tissue (Jaffe and Poo, 1979) can be controlled by externally applied electric fields both support the notion that the coupling of extracellular electrical currents to cellular function is physiologically important. The search for an understanding of the mechanisms and sites of coupling of these electric fields to living cells has led to a new probe of both cellular architecture and function. We report here on some of our work on one physical interaction induced by exogenous electric fields: the redistribution of cell surface membrane components by surface electrophoresis.

Materials and Methods

Most details of the experiments have been previously described (Ryan *et al.*, 1988). Briefly, tumour mast cells that were grown, harvested, and labeled with FITC-IgE (Taurog *et al.*, 1979; Barsumian *et al.*, 1981) were plated on #1 glass coverslips, mounted in an electrophoresis chamber (Gross *et al.*, 1986) modified for an inverted microscope, and exposed to an applied electric field E_0. Equilibration of the surface distribution was verified by following its time course after applying the field. The digital fluorescence images of the distribution of fluorescence-labeled proteins on the surface of rat basophilic leukemia (RBL) cells were recorded with a Zeiss 100× Neofluar 1.3NA oil objective on a Zeiss IM-35 epi-illuminated fluorescence microscope (with appropriate excitation-dichroic-barrier filter combinations for fluorescein or rhodamine) coupled to a Venus Scientific TV2 or TV3 intensified video camera. Neutral density filters were used in the optical path of the excitation source (a 100 watt mercury arc lamp) to maintain the fluorescence intensity within the linear range of the camera. Photobleaching was negligible. The images were digitized and typically averaged over 30 frames in a Trappix 5500 image processor (Recognition Concepts, Inc.). The time course of the relaxation of electric field induced segregation after switching of the field was followed to obtain a measure of molecular diffusibility. Several different fields of view were recorded at each time point (over ~1–2 min window) to provide ~25–30 cells for averaging. For experiments performed on cross-linked receptors, the cells mounted in the electrophoresis chamber were perfused 15 min prior to electrophoresis with the monoclonal antibody A2 (Menon *et al.*, 1986) at a concentration of 20 μg/ml. All experiments were carried out at room temperature unless otherwise noted.

Results and Discussion

The hypothesis that externally applied electric fields redistribute the cell surface distribution of important cell membrane components, and hence potentially provides a spatial polarization that might serve as a guidance cue for cellular migration or growth, was first put forth by Jaffe (1977). The qualitative aspects of this redistribution were verified by Poo and Robinson (1977) and found to support the notion that applied external currents do in fact induce spatial concentration gradients of cell surface proteins.

By applying techniques of quantitative digital fluorescence microscopy to the analysis of the equilibrium distribution of fluorescence labeled surface proteins under

electrical potential gradients, we have recently shown that the general surface protein population does not behave as an ideal solution. Instead, the thermodynamic activities are strongly enhanced (up to a factor of 4 in our experiments).

The model system chosen for these studies is a tumor mast cell line, the rat basophilic leukemia (RBL) cell line which expresses $2\text{–}3 \times 10^5$ receptors with high affinity for the Fc portion of immunoglobulin E (IgE). Figure 1 is a digital fluorescence microscope image of a field of view of RBL cells after equilibration in the presence of an externally applied electric field of 10 V/cm. It shows the field induced asymmetric distribution of fluorescein-conjugated IgE-receptor complexes. One of the most convenient aspects of this model cellular system is the fact that the labeling procedure leaves the IgE-receptor complex as a monomeric unit, greatly simplifying studies on surface interactions and lateral diffusion. The concentration profile obtained by scanning the fluorescence intensity of the cell along the periphery as a function of angle θ with respect to the direction of the applied field E_0 is displayed in Figure 2. The solid line in the figure represents an attempted best fit to the ideal solution theory put forth by Jaffe (1977) and later in the following form by Poo (1981):

$$\frac{C_T(\theta)}{C_{0T}} = \frac{\frac{2\beta}{kT}\exp\frac{-\beta(1+\cos\theta)}{kT}}{1-\exp\left(\frac{-2\beta}{kT}\right)}(1-I_{im}) + I_{im} \qquad (1)$$

where C_{0T} is the average prefield concentration, k is Boltzmann's constant, I_{im} is a possible electro-immobile fraction and $\beta = (3/2)ZeE_0r$ (r is the cell radius and Ze the effective charge of the electromobile proteins).

The discrepancy that arises between the data and the ideal solution theory is evidence that at least one of the underlying assumptions is inappropriate in the description of the proteins as non-interacting and point-like particles. Since the high concentration region in Figure 2 appears to be saturating with respect to the predicted distribution, we invoked simple steric exclusion to account for the differences. Analogous exclusion principles generate the Fermi distribution and the Langmuir adsorption isotherm. In this case, the predicted field-induced concentration profile of a population of surface proteins which, averaging over the entire cell, occupies a fraction f_0 of the surface area available to diffusion takes the form:

$$\frac{C_T(\theta)}{C_{0T}} = \frac{\frac{1-I_{im}}{f_0}}{\exp\left(\frac{\beta\cos\theta}{kT}\right)\exp\left(\frac{-\mu}{kT}\right)+1} + I_{im} \qquad (2)$$

where

$$\exp\left(\frac{\mu}{kT}\right) = \frac{\exp\left(\frac{\beta}{kT}\right) - \exp\frac{\beta(1-2f_0)}{kT}}{\exp\left(\frac{2\beta(1-2f_0)}{kT}\right)-1} \qquad (3)$$

Independent fits of this theory to the measured concentration profiles at four different field strengths are shown in Figure 3 and indicate that the cell surface proteins are responding to the electric field as if ~45% of the area available to diffusion is covered by mobile proteins. It is important to note that in this study we have assumed that the IgE receptor is behaving as a representative marker of the general surface population. This is supported by our measurements of other more general markers of cell surface proteins (Ryan *et al.*, 1988) which give similar fitting parameters as those above. The details of the fitting procedure as well as parameters used are reported elsewhere (Ryan *et al.*, 1988).

Quantitation of the kinetics of the redistribution of fluorescence-modified surface molecules after termination of the electric field has provided estimates of the lateral diffusibility (Pool, 1981) of these molecules. Estimates of the lateral diffusion coefficient derived from post-electrophoresis recovery experiments (D_{PER}) have been widely used in comparison with those obtained from fluorescence photobleaching recovery (FPR) experiments (D_{FPR}) (Axelrod *et al.*, 1976; Jacobsen *et al.*, 1982). Most available data suggest that D_{PER} is an order of magnitude larger than D_{FPR} (Poo, 1981; Tank *et al.*, 1985) and this discrepancy has led to speculation about possible perturbations on the cell membrane organization induced by the electrophoresis. These differences cannot be attributed to perturbations induced by the photobleaching light pulse itself since extensive studies have shown (Wolf *et al.*, 1980) that neither repeated bleaching pulses in the same spot nor measurements of lateral diffusion using a combination of fluorophores as markers reveal any photo-induced membrane damage.

We point out some complications in the comparison of these two diffusion coefficients. One essential distinction is the basic difference between self (or tracer) diffusion and mutual (or inter) diffusion which governs statistical mixing and which relaxes a macroscopic concentration gradient in solution. The usual FPR experiment on cell membranes measures the self diffusion of labeled lipids or proteins while observation of PER or fluorescence correlation spectroscopy (FCS) (Magde *et al.*, 1972, 1974a, b) measures the mutual diffusion coefficient. The basic difference arises because in one case one measures the relaxation of a physical gradient of a material (PER, FCS), while in the other one is observing the randomiza-

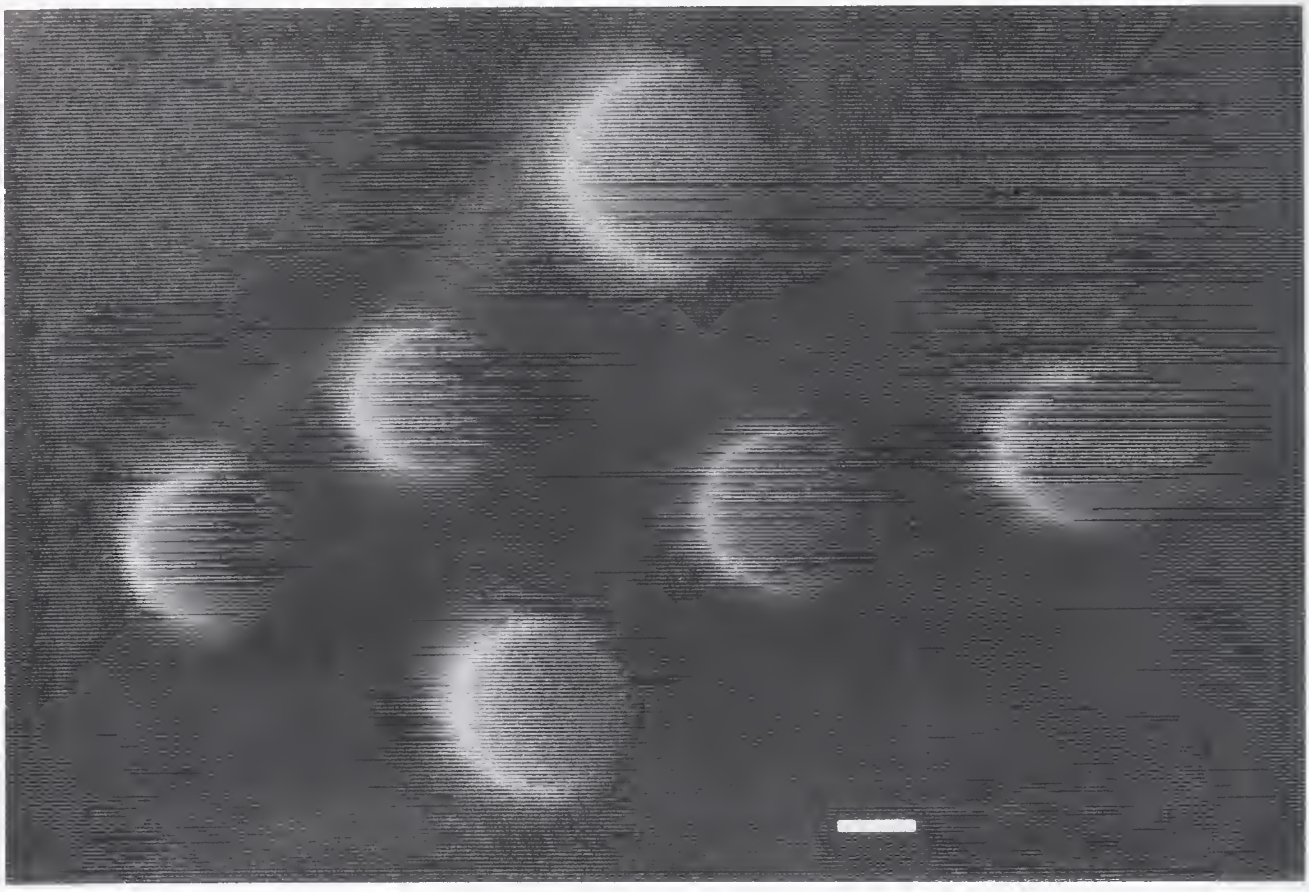

Figure 1. This fluorescence image shows the distribution of fluorescein isothiocyanate (FITC)-labeled rat IgE-receptor complexes (IgE-R) on the surface of live RBL cells (2H3 subline) after electrophoresis. Reprinted from *Science* (Ryan *et al.*, 1988) copyright 1988 by the American Association for the Advancement of Science (AAAS). Scale bar is 5 μm.

tion of a gradient of the concentration of an equivalent marker of proteins and not a gradient in the thermodynamic activities of proteins (FPR).

In an ideal binary mixture, the mutual diffusion coefficient D relative to a frame fixed at the centroid of the system can generally be expressed in terms of molecular fractions X_A (solvent) and X_B (solute) and the concentration dependent self-diffusion coefficients D_A and D_B as (Darken, 1948; Bardeen, 1949):

$$\tilde{D} = X_A D_B + X_B D_A \tag{4}$$

This equation expresses the consequences of the induced flow with velocity V which is required by simple continuity to maintain a stationary centroid for the material. Neglecting molecular volume differences a local flow velocity

$$V(y) = \frac{(D_A - D_B)\left(\frac{\partial X_B}{\partial y}\right)}{\Omega} \tag{5}$$

is induced by a diffusive relaxation of a concentration gradient (dX_B/dy) in a solution where $D_A \neq D_B$ and Ω is the volume/molecule. In the case where the diffusing species exhibit non-ideal behavior due to solute-solute repulsion, as we have found for proteins in cell membranes, the diffusion process is modified by an extra driving force which can be expressed in terms of the concentration dependent activity coefficient γ_B resulting in a correction for D_B in Eq. (4) by a factor (Darken, 1948) $[1 + X_B(\partial \ln \gamma_B/\partial X_B)]$. By the Gibbs-Duhem relation, the activity coefficient for the solvent (lipid) can be calculated, which gives

$$\left[1 + X_B \frac{\partial \ln \gamma_B}{\partial X_B}\right] = \left[1 + X_A \frac{\partial \ln \gamma_A}{\partial X_A}\right] \tag{6}$$

such that the mutual diffusion coefficient is multiplied by an overall factor $[1 + X_B(\partial \ln \gamma_B/\partial X_B)]$. In our case we have shown (Ryan *et al.*, 1988) that $\gamma_B \equiv 1/(1 - f)$ (where $f = X_B$) so

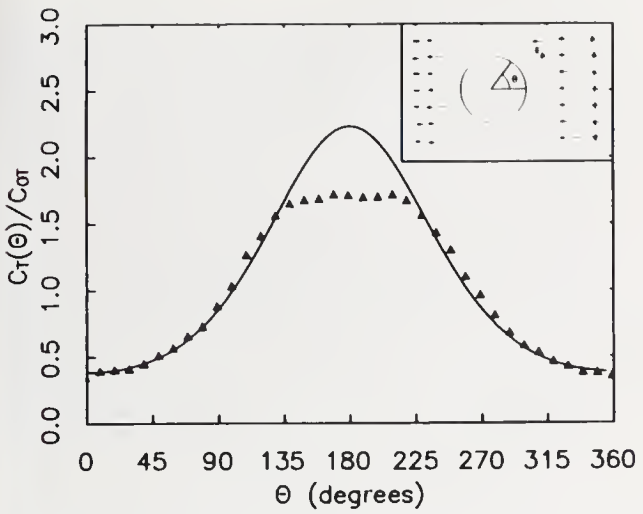

Figure 2. The relative surface concentration profile $[C_T(\theta)/C_{0T}]$ of IgE-R on RBL cells equilibrated in an applied field of $E_0 = 15$ V/cm. Shown is the average over an ensemble of about 30 cells like those displayed in Figure 1. $[C_T(\theta)/C_{0T}]$ is displayed as a function of angle θ with respect to the direction of the applied field E_0 (see insert). The standard deviation of the mean values for the data points shown was typically ~10%. The solid line is an attempted fit to Boltzmann statistics including an immobile fraction. Reprinted from *Science* (Ryan *et al.*, 1988), copyright 1988 by the AAAS.

$$\tilde{D} = \frac{1}{1 - X_B}[X_A D_B + X_B D_A] = \frac{D_B + X_B(D_A - D_B)}{1 - X_B} \tag{7}$$

The relaxation process is further complicated by the fact that both D_A and D_B are also likely to be concentration dependent. Saxton (1987) has recently calculated the concentration dependence of tracer diffusion from Monte Carlo simulations of molecular motion on a lattice and finds

$$\frac{D(c)}{D(0)} = 1 - 2.1817c + 1.8025c^2 + \cdots \tag{8}$$

where D(0) is the tracer diffusion in the infinite dilution limit of the concentration c (here $c \equiv X_B$). Neglecting high order terms, we see that in this case the effects of the non-ideal activity coefficient in the extra driving force is roughly compensated for by the slowing of diffusion by crowding.

In most cell membranes of high protein concentration ($X_B \sim 0.5$) typical values for $D_A \sim 10^{-8}$ cm^2/s and $D_B \leq 10^{-10}$ cm^2/s imply $\tilde{D}$ an order of magnitude larger than D_B. This result is apparently confirmed by most available data on cell membranes. The one known exception is the case of IgE-R on RBL cells (Wolf *et al.*, 1980; Menon *et al.*, 1986; McCloskey *et al.*, 1984) where experiments show clearly that $D_{PER} \sim D_{FPR}$. The reason for this exception is not clear. Nevertheless, we conclude that observed differences between D_{PER} and D_{FPR} are consistent with the general macroscopic foundation and do not necessarily imply membrane perturbations during electrophoresis such as dissociation from cytoskeletal attachments. The interactions with cell substrate and stationary cytoskeleton that establish a frame of reference for the centroid of the cell membrane are, however, explicitly implicated by this analysis of the continuity of the diffusive fluxes. Recently, Abney *et al.* (1988) presented a computational analysis of diffusion models that also reveals differences between self and mutual diffusion in the presence of explicit protein-protein interactions. Their results of an entirely different approach agree with the general macroscopic foundation presented here.

Prolonged exposures to electric fields do, however,

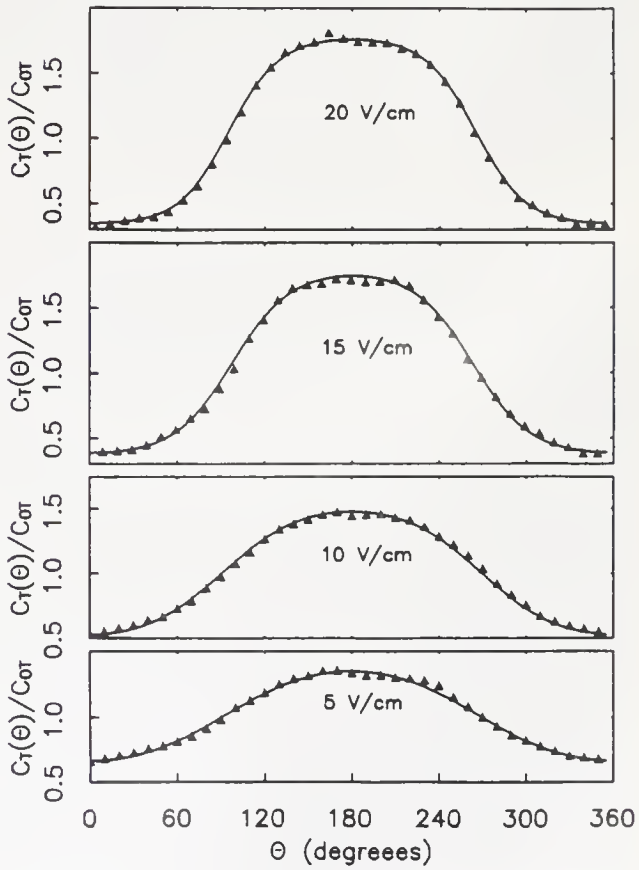

Figure 3. Equilibrium relative cell surface concentration profiles of IgE-R on RBL cells in applied electric fields are accurately fit by the exclusion principle theory for crowding (Eq. 2). Like Fig. 2, $[C_T(\theta)/C_{0T}]$ is plotted for angle θ with respect to E_0. At each applied electric field E_0, the data set was fit independently to Eq. (8) to determine β, I_{im} and f_0 by a nonlinear least squares procedure. Reprinted from Science (Ryan *et al.*, 1988), copyright 1988 by the AAAS.

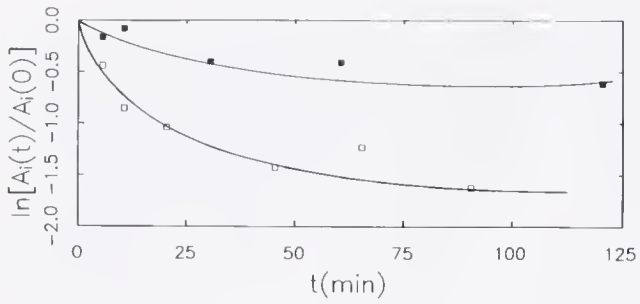

Figure 4. Post-field relaxation curves plotted as ln $[A_i(t)/A_i(0)]$ (A_i as defined in the text) as a function of time for monomeric IgE-R complexes (unfilled squares) and antibody cross-linked IgE-R complexes (filled squares). Both data sets were obtained for exposures at 10 V/cm for 120 min prior to relaxation. Typical standard deviations for A_i were ~10%. The solid lines are provided to guide the eye, and are not fits to the data.

seem to induce some irreversible or slowly reversible effects. Figure 4 (open squares) depicts the relaxation of a distribution of IgE-R complexes after exposure to a field of 10 V/cm for 120 minutes (~10 times the rise time for equilibration of the concentration profile) as a semilog plot of the asymmetry index (Poo, 1981)

$$A_i = \frac{C(180°) - C(0°)}{C(180°) + C(0°)}$$

versus time. The initial slope yields $D_{PER} \sim 2 \times 10^{-10}$ cm^2/s and is consistent with previous reports (McCloskey, 1984). The slope of the recovery at later times, however, differs significantly from that at early times. The precise magnitude of this effect has varied from day to day, but it was generally observed to be more pronounced for prolonged exposures than for brief exposures. One must be very cautious in interpreting relaxation data analyzed in this fashion since the original assumptions underlying the approximations used to obtain a single relaxation rate in the decay of A_i are not valid. Since the initial condition prior to relaxation does not conform to simple ideal solution theory (but is instead a Fermi distribution), the original derivation (Poo, 1981) no longer applies. However, the corrections to the slope in Figure 4 should decrease at later times. Instead, the observed cessation of recovery is consistent with an immobilization of a fraction of the proteins occurring during electrophoresis over a time scale much longer than that required to reach equilibrium in the field, as suggested by Poo *et al.* (1979). This is further supported by the data presented in Figure 4 (filled squares) which depicts the post-field relaxation of IgE-R complexes which have been cross linked by a monoclonal anti-IgE antibody present in concentrations greatly in excess of surface IgE concentrations. Under similar conditions the IgE-R complexes have been shown from FPR measurements to be virtually immobilized (Menon *et al.*, 1986). The slope of the dashed line at early times suggests that for the cross linked receptor D_{PER} ($\sim 3 \times 10^{-11}$ cm^2/s) > D_{FPR} ($<10^{-12}$ cm^2/s), unlike the monomeric IgE-R complexes where, as discussed, $D_{FPR} \sim D_{PER}$. The vanishing slope at later times again is consistent with the immobilization of some large fraction of the population during retention in the electrophoresed high concentration. This mechanism seems likely since cross-linking reactions are progressing throughout the experiment. Hence, these data raise the interesting possibility that, over prolonged exposures to electric fields, the membrane surface proteins may be reordering themselves to produce stable configurations or associations which persist after removal of the electric field.

It is still unknown whether the membrane reorganization induced by electric fields can be directly related to physiological cell responses reported in many systems. Since our studies have shown that even at typical membrane protein concentrations strong steric constraints are manifest, it is possible that small shifts away from equilibrium concentrations alone could prove to have profound effects on cellular physiology. For example, Grassberger *et al.* (1986) have estimated that the equilibrium binding constant for protein self association is significantly enhanced in the presence of large area fractions of inert proteins. It is also possible that any membrane diffusion mediated signal transduction events could be eliminated or slowed in the high concentration region by virtue of the fact that the surface area coverage is so high that self-diffusion coefficients may be quite small. This could provide a polarization in the cell's signal transduction abilities since on the side of the cell where the concentration has decreased, diffusion may be faster.

Acknowledgments

We are grateful to Dr. Barbara Baird and Dr. David Holowka for stimulating discussions during the course of this work. Supported by the Office of Naval Research, the National Science Foundation, and the Cornell Biotechnology Program.

Literature Cited

Abney, J., B. Scalettar and J. Owicki. 1988. *Proc. Natl. Acad. Sci. USA* **85:** 6726–6729.

Axelrod, D., D. E. Koppel, J. Schlessinger, E. Elson, and W. W. Webb. 1976. *Biophys. J* **16:** 1055–1069.

Bardeen, J. 1949. *Phys. Rev.* **76:** 1403–1405.

Barsumian, E. L., C. Isersky, M. G. Petrino, and R. Siraganian. 1981. *Eur. J Immunol.* **11:** 317–323.

Darken, L. S. 1948. *Met. Tech. Paper* **2311:** 1–11.

Grassberger, B., A. P. Minton, C. DeLisi, and H. Metzger. 1986. *Proc. Natl. Acad. Sci. USA* **83:** 6258–6262.

Gross, D., L. M. Loew, T. A. Ryan, and W. W. Webb. 1986. *Ionic Currents in Development,* R. Nuccitelli, ed. Alan R. Liss, Inc., New York. Pp. 263–270.

Jacobsen, K., E. Elson, and W. W. Webb. 1982. *Nature* **295:** 283–284.

Jaffe, L. 1977. *Nature* **265:** 600–602.

Jaffe, L. F., and M-M. Poo. 1979. *J. Exp. Zool.* **209:** 115–128.

Jaffe, L. F., and C. D. Stern. 1979. *Science* **206:** 569–571.

McCloskey, M., Z-Y. Liu, and M-M. Poo. 1984. *J. Cell Biol.* **99:** 778–787.

Magde, Douglas, Elliot Elson, and Watt W. Webb. 1974a. *Biopolymers* **13:** 29–61.

Magde, Douglas, and Elliot Elson. 1974b. *Biopolymers* **13:** 1–27.

Magde, D., E. Elson and W. W. Webb. 1972. *Phys. Rev. Lett.* **29:** 705–708.

Menon, A. K., D. Holowka, W. W. Webb, and B. Baird. 1986. *J. Cell Biol.* **102:** 541–550.

Poo, M-M. 1981. *Ann. Rev. Biophys. Bioeng.* **10:** 245–276.

Poo, M-M., and K. Robinson. 1977. *Nature* **265:** 602–605.

Poo, M-M., J. W. Lam, N. Orida, and A. W. Chao. 1979. *Biophys. J.* **26:** 1–22.

Ryan, T. A., J. Myers, D. Holowka, B. Baird, and W. W. Webb. 1988. *Science* **239:** 61–64.

Saxton, Michael J. 1987. *Biophys. J.* **52:** 989–997.

Tank, D. W., W. J. Fredericks, L. S. Barak, and W. W. Webb. 1985. *J. Cell Biol.* **101:** 148–157.

Taurog, J. D., C. Fewtrell, and E. Becker. 1979. *J. Immunol.* **122:** 2150–2153.

Wolf, D., M. Edidin, and P. R. Dragsten. 1980. *Proc. Natl. Acad. Sci. USA* **77:** 2043–2045.

Reference: *Biol. Bull.* **176(S)**: 170–178. (April, 1989, Suppl.)

Experiments on the Interaction of Electromagnetic Fields with Mammalian Systems

W. C. PARKINSON[1] AND C. T. HANKS[2]

[1]*Department of Physics and* [2]*School of Dentistry, University of Michigan, Ann Arbor, Michigan 48109*

Abstract. The results of a series of measurements on the interaction of electromagnetic fields with cell ensembles *in vitro* are described. The measurements include the effect of fields on population doubling time, ^{3}H-TdR uptake, membrane transport, and galvanotropism. No measureable effect of AC fields was found, and in particular no evidence was found for a cyclotron-resonant mechanism in the ion transport across cell membranes.

Introduction

There is now considerable experimental evidence for the interaction of low energy, non-ionizing electromagnetic fields with mammalian cell systems. The evidence can be separated according to the type of field: DC magnetic field, DC electric field, both steady and pulsed, and low frequency AC field, both sinusoidal and pulsed. The evidence for the interaction of DC electric fields is firm. The evidence for the AC interaction remains highly controversial, in part because there is a lack of duplication of crucial experiments, which in turn can lead to the quoting of unconfirmed results as fact.

The purpose here is to describe a series of experiments carried out over the past six years that have had as their objective the measurement of the electromagnetic interaction with transformed cell ensembles, in particular L929, Chinese hamster ovary (CHO), Balb/c 3T3, and rat osteosarcoma (ROS). The only primary cells investigated were quail somite and fetal rat calvarium, and for these only the response to DC electric fields was measured.

The experiments fall into four categories: (1) measurements of the effects of DC magnetic and AC electromagnetic fields on population doubling time, (2) effects of AC and pulsed fields on ^{3}H-TdR uptake, (3) effects of AC fields on membrane transport, and (4) galvanotropic effects of DC electric fields.

Methods and Results

The population doubling time with a 3 mT DC magnetic field and with a 3 mT rms 60-Hz field have been measured for L929 cells. We know of no data, duplicated in at least a second laboratory, that shows any effect of *static* magnetic fields in the mT range on cell growth or doubling time. Graphs of the doubling time for three values of the induced electric field at 60 Hz are shown in Figure 1. There is no significant difference between field on and field off as determined by comparison of the linear regression coefficients. The three linear regression lines of Figure 1 were obtained by a least squares fit to the data and give the rate of cell growth over the interval from zero to 129 h. To test whether the electric field had a significant effect on the growth rate linear regression coefficients were determined (by least squares) for each of the three regions in time, and for each of the three values of the applied electric field. In the time interval 0–38 h, with no field applied, the rates should be the same within statistical fluctuation. The three values with standard error are $b_{21} = (15.5 \pm 2.3) \times 10^{-3}$, $b_{10} = (15.0 \pm 2.3) \times 10^{-3}$, and $b_{151} = (17.7 \pm 2.1) \times 10^{-3}$ for E = 2.2 mV/m, 10.2 mV/m, and 15.5 mV/m, respectively. In the time interval 38–90 h, with the field applied, the corresponding values are $b_{22} = (17.2 \pm 1.21) \times 10^{-3}$, $b_{102} = (15.5 \pm 1.21) \times 10^{-3}$, and $b_{152} = (15.6 \pm 1.0) \times 10^{-3}$. For the time interval 90–129 h, with the field off, the values are $b_{23} = (18.6 \pm 1.4) \times 10^{-3}$, $b_{103} = (16.2 \pm 2.8) \times 10^{-3}$, and $b_{153} = (16.5 \pm 2.0) \times 10^{-3}$. In a further test of significance, a comparison of the regression coefficients was made. The standard error of the differences was determined and using the "student" t, the confidence levels determined. They varied from 0.2 to 0.85. Thus it is concluded that the variation in growth rate cannot be regarded as significant. There is not sufficient

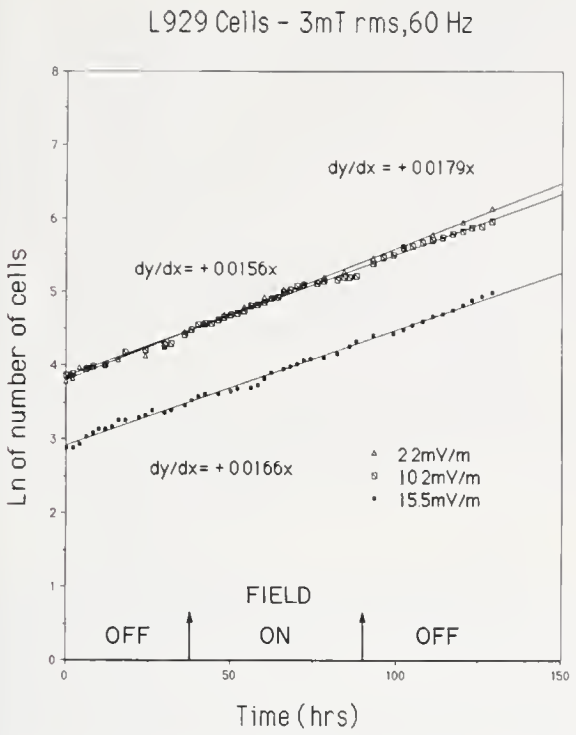

Figure 1. Doubling time of L929 cells for 3 values of the electric field induced by a 30 gauss (rms), 60 Hz magnetic field at T = 37°C. The field was off for the first 38 h, on for 52 h, then off for 39 h.

evidence to assert that the growth rate was influenced by the applied electric field. It might be noted that in general an increase in initial growth rate is to be expected because of the "conditioning of the medium" effect (Parkinson 1983). In such measurements it is critical that the temperature be maintained constant with field on and off since the doubling time is an exponential function of temperature. [See for example the measured dependence of the mitotic period for L929 cells in Parkinson (1983).]

It has been reported that appropriately pulsed electromagnetic fields (Bassett *et al.*, 1981) promote osteogenesis and wound healing. There is also a report that pulsed electromagnetic fields stimulate DNA synthesis in fetal rat calvarial osteoblasts grown in culture (Hanley *et al.*, 1981). There is, to our knowledge, only one report in a refereed journal of a response by transformed cells (Colacicco and Pilla, 1983). We have measured the uptake of tritiated thymidine (^{3}H-TdR) by cultures of finite cell lines and continuous cell lines in response to pulsed electromagnetic fields (PEMF) using both the Bassett waveform ("c"-signal) and a repetitive rectangular pulse train. The finite cell lines were quail somite fibroblasts and periosteal cells from fetal rat calvarium; the continuous cell lines were L-929, Balb/c 3T3, Chinese hamster ovary (CHO), and rat osteosarcoma [ROS 17/2.8]. The apparatus for generating the pulsed electrical field is the same as that described earlier (Parkinson and Hanks, 1986). In that work, 24 well tissue culture dishes were used. The values given for the induced electric field were not correct because the centers of the wells were not coaxial with the coils. The old data has been re-evaluated and some of the experiments repeated using 80-mm plastic culture dishes carefully aligned co-axially with the coils so that the induced electric field at the position of the cells is accurately known. The results after re-evaluation for fetal rat calvarial periosteal cells are shown in Figure 2 together with the results for Balb/c 3T3 using the 80-mm dishes. We did not find a statistically significant difference in the uptake of any of these cell lines from that of control ensembles. The regression coefficients for the data for Rat Calvariun for 1 min and 24 h exposure are $b_1 = (12.9 \pm 28.7) \times 10^{-3}$ and $b_{24} = (-41.9 \pm 39.3) \times 10^{-3}$ with corresponding confidence intervals of 0.65 and 0.33, respectively. For the Balb/c3T3 the values are $b_9 = (1.2 \pm 3.9) \times 10^{-3}$ and $b_0 = (1.81 \pm 1.2) \times 10^{-3}$ with confidence levels of 0.75 and 0.2, respectively. There is not sufficient evidence to assert that the uptake of ^{3}H-TdR was influenced by the applied electric field.

Reports (Bawin and Adey, 1976; Blackman, 1985) that efflux and/or influx of Ca^{++} ions from brain tissue display a resonance type response to an applied electromagnetic field has led to a cyclotron-resonance model for the interaction (Blackman, 1985; Chiabrera *et al.*, 1985; Liboff, 1985). We have done two experiments. The first searched for resonances in Ca^{++} transport in Balb/c 3T3, L929, V79 and ROS 17/2.8 cells by measuring changes in the cytosolic Ca^{++} concentration using fluorescence spectroscopy on cells loaded with the fluorescent chelating agent fura2 (Parkinson and Hanks, 1988). The second experiment searched for resonances in the ion transport across turtle colon (Liboff and Parkinson, 1988). The apparatus for the fluorescent studies is shown in Figure 3. The spectral emission from an ensemble of L929 cells is shown in Figure 4. Figure 5 shows the emission intensity as a function of time and illustrates the chelation of Ca^{++}, while Figure 6, a time scan of the fluorescent intensity, shows the action of ionomycin and EGTA. The movement of Ca^{++} into and out of the cytoplasm under the action of ionomycin and EGTA caused extreme changes in the fluorescent intensity. (Ionomycin makes the membrane permeable to calcium while EGTA is a calcium chelator.) Conversely no change in fluorescence was observed when the DC field (50 μT) and the AC magnetic fields (50 μT amplitude, f = 38.15 Hz) were applied at the resonant conditions in which the DC field is comparable to the geomagnetic field (McLeod and Liboff; 1986). Because the "effective-mass" for Ca-ions may be quite different from the free-space mass, the frequency was varied over the range from one to 100 Hz,

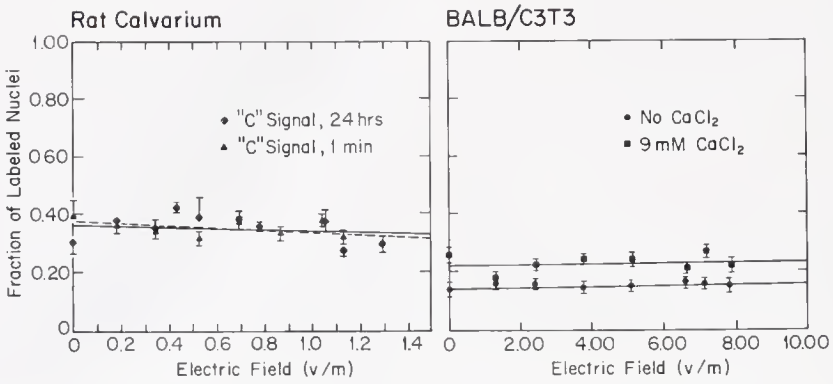

Figure 2. The uptake of ^{3}H-TdR by fetal rat calvarial periosteal cells and of Balb/c 3T3 cells in response to pulsed electromagnetic fields. The lines represent a linear least squares fit to the data. The error bars are from counting statistics only and do not include systematic reader errors. The pulsed field for the Balb cells was a continuous 25 μs square wave.

and the amplitudes varied over a large range. It is estimated that a 1% change in Ca^{++} concentration would have been detected. A very rough estimate of the time constant and of the sensitivity of the measurements to changes in cytosolic Ca^{++} concentration $[Ca^{++}]_c$ can be made on the following basis: assuming the normal cytosolic concentration to be 100–200 nM, as predicted by the Nernst equation (also Rasmussen and Barrett, 1984) then in the volume of a cell, taken as 4×10^{-16} m^3, there would be of the order of 4×10^4 Ca^{++} ions. The number

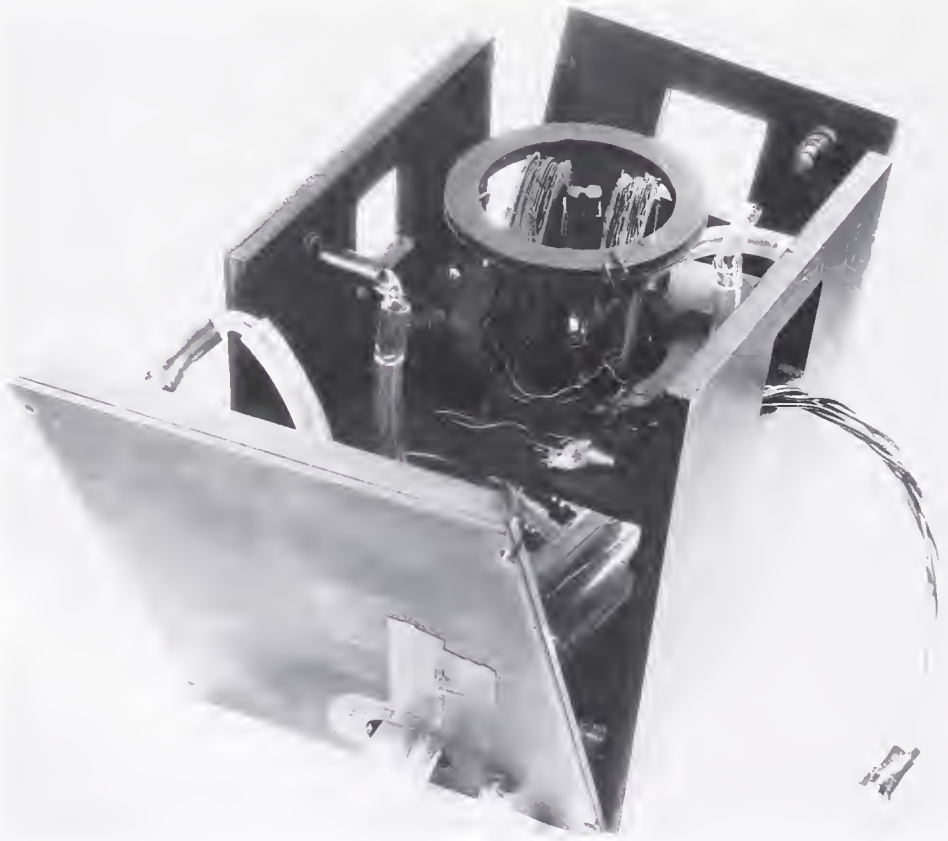

Figure 3. Apparatus for fluorescent spectroscopy. An exploded view of the heating panels, Helmholtz-like coils and sample holder that fit snugly into the sample volume of the SLM-8000C spectrofluorometer.

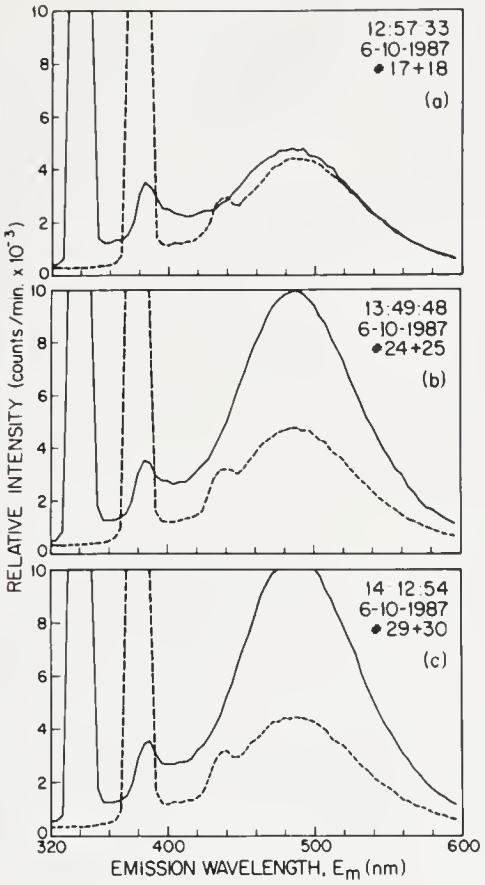

Figure 4. Spectral emission from an ensemble of L929 cells illustrating the chelation of Ca^{++}. Each graph contains two superimposed plots, one for excitation wavelength E_x = 340 nm (solid curve), and one for E_x = 380 nm (dashed curve). The large peaks at the left, centered at E_m = 340 nm and E_m = 380 nm, are reflections by the sample holder of the incident radiation. The small peaks (E_m = 385 nm and 440 nm) are artifacts, probably Raman scattering. The broad peaks, centered between E_m = 480 nm and 500 nm, indicate the relative fluorescence emission. The cells were loaded for 1.5 hours in 3 μM fura2AM in 3 ml of Ca-free buffer, washed three times in buffer, and mounted in a cuvette containing 3 ml of Ca-free buffer. (a) Spectra immediately after mounting (clock time = 12:57:33); (b) The same cell ensemble 52 minutes later (clock time 13:49:48) after again washing the cells in Hallam's, mounting in new cuvette with fresh buffer and 2.6 mM $CaCl_2$; (c) The same ensemble 23 min later (clock time 14:12:54) with 5.2 mM $CaCl_2$. The temperature was maintained at T = 37°C.

of calcium channels per cell is not known, but based on the number of Na-channels (Darnell *et al.*, 1986), 400 is a reasonable number. Thus to reduce the cytosolic Ca^{++} concentration by 200 nM requires that each channel on the average transport 100 ions. Calculations based on NMR-derived rate constants for gramicidin channels (Urry *et al.*, 1980) suggest a conduction of 10^7 ions/s/channel for a 1 M external to 10^{-7} M internal concentration gradient. Thus for 10^{-3} M external to 10^{-7} M internal concentration a conduction of 10^4 ions/s/channel would seem to be a very conservative estimate. This leads to a transient time constant of the order of milliseconds, as is observed via patch clamp techniques.

A change in fluorescent intensity of the order of 3% would be detectable in the data of Fig. 5. The addition of EGTA (Fig. 6) results in a factor of 3.1 decrease in intensity, a decrease due to reduction of $[Ca^{++}]_c$. Again for a normal cytosolic concentration of 200 nM, then a

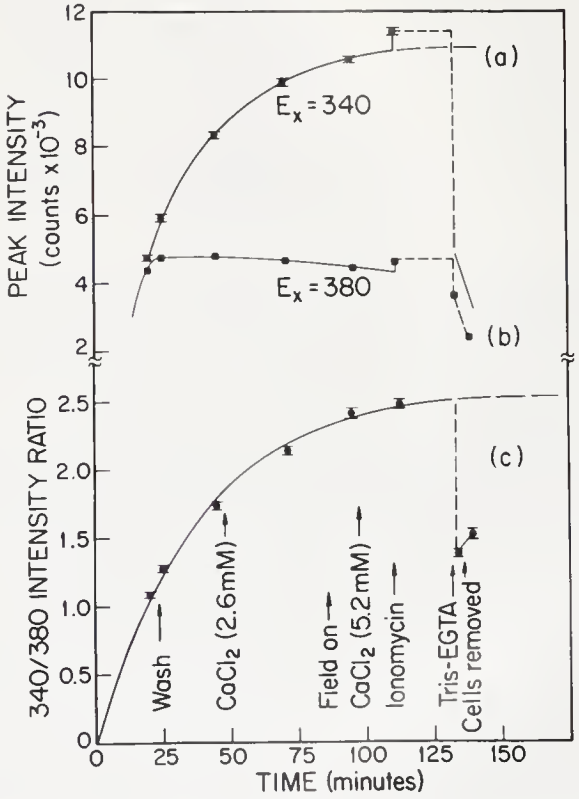

Figure 5. (a) The emission intensity at E_m = 490 nm for E_x = 340 nm as a function of time. The data points are taken from eight graphs, including the three of Figure 4. The solid curve is given by $I = I_s(1 - e^{-t/\tau})$ fitted by least squares to the data, where I_s = 11,300, τ = 34.3 min, and $\chi^2 = 23 \times 10^3$, where χ^2 is the sum of the squares of the deviations of the data points from the calculated curve. Note particularly the increase in intensity following the addition of Ionomycin, and the decrease following the addition of Tris-EGTA. (b) The emission intensity at E_m = 490 nm for E_x = 380 nm. The line is drawn just to connect the points. (c) The 340/380 ratio for E_m = 490 nm calculated from the data points in (a) and (b). The arrows indicate changes in the experimental conditions. The solid curve, again of the form $I = I_s(1 - e^{-t/\tau})$, when fitted by means of least squares yields I_s = 2.6, τ = 38.6 min, and $\chi^2 = 2.9 \times 10^{-3}$. The time t = 0 corresponds to 70 min after the start of loading. The exponential form and long time constant suggest a slow hydrolysis of the fura ester to the acid, or the diffusion of Ca^{++} from internal stores (organelles) to the cytosol and not membrane transport, since washing at t = 5 min, the addition of $CaCl_2$ at t = 48 min and the application of the EMF at t = 86 min did not alter the rate of change of the emission intensity.

The uncertainties associated with the data points are calculated from the statistics of counting only. Note that while the intensities change significantly on the addition of ionomycin the ratio did not change.

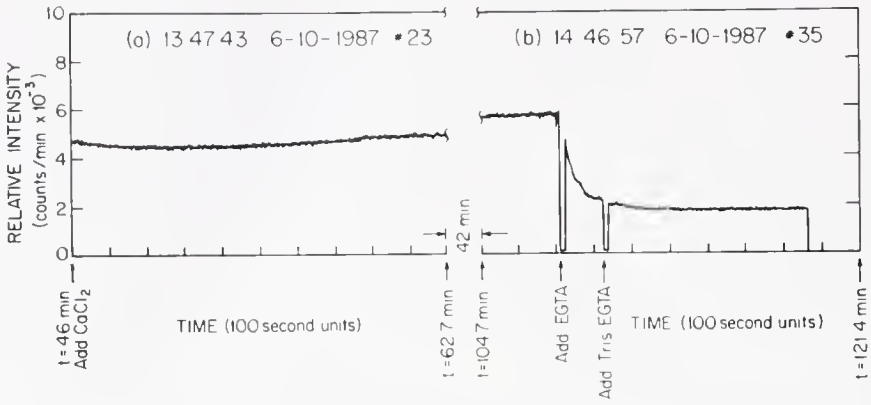

Figure 6. Slow kinetics scan of the E_m = 490 fluorescence intensity for E_λ = 340 nm. The times of addition of $CaCl_2$, ionomycin, EGTA and Tris-base EGTA are shown by arrows.

change of 2 n*M* concentration is just detectable, or $[\Delta Ca^{++}]_c/[Ca^{++}]_c$ = 1%. This requires on the average only one ion/s/channel, a remarkably low number. At the other extreme, say only one calcium channel per cell, a transport of only 400 ions/s/channel would be required. This excellent sensitivity is due to the properties of fura2, and represents a significant improvement over the ionophore quin2. These conclusions are consistent with the calibration of the fluorescence of fura2 by Grynkiewicz *et al.* (1985). It might be noted that Bawin and Adey (1976) report an 11–15% effect at the "window." Blackman *et al.* (1985) report 15–20% effect, while McLeod *et al.* (1987) report an increase in the ratio of ^{45}Ca uptake of a factor of three at resonance. As discussed more fully below, it would be surprising to observe a resonant response in view of the fact that the random thermal energy of the ions ($\frac{3}{2}$ kT) is orders of magnitude larger than the energy derived from the electromagnetic field. As a result, any cyclotron motion would be completely masked. The time between collisions of the ions with the molecules of the medium (randomizing collisions) is very much shorter ($\sim 10^{-12}$ s) than the period of the electromagnetic field ($\sim 10^{-2}$ s).

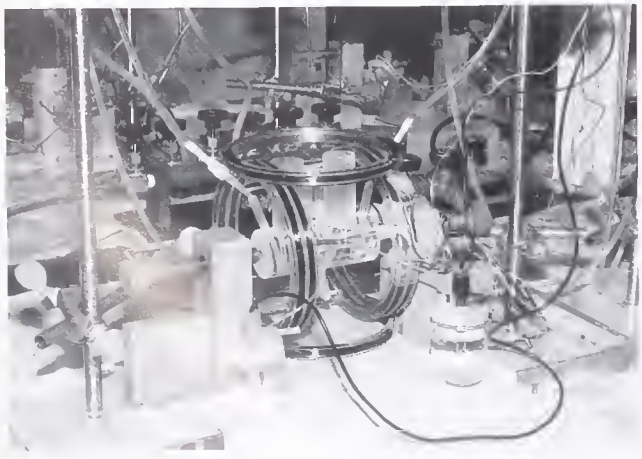

Figure 7. Apparatus for ion transport measurements across turtle colon. The colon is clamped in an Ussing chamber, which is surrounded by three pairs of Helmholtz-like coils.

The search for a cyclotron resonant effect on ion transport across an epithelial membrane, turtle colon, used the method described by Dawson (1987a, b) and was carried out in his laboratory using his experimental apparatus suitably modified. The arrangement is shown in Figure 7. The turtle colon is a sodium-absorbing epithelium in which Na enters the cell across the apical membrane via Na-channels and exits the cell through an electrogenic pump which exchanges Na for K. Colons were excised from turtles (*Pseudemys scripta*), stripped of serosal muscular layers, washed, and clamped in an Ussing chamber. The transmembrane current was measured in the voltage clamp condition and also under the influence of a 10 mV transmembrane pulse. Magnetic fields were then applied using three pairs of Helmholtz-like coils, one to buck the local vertical field and the other two to provide collinear DC and AC fields in the horizontal direction normal to the plane of the membrane.

With a DC magnetic field (50 μT) parallel to an ac electromagnetic field (50 μT amplitude), with both being perpendicular to the plane of the membrane and with the transepithelial potential clamped, the baseline short circuit current was recorded. The change in current was measured following transmembrane 10 mV pulses (length 1–20 s) with and without the ion cyclotron resonant fields for a variety of ions (H^+, Li^+, Na^+, K^+, Mg^{++}, Ca^{++}, Cl^-). The frequencies were varied over a wide range (3–770 Hz), and the magnetic fields from 10 to 200 μT DC, and from 1 to 200 μT peak AC. Three combinations of bathing solutions were used on the lumen and

Table I

Response of cell lines to DC electric fields

Cell type	Substrate*	Temp °C	E (V/cm)	Medium	Result
Quail somite fibrobl.	G	37	4.5	F-12/FCS10/CEE3	+
Balb/c 3T3	G	37	4.5	Dulbecc. MEM/FCS10	−
Prim. rat calv. osteobl.	G	37	4.5	F-12/FCS10	−
CHO	G	37	4.5	F-12/FCS10	−
L929	G	37	4.5	F-12/FCS10	−
ROS 25/1	G	36.1	5.0	F-12/FCS3	−
ROS 17/2.8	G	37	7.0	F-12/FCS10	+
ROS 17/2.8	G	24.5	13	F-12/FCS3	+
ROS 25/1	G	24.5	13	F-12/FCS3	+
ROS 17/2.8	T	24.5	13	F-12/FCS3	+
ROS 25/1	T	24.5	13	F-12/FCS3	+
L929	G	24.5	13	F-12/FCS3	+
ROS 17/2.8	G	24.5	13	Hallam BSS/1.3 mM Ca^{++}	±
ROS 17/2.8	G	24.5	13	Hallam BSS/w/o Ca^{++}	−
ROS 25/1	G	24.5	13	Hallam BSS/w/o Ca^{++}	−

* G = glass; T = Thermonox; (+) = alignment, (−) = no response, (±) indicates cells appeared to be aligning at 240 min, but were lifting off the substrate.

apical sides of the membrane: Ringers/Ringers, K-gluconate/K-gluconate, and K-gluconate/Ringers. A very rough estimate of the sensitivity can be made. The sample area of 5.2 cm^2 contains approximately 10^6 cells. If a change of current of 1 μA is just detectable, and again assuming $\sim$100 channels/$(\mu m)^2$ (Darnell *et al.*, 1986) or a total of 5×10^6 channels in the sample area, the minimum detectable current per channel is 3.2×10^{-16} amperes, or 100 ions/s/channel if all channels were simultaneously affected. Normal ion fluxes are estimated to be 10^7 ions/s/channel (Darnell *et al.*, 1986) for 1 M external to 10^{-7} internal concentration, a conservative estimate which assumes a linear response to molarity, then only one channel in 10^2 would have to be affected at resonance for an effect to be detected. It should be noted again that the time response would be rapid, on the order of milliseconds. No change in ion current (to less than 1%) was observed for any of the ion resonant conditions. At least three possible reasons exist to explain these negative results: Na and K-channels may not exhibit such resonances, the sensitivity of the measurement may not be sufficient, or the proposed model may not be realistic.

The galvanotropic and galvanotactic responses of several cell types are well known. We reported at this conference three years ago (Parkinson and Hanks, 1986) on the positive response we found for embryonic quail somitic fibroblasts and for ROS 17/2.8 cells at 4.5 volts/cm, and the negative response for L929, CHO, Balb/c 3T3, and fetal rat calvarium cells at the same 4.5 volts/cm. We have recently looked again at L929 cells at 13.1 volts/cm and at ROS 17/2.8 osteoblasts and ROS 25/1 fibroblasts with and without calcium in the medium. Two values of the electric field were used for the ROS cells; 5.0 volts/cm and 13.1 volts/cm. The results are summarized in Table I and the response of ROS 17/2.8 at E = 13.1 volts/cm is reproduced in Figure 8. Cell alignment was determined as a function of time from time-lapse photography by projecting a frame onto a viewing table and, using a protractor, measuring the angle between the long axis of a cell and the direction of the electric field. In general if alignment occurs a large fraction of the cells, as in Figure 8, will align to within a few degrees of the field direction. For "no response" essentially no cells show a change in angle during the time of exposure to the field.

The galvanotropic response at the low field value is minimal, while at the higher value the response is significant, but only if calcium is present. This is in agreement with the results of Cooper and Schliwa (1986) and Onuma and Hiu (1986), who pointed out the essentiality of calcium. These measurements are preliminary to measurements on the change in cytosolic calcium, measured with the fura2 technique, under the action of a DC electric field, a pulsed DC field, and a pulsed AC electric field. The galvanotaxis chambers shown in Figure 9, necessarily designed with thin plastic windows, have the disadvantage in that there is no heat sink for the power developed in the channel and as a result it is difficult to control the temperature. The chamber in Figure 9(a) is horizontal and was used in the time lapse studies reported here. The vertical chamber in Figure 9(b) is designed for use in the SLM-8000C spectrofluorometer. The 2% agar bridges were made with either ROS culture medium,

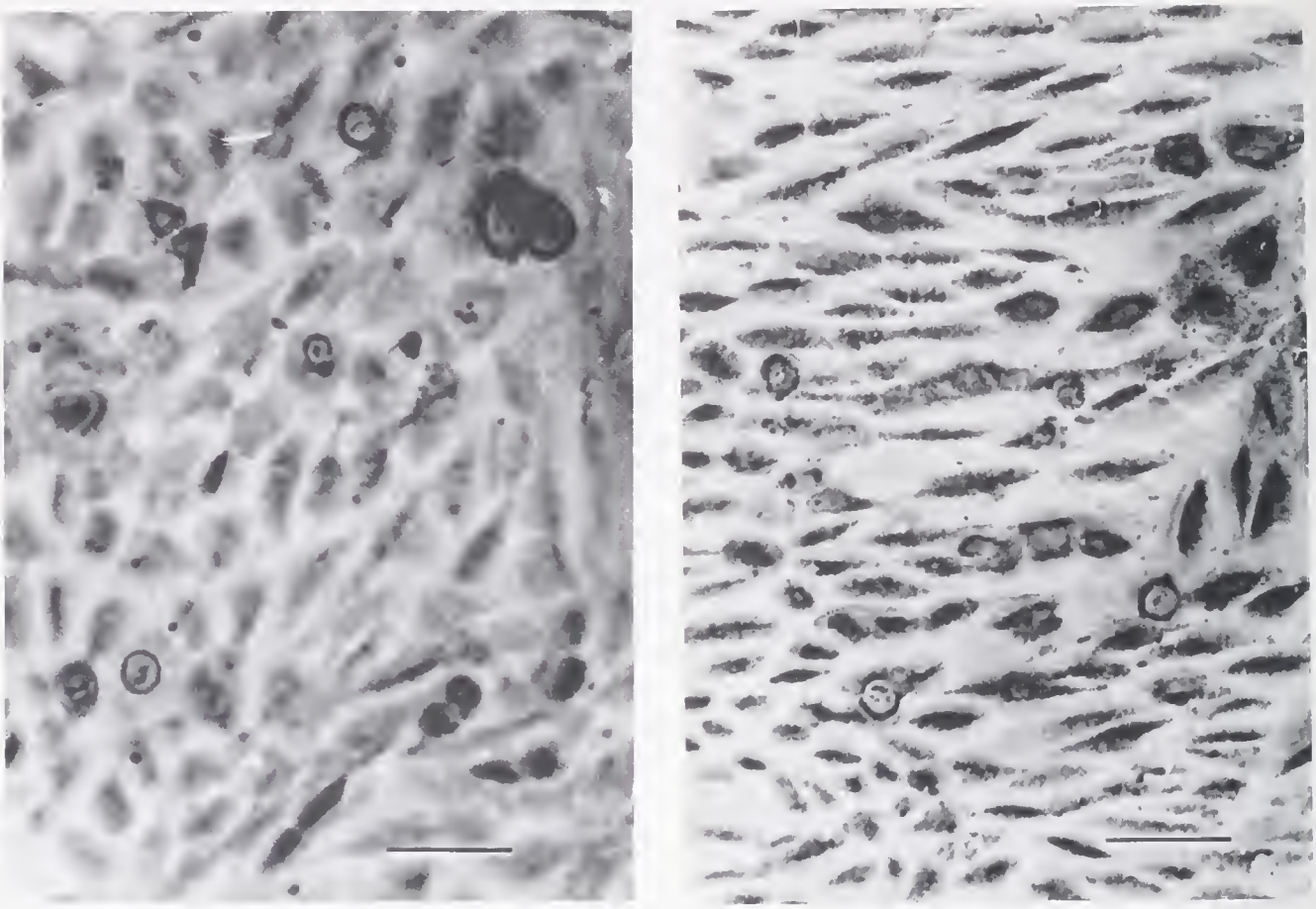

Figure 8. Galvanotropic response of ROS osteoblasts 17/2.8 at 13.1 V/cm. (Left) t = 0 before field; (right) at t = 260 min.

Hallam's with 1.3 m*M* calcium added, or Hallam's without calcium. Because the Noble agar contained 11.0 μg/ml calcium, it was dialyzed, reducing the calcium concentration to 0.05 μg/ml before being used.

Conclusions and Discussion

In our various measurements we find no effect of AC electromagnetic fields on mammalian cells. The many reported effects of the interaction of *induced* fields (thus no DC component) with the cell system are puzzling since the induced field can produce a net displacement of an ion only through a non-linear response (Parkinson, 1985). It can be shown that a non-linear response can occur, but the DC component will be very small. Consider the ion motion that results from the application of a time-varying magnetic field. Assume an ion of charge q and mass m is immersed in liquid in the midplane of a Helmholtz configuration so that the magnetic field [$B = B_0 + B_1 \sin \omega t$] has only a z-component and therefore the induced electric field $E = E_\phi$ has only a ϕ-component. The forces acting on the ion are the Lorentz force, $q(\vec{E} + \bar{v} \times \bar{B})$, the viscous drag $-f\bar{v}$ and the random molecular bombardment K(t). These forces then give the ion an acceleration, so that

$$m \frac{d\bar{v}}{dt} = -f\bar{v} + K(t) + q(\vec{E} + \bar{v} \times \bar{B}) \qquad (1)$$

where f is the friction coefficient for the viscous drag, K(t) is a fluctuating force of which the average value is zero and which has a sharp correlation function and, thus, essentially a white spectrum. The ratio of the frictional force to the inertial force may be written in terms of $\beta = f/m = 1/\tau$, where τ has the dimensions of time and measures their relative importance. If τ is large (f small or m large, large inertia) the particle will move an appreciable distance in the observation time t under the influence of the driving force. If however the time between collisions is very short then the friction term is large, the inertial term small, and the particles diffuse according to the well known diffusion equation of Einstein. Thus we

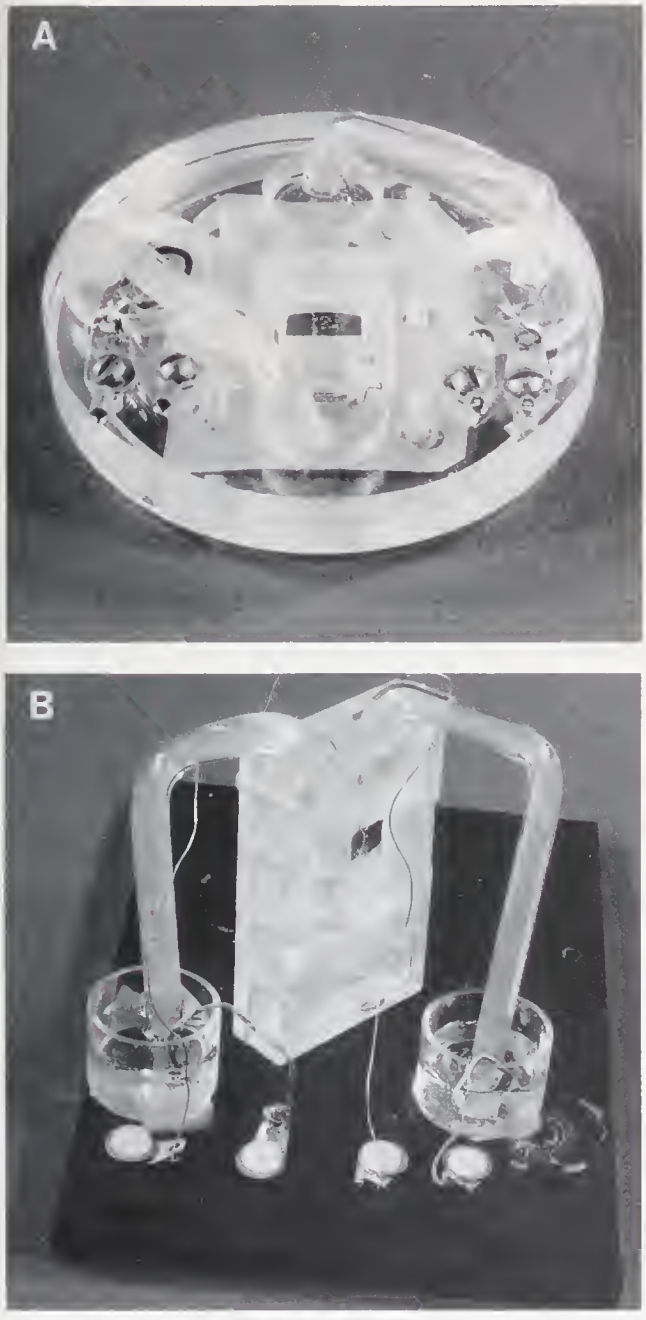

Figure 9. Galvanotaxis chambers (A) horizontal model; (B) vertical model for use in SLM-8000C spectrofluorometer.

have to look at the magnitude of $\beta = 1/\tau$ in liquid. In a gas the assumptions under which the mean free path (λ) and the collision time (τ) are calculated are well justified. In a liquid, while the situation is more complicated, there is evidence for the validity of the random walk model for diffusion (Hildebrand *et al.*, 1970) and the diffusion constant can be related to λ and τ. These considerations give an estimate of $\lambda \sim 10^{-10}$ m, a fraction of a molecular diameter, and $\tau \sim 10^{-13}$ s. The diffusion coefficients and electrophoretic mobility for concanavlin A receptors have been measured by Poo *et al.* (1976) who found values from 10^{-12} and 10^{-14} m^2/s and 2×10^{-5} $\mu m/s/volt/meter$, respectively. The point then is that the inertial term is unimportant. Chiabrera *et al.* (1985) showed, and we have verified*, beginning with equation (1), that there is indeed rectification, that is, a DC term appears in the velocity. The non-linearity necessary to produce the DC component comes through the ($\sin^2 \omega t$) term from the interaction of v_ϕ and B_1. It will be *very* small, however, since its magnitude is proportional to $1/\beta$.

In view of the large value of β, it is difficult to visualize any mechanism for an ion cyclotron resonance (ICR). A cyclotron *resonance* implies that energy is fed into the ion motion at the orbital frequency in such a way as to continue the orbital motion. [If the alternating component of the magnetic field is essential for ICR as suggested by McLeod and Liboff (1986), then the resonance has to be a betatron type acceleration where the energy is fed in during the time of the increasing magnetic field and taken out (the ion deaccelerated) during the alternate half cycle when the field is decreasing.] If the orbital frequency is an integral number higher, so that the ion makes several turns during the rise of the field then energy can be absorbed. This is the case in "cyclotron resonance" in metals. But in metals the mean free path of an electron is much longer than the orbit circumference, or $\omega_c \tau \gg 1$ where $\omega_c = (qB)/m$. However in a metal, and as for our case, if $\omega_c \tau \ll 1$ there will be no resonance. The ion will traverse a small fraction of an orbit before making a collision, it will be scattered, and start again on a new orbit. For the numbers $B_0 = 38$ μT and $f = 29.4$ Hz the radius of curvature of a Ca^{++} ion at rms thermal velocity is 2.2 m. For a radius of curvature corresponding to a channel radius ($\sim 10^{-10}$ m) the component of velocity perpendicular to the magnetic field would be $\sim 2 \times 10^{-8}$ m/s, a very small number. While Ca^{++} ions will find and move through open channels of a few angstroms diameter (such as along the axis of a gramidicin bridge), it is not clear how a "cyclotron resonance" can significantly enhance the process.

It is possible to suggest a simple model that could produce the necessary non-linearity for bone repair. Ions in the medium between bone ends will experience a force due to the AC field (pulsed or sinusoidal) tending to cause the ion to move back and forth. It will, of course, make many collisions with the molecules of the medium, but as for electrical conductivity in a metal there will be a small average displacement. An ion driven to left, say, may be trapped by the bone matrix, which may exert a greater (binding) force on it than the force due to the elec-

* We are indebted to A. C. T. Wu for carrying out this non-trivial calculation.

tric field. This reduces the concentration of the free ions in the medium and because of the concentration gradient, additional ions diffuse into the region. Thus Ca^{++} (or other ions) become available for forming a bolus. It is the randomness of the ion motion, superimposed on the sinusoidal motion due to the electric field, that causes some ions to be trapped by the bone matrix. Note also that ions should be trapped at *each* bone end. Two consequences of this simple model can be tested. First, the time for repair using pulsed EMF should be *much* longer than that required for the DC currents used in invasive surgery, and second, the calcium bolus should build up at *both* ends of the fracture, not just the cathodal end as for the DC case.

Literature Cited

Bassett, C. A. L., S. N. Mitchell, and S. R. Gaston. 1981. Treatment of ununited tibial diaphyseal fractures with pulsing electromagnetic fields. *J. Bone Joint Surg.* **63A:** 511–523.

Bawin, S. A., and W. R. Adey. 1976. Sensitivity of calcium binding in cerebral tissue to weak environmental electrical fields oscillating at low frequency. *Proc. Natl. Acad. Sci. USA* **73:** 1999–2003.

Blackman, C. F. 1985. Biological influences of low frequency sinusoidal electromagnetic signals alone and superimposed on RF carrier waves. Pp. 521–535 in *Interactions Between Electromagnetic Fields and Cells,* A. Chiabrera, C. Nicolini and H. P. Schwann, eds. Plenum, London.

Blackman, C. F., S. G. Benane, J. R. Rabinowitz, D. E. House, and W. T. Joines. 1985. A role for the magnetic field in the radiation-induced efflux of calcium ions from brain tissue *in vitro*. *Bioelectromagnetics* **6:** 327–337.

Chiabrera, A., F. Caratozzolo, G. Giannetti, M. Grattarola, G. Nebiacolombo, and B. Bianco. 1985. Effects of Magnetic Fields on Bioelectrochemical Processes. Trans. of the 5th Bioelectrical Repair and Growth Society Meeting, Boston. P. 17.

Colacicco, G., and A. A. Pilla. 1983. Electromagnetic modulation of biological processes: ATPase function and DNA production by *Raji* cancer cells *in vitro*. *Z. Naturforsch.* **38C:** 468–470.

Cooper, M. S., and M. Schliwa. 1986. Transmembrane Ca^{2+} fluxes in the forward and reversed galvanotaxis of fish epidermal cells. Pp. 311–318 in *Ionic Currents in Development,* R. Nuccitelli, ed. Alan R. Liss, Inc., New York.

Darnell, J., H. Lodish, and D. Baltimore. 1986. *Molecular Cell Biology.* Scientific American Books. 732 pp.

Dawson, David C. 1987a. Cellular mechanisms for K transport across epithelial cell layers. *Sem. Nephrol.* **7:** 185–192.

Dawson, David C. 1987b. Properties of epithelial potassium channels. *Curr. Top. Mem. Trans.* **28:** 41–71.

Erickson, C. A., and R. Nuccitelli. 1984. Embryonic fibroblast motility and orientation can be influenced by physiological electric fields. *J. Cell Biol.* **98:** 296–307.

Grynkiewicz, G., M. Poenie, and R. Y. Tsien. 1985. A new generation of Ca^{2+} indicators with greatly improved fluorescence properties. *J. Biol. Chem.* **260:** 3440–3450.

Hanley, K., L. A. Norton, and G. A. Rodan. 1981. Electromagnetic field effects on periosteal and osteoblast-like cells. *J. Dent. Res.* **60**(A): 402.

Hildebrand, J. H., J. M. Prausnitz, and R. L. Scott. 1970. *Regular and Related Solutions.* Van Nostrand, New York. Pp. 36–39.

Liboff, A. R. 1985. Geomagnetic cyclotron resonance in living cells. *J. Biol. Phys.* **13:** 99.

Liboff, A. R., and W. C. Parkinson. 1988. Search for ion cyclotron resonance in turtle colon. *Bioelectromagnetics* (in press).

McLeod, B. R., and A. R. Liboff. 1986. Dynamic characteristics of membrane ions in multifield configurations of low-frequency electromagnetic radiation. *Bioelectromagnetics* **7:** 177–189.

McLeod, B. R., S. D. Smith, K. E. Cooksey, and A. R. Liboff. 1987. Ion cyclotron resonance frequencies enhance Ca^{++}-dependent motility in diatoms. *J. Bioelectricity* **6:** 1–12.

Onuma, E. K., and S. W. Hui. 1986. The effects of calcium on electric field-induced cell shape changes and preferential orientation. Pp. 319–327 in *Ionic Currents in Development,* R. Nuccitelli, ed. Alan R. Liss, Inc., New York.

Parkinson, W. C. 1983. Motility of mouse fibroblasts in tissue culture. *Biophys. J.* **42:** 17–23.

Parkinson, W. C. 1985. Electromagnetic fields in biological studies. *Ann. Biomed. Eng.* **13:** 491–514.

Parkinson, W. C., and C. T. Hanks. 1986. Response of primary and transformed cells to electromagnetic fields. Pp. 329–336 in *Ionic Currents in Development,* R. Nuccitelli, ed. Alan R. Liss, New York.

Parkinson, W. C., and C. T. Hanks. 1988. Search for cyclotron resonance in cells *in vitro*. *Bioelectromagnetics* **10**(2).

Poo, M. M., W. H. Poo, and J. W. Lam. 1978. Lateral electrophoresis and diffusion of concanavalin A receptors in the membrane of embryonic muscle cell. *J. Cell Biol.* **76:** 483–501.

Rasmussen, H., and P. Q. Barrett. 1984. Calcium messenger system: an integrated view. *Physiol. Rev.* **64:** 938–984.

Urry, D. W., C. M. Venkatachalam, A. Spisni, P. Läuger, and M. A. Khaled. 1980. Rate theory calculations of gramicidin single-channel currents using NMR-derived rate constants. *Proc. Natl. Acad. Sci. USA* **77:** 2028–2032.

Reference: *Biol. Bull.* **176(S):** 179–183. (April, 1989, Suppl.)

Electrical Fields in the Vicinity of Small Wounds in *Notophthalmus viridescens* Skin

MEICHENG CHIANG[1], E. J. CRAGOE JR.[2], AND JOSEPH W. VANABLE JR.[1]

[1]*Department of Biological Sciences, Purdue University, West Lafayette, Indiana 47907 and*
[2]*2211 Oak Terrace Drive, Lansdale, Pennsylvania 19446*

Abstract. The transepithelial potential (TEP) across the skin of *Notophthalmus viridescens* hindlimb digits was measured in animals immersed in artificial pond water (APW) that was 1.5 m*M* in NaCl, 0.06 m*M* in KCl, and 0.1 m*M* in $CaCl_2$, before and after making a wound in the digit tip. Before wounding, the TEP of the digit skin averaged 35.3 mV ± 5.5 mV (S.E.M.), inside positive. After wounding, the TEP at locations distant from the wound approximated the TEP before wounding, but, at points progressively closer to the wound surface, the measured TEP was progressively less. The slope of this change in TEP, the lateral wound potential, averaged 41.7 mV/mm ± 9.5 mV/mm, with the regions closer to the wound being more negative than those away from the wound. When the Na^+ channels of the outer surface of the external epidermal cells were blocked with benzamil (30 μM in APW), the TEP of the unwounded skin was reversed, to an average of −14.1 mV ± 3.7 mV (inside negative). After benzamil-blocked digits were wounded, the lateral wound potentials averaged −21.5 mV/mm ± 4.0 mV/mm, with the polarity reversed: regions close to the wound were more positive than those away from the wound. The magnitudes of both the normal and the reversed wound fields are greater than those known to promote the migration of cells *in vitro*. What remains to be determined is how *Notophthalmus viridescens* epidermal cells and fibroblasts behave in such fields, and how this behavior relates to the process of wound healing under normal and modulated wound field conditions.

Introduction

Wound healing is a process that is simpler than most developmental events, but it nevertheless is crucial for the well-being of organisms (Needham, 1964). Breaks in the integument that compromise the protective barrier it provides against the external world must be repaired. It is therefore of some interest to discover ways in which this repair process can be facilitated, particularly under pathological conditions that interfere with normal wound healing. Over the past 20 years, reports have appeared in the literature that describe an acceleration of mammalian wound healing by applying relatively steady electrical currents to wounds (reviewed by Carley and Wainapel, 1985, and by Vanable, 1989). However, the development of a rationale for why electric fields should promote wound healing is in its infancy, and controlled experiments exploring this issue have just begun.

The skin of vertebrates maintains a transepithelial potential (TEP) across itself, chiefly by virtue of the ability of its epidermis to transport Na^+ electrogenically from the water in which it is immersed into the interior (Kirschner, 1983). This TEP provides the electromotive force to drive currents from wounds made in the skin. L. R. Robinson (1985) described a reduction in the rate of healing of wounds made in the skin of adult *Notophthalmus viridescens* when these wound currents are attenuated by benzamil blocking of the channels through which the transported Na^+ enters the outer epidermal cells (Eltinge *et al.*, 1986). More recently, Stump and K. R. Robinson (1986) and Rajnicek *et al.* (1988) found that wound healing of *Xenopus* embryos is retarded or prevented when these Na^+-dependent currents are reduced, either by blocking of Na^+ transport with ouabain, by substituting choline for Na^+, or by Na^+ channel blocking with amiloride or benzamil. These observations are consistent with the hypothesis that there is an electrical component to wound healing.

However, it is not likely that the wound currents themselves are instrumental in promoting wound healing.

Rather, cells are able to respond to electrical fields, by growing or migrating toward one pole or the other (reviewed by K. R. Robinson, 1985). Generally speaking, a response to such imposed fields by cells in culture can first be detected at field strengths of 5 to 10 mV/mm; at somewhat higher field strengths, the response becomes more robust. Therefore, worthwhile questions to ask are whether fields exist in the tissue bordering wounds that are sufficient to promote the cell migration that must occur during wound healing, and, if so, what effect modulating such fields has on wound healing. Such fields would have to be proximo-distal, and, at least as a first approximation, have strengths of at least 5 to 10 mV/mm to be reasonable candidates for promoting cell migration from the non-wounded area into the wound. The polarity of such wound fields should be a consideration, also (Vanable, 1989), since cells usually migrate to one pole or the other in a field. (However, there are hints that epidermal cells may migrate both to the anode and cathode in culture [K. R. Robinson, 1985].)

Barker *et al.* (1982) measured such lateral fields in the skin of guinea pigs, and found them to be of ample strength: *ca.* 150 mV/mm. However, except for the measurements of McGinnis and Vanable (1986b) made in the vicinity of the very drastic wounds made by limb amputation, data for lateral wound fields in amphibians, with which most of the controlled experiments on electrical aspects of wound healing have been done, are lacking.

We report here our early results with measuring lateral fields in the vicinity of relatively small wounds made in the skin of *Notophthalmus viridescens*, and the effect that is produced on these lateral fields by interfering with the skin's ability to generate a normal Na^+-dependent TEP with the Na^+ channel blocker, benzamil.

Materials and Methods

Notophthalmus viridescens adults, purchased from Charles D. Sullivan Co., Inc., Nashville, Tennessee, were maintained in tap water conditioned with Novaqua (Kordon, Hayward, California) and fed liver twice a week. They were anesthetized in 0.02% benzocaine dissolved in an artificial pond water (APW) with 1% ethanol (Vanable, 1985). The APW used for measuring the lateral potentials was 1.5 m*M* in NaCl, 0.06 m*M* in KCl, and 0.1 m*M* in $CaCl_2$ (anhydrous; contains 1% Mg salts). Na^+ channels were blocked by immersion in 30 μM benzamil, which is 3,5-diamino-6-chloro-*N*-{amino[(phenylmethyl)amino]-methylene}pyrazinecarboxamide, in this APW. Benzamil was synthesized by the method of Cragoe *et al.* (1967), and isolated as the hydrochloride sesquihydrate. The effects of benzamil on Na^+ channels and Na^+-dependent currents are described by Cuthbert and Fanelli (1978) and by Eltinge *et al.* (1986). Wounds *ca.* 0.25 mm in diameter were made by slicing the tip of a hindlimb digit with a piece of a razor blade (Gillette Super Blue Blade). Lateral potentials were measured by essentially the same standard microelectrode technique used by McGinnis and Vanable (1986a, b): the TEP across the skin was measured before wounding, and then again after wounding, at five positions: at the cut surface of the wound, and at 0.25, 0.5, 1.0, and 2.0 mm from the cut surface. To facilitate the microelectrode penetrations, the digit was gently kept in place by a fine glass rod imbedded in dental wax affixed to the bottom of the measuring chamber to either side of the foot. The microelectrodes used to penetrate the skin had a resistance of 1 to 3 megohms, and were pulled from WPI 1B120F 1.2 mm capillary tubing, back-filled with 3 *M* KCl, and connected to a differential electrometer (Model 750 Dual Microprobe Amplifier, WPI, Inc., New Haven, Connecticut) via a Ag/AgCl half cell in a WPI microelectrode holder. These relatively low-resistance electrodes had low tip potentials (less than 1 mV difference between intact and broken electrode readings) and salt sensitivity (less than 1 mV difference between APW and 3 *M* KCl readings). The reference electrode, positioned in the water in which the animal was immersed, was a very low resistance broken microelectrode similarly connected to the other input of the electrometer. Previous experiments (McGinnis and Vanable, 1986a) have shown that TEPs measured with an external reference electrode do not differ from those made with an internal reference (Silastic tubing filled with Ringer's). The external reference was used in the present experiments because it is less debilitating to the animal than such an internal reference. The electrometer was grounded to the bath via a large Ag/AgCl electrode. The measured potentials were displayed on a digital storage oscilloscope (Model 2221, Tektronix, Portland, Oregon). They are reported here as the mean ± S.E.M. For repeated measurements as healing occurred, animals were kept anesthetized by periodic immersions in benzocaine, so as to avoid damage to the healing wound by ambulatory movements.

Results

The TEP of the digit skin before wounding averaged 35.3 mV ± 5.5 mV (range, 8.2 to 54.3 mV). This is somewhat lower than the 66 mV ± 3 mV found for limb skin by McGinnis and Vanable (1986b), possibly because of the lower $[Ca^{++}]$ used in the APW of the present experiments (Eltinge *et al.*, 1986). However, the lateral potentials found under the skin in the vicinity of digit tip wounds (Fig. 1) were similar to those found in the vicinity of the much larger wounds produced by limb amputation: the average lateral potential in the distal-most 0.25

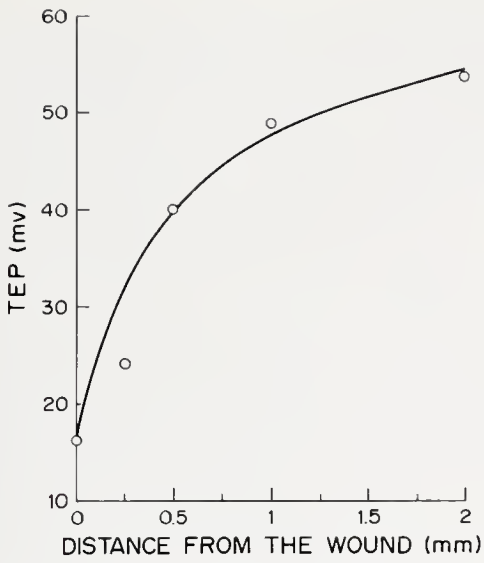

Figure 1. Lateral wound potential in normal newt skin. A wound *ca.* 0.25 mm in diameter was made in the middle hindlimb digit tip, and the transepithelial potential of the skin was measured at 0, 0.25, 0.5, 1, and 2 mm from the edge of the wound. The slope of the potential difference between the edge of the wound and a point 0.25 mm away from the wound is taken as the lateral wound potential. In this case, the lateral wound potential was 66 mV/mm.

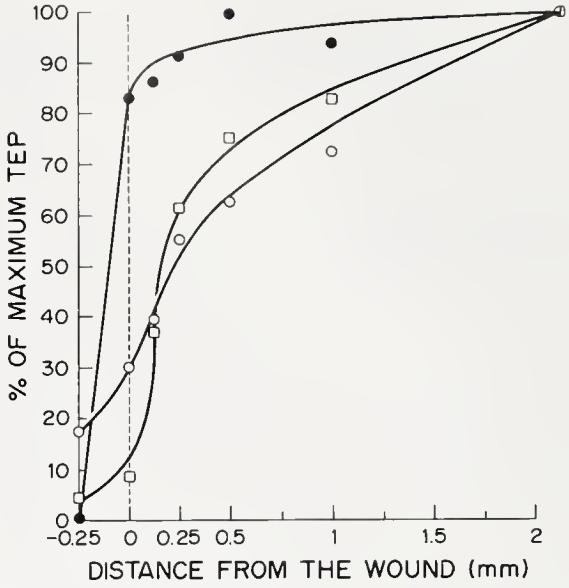

Figure 2. Change in lateral wound potential with healing. ○, within ½ hour after wounding; □, 1½ hours after wounding; ●, 3½ hours after wounding. The vertical dashed line represents the wounding plane. A wound *ca.* 0.25 mm in diameter was made in the middle hindlimb digit tip, and the transepithelial potential of the skin was measured at 0, 0.25, 0.5, 1, and 2 mm from the edge of the wound at the times indicated above. An additional measurement of the potential between the recording electrode and the reference in the bath was taken 0.25 mm away from the surface of the wound. As healing nears completion, most of the potential drop between the subintegumentary region and the bath occurs across the epithelium that covers the wound.

mm of the wounded digit tip one-half hour after wounding was 41.7 mV/mm ± 9.5 mV/mm (range, 10 mV/mm to 88 mV/mm; n = 10). The comparable value for the stump fields was *ca.* 48 mV/mm (calculated from McGinnis and Vanable, 1986b). As wound healing occurred, more and more of the lateral potential drop occurred across the wound epithelium, rather than along the distal-most skin proximal to the wound (Fig. 2), as was the case with the healing of the limb amputation wounds studied by McGinnis and Vanable (1986b).

When sodium channels were blocked with 30 μM benzamil in APW containing 0.1 mM $CaCl_2$, the overall TEP diminished drastically, and usually reversed, so that the subintegumentary region was negative with respect to the outside (Fig. 3). A series of 8 measurements yielded a value of −14.1 mV ± 3.7 mV (range, −29.0 mV to +1.6 mV) for the TEP of the digit skin before wounding. One-half hour after wounding, the lateral potential in the first 0.25 mm from the edge of the wound averaged −21.5 mV/mm ± 4.0 mV/mm (that is, in contrast to the normal situation, the region close to the wound's edge was more positive than regions away from the edge), with a range of −35.2 mV/mm to −4.0 mV/mm.

Discussion

If the cells that migrate to heal wounds in newt skin are as sensitive to electrical fields as typically are cells *in vitro*, then the normal lateral wound fields that were observed here should be of sufficient strength to have an effect on their migration. The value of 42 mV/mm in the

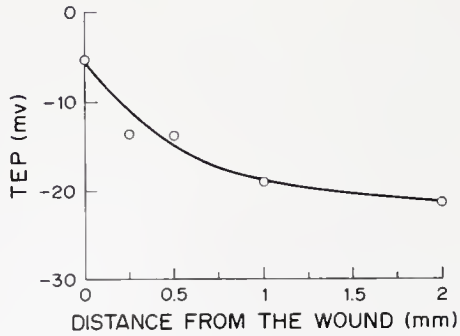

Figure 3. Lateral wound potential with the Na^+ channels of the outer cells of the epidermis blocked with 30 μM benzamil. A wound *ca.* 0.25 mm in diameter was made in the middle hindlimb digit tip, and the transepithelial potential of the skin was measured at 0, 0.25, 0.5, 1, and 2 mm from the edge of the wound. The slope of the potential difference between the edge of the wound and a point 0.25 mm away from the wound is taken as the lateral wound potential. In this instance, the lateral wound potential was −21.6 mV/mm (the negative sign conveys the fact that the polarity of this field is opposite that of the normal wound potentials).

first 0.25 mm is actually somewhat conservative; in the case of measurements of limb stump fields (McGinnis and Vanable, 1986b) in which TEP readings were made at 0.125 mm from the edge of the wound, the average lateral field between the surface of the wound and this point was *ca.* 60 mV/mm, while the field between the surface of the wound and 0.25 mm was *ca.* 48 mV/mm. Therefore, the magnitude of the fields we measured was at least 3 to 4 times greater than the *ca.* 10 mV/mm typically seen as the field strength to which cells just begin to respond *in vitro* (K. R. Robinson, 1985). Furthermore, it is conceivable that *in vivo,* cells could be more responsive to fields than they are *in vitro* (Borgens *et al.,* 1983).

In the vicinity of wounds made in skin immersed in APW that was 30 μM in benzamil, the average lateral field strength of *ca.* −22 mV/mm was less in absolute value than that measured without Na^+ channel blocker, but still greater than the field strengths that affect cell migration *in vitro.* However, it must be emphasized that the polarity of these fields, more positive at the wound than at locations away from the wound, is the opposite of those in animals with normally functioning Na^+ channels. This is because the overall polarity of the TEP is reversed (it is inside negative), probably because Cl^- transport is dominating under the conditions of Na^+ channel blocking and the relatively low Ca^{++} (0.1 mM) in the APW used in these experiments (Eltinge *et al.,* 1986).

In vitro, cells whose migration is affected by the imposition of fields typically migrate towards the cathode (K. R. Robinson, 1985). That is, their migration would be appropriate in fields of the polarity found in animals with normally functioning Na^+ channels. However, this is not true for all the cell types that contribute to wound healing. While Cooper and Schliwa (1985) found that epidermal cells isolated from fish scales migrate toward the cathode in field strengths ranging from 50 to 1500 mV/mm, Muncy and Robinson (unpub.; discussed by K. R. Robinson, 1985) observed significant numbers of epidermal cells isolated from *Xenopus* larval skin migrating to the anode, as well as toward the cathode. Fibroblasts (from embryonic quail somites) migrate toward the cathode, even (in half the trials) at field strengths as low as 1 mV/mm (Nuccitelli and Erickson, 1984; Erickson and Nuccitelli, 1984). On the other hand, macrophages may well migrate toward the anode (Dineur, 1892; Orida and Feldman, 1982), as do leucocytes (Fukushima *et al.,* 1953), although activated macrophages apparently migrate preferentially to the cathode (Dineur, 1892).

Therefore, in comparing newt wound healing under normal and reversed-field conditions, one might expect that epithelization could occur in both situations, if the *Xenopus* observations cited above hold in this instance. On the other hand, the expectation would be that fibroblast migration into the wound to produce connective tissue should (if quails may serve as a model) be enhanced in normal wound fields, but impaired in fields that are reversed. Leucocytes and unactivated macrophages should be caused to migrate away from the wound region under normal conditions, but the migration of activated macrophages into the wound region should be promoted, if the observations described above apply to newts.

Epithelization is perhaps the most readily studied aspect of wound healing, and there are observations with amphibians that suggest that this process is promoted by wound fields: when the skin's generation of a TEP is impaired, either by Na^+ channel blocking (L. R. Robinson, 1985; Stump and K. R. Robinson, 1986; Rajnicek *et al.,* 1988), or by inhibition of Na^+ transport with ouabain and by substitution of choline for Na^+ (Stump and K. R. Robinson, 1986; Rajnicek *et al.,* 1988), epithelization is impaired. Stump and K. R. Robinson (1986) have, in addition, carried out early experiments in "rescuing" wound healing in diminished-current *Xenopus* neurulae by injecting current via a microelectrode.

However, measurements of lateral wound potentials were not made in any of these experiments, although Rajnicek *et al.* confirmed that blocking Na^+ channels of the epidermis of their wounded neurulae with 10 μM amiloride decreased the normal TEP by 70%, and resulted in a 70% decrease in their wound currents. In L. R. Robinson's experiments (1985), wound currents were measured and used as an index of healing: as the epidermis covers the wound, it impedes the flow of current (McGinnis and Vanable, 1986a). In these experiments, APW that was 0.5 mM in Ca^{++} was used, and wound currents of reversed direction were observed when Na^+ channels were blocked with benzamil. Therefore, the TEPs and lateral wound potentials would also have been reversed under these conditions. However, it is likely that, with 0.5 mM Ca^{++} in the APW, the magnitude of the reversed TEPs and the lateral wound potentials would not have been as great as in the present series of measurements with 0.1 mM Ca^+ APW. These experiments must be extended by modulating TEPs so that they range from strongly positive (for instance, with increased Na^+ and Ca^{++}, and with salts in which nonpermeant gluconate ion is substituted for Cl^-) through strongly negative (for instance, by increasing the Cl^- with greater than 1.5 mM NaCl while still blocking Na^+ channels). It should also be possible to modulate TEPs, and therefore also the lateral wound potentials and healing rates, with current injected from an external source. By examining the rate of wound healing under these conditions of strong normal and reversed fields, as well as with fields whose strengths are close to zero, it should be possi-

ble to clarify the role of electrical fields and their polarity in the process of wound healing. It is also important to initiate studies of the behavior of cultured newt cells when fields are imposed on them, particularly epidermal cells and fibroblasts, since they are so crucial for wound repair. Knowing this behavior will be essential for properly interpreting the effect of modulating *in vivo* wound fields on wound healing.

Understanding mammalian wound healing must be one of the ultimate goals of this research. The data provided by Barker *et al.* (1982) are a good beginning, but differences in mammalian skin circuitry (discussed in Vanable, 1989) raise the question of which direction mammalian epidermal cells should migrate in an imposed field. Since the lateral fields measured by Barker *et al.* were on the return leg of the current path, their polarity is opposite to that measured in the newts (Jaffe and Vanable, 1984; Vanable, 1989). Therefore, it is of considerable interest to examine the behavior of cultured mammalian epidermal cells in imposed fields, as well as to examine mammalian wound healing with modulation of their lateral wound fields *in vivo*.

The fruit of these endeavors, in addition to clarifying our understanding of aspects of cell and developmental biology, should be the development of a rationale for the existing but little-used clinical protocols for the promotion of wound healing by supplying steady direct currents to these wounds. With a more solid footing, the potential exists for improving these procedures and their acceptance by clinicians.

Acknowledgments

Supported by NSF grant PCM 8311002, and by gifts from R. J. Platt Sr. and the Exxon Corporation.

Literature Cited

Barker, A. T., L. F. Jaffe, and J. W. Vanable Jr. 1982. The glabrous epidermis of cavies contains a powerful battery. *Am. J. Physiol.* **242:** R358–R366.

Borgens, R. B., M. F. Rouleau, and L. E. DeLanney. 1983. A steady efflux of ionic current predicts hind limb development in the axolotl. *J. Exp. Zool.* **228:** 491–503.

Carley, P. J., and S. F. Wainapel. 1985. Electrotherapy for acceleration of wound healing: Low intensity direct current. *Arch. Phys. Med. Rehabil.* **66:** 443–446.

Cooper, M. S., and M. Schliwa. 1985. Electrical and ionic controls of tissue cell locomotion in DC electric fields. *J. Neurosci. Res.* **13:** 223–244.

Cragoe, E. J., Jr., O. W. Woltersdorf Jr., J. B. Bicking, S. F. Kwong, and J. H. Jones. 1967. Pyrazine diuretics. II. N-amidino-3-amino-5-substituted-6-halopyrazinecarboxamides. *J. Med. Chem.* **10:** 66–75.

Cuthbert, W. W., and G. M. Fanelli. 1978. Effects of some pyrazinecarboxamides on sodium in frog skin. *Br. J. Pharmacol.* **63:** 139–149.

Dineur, E. 1892. Note sur la sensibilité des leucocytes à l'électricité. *Bull. Seances Soc. Belge Microscop. (Bruxelles)* **18:** 113–118.

Eltinge, E. M., E. J. Cragoe Jr., and J. W. Vanable Jr. 1986. Effects of amiloride analogues on adult *Notophthalmus viridescens* limb stump currents. *Comp. Biochem. Physiol.* **89A:** 39–44.

Erickson, C. A. and R. Nuccitelli. 1984. Embryonic fibroblast motility and stimulation can be influenced by physiological electric fields. *J. Cell Biol.* **98:** 296–307.

Fukushima, K., N. Senda, H. Inui, H. Miura, Y. Tamai, and Y. Murakami. 1953. Studies on galvanotaxis of leukocytes. I. Galvanotaxis of human neutrophilic leukocytes and methods of its measurement. *Med. J. Osaka Univ.* **4:** 195–208.

Jaffe, L. F., and J. W. Vanable Jr. 1984. Electric fields and wound healing. *Clin. Dermatol.* **2:** 34–44.

Kirschner, L. B. 1983. Sodium chloride absorption across the body surface: frog skins and other epithelia. *Am. J. Physiol.* **244:** R429–R443.

McGinnis, M. E., and J. W. Vanable Jr. 1986a. Wound epithelium controls stump currents. *Dev. Biol.* **116:** 174–183.

McGinnis, M. E., and J. W. Vanable Jr. 1986b. Electrical fields in *Notophthalmus viridescens* limb stumps. *Dev. Biol.* **116:** 184–193.

Needham, A. E. 1964. Biological considerations of wound healing. Pp. 1–29 in *Advances in Biology of Skin, Vol. 5, Wound Healing,* W. Montagna and R. F. Billingham, eds., Pergamon Press, Oxford.

Nuccitelli, R., and C. W. Erickson. 1983. Embryonic cell motility can be guided by physiological electrical fields. *Exp. Cell Res.* **147:** 195–201.

Orida, N., and J. D. Feldman. 1982. Directional protrusive pseudopodial activity and motility in macrophages induced by extracellular electric fields. *Cell Motility* **2:** 243–255.

Rajnicek, A. M., R. F. Stump, and K. R. Robinson. 1988. An endogenous sodium current may mediate wound healing in *Xenopus* neurulae. *Dev. Biol.* **128:** 290–299.

Robinson, K. R. 1985. The responses of cells to electrical fields: a review. *J. Cell Biol.* **101:** 2023–2027.

Robinson, L. R. 1985. The effects of electrical fields on wound healing in *Notophthalmus viridescens.* M.S. Thesis, Purdue University, viii + 48 pp.

Stump, R. F. and K. R. Robinson. 1986. Ionic current in *Xenopus* embryos during neurulation and wound healing. Pp. 223–230 in *Ionic Currents in Development,* R. Nuccitelli, ed. A. R. Liss, New York.

Vanable, J. W., Jr. 1985. Benzocaine: an excellent amphibian anesthetic. *Axolotl Newsletter* **14:** 19–21.

Vanable, J. W., Jr. 1989. Integumentary potentials and wound healing. Pp. 171–224 in *Electric fields in Vertebrate Repair,* R. B. Borgens, K. R. Robinson, J. W. Vanable Jr., and M. E. McGinnis, eds. Alan R. Liss, New York.

INDEX

A

Algae, 5
Applied electric fields, 150

B

Bioelectrical current, 31
BJÖRKMAN, THOMAS, The use of bioelectric currents to study gravity perception in roots, 49
Blattella germanica, 96
BOWDAN, E., see J. G. Kunkel, 96
BROWNLEE, COLIN, Visualizing cytoplasmic calcium in polarizing zygotes and growing rhizoids of *Fucus serratus,* 14
Bryopsis, 41

C

Calcium and early development in fucoid algae, 5
Calcium buffer injections arrest fucoid egg development by suppressing calcium gradients, 9
Calcium concentration gradients in development, 5–30
Calcium control of pollen tube tip growth, 18
Calcium wave in activating hamster eggs, 21
Calcium, 103
Cell cycle, 103
Cell motility, 130
Charge-dependent molecular movement through intercellular bridges in *Drosophila* follicles, 71
CHEN, T.-H., see J. E. Speksnijder, 9
CHIANG, MEICHENG, E. J. CRAGOE JR., AND JOSEPH W. VANABLE JR., Electrical fields in the vicinity of small wounds in *Notophthalmus viridescens* skin, 179
Closterium, 36
COOPER, MARK S., JOHN P. MILLER, AND SCOTT E. FRASER, Electrophoresis of cytoplasmic molecules through gap junctions by externally applied electric fields, 150
CORK R. J., A. F. STRAUTMAN, AND K. R. ROBINSON, Measuring cytoplasmic calcium: a review of three methods with emphasis on the practical aspects of their use, 25
CRAGOE, E. J., JR., see Meicheng Chiang, 179
Cyclotron resonance, 170
Cytoskeleton, 145

D

DE LOOF, ARNOLD, see Barend Verachtert, 91
Desmids, 36
DIEHL-JONES, W., AND E. HUEBNER, Pattern and composition of ionic currents around ovarioles of the hemipteran, *Rhodnius prolixus* (Stahl), 86
DOHMEN, M. R., see D. Zivkivic, 103
DOVER, PHILIPPA J., see Colin D. McCaig, 140
Drosophila egg chamber: external ionic currents and the hypothesis of electrophoretic transport, the, 79
Drosophila follicles, 71

E

Electric currents associated with directed migration of fibroblasts, 123
Electric field, 110
Electric field-induced redistribution of ACh receptors on cultured muscle cells: electromigration, diffusion, and aggregation, 151
Electric fields, 145
Electrical fields in the vicinity of small wounds in *Notophthalmus viridescens* skin, 179
Electromagnetic fields, 170
Electrophoresis of cytoplasmic molecules through gap junctions by externally applied electric fields, 150
Electrophoretic transport, 79
Elongation of initially non-polar protoplasts is oriented by electric fields, 145
Experiments on the interaction of electromagnetic fields with mammalian systems, 170
Extracellular calcium levels strongly influence neural crest cell galvanotaxis, 130
Extracellular electrical currents in the chick blastoderm, 118

F

FRASER, SCOTT, E., see Mark S. Cooper, 150; Jes Stollberg, 157
Fucus serratus, 14
Fungal growth, 31

G

Galvanotaxis, 130
Galvanotropism and galvanotaxis in development and regeneration, 130–183
Gap junctions, 150
GOW, NEIL, A. R., Relationship between growth and the electrical current of fungal hyphae, 31
Gravitropism, 49

H

HANKS, C. T., see W. C. Parkinson, 170
HISHINUMA, TASUKU, see Tomoki Nawata, 41
HUEBNER, E., see W. Diehl-Jones, 86
HUSH, JULIA M., AND ROBYN L. OVERALL, Steady ionic currents around pea (*Pisum sativum* L.) root tips: the effects of tissue wounding, 56

I

Intercellular bridges, 71
Intra- and extracellular electrical fields of vitellogenic polytrophic insect follicles, 91
Ion currents and cell polarity in insects, 71–102
Ion currents and cell polarity in other animal systems, 103–129
Ion currents and cell polarity in plant systems, 31–70
Ion currents and growth regulators in plant root development, 65

Ionic control of postsynaptic differentiation in muscle, 126
Ionic currents around developing embryos of higher plants in culture, 46
Ionic currents during regeneration of thallus and rhizoid from cell segments isolated from the marine alga *Bryopsis,* 41
Ionic currents in *Lymnaea stagnalis* eggs during maturation divisions and first mitotic cell cycle, 103

J

JAFFE, L. F., see Speksnijder, 9; Preface, 1

K

KROPF, DARRYL L., Calcium and early development in fucoid algae, 5
KŮCERA, PAVEL, AND YVES DE RIBAUPIERRE, Extracellular electrical currents in the chick blastoderm, 118
KUNKEL, J. G., AND E. BOWDAN, Modeling currents around vitellogenic oocytes of the cockroach, *Blattella germanica,* 96

L

Large ionic currents leave the primitive streak of the 7.5-day mouse embryo, 110
Lymnaea stagnalis, 103

M

MCCAIG, COLIN D., On the mechanism of nerve galvanotropism, 136
MCCAIG, COLIN D., AND PHILIPPA J. DOVER, On the mechanism of oriented myoblast differentiation in an applied electric field, 140
Measuring cytoplasmic calcium: a review of three methods with emphasis on the practical aspects of their use, 25
Membrane transport, 170
Micrasterias, 36
MILLER, ANDREW L., Ion currents and growth regulators in plant root development, 65
MILLER, JOHN P., see Mark S. Cooper, 150
MIYAZAKI, SHUN-ICHI, Calcium wave in activating hamster eggs, 21
Modeling currents about vitellogenic oocytes of the cockroach, *Blattella germanica,* 96
Molecular interactions on the cell surface revealed by electrophoresis, 164
Mollusca, 103
MYERS, JEFFREY, see Timothy Ryan, 164

N

NAWATA, TOMOKI, TASUKU HISHINUMA, AND SHUNJI WADA, Ionic currents during regeneration of thallus and rhizoid from cell segments isolated from the marine alga, *Bryopsis,* 41
Neural crest cells, 130
Notophthalmus viridescens, 179
NUCCITELLI, RICHARD, AND TANYA SMART, Extracellular calcium levels strongly influence neural crest cell galvanotaxis, 130
NUCCITELLI, RICHARD, see Glen K. Winkel, 110

O

OHNO-SHOSAKU, TAKAKO, see Shigetoshi Oiki, 123
OIKI, SHIGETOSHI, TAKAKO OHNO-SHOSAKU, AND YASUNOBU OKADA, Electric currents associated with directed migration of fibroblasts, 123
OKADA, YASUNOBU, see Shigetoshi Oiki, 123
On the mechanism of nerve galvanotropism, 136
On the mechanism of oriented myoblast differentiation in an applied electric field, 140
Oogenesis, *Drosophila,* 79
Ovariole, 86
OVERALL, ROBYN L., see Julia M. Hush, 56; Rosemary G. White, 145

P

PARKINSON, W. C., AND C. T. HANKS, Experiments on the interaction of electromagnetic fields with mammalian systems, 170
Pattern and composition of ionic currents around ovarioles of the hemipteran, *Rhodnius prolixus* (Stahl), 86
Pea (*Pisum sativum* L.), 56
PENG, H. BENJAMIN, AND DING-LIANG ZHU, Ionic control of postsynaptic differentiation in muscle, 126
Polarity, 103, 145
Polarized movement, 71

R

RATHORE, KEERTI S., AND KENNETH R. ROBINSON, Ionic currents around developing embryos of higher plants in culture, 46
Relationship between growth and the electrical current of fungal hyphae, 31
Rhodnius prolixus, 86
DE RIBAUPIERRE, Yves, see Pavel Kůcera, 118
ROBINSON, K. R., see R. J. Cork, 25; Keerti S. Rathore, 46
Roots, 49, 56
RYAN, TIMOTHY, JEFFREY MYERS, AND WATT W. WEBB, Molecular interactions on the cell surface revealed by electrophoresis, 164

S

Skin, 179
SMART, TANYA, see Richard Nuccitelli, 130
SPEKSNIJDER, J. E., M. H. WEISENSEEL, T.-H. CHEN, AND L. F. JAFFE, Calcium buffer injections arrest fucoid development by suppressing calcium gradients, 9
Steady ionic currents around pea (*Pisum sativum* L.) root tips: the effects of tissue wounding, 56
STEER, MARTIN W., Calcium control of pollen tube tip growth, 18
STOLLBERG, JES, AND SCOTT E. FRASER, Electric field-induced redistribution of ACh receptors on cultured muscle cells: electromigration, diffusion, and aggregation, 157
STRAUTMAN, A. F., see R. J. Cork, 25
SUN, YI-AN, AND ROBERT J. WYMAN, The *Drosophila* egg chamber: external ionic currents and the hypothesis of electrophoretic transport, 79

T

Tip growth, 18, 31, 36
Transcellular ionic currents during primary cell wall morphogenesis in *Micrasterias* and *Closterium,* 36
TROXELL, CYNTHIA L., Transcellular ionic currents during primary cell wall morphogenesis in *Micrasterias* and *Closterium,* 36

U

Use of bioelectric currents to study gravity perception in roots, the, 49

V

VANABLE, JOSEPH W., JR., see Meicheng Chiang, 179
VERACHTERT, BAREND, AND ARNOLD DE LOOF, Intra- and extracellular electrical fields of vitellogenic polytrophic insect follicles, 91

Vibrating probe, 79
Visualizing cytoplasmic calcium in polarizing zygotes and growing rhizoids of *Fucus serratus*, 14
Vitellogenesis, 79

W

WADA, SHUNJI, see Tomoki Nawata, 41
WEBB, WATT W., see Timothy Ryan, 164
WEISENSEEL, M. H., see J. E. Speksnijder, 9
WHITE, ROSEMARY G., AND ROBYN L. OVERALL, Elongation of initially non-polar protoplasts is oriented by electric fields, 145
WINKEL, GLEN K., AND RICHARD NUCCITELLI, Large ionic currents leave the primitive streak of the 7.5-day mouse embryo, 110
WOODRUFF, RICHARD I., Charge-dependent molecular movement through intercellular bridges in *Drosophila* follicles, 71
Wound healing, 56
Wounding, 56
WYMAN, ROBERT J., see Yi-An Sun, 79

Z

Zea, 49
ZHU, DING-LIANG, see H. Benjamin Peng, 126
ZIVKOVIC, D., AND M. R. DOHMEN, Ionic currents in *Lymnaea stagnalis* eggs during maturation divisions and first mitotic cell cycle, 103

GALVANOTROPISM AND GALVANOTAXIS IN DEVELOPMENT AND REGENERATION

Nuccitelli, Richard, and Tanya Smart
Extracellular calcium levels strongly influence neural crest cell galvanotaxis 130

McCaig, Colin D.
On the mechanism of nerve galvanotropism 136

McCaig, Colin D., and Philippa J. Dover
On the mechanism of oriented myoblast differentiation in an applied electric field 140

White, Rosemary G., and Robyn L. Overall
Elongation of initially non-polar protoplasts is oriented by electric fields 145

Cooper, Mark S., John P. Miller, and Scott E. Fraser
Electrophoresis of cytoplasmic molecules through gap junctions by externally applied electric fields .. 150

Stollberg, Jes, and Scott E. Fraser
Electric field-induced redistribution of ACh receptors on cultured muscle cells: electromigration, diffusion, and aggregation 157

Ryan, Timothy, Jeffrey Myers, and Watt W. Webb
Molecular interactions on the cell surface revealed by electrophoresis 164

Parkinson, W. C., and C. T. Hanks
Experiments on the interaction of electromagnetic fields with mammalian systems 170

Chiang, Meicheng, E. J. Cragoe Jr., and Joseph W. Vanable Jr.
Electrical fields in the vicinity of small wounds in *Notophthalmus viridescens* skin 179

Index 184

CONTENTS

Preface 3

CALCIUM CONCENTRATION GRADIENTS IN DEVELOPMENT

Kropf, Darryl L.
Calcium and early development in fucoid algae ... 5
Speksnijder, J. E., M. H. Weisenseel, T.-H. Chen, and L. F. Jaffe
Calcium buffer injections arrest fucoid egg development by suppressing calcium gradients 9
Brownlee, Colin
Visualizing cytoplasmic calcium in polarizing zygotes and growing rhizoids of *Fucus serratus* 14
Steer, Martin W.
Calcium control of pollen tube tip growth 18
Miyazaki, Shun-Ichi
Calcium wave in activating hamster eggs 21
Cork, R. J., A. F. Strautman, and K. R. Robinson
Measuring cytoplasmic calcium: a review of three methods with emphasis on the practical aspects of their use 25

ION CURRENTS AND CELL POLARITY IN PLANT SYSTEMS

Gow, Neil A. R.
Relationship between growth and the electrical current of fungal hyphae 31
Troxell, Cynthia L.
Transcellular ionic currents during primary cell wall morphogenesis in *Micrasterias* and *Closterium* .. 36
Nawata, Tomoki, Tasuku Hishinuma, and Shunji Wada
Ionic currents during regeneration of thallus and rhizoid from cell segments isolated from the marine alga *Bryopsis* 41
Rathore, Keerti S., and Kenneth R. Robinson
Ionic currents around developing embryos of higher plants in culture 46
Björkman, Thomas
The use of bioelectric currents to study gravity perception in roots 49
Hush, Julia M., and Robyn L. Overall
Steady ionic currents around pea (*Pisum sativum* L.) root tips: the effects of tissue wounding 56
Miller, Andrew L.
Ion currents and growth regulators in plant root development 65

ION CURRENTS AND CELL POLARITY IN INSECTS

Woodruff, Richard I.
Charge-dependent molecular movement through intercellular bridges in *Drosophila* follicles 71
Sun, Yi-An, and Robert J. Wyman
The *Drosophila* egg chamber: external ionic currents and the hypothesis of electrophoretic transport 79
Diehl-Jones, W., and E. Huebner
Pattern and composition of ionic currents around ovarioles of the hemipteran, *Rhodnius prolixus* (Stahl) 86
Verachtert, Barend, and Arnold De Loof
Intra- and extracellular electrical fields of vitellogenic polytrophic insect follicles 91
Kunkel, J. G., and E. Bowdan
Modeling currents about vitellogenic oocytes of the cockroach, *Blattella germanica* 96

ION CURRENTS AND CELL POLARITY IN OTHER ANIMAL SYSTEMS

Zivkovic, D., and M. R. Dohmen
Ionic currents in *Lymnaea stagnalis* eggs during maturation divisions and first mitotic cell cycle 103
Winkel, Glen K., and Richard Nuccitelli
Large ionic currents leave the primitive streak of the 7.5-day mouse embryo 110
Kůcera, Pavel, and Yves de Ribaupierre
Extracellular electrical currents in the chick blastoderm 118
Oiki, Shigetoshi, Takako Ohno-Shosaku, and Yasunobu Okada
Electric currents associated with directed migration of fibroblasts 123
Peng, H. Benjamin, and Ding-Liang Zhu
Ionic control of postsynaptic differentiation in muscle 126

(Continued Cover 3)

MBL/WHOI LIBRARY
WH 1B2F Z